IMPLEMENTING METABOLOMICS TOOLS IN THE SEARCH FOR NEW ANTI-PROLIFERATIVE AGENTS FROM THE PLANT-ASSOCIATED ENDOPHYTES

A THESIS PRESENTED FOR THE DEGREE OF DOCTOR OF PHILOSOPHY IN

THE FACULTY OF SCIENCE

THE UNIVERSITY OF STRATHCLYDE

BY

YAHIA ZAKARIA ABDELQADER TABAZA

B.Sc., M.Sc.

Strathclyde Institute of Pharmacy and Biomedical Sciences

University of Strathclyde

161 Cathedral Street

Glasgow

G4 0RE

United Kingdom

May 2018

This thesis is the result of the author's original research. It has been composed by the author and has not been previously submitted for examination which has led to the award of a degree.

Signed:

Date:

Acknowledgements

First, I would like to express my deepest gratitude to the Almighty God for giving me the strength to complete this study and blessing me through all my life. I would have never become what I am without his blessings, care and guidance.

I would like to express my sincere gratitude to my supervisor Dr. RuAngelie Edrada-Ebel for giving me the opportunity to be one of her students and for her immense knowledge, patience and motivation. I owe her a lot for growing as a researcher. Her encouragement, advices, support and guidance were invaluable. She is the best supervisor that I ever could have! I wish to present my special thanks as well to my second supervisor Dr. David Watson for his assistance in LC-HRMS and to my third supervisor Mrs. Louise Young for her help in tissue culture and anti-proliferative assays.

I would like also to pay my regards to Dr. Rothwelle Tate for his help in PCR and ITS gene sequencing, Ms. Grainne Abbott for teaching me anti-proliferative assays, Mr. Craig Irving and Dr. John Parkinson for allowing me to use their NMR facility in the department of Pure and Applied Chemistry and for Mr. Gavin Bain for helping me in optical rotation experiments. Moreover, I wish to present my special thanks to Mr. Ismael Abaza for helping me in collecting the plant material and to the taxonomist Prof. Dawud Al-Eisawi for identifying the collected plants.

I am extremely grateful for the University of Jordan (JU) for generously funding my Ph.D. study and for the professors of the School of Pharmacy at JU for their constant support and encouragement.

I thank my fellow labmates in the Natural Products Metabolomics Group: Dr. Lynsey McIntyre, Dr. Ahmed Tawfike, Dr. Chiara Viegelmann, Dr. Noorwini Mazlan, Dr. Nurkhalida Kamal, Dr. Nashwa Tawfike, Prof. Venugopal Mukku, Weqas, Kirsty, Bela, Yus, Hanan, Mohamed, Bish, Iain, Ewan, Dennis and Saif for their friendship and help. I wouldn’t have enjoyed my last three years if you weren’t there!

A very special gratitude goes out to Steve, Ibrahim and Mohammad for helping me settle in Glasgow, and for all other friends that I met in this beautiful city!

And last but not least, I dedicate my heartfelt thanks to my family; mom and dad, my fiancée Rowaa and my siblings Noor, Moath and Haya for their endless love, support and prayers. I am very blessed to have you in my life. I love you all! You mean the world to me!

Table of Contents

Abbreviations

^{13}C NMR	Carbon NMR
^{1}H NMR	Proton NMR
A549	Human Caucasian Lung Carcinoma
ACAT	acyl-CoA: Cholesterol AcylTransferase
ACN	Acetonitrile
BLAST	Basic Local Alignment Search Tool
bp	Base Pair
CA	*Curvularia australiensis*
CNS	Central Nervous System
COSY	Correlation Spectroscopy
CS	*Chaetomium subaffine*
DCM	Dichloromethane
DEPT	Distortionless Enhancement by Polarisation Transfer
DMAT	Dimethylallyltryptophan
DMFD	7-Desmehtyl Fusarin C Derivative
DMSO	Dimethyl Sulfoxide
DNA	Deoxyribonucleic Acid
DNP	Dictionary of Natural Products
DPPH	2,2-diphenyl-1-picrylhydrazyl
ELSD	Evaporative Light Scattering Detector
EtOAc	Ethyl Acetate
EtOH	Ethanol
FA	*Fusarium acuminatum*
FBS	Foetal Bovine Serum
FC	Flash Chromatography
FDA	The US Food and Drug Administration
GC-MS	Gas Chromatography-Mass Spectroscopy
HBS	Hanks' Balanced Salt Solution
Hex	Hexane
HMBC	Heteronuclear Multiple-Bond Correlation
HMG-CoA	Hydroxymethylglutaryl-CoA
HMQC	Heteronuclear Multiple-Quantum Correlation

HPLC	High Performance Liquid Chromatography
HSQC	Heteronuclear Single Quantum Correlation
Hylv	D-2-hydroxyisovaleric acid
ITS	Internal Transcribed Spacer
JMod	J-Modulated Spin
LC-HRMS	Liquid Chromatography-High Resolution Mass Spectroscopy
MA	Malt-Agar
MeOH	Methanol
min	Minute
MPLC	Medium Pressure Liquid Chromatography
MTPA-Cl	Methoxy-α-Triflouro-methylphynylacetyl Chloride
MWt	Molecular Weight
NCBI	National Center for Biotechnology
NMeIle	*N*-methylisoleucine
NMeVal	*N*-methylvaline
NMR	Nuclear Magnetic Resonance
nOe	Nuclear Overhauser Effect
NOESY	Nuclear Overhauser Effect Spectroscopy
O2-PLS	Modified Orthogonal Projections to Latent Structures
OPLS-DA	Orthogonal Partial Least squares Discriminant Analysis
OSMAC	One Strain Many Compounds
PC	Principal Component
PCA	Principal Component Analysis
PCR	Polymerase Chain Reaction
PLS-DA	Partial Least Squares, or Projections to Latent Structures-Discriminant Analysis
PNT2	Human Normal Prostate Epithelium
PTLC	Preparative Thin Layer Chromatography
ROESY	Rotating-Frame NOE Spectroscopy
rRNA	Ribosomal Ribonucleic Acid
SI	Selectivity index
SIMCA	Soft Independent Modelling by Class Analogy
Semiprep-HPLC	Semi-preparative High Performance Liquid Chromatography
TBE	TrisBorateEDTA

TLC	Thin Layer Chromatography
TOCSY	Total Correlation Spectroscopy
UK	United Kingdom
US	United States
UV	Ultraviolet
ZR-75	Human Caucasian Breast Carcinoma

Publications and conferences' presentations

25 – 26 September 2017:	International Conference on Natural Product Biotechnology. Aberdeen, UK. **Short lecture:** "Implementing metabolomic tools in the search for new cytotoxic agents from the endophyte *Chaetomium subaffine*"
3 – 7 September 2017:	The 65th International Congress and Annual Meeting of the Society for Medicinal Plant and Natural Product Research (GA). Basel, Switzerland **Short lecture:** "Implementing metabolomic tools in the search for new cytotoxic agents from the endophyte *Chaetomium subaffine*"

Abstract

In the search for new anticancer agents of natural origin against breast and lung cancer (ZR-75 and A549 cancer cell lines, respectively), plant-associated endophytes could be a good source for bioactive secondary metabolites. Twenty six endophytes were obtained from four different Jordanian plants; *Anchusa strigosa*, *Anthemis palestina*, *Euphorbia peplus* and *Rumex cyprius*. Internal transcribed spacer (ITS) gene sequencing was implemented to identify the obtained endophytes. Based on their biological activity and chemical profile, three endophytes namely *Curvularia australiensis*, *Chaetomium subaffine* and *Fusarium acuminatum* were chosen for the scale-up. These endophytes were cultured in liquid and rice media at different time periods to optimise their growth and production of compounds, employing both NMR and mass spectrometry-based metabolomics. The medium that afforded better yield, more chemical diverse extract and more potent biological activity was chosen for scaling-up purposes.

Each of the scaled-up extracts was subjected to liquid-liquid partitioning followed by fractionation using a high-throughput flash-chromatography system. The fractions obtained from the first chromatography step were tested *in-vitro* against both breast and lung cancer (ZR-75 and A549 cell lines, respectively) and analysed using both proton nuclear magnetic resonance (NMR) and liquid chromatography-high resolution mass spectrometry (LC-HRMS). The HRMS data were processed with MZmine then subjected to Orthogonal Partial Least Square-Discriminant Analysis (OPLS-DA). The OPLS-DA results pinpointed the biologically active secondary metabolites. Metabolomics-guided isolation work targeted the bioactive secondary metabolites. As a result, five new compounds and ten known compounds were obtained from the three scaled-up endophytes. The isolated compounds were elucidated by employing 1D and 2D NMR then tested against ZR-75 and A549 cell lines. Twelve compounds were found active against ZR-75 cell line, which included five new compounds. Six compounds were found active against A549 cell line that included one of the new natural products isolated.

Chapter 1: Introduction

1. Introduction

1.1 Drug discovery

It's no secret that the process of drug discovery and drug development is continuous and the need for novel chemical compounds to be utilised as therapeutic agents is increasing. Many reasons push this unceasing process and the advances that are taking place in the field of drug discovery. The surge of the number of multi-drug resistant microbes is one of the reasons that are boosting the field of discovering new antibiotics (Strobel, 2003, Yu *et al*., 2010, Alvin *et al*., 2014, Wu *et al*., 2015). Moreover, new life-threatening infections, cancers and diseases are playing a major role in keeping the truck of drug discovery moving on (Alvin *et al*., 2014).

The road of drug discovery diverges into three pathways. The first pathway is rational drug design, where a drug is tailored to fit its suggested target (Mandal *et al*., 2009). The second pathway is combinatorial chemistry, where huge number of compounds is prepared *in silico* to form a combinatorial library, which, in turn, is tested against the suggested target to determine the most potent and active compounds (Gallop *et al*., 1994, Liu *et al*., 2017b). The third pathway is the phenotypic screening of natural product in drug discovery (Alvin *et al*., 2014). Phenotypic screening allows the evaluation of the activity of natural products at the cellular, tissue, or whole organism level without the need of prior understanding of the molecular mechanism of action of those natural products (Swinney and Anthony, 2011, Chang and Kwon, 2016). In the past few years, pharmaceutical companies and research centres became more interested in the first two pathways which utilise the latest technologies of research, *i.e.* 3D X-ray crystallography, drug-docking and computer based tools in their favour (Mueller, 2009).

However, there are still some striking disadvantages in employing rational drug design and combinatorial chemistry. Laboratory synthesised compounds and combinatorial outcomes have limited structural rigidity and complexity while lots of purification work and bioactivity testing are still needed to identify the bioactive compounds (Baker *et al*., 2000). Furthermore, it will be difficult to select potential targets for structure-guided drug design until the detailed mechanisms of targeted cell death and survival are first fully elucidated (Barry and Blanchard, 2010). All these hurdles make it worthy to knock on the door of natural products research and to get back to the fundamental role they used to play in pharmaceuticals.

1.2 Natural Products

1.2.1 Introduction to natural products

Natural products are chemical compounds produced by a living organism. Although the plant kingdom is considered as the most common source of natural products, innovative resources also cover natural products from animals, fungi, and bacteria (Harvey, 2008, Sarker and Nahar, 2012, Alvin *et al*., 2014). Natural products are divided into two groups, primary metabolites and secondary metabolites. Primary metabolites are compounds produced by a living organism that are essential for its life and growth, like starch and cellulose. In contrast, secondary metabolites are low molecular weight compounds that are not required for the growth of an organism, but are produced for adaptation for its specific functions in nature and are considered a phenotype of the organism, as these metabolites are produced as a result of a gene translation process (Harvey *et al*., 2015, Nisa *et al*., 2015).

Historically, natural products were the exclusive source of all therapeutic preparations. Natural products, including terrestrial higher plants and herbs, were used as therapeutic agents in ancient Mesopotamia, Greece, India, and China (Harvey, 2008, Sarker and Nahar, 2012). Even in the ages of industrial revolution and world wars, the discovery of important therapeutic agents from natural origin was continuum and resulted in the discovery of important drugs. For example (Figure 1.1), digoxin from foxglove discovered by William Withering was used as a cardiotonic; morphine from poppies discovered by Freidrich Serturner was used as a pain killer; aspirin, from salicylic acid of willow bark, was synthesised by Felix Hoffmann and, of course, the famous penicillin that was discovered by Alexander Fleming from mould was among the first antibiotics discovered (Rishton, 2008).

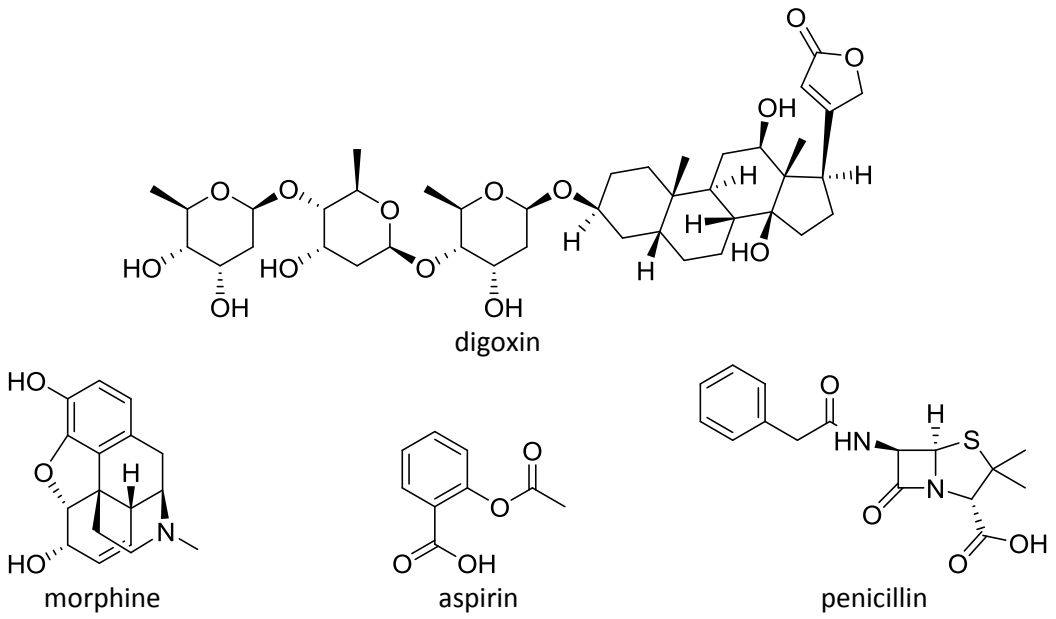

Figure 1.1: Drugs from natural origin isolated at 1785 – 1928.

Nowadays, natural products provide leads for compounds that are being submitted to clinical trials, especially anticancers and antimicrobials (Harvey *et al*., 2015). Nonetheless, there are few misconceptions about natural products. An example of those misconceptions is the belief that natural products are old fashioned and incompatible with the latest technologies that are utilised in drug discovery and those that are based on high-throughput screening directed at molecular targets. Another example is the overestimation of the difficulties of isolating and purifying natural products from their origin (Harvey *et al*., 2015). But fortunately, these misconceptions haven't stopped the research of natural products for drug discovery.

Despite the trend of favouring totally synthesised compounds and combinatorial chemistry outcomes, 44% of all new approved drugs were still either biological macromolecules, unaltered natural products, botanical drugs (defined mixture) or natural product derivatives (Newman and Cragg, 2016). In addition to that, 21% were synthetics that mimic natural products (Figure 1.2). Therefore, in spite of the major role that combinatorial chemistry plays in drug development and discovery process, the trend toward the synthesis of complex natural product-like libraries is also persevering (Newman and Cragg, 2016). Codes used in Figures 1.2, 1.4 and 1.5 are listed in (Table 1.1).

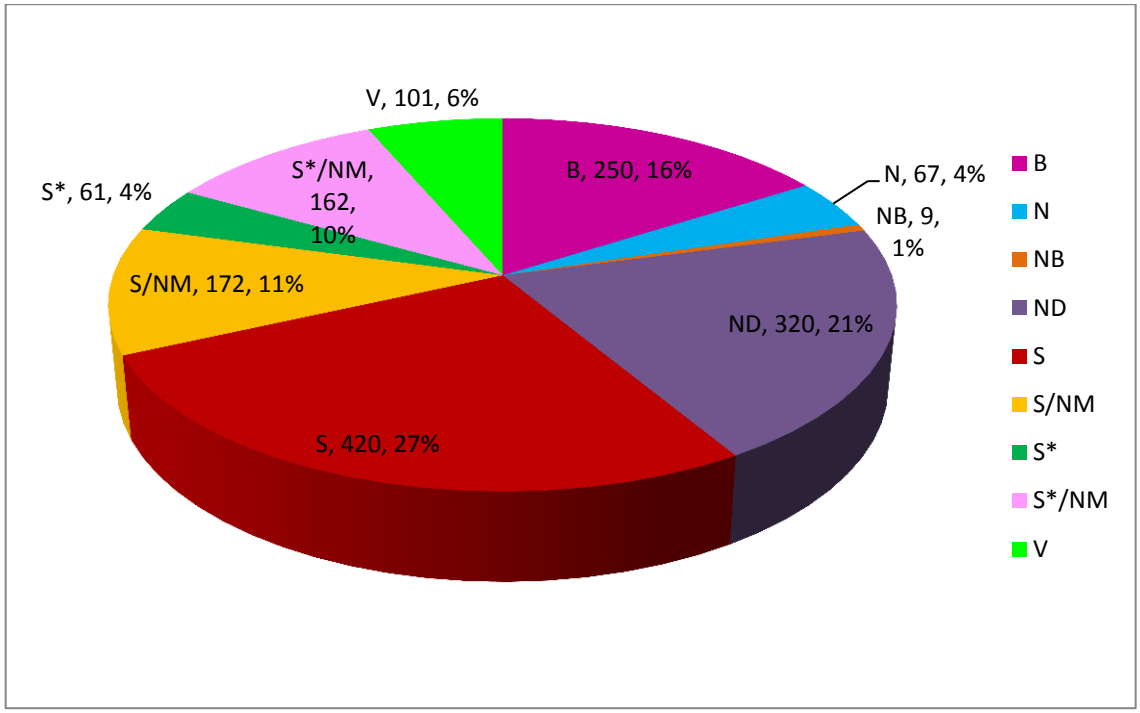

Figure 1.2: All new approved drugs 1981 – 2014; *n* = 1562 (Newman and Cragg, 2016).

Table 1.1: Codes used in Figures 1.2, 1.4 and 1.5.

Code	Brief definition, year
B	Biological macromolecule, 1997
N	Unaltered natural product, 1997
NB	Botanical drug (defined mixture), 2012
ND	Natural product derivative, 1997
S	Synthetic drug, 1997
S*	Synthetic drug (NP pharmacophore), 1997
V	Vaccine, 2003
/NM	Mimic of natural product, 2003

Treatment of cancer, infectious diseases, and diabetes are of great potential for natural products and are the most promising fields for natural products to be employed in (Harvey, 2008, Harvey *et al*., 2015). This is referred to the boundless diversity of the chemical structures in natural products (Harvey, 2008). The significant numbers of antitumors, antibacterials and antifungals that have been approved from 2006 to 2010 confirm this, as half of them were natural products or their derivatives (Newman and Cragg, 2012). And of the thirteen new approved natural-product related drugs between 2005 and 2007, five compounds were the

first members of new classes of drugs, the peptides exenatide (4.19 kDa) and ziconotide (2.64 kDa) in addition to ixabepilone, retapamulin and trabectedin (Figure 1.3) (Harvey, 2008). This confirms the great potential of natural products to provide leads and novel compounds to the area of drug discovery. In particular, those compounds that are currently undergoing clinical trials, the biggest portion of which are mostly of plant or microbial origin (Harvey, 2008).

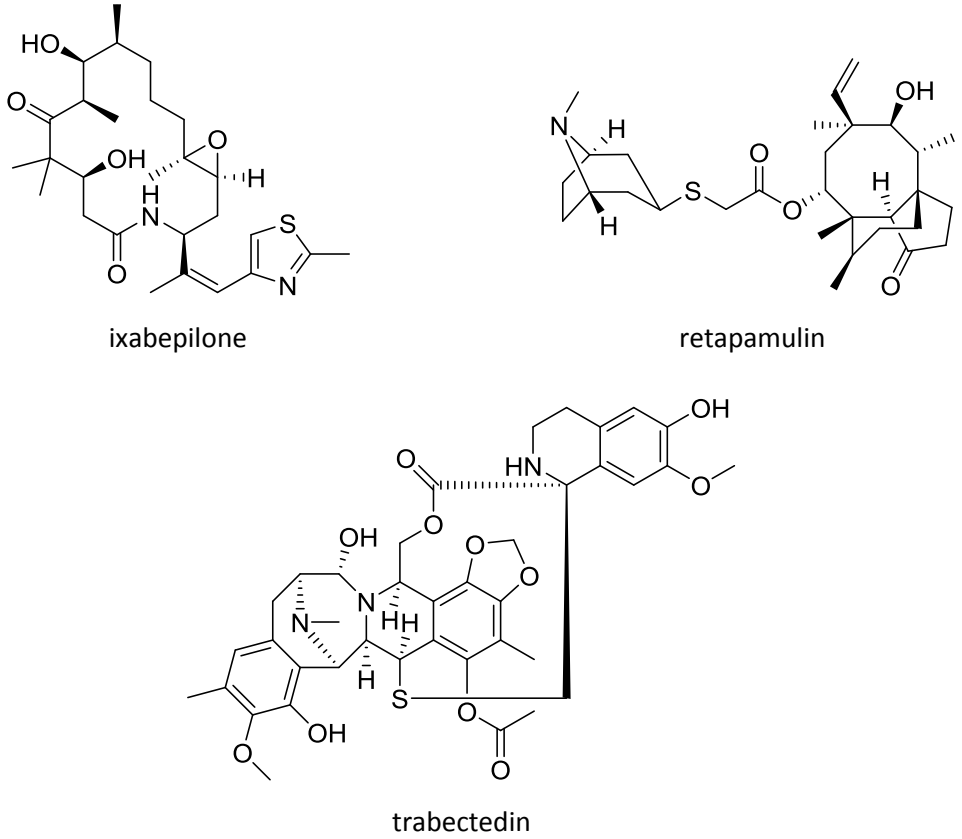

Figure 1.3: Secondary metabolites discovered at 2005 – 2007 and represented new classes of drugs.

Specifically new for anticancer drugs, between 1981 and 2014, 52% of all new approved drugs were of natural origin and 25% were synthetics that mimic natural products (Figure 1.4). For the period, 1940 to 2014, 51% of all new approved anti-cancer drugs were of natural origin while 19% were synthetics that mimic natural products (Figure 1.5) (Newman and Cragg, 2016). This indicates the importance of natural products as a source for new cytotoxic, anti-proliferative and anticancer agents.

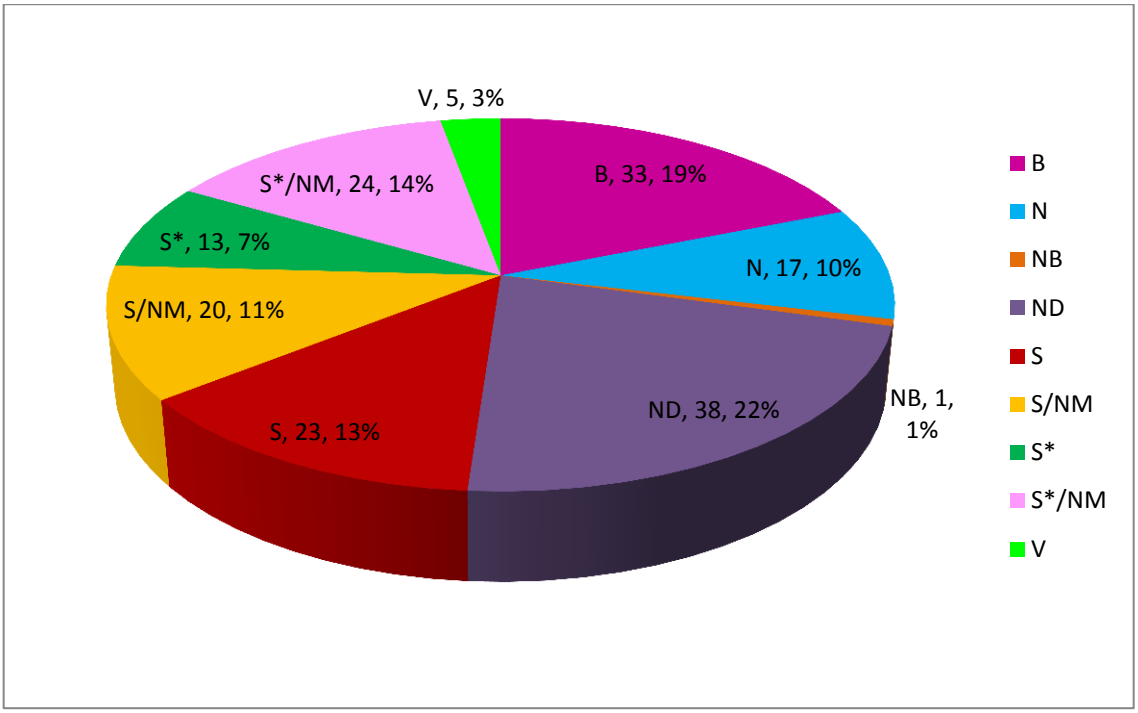

Figure 1.4: All anticancer drugs 1981 – 2014; *n* = 174 (Newman and Cragg, 2016). Codes are mentioned in Table 1.1.

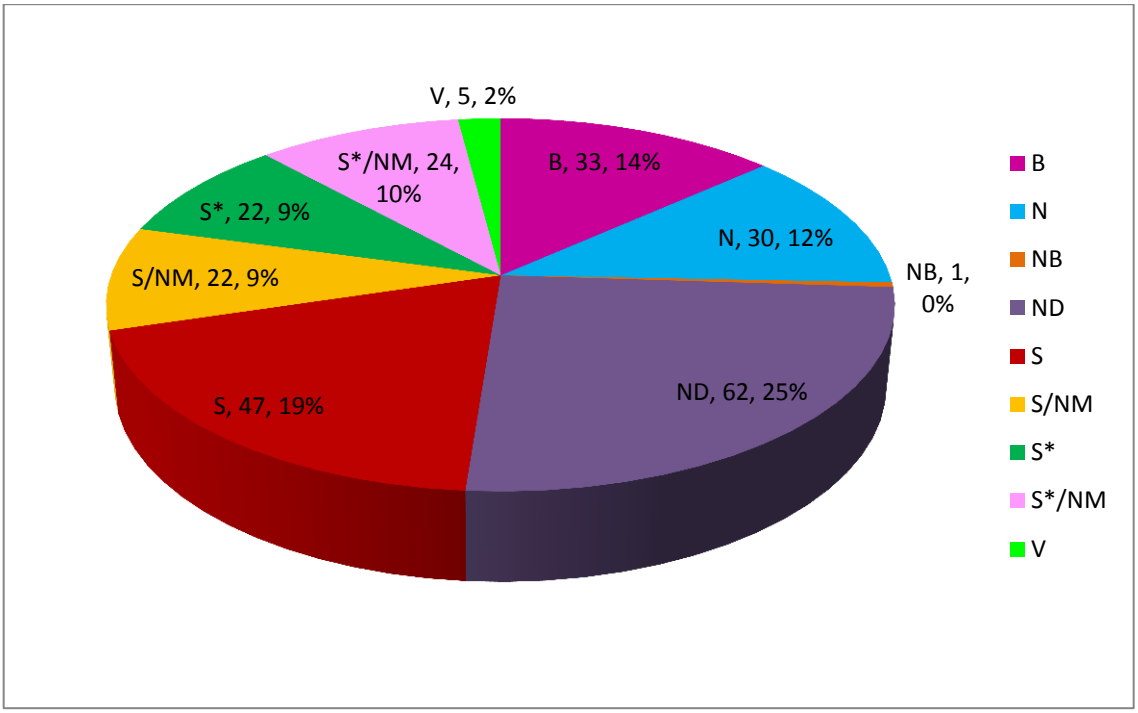

Figure 1.5: All anticancer drugs 1940s – 2014; *n* = 246 (Newman and Cragg, 2016). Codes are mentioned in Table 1.1.

Still, one shall not overlook the anticipated decreasing interest of pharmaceutical companies on natural products, especially in the 1990s and 2000s (Baker *et al*., 2007). The limitations of natural products include the complexity of their chemistry that may hinder their usage, decrease their solubility and limit their use in parenteral preparations or decrease their stability (Harvey, 2008, Chen *et al*., 2015). Nonetheless, chemical and structural modifications could be introduced to overcome those challenges, to improve their physicochemical properties, their plasma stability, their potency and their selectivity and even their ability to cross blood brain barrier (Chen *et al*., 2015). Moreover, the availability of enough supply of chemical compounds for development and market needs is still an issue when accessing some natural products' sources or maintaining their sustainability and cultivability (McChesney *et al*., 2007). Furthermore, concerns about the intellectual property rights and getting legal access and use of the natural resources outside the supplier's zone of jurisdiction are still an issue to be solved (Mays and Mazan, 1996, Harvey, 2008). The United Nations Convention on Biological Diversity stated that countries have sovereign rights over the genetic resources in their territories, and

the access to genetic resource by foreigners will require the authorisation of the source country. The source country should be involved in researches that take place on its genetic resources and benefit from technology transfer and from the genetic resources it possesses (Monge *et al*., 2000, Baker *et al*., 2007, Harvey, 2008, Harvey *et al*., 2015). This will alienate pharmaceutical companies and investors who still prefer to use combinatorial chemistry as superior to natural products in meeting the demands of automated high-throughput screening programs and creating large sets of chemical derivatives and families that could be utilised as drugs (Baker *et al*., 2007, Harvey, 2008).

On the other hand, natural products possess structural diversity that makes them suitable for lots of targets and receptors as well as appropriate models for drug design (Chen *et al*., 2017). They also have a wide range of pharmacophores and a vastness of stereochemistry, which enable them to provide hits against screening targets, even for the more difficult protein-protein interactions (Drewry and Macarron, 2010, Gray *et al*., 2012, Chang and Kwon, 2016). Furthermore, they have the advantage of being good substrates for many cellular transporter systems which give them the ability to act intracellularly (Harvey *et al*., 2015, Chatzikonstantinou *et al*., 2017). This is referred to the fact that 83% of their core scaffolds are not present in commercially available synthetic molecules and screening libraries (Chen *et al*., 2015). In addition to that, natural products cover parts of the chemical space that are not represented by synthetic compounds, suggesting more novel potential interaction between the natural product and biological structure space of some targets (Gray *et al*., 2012, Harvey *et al*., 2015). Moreover, on average, natural products are more readily absorbed from the gastrointestinal tract than synthetic drugs when they conform to the Lipinski's rule of five and will have broader dispersion in structural and physicochemical properties than synthetic compounds (Harvey, 2008, Quinn *et al*., 2008, Chen *et al*., 2015).

1.2.2 New approaches and technologies in utilising natural products for medical uses

The traditional approach of bioassay-guided isolation of natural products is being modified nowadays to make use of technological advances, to adapt current understanding in medicinal chemistry and to utilise cheminformatics approaches in designing libraries to explore biologically relevant chemical space. Advances such as the use of pre-fractionation high-

throughput strategies has improved the applicability of natural-product-based screening collections, and eased the comprehensive removal of compounds that are likely to cause artefacts and interferences (Abel *et al*., 2002, Gray *et al*., 2012, Harvey *et al*., 2015). The pharmaceutical company, Wyeth, made use of the high-throughput screening that was introduced into drug discovery and created a pre-fractionated natural product library for drug or lead likeness (Wagenaar, 2008). Furthermore, metabolomics and chemometrics could be applied to natural products (Harvey, 2008, Yuliana *et al*., 2011). Metabolomics can explore the phenotypic ability of an organism to produce secondary metabolites, cut down purification work by pinpointing the interesting and bioactive compounds and prioritising fractions for further purification, optimise fermentation and production conditions for secondary metabolites that are obtained from microorganisms and predict biosynthetic precursors that can aid in engineering pathways to produce more of the desired natural product (Bochner, 2009, Tawfike *et al*., 2013, Macintyre *et al*., 2014, Harvey *et al*., 2015). Other new approaches include the use of molecular biology and genetic engineering to render bacteria capable of producing drug-like compounds (Chang and Keasling, 2006, Watanabe and Oikawa, 2007) and metagenomic approach that involves sampling bacterial DNA from an environmental sample and cloning it in a industrially robust host organisms (Gillespie *et al*., 2002, Sanka Loganathachetti and Muthuraman, 2015). Moreover, a mutasynthetic approach was introduced, and it is used to produce natural products by applying a combination of synthetic and natural enzymatic methods (Kopp and Marahiel, 2007, Knobloch *et al*., 2012). And of most importance is the role of microbes themselves as sources of novel bioactive drugs. There are molecules that depend on the interaction among organisms in their production. An example of these interactions include the activation of silent gene clusters in fungi, the activation of natural products synthesis in one organism by another and the role of endophytes in producing natural products (Newman and Cragg, 2012).

1.3 Endophytes as sources of secondary metabolites

Despite being sessile, plants have a mutualistic network that connects them with their exterior environment and ensures their interaction with different organisms. Thus, plants are in continuous interspecies cross talk with many microorganisms, including endophytes (Kusari *et al*., 2014). In 1866, the term "Endophyte" was first introduced by the German botanist and

microbiologist Heinrich Anton (Nisa *et al*., 2015). Endophytes are microorganisms that colonise intercellular and intracellular regions of healthy plant tissues without causing an apparent harm to those tissues while eliciting strong defence responses (Yu *et al*., 2010, Reinhold-Hurek and Hurek, 2011, Alvin *et al*., 2014, Kusari *et al*., 2014). In the most cases, those endophytes are fungi, one of the most diverse lifeforms on the planet. However, they could be bacterial as well, particularly, actinomycetes (Bhimba *et al*., 2012, Nisa *et al*., 2015, Shah *et al*., 2017). Plants provide a store for a huge number of endophytes that could be found in almost all plants from herbs to trees and even in algae (Strobel, 2003, Samaga and Rai, 2016).

In fact, the endophytic-plant symbiosis is not the only kind of symbiosis occurring between plants and fungi. Fungi-plant symbioses are subcategorised into two groups, mycorrhizal and endophytic. Mycorrhizal associations are more common than the endophytic ones and include the interaction between the plant, the mutualistic fungi and the soil factors. Mycorrhizal associations are usually non-pathogenic and may enhance the production of certain metabolites by the plant by the transmission of chemical signals between the root of the plant and the mycorrhizal fungus (Yuan *et al*., 2007). On the contrary, endophytic associations are more complicated and take place usually in the above ground plant parts. Nonetheless, roots could contain endophytes as well (Yuan *et al*., 2007). In the case of endophytic-plants associations, the metabolites could be either produced by the endophyte itself, by the plant as a result of endophytic eliciting factors that induce the production in the plant tissues or by complex interaction between the endophyte and the plant that result in either structural modifications or partial synthesis of the compound that is produced by one life form by the other (Ludwig-Muller, 2015, Wani *et al*., 2015).

Plant endophyte symbiosis and interactions attracted researchers in the past few years for their potential in providing good candidates and unique metabolites for drug discovery and novel leads for new classes of drugs (Strobel, 2003, Aly *et al*., 2011). The interest in studying plant associated endophytes is increasing as they represent a relatively unexplored area of biochemical diversity. Moreover, the role that endophytes play in the protection of plants against harmful microbes and pathogens could be directed to the discipline of creating new antibiotics and anti-infective agents. In addition to that, as the plant is a eukaryotic system in which the endophyte resides, the compounds that endophytes produce may have reduced cell

toxicity (Strobel and Daisy, 2003, Strobel, 2003, Chadha *et al*., 2015). Furthermore, the interaction of endophytes with their environment may grant them the ability to produce novel secondary metabolites (Schulz *et al*., 2002).

1.3.1 Plant-endophyte interactions

Endophytes don't cause apparent harm on the hosts' tissues and their relation with plant is mutually beneficial (Grayer and Kokubun, 2001). Nevertheless, plant-microbe interactions are not always endophytic. Depending on their effects on the plant, these interactions could be pathogenic, saprophytic or beneficial (Lugtenberg *et al*., 2002). The plant-endophyte relationship is old, as evidences of plant-associated microbes has been discovered in the fossils of plants' stems and leaves (Taylor and Taylor, 2000). So, there are beliefs that a horizontal genetic information transfer might happen between host plants and endophytes (Stierle *et al*., 1993b, Taghavi *et al*., 2005). Thus, the same biosynthetic pathway may have been developed in both the host plant and endophyte and lead to the production of similar secondary metabolites from both organisms (Bomke and Tudzynski, 2009, Alvin *et al*., 2014). Nonetheless, well-matched architectural, morphological and physiological traits of endophyte and host plant are required for a highly integrated and specialised symbiosis to persist (Saikkonen *et al*., 1998, Saikkonen *et al*., 2004).

It's challenging to understand the behaviour of microbes and their interactions in their natural and complex habitats, and plant-endophytes interactions are no exception. The first step in order for plant-microbe interaction to take place is the recognition of the plant by microbes. It is a key to initiate a plant's response to the microbes. This response could be either a physical interaction that involves adhesins, fimbriae or flagella or a chemical interaction that involves the use of signalling molecules, followed by spore germination, penetration of the epidermis by the endophyte and the colonisation of plant tissues by the endophyte (Lugtenberg *et al*., 2002, Hardoim and Van Elsas, 2013). Good colonisation requires a strong defence by the microbe's cells, an efficient uptake of nutrients and a weakening or destruction of the competing organisms that are attempting to colonise the same plant (Lugtenberg *et al*., 2002, Sieber, 2007, Nisa *et al*., 2015). Furthermore, phase variation may be involved to escape the host's

immune system. Finally, the synthesis of extracellular enzymes and the secondary metabolites by the microbe could begin (Lugtenberg *et al*., 2002).

Endophytic fungi and bacteria are living organisms that lack chlorophyll, and hence, they lost their ability of photosynthesis. Therefore, they spend the whole or part of their life cycles colonising host organisms, especially plants, for their carbon and energy sources without causing any apparent symptoms of diseases (Grayer and Kokubun, 2001, Nisa *et al*., 2015, Behie *et al*., 2017). On the other side, plants benefit from the secondary metabolites that are produced by the endophytes as well. It is believed that a plant's ability to adapt to biotic and abiotic stress factors depends on the secondary metabolites produced by the endophytes (Giordano *et al*., 2009, Aly *et al*., 2011). Accordingly, the biological defence of a plant against foreign pathogens is supported by this symbiotic relationship with its endophytes (Alvin *et al*., 2014). This could be achieved by the release of antibacterial, antifungal, antiviral or insecticidal secondary metabolites by the endophyte to directly attack the pathogens and lyse the affected cells or by the induction of the plant's defence mechanism and promotion of its growth to compete for cell apoptosis that will enhance the growth and the competitiveness of the host plant in nature (Strobel, 2003, Berg and Hallmann, 2006, Kloepper and Ryu, 2006, Alvin *et al*., 2014, Nisa *et al*., 2015). Moreover, endophytes' secondary metabolites can help the host plant to adapt to its adverse environmental conditions (Aly *et al*., 2010). Furthermore, the growth of plants colonised by certain endophytes is accelerated by the production of phytohormones (Owen and Hundley, 2004).

1.3.2 The applications and uses of plant-endophyte interactions

The secondary metabolites that are produced by endophytes and involved in the host-endophyte relationship are of great potential in drug discovery and proved to be a promising reservoir of medical natural products (Strobel, 2003, Wani *et al*., 2016). Those endophytes have unique genetic and biological systems that granted them the applicability to be used outside their host plants (Strobel, 2003). Diverse chemical classes like steroids, xanthones, phenols, coumarines, quinones and terpenes have been isolated from endophytic fungi explaining their important role in drug discovery (Geris dos Santos *et al*., 2003, Schulz and Boyle, 2005, Verma *et al*., 2009, Nisa *et al*., 2015). Moreover, the ability of endophytic secondary metabolites to

work as antibiotics, anticancers, antioxidants, and anti-inflammatories has integrated their role in drug discovery (Chow and Ting, 2014, Sudha *et al*., 2016, Zhang *et al*., 2016).

Many plants and natural products producers such as marine invertebrates are considered as a rich source of novel metabolites. However, they are uncultivable and unsustainable, which limit their possible commercial success. Fortunately, their metabolites could be produced through biotechnology and fermentation techniques by scaling up cultures of their resident endophytes which, in turn, could act as a supplier for novel bioactive metabolites (Reinhold-Hurek and Hurek, 2011, Alvin *et al*., 2014, Kusari *et al*., 2014, Macintyre *et al*., 2014, Harvey *et al*., 2015).

Another possible application is the *in vivo* or *in vitro* co-culture system of plant tissues, fungi and bacteria. This approach was inspired by the endophytic infection of plants that is assumed to be an effective tool for biotic elicitation of their secondary metabolites (Yuan *et al*., 2007). Several studies have shown that the inoculation of generated plants *in vitro* with endophytic fungi promoted the biomass and enhanced the production of secondary metabolites in plant suspension cells (Mucciarelli *et al*., 2003, Sherameti *et al*., 2005, Wan, 2015). Moreover, co-culture of different endophytes could initiate the expression of silent gene clusters that may code for the synthesis of novel and biologically active metabolites or enhance the production of known metabolites and increase their yield (Ola *et al*., 2013). Furthermore, some novel and biologically active secondary metabolites occur as minor components. This problem could be solved by overexpressing their biosynthetic gene clusters in cultivable organisms such as endophytes (Kalaitzis, 2013, Nah *et al*., 2013, Stevens *et al*., 2013).

The close biological associations that were developed in plant-endophyte symbiotic systems make them superior to epiphytes and soil-related organisms in the terms of number and chemical diversity of the produced secondary metabolites, and hence, more appealing to study (Strobel, 2003). Mycorrhizal fungi are higher in their compatibility with the host plants than endophytic fungi. However, they have less host specificity; as a result, mycorrhizal fungi were considered inferior to endophytic fungi in terms of producing novel and biologically active secondary metabolites (Bacon and White, 2000).

1.3.3 Some of the hurdles that limit working with plant-associated endophytes

Nevertheless, there are some problems that need to be dealt with when plant-associated endophytes are to be studied. Firstly, it is crucial to correctly identify the fungal endophyte. This might not be always an easy task as many fungi exhibit different anamorphs and teleomorphs in plants and *in vitro* (Webster and Weber, 2007). Thus, the classical taxonomic identification is not enough for fungal endophytes and the sequencing of the internal transcribed spacer (ITS) region of ribosomal ribonucleic acid (rRNA) should be performed for a correct identification (Gardes and Bruns, 1993, Horton and Bruns, 2001, Kusari *et al*., 2014). ITS region has several advantages over other regions; only little amount of it is needed for amplification, it has a well-conserved fungal specific priming sites that are directly adjacent to highly variable regions which allow the use of same primers to identify different genera and species, the availability of comparison sequences in addition to its correlation with the morphologically defined species (Peay *et al*., 2008). On the other hand, with the identification of bacterial endophytes, the implementation of 16S rRNA-based phylogenetic analysis is deemed necessary (Hentschel *et al*., 2001, Macintyre *et al*., 2014).

Furthermore, it's difficult to allow constant expression of the biosynthetic genes that are required for the production of novel bioactive secondary metabolites in certain fermentation conditions. Repeated subculturing diminishes the production of secondary metabolites, especially if monoculture techniques were used. Such standard culture conditions do not activate the expression of certain cryptic gene clusters of the endophyte, and hence, will lead to the production of less diverse secondary metabolites than expected (Scherlach and Hertweck, 2009, Kusari and Spiteller, 2011, Kusari *et al*., 2014).

1.3.4 Examples of drugs obtained from endophytes

The most prominent example of drugs obtained from endophytes is the happy story of the multibillion dollar anticancer drug taxol (Figure 1.6). It was first isolated from the traditional medicinal plant Pacific yew tree, *Taxus brevifolia* (Wani *et al*., 1971). Taxol was isolated from other species of *Taxus* as well, however, this genus is slow-growing, limited geographically and cannot be cultivated in an economical scale. Nonetheless, the discovery of the endophyte

Taxomyces andrenae from this plant provided a more reasonable source of taxol without the mass destruction of ancient yew trees (Stierle *et al*., 1993a, Stierle *et al*., 1995).

Furthermore, native people of North Australia used the ground-up mass of a medicinal plant known as snakevine (*Kennedia nigricans*) for both treating infections and wound healing. This plant was harvested and searched for endophytes. One of the endophytes that were isolated from this plant is *Streptomyces* sp. NRRL 30562 which showed to be active when tested against several microorganisms. This bacterial endophyte produced novel peptide antibiotics named as munumbicins. They possessed wide spectrum activity against many human and plant pathogenic microorganisms. For example, munumbicin B (1.27 kDa) was found active against a methicillin resistant strain of *Staphylococcus aureus* with a minimal inhibitory concentration of 2.5 µg/mL and munumbicin D (1.31 kDa) was found active against the malarial parasite *Plasmodium falciparum* with an IC_{50} of 4.5 ng/mL (Castillo *et al*., 2002).

Moreover, the endophytic fungus *Cryptosporiopsis cf. quercina* was isolated from the medicinal plant *Tripterigeum wilfordii* and was able to produce the novel peptide cryptocandin that possessed activity against the pathogenic fungi *Sclerotinia sclerotiorum* and *Botrytis cinerea* (Figure 1.6) (Strobel *et al*., 1999).

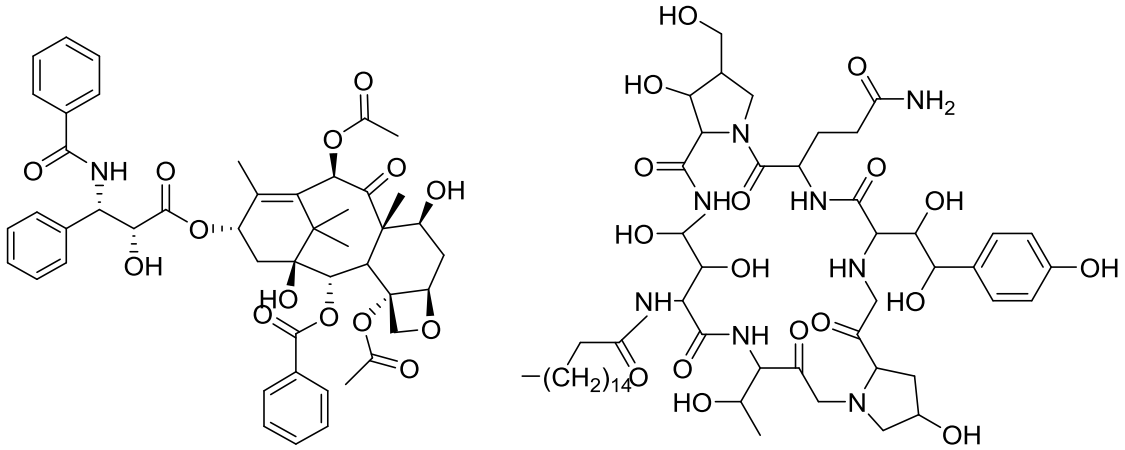

Figure 1.6: Bioactive secondary metabolites obtained from endophytes.

1.4 Plants used for this project

When plant-endophyte symbiosis is studied and new secondary metabolites from endophytes are targeted, the importance of natural plant selection cannot be overlooked. This is referred to the correspondence of secondary metabolites that certain fungus might synthesise to its respective ecological niche (Gloer, 2007). In addition to that, the metabolic interactions an endophyte might have with its environment will affect the secondary metabolites it produces in the terms of type and quantity (Schulz *et al*., 2002). Moreover, plants that live in unique environments, especially those that possess survival strategies for survival of harsh conditions, should be considered for study, as endophytes and their secondary metabolites may be responsible for the survival and adaptation of the host plant (Strobel *et al*., 2004, Yu *et al*., 2010). Furthermore, plants that grow in areas of great biodiversity could be hosting endophytes of great biodiversity as well (Strobel *et al*., 2004). Healthy plants surrounded by pathogen-infected plants could be a host for interesting endophytes that produce antimicrobial secondary metabolites (Tuntiwachwuttikul *et al*., 2008). Other good options are plants that have ethnobotanical history and were used in traditional medicine, as their activity might be related to secondary metabolites produced by the endophytes they contain (Ji *et al*., 2005). Additionally, plants that have exceptional longevity or those that occupied certain ancient land mass could host endophytes with active secondary metabolites (Strobel and Daisy, 2003).

When a suspected plant is collected and its endophytes are isolated, a crude extract from the fermentation of each endophyte should be tested *in vitro*. Following that, the isolation work and the separation of active metabolites will take place, followed by further biological screening and identification of interesting and bioactive compounds (Yu *et al*., 2010).

Four different plants of Jordan flora were selected for this project, *Anchusa strigosa* [Soland.] (Boraginaceae), *Anthemis palestina* Reut. ex Boiss. (Asteraceae), *Euphorbia peplus* L. (Euphorbiaceae) and *Rumex cyprius* Murb. (Polygonaceae).

1.4.1 *Anchusa strigosa* [Soland.]

Anchusa strigosa [Soland.] is a member of Boraginaceae family. It is used locally in Jordan to treat fever, skin and respiratory system diseases, weariness, exhaustion, burns, wounds, ulcers,

cough, rheumatic pain and to clean blood. Its leaves are used as counter-irritants and for bone fractures and its roots extract is used for abdominal pain and as a diuretic (Al-Khalil, 1995, Qasem, 2015).

Alali and his colleagues screened 95 plant species from Jordan's flora for antioxidant activity. Two species of *Anchusa*; *Anchusa italica* and *Anchusa strigosa* exhibited antioxidant activity when screened by Trolox equivalent antioxidant capacity assay. A linear correlation was detected between the phenolic content of a screened extract and its antioxidant activity (Alali *et al*., 2007).

Chloroform extract of flowers of Iranian *Anchusa strigosa* yielded four aliphatic hydrocarbons, while the methanolic extract was rich in amino acids and proteins (Kohli and Ali, 2003). Two anthocyanidins; malvidin and pelargonidin were also isolated and deemed responsible for the pink-violet colour of this plants' flowers (Figure 1.7) (Kohli and Ali, 2003). These anthocyanidins were used in folk medicine as anti-infective agents (Borras-Linares *et al*., 2015). Other studies showed that the anticancer activity of anthocyanidins is correlated to the inhibition of cyclooxygenase enzyme and their antioxidant activities (Hou *et al*., 2004, Thomasset *et al*., 2009).

Anchusa strigosa that was collected from Amman, Jordan afforded six pyrrolizidine alkaloids, including four retronecine derivatives, one trachelanthamidine derivative and one supinidine derivative (Figure 1.7) along with several known compounds (Braca *et al*., 2003). The previously isolated pyrrolizidine alkaloids found to be active against *Spodoptera exigua* and *Pieris brassicae* larvae. All compounds showed antifeedant activity against the tested herbivores (Siciliano *et al*., 2005).

The aqueous extract of the roots of Jordanian *Anchusa strigosa* inhibited pepsin enzyme (Abuereish, 1998). Furthermore, oral administration of this extract protected stomachs of the tested rats against the induced ulcers as well as treated induced ulcer in guinea pigs. However, symptoms of depression were observed when it was administered in higher concentrations (Disi *et al*., 1998). The ethanolic extract of Iraqi *Anchusa strigosa* showed inhibitory effects on aryl hydrocarbon hydroxylase in rats, an enzyme that is responsible for converting inert

polycyclic aromatic hydrocarbons into reactive intermediates that bind to cellular macromolecules causing cancer (Alwan *et al*., 1989).

Flower extract of *Anchusa strigosa* from India yielded glucose, rhamnose and ribose. Moreover, a semi-purified glycoside was isolated and showed a mild to moderate hypotensive activity when tested in cats (Garg *et al*., 1970).

No published work was found regarding the endophytes of *Anchusa strigosa* or any other species of the genus *Anchusa*. However, from another member of the Boraginaceae family, 12 fungal endophytes were isolated from *Symphytum officinale*, four endophytes were active when tested *in vitro* against the plant pathogen *Sclerotinia sclerotiorum* that damages bean crops. These endophytes included *Candida pseudotropicalis*, *Candida tropicalis*, *Trichophyton* sp. and *Chrysosporium* sp. (Rocha *et al*., 2009).

Based on its uses in folk medicine and previous research, *Anchusa strigosa* could be a lodge for endophytes that produce interesting and biologically active secondary metabolites, as they haven't been obtained or investigated before. Thus, the endophytes of this plant were considered in this project.

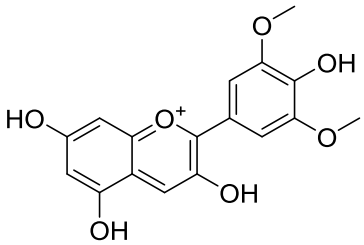
malvidin

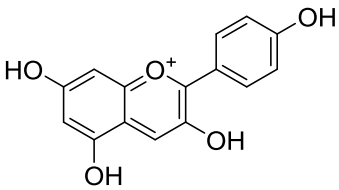
pelargonidin

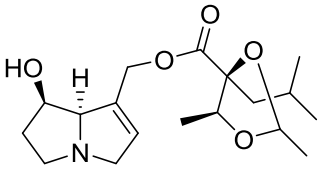
retronecine derivative-1

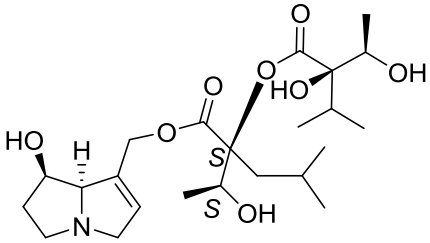
retronecine derivative-2

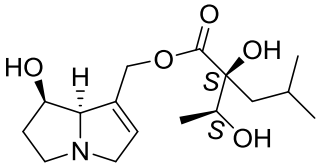
retronecine derivative-3

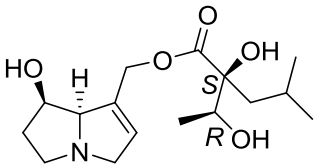
retronecine derivative-4

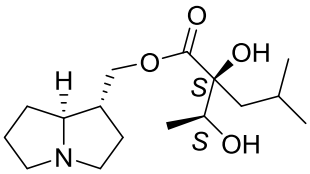
trachelanthamidine derivative

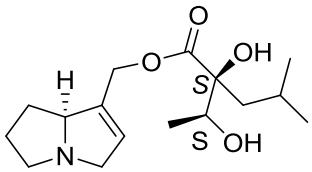
supinidine derivative

Figure 1.7: Secondary metabolites isolated from *Anchusa strigosa*.

1.4.2 *Anthemis palestina* Reut. ex Boiss.

Anthemis palestina Reut. ex Boiss. is a member of the family Compositae (Asteraceae). It is used locally in Jordan and Palestine as an antispasmodic, antibacterial, anti-inflammatory and antioxidant (Bardaweel *et al*., 2014, Jaradat *et al*., 2016a). Hydro-distillation of the flowers of *Anthemis palestina* collected from Northern Jordan yielded essential oil (Tawaha *et al*., 2015). The essential oil was analysed by gas chromatography-mass spectroscopy (GC-MS) and contained 109 compounds, of which, most were terpenes. The principal oil components were spathulenol, germacrene-D and caryophyllene oxide (Figure 1.7). The essential oil was cytotoxic when tested using Brine Shrimp Lethality test with an LC_{50} of 12.0 mg/mL (Tawaha *et al*., 2015).

Furthermore, Hydro-distillate of dried flowers of *Anthemis palestina* afforded essential oil exhibiting antioxidant activities *in vitro*, as well as antibacterial activities against both gram positive bacteria (*Bacillus subtilis, Staphylococcus aureus* and *Staphylococcus epidermidis*) and gram negative bacteria (*Escherichia coli, Pseudomonas aeuriginosa* and *Xanthomonas vesicatoria*). Moreover, the oil showed moderate antifungal activity against *Candida albicans*, *Candida glabrata* and *Candida krusei*. In addition to that, it possessed cytotoxic activity against human cervix adenocarcinoma (HeLa), human Burkitt lymphoma B (BJAB) and human colon adenocarcinoma (Caco-2) cell lines (Bardaweel *et al*., 2014).

Methanolic extracts of *Anthemis palestina* along with other 22 Jordanian plants were tested *in vitro* to search for novel xanthine oxidase inhibitors. The extract of *Anthemis palestina* was found the second most active one with an IC_{50} of 168.0 µg/mL. This could reveal the importance of *Anthemis palestina* in the treatment of gout and other xanthine oxidase related diseases (Hudaib *et al*., 2011). However, the same extract of *Anthemis palestina* was evaluated for its hormone sensitive lipase inhibitory potential and showed very weak inhibition (Bustanji *et al*., 2011). An extract of *Anthemis palestina* was found inactive as inhibitor of α-amylase activity when it was tested along with 35 Jordanian plants (Hamdan and Afifi, 2008). *Anthemis palestina* was also screened with 51 Jordanian plants for their total phenolic content from both aqueous and methanolic extracts in parallel to their antioxidant activities. Those antioxidant activities were in positive linear correlation to the phenolic content of the extracts. Thus, this plant could be used as a source for free radical scavenging compounds (Tawaha *et al*., 2007).

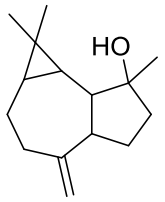

spathulenol

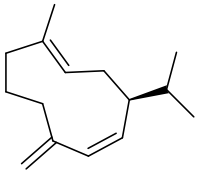

germacrene-D

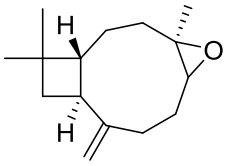

caryophyllene oxide

Figure 1.7: Secondary metabolites isolated from *Anthemis palestina*.

No published work was found for endophytes of *Anthemis palestina* or any other species of the genus *Anthemis.* Nonetheless, the Asteraceae family is known to be one of the biggest hosts for

plant-associated endophytes (Martinez-Klimova *et al*., 2017). Thus, other genera of Asteraceae were associated with endophytes and studied.

The endophytic fungus *Aspergillus calidoustus* was isolated from the Brazilian plant *Acanthospermum australe* (Rodrigues de Carvalho *et al*., 2015). The bioassay directed fractionation resulted in the isolation of the two compounds ophiobolin K and 6-epi-ophiobolin K that possessed antifungal, antiprotozoal and cytotoxic activities when tested *in vitro* (Figure 1.8) (Rodrigues de Carvalho *et al*., 2015). Moreover, 180 endophytic fungi of 25 different taxa from the phyla *Ascomycota* and *Basidiomycota* were isolated from the Brazilian medicinal plant *Baccharis trimera* (Vieira *et al*., 2014). The obtained endophytes were cultured and screened for antimicrobial activities, from which, 23 extracts exhibited bioactivity.

Closely related genera to *Anthemis* are *Chamaemelum* and *Matricaria*. No endophytes were obtained from *Chamaemelum.* However, microbial endophytes from *Matricaria* have been reported. Bacterial endophytes including rare actinomycetes were obtained from the leaves of *Matricaria matricarioides* collected from the Moscow region (Machavariani *et al*., 2014). Moreover, the endophyte *Paenibacillus polymyxa* Strain Mc5Re-14 got its genome sequenced after it was isolated from the roots of *Matricaria chamomilla* that was cultivated in Northern Egypt (Koberl *et al*., 2015).

Apart from the evaluation of volatile oils of *Anthemis palestina*, no other research was conducted on this plant. Therefore, *Anthemis palestina* was considered a valuable plant species to be investigated, particularly, as it has been described to be used in folk medicine while earlier screening results demonstrated biological activity.

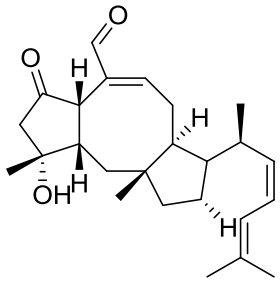

ophiobolin K

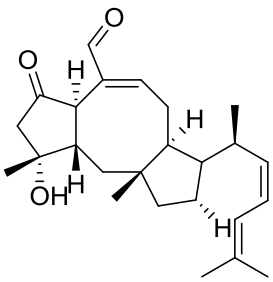

6-epi-ophiobolin K

Figure 1.8: Secondary metabolites isolated from the endophytes associated with Asteraceae.

1.4.3 *Euphorbia peplus* L.

Euphorbia peplus L. is a very common plant. The latex of *Euphorbia peplus* is applied topically to the skin and used as home treatment for actinic keratosis skin cancer. Moreover, this plant is used as antimicrobial, vasoactive, immunomodulatory, anti-inflammatory, antiproliferative and neuroprotective agent (Ernst *et al*., 2015). Ingenol mebutate (or ingenol-3-angelate) is a cytotoxic diterpene ester (Figure 1.9) obtained from *Euphorbia peplus*, formulated as a gel and has been approved by the US Food and Drug Administration (FDA) and the European Medicines Agency (EMA) for the treatment of actinic keratosis and superficial basal cell carcinoma (Beres *et al*., 2017, Diluvio *et al*., 2017). It began to bring attention since 1986, when a survey was conducted in Nambour, Australia. 164 respondents out of the 2000 surveyed residents claimed that they self-treated skin cancer and actinic keratosis. Many of them used the sap of *Euphorbia peplus* for this purpose (Green and Beardmore, 1988). The mechanism of action of this secondary metabolite relies on inducing primary necrosis and initiating inflammatory responses in the treated area (Zarchi and Jemec, 2015).

The methanolic extract of *Euphorbia peplus* was found to be the most active amongst 15 Egyptian plants tested *in vitro* against *Leishmania donovani* (Amin *et al*., 2017). The plant extract was then subjected to bioassay-guided fractionation and four pure compounds were isolated, which included simiarenol, 1-hexacosanol, β-sitosterol and β-sitosterol-3-*O*-glucoside (Figure 1.9). Investigation of the latex of *Euphorbia peplus* afforded twelve diterpenes and one triterpene that showed antifeedant activities against the plant pathogen *Helicoverpa armigera* (Hua *et al*., 2017). The acetone extract of *Euphorbia peplus* yielded twelve diterpenoids, paralianones A – D and pepluanols A – H (Figure 1.9). Paralianone D and pepluanol G were moderately active in inhibiting nitric oxide production in the lipopolysaccharide-stimulated mouse macrophage cellular model (Wan *et al*., 2016). A jatrophane diterpene named euphopeplin A (Figure 1.9) was also isolated from *Euphorbia peplus* (Song *et al*., 2010). Cerebrosides 1 and 2 (Figure 1.9) were also obtained from *Euphorbia peplus* collected from North Italy (Cateni *et al*., 2010). The isolated compounds showed antiproliferative activities against human cervix (HeLa contaminanted) carcinoma (KB) and human neuroblastoma (IMR-32) cell lines.

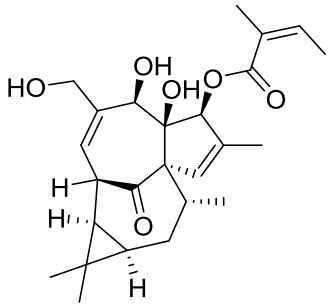

ingenol mebutate

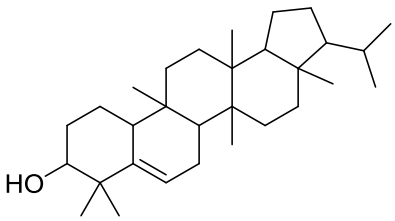

simiarenol

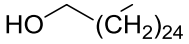

1-hexacosanol

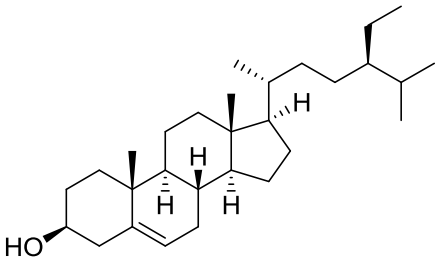

β-sitosterol

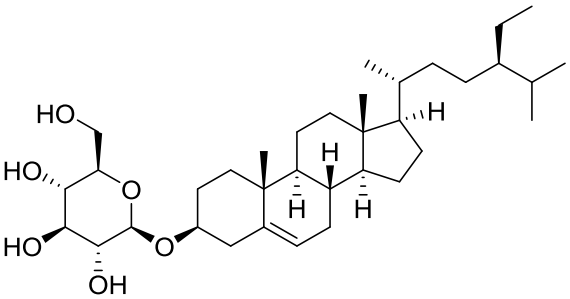

β-sitosterol-3-*O*-glucoside

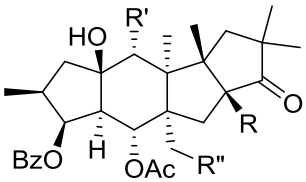

	R	R'	R"
A	OH	OAc	H
B	OAc	OAc	OAc
C	H	OAc	H
D	H	=O	H

paralianones A – D

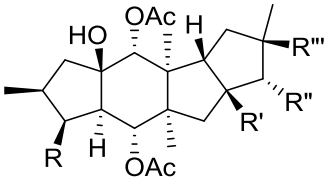

	R	R'	R"	R'''
A	OBz	OAc	OH	OH
B	OBz	OH	OAc	OH
C	OH	OAc	OAc	OH

pepluanols A – C

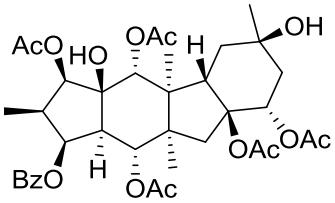

pepluanol D

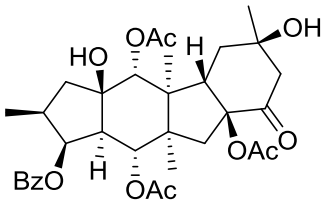

pepluanol E

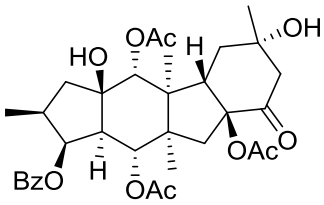

pepluanol F

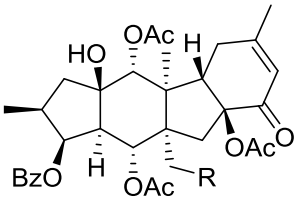

G: R = H
H: R = OAc

pepluanols G – H

Figure 1.9: Secondary metabolites isolated from *Euphorbia peplus*.

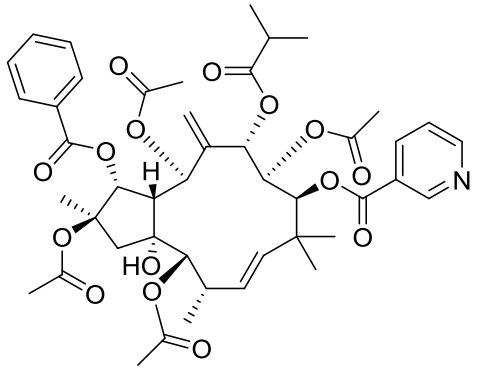

euphopeplin A

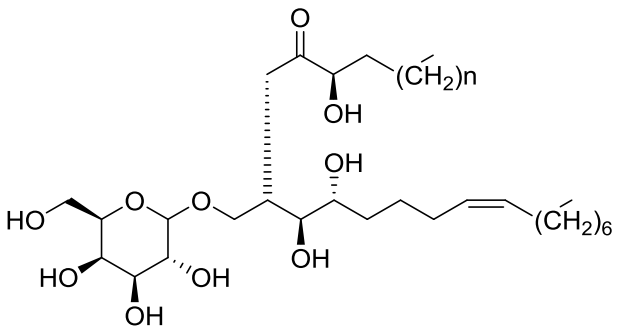

1: n = 21
2: n = 18

cerebrosides 1 and 2

Figure 1.9 (continued): Secondary metabolites isolated from *Euphorbia peplus*.

No studies have been published on endophytes of *Euphorbia peplus*. However, some of the endophytes from other species of the genus *Euphorbia* have been previously reported. The endophytic fungus *Achaetomium* sp. from the roots of *Euphorbia hirta* was cultivated in potato dextrose agar petri dishes (Uma and Mythili, 2017). The ethyl acetate extract of *Achaetomium* sp was hepatoprotective, antioxidant, and exhibited antibacterial activities against *Staphylococcus aureus*, *Pseudomonas aeroginosa*, and *Klebsiella pneumoniae*. Endophytic actinomycetes obtained from *Euphorbia hirta* were screened for antimicrobial activity. Five isolates out of the 46 obtained actinomycetes were active. Thus, the strain that displayed the most significant activity was selected, fermented and extracted by ethyl acetate. The acquired extract was active when tested against *Bacillus subtilis*, *Escherichia coli*, *Candida albicans*, *Staphylococcus epidermis*, *Aspergillus flavus* and *Fusarium oxysporum* (Syed *et al*., 2015). The fungal endophyte *Guignardia* sp was obtained from the leaves of *Euphorbia sieboldiana*. *Guignardia* sp was grown in a rice medium and afforded nine meroterpenes, one dioxolanone derivative and seven other known compounds. Both guignardone N and guignardic acid (Figure 1.10) were active in inhibiting the growth of *Candida albicans*, especially when combined with fluconazole (Li *et al*., 2015b). From the roots of *Euphorbia nematocypha,* 41 strains of endophytic fungi were isolated. Nine of the obtained strains exhibited antibacterial activity against *Escherichia coli* (Luo *et al*., 2007).

Euphorbia peplus is one of the most widely spread plants, as it is native to Europe and the Mediterranean but considered invasive in Australia, New Zealand and North America, *E. peplus* has been studied extensively. However, no studies were conducted on its endophytes. Thus, investigating those endophytes could provide a more convenient and sustainable source for secondary metabolites. Notably, those with anticancer activities.

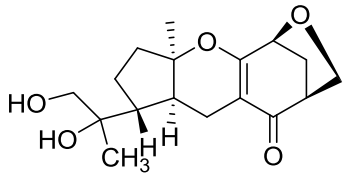

guignardone N

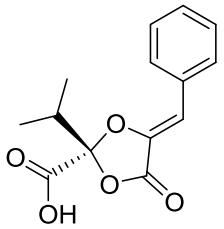

guignardic acid

Figure 1.10: Secondary metabolites isolated from the endophytes associated with *Euphorbia*.

1.4.4 *Rumex cyprius* Murb.

Rumix cyprius Murb. is an annual plant that belongs to the family Polygonaceae. In Jordan, this plant is usually found in dry and salty soils, that is why it is very commonly found in areas close to the Dead Sea. It is used in folk medicine in Jordan and Palestine to treat skin diseases (Jaradat *et al*., 2016a, Al Khateeb *et al*., 2017).

The antioxidant activities of the methanolic extracts of three Palestinian plants *Urtica urens*, *Rumex cyprius* and *Borago officinalis* using 2,2-diphenyl-1-picryl-hydrazylhydrate method were evaluated (Jaradat *et al*., 2016b). The extract of *Rumex cyprius* exhibited the highest antioxidant activity with an IC_{50} value of 5.07±0.49 µg/mL. The methanolic extract of *Rumex cyprius* showed good antibacterial activities against both *Syncephalastrum racemosum* and *Streptococcus pneumoniae* (Abdelwahab *et al*., 2016). Moreover, this extract afforded three flavones isoorientin, vitexin and cynarosid (Figure 1.11). The ethanolic extract of the Palestinian *Rumex cyprius* displayed fungicidal activities against *Microsporum canis*, *Trichophyton mentagrophytes*, *Trichophyton rubrum* and *Ascophaera apis* (Husein *et al*., 2012). Therefore, the plant extract was fractionated and isolated the antifungal compound, 1,3,8-trihydroxy-6-methylanthracene-9,10-dione (Figure 1.11).

The Egyptian *Rumex cyprius* yielded polyphenolic compounds that included vitexin, isovitexin, orientein, isoorientein and emodin (Figure 1.11) (Arafa, 2005). Emodin is a naturally occurring anthraquinone that possess antiproliferative activities, and has been earlier isolated from the same species (El-Fattah, 1989, Al-Nuri *et al*., 1996). In addition to emodin, chrysophanol, another anthraquinone, and four other flavonoids; sovitexin, orientin, isoorientin and quercetin (Figure 1.11) were isolated from the aerial parts of Egyptian *Rumex cyprius* (El-Fattah, 1989). The alcoholic extract of *Rumex cyprius* has been described to exhibit the best antimicrobial activity when tested amongst 15 other Jordanian ethanolic plant extracts by inhibiting the growth of both *Bacillus subtilis*, and *Saccharomyces pastorianus* (Salim *et al*., 1996). Amongst 41 Egyptian plants assayed, the extract of the fruits of *Rumex cyprius* was among the five most active tested extracts against human immunodeficiency virus-1 reverse transcriptase (El-Mekkawy *et al*., 1995). Moreover, the ethanolic extract of *Rumex cyprius* inhibited the activity of hyaluronidase and acted as an antioxidant. Thus, it is used as a skin-lightening and anti-wrinkle agent in cosmetics (Nanba *et al*., 1996).

The endophytes of *Rumex cyprius* have not been investigated before. Yet, some of the endophytes from other species of the genus *Rumex* have been reported. A high performance liquid chromatography (HPLC) method was developed to screen the endophytic fungi of the Chinese *Rumex gmelini* for anthraquinones. The fungal cultures were able to produce emodin, rhein and aloe-emodin (Figures 1.11 and 1.12) (Guo *et al*., 2014). The endophytic fungus coded RGT-S11 was isolated from the Chinese *Rumex gmelini* (Wang *et al*., 2012). By implementing column chromatography, the fungal endophyte yielded benzoic acid, palmitic acid, oleinic acid, gallic acid, adenosine, guanosine and ergosta-5,7,22-trien-3β-ol (Figure 1.12). Moreover, the endophytic fungus *Fusarium tricinctum* was obtained from the roots of *Rumex hymenosepalus* (Bashyal and Leslie Gunatilaka, 2010). Two sesqueterpenes tricinonoic acid and tricindiol in addition to the two furanopyrrolidones NG-391 and NG-393 (Figure 1.12) were obtained from this *R. hymenosepalus* endophyte.

Rumex cyprius is considered a source of many flavonoids and anthraquinones that could be used as antibacterials, anti-proliferative agents, and antioxidants. The endophytes of other species of *Rumex* were investigated and also showed to produce flavonoids, anthraquinones

and terpenes. However, the endophytes of *Rumex cyprius* in particular have not been studied. Yet, they could be source to novel anti-proliferative compounds.

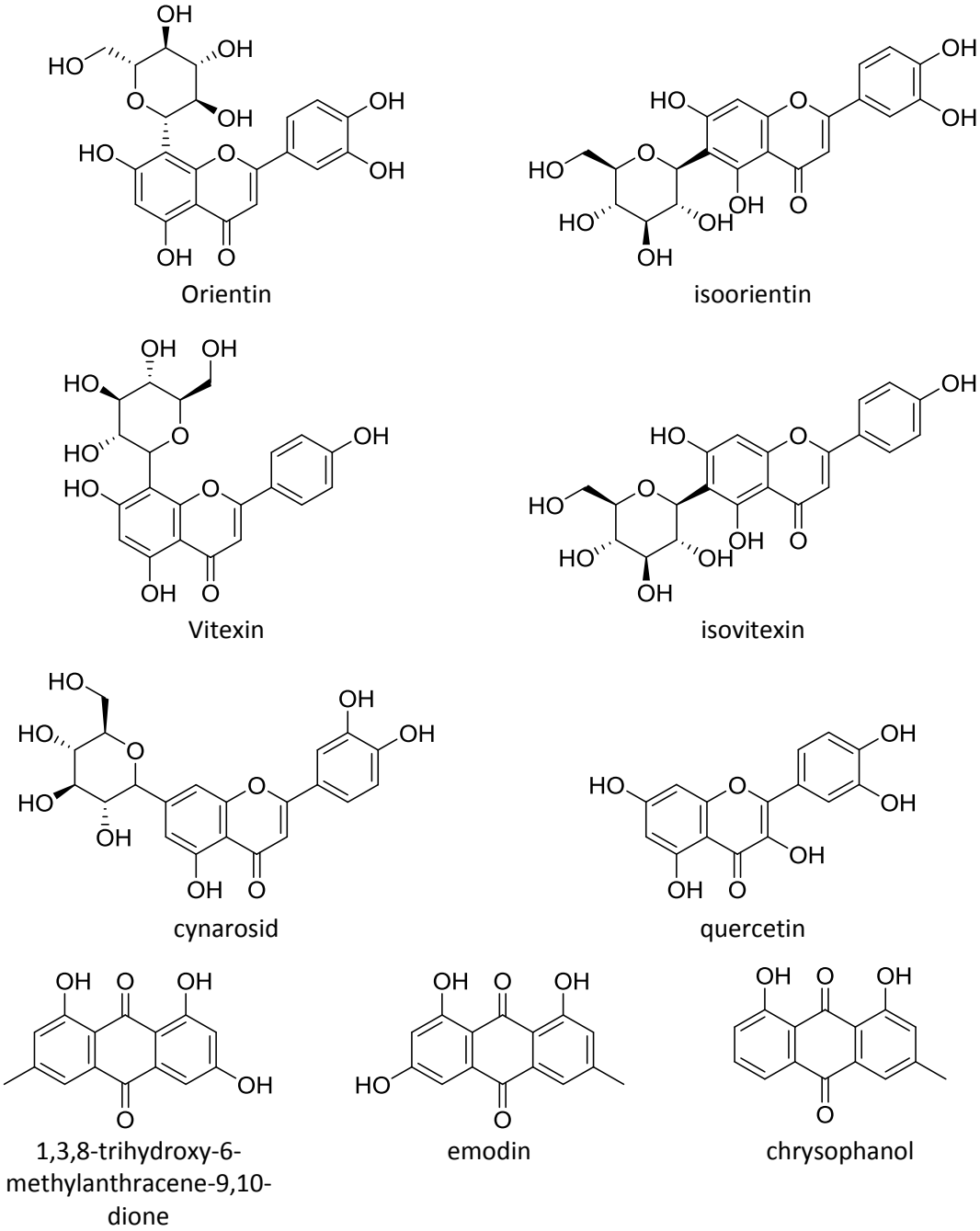

Figure 1.11: Secondary metabolites isolated from *Rumex cyprius*.

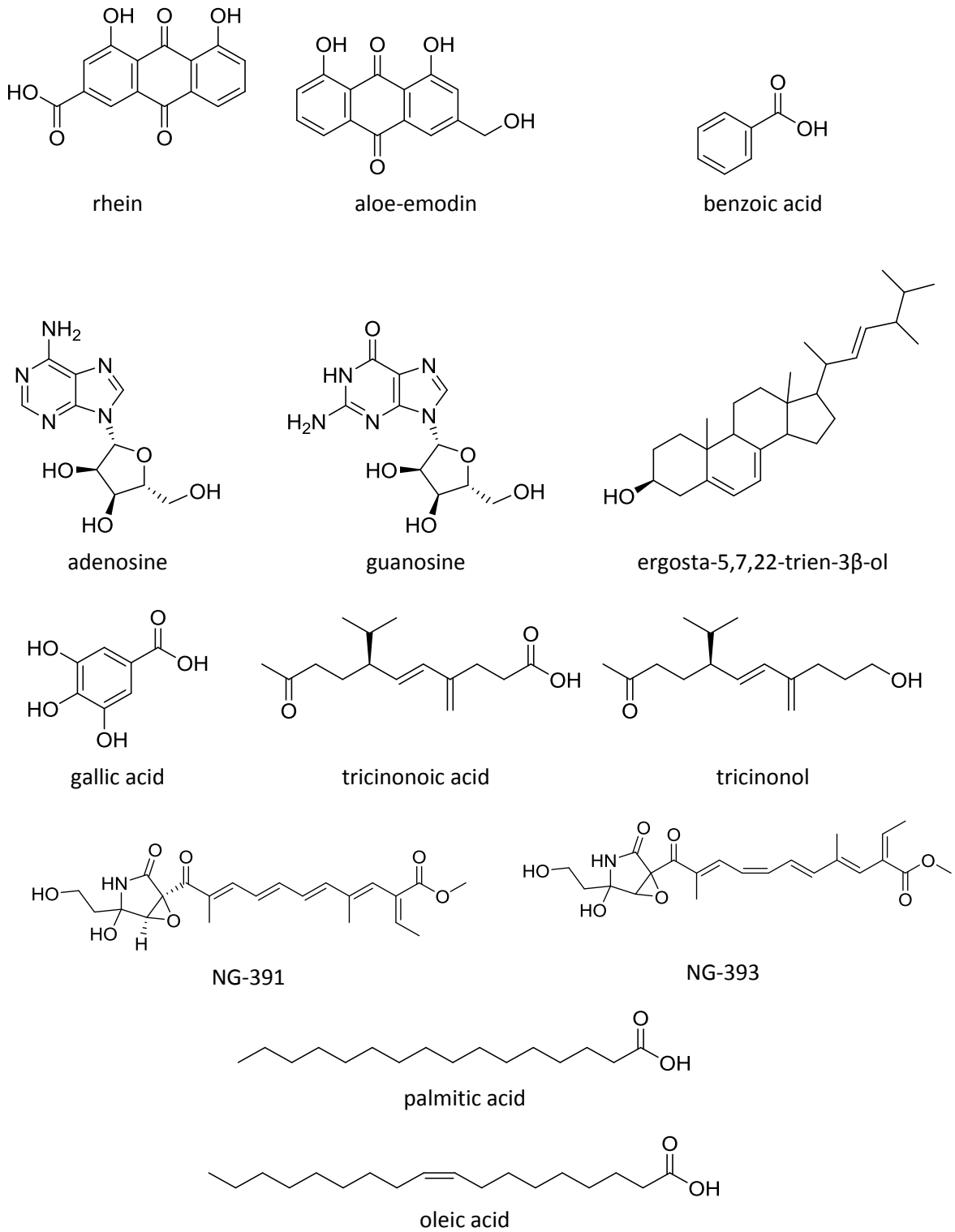

Figure 1.12: Secondary metabolites isolated from the endophytes associated with *Rumex*.

1.5 Metabolomics

Metabolomics is defined as the holistic systematic qualitative and quantitative analysis of all metabolites contained in an organism, or a part of, at a specific time and under specific conditions (Rochfort, 2005, Maree *et al*., 2014, Harvey *et al*., 2015). As metabolomics is the study of the end product of a gene expression process, it is considered among the handiest approaches in monitoring both gene functions and biochemical status of an organism (Yuliana *et al*., 2011). At the biochemical level, the metabolites produced by an organism, and thus, its metabolome, are related to its phenotype (Macintyre *et al*., 2014).

Metabolomics studies are divided into nontargeted and targeted. As its name indicates, nontargeted metabolomics is used for holistic study of all measurable analytes in a sample and it should be coupled to chemometric methods that are able to visualise data in a small set of signals. Whereas targeted metabolomics is designed to study a certain pathway or limited predefined or expected metabolites (Griffiths *et al*., 2010).

Metabolomics is considered the endpoint of the "omics" cascade that contains genomics, transcriptomics and proteomics (Figure 1.13) (Rochfort, 2005, Dettmer *et al*., 2007). However, the dependence on transcriptomics and proteomics to study gene functions is uncertain and limited. This is due to the fact that changes in transcriptome and proteome do not always result in changes to its biochemical phenotypes. Moreover, not all translated proteins are active as enzymes. Furthermore, the identification of mRNA and proteins relies heavily on the sequence similarity and database matching. Therefore, it is affected by any lack of database sources. As a result, metabolomics is considered the most functional approach amongst all other omics approaches (Sumner *et al*., 2003, Rochfort, 2005, Nobeli and Thornton, 2006, Yuliana *et al*., 2011).

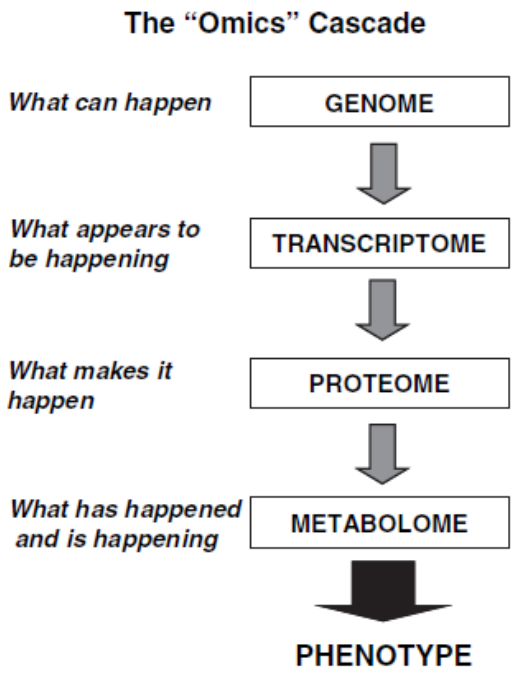

Figure 1.13: The omics cascade reveals the information that could be acquired from each type of analysis. The metabolome is the most representative of the phenotype. Adopted from (Dettmer *et al*., 2007).

Due to their structural complexity and variability in their physicochemical properties, it is challenging to identify and quantify secondary metabolites that are present in a certain natural product extract. Thus, reliable, robust and selective analytical methods are required (Tawfike *et al*., 2013). Both liquid chromatography-high resolution mass spectroscopy (LC-HRMS) and nuclear magnetic resonance (NMR) spectroscopy are commonly used in metabolomics. LC-HRMS has the advantage of being more sensitive than the NMR, detecting compounds that are present at femtogram levels in the extracts. Moreover, LC-HRMS data are able to assist in the identification of compounds based on their exact mass and fragmentation pattern as well as with the addition of other parameters such as retention time that could enhance the identification process. However, the ionisation capability of the metabolites limits the employment of LC-HRMS in the identification of such metabolites (Griffiths *et al*., 2010, Tawfike *et al*., 2013, Krug and Muller, 2014). On the other hand, NMR is more reproducible and better for structure elucidation. Nevertheless, it is not sensitive enough to detect minor metabolites that are present at lower concentrations.

Dereplication is defined as the process of implementing spectroscopy in the identification of known metabolites in the early stages of isolation (Krug and Muller, 2014, Harvey *et al*., 2015). This is achieved by using LC-HRMS, where hits with certain *m/z* values are compared to available databases like AntiMarin and Dictionary of Natural Products (DNP). Along with multivariate analysis, the active compounds are pinpointed; this allows prioritising fractions for further purification work and helps save time and resources in the process of isolating novel bioactive compounds. Combining data attained by LC-HRMS and/or NMR to a multivariate data analysis tool allows the comparison and detection of differential metabolites in biological samples which, in turn, will narrow the search of potential biomarkers and will avoid chemical redundancy at the very beginning of the research (Wu *et al*., 2015). By implementing multivariate analysis, a metabolomics dataset can be analysed and visualised to identify significant correlations that lies within it (Covington *et al*., 2017).

1.5.1 Chemometrics and multivariate analysis

Chemometrics is defined by Wold as "The art of extracting chemically relevant information from data produced in chemical experiments, and it's heavily dependent on the use of different kinds of mathematical models. The main issue is to structure the chemical problem to a form that can be expressed as a mathematical relation. It is a process of extracting chemically relevant information out of measured chemical data, representing and presenting this information, and interpreting such data into information" (Wold and Sjostrom, 1998). It includes the application of both mathematical and statistical techniques in retrieving more information from complex datasets and could be used as a tool for clearing up patterns in complicated chemical matrices (Mok and Chau, 2006, Maree *et al*., 2014).

Multivariate data analysis is a chemometrics tool that is applied to extract relevant information from measured data. Thus, visualising this data and enabling the prediction of its outcomes. The use of common instrumental analysers produces multivariate collinear data. Measured variables, which describe the system, provide similar information content. These collinear variables and thus, the structure of data, could be combined and described by fewer factors, called latent variables or principal components (Rajalahti and Kvalheim, 2011).

Different approaches in multivariate analysis include; principal component analysis (PCA), soft independent modelling by class analogy (SIMCA), partial least squares, or projections to latent structures, discriminant analysis (PLS-DA), orthogonal partial least squares discriminant analysis (OPLS-DA) and modified orthogonal projections to latent structures (O2-PLS). Those approaches are summarised in Table 1.2 (Wiklund, 2008).

Table 1.2: Some of the approaches used in multivariate analysis (Wiklund, 2008).

PCA: **Overview**	**SIMCA:** **Classification**	**PLS-DA and OPLS-DA:** **Discrimination**	**O2-PLS:** **Regression**
Trends Outliers Quality control Biological diversity Patient monitoring	Pattern recognition Diagnostics Healthy/diseased Toxicity mechanisms Disease progression	Discriminating between groups Biomarker candidates Comparing studies or instrumentation	Comparing blocks of omics data Metabolomic vs proteomic vs genomic Correlation spectroscopy
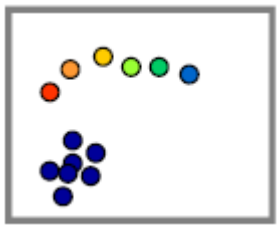		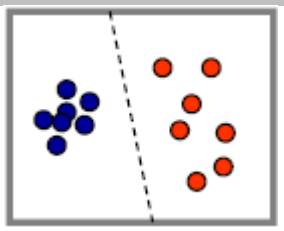	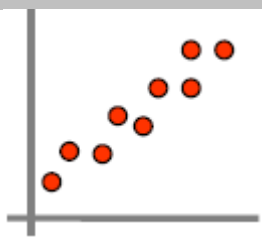

Two of the most used multivariate approaches for metabolomics data analysis are PCA and OPLS-DA (Covington *et al*., 2017). Visualise measuring "K" number of variables for "I" number of objects, this will result in a big data matrix of size I×K as shown in Figure 1.14. Using principal component analysis (PCA) could reduce this huge matrix to smaller matrices I×A and A×K which are easier to interpret and understand (Geladi, 2003). PCA converts the large data space that is present in I×K matrix into a smaller space as showed in the figure, where X = I×K = I×A + A×K + E. Each term (I×A) and (A×K) is called principal component (PC) or latent variable and E is the residual matrix. Usually, many principal components are obtained; however, two could be enough to represent the data in an efficient descriptive way.

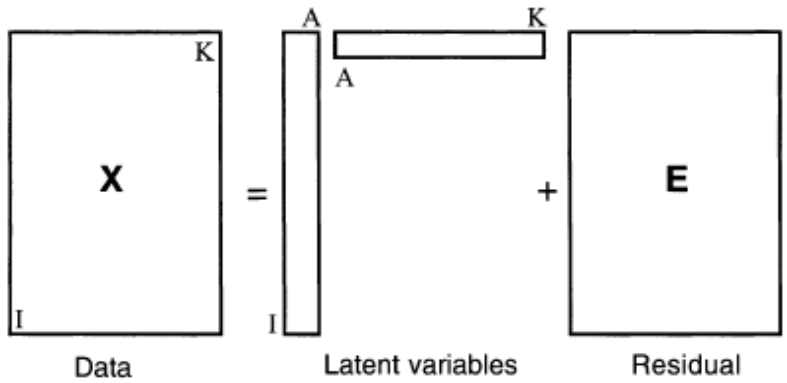

Figure 1.14: "A data matrix of size I×K is reduced to smaller matrices of size I×A and A×K (A<<min(I, K)) that are easier to interpret and understand and contain all the relevant information. Noise and other disturbances are left in the residual matrix of size I×K. A general name for the reduced data is latent variables". Adopted from (Geladi, 2003).

Two types of plots are usually used for PCA, the scores plot and the loadings plot. The scores plot summarises the observations (samples) and the loadings plot summarises the variables responsible for the pattern of observations in the scores plot. Figure 1.15 illustrates an example of scores plots for two PCs (latent variables) (Geladi, 2003). As the figure depicts, cluster A shows less variation, as it's denser than the spread-out cluster B that shows larger variation. In some situations outliers might be observed as well as a gradient between the pure classes A and B (Geladi, 2003).

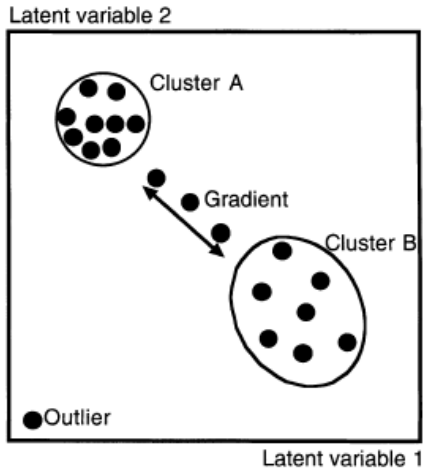

Figure 1.15: Example of a scores plot that represents some of phenomena in the data. Adopted from (Geladi, 2003).

PCA is an unsupervised analysis that doesn't make assumptions about the data and identifies the sources of variation among the observations, and thus, observations are classified in scores plot depending on the variables of the loadings plot (Covington *et al*., 2017). On the other hand, PLS-DA approach is supervised. Thus, separate groups of observations are defined by the user and are accordingly clustered in the scores plot, whereas the variables in the loadings plot are grouped so they are responsible for the observations separation in scores plot (Covington *et al*., 2017). To improve separation between predictive and nonpredictive variation, orthogonal signal corrections are applied to PLS regressions (Bylesjoe *et al*., 2007).

1.5.2 Applications of metabolomics in natural products

In searching natural products for drug discovery, metabolomics introduced quite important applications either on the level of tracking novel compounds and active metabolites or on the level of optimising the production of secondary metabolites. Both PCA and OPLS-DA could be used to guide the isolation of compounds and prioritise fractions for further work which will save time and resources and will direct the work toward the novel and bioactive compounds (Tawfike *et al*., 2013, Harvey *et al*., 2015, Covington *et al*., 2017). This is based on the ability of metabolomics to compare and screen secondary metabolites, rapidly revealing the outliers, the differences and biomarkers among experimental groups either they were of different sources or different fractions related to the same source. This will help track the production of possible novel and bioactive target metabolites and/or biomarkers available at the earlier stages of the work (Tawfike *et al*., 2013, Wu *et al*., 2015). Then, the target metabolites are isolated while structural information provided by the NMR or LC-HRMS is compared with the database or library for identification of known versus unknown metabolites to reduce dereplication time (Wu *et al*., 2015). If the core structure is known but not the functional groups then 2D NMR and fragmentation pattern in MS/MS spectra in conjugation with molecular networking evaluation could be used to identify the compound. However, if its nucleus is unique, then a full de novo NMR structural characterisation is needed (Tawfike *et al*., 2013).

Furthermore, metabolomics could be utilised to optimise fermentation conditions and to detect and sustain the production of interesting secondary metabolites during the scaling-up process (Schulz *et al*., 2002, Harvey *et al*., 2015). Moreover, the real time metabolomics could

aid in studying, exploring and validating relationships between culture methods, diversity, bioactivity and metabolome evaluation in the microbial isolate (Jorda *et al*., 2012, Zhu *et al*., 2013, Abdelmohsen *et al*., 2014, Hubert *et al*., 2014). When changing specific fermentation parameters, the metabolic production could be checked by metabolomics. This gives metabolomics the ability to work as a quality control tool (Tawfike *et al*., 2013, Toya and Shimizu, 2013, Wu *et al*., 2015). Metabolomics could also be used as a quality control tool for phytomedicines. Interspecies variations, adulterations, environmental changes, post harvesting treatment and extraction may all lead to different metabolite profile and significantly affect the efficacy of phytomedicines. All these changes could be detected by PCA (Yuliana *et al*., 2011). In addition to that, metabolomics could be used to link chemical profile and bioactivity pattern of certain phytomedicines where the activity is a result of synergism of many individually inactive chemical constituents. In such cases, the bulk of chemical constituents, *i.e.,* the metabolome is monitored (Yuliana *et al*., 2011). Further, metabolomics data can be mined in search for biosynthetic precursors that might be used to increase the production of a certain functional novel product (Harvey *et al*., 2015).

1.6 Hypothesis and aims of the study

In the last decades, cancer became a worldwide overwhelming problem. In the United States, 1,688,780 new cancer cases were projected to occur in 2017. Breast cancer is estimated to be the most common type of cancer among females with 252,710 cases (30%), followed by lung and bronchus cancer with 105,510 new incidences. On the other hand, prostate cancer is estimated to top the new cancer incidences in males with 161,360 cases (19%), followed by lung and bronchus cancer with 116,990 cases (14%). However, lung and bronchus cancer is estimated to be the deadliest among other cancer types in both females (25%) and males (27%) (Siegel *et al*., 2017). In the United Kingdom, more than 360,000 new cancer cases are recorded yearly. Breast (15.3%), prostate (13.1%), lung (12.9%) and bowel (11.6%) cancers were the most common types and made 53% of all new cancer cases in the year 2015. The most common type of cancer in females was breast cancer (30.9%), followed by cervix (17.2%) and lung (12.3) cancers. However, prostate cancer was the most common cancer type in males (25.8%), followed by lung cancer and bowel cancer with 13.4% and 12.6% of incidences, respectively (Cancer Research UK, 2018).

In the year 2012, there were 14.1 million new cases of cancer worldwide, out of which, 42% were lung (13.0%), female breast (11.9%), bowel (9.7%) or prostate (7.9%) cancers (Torre *et al*., 2015). Jordan was no exception. According to the statistical report "Cancer incidence in Jordan - 2012", the number of new cases diagnosed as cancer has increased by 46% in the years 2000 to 2012, jumping from 3362 cases in the year 2000 to 5013 in the year 2012 (Al-Sayaideh *et al*., 2012). This resulted in having 78 people out of each 100,000 Jordanians suffer from cancer. Speaking of cancer types in Jordan, breast cancer was considered the most common type as 20.1% of cancer patients in Jordan suffered from breast cancer, followed by colorectal cancer (11.3%) and lung cancer (7.4%) (Figure 1.16).

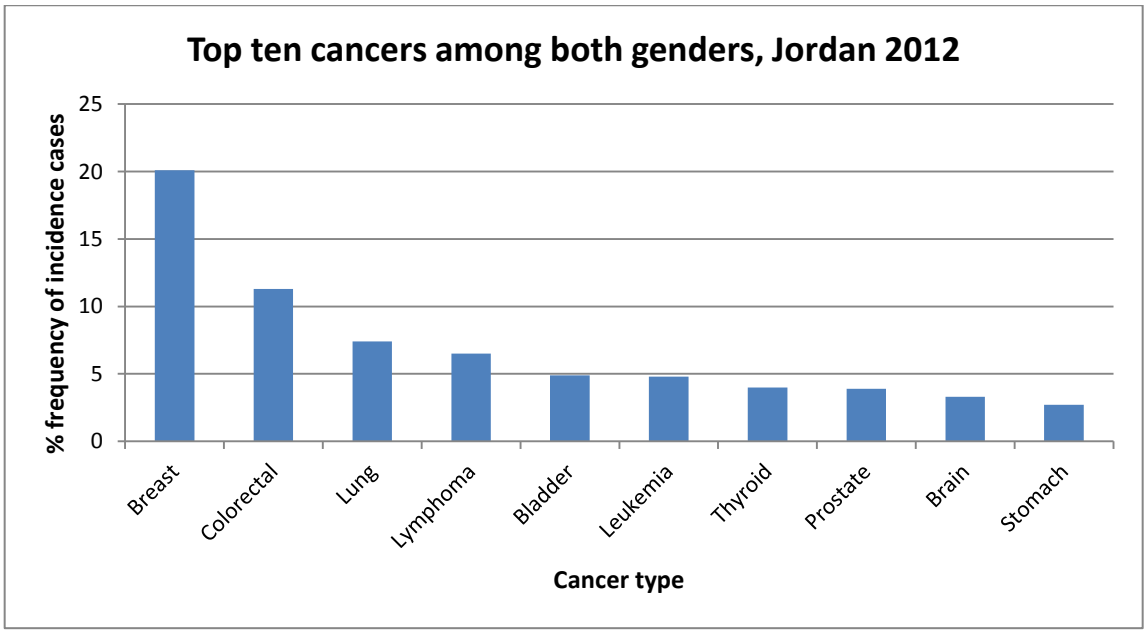

Figure 1.16: Top ten cancers among both genders, Jordan 2012.

On the gender level; breast cancer was the most common type in female Jordanian cancer patients with 37.7% of incidence cases, followed by colorectal (10.7%) and thyroid (5.9%) cancers (Figure 1.17).

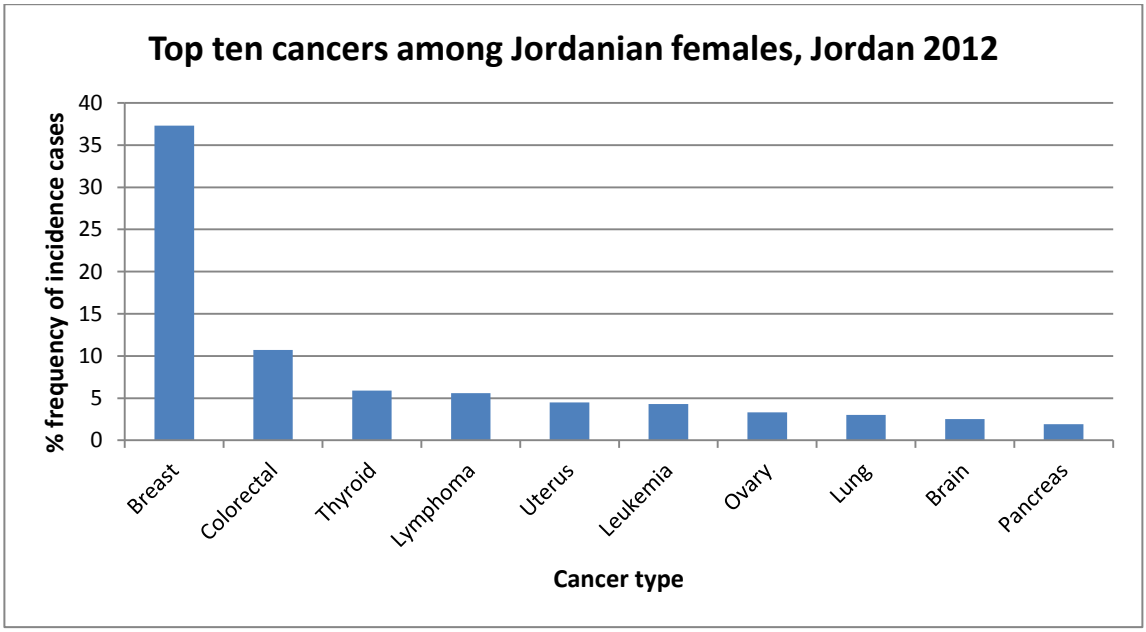

Figure 1.17: Top ten cancers among females, Jordan 2012.

On the other hand, lung cancer was the most common cancer type among males in Jordan (12.4%), followed by colorectal (12.0%) and bladder (9.2%) cancers (Figure 1.18).

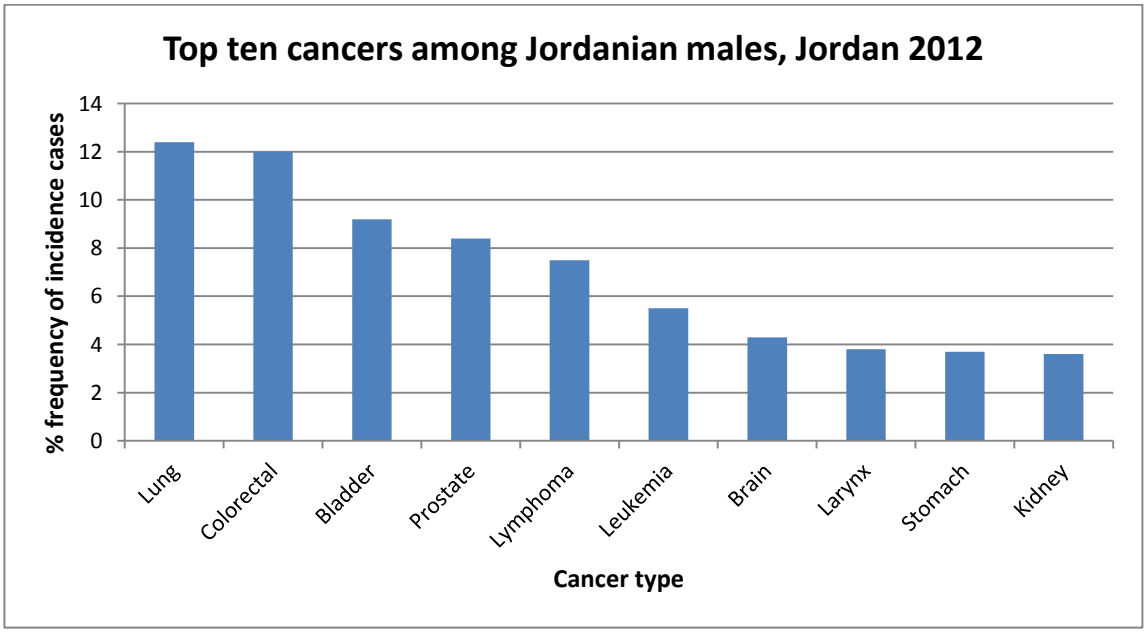

Figure 1.18: Top ten cancers among males, Jordan 2012.

As cancer incidences are increasing in Jordan and worldwide, the need for new therapeutic agents for cancer is still persistent. Breast cancer was selected as a main target for this study because it both tops cancer incidences in Jordan, UK and the US and was among the fastest four types of cancer spreading worldwide. Furthermore, lung cancer was the third most common type of cancer in Jordan and the most common cancer type among males in Jordan, as well as being the fastest type of cancer spreading worldwide; therefore, it was added as a second target to study the selectivity of the isolated compounds.

Hypothesis: Applying metabolomics, and hence, OPLS-DA in the search for anti-proliferative agents for breast cancer and lung cancer from plant-associated endophytes will facilitate pinpointing the biologically active compounds in the first fractionation step. Thus, saving the time consumed in the traditional bioassay-guided isolation where all fractions should be assayed for their biological activity after each fractionation step, so the biologically active fractions, and hence, the biologically active compounds are tracked and isolated. The pinpointed compounds obtained and defined by multivariate analysis will be targeted for isolation work, structurally elucidated and tested to validate their activity. The isolation work will not involve a step-by-step bioassay tests prior to each fractionation stage. Moreover, early stage dereplication will help in isolating new compounds.

The aim of this study is to isolate anti-proliferative compounds from the plant-associated endophytes. Four Jordanian medicinal plants, *Anchusa strigosa*, *Anthemis palestina*, *Euphorbia peplus* and *Rumex cyprius* were chosen for this purpose. For the sake of this, the following objectives were accomplished:

1. The endophytes were isolated from the studied plants and identified using ITS gene sequencing.
2. The obtained endophytes were screened for biological activity. Three endophytes were scaled-up based on their biological activity and chemistry.
3. Two types of media were used for the scaling-up. Thus, media optimisation took place for each endophyte. The medium that afforded better yield, more chemical diverse extract and more potent biological activity was chosen for scaling-up.

4. A metabolomics-bioassay guided approach was developed for each of the scaled-up endophytes to pinpoint the biologically active compounds against breast cancer and lung cancer.
5. Fractionation took place to isolate the pinpointed compounds.
6. Nuclear magnetic resonance (NMR) and liquid chromatography-high resolution mass spectroscopy (LC-HRMS) were implemented to identify the isolated compounds.
7. The isolated compounds were tested against breast cancer (ZR-75) and lung cancer (A549) cell lines to confirm their activity.

Chapter 2: Materials, instruments and methods

2 Materials, instruments and methods

2.1 Isolation and identification of endophytes from the selected plants

2.1.1 Materials, reagents and instruments

For the preparation of the nutrient malt-agar (MA) medium, both Malt Extract and Nutrient Agar were purchased from Oxoid, UK. Chloramphenicol from Acros Organics, Belgium was used as an antibacterial. Isopropanol (HPLC grade) from Sigma-Aldrich, Poland, prepared as 70% solution in water and Sagrotan Spray Disinfectant from Sagrotan, Germany was used as an antimicrobial agents and disinfectants for the working space.

The pH meter used was purchased from Jenway, UK. Sodium hydroxide was obtained from Sigma-Aldrich, US. The magnetic mixer was procured from Stuart, UK. Vortex Genie 2 was obtained from Scientific Industries, US. The incubator was bought from Vindon Scientific, UK and kept at 27°C. The Petri dishes were purchased from Thermo Scientific, US. The utilised laminar flow hood (BioMAT^2) was obtained from Medical Air Technology, UK.

Twenty six fungal strains were obtained from the MA plates and identified by sequencing the internal transcribed spacer (ITS) region that lies between 18S and 5.8S (ITS1) and 5.8S and 28S (ITS2) rRNA genes of their DNAs. Thus, UltraPure™ TBE Buffer 10X from Life Technologies, UK was used. In addition to that, ethidium bromide 10 mg/mL solution, Water-Molecular Biology Reagent, REDExtract-N-Amp™ PCR ReadyMix™, Extraction Solution and Dilution Solution were all obtained from Sigma-Aldrich, US. Agarsoe-Molecular Grade, HyperLadder II and Sample Loading Buffer were all obtained from Bioline, US. The primers ITS1 (5'-TCC-GTA-GGT-GAA-CCT-GCG-G-3') and ITS4 (5'-TCC-TCC-GCT-TAT-TGA-TAT-GC-3') were procured from Integrated DNA Technologies, US.

For measuring the concentration of the extracted and amplified genes, GenElute™ Gel Extraction Kit was purchased from Sigma-Aldrich, US. It contained Wash Solution, Gel Solubilisation Solution, Column Preparation Solution, Elution Solution, GenElute™ Binding Column G and Collection Tubes.

Two thermal cyclers were used, including Primus 96 Thermal Cycler that was purchased from MWG AG Biotech, Germany and DNA Thermal Cycler 480 Manual from Perkin Elmer, US. The agarose gel plates were purchased from Bioscience Services, UK. The voltage source BioMax MBP300 was obtained from Kodak, Japan. For gel imaging, INGENIUS gel documentation system was obtained from Syngene, UK. For the process of extracting the gene, both the DRI-BLOCK® DB-2A that was obtained from Techne, UK and the Centrifuge 5415 D that was purchased from Eppendorf, Germany were used. Nanodrop 2000C Spectrophotometer was purchased from Thermo Scientific, Germany to measure the concentration of the obtained and amplified genes. For the identification of endophytes, FinchTV 1.4.0 software that was developed by Geospiza, and Basic Local Alignment Search Tool (BLAST) that is available online by the National Center for Biotechnology (NCBI), US were employed.

2.1.2 Methods

2.1.2.1 Collection of plant samples

Three plants, namely, *Anchusa strigosa* [Soland.] (201505-01-ANS, Boraginaceae), *Anthemis palestina* Reut. ex Boiss. (201505-02-ANP, Asteraceae), and *Euphorbia peplus* L. (201505-03-EUP, Euphorbiaceae) were collected from The University of Jordan, Amman, Jordan. The fourth plant, *Rumex cyprius* Murb. (201505-04-RUC, Polygonaceae) was collected from Dier Alla, Balqa, Jordan. All plants were identified by the taxonomist Prof. Dawud Al-Eisawi, Department of Biology, Faculty of Science, The University of Jordan. Their voucher specimens were kept in the herbarium collection, Department of Pharmaceutical Sciences, Faculty of Pharmacy, The University of Jordan. The plant material was collected in May 2015, four days prior to isolation of the fungal endophytes, kept in plastic bags and stored at 2–8°C.

2.1.2.2 Preparation of nutrient malt agar (MA) medium and incubation of plants' parts

The nutrient malt agar medium composed of 10 g of agar extract, 7.5 g malt extract and 0.1 g chloramphenicol. All components were weighed and solubilised in 500 mL of deionised water. The pH was adjusted to 7.4 by the addition of sodium hydroxide. The prepared medium was autoclaved and poured into 21 petri dishes in a disinfected laminar flow hood.

The laminar flow hood was disinfected with 70% isopropanol solution and Sagrotan Spray Disinfectant before inoculating the plant parts to petri dishes. The plant parts listed in Table 2.1 were washed with 70% isopropanol then with sterile deionised water to get rid of all contaminants and epiphytic microorganisms. Moreover, each plant part was dissected to expose the inner tissues. The exposed inner tissues of the respective plant parts were inoculated on MA medium. Each plant part was inoculated three times in two different dishes. During the inoculation process, one petri dish was left open in the laminar flow hood as a control. All samples and the control were incubated at 28°C for seven days.

Table 2.1: Plant parts incubated.

Plant	Parts incubated
Anchusa strigosa	Stems and flowers
Anthemis palestina	Stems, flowers and roots
Euphorbia peplus	Middle stems, upper stems and roots.
Rumex cyprius	Stems and flowers

2.1.2.3 First Inoculation of endophytes

1000 mL of MA medium was prepared by dissolving 20 g of agar extract, 15 g of malt extract and 0.2 g of chloramphenicol in water that was added up to 1000 mL. Chloramphenicol was added to inhibit bacterial growth. After that, pH was adjusted to 7.4 by adding sodium hydroxide. The mixture was sent to autoclave and poured into 42 petri dishes in the laminar flow hood. The endophytes were collected from the previously incubated petri dishes (described under 2.1.2.2). They were classified depending on their origin, colour and morphological characteristics. Each endophyte was inoculated in duplicate and incubated at 28°C for five days.

2.1.2.4 Second inoculation of endophytes

Another 1000 mL of MA medium were prepared as described under 2.1.2.3 for further re-inoculation and incubation of pure endophyte isolates based on their morphology after 5 days of incubation at 28°C. Twenty six different endophytes were isolated from the four studied plants and listed in Table 2.2.

Table 2.2: Morphological description of endophytes isolated from the studied plants.

Plant	Number	Plant Part	Colour and appearance of the endophyte	
			First incubation	Second incubation
Anthemis palestina	1	Flower	White	White, fluffy
	2	Root	Green	Green centre, white edges
	3	Root	Red	Red bottom, white hard top
	4	Root	White	White, water like
	5	Root	White	White, fluffy
	6	Flower	Pink	White centre, red and white edges
	7	Flower	Black	Green centre, white edges
	8	Flower	Black	White, fluffy
	9	Flower	Black	Light green
	10	Flower	Black	White, water like
	11	Stem	White	Thick white
Anchusa strigosa	12	Stem	White	Thick white
	13	Flower	Black	Dark green
	14	Flower	Black	White
	15	Flower	White	Colorless, water like
	16	Flower	White	Yellow, water like
Euphorbia peplus	17	Upper stem	White	Red, water like
	18	Upper stem	White	Red
	19	Root	Green	Green centre, white edges
	20	Root	White	White, fluffy
	21	Middle stem	White	Soft white, water like
	22	Middle stem	White	White, cotton like
	23	Middle stem	Green	Green centre, white edges
	24	Middle stem	Red	Red centre, white edges
	25	Middle stem	Red	White, water like
Rumex cyprius	26	Stem	White	Thick white

2.1.2.5 ITS gene extraction and amplification

From the second incubation of each endophyte, a fungal layer was cut and transferred to a 0.5 mL Eppendorf tube. This was followed by the addition of 100 µL of extraction solution and a vigorous mixing. The contents of Eppendorf tubes were incubated in the DNA Thermal Cycler 480 Manual at 95°C for 10 minutes. After that, 100 µL of the dilution solution was added to each tube.

For the polymerase chain reaction (PCR) and amplification of the gene, 4 µL of the gene product was added to a mixture of 25 µL of REDExtract-N-Amp™ PCR ReadyMix™, 3 µL of the forward primer ITS1, 3 µL of the reverse primer ITS4 and 18 µL of water-molecular biology reagent. The previous mixture was subjected to a PCR reaction on Primus 96 Thermal Cycler as explained in Table 2.3. After the PCR was finished, 2 µL of sample loading buffer was added to each sample.

Table 2.3: PCR cycles.

Step	Temperature (°C)	Duration (min)	Cycles
Initial denaturation	95	3	1
Denaturation	95	1	-
Annealing	56	1	35
Extension	72	1	-
Final extension	72	10	1
Hold	4	-	-

2.1.2.6 Gel electrophoresis

The agarose gel was prepared by dissolving 0.5 g of agarose and 2 µL of ethidium bromide in 50 of 1x diluted TrisBorateEDTA (TBE) buffer. After that, the gel was poured into gel electrophoresis plate and allowed to solidify. Then, the plate was filled with the TBE 1x diluted buffer. 6 µL of HyperLadder II was inserted to one of the wells of the plate. 15 µL of the blank and amplified genes were inserted to the other wells multiple times to get a reasonable amount of genes for sequencing. The gel was run for 45 minutes under the voltage of 60 volts. After the run was finished, the gel was examined under the UV and the amplified gene bands were cut and stored in the fridge at 2–8°C. The band size of each endophyte's gene was determined by comparison to the HyperLadder II reference.

2.1.2.7 Extracting, measuring the concentration and the sequencing of the obtained PCR product

For the extraction of the amplified genes, the protocol of GenElute™ Gel Extraction Kit was used. For each sample, the agarose gel pieces that contained the gene fragments were weighed. Then the solubilisation solution was added to them in three times their volume. Subsequently, the mixture was incubated in DRI-BLOCK® for 10 minutes with occasional mixing

by a vortex mixer. Later, equal volume of isopropanol was added to the solubilised gene-agarose mixture and homogenised by a vortex mixer. Meanwhile, the GenElute™ Binding Columns were prepared. Each binding column was placed in a 2 mL collection tube. After that, 500 µL of the column preparation solution was added to each binding column followed by 1 minute of centrifugation. The preparation solution was drained into the collection tube and discarded. Then, the solubilised gel solution mixture was loaded into the binding column and centrifuged for 1 minute. After centrifugation, the solution collected in the collection tube was discarded. Later, 700 µL of the wash solution was added to the binding column. This was followed again by centrifugation for 1 minute. After finishing, the solution was discarded along with the collection tubes. Next, the binding columns were placed in a new collection tubes, had 25 µL of a previously heated Elution Solution added into them and centrifuged for 1 minute. After that, the binding columns were discarded and the genes were solubilised in the Elution Solution and collected in the collection tubes. Finally, the concentration of the genes solution was measured using the Nanodrop spectrophotometer and sent for sequencing. The received sequences were read using the FinchTV software and compared to hits of the databases available on the Basic Local Alignment Search Tool (http://blast.ncbi.nlm.nih.gov/Blast.cgi). The identified endophytes are listed in Table 2.4.

Table 2.4: The obtained endophytes and their identity.

Sample ID	Concentration (ng/µL)	Band Size (bp)	Endophyte
1	4.7	1800-2000	Sequencing failed
2	15.4	500-700	*Ulocladium* sp.
3	10.2	500-700	*Fusarium acuminatum*
4	7.5	1800-2000	Sequencing failed
5	5.6	1800-2000	Sequencing failed
6	9.6	1800-2000	*Alternaria alternata*
7	24.3	500-700	*Curvularia australiensis*
8	6.8	1800-2000	Sequencing failed
9	7.9	500-700	*Chaetomium subaffine*
10	9.9	1800-2000	Sequencing failed
11	6.5	1800-2000	Sequencing failed
12	5.0	500-700	*Aureobasidium pullulans*
13	6.8	500-700	*Alternaria tenuissima*
14	5.8	500-700	*Alternaria alternata*
15	16.7	1800-2000	*Aureobasidium pullulans*
16	4.3	1800-2000	Sequencing failed
17	8.1	1800-2000	Sequencing failed
18	7.2	500-700	*Fusarium acuminatum*
19	8.2	500-700	*Alternaria multiformis*
20	5.0	500-700	*Fusarium equiseti*
21	2.9	1800-2000	Sequencing failed
22	3.5	1800-2000	*Aspergillus flavus*
23	5.0	500-700	*Pleosporales* sp.
24	3.3	500-700	*Fusarium* sp.
25	7.1	1800-2000	Sequencing failed
26	5.2	500-700	*Chaetomium subaffine*

2.2 Screening and dereplication of the endophytes

2.2.1 Materials, reagents and instruments

For the preparation of the nutrient media, the same reagents and instruments that were described in 2.1.1 were used. Ethyl acetate (HPLC grade) was obtained from Sigma-Aldrich, Poland. Acetone (analytical grade) was purchased from VWR chemicals, France.

A non-absorbent cotton wool was purchased from Fisher Scientific, US. The homogeniser (IKA® T18 basic ULTRA-TURRAX) was obtained from IKA, Germany. The rotary evaporator R-110 was obtained from Buchi, Switzerland. A Block Heater SBH130D/3 and Sample Concentrator

SBHCONC/1 that were obtained from Stuart, UK were used to evaporate solvents from sample vials. The Ultrawave Sonicator was procured from Scientific Laboratory Supplies, UK.

2.2.2 Methods

2.2.2.1 Preparation of MA medium and incubation of endophytes

2000 mL of MA medium was prepared as described under 2.1.2.3. Each of the 26 endophytes was inoculated in triplicate and incubated at 28°C for one or two weeks, depending on their growth rate.

2.2.2.2 Extraction of metabolites from the incubated endophytes

After the incubation, each plate of the three plates of each endophyte was cut into six parts and had all its components *i.e.* both the endophyte and the medium, transferred into a 500 mL conical flask. Then, 200 mL of the extracting solvent, ethyl acetate was added and left overnight. The following day, the flask was homogenised using the IKA homogeniser and vacuum filtered. Another two 200 mL portions of ethyl acetate were added to the residue increasing the number of extractions to exhaustion. Then, the homogenised mixture was vacuum filtered again. The exhausted residue was discarded and the pooled ethyl acetate filtrates were evaporated by rotary evaporator. The temperature of water bath was set to 40 °C. The dry concentrated extract was reconstituted in the least amount possible of acetone (1 – 5 mL) and transferred into a tared capped small vial. All vials were placed in the heat block to evaporate the acetone. The dry extract was weighed and samples for LC-HRMS, NMR and bioassay screening were prepared as listed in Table 2.5.

Table 2.5: Samples prepared for analysis and bioassay screening.

Purpose	Concentration	Solvent
LC-HRMS	1 mg/mL	Methanol
NMR	5 mg/600 µL	DMSO-$_{d6}$
Bioassay	10 mg/mL	DMSO

2.3 Media optimisation and up scaling the endophytes

2.3.1 Materials, reagents and instruments

For the preparation of the MA and liquid-Wickerham nutrient media, the same reagents, solvents and instruments that were described in 2.1.1 and 2.2.1 were used. Peptone was obtained from Fisher Scientific, UK. Glucose monohydrate was purchased from Alfa Aesar, England. The rice was purchased from Aldi, UK. HPLC grade Hexane (Hex) and Methanol (MeOH) were obtained from VWR chemicals, France.

A non-absorbent cotton wool was procured from Fisher Scientific, US and used for filtration. Two homogenisers were obtained from IKA, Germany; IKA® T18 basic ULTRA-TURRAX was utilised for the liquid-Wickerham media samples and IKA® RW16 basic was used for solid-rice media's samples. Buchi R-110 rotary evaporator was obtained from Buchi, Switzerland. The block heater, the sample concentrator and the Ultrawave sonicator that were described in 2.2.1 were used to dry the samples in vials.

2.3.2 Methods

2.3.2.1 Preparation of Wickerham medium for liquid cultures

Each 2 L conical culture flask used for up scaling composed of 3 g of yeast extract, 3 g of malt extract, 5 g of peptone and 10 g of glucose. Water was added up to 1000 mL. For media optimisation, 500 mL flasks were used and composed of 0.6 g of yeast extract, 0.6 g of malt extract, 1 g of peptone, 2 g of glucose and water that was added up to 200 mL. For both purposes, the pH was adjusted to 7.4 by the addition of 0.1 M sodium hydroxide. The media was then autoclaved under 15 psi at 121 °C.

2.3.2.2 Preparation of rice medium for solid cultures

For both media optimisation and up scaling, 500 mL conical culture flasks were used. Each conical culture flask composed of 100 g of rice and 100 mL of water. Components were left to stand overnight prior to autoclaving.

2.3.2.3 Cultivation

For media optimisation, the selected endophytes were grown in 500 mL flasks of liquid-Wickerham media and solid rice media for three incubation periods, 7, 15 and 30 days. For the up-scaling, depending on the results of media optimisation, the selected endophytes were reinoculated and grown again for either 7, 15 or 30 days in 15x 2 L or 500 mL conical culture flasks; each 2 L conical flask contained 1000 mL of liquid-Wickerham media and each 500 mL conical flask contained 100 g solid-rice media. All incubations took place at room temperature away from light.

2.3.2.4 Extraction of fungi grown in liquid-Wickerham medium

The incubation was ended by adding ethyl acetate to each flask and left to stand overnight to extract the produced metabolites (200 mL for media optimisation flasks, 1000 mL for up-scaling flasks). The ethyl acetate saturated culture mycelia was homogenised and kept overnight. The following day, the culture flasks were filtered through a filter paper under vacuum using a Buchner funnel and collected in collection flasks. The filtrate was then partitioned in a separatory funnel between water and ethyl acetate to separate medium contents from the produced metabolites. The partitioning step was performed thrice with new portion of ethyl acetate added each time to extract the most amounts of metabolites possible. Then, the ethyl acetate was evaporated with a rotary evaporator; the dried extracts were collected in a vial and weighed.

2.3.2.5 Extraction of fungi grown in solid-rice medium

Ethyl acetate was initially added to each flask to kill the endophyte and extract the secondary metabolites. The mycelia and the rest of the media was homogenised with 200 mL of ethyl acetate then filtered through a cotton wool into collection flasks. This step was repeated seven times to maximise the extraction of the metabolites. The ethyl acetate filtrate was evaporated and concentrated using a rotary evaporator. The dried ethyl acetate extract was then weighed and reconstituted in 130 mL of 10% aqueous methanol and subjected to partitioning in a separatory funnel with equal volume of hexane to separate the lipophilic fatty acids that will partition mainly in the non-polar solvent hexane from the other types of compounds. The

partitioning was repeated seven times before evaporating the solvents and concentrating the extracts from the two solvent phases. The dried extracts were again weighed.

2.4 Analysis methods

2.4.1 Materials, reagents, instruments and software

2.4.1.1 LC-HRMS spectroscopy and multivariate analysis

For liquid chromatography-high resolution mass spectrometry (LC-HRMS) both HPLC grade methanol and acetonitrile were purchased from VWR chemicals, European Community. Analytical grade formic acid was obtained from Fisher Chemicals, UK. The HPLC grade water was obtained from Direct-Q® water purification system, a product of Merck Millipore, US. The ACCELA HPLC system (autosampler and 600 pump) was coupled to the Exactive Mass spectrometer from Thermo Scientific, Germany. Thermo Xcalibur 2.1 software from Thermo Fisher Scientific, Germany was used to operate the process. The reversed phase column ACE 5 C18 5 µm x 75 mm x 3.0 mm was purchased from Hichrom, UK. Its particle and pore sizes were 5 µm and 100 °A, respectively. All runs were operated under at 37 bar pressure and 22 °C. The obtained data were acquired using Xcalibur 2.2 released by Thermo Scientific, Germany. MassConvert developed ProteoWizard, US was used to split the raw data to separate positive and negative ionisation files that were imported to MZmine 2.10 developed by Matej Orešič and Mikko Katajamaa from VTT, Finland. The data were then analysed using SIMCA-P 14.0 obtained from Umetrics, Sweden. The macro was developed *in-house* by Dr. Tong Zhang and coupled to the dictionary of natural products (DNP) database. The prepared samples were kept in vials obtained from Kinesis, UK.

2.4.1.2 NMR spectroscopy

Nuclear magnetic resonance (NMR) spectroscopy was carried out on four different instruments. The first instrument was the 400 MHz spectrometer JNM-LA400 manufactured by Joel, Japan. The magnet was Oxford AS400 model EUR0034 from Oxford, UK. The NMR has a Pulse-Field Gradient "Autotune"™ probe 40TH5AT/FG broadband high sensitivity probe for 5mm tubes. Furthermore, it has FG coils, 2H lock channel and can operate at different temperatures.

Moreover, Bruker Avance AV3 400 was used. It has a 9.4 T Ultrashield magnet, a BACS 120 autosampler and a Prodigy Cryoprobe. It is also DQD-equipped. In addition to that, Avance AVIIIHD 500 was used. It has a 9.4 T Bruker UltraShield magnet, a 11.74 T Ascend magnet, a Sampl Casease autosampler and a PA BBO 500S2 Smart Probe. The third Bruker Avance instrument was an AV 600 with a 14.1 T Bruker UltraShield magnet. It has a 24 position autosampler, 3 channel console, is DQD and Waveform-equipped and can use either a BBO-z-ATMA-[^{31}P-^{183}W/^{1}H] probe or a TBI-z-[^{1}H, ^{13}C, ^{31}P-^{15}N] probe. Both AVIIIHD 500 and AV 600 are equipped with a BCU-05 unit for automatic cooling of probes to 0 °C. All Bruker Avance instruments were obtained from Bruker, US and are in the Department of Pure and Applied Chemistry at The University of Strathclyde.

Samples were dissolved in either dimethyl sulfoxide-d_6 (DMSO-d_6) or pyridine-d_5 that were purchased from Aldrich, US. The obtained spectra were examined using MestReNova 10.0.2 developed by Mestrelab Research, Spain. NMR tubes were obtained from Norell, US. Wilmad® NMR capillary tubes were procured from Sigma-Aldrich, US and used for samples weighing less than 5 mg.

(*S*)-(+)-Methoxy-α-triflouro-methylphynylacetyl chloride ((*S*)-(+)-MTPA-Cl) and (*R*)-(–)-Methoxy-α-triflouro-methylphynylacetyl chloride ((*R*)-(–)-MPTA-Cl) were obtained from Sigma-Aldrich, US and used for Mosher ester analysis for determining the absolute configuration of stereogenic carbinol carbons.

2.4.1.3 Medium pressure liquid chromatography (MPLC)

HPLC grade Methanol (MeOH), Hexane (Hex), acetonitrile (ACN) and isopropanol were obtained from VWR chemicals, France. HPLC grade Ethyl acetate (EtOAc) and acetone were purchased from Sigma-Aldrich, Poland. HPLC grade Dichloromethane (DCM) was procured from Fisher Scientific, UK. HPLC grade water was obtained from Direct-Q® water purification system, a product of Merck Millipore, US. Celite® 545AW-Reagent Grade was obtained from Supelco, US.

Two Buchi C-601 pumps were connected to the pump manager Buchi C-615. All obtained from Buchi, Switzerland. This system allowed binary solvent gradients with flow rates from 2.5 to

250 mL/min to be run. VersaFlash, VersaPak cloumns were made of spherical silica (20–45 µm), 40 x 75 mm (48 g), brought from Supelco, US.

The Reveleris® Flash Forward system from Grace Davison Discovery Sciences, UK was used for MPLC as well. The system is equipped with two detectors, an evaporative light scattering detector (ELSD) and an ultraviolet (UV) detector with a wavelength ranging from 200 to 500 nm. This leads to greater sensitivity, selectivity and detection of UV inactive compounds. Moreover, this system allowed binary solvent gradient too. Yet, four different solvents could be used in a single run as there are four solvent channels. The flow rate could be set from 4 to 200 mL/min and it would be automatically adjusted if the pressure exceeded the limit. The fraction collector was automated and built into the system. In addition to that, the chromatogram could be saved and printed. The used columns were obtained from Reveleris, US. All were normal phase, made of 12 – 48 g of silica, with diameter of 40 µm.

2.4.1.4 Semi-preparative high performance liquid chromatography (Semiprep-HPLC)

VisionHT C18 HighLoad column, 5 µm was procured from Dr. Maisch, Germany. Its diamensions were 150 mm x 10 mm. ACN and water were used as solvents and described in 2.5.1.3. The samples were filtered through 0.22 µm Millex®GP filters that were obtained from Merck Millipore, Ireland before injecting them into the system.

The Reveleris® Prep Flash Forward system from Grace Davison Discovery Sciences, US was used for semiprep-HPLC. Its specifications are similar to the Reveleris® Flash Forward system that was described in 2.5.1.3. However, HPLC columns could be installed to the Reveleris® Prep system and liquid samples could be injected into the system.

2.4.1.5 Thin layer chromatography (TLC) and preparative thin layer chromatography (PTLC)

Both normal TLC plates (TLC silica gel 60 F_{254} plates) and preparative TLC plates (TLC silica gel 60 F_{254} on 20x20 cm aluminum sheets) were obtained from Merck, Germany. The capillary tubes were obtained from Hirschmann, Germany. The UV lamp operated at 254 nm (short UV) and 365 nm (long UV). It was of the model UVGL-55 Handheld and purchased from UVP, UK. For the preparation of the spraying reagent, sulfuric acid was obtained from Fisher Scientific, UK. Acetic acid was purchased from Sigma-Aldrich, US. Anisaldehyde was obtained from Acros Organics,

Belgium. The heating gun HL 2010 E was obtained from Steinel, UK. The same HPLC grade solvents that were described in 2.5.1.3 were used for TLC and PTLC. The magnetic mixer was purchased from Stuart, UK.

2.4.1.6 Optical rotation

Perkin Elmer 341 Polarimeter was obtained from PerkinElmer, US. Ethanol and chloroform were purchased from Fisher, UK. Methanol was procured from VWR chemicals, France.

2.4.2 Methods

2.4.2.1 LC-HRMS spectroscopy and multivariate analysis

Each sample was prepared at a concentration of 1 mg/mL in methanol. Methanol was used as a blank for the run. ACE 5 C18 column was used. Two solvents were used for mobile phase; 0.1% formic acid in water (solvent A) and 0.1% formic acid in acetonitrile (solvent B). The injection volume was 10 µL and the flow rate was 300 µL/min. The gradient is described in Table 2.6. High resolution mass spectrometry analysis was performed in both positive and negative modes in a mass range that varied from *m/z* 150 to 1500. The spray voltage was 4.5 kV. The capillary temperature was 320 °C.

Table 2.5: Mobile phase used for LC-HRMS.

Time (minutes)	% A	% B
0	90	10
30	0	100
35	0	100
36	90	10
45	90	10

The LC-HRMS chromatograms and spectra were viewed in Thermo Xcalibur 2.1. The files were splitted into positive or negative ionisation modes using the MassConvert before they were imported to MZmine 2.10 for processing. The splitting was essential due to the inability of MZmine to process both negative and positive data modes sets at once (Pluskal *et al*., 2010).

In MZmine, the centroid mass detector was used for peak detection where the noise level set to $1.0E^4$ and the MS level to 1. The chromatogram builder function was set to a minimum time

span of 0.2 min, minimum height of $1.0E^4$ and *m/z* tolerance of 0.001 *m/z* or 5.0 ppm. Local minimum search algorithm was used for chromatogram deconvolution. The chromatographic threshold was set to 5.0%, the minimum search for the retention time (t_R) range was set to 0.4 minutes, the minimum relative height to 5.0%, the minimum absolute height to 10000, the minimum ratio of peak top/edge to 3 and the peak duration range to 0.2 – 5.0 min. Isotopic peak grouper was used for detecting isotopes. The tolerances for both t_R and *m/z* were set to 0.1 min and 0.001 *m/z*, respectively. The maximum charge was set to 2 and the representative isotope chosen was the most intense. After that, the chromatograms were cropped to 5.0 – 40.0 min using the peak list row filtering function. Then, join aligner was used to align the peak list, in which, *m/z* tolerance was set to 0.001 *m/z* or 5 ppm, t_R tolerance to 5 relative % and weight for t_R and *m/z* to 20. Later, gap filling took place where the m/z tolerance was set to 0.001 *m/z* too, intensity tolerance to 30%, t_R tolerance to 0.5 minutes and *m/z* tolerance to 0.001 *m/z* or 5 ppm. Adduct search was performed with t_R tolerance of 0.2 min, *m/z* tolerance of 0.001 *m/z* or 5 ppm and maximum relative adduct peak height of 30%. The adducts searched for were Na, K, NH_4 in positive mode and formate in negative mode. ACN was searched for in both modes. Furthermore, a complex search was performed using $[M+H]^+$ for the positive mode and $[M-H]^-$ for the negative mode. The tolerance of t_R was set to 0.2 min, *m/z* tolerance of 0.001 *m/z* or 5 ppm and maximum complex peak height to 50%. Moreover, the formula prediction function was used to search for unknowns where again *m/z* tolerance was 0.001 *m/z* or 5 ppm. Finally, the data were exported as a CSV excel file for further clean up using the *in-house* developed macro. The exported parameters were Row ID, *m/z*, t_R, identification method, predicted chemical formula and the peak area. In macro, data preparation took place where both positive and negative outputs were combined again in one data set. This was followed by the removal of media and solvent effects and dereplication. This resulted in a data set prepared to be analysed using SIMCA-P software. The data were imported into SIMCA-P. Polarity and MZmine ID were merged and set to be the primary identifier and *m/z*, t_R, molecular formula and molecular weight (MWt) were selected as secondary identifiers. Either Principal Component Analysis (PCA) or Orthogonal Partial Least Squares Discriminant Analysis (OPLS-DA) was performed depending on the purpose of the study. Scores plots, loadings plots and S plots were then generated (Macintyre *et al*., 2014). Permutation test was performed for OPLS-DA models. This test calculates the model's fitness (R2) and predictive power (Q2). A strong model

have its R2 value close to 1, its Q2 value around 0.5, its R2Y intercept less than 0.4, and its Q2Y intercept less than zero (Ali *et al*., 2013, Triba *et al*., 2015). Moreover, the optimum difference between R2Y and Q2 values should be no more than 0.3 (Wiklund, 2008).

2.4.2.2 NMR spectroscopy

Samples were dissolved in 600 µL of DMSO-$_{d6}$ and transferred to NMR tubes, 5 mg was used for fractions, while the entire amount obtained (up to 30 mg) was used for pure compounds. Quantities less than 5 mg were dissolved in 200 µL DMSO-$_{d6}$ and transferred to capillary NMR tubes or 3 mm tubes. For Mosher ester analysis, 1 mg aliquots of each sample were dissolved in 600 µL of pyridine-$_{d5}$, transferred to an NMR tube and had their ^{1}H and ^{1}H–^{1}H COSY NMR spectra recorded. After that, either (*S*)-(+)-MTPA-Cl or (*R*)-(–)-MTPA-Cl were added to these aliquots. 5 µL of each reagent was added for each hydroxyl group in the sample. The tubes were shaken thoroughly and allowed to stand for 72 hours. The reaction was monitored by ^{1}H and ^{1}H–^{1}H COSY NMR each 12 hours.

All experiments were processed using MestReNova 10.0.2.

2.4.2.3 Medium pressure liquid chromatography (MPLC)

MPLC or flash chromatography (FC) is a separation technique that is very similar to open column chromatography; however, a pressure is applied to elute the sample faster from the column. The solvent system was chosen after being tested on a TLC plate.

In both Buchi and Reveleris® Flash Forward systems, normal phase columns were used and conditioned with the starting solvent system before loading dry samples that were mixed with celite. Fractions were collected manually in 100 mL Erlenmeyer flasks if Buchi system was used and were collected automatically in test tubes if Reveleris® Flash Forward system was used. After that, TLC analysis was done for all fractions so the similar fractions were pooled together. The conditions, parameters and mobile phases used are mentioned in results and discussion.

2.4.2.4 Semi-preparative high performance liquid chromatography (Semiprep-HPLC)

Preparative HPLC is a technique that is used to purify compounds from mixed solutions. It could be utilised to purely isolate secondary metabolites from natural extracts. Prep-HPLC was implemented in this project to purify enniatins that were difficult to purify using MPLC. Samples were dissolved in the least amount possible (up to 5 mL) of the starting solvent system and injected to Reveleris® Prep Flash Forward system. Reversed phase columns were used. Fractions were collected automatically in test tubes. The conditions, parameters and mobile phases used are mentioned in results and discussion.

2.4.2.5 Thin layer chromatography (TLC) and preparative thin layer chromatography (PTLC)

Thin layer chromatography (TLC) could be used as analytical tool to identify compounds based on their R_f value and colour either under UV light or upon reaction with different spraying agents. Moreover, it could be used to determine the purity of a sample and to estimate the number of compounds it's composed of. Furthermore, it could be used to determine the suitability of solvent systems for flash chromatography. In addition to all of that, it could be used as a preparative tool to purify compounds.

For analytical TLC purposes, fractions were all dissolved in acetone and spotted 1 cm above the bottom edge of the TLC plate. The mobile phase was allowed to develop in a TLC chamber. The run of the plates was 5 – 6 cm. After that, the spots were detected under short and long UV lights. Compounds that quenched flourescene or phosphorescene could be detected as dark spots under the short UV light. Conjugated double bond systems and aromatics could be detected as coloured spots under short UV light as well. Alkaloids, flavonoids and other analytes could be detected under long UV light (Wall, 2005). Then, TLC plates were sprayed with anisaldehyde/sulfuric acid reagent (Table 2.6) and heated to 200 °C by heat gun. This spraying reagent is used to detect many natural products like essential oil components, steroids, terpenes, sugars, phenolic compounds, and sapogenins (Wall, 2005). The mobile phases used are mentioned in results and discussion.

For PTLC, 10 mg of sample was dissolved in 150 µL of acetone and applied to each plate as a band 2 cm above the bottom edge of the plate. Before the elution of plates, filter papers were

placed inside the chamber, so the mobile phase would run up the papers and saturate the chamber, fastening the equilibration of the chamber. This is very important, otherwise, the solvent front would evaporate from the plates, its velocity would decrease and the solvent front would be uneven and concavely shaped. After the mobile phase was allowed to develop on the plates, the bands were viewed under UV light. Moreover, the plates were covered by aluminum foil, allowing a little bit of their right edge to be uncovered and sprayed by anisaldehyde/sulfuric acid reagent. The bands were marked with a pencil, cut and recovered by acetone. The mobile phases used are mentioned in results and discussion.

Table 2.6: The components of anisaldehyde/sulfuric acid spray reagent.

Component	Volume (mL)
Anisaldehyde	0.5
Methanol	85
Glacial acetic acid	10
Concentrated sulfuric acid	5

2.4.2.6 Optical rotation

Enantiomers could be differentiated into – or + depending on their interaction with linear polarised light. The (+) isomer rotates linearly polarised light clockwise and the (–) isomer rotates it counter-clockwise. All samples were prepared as 0.1 g/100 mL solutions. The specific optical rotation at 589 nm (the wavelength of the sodium D-line) could be calculated using the following equation:

$$[\alpha]_D^{20} = \frac{100\,\alpha}{l \times c}$$

Where α is the average of the measured rotation (°) as 10 measures were taken, l is the path length (dm) and *c* is the concentration of the solution (g/mL). Measures were done at 20 °C.

2.5 Biological activity: Anti-proliferative activity assay

2.5.1 Materials, reagents, instruments and software

Screening for potential bioactive anticancer compounds, anti-proliferative assay was preliminary done on Human Caucasian Breast Carcinoma (ZR-75). For pure compounds and

selected fractions and extracts, bioassays were performed against Human Caucasian Breast Carcinoma (ZR-75), Human Caucasian Lung Carcinoma (A549), and Human Normal Prostate Epithelium (PNT2) cell lines. The additional cell lines were used to investigate the compounds' selectivity and anti-proliferative activity. All of those cell lines were epithelial, adherent and obtained from ATCC, US. RPMI 1640 and DMEM media were bought from BioWhittaker Lonza, Belgium. Foetal bovine serum (FBS), glutamine and penicillin/streptomycin solution were all obtained from Invitrogen, UK. TrypLE Express was procured from GIBCO, UK. Hanks' balanced salt solution (HBS) and Trytox X-100 were brought from Sigma, US. AlamarBlue BUF012B was obtained from Bio-Rad, UK. Samples were solubilised in Dimethyl Sulfoxide (DMSO) assay grade that was produced by Fisher Scientific, US. 96-well plates were purchased from TRP, Switzerland and Greiner bio-one, Austria. Falcon tubes and incubation flasks were produced by Corning, Mexico.

Napco 5410 incubator was humidified, kept at 37 °C in the presence of 5% CO_2 and obtained from Napco, US. SterilGard biological safety cabinet was purchased from The Baker Company, US. The IEC Medispin centrifuge was procured from Thermo Scientific, Germany. Bright-Line hemocytometer was obtained from Reichert, US. The water bath was from Clifton, UK. The microscope was obtained from Olympus Optical, Japan. Wallac Victor 2 was used for measuring fluorescence and obtained from PerkinElmer, UK. Bar charts were plotted by Microsoft Excel 2010 whereas dilution curves were plotted by Prism 4.03 that was developed by GraphPad Software, US.

2.5.2 Methods

2.5.2.1 Sample preparation

All samples were prepared by the use of DMSO as a solvent and kept at -20 °C.

2.5.2.2 Media preparation

Both RPMI 1640 and DMEM medium were prepared as the following protocol:

- 60 mL were taken out of the 600 mL medium bottle and discarded.
- 5 mL of Penicillin/Streptomycin (5000 IU/µL – 5000 µg/µL) were added.

- 5 mL of L-Glutamine 200 mM (× 100) were added.
- The pH was adjusted to 7.4 by the addition of Sodium hydroxide.
- Finally, 50 mL of FBS were added.

2.5.2.3 Cell splitting and seeding

The used cell lines were stored at -80°C. They were thawed at 37°C in a water bath. After that, 5 mL of medium were added to small seeding flasks and had the cells poured into them. When the cells adhered to the walls of the flasks, they were split. The medium was taken out of the seeding flask while the cells were attached to the walls of the flask. HBS was added to the flask, shaken gently and removed. This was followed by the addition of TrypLE Express that caused cells to detach. The flask was shaken gently and incubated for 6 minutes. After that, medium was added to stop the effect of TrypLE Express. The mixture was then transferred to a falcon tube and centrifuged. After centrifugation, the supernatant was discarded and the cells were kept in the tube. Then, a known volume of medium that was kept at 37°C was added and shaken, causing cells to suspend. The suspended cells were counted by the hemocytometer. The volume of the suspension that was transferred to a new seeding flask is calculated as follows:

$$v = \frac{seeding\ density\ \left(\frac{cells}{cm^2}\right)}{cell\ count\ \times\ 10^4 \left(\frac{cells}{ml}\right)} \times area\ of\ the\ flask\ (cm^2)$$

The volume of suspension that was transferred to a new falcon tube to seed a 96-well plate is calculated as follows:

$$v = \frac{seeding\ density\ \left(\frac{cells}{cm^2}\right)}{cell\ count\ \times\ 10^4 \left(\frac{cells}{ml}\right)} \times 10$$

Where v is the volume in mL. Volume of cell suspension taken to seed a 96-well plate seeding was completed to 10 mL by the addition of medium. The seeding densities for the tested cell lines are mentioned in Table 2.7. Then, seeded flasks and 96-well plates were incubated at 37°C and 5% CO_2 in a humidified incubator.

Table 2.7: Seeding densities (cells/cm^2) for the used cell lines.

Cell line	ZR-75	A549	PNT2
Flask	8×10^3	7×10^3	3×10^3
96-well Plate	2×10^4	5×10^4	5×10^4

2.5.2.4 AlamarBlue assay

Extracts and fractions were tested at a concentration of 30 µg/mL. However, for the creation of dilution curves for pure compounds, samples were added at a concentration range of 0.001 µM to 30 µM. TrytonX was used as a negative control whereas a column of cells was left with no samples as positive control. All tested samples were added to the tested cell lines in 96-well plates and incubated for 48 hours. Cell viability was assessed using AlamarBlue that was added to the wells in 10% of their volume. After 6 hours of the addition, the fluorescence was measured using a Wallac Victor 2 fluorometer. The bar charts for extracts and fractions were plotted by Microsoft Excel 2010, while the dilution curves and IC_{50} values for pure compounds were determined by Prism 4.03. A fraction or extract was considered active if it resulted in 40% viability of the tested cells or less. Results were confirmed by being microscopically inspected.

2.5.2.5 Selectivity index

If the IC_{50} value of any of the isolated compounds against the normal prostate PNT2 cells was obtained from the dilution curve, then its selectivity index was calculated according to following equation:

$$SI = \frac{IC_{50}\ against\ PNT2\ cells\ (\mu M)}{IC_{50}\ against\ cancer\ cells\ (\mu M)}$$

Where SI is the selectivity index. The selectivity index was calculated whenever there was a presumed activity. Thus, it was calculated when the value of IC_{50} for the tested compound was equal or less than 30 µM against the tested cancer cell line. If the SI value was greater than 2 or if the IC_{50} value of a compound against the normal prostate PNT2 calls was not obtainable from the dilution curve then the compound was considered selective.

Chapter 3: Bioassay-metabolomics guided approach to select three endophytes for the large scale fermentation

3 Bioassay-metabolomics guided approach to select three endophytes for the large scale fermentation

3.1 Small scale fermentation and extraction

All of the 26 obtained endophytes that are listed in Table 3.1 were incubated in malt-agar medium and extracted as described in Section 2.2.2. For, preliminary screening, all extracts were subjected to anti-proliferative assay against breast cancer (ZR-75) cell line as well as both ^{1}H NMR analysis and LC-HRMS analysis.

Table 3.1: The obtained endophytes and their plant sources.

Plant source	Sample ID	Endophyte
Anthemis palestina	1	Sequencing failed
	2	*Ulocladium* sp.
	3	*Fusarium acuminatum*
	4	Sequencing failed
	5	Sequencing failed
	6	*Alternaria alternata*
	7	*Curvularia australiensis*
	8	Sequencing failed
	9	*Chaetomium subaffine*
	10	Sequencing failed
	11	Sequencing failed
Anchusa strigosa	12	*Aureobasidium pullulans*
	13	*Alternaria tenuissima*
	14	*Alternaria alternata*
	15	*Aureobasidium pullulans*
	16	Sequencing failed
Euphorbia peplus	17	Sequencing failed
	18	*Fusarium acuminatum*
	19	*Alternaria multiformis*
	20	*Fusarium equiseti*
	21	Sequencing failed
	22	*Aspergillus flavus*
	23	*Pleosporales* sp.
	24	*Fusarium* sp.
	25	Sequencing failed
Rumex cyprius	26	*Chaetomium subaffine*

3.2 Anti-proliferative activity screening of the obtained endophytes against breast cancer (ZR-75) cell line

As depicted in Figure 3.1, out of the 26 tested endophytes, only six endophytes possessed activity and afforded less than 40% viability of the tested cells. The active fungal extracts included *Fusarium acuminatum* (no. 3), *Curvularia australiensis* (no. 7), an unknown endophyte (no. 8) *and Chaetomium subaffine* (no. 9) that were obtained from *Anthemis palestina;* As well as *Fusarium* sp. (no. 24) and *Chaetomium subaffine* (no. 26) from *Euphorbia peplus and Rumex cyprius*, respectively.

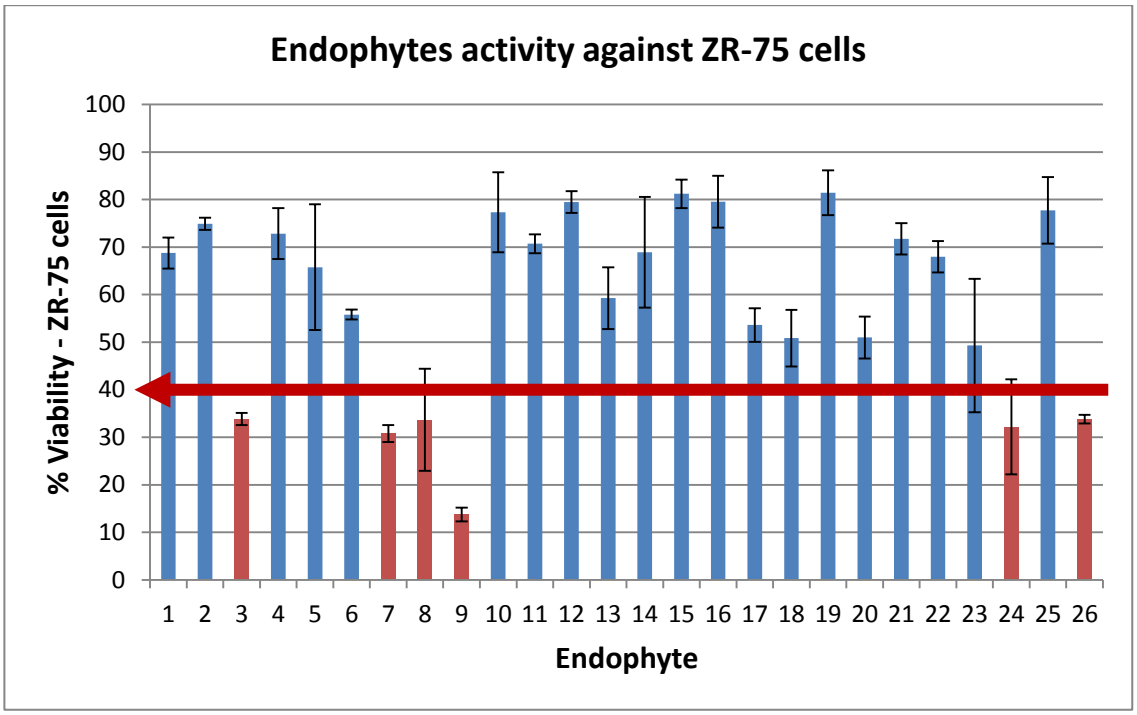

Figure 3.1: The biological activity of the extracts (30 µg/mL) of the obtained endophytes against ZR-75 cell line. Endophyte numbers refer to the corresponding endophyte that is mentioned in Table 3.1. Red line indicated the bioactivity threshold for 40% viability of the tested cells.

Four out of the six active endophytes were obtained from the plant *Anthemis palestina*. Moreover, two *Fusarium acuminatum* endophytes were obtained, but only the one obtained from *Anthemis palestina* was anti-proliferative against the tested cell line. Furthermore, two *Chaetomium subaffine* endophytes were obtained and found active. Yet, the one obtained from the plant *Anthemis palestina* was found to be more active as it yielded 13% viability of the

tested cells, whereas the one obtained from *Rumex cyprius* yielded 33% viability of the tested cells. These findings could be denoted to certain specific host-endophyte interactions like those between the plant host *Anthemis palestina* and its endophytes, which lead to the synthesis of anti-proliferative secondary metabolites that resulted to the detected bioactivity. However, this could not be confirmed until it is fully investigated.

3.3 ^{1}H NMR screening of the obtained endophytes

As illustrated in Figure 3.2, most of the peaks, those marked within the red boxes, are medium components while peaks highlighted within the blue boxes represented the produced secondary metabolites. The huge difference in concentration between the media components and the secondary metabolites that were produced by the endophytes rendered ^{1}H NMR spectral data not useful enough to compare the extracts. However, seven endophytes were poor in producing secondary metabolites as no other peaks other than those from the media could be detected in their respective ^{1}H NMR spectra. Thus, these endophytes could be excluded from the scale-up. They included *Ulocladium* sp. (no. 2), unknown endophyte (no. 11), *Aureobasidium pullulans* (no. 12), *Pleosporales* sp. (no. 23), *Fusarium* sp. (no. 24), an unknown endophyte (no. 25) and *Chaetomium subaffine* (no. 26). Out of those seven endophytes, both *Fusarium* sp. (no. 24) and *Chaetomium subaffine* (no. 26) possessed activity against breast cancer. This indicated their ability of producing potent anti-proliferative metabolites, as they were found to be biologically active despite their low yield.

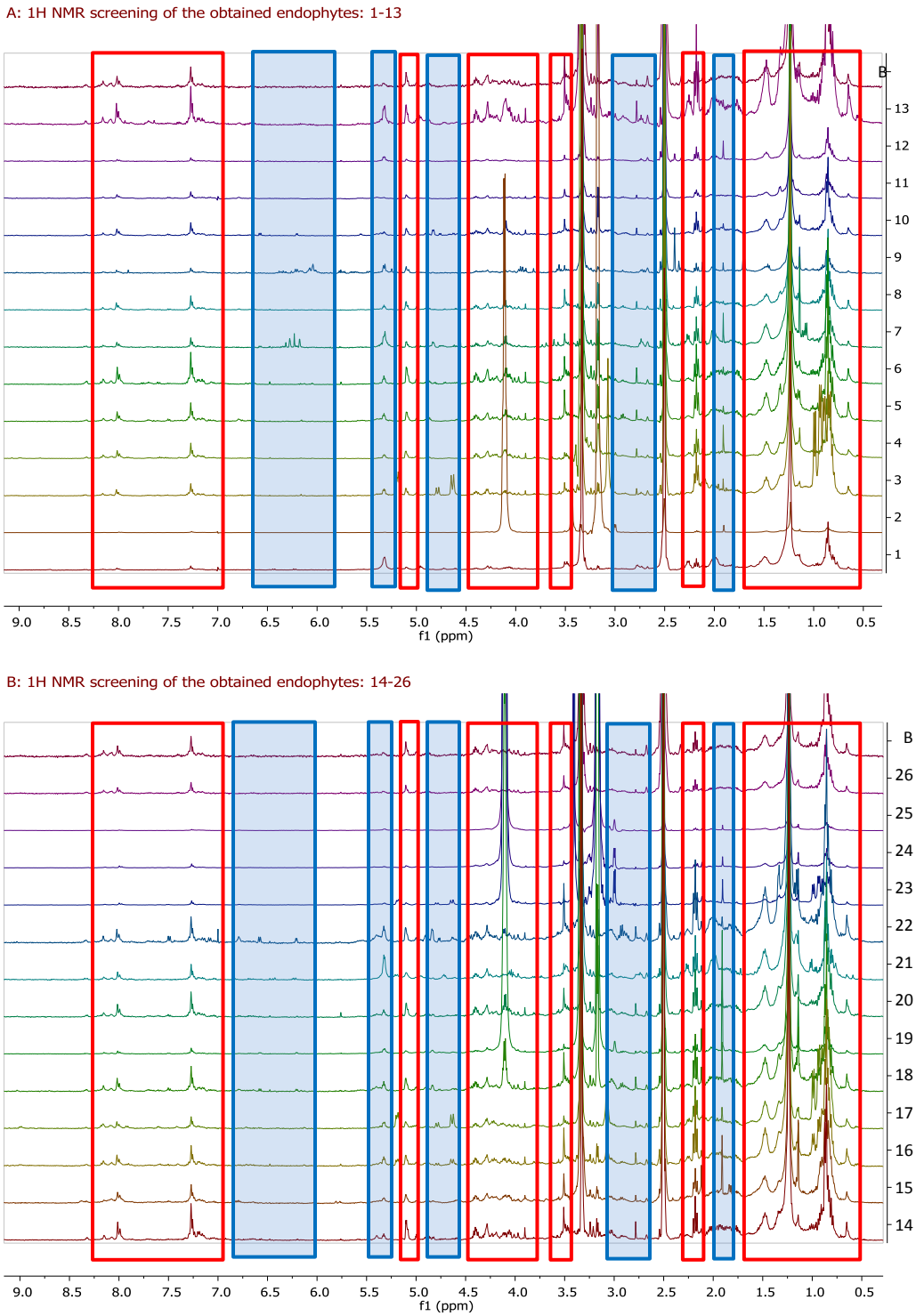

Figure 3.2: The ^{1}H NMR data of the obtained endophytes. Numbers on Y-axis indicated the number ID of the respective endophyte as listed in Table 3.1, while (B) is for MA medium blank. 5 mg of each sample were dissolved in DMSO-$_{d6}$, (400 MHz).

3.4 LC-HRMS and metabolomics screening of the obtained endophytes

PCA analysis was performed as described in section 2.5.2.1. Figure 3.3 included all obtained endophytic extracts. As shown in Figure 3.3, three clusters could be discerned. The first cluster is encircled in red and contained most of the obtained endophytes. The second cluster is circled in blue and contained three out of the four *Fusarium* spp. obtained; *Fusarium acuminatum* (no. 3 and 18), *Fusarium* sp. (no. 24) and an unknown endophyte (17). This may lead to identify the unknown endophyte (17) as a *Fusarium* sp. as well; especially that it shared the red morphological colour of the other endophytes of *Fusarium* genus (Table 2.2). And hence, PCA could be utilised as an identification tool. The clustering itself is referred to the similarity of the chemical profile of these endophytes; as *Fusarium* spp. are known to produce unique but characteristic classes of mycotoxins, including enniatins and beauvericin (Firakova *et al*., 2007). The third cluster is circled in black and included the single endophyte *Ulocladium* sp. (2).

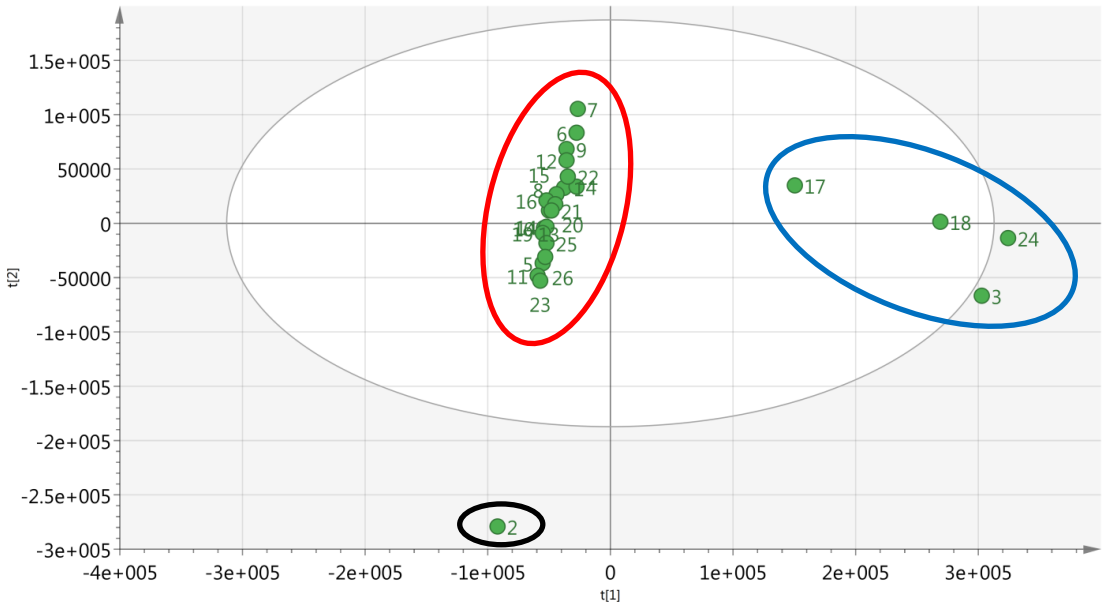

Figure 3.3: Scores plot of the obtained endophytes. Numbers refer to the corresponding endophyte that is mentioned in Table 3.1. R2X=0.415, Q2=0.131.

The outliers of the previous model were excluded and a new PCA model was created (Figure 3.4). As shown in the scores plot, the unknown endophyte (no. 4) formed a new distinct outlier in addition to *Alternaria alternata* (no. 6) and *Curvularia australiensis* (no. 7). Other endophytes

were scattered randomly with no specific pattern or clustering. This suggested the variation in the secondary metabolites that were produced.

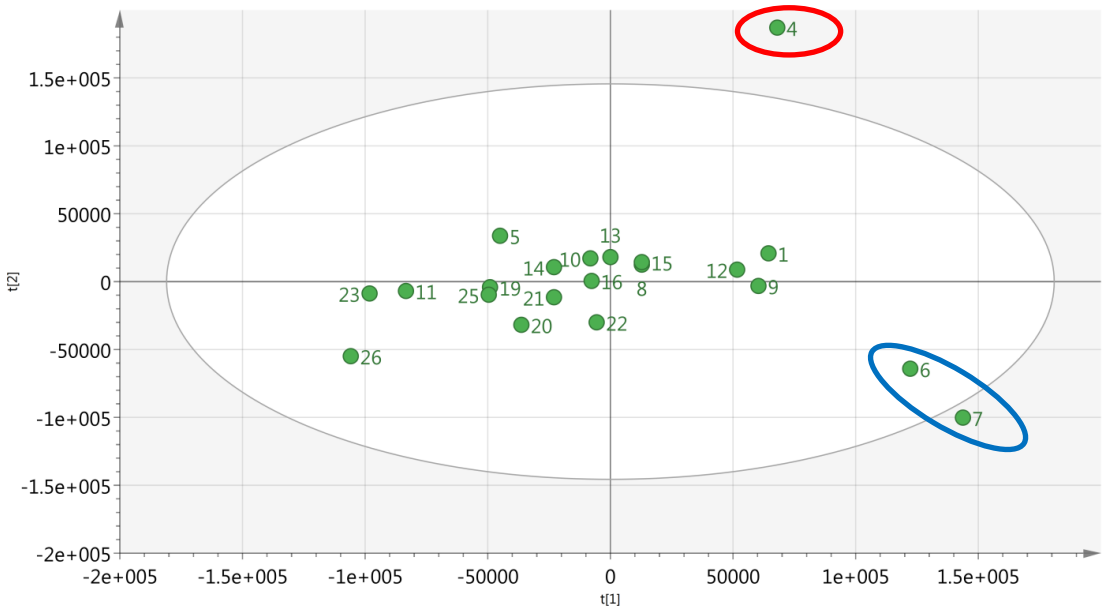

Figure 3.4: Scores plot of the obtained endophytes, excluding 2, 3, 17, 18 and 24. Numbers refer to the corresponding endophyte that is mentioned in Table 3.1. R2X=0.274, Q2=-0.0384.

A third PCA model was generated for the active metabolites (Figure 3.5). All endophytes clustered together (red circle) except the two *Fusarium* spp. that formed two distinct outliers; *Fusarium acuminatum* (no. 3) and *Fusarium* sp. (no. 24).

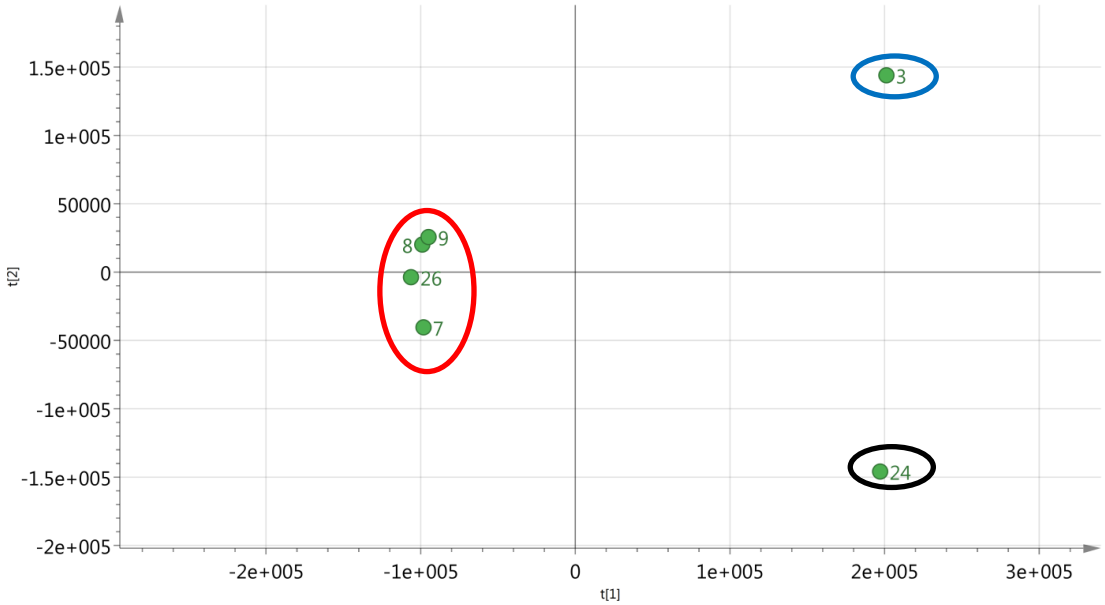

Figure 3.5: Scores plot of the endophytes that were active against ZR-75 cell line. Numbers refer to the corresponding endophyte that is mentioned in Table 3.1. R2X=0.698, Q2=0.196.

3.5 The selection of three endophytes for the large scale fermentation

The selection of three endophytes for the large scale fermentation for this project was limited to the ones that were active against breast cancer as discussed in 3.2. From those, the unknown endophyte (no. 8) was excluded as it couldn't be identified using ITS gene sequencing. This reduced the selection to the five endophytes that were listed in Table 3.2. Those five endophytes included three species, *i.e.* one *Curvularia* species, two *Fusarium* species and the two strains of *Chaetomium subaffine*. Both *Fusarium* sp. (no. 24) and *Chaetomium subaffine* (no. 26) afforded poor ^{1}H NMR spectrum, and hence, poor production of secondary metabolites. Thus, they were excluded as well. As a result, three endophytes that belonged to three different genera remained, and therefore, were chosen to be scaled-up. Those endophytes were *Fusarium acuminatum* (no. 3), *Curvularia australiensis* (no. 7) and *Chaetomium subaffine* (no. 9) that were all obtained from the plant *Anthemis palestina.*

Table 3.2: Endophytes considered for up-scaling.

Plant source	Sample ID	Endophyte
Anthemis palestina	3	*Fusarium acuminatum*
Anthemis palestina	7	*Curvularia australiensis*
Anthemis palestina	9	*Chaetomium subaffine*
Euphorbia peplus	24	*Fusarium* sp.
Rumex cyprius	26	*Chaetomium subaffine*

3.6 Metabolomics-bioassay guided approach to select the most suitable conditions for culturing the selected fungal endophytes for large-scale fermentation

Metabolomics workflow was designed to isolate anti-proliferative metabolites from the studied endophytes. It is illustrated in Figure 3.6.

In order to optimise the best conditions for scale-up, the respective fungal endophytes were incubated in two types of media; liquid-Wickerham and solid-rice media. Both the composition of the medium and the incubation period are important for determining the compounds that are produced by the endophyte. Therefore, depending on the life cycle of the Ascomycota, three incubation periods were chosen for testing and choosing the most optimal growth conditions (Webster and Weber, 2007). Incubating the fungi for 7 days will represent the germination phase; while 15 days of incubation will represent the hyphal growth phase and 30 days of incubation will represent the sporing phase.

Three parameters were monitored in order to decide the optimum conditions for the large-scale fermentation:

1. The weight or yield of the extract that was produced by the endophyte.

2. Its chemical composition and diversity, which was determined by implementing both LC-HRMS and NMR.

3. Its bioactivity against ZR-75 (human breast carcinoma) and A549 (human Caucasian lung carcinoma) cell lines.

After the large-scale fermentation was carried out, a metabolomics-guided approach was conducted to target the bioactive secondary metabolites by utilising both the biological assay

results and the LC-HRMS data. The LC-HRMS data were subjected to Orthogonal Partial Least Square-Discernment analysis (OPLS-DA). The active fractions were grouped together apart from the inactive fractions then a permutation test was conducted to test the validity of the model. The LC-HRMS data were set as the X independent variable and supervised by the set of bioactive fractions as the Y variable. Loadings S-plot was generated from the OPLS-DA score plot model, in which, the extreme loadings of the metabolites (in *m/z*) were correlated to the activity of the fractions. An S plot was generated from each OPLS-DA model.

Significance thresholds for R2 and Q2 values are strongly application-dependent. Concerning the Q2 parameter, a significance threshold of 0.5 is generally admitted (Triba *et al*., 2015). The SIMCA users' guide has assigned Q2>0.5 for good predictability. However, many PLS-DA/OPLS-DA models built using SIMCA have published Q2 values less than 0.5 as frequently encountered in metabolomics (Triba *et al*., 2015). The R2 and Q2 values strongly depend on the individuals that constitute the validation subsets. When the Q2 values are lower than 0.5, the quality parameters were verified to be stable towards permutation of the rows in their dataset. Q2<0.4 are models with poor predictability and are validated by a permutation test that consisted of comparing the Q2 obtained for the original dataset with the distribution of Q2 values calculated when original Y values are randomly assigned to the individuals. The Y intercept on the permutation graph is a measure of the overfit. A clear indication that the original model is valid and does not happen by coincidence is when the Q2 values of the permuted Y models are less than zero on the permutation plot test (Eriksson *et al*., 2006). Generally, two principal components and 100 permutations were used for the OPLS-DA models of this project.

The loadings on the S plot depicted all metabolites contained in all fractions. The metabolites were differentiated by their presence or absence in either the active or the inactive fractions. The "endpoint" metabolites indicated on the S-plot were assigned as the target bioactive metabolites and were dereplicated. The putative metabolites predicted as "hits" from the DNP database were filtered according to the fungal source and the host plant genus *Anthemis* as source.

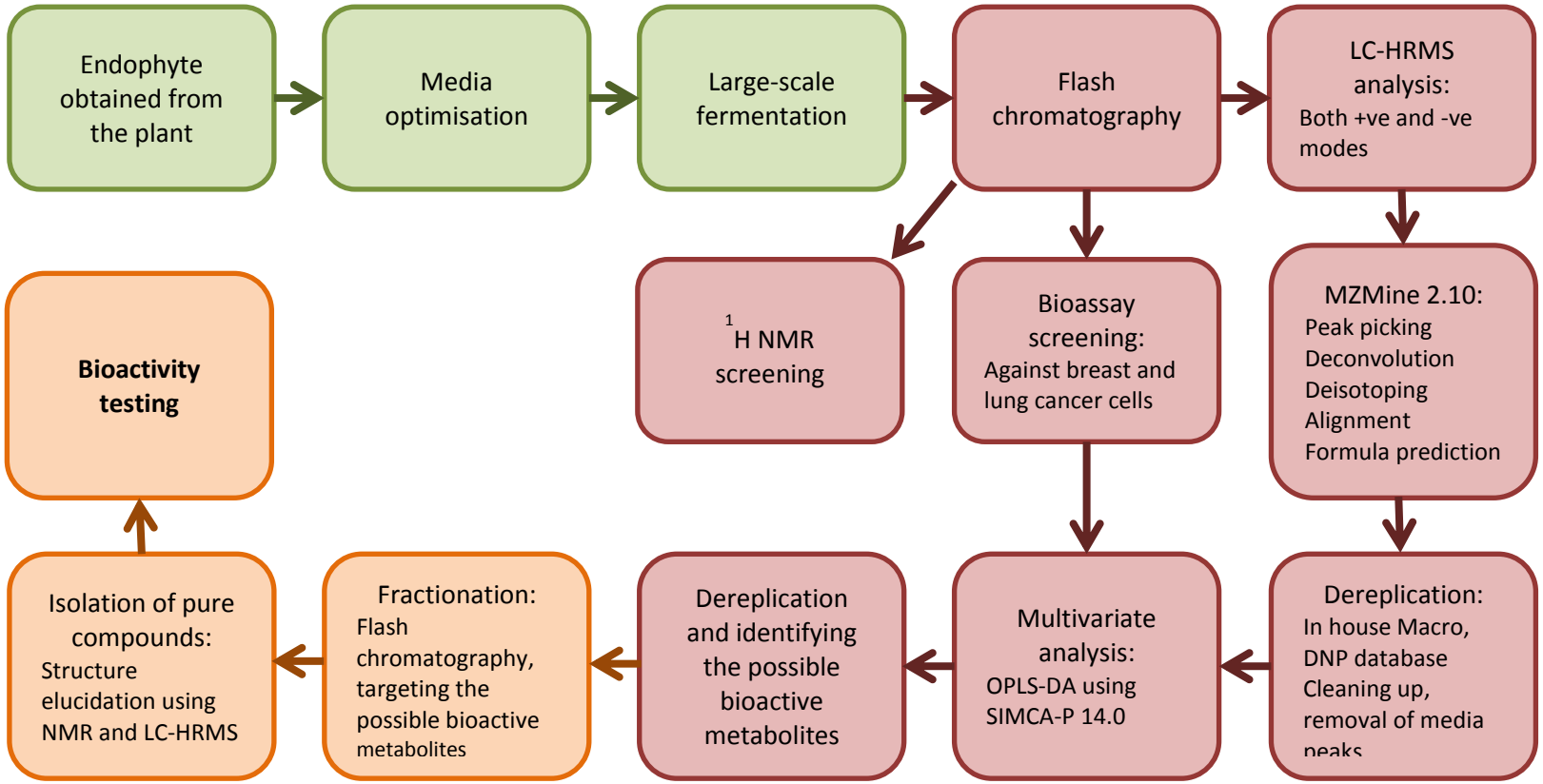

Figure 3.6: Implementing metabolomics in the search for anti-proliferative agents from the selected endophytes.

Chapter 4: *Curvularia australiensis*

4. *Curvularia australiensis*

4.1 Introduction

4.1.1 Secondary metabolites isolated from *Curvularia* spp

Curvularia is a genus of the family Pleosporaceae (phylum Ascomycota). It is an anamorph associated with the plant pathogen genus *Cochliobolus* (Webster and Weber, 2007). The genus *Curvularia* contains more than 80 species, of which, most are either plant or soil pathogens (da Cunha *et al*., 2013). However, some of these species caused infections in animals and humans as well (da Cunha *et al*., 2013).

Curvularia borreriae strain HS-FG-237 yielded androstanoid 4α-methyl-9α-methoxyandrosta-8, 15-diene-3,17-dione (Figure 4.1), which possessed weak anti-proliferative activity against HCT-116 cell line as well as weak anti-inflammatory activity against ANA-1 murine macrophages model (Liu *et al*., 2017a). Moreover, rice cultures of *Curvularia* sp. strain M12 obtained from the plant *Murraya koenigii* afforded murranofuran A, murranolide A, murranopyrone and murranoic acid A in addition to six earlier known metabolites that included curvularin and (*S*)-dehydrocurvularin (Figure 4.1). Both murranolide A and murranopyrone impaired the motility of *Phytophthora capsici* zoospores. (Mondol *et al*., 2017). Furthermore, three compounds *N*-acetylphenylalanine, the dipeptide *N*-acetylphenylalanyl-L-phenylalanine and the tripeptide *N*-acetylphenylalanyl-L-phenylalanyl-L-leucine (Figure 4.1) were isolated from the endophyte *Curvularia* sp. obtained from the leaves of *Terminalia laxiflora* (Tawfike *et al*., 2017). The isolated peptides were tested against NF-κB's antiapoptotic transcription factors in K562 cell line (human Philadelphia chromosome-positive chronic myelogenous leukemia cells) and only *N*-acetylphenylalanine was found to be active (Tawfike *et al*., 2017). Cultures of the marine fungus *Curvularia inaequalis* yielded (+)-phomalactone, cinodontin, curvulapyrone, radicinin and ergosterol peroxide (Figure 4.1). The compounds (+)-phomalactone, curvulapyrone and radicinin possessed anti-proliferative activity against Ehrlich ascites carcinoma cells in mice (Yurchenko *et al*., 2013). In addition, the same species *Curvularia inaequalis* (strain HS-FG-257) obtained from a soil sample, incubated in potato starch and peptone afforded curvularone A and 4-hydroxyradianthin (Figure 4.1) (Pang *et al*., 2013). Both compounds exhibited anti-proliferative activities against ACHN (Human renal adenocarcinoma) and HepG2 (Human

Caucasian hepatocyte carcinoma) cell lines (Pang *et al*., 2013). Nonetheless, no metabolites were previously reported from *Curvularia australiensis* (Synonym: *Bipolaris australiensis).*

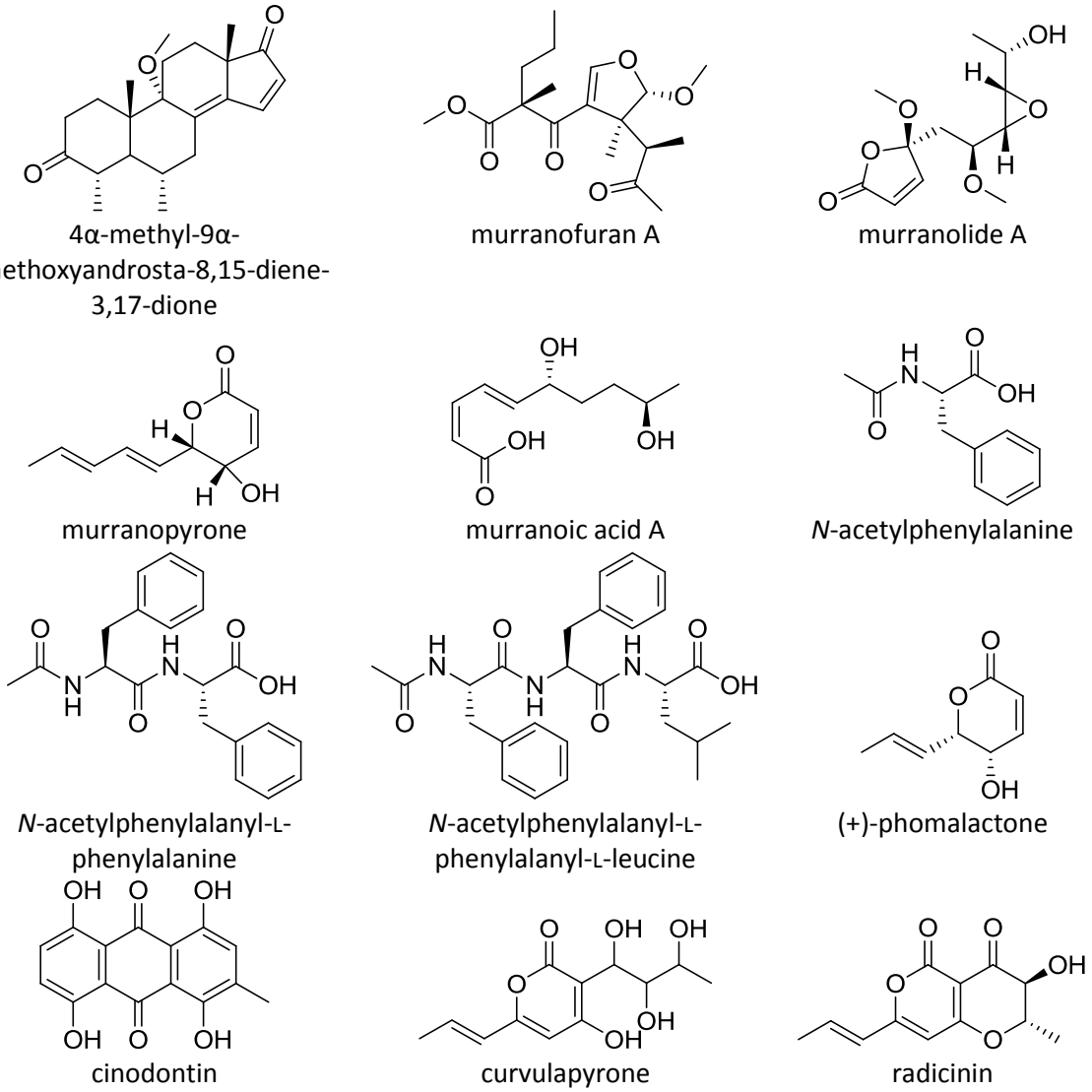

Figure 4.1: Secondary metabolites isolated from various species of *Curvularia*.

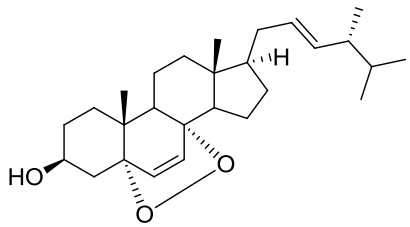

ergosterol peroxide

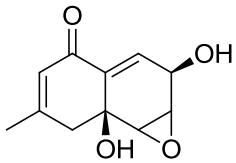

curvularone A

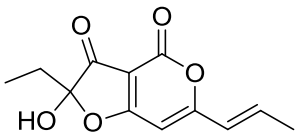

4-hydroxyradianthin

Figure 4.1 (continued): Secondary metabolites isolated from *Curvularia* spp.

4.1.2 Curvularin-type derivatives isolated from microorganisms

The polyketide curvularin was isolated for the first time in 1956 from, then, a new species of *Curvularia* that was grown in a medium composed of glucose, peptone and mineral salts (Musgrave, 1956). Moreover, it was shown that the biosynthesis of curvularin required eight acetic acid units (Birch *et al*., 1959). The first biological activity of curvularin was described in 1977 indicating weak anti-proliferative activity against HeLa (Human cervix epitheloid carcinoma) cell line (Horakova and Betina, 1977).

Later, in 1962, curvulin and curvulinic acid (Figure 4.2) were isolated for the first time from the fungus *Curvularia siddiqui* (Kamal *et al*., 1962). After that, in 1967, Munro, Musgrave and Richard were able to isolate 10,11-didehdrocurvularin (αβ-dehydrocurvularin) (Figure 4.2) from *Curvularia* sp. (Munro *et al*., 1967). In 1976, both αβ-dehydrocurvularin and β-hydroxycurvularin (Figure 4.2) were purified from the extract of *Alternaria tomato*, another fungus of the family Pleosporaceae (Hyeon *et al*., 1976). The compounds suppressed both sporulation and spore germination activities of *A. tomato* (Hyeon *et al*., 1976). Along with curvularin and dehydrocurvularin 11-methoxycurvularin, that was named 8-methoxycurvularin (Figure 4.2), was isolated from *Penicillium* sp. A-5-1 (Kobayashi *et al*., 1985). These three compounds blocked the first cleavage in the cell division process by giving barrel-like spindles and dispersing the microtubule organising centre (Kobayashi *et al*., 1985). In 1989, *cis*-dehydrocurvularin, 11α-hydroxycurvularin, 12-oxocurvularin and citreofuran (Figure 4.2) were isolated from *Penicillium citreo-viride* B (Lai *et al*., 1989). In 1991, the same research group were able to identify and isolate the two stereoisomers 11-α-methoxycurvularin and 11-β-methoxycurvularin along with 11,12-dihydroxycurvularin and 12-hydroxy-10,11-*trans*-

dehydrocurvularin (Figure 4.2) from the hybrid strain ME 0005 derived from *P. citreo-viride* B. IFO 4692 and 6200 (Lai *et al*., 1991). Nineteen years later, curvulone A and curvulone B (Figure 4.2) were reported from *Curvularia* sp. that was obtained from the marine alga *Gracilaria folifera*. The isolated congeners showed antimicrobial activity against the gram-positive bacterium *Bacillus megaterium*, the fungi *Microbotryum violaceum* and *Septoria tritici* and the alga *Chlorella fusca* (Dai *et al*., 2010).

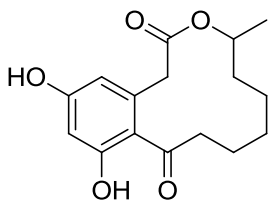

curvularin

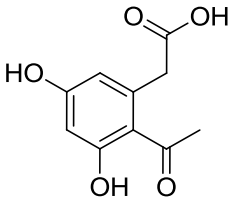

curvulin

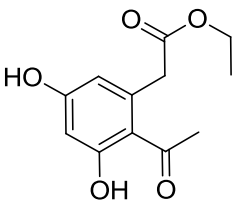

curvulinic acid

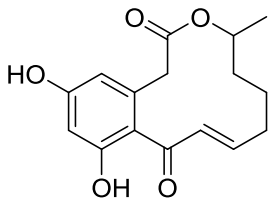

10,11-didehydrocurvularin

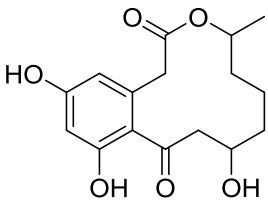

11-hydroxycurvularin

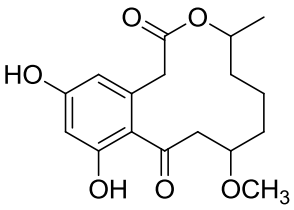

11-methoxycurvularin

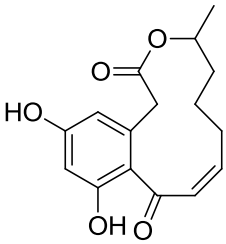

cis-dehydrocurvularin

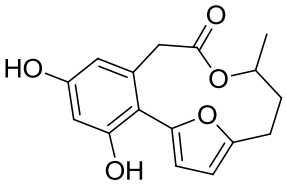

citreofuran

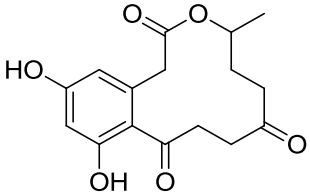

12-oxocurvularin

Figure 4.2: Curvularin-type derivatives isolated from microorganisms.

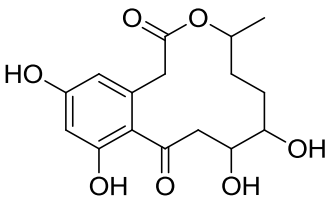

11,12-dihydroxycurvularin

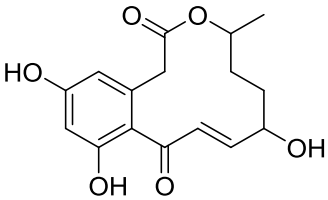

12-hydroxy-10,11-*trans*-dehydrocurvularin

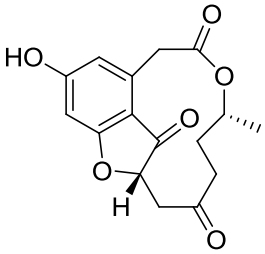

curvulone A

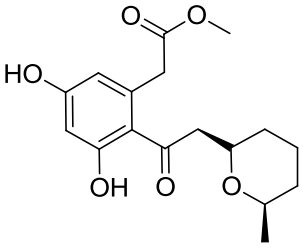

curvulone B

Figure 4.2 (continued): Curvularin-type derivatives isolated from microorganisms.

4.2 Medium optimisation to select the most suitable conditions for culturing *Curvularia australiensis*, medium-scale fermentation

As seen in table 4.1, the growth of *Curvularia australiensis* was at its optimum when incubated in solid-rice medium, as proven by the higher yields obtained from those cultures. On the other hand, the growth of the endophyte in the liquid-Wickerham medium was inferior to that of solid-rice medium as the yields obtained were less.

Table 4.1: Weights of *Curvularia australiensis* extracts cultured in two types of media harvested at various incubation periods.

Medium	Incubation period (days)	Weight of extract (mg) per 200 mL (liquid) or 100 g (solid)
Liquid-Wickerham	7	70
Liquid-Wickerham	15	106
Liquid-Wickerham	30	120
Solid-Rice	7	275
Solid-Rice	15	478
Solid-Rice	30	792

Both ^{1}H NMR and LC-HRMS data were implemented to investigate the chemical composition of the previously mentioned extracts. As depicted by the ^{1}H NMR spectra (Figure 4.3.A) for liquid-Wickerham medium extracts, the biosynthesis of the secondary metabolites was observed from day seven. The secondary metabolites included aromatics that are indicated by the red box in figure 4.3.A (δ_H 6.00 – 7.00). These aromatics were substituted by electron donating groups that shifted the protons of the benzene ring upfield to 7.24. Furthermore, peptides were detected from resonances at δ_H 4.00 – 5.50 (marked by the orange box in figure 4.3.A), representing the α-protons of an amino acid. These signals can be deduced from peptone as nitrogen source in liquid-Wickerham medium. More signals could be noticed in the aliphatic region at δ_H 0.50 – 2.50 (the green box), representing aliphatic parts of the peptides. Additionally, incubating the endophyte for either 15 or 30 days, increased the concentration and diversity of secondary metabolites produced. This was implied by the presence of additional signals in the ^{1}H spectra of the 15 and 30 days extracts as seen in the black boxes. However, some media signals remained even after 30 days of incubation, indicated by the blue box in at δ_H 7.20 – 8.30. These signals could be attributed to some aromatic amino acids such as phenylalanine and tyrosine, which might be present in some of the peptides that were produced by *Curvularia australiensis*.

On the other hand, the production of compounds was very poor when the endophyte was incubated in solid-rice medium. As shown in Figure 4.3.B, most signals observed in the ^{1}H NMR spectra of the solid-rice culture extracts were coming from the medium components (highlighted in green boxes). Moreover, fatty acid signals were also detected. The huge broad signal at δ_H 1.00 – 1.50 is characteristic of long chain methylene units of a fatty acid. In addition to that, the olefinic protons that existed in unsaturated fatty acids were found at δ_H 5.00 – 5.50. Furthermore, the α-protons of the carboxylic end resonated at δ_H 2.10 – 2.40. Nevertheless, after 15 days of incubation, the endophyte started to produce a small amount of aromatic compounds, which increased after 30 days of incubation. This is depicted in the violet box at δ_H 6.00 – 6.50. However, the yield of these compounds was very low compared to the fatty acids as noticeable by their differences in signals intensity.

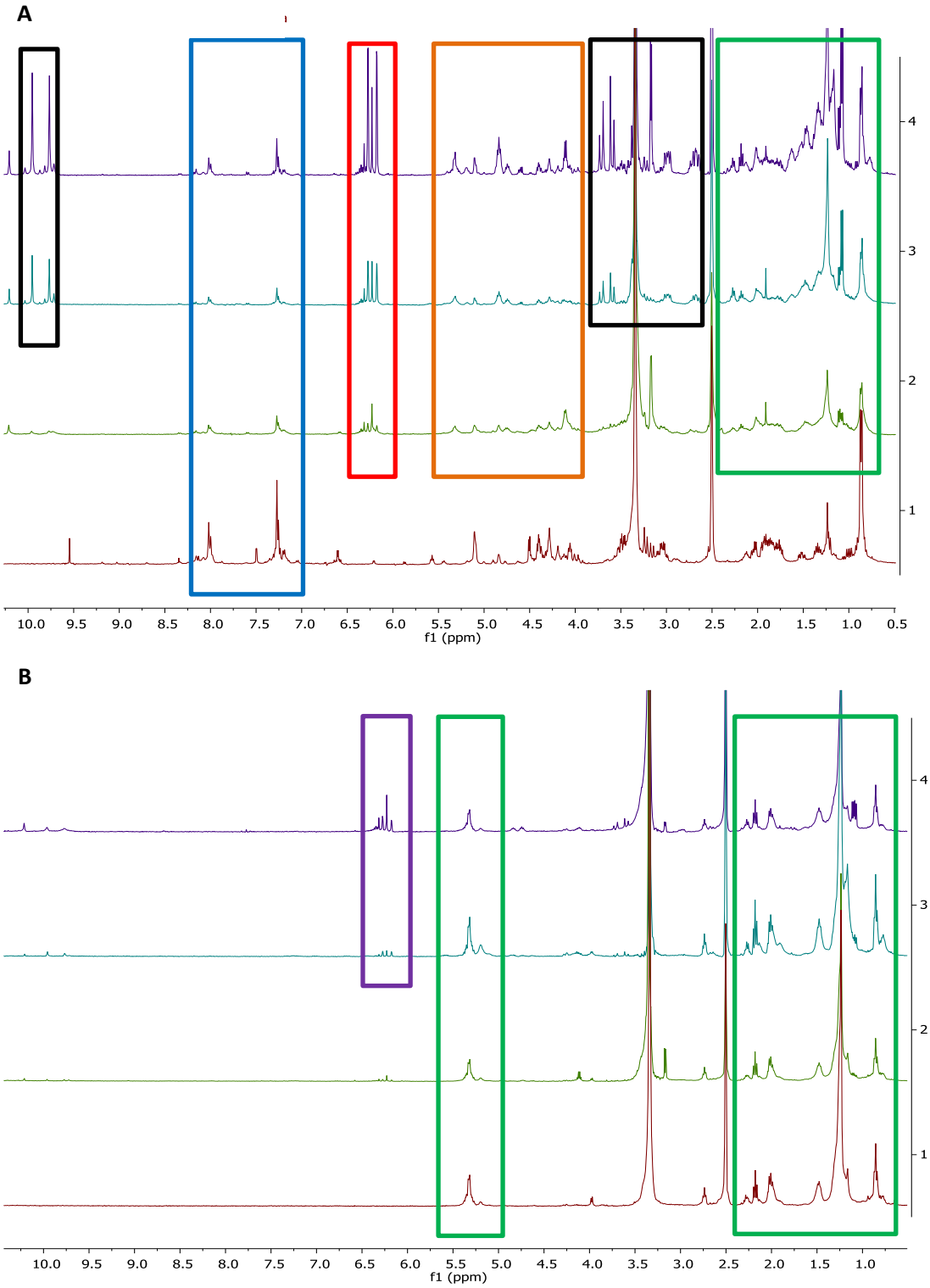

Figure 4.3: ^{1}H NMR (400 MHz) data obtained for *Curvularia australiensis* extracts after incubation in (A): liquid media and (B): solid media. Spectrum 1 is the medium blank, 2 is 7 days incubation, 3 is 15 days and 4 is 30 days. All were measured in DMSO-d_6.

While the ^{1}H NMR data provided information about major compounds that existed in each extract, a more detailed insight for the chemical composition of each extract could be obtained from the LC-HRMS data. The scatter plots that were generated from the LC-HRMS data confirmed the findings of the ^{1}H NMR data in the terms of chemical richness of the extracts. As seen in (Figure 4.4), the chemical composition of the liquid-Wickerham's extracts was richer. Yet, the extracts of the three incubation periods looked very similar. This was illustrated by the scattering pattern that could hardly differentiate the extract obtained after 7 and 15 days as well as between 15 and 30 days. However, a slight increase in the scattering pattern could be perceived between the 7 and 15 days for incubation. Nonetheless, almost no change in pattern was observed when comparing the extracts obtained after 15 and 30 days of incubation.

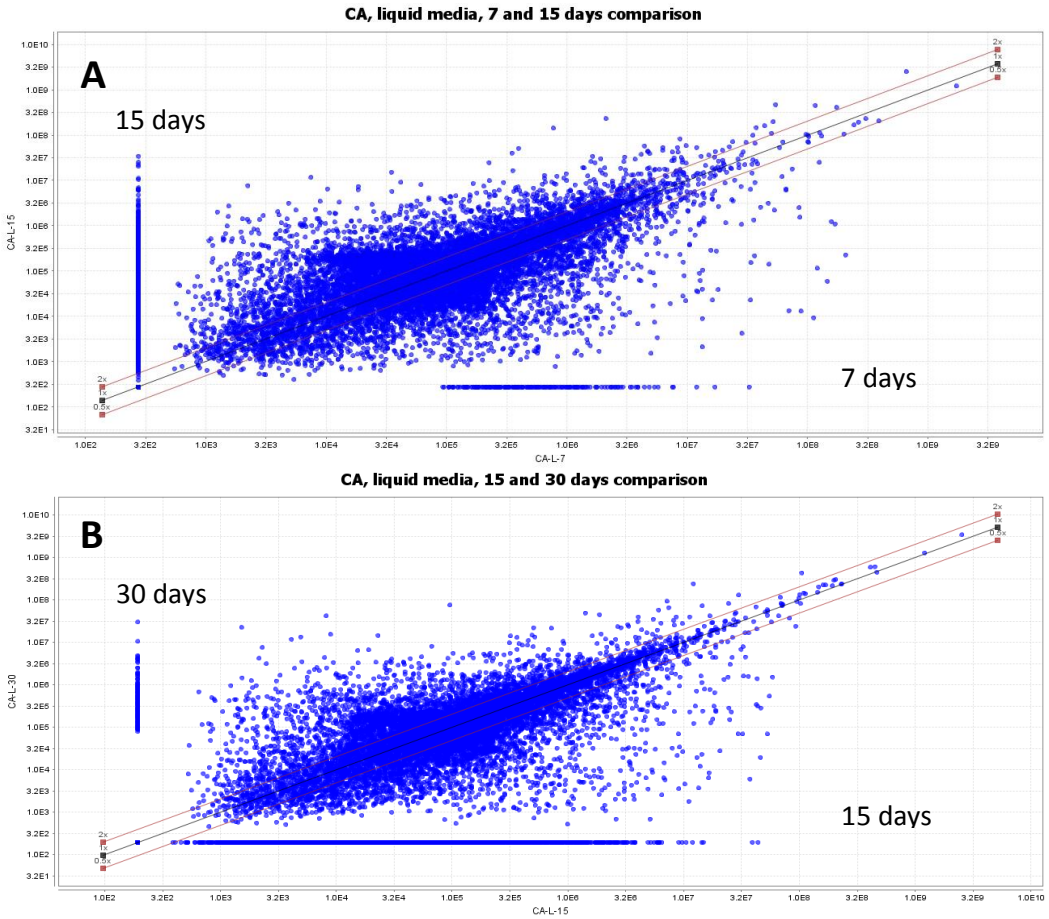

Figure 4.4: Scatter plots of the LC-HRMS data of *Curvularia australiensis* extracts obtained at different incubation periods in liquid-Wickerham medium, comparing (A): 7 with 15 days and (B): 15 with 30 days of incubation.

On the other hand, in the case of the solid-rice medium, a noticeable difference in the scattering pattern could be seen between 7 and 15 days of incubation (Figure 4.5.A). As the figure depicts, the scattering pattern was in favour for the 7 days of incubation. This is explained by the slow growth of *Curvularia australiensis* in solid-rice medium. As a result, the components of the medium were richer chemically than the extract itself because the endophyte consumed the medium components and did not produced metabolites efficiently. However, the extract of 30 days of incubation was chemically richer than the extract obtained after 7 days of incubation. This was illustrated by the scattering pattern in the scatter plot (Figure 4.5.B). Moreover, it is confirmed by the ^{1}H NMR data findings that the efficient production of aromatic compounds could be discerned 30 days after the start of incubation.

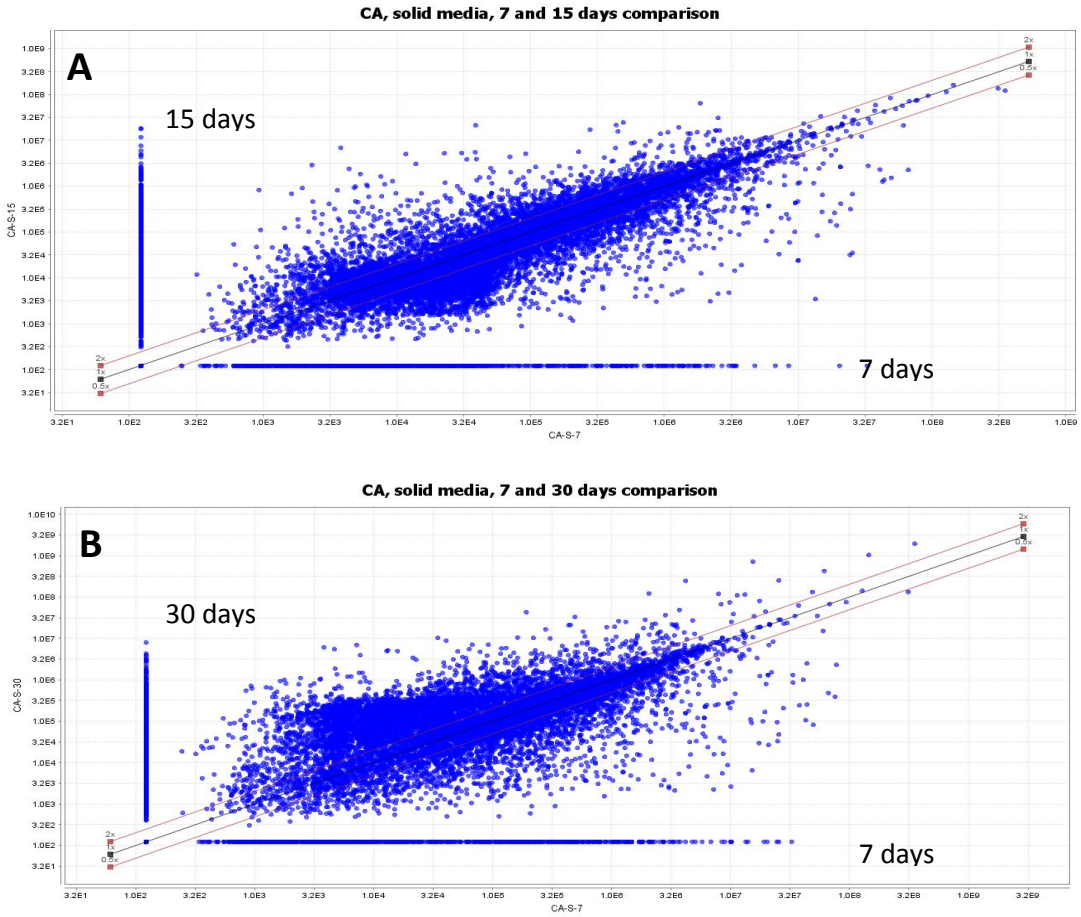

Figure 4.5: Scatter plots of the LC-HRMS data of *Curvularia australiensis* extracts obtained from solid rice media at different incubation periods, comparing (A): 7 with 15 days and (B): 15 with 30 days of incubation.

The findings from the scatter plots were supported by the clustering pattern that is seen in the scores plot of the PCA of the LC-HRMS data of the media optimisation extracts (Figure 4.6). The red circle contained the chemically rich extracts from the 15 and 30 days of incubation in liquid-Wickerham medium, indicating their similarity. On the contrary, on the left side of the Y-axis of the plot, the blue circle contained the chemically poor extracts at 7 and 15 days incubation in solid-rice medium, indicating their similarity as well. The extract from seven days of incubation in liquid-Wickerham medium was separated from the other liquid-Wickerham culture extracts because it contained less diverse compounds as shown by its ^{1}H NMR spectrum. On the contrary, the 30 days extract from solid-rice medium was separated from the other rice culture extracts because it was chemically richer as indicated by both its ^{1}H NMR spectral data and LC-HRMS scatter plots.

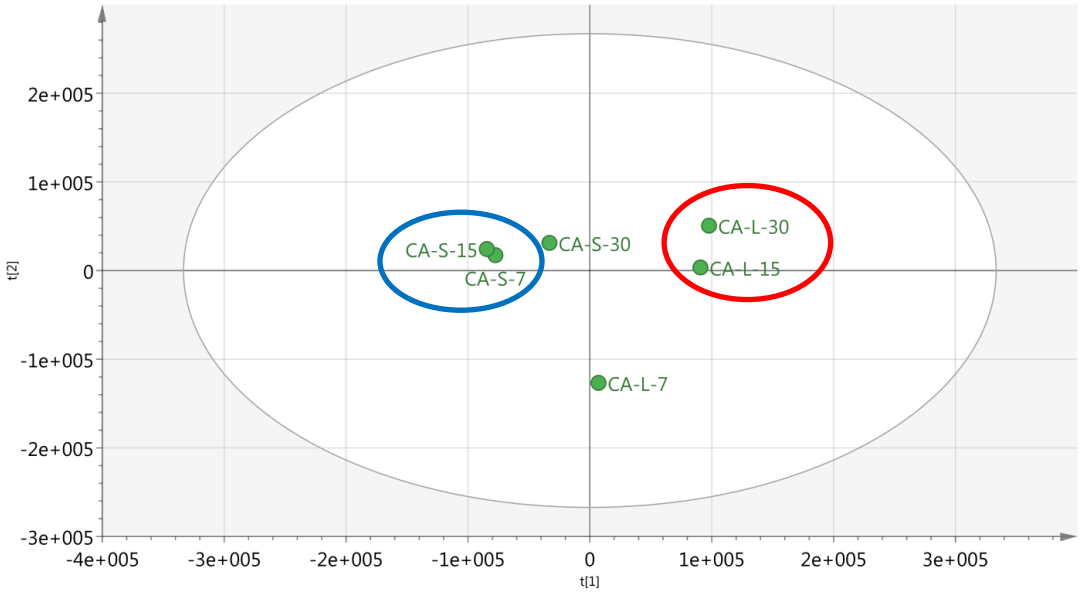

Figure 4.6: Scores plot based on the PCA of the LC-HRMS data for the various *Curvularia australiensis* extracts. "CA" refers to the endophyte *Curvularia australiensis*. The letter "S" is for the solid-rice medium and "L" is for the liquid-Wickerham medium. While the numbers "7, 15, and 30" indicate the incubation period. R2X=0.736, Q2=0.115.

Finally, the *in-vitro* biological activity of media optimisation extracts of the *Curvularia australiensis* against both breast cancer (ZR-75) and lung cancer (A549) cell lines was tested as the third parameter that was considered before the most suitable medium conditions for the large-scale fermentation were chosen (Figure 4.8).

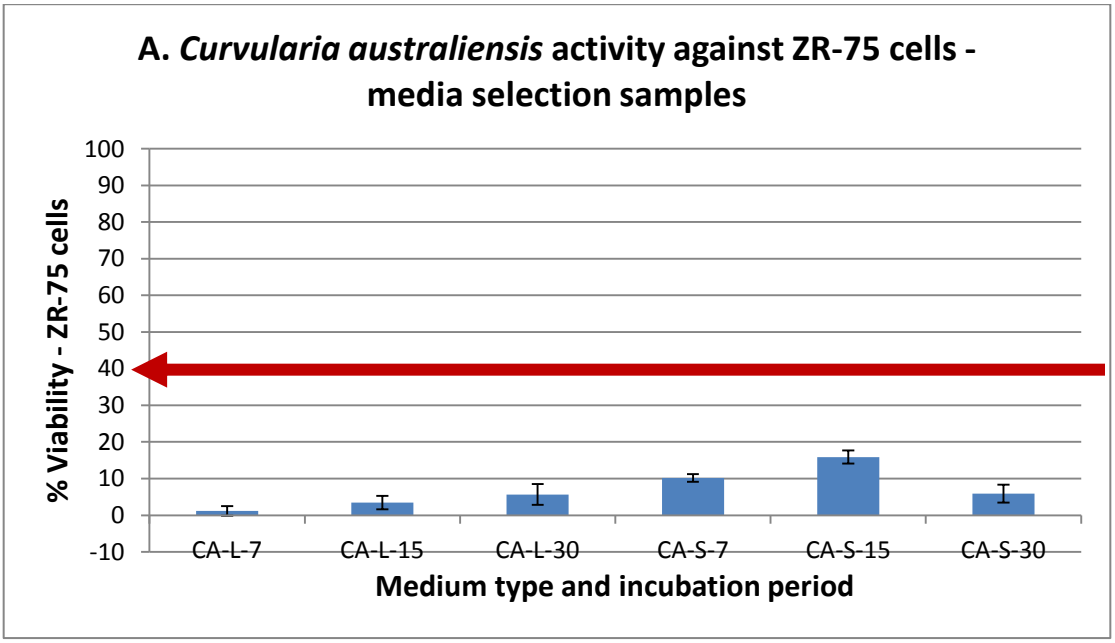

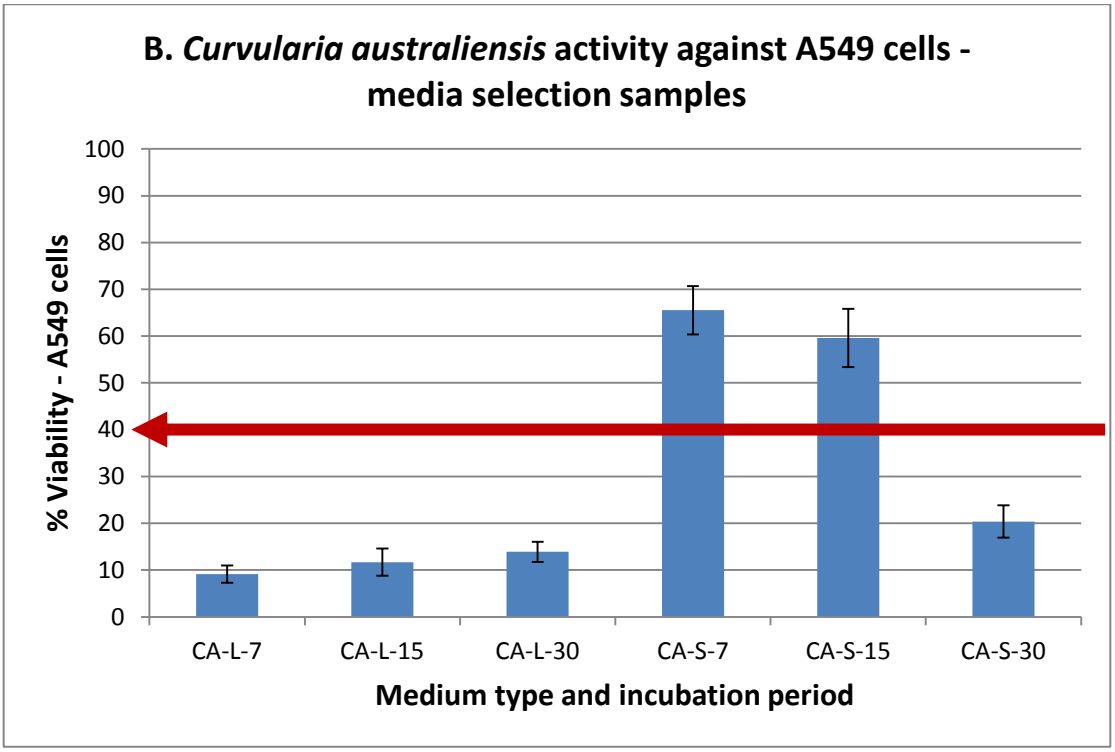

Figure 4.7: The biological activity for *Curvularia australiensis* extracts at 30 µg/mL against (A): breast cancer (ZR-75) cell line and (B): lung cancer (A549) cell line. "CA" refers to the endophyte *Curvularia australiensis*. The letter "S" is for the solid-rice medium and "L" is for the liquid-Wickerham medium. The numbers "7, 15 and 30" indicate the incubation period in days. The red line indicates the bioactivity threshold.

As shown in figure 4.7.A, all extracts were strongly active against breast cancer (ZR-75) cell line, where percent cell viability was less than 20% for all of the tested extracts. On the other hand, the extracts obtained with the liquid-Wickerham medium were all strongly active against lung cancer (A549) cell line; giving a percent viability of less than 15% (Figure 4.7.B). However, two of the solid-rice extract samples were inactive; giving a percent viability more than 40% of the cells. Nevertheless, incubating the endophyte for 30 days in solid-rice medium resulted in an active extract against the lung cancer cell line.

When a comparison of the metabolite yield and diversity was recorded between the employment of liquid-Wickerham and solid-rice media, an increase in chemical diversity was observed with the liquid-Wickerham medium as depicted in Figure 4.8. Figure 4.8 compares the scattering pattern between the best incubation periods between the Wickerham and rice culture extracts, in terms of both chemistry and activity, for both media types, *i.e.*, 15 days of incubation in liquid-Wickerham medium to 30 days of incubation in solid-medium. The scatter plot favoured the 15 days of incubation period in the liquid-Wickerham medium. This concluded that the extract of 15 days of incubation in liquid-Wickerham medium afforded more diverse chemistry.

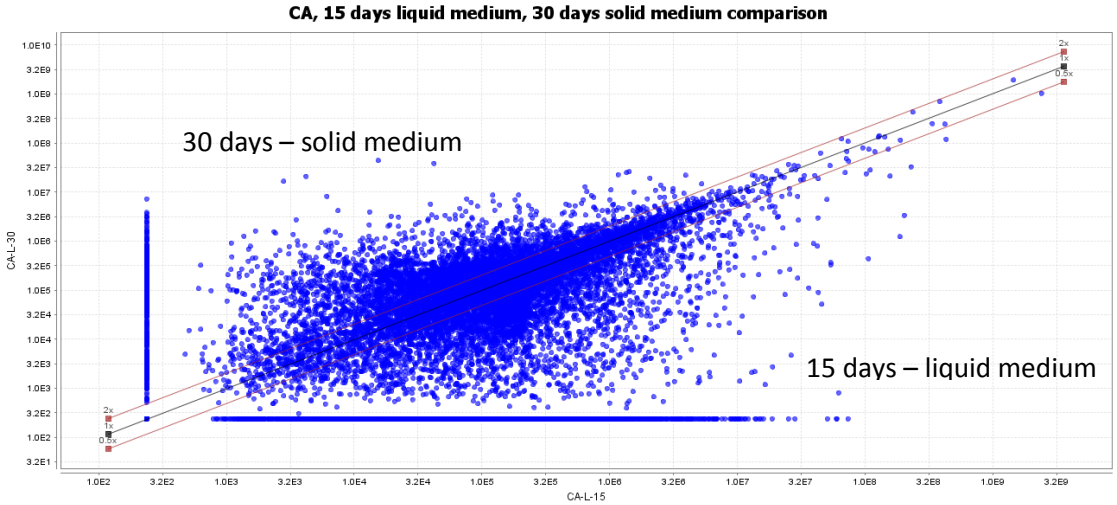

Figure 4.8: Scatter plot of LC-HRMS data of *Curvularia australiensis* extracts, comparing 30 days of incubation in solid-rice medium to 15 days of incubation in liquid-Wickerham medium.

As a conclusion, depending on the chemistry, culturing the endophyte in liquid-Wickerham medium for either 15 or 30 days were the best options for the scale-up because they have the

richest chemical composition among the tested samples as shown by their ^{1}H NMR spectral data and scatter plot analyses of the LC-HRMS data. In the terms of biological activity, 7 days of incubation in liquid-Wickerham medium was the strongest, followed by the 15 and 30 days of incubation, respectively. However, as 15 days of incubation afforded more yield and more diverse chemistry than the extract of 7 incubation days, it was chosen as the incubation duration period for the large-scale fermentation.

4.3 Large scale fermentation and first fractionation of the extract of *Curvularia australiensis*

For the large-scale fermentation, fifteen litres of liquid-Wickerham medium were prepared and inoculated with *Curvularia australiensis*. The fermentation flasks were prepared as described in 2.3.2.1. After 15 days of incubation, 500 mL of ethylacetate were added to each flask to extract the metabolites that were produced. This was followed by homogenisation, partitioning, filtration, and solvent evaporation. At the end, the weight of the obtained extract was 4.5310 g.

The total crude organic extract was fractionated by gradient flash chromatography through a Büchi system as mentioned in 2.5.2.3. A normal phase VersaPak™ (48 g), spherical silica (20-45 µm) column was used with a flow rate of 100 mL/min. The mobile system is detailed in Table 4.2. The 100 mL fractions were collected in conical flasks then pooled using TLC. A total of 17 fractions were obtained in addition to the segregated crystals from fraction 6 (Figure 4.9 and Table 4.3).

Table 4.2: Mobile phase used for the first fractionation of the extract of the endophyte *Curvularia australiensis.*

Time (minutes)	% Hexane	% EtOAc	% MeOH
0	100	0	0
10	100	0	0
70	0	100	0
75	0	100	0
105	0	50	50
120	0	50	50

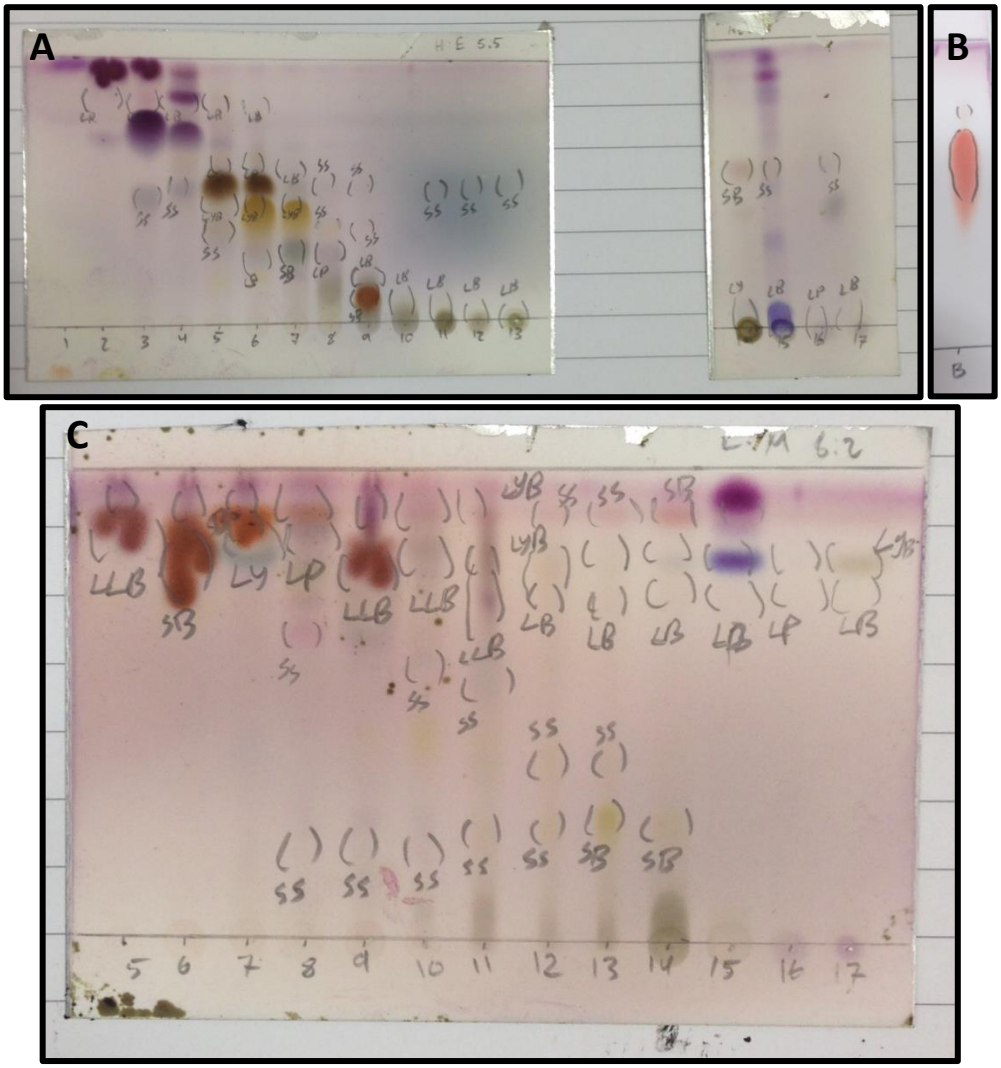

Figure 4.9: Summary TLC plate for the first fractionation step (C.n) of *Curvularia australiensis* after spraying with anisaldehyde reagent. (A): EtOAc 50:50 Hex, (B): C.C in EtOAc 50:50 Hex, and (C): EtOAc 80:20 MeOH.

Table 4.3: Weights of fractions obtained from the first chromatographic fractionation of *Curvularia australiensis*.

Fraction	Weight (mg)	Fraction	Weight (mg)
C.1	19	**C.9**	329
C.2	147	**C.10**	287
C.3	201	**C.11**	878
C.4	75	**C.12**	73
C.5	339	**C.13**	246
C.6	645	**C.14**	109
C.C	556	**C.15**	55
C.7	181	**C.16**	4
C.8	69	**C.17**	15

In order to determine the class of major compounds that each fraction has, the fractions were inspected by ^{1}H NMR spectroscopy (Figure 4.10). Analysis of the ^{1}H NMR spectral data categorised the fractions into four groups, depending on the observed resonances. The first category included fractions C.1 – C.4 that were rich in fatty acids and other non-polar compounds. This was referred to the presence of both methylene resonances at δ_H 1.00 – 1.50 and α-protons at δ_H 2.10 – 2.40 ppm (the violet box). However, fractions C.2 – C.4 contained unsaturated fatty acids. This was indicated by the presence of the olefinic proton resonances at δ_H 5.00 – 5.50 (orange box). The second category involved fractions C.5 – C.8 that were composed mainly of aromatic polyketides. This could be explained by the presence of protons at α position relative to a carbonyl carbon detected at δ_H 2.50 – 4.00 (blue box) and aromatic protons adjacent to an electron donating substituent observed at δ_H 6.00 – 6.50 (red box). The third category is composed of fractions C.9 – C.14 that consisted of amino acids and peptides. This was afforded by α-protons that were detected at δ_H 4.00 – 5.50 (the black box). The fourth category included fractions C.15 – C.17 that composed of various aliphatic compounds, as their ^{1}H NMR signals resonated mainly at δ_H 0.50 – 3.00.

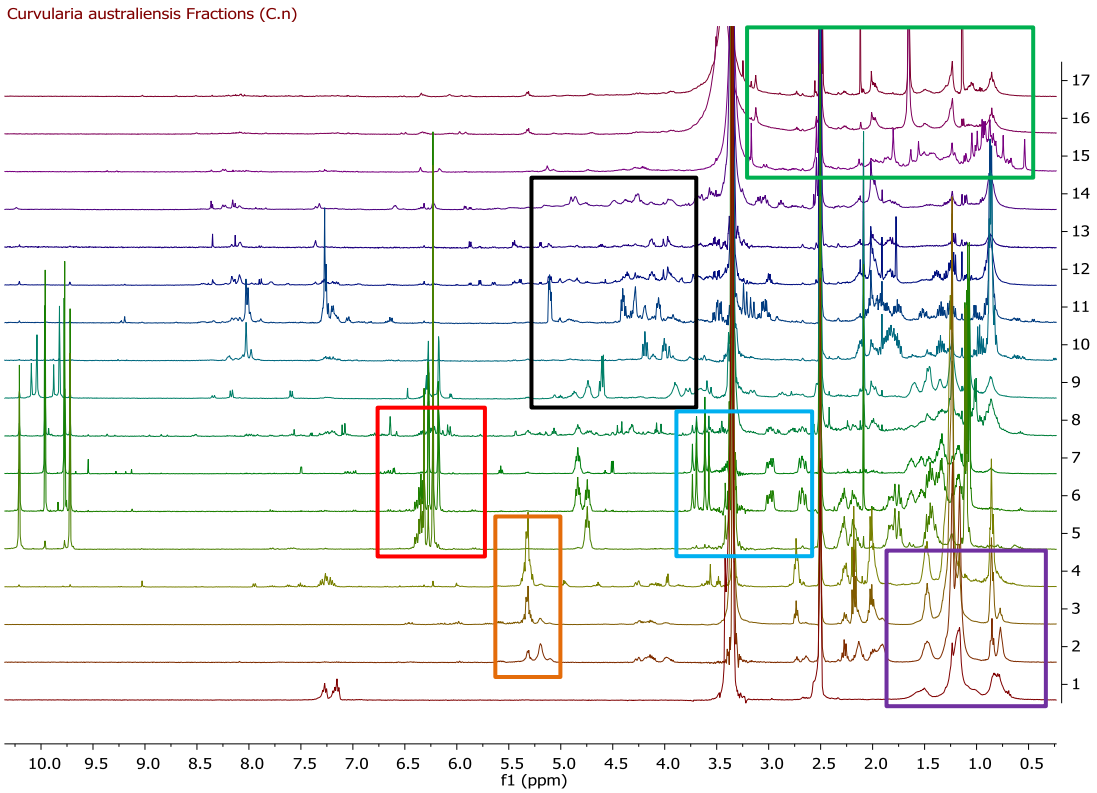

Figure 4.10: The ^{1}H NMR (400 MHz) data obtained for the first chromatographic fractions of *Curvularia australiensis* (C.n). Numbers on Y axis indicate respective fractions. 5 mg of each sample were dissolved in DMSO-d_6,

Furthermore, all fractions were assayed against breast cancer (ZR-75) and lung cancer (A549) cell lines (Figure 4.11). Interestingly, all fractions were found active against breast cancer cells, resulting in less than 40% viability of the cells tested. However, fractions C.5 to C.9, C.14, and C.17 exhibited more activity as they resulted in less than 10% viability of the tested cells. Interestingly, C.C was less active than C.6. This could be due to two reasons, either the segregated impurities in C.6 were more active than the pure compound C.C was, or the presence of these impurities had a synergistic effect. On the other hand, fewer fractions exhibited activity against the lung cancer cell line. The active fractions were the ones that belonged to the polyketide category as revealed by the ^{1}H NMR data analysis. These included fractions C.5 to C.8 along with C.C (crystals from C.6), C.9 that contained aromatic polyketides, and C.17, which was the column wash.

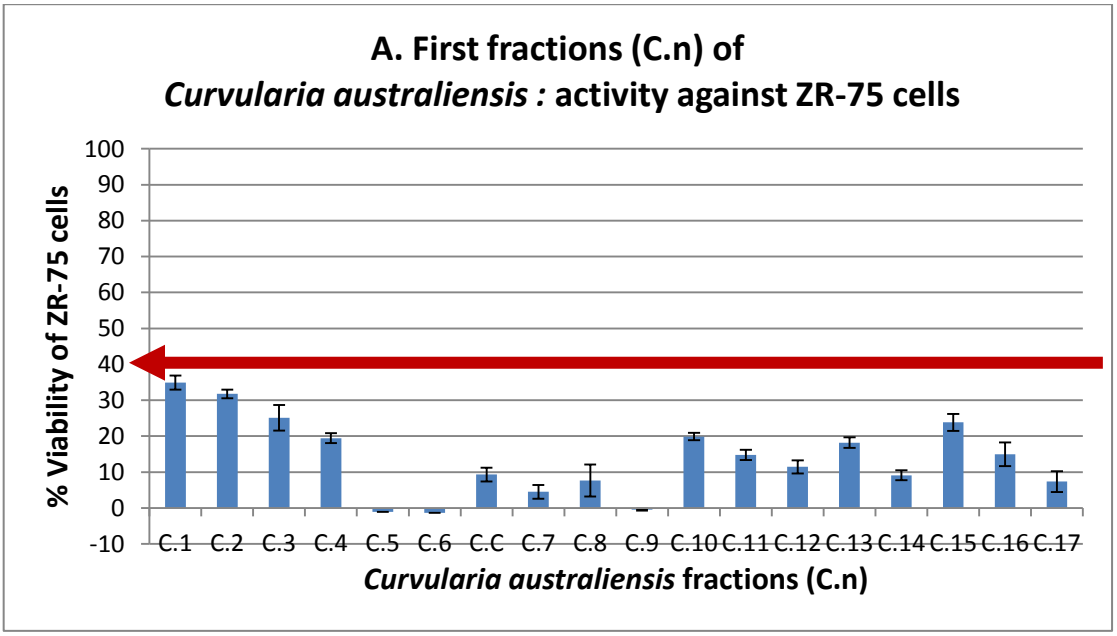

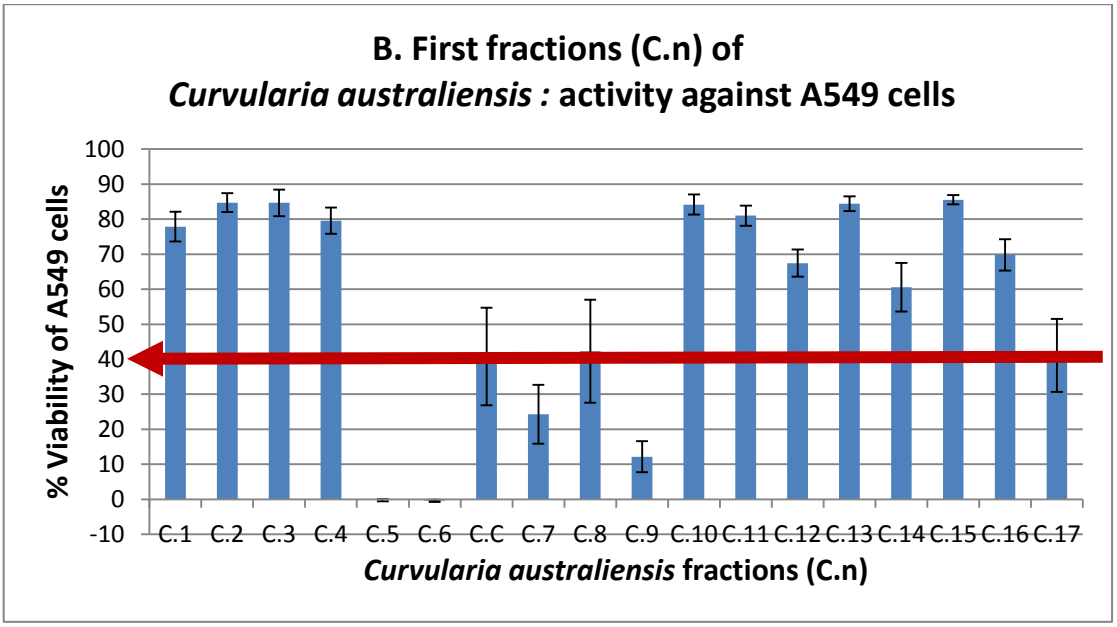

Figure 4.11: Biological activity for first chromatographic fractions of *Curvularia australiensis* (C.n) at 30 µg/mL against (A): breast cancer (ZR-75) and (B): lung cancer (A549) cell lines. The red line indicates the bioactivity threshold.

4.4 The creation of metabolomics-bioassay guided approach to pinpoint the bioactive metabolites of *Curvularia australiensis* at the initial chromatographic separation step

A loadings S-plot was generated from the OPLS-DA score plot model, in which, the extreme loadings of the metabolites (in *m/z*) were correlated to the activity of the fractions. As all fractions were found active against ZR-75 cell line, the Y variable will not be able to differentiate between fractions and no OPLS-DA could be performed, and hence the active metabolites against ZR-75 could not be identified. However, one model, and hence, one study was conducted to pinpoint the metabolites predicted to be responsible for the activity against the lung cancer (A549) cell line.

In order to target the bioactive metabolites against lung cancer (A549) cell line, the active fractions C.5, C.6, C.C, C.7, C.8, C.9 and C.17 were grouped together apart from the inactive fractions (Figure 4.12). This was followed by the conduction of a permutation test to test the validity of the model (Figure 4.13). In the generated model, the R2 was 0.87 and Q2 was 0.47, while the R2Y intercept was 0.674 and Q2Y intercept was -0.331. These values indicated good fitting and good prediction as the R2 and Q2 values were close to 1 and 0.5, respectively, while the Q2Y intercept was -0.331, which is less than zero indicating the validity of the permutation test. Moreover, the difference between Q2 and R2Y was 0.202 which is less than 0.3, indicating the absence of overfitting.

An S plot was generated from the OPLS-DA model (Figure 4.14). The “endpoint” target bioactive metabolites were found left of the Y-axis as shown in Figure 4.14.A. The targeted metabolites were dereplicated and listed in Table 4.4.

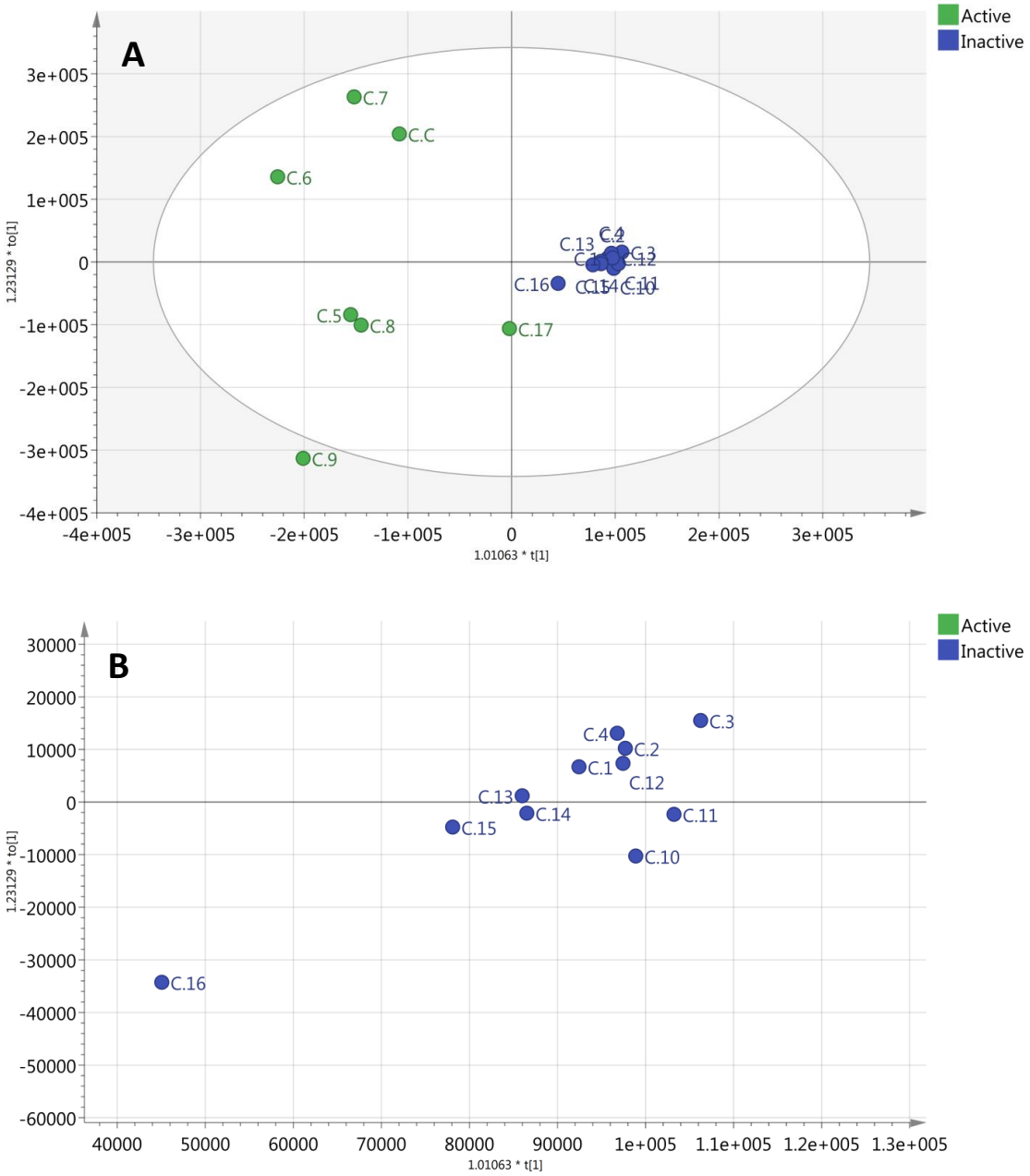

Figure 4.12: (A): Scores plot of *Curvularia australiensis* (C.n) fractions. Samples were grouped into active (greens) and inactive (blues) depending on their activity against lung cancer (A549) cell line. R2X=0.436, R2Y=0.869, Q2=0.47. (B): Expanded view for the inactive scores of the scores plot presented in (A).

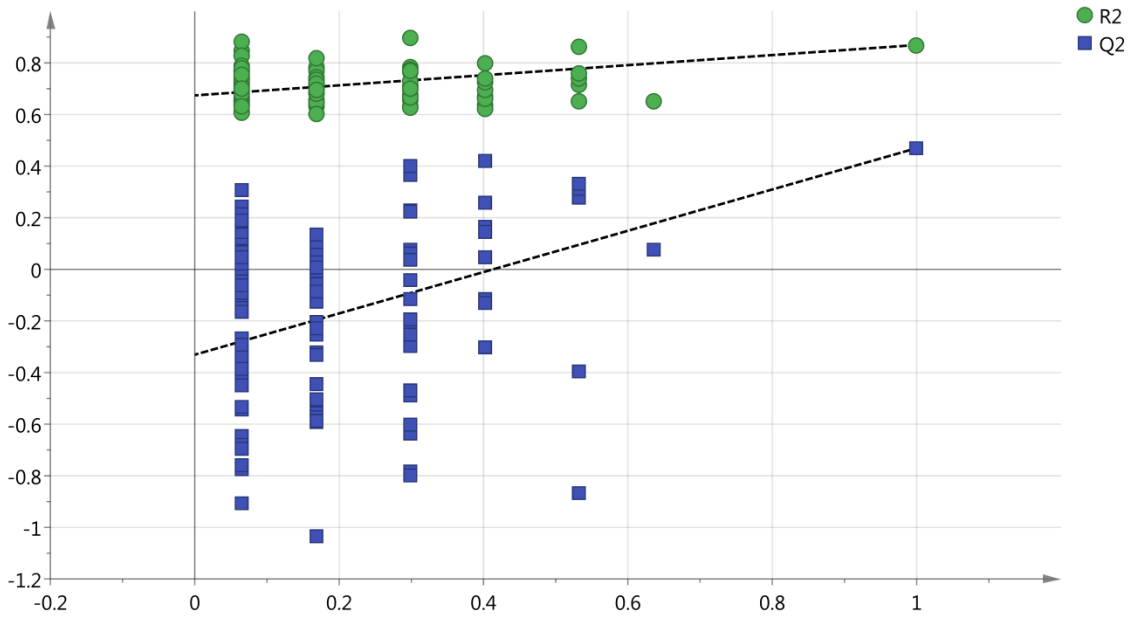

Figure 4.13: Permutation test (100 permutations) for *Curvularia australiensis* (C.n) fractions for the OPLS-DA model of their activity against lung cancer (A549) cell line.

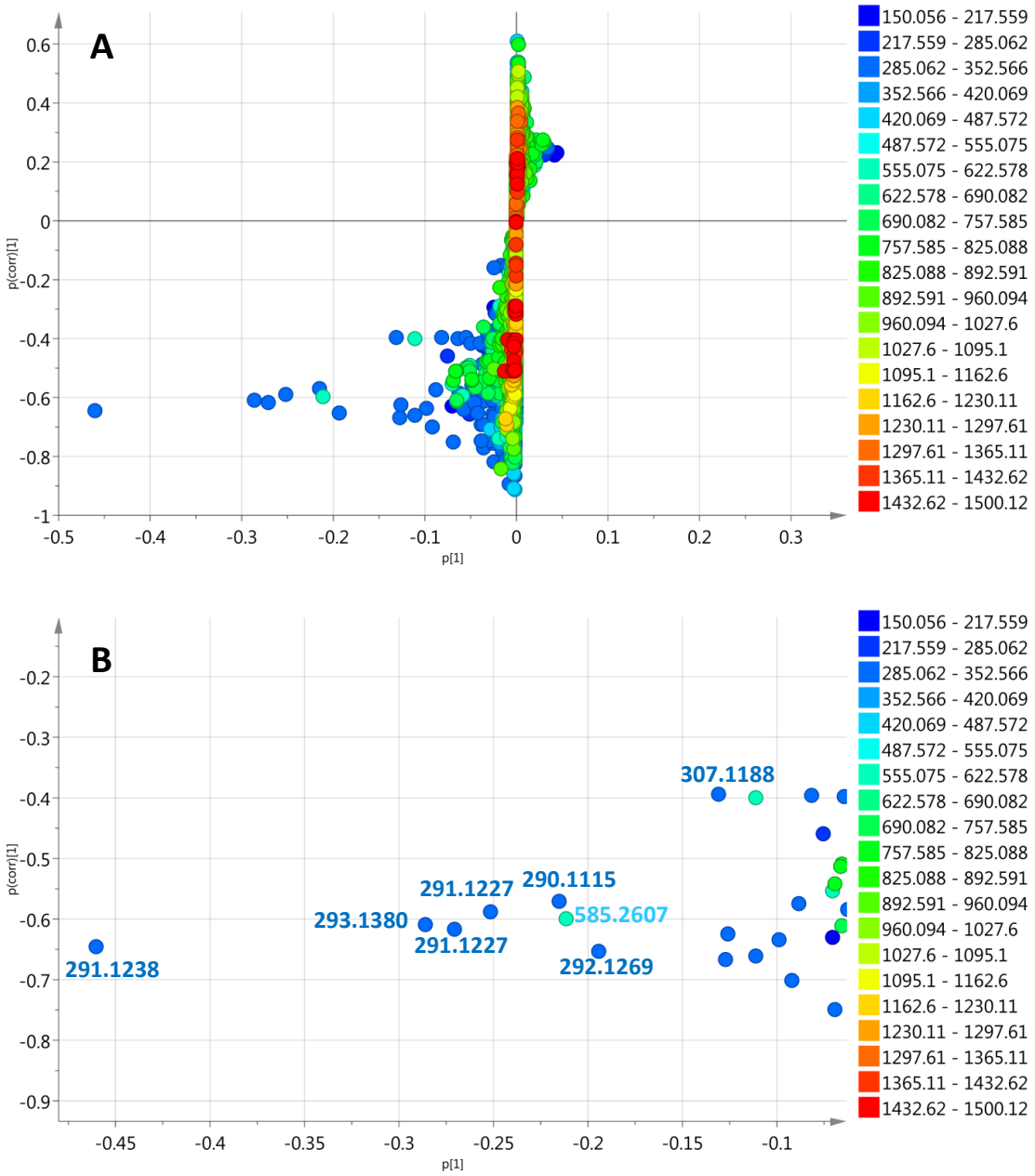

Figure 4.14: (A): S plot for *Curvularia australiensis* (C.n) fractions acquired from an OPLS-DA model (Figure 4.12) for their activity against lung cancer (A549) cell line. (B): expanded view for the end-points metabolites, the isolated metabolites and the outliers are labelled by their *m/z* value.

Table 4.4: Dereplication of target bioactive metabolites against A549 cell line as predicted by OPLS-DA loadings S-plot. Highlighted rows represent compounds that were isolated from the fungal extracts.

t_R(min)	MZMine ID	*m/z*	Predicted Molecular formula	Fraction yielding highest peak intensity	Peak intensity	MWt	Name	Source
7.50	N_1698	615.2453	$C_{33}H_{36}N_4O_8$	C.9	4.95E+09	616.2526	RP 66453	*Streptomyces* sp. A9738
7.50	N_2664	308.1220	$C_{10}H_{15}N_9O_3$ $C_9H_{19}N_5O_7$	C.9	1.26E+09	309.1293	unknown	unknown
7.57	N_1225	307.1188	$C_{16}H_{20}O_6$	C.9	7.08E+09	308.1260	curvularin; (*R*)-form, 11α-hydroxy	a marine-derived *Curvularia* sp. (strain 768)
							curvularin; (*R*)-form, 11β-hydroxy	a marine-derived *Curvularia* sp. (strain 768)
							curvularin; (*S*)-form, 11α-hydroxy	*Penicillium citreo-viride*
							curvularin; (*S*)-form, 11β-hydroxy	*Penicillium citreo-viride* and *Alternaria tomato*
10.33	N_673	249.1132	$C_{14}H_{18}O_4$	C.5	1.71E+09	250.1204	deliquinone	*Russula delica*
							3,4-dihydro-8-hydroxy-3-(4-hydroxypentyl)-1H-2-benzopyran-1-one; (3*R*,4'*S*)-form	a marine-derived *Aspergillus* sp. and *Penicillium* sp. MWZ14-4
							3,4-dihydro-8-hydroxy-3-(4-hydroxypentyl)-1H-2-benzopyran-1-one; (3ξ,4'ξ)-form	*Talaromyces verruculosus*
							2,3-dihydroxy-4-methyl-5-(3-methyl-2-butenyl)benzoic acid; 3-Me ether	*Pestalotiopsis photiniae* L328
							2,4-dihydroxy-6-methyl-3-	*Polyporus dispansus*

							prenylbenzoic acid; Me ester	
							flammulinolide B; 1-Ketone	*Flammulina velutipes*
							gregatin B; (*R*)-form	*Cephalosporium gregatum* and *Aspergillus panamensis*
							3-hexyl-3,7-dihydroxy-1(3H)-isobenzofuranone; (±)-form	*Corollospora maritima*
							1-[3-hydroxy-4-(hydroxymethyl)phenyl]-1,5-heptadiene-3,4-diol; (1*E*,3*R*,4*S*,5*E*)-form	*Pyricularia oryzae*
							1-[3-hydroxy-4-(hydroxymethyl)phenyl]-1,5-heptadiene-3,4-diol; (1*E*,3*S*,4*S*,5*E*)-form	*Pyricularia oryzae*
							4-hydroxy-2-methoxy-5-(1-oxo-2,4-hexadienyl)benzaldehyde; 2',3'-Dihydro, 7-alcohol	*Phaeoacremonium* sp. (NRRL 32148)
							parvulenone; 1'-Et ether	*Aspergillus parvulus*
							penicillone B; 4-Ketone	*Penicillium terrestre*
							penicitrinol F; 1,15-Diepimer, O-de-Me	*Penicillium citrinum*
							prospiciferone	a marine-derived *Microsphaeropsis* sp. strain 6288
							sohirnone B; 2',3'-Dihydro	*Penicillium notatum* (GWP A)
							vertinolide	*Trichoderma viride*
11.96	N_1230	335.1137	$C_{17}H_{20}O_7$	C.3	2.18E+08	336.1209	euparvilactone	*Eupenicillium parvum*
							fusarubin; 4aα,10aα-dihydro, 3-Et ether	*Fusarium solani*

							fusarubin; 4aα,10aβ-dihydro, 3-Et ether	*Fusarium martii*
							fusarubin; 4aβ,10aα-dihydro, 3-Et ether	*Nectria haematococca*
							7-hydroxy-6-[2-hydroxy-2-(tetrahydro-2-methyl-5-oxo-2-furyl)ethyl]-5-methoxy-4-methylphthalide,8Cl	*Penicillium brevi-compactum*
							islandic acid II; 3'''-alcohol, 1'-O-(2*Z*,4*E*-hexadienoyl)	*Allantophomopsis lycopodina* KS-97
							6-Methyl-1,3,8-naphthalenetriol; 1-Me ether, 3-O-α-D-ribofuranoside	a marine-derived *Aspergillus glaucus*
							mycophenolic acid; 4'*S*-hydroxy	*Eupenicillium parvum* and the marine-derived *Penicillium* sp. SOF07
							1,8-naphthalenediol; mono-Me ether, O-β-D-glucopyranoside	*Xylaria* sp.
							terreumol D; 6*S*,7*R*-epoxide	*Tricholoma terreum*
11.99	N_675	290.1115	$C_{23}H_{15}$ $C_{10}H_{13}N_9O_2$ $C_9H_{17}N_5O_6$	C.5	1.34E+09	291.1187	unknown	unknown
12.09	P_4516	291.1227	$C_{16}H_{18}O_5$	C.5	1.01E+10	290.1154	curvularin; (*R*)-form, 10,11-didehydro(*E*-)	a marine-derived *Curvularia* sp. (strain 768)
							curvularin; (*S*)-form, 10,11-didehydro(*E*-)	*Curvularia spp., Cercospora scirpicola , Ascochytula obiones, Alternaria zinniae, Drechslera australiensis, Alternaria cinerariae, Alternaria macrospora* and *Penicillium citreo-viride*

12.53	N_652	585.2607	$C_{27}H_{65}N_{14}$ $C_{37}H_{69}N_4O$	C.7	4.20E+08	586.2680	No hits produced by fungi	No hits produced by fungi
12.55	N_430	291.1237	$C_{16}H_{20}O_5$	C.C	2.11E+10	292.1310	curvularin; (*S*)-form	*Curvularia spp., Penicillium steckii, Penicillium citreo-viride, Alternaria macrospora, Alternaria cinerariae, Penicillium gilmanii, Penicillium baradicum, Alternaria zinniae , Drechslera australiensis* and *Cochliobolus* sp.
							curvularin; (*R*)-form	unknown
							curvularin; (±)-form	unknown
							curvularin	unknown
							1893B	a marine endophytic fungus no. 1893
							lasiodiplodin; (*R*)-form, 6-Oxo, O-de-Me	a marine-derived endophytic fungus (No. ZZF36) and *Syncephalastrum racemosum*
							malettinin C	NRRL 29110 isol. from the stromata of a *Hypoxylon* sp.
							malettinin C; 9-Epimer	imperfect fungus NRRL 29110 isol. from the stromata of a *Hypoxylon* sp.
12.55	N_650	292.1269	$C_9H_{19}N_5O_6$	C.7	4.01E+09	293.1342	resorcylide; (*S,E*)-form, 7,8-dihydro	*Acremonium aeae* NRRL 45893
12.56	N_653	327.1005	$C_{16}H_{21}ClO_5$	C.6	3.52E+08	328.1077	chaetomugilin R	a marine-derived *Chaetomium globosum*

								OUPS-T106B-6
12.56	N_651	337.1292	$C_{17}H_{22}O_7$	C.7	1.30E+09	338.1365	acremonin A; (+)-form, 6-O-β-D-Glucopyranoside	*Acremonium* sp.
							cyclocalopin A; 7-Ac	*Boletus* spp.
							7,8-Epoxy-9,17-dihydroxy-13,14,15,16-tetranor-12,17:19,6-labdanediolide; (6β,7α,8α,9α,17α)-form, 17-Me ether	*Oidiodendron* spp.
							fusaquinone B; 4α-epimer, 1-deoxy, O10-Me	*Nigrospora* sp.
							1,3,4,4α,5,10α-hexahydro-3,5,6,7,9-pentahydroxy-3-methyl-10H-naphtho[2,3-c]pyran-10-one; (3*R*,4α*S*,5*S*,10α*R*)-form, 3,5,7-tri-Me ether	*Fusarium* sp.
							1,3,4,4α,5,10α-hexahydro-3,5,6,7,9-pentahydroxy-3-methyl-10H-naphtho[2,3-c]pyran-10-one; (3*R*,4α*S*,5*R*,10α*S*)-form, 3,5,7-tri-Me ether	*Fusarium* sp.
							4-hydroxybenzyl alcohol; 4-O-(2,3-butadienyl), α-O-α-D-glucopyranoside	*Neurospora terricola*
							4-hydroxybenzyl alcohol; 4-O-(2,3-butadienyl), α-O-β-D-mannopyranosyl	*Neurospora terricola*
							3,7,8,15-scirpenetetrol; 8-ketone, 15-Ac	*Fusarium graminearum* and *Gibberella zeae*
							3,7,15-trihydroxy-8-scirpenone; (3α,7α)-form, 3-	*Fusarium culmorum*

							Ac	
							3,8,9,10-tetrahydroxy-4,11(13)-guaiadien-12,6-olide; (1α,3α,6α,8α,9α,10α)-form, 8-Ac	*Anthemis carpatica*
							1,3,8-trihydroxy-4,10(14),11(13)-germacratrien-12,6-olide; (1β,3β,4E,6α,8β)-form, 1-Hydroperoxide, 3-Ac	*Anthemis aetnensis*
							4,9,10-trihydroxy-2,11(13)-guaiadien-12,6-olide; (4α,6α,9α,10α)-form, 4-hydroperoxide, 9-Ac	*Anthemis carpatica*
12.60	P_251	311.1486	$C_{16}H_{22}O_6$	C.7	1.08E+09	310.1413	fusarentin; 6,7-di-Me ether	*Fusarium larvarum* and a *Colletotrichum* sp.
							fusarentin; 6,8-di-Me ether	*Fusarium larvarum*
							7-[3-(hydroxymethyl)-4-methoxy-2-oxo-2H-pyran-6-yl]-5-methyl-6-octenoic acid	a marine-derived *Petriella* sp. TUBS 7961
							nivefuranone A; (ξ)-form, 1'',2''-Dihydro, 2''ξ,5'ξ-dihydroxy, Me ester	*Penicillium daleae*
							pyrenophorol; monoketone	*Drechslera avenae*
							pyrenophorol; 2*Z*-isomer, 4-ketone	*Phoma* sp, strain No. 8874
12.64	P_519	169.0496	$C_8H_8O_4$	C.6	5.17E+08	168.0423	6-acetyl-4-methoxy-2H-pyran-2-one	a marine-derived *Nigrospora* sp. PSU-F18
							2,5-dihydroxy-1,4-benzoquinone; Di-Me ether	*Polyporus fumosus*; also isol. from cultures of *Lenzites thermophila, Trichoderma pseudokoningii* and

								Gloeophyllum sepiarum. Also isol. from higher plants *Acorus calamus, Cassia obtusifolia*, *Dalbergia melanoxylon*
							2,6-dihydroxy-1,4-benzoquinone; di-Me ether	*Dendryphiella salina*
							2,3-dihydroxy-5,6-dimethyl-1,4-benzoquinone	*Gliocladium roseum*
							2,4-dihydroxy-6-(hydroxymethyl)benzaldehyde	*Aspergillus rugulosus*
							2,4-dihydroxy-6-methylbenzoic acid	*Penicillium* spp., *Hypoxylon* spp., a marine-derived *Chaetomium* sp.
							2,6-dihydroxy-4-methylbenzoic acid	*Phoma* sp.
							2,3-dihydroxy-5-methyl-1,4-benzoquinone; 3-Me ether	*Aspergillus fumigatus*
							2,3-dihydroxy-5-methyl-1,4-benzoquinone; 2-Me ether	*Aspergillus fumigatus*
							2,5-dihydroxy-3-methyl-1,4-benzoquinone; 5-Me ether	*Xylaria* sp. PBR-30
							(2,5-dihydroxyphenyl)acetic acid	*Penicillium* spp., *Aspergillus* spp.
							(3,4-dihydroxyphenyl)acetic acid	*Polyporus tumulosus*
							4-ethyl-2-oxo-2H-pyran-6-carboxylic acid	*Ophiostoma crassivaginata*
							2-hydroxy-2-(4-hydroxyphenyl)acetic acid; (*R*)-form	*Pisolithus tinctorius*
							5-methyl-1,2,3,4-benzenetetrol; 2,3-Methylene ether	*Antrodia camphorata*

							phaeofuran A	*Phaeoacremonium* sp. (NRRL 32148)
							xanthofusin	*Fusicoccum* sp. Imi 351573
33.00	N_18443	765.6367	$C_{42}H_{78}N_{12}O$ $C_{46}H_{82}N_6O_3$ $C_{50}H_{86}O_5$ $C_{41}H_{82}N_8O_5$ $C_{45}H_{86}N_2O_7$	C.7	9.58E+08	766.6439	unknown	unknown
34.30	N_13377	744.6181	$C_{52}H_{79}N_3$ $C_{54}H_{81}O$ $C_{37}H_{75}N_{15}O$ $C_{47}H_{79}N_5O_2$ $C_{36}H_{79}N_{11}O_5$ $C_{46}H_{83}NO_6$	C.7	3.04E+08	745.6254	unknown	unknown

4.5 Implementing metabolomics for the isolation of the pure secondary metabolites from the endophyte *Curvularia australiensis*

The fractionation work was designed to isolate the "pinpointed" metabolites that possessed the activity against both the lung cancer (A549) cell line. So, the fractions that contained the predicted target bioactive metabolites were prioritised for further fractionation. This resulted in the isolation of the three pure curvularin-type compounds that are listed in Table 4.5. Moreover, the diketopiperazine, cyclo(L-prolylglycyl), was isolated. However, as it was not a target metabolite, it possessed no biological activity against the tested cell lines.

Table 4.5: The metabolites that were isolated from *Curvularia australiensis.*

Cpd No.	Name	New / Known	t_R (min)	*m/z*	MWt	Source	Weight (mg)	% Yield
1	(-)-(*S*)-curvularin	known	12.55	291.1229	292.3270	C.C	556.0	12.27
2	dehydrocurvularin	known	11.94	291.1237	290.3111	C.5	339.0	7.48
3	11α-hydroxycurvularin	known	7.58	307.1181	308.3264	C.9	9.2	0.20
4	cyclo(L-prolylglycyl)	known	1.21	155.0816	154.1665	C.13	26.1	0.58

Flash chromatography was utilised to isolate the pure compounds (Figure 4.15). The parameters and conditions applied for flash chromatography-1 (FC-1) are described under section 4.3, while those for the other flash chromatography experiments (2 and 3) are mentioned in Table 4.6. The solvent systems that were used as mobile phases are listed in tables 4.7 and 4.8.

Table 4.6: The chromatographic conditions that were used in isolating the pure compounds from the extract of *Curvularia australiensis.*

Column	Reveleris® Silica 24 g
Flow rate	15 mL/min
ELSD Threshold	20 mV
UV Threshold	0.05 AU
UV1 Wavelength	254 nm
UV2 Wavelength	280 nm

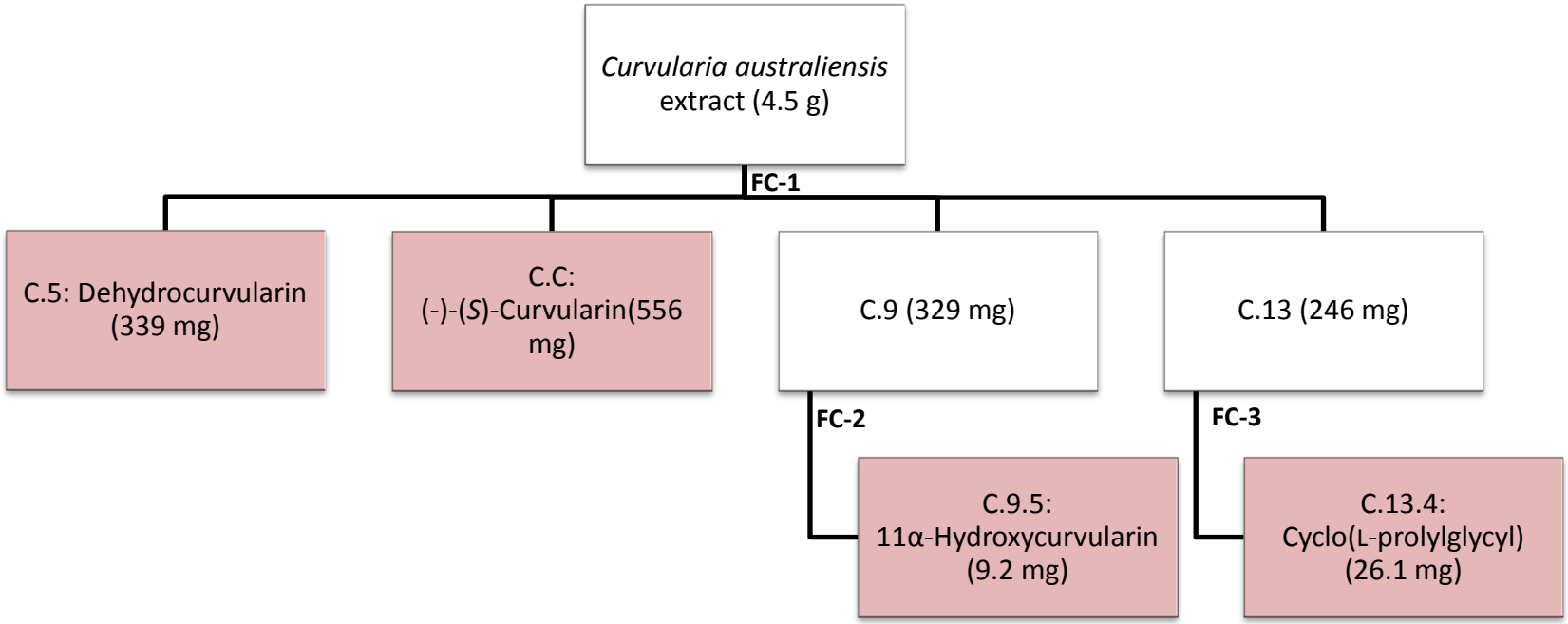

Figure 4.15: The workflow for isolating the bioactive target metabolites from *Curvularia australiensis* extract. FC: Flash chromatography.

Table 4.7: Mobile phase used for flash chromatography-2 (FC-2).

Time (minutes)	% DCM	% Methanol
0	100	0
60	70	30
65	70	30

Table 4.8: Mobile phase used for flash chromatography-3 (FC-3).

Time (minutes)	% DCM	% Methanol	% EtOAc
0	99	1	0
5	99	1	0
50	95	5	0
70	95	5	0
90	70	30	0
120	0	40	60

4.6 Structure elucidation of the pure secondary metabolites from the endophyte *Curvularia australiensis*

4.6.1 (-)-(*S*)-Curvularin (1)

(-)-(*S*)-Curvularin
Fraction: C.C, segregated from C.6 Retention time: 12.55 min Synonym(s): • (*4S*)-4,5,6,7,8,9-Hexahydro-11,13-dihydroxy-4-methyl-2*H*-3-benzoxacyclododecin-2,10(1*H*)-dione • (-)-(*S*)-Curvularin Source: endophytic *Curvularia australiensis* from *Anthemis palestina* Amount of sample: 556.0 mg Percent yield: 12.27% Percent purity: 100% Physical description: White crystals Molecular formula: $C_{16}H_{20}O_5$ Molecular weight: 292.3270 g/mol Optical rotation: $[\alpha]_D^{20}$ = -19 (0.1 g/100 mL, EtOH)
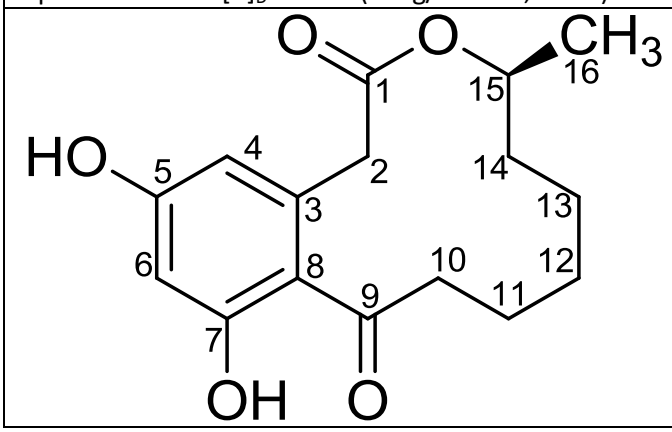

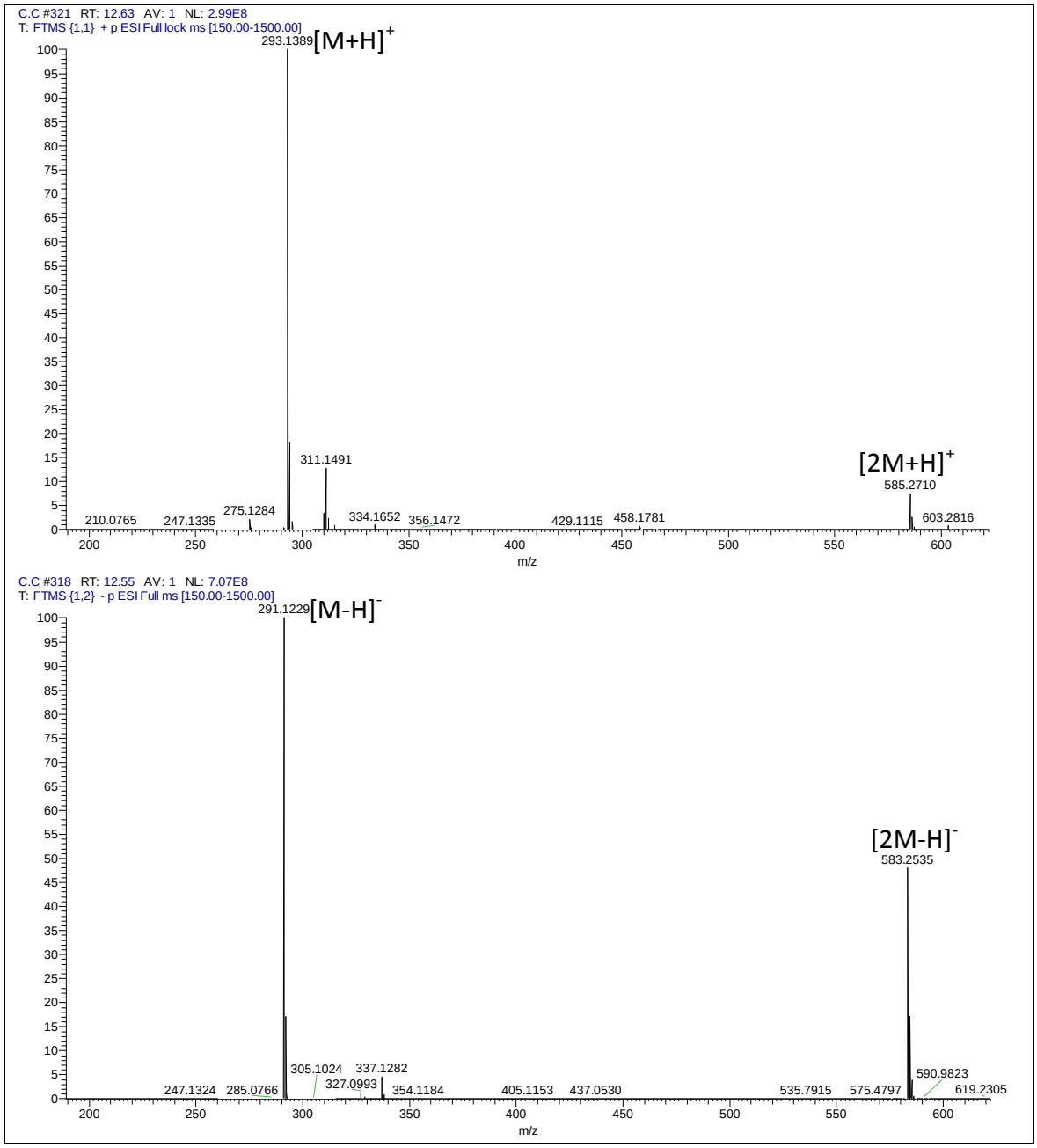

(-)-(*S*)-curvularin was isolated as white crystals with a yield of 12.27% (556.0 mg). LC-HRMS data exhibited a pseudomolecular ion at *m/z* 293.1389 $[M+H]^+$ and 291.1229 $[M-H]^-$, suggesting a molecular weight of 292.3270 g/mol. The molecular formula afforded by HRMS is $C_{16}H_{20}O_5$.

Two doublets were detected in the ^1H NMR spectrum for the *meta* positioned H-6 (δ_H 6.27, *J*=2.2 Hz) and H-4 (δ_H 6.18, *J*=2.2 Hz) that coupled to each other via ^1H-^1H COSY experiment,

indicating a shielding effect by electron donating substituents (Figure 4.16, Figure A.II.2). These electron donating substituents included the two hydroxyl groups 5-OH (δ_H 9.96) and 7-OH (δ_H 9.77) that are attached *ortho* to both H-6 and H-4. The proton H-15 resonated at δ_H 4.84 (ddt, *J*=9.0, 6.3, 3.9). This is referred to the attachment of an oxygen atom to C-15. The splitting pattern of H-15's signal is caused by its neighbouring protons, the doublet for methyl CH_3-16 (δ_H 1.08, *J*=6.3 Hz) and the two multiplets for H-14a (δ_H 1.33) and H-14b (δ_H 1.54). The signals of the geminal protons CH_2-2 were detected as two doublets at δ_H 3.60 (H-2a, *J*=15.6 Hz) and δ_H 3.71 (H-2b, *J*=15.6) that are coupled to each other as a ^{1}H-^{1}H COSY expierement showed (Figure 4.18). Furthermore, the signals of another geminal protons of the methyl CH_2-10 were detected as a doublet of doublet of doublet at δ_H 2.68 (H-10a, *J*=15.4, 6.5, 2.6 Hz) and a multiplet δ_H 2.98 (H-10b), both coupled to each other as detected in the ^{1}H-^{1}H COSY spectrum (Figure A.II.3). The connection of these two methylene protons, CH_2-10 to the carbonyl carbon resulted in their deshielding, and thus, their signals were detected downfield to the other methylene protons, *i.e.*; CH_2-11 to CH_2-14 that were detected at (δ_H 1.10 – 1.70).

The proton – carbon assignments were settled using ^{13}C, DEPT and ^{1}H-^{13}C HMQC experiments (Figures 4.18, A.II.5 and A.II.6). The signals for the carbonyl carbons resonated at δ_C 206.6 and δ_C 170.8 corresponding to the ketone unit for C-9 and the ester moiety C-1, respectively. The phenolic carbons of the benzene ring were detected at 159.7 (C-5) and 157.9 (C-7). The carbon C-3 is positioned *γ* to the carbonyl C-9. This caused it to resonate at δ_C 135.8 and to be more deshielded than the carbon C-8 that resonated at δ_C 120.2. The attachment of oxygen to C-15 was responsible for the methine signal at δ_C 72.0, while C-10 that is vicinal to the carbonyl unit caused its signal to be detected at δ_C 43.5.

The connectivity of the substructures was afforded by running a ^{1}H-^{13}C HMBC NMR experiment (Figure A.II.7). Starting with the aromatic protons, ^3J correlations were found going from H-4 to C-2, C-6 and C-8 and from H-6 to both C-4 and C-8. Moreover, ^2J correlations were detected from both H-4 and H-6 to C-5. Furthermore, a ^4J (*W*) correlation was revealed with the cross peak of H-6 with C-9. For the aliphatic protons, ^2J correlations were observed from CH_2-2 to both C-1 and C-3 as well as ^3J correlations from CH_2-2 to C-4 and from H-15 to the carbonyl C-1. Furthermore, ^3J correlations were detected from CH_3-16 to C-14 and from CH_2-10 to C-12. Moreover, ^2J correlations were also found from CH_3-16 to C-15, from H-11 to C-12 and from

both H-10 and H-12 to C-11. In addition, another ^{4}J (*W*) correlation could be detected from H-14 to C-11.

The structure was confirmed as (-)-(*S*)-curvularin by comparing both its ^{1}H and ^{13}C NMR data to the literature (Elzner *et al*., 2008) (Table 4.9).

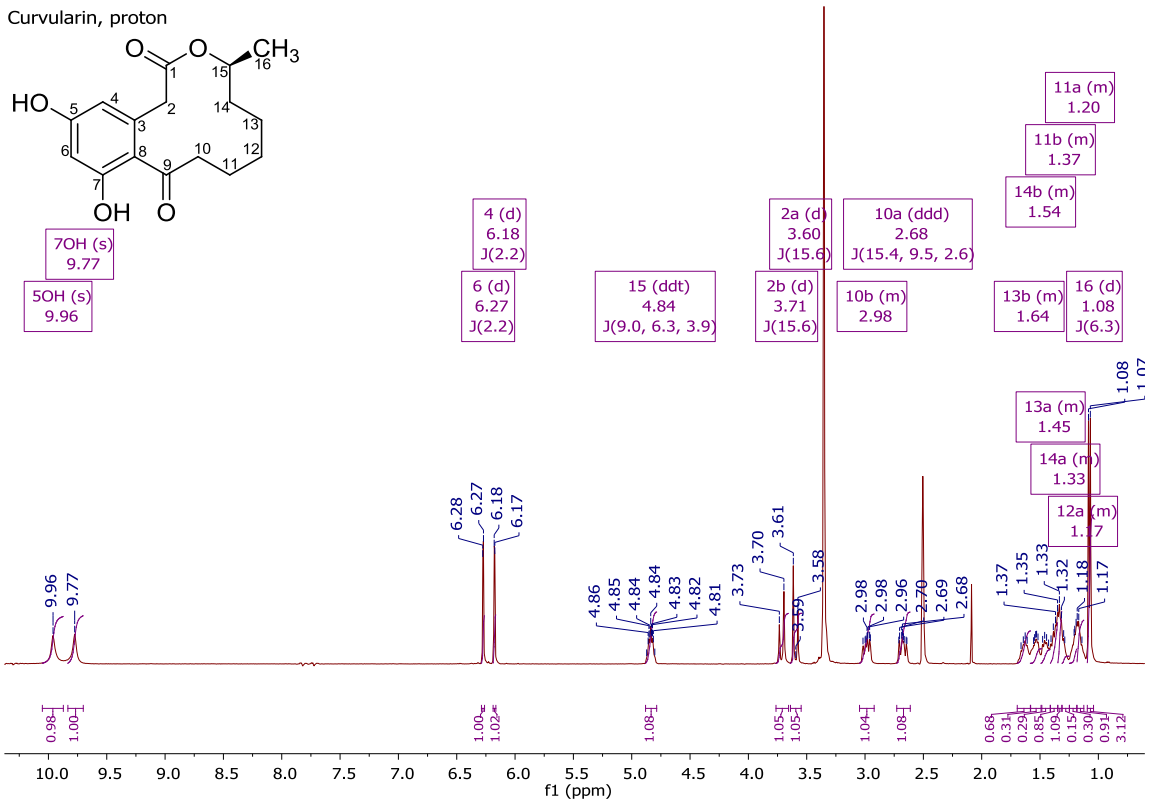

Figure 4.16: ^{1}H NMR (400 MHz) spectrum for (-)-(*S*)-curvularin, measured in DMSO-d_6.

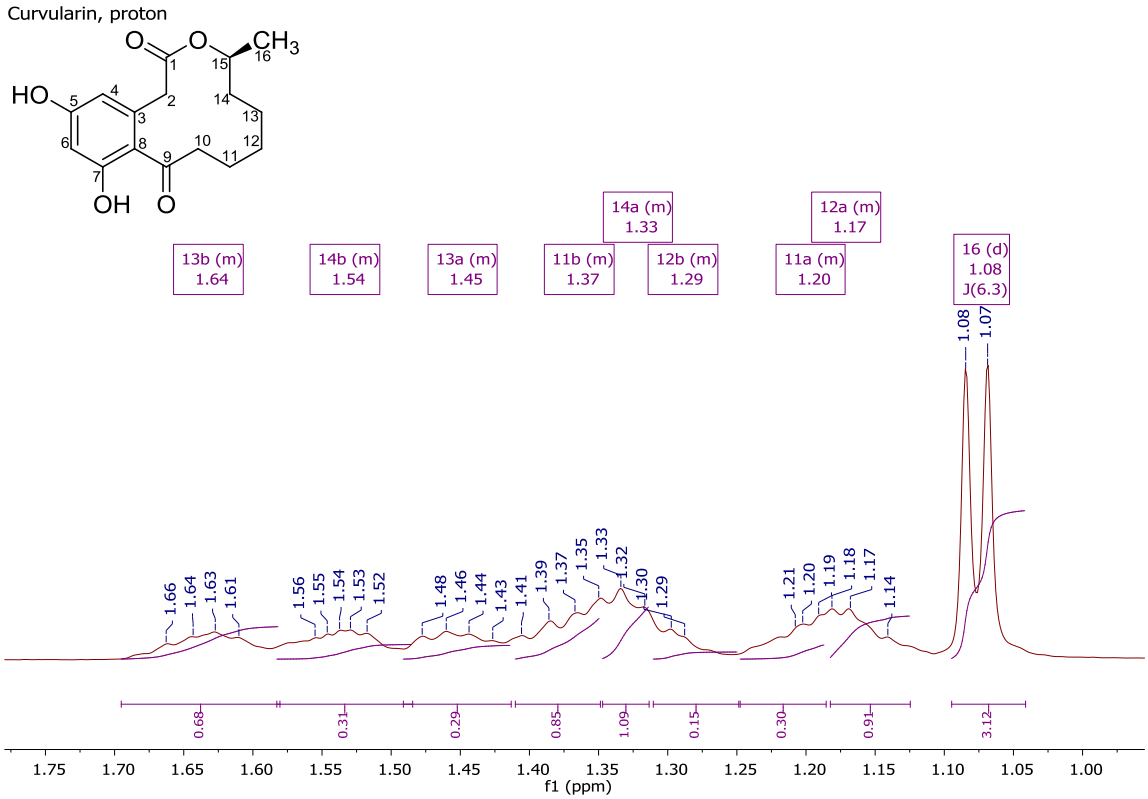

Figure 4.17: Expansion for the region δ_H 1.00-1.70 of the ^{1}H NMR (400 MHz) spectrum for (-)-(*S*)-curvularin, measured in DMSO-d_6.

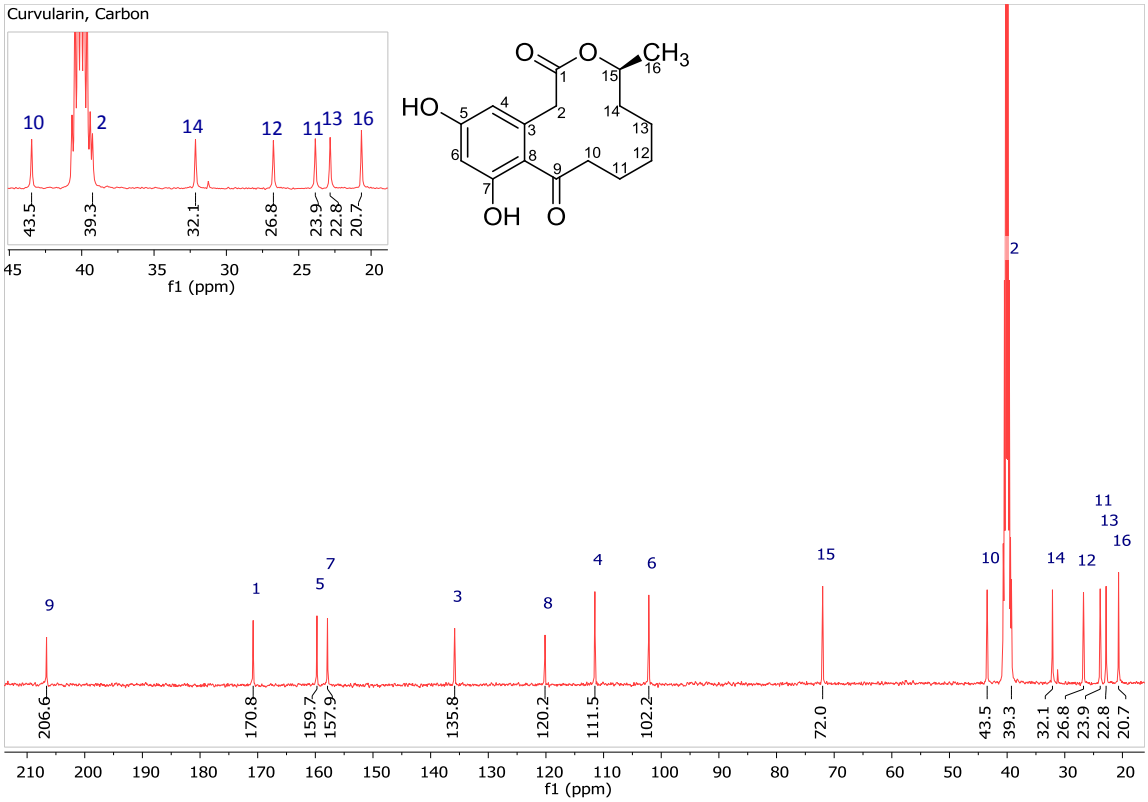

Figure 4.18: ^{13}C NMR (100 MHz) spectrum for (-)-(*S*)-curvularin, measured in DMSO-d_6.

Table 4.9: ^{1}H and ^{13}C NMR data for (-)-(*S*)-curvularin compared to the literature.

	(-)-(*S*)-curvularin in DMSO-d_6						**(-)-(*S*)-curvularin (Elzner *et al.*, 2008) in acetone-d_6**				
	^{1}H NMR data, (400 MHz)				^{13}C NMR data, (100 MHz)		^{1}H NMR data, (300 MHz)				^{13}C NMR data, (75.5 MHz)
Atom no.	δ_H (ppm)	Integration	Multiplicity	*J* (Hz)	δ_C (ppm)	Multiplicity	δ_H (ppm)	Integration	Multiplicity	*J* (Hz)	δ_C (ppm)
1					170.8	C					171.0
2	3.71 3.60	1H 1H	d d	15.6 15.6	39.3	CH_2	3.77 3.68	1H 1H	d d	15.5 15.5	39.7
3					135.8	C					136.9
4	6.18	1H	d	2.2	111.5	CH	6.33	1H	d	2.2	112.2
5					159.7	C					160.1
6	6.27	1H	d	2.2	102.2	CH	6.38	1H	d	2.2	102.4
7					157.9	C					158.2
8					120.2	C					121.3
9					206.6	C					206.7
10	2.98 2.68	1H 1H	m ddd	 15.4, 9.5, 2.6	43.5	CH_2	3.10 2.75	1H 1H	ddd ddd	15.5, 8.5, 2.9 15.5, 9.6, 2.9	44.0
11	1.37 1.20	1H 1H	m m		23.9	CH_2	1.78 – 1.70 1.63 – 1.22	1H 1H	m m		23.5
12	1.29 1.17	1H 1H	m m		26.8	CH_2	1.63 – 1.22	2H	m		27.5
13	1.64 1.45	1H 1H	m m		22.8	CH_2	1.63 – 1.23	2H	m		24.6
14	1.54 1.33	1H 1H	m m		32.1	CH_2	1.63 – 1.24	2H	m		32.9
15	4.84	1H	ddt	9.0, 6.3, 3.9	72.0	CH	4.94 – 4.87	1H	m		72.6
16	1.08	3H	d	6.3	20.7	CH_3	1.10	3H	d	6.3	20.6
5-OH	9.96	1H	s				9.17	1H	brs		
7-OH	9.77	1H	s				8.75	1H	brs		

4.6.2 Dehydrocurvularin (2)

Dehydrocurvularin
Fraction: C.5 Retention time: 11.94 min Synonym(s): • (4*S*,8*E*)-4,5,6,7-Tetrahydro-11,13-dihydroxy-4-methyl-2*H*-3-benzoxacyclododecin-2,10(1*H*)-dione • (10*E*,15*S*)-10(11)-Dehydrocurvularin • 10,11-Dehydrocurvularin Source: endophytic *Curvularia australiensis* from *Anthemis palestina* Amount of sample: 339.0 mg Percent yield: 7.48% Percent purity: 95.3% Physical description: White amorphous powder Molecular formula: $C_{16}H_{18}O_5$ Molecular weight: 290.3111 g/mol Optical rotation: $[\alpha]_D^{20}$ = -31 (0.1 g/100 mL, EtOH)
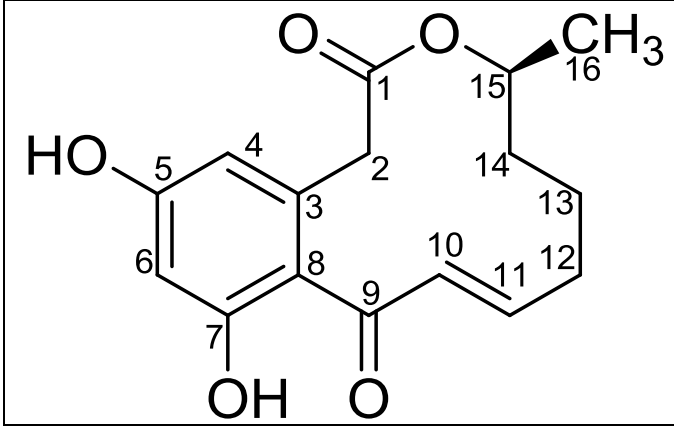

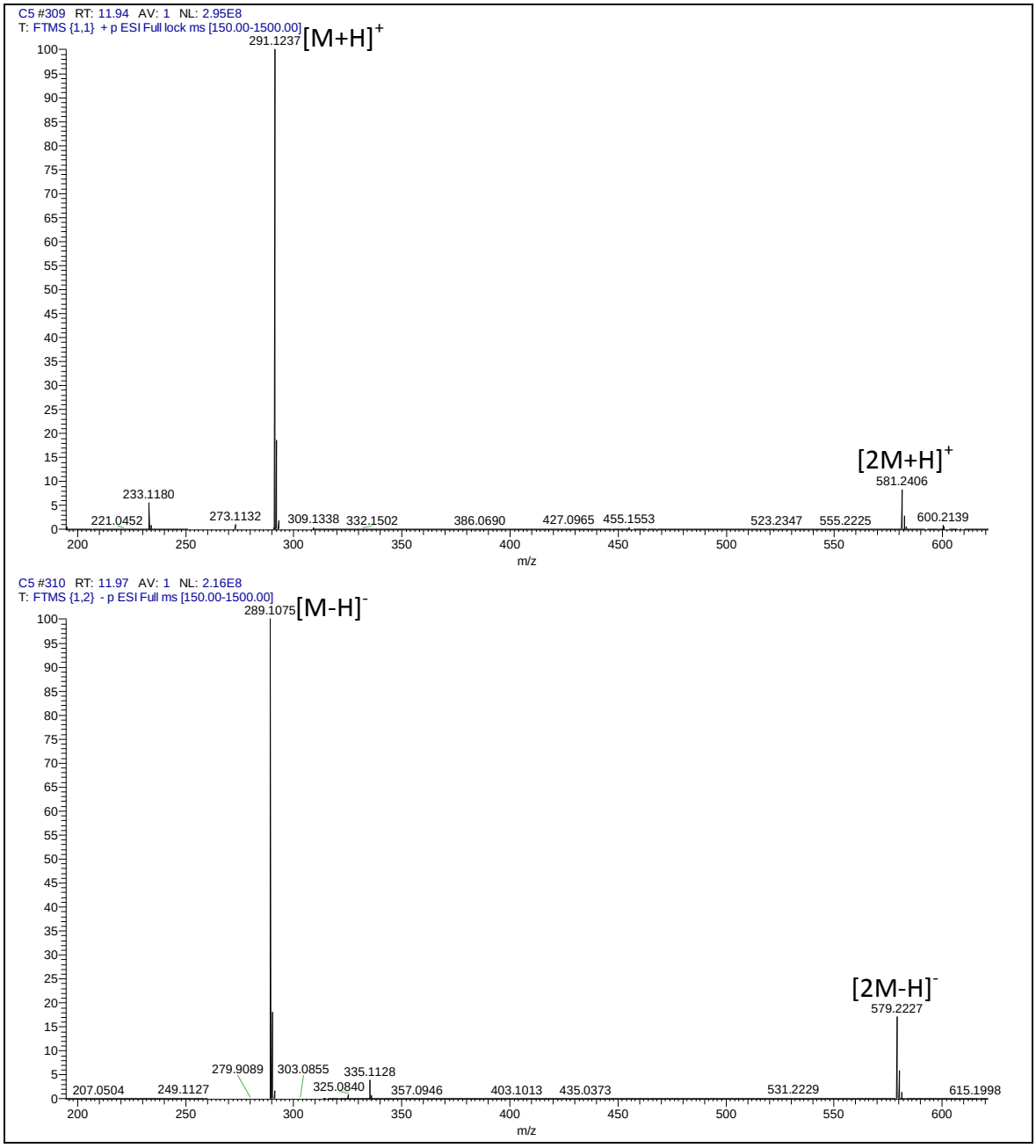

Dehydrocurvularin was isolated in the form of white crystals. Its yield was at 7.48% (339.0 mg). LC-HRMS data afforded a pseudomolecular ion at *m/z* 291.1237 $[M+H]^+$ and 289.1075 $[M-H]^-$, indicating a molecular weight of 290.3111 g/mol. The molecular formula predicted by HRMS is $C_{16}H_{18}O_5$.

Dehydrocurvularin is a didehydrogenated derivative of (-)-(*S*)-curvularin. Thus, both compounds possess very similar ^{1}H and ^{13}C NMR data and were compared in Table. 4.10. Nevertheless, their signals differ at positions 10, 11 and 12. The protons H-10 (δ_H 6.29) and H-11 (δ_H 6.35) in Dehydrocurvularinare more deshielded, and so, more downfield than those of (-)-(*S*)-curvularin (Figure 4.19). This was referred to the addition of a double bond as a result of the dehydrogenation that took place at both carbons C-10 (δ_C 133.0) and C-11 (δ_C 154.2) that were shifted downfield as well (Figure 4.20). Nonetheless, C-11 was detected at more downfield position than C-10. This was a result for its *γ* position to carbonyl C-9. Thus, it was more deshielded than C-10. The configuration of the double bond was set to *(E)* as the coupling constant of the proton H-10 is *J*=15.7 Hz (Lai *et al*., 1989). In addition to that, the creation of the double bond at position 11 inductively deshielded position 12, shifting its protons and carbon more downfield compared to (-)-(*S*)-curvularin. As a result, H-12a was detected at δ_H 2.16 and H-12b was detected at δ_H 2.28, while the carbon C-12 resonated at δ_C 33.2.

The structure was confirmed as dehydrocurvularin by comparing both its ^{1}H and ^{13}C NMR data to the literature (Zhan *et al*., 2004) (Table 4.11).

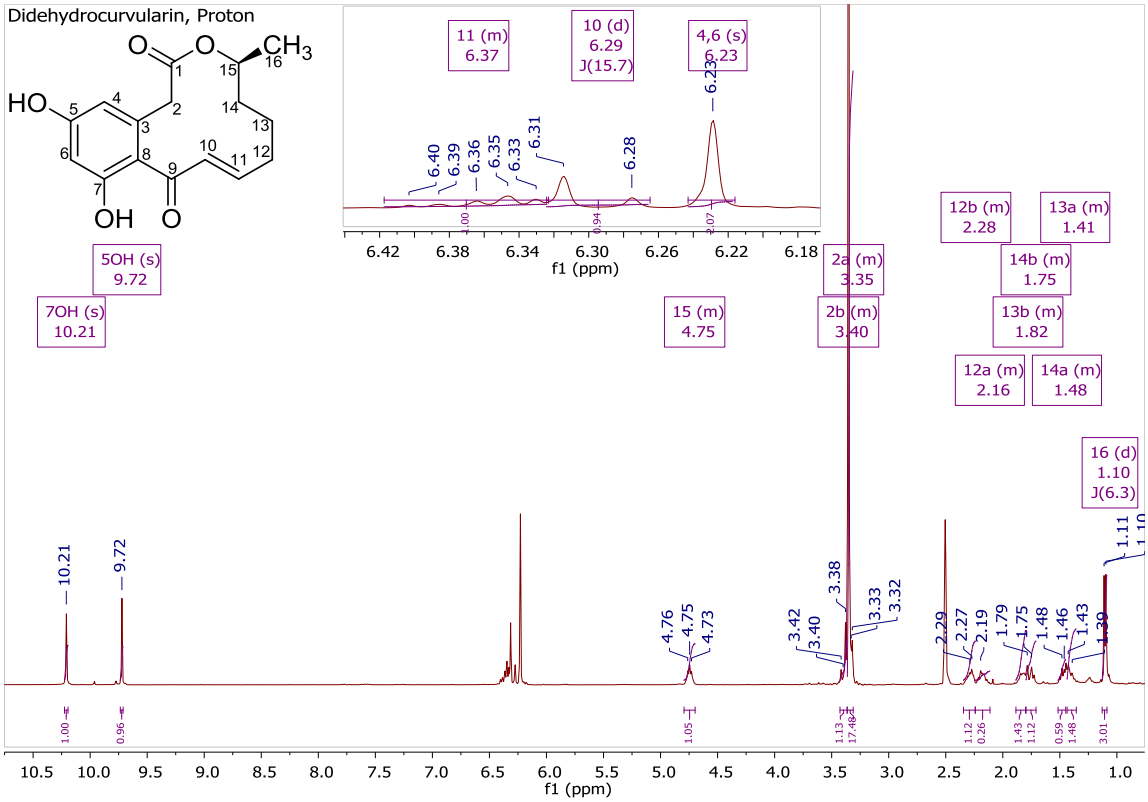

Figure 4.19: ^{1}H NMR spectrum (400 MHz) for dehydrocurvularin, measured in DMSO-d_6.

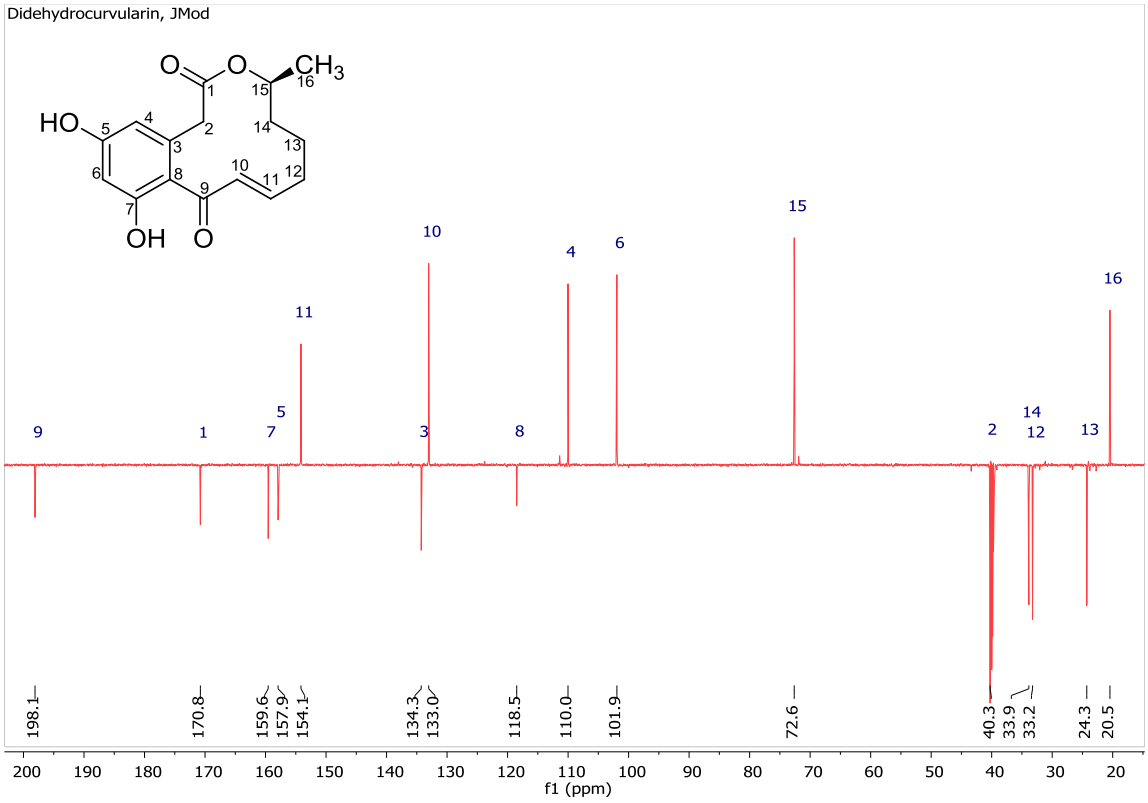

Figure 4.20: JMod NMR (100 MHz) spectrum for dehydrocurvularin, measured in DMSO-d_6.

Table 4.10: ^{1}H and ^{13}C NMR data for dehydrocurvularin compared to (-)-(*S*)-curvularin.

	(-)-(*S*)-curvularin in DMSO-d_6						**dehydrocurvularin in DMSO-d_6**					
	^{1}H NMR data, (400 MHz)				^{13}C NMR data, (100 MHz)		^{1}H NMR data, (400 MHz)				^{13}C NMR data, (100 MHz)	
Atom no.	δ_H (ppm)	Integration	Multiplicity	*J* (Hz)	δ_C (ppm)	Multiplicity	δ_H (ppm)	Integration	Multiplicity	*J* (Hz)	δ_C (ppm)	Multiplicity
1					170.8	C					170.8	C
2	3.71, 3.60	1H, 1H	d, d	15.6, 15.6	39.3	CH_2	3.40, 3.35	1H, 1H	d, overlapped by water	15.4	40.3	CH_2
3					135.8	C					134.3	C
4	6.18	1H	d	2.2	111.5	CH	6.23	1H	overlapped by H-6		110.0	CH
5					159.7	C					157.9	C
6	6.27	1H	d	2.3	102.2	CH	6.23	1H	overlapped by H-4		101.9	CH
7					157.9	C					159.6	C
8					120.2	C					118.5	C
9					206.6	C					198.1	C
10	2.98 2.68	1H 1H	m ddd	15.4, 9.5, 2.6	43.5	CH_2	6.29	1H	d	15.7	133.0	CH
11	1.37 1.20	1H 1H	m m		23.9	CH_2	6.35	1H	m		154.2	CH
12	1.29 1.17	1H 1H	m m		26.8	CH_2	2.28 2.16	1H 1H	m m		33.2	CH_2
13	1.64 1.45	1H 1H	m m		22.8	CH_2	1.82 1.41	1H 1H	m m		24.3	CH_2
14	1.54 1.33	1H 1H	m m		32.1	CH_2	1.75 148	1H 1H	m m		33.9	CH_2
15	4.84	1H	ddt	9.0, 6.3, 3.9	72.0	CH	4.75	1H	m		72.6	CH
16	1.08	3H	d	6.3	20.7	CH_3	1.10	3H	d	6.3	20.5	CH_3
5-OH	9.96	1H	s				9.72	1H	s			
7-OH	9.77	1H	s				10.21	1H	s			

Table 4.11: ^{1}H and ^{13}C NMR data for dehydrocurvularin compared to the literature.

	dehydrocurvularin in DMSO-d_6						**dehydrocurvularin (Zhan *et al.*, 2004) in acetone-d_6**				
	^{1}H NMR data, (400 MHz)				^{13}C NMR data, (400 MHz)		^{1}H NMR data, (500 MHz)				^{13}C NMR data, (125 MHz)
Atom no.	δ_H (ppm)	Integration	Multiplicity	*J* (Hz)	δ_C (ppm)	Multiplicity	δ_H (ppm)	Integration	Multiplicity	*J* (Hz)	δ_C (ppm)
1					170.8	C					172.3
2	3.40 3.35	1H 1H	m overlapped by water		40.3	CH_2	4.08 3.61	1H 1H	d d	17.3, 17.7	44.2
3					134.3	C					140.0
4	6.23	1H	overlapped by H-6		110.0	CH	6.36	1H	d d	2.4	114.2
5					157.9	C					163.6
6	6.23	1H	overlapped by H-4		101.9	CH	6.31	1H	d d	2.4	103.3
7					159.6	C					166.5
8					118.5	C					116.2
9					198.1	C					197.7
10	6.29	1H	d	15.7	133.0	CH	6.78	1H	d	15.5	133.1
11	6.35	1H	m		154.2	CH	6.57	1H	dq	15.5, 4.8	150.1
12	2.28 2.16	1H 1H	m m		33.2	CH_2	2.42 2.35	1H 1H	m m		33.7
13	1.82 1.41	1H 1H	m m		24.3	CH_2	1.99 1.67	1H 1H	m m		25.5
14	1.75 148	1H 1H	m m		33.9	CH_2	1.85 1.62	1H 1H	m m		35.3
15	4.75	1H	m		72.6	CH	4.73	1H	m		73.4
16	1.10	3H	d	6.3	20.5	CH_3	1.19	3H	d	6.4	22.8
5-OH	9.72	1H	s								
7-OH	10.21	1H	s								

4.6.3 11α-Hydroxycurvularin (3)

11α-Hydroxycurvularin
Fraction: C.9.5 Retention time: 7.58 min Synonym(s): • (4*S*,8*S*)-4,5,6,7,8,9-Hexahydro-8,11,13-trihydroxy-4-methyl-2*H*-3-benzoxacyclododecin-2,10(1*H*)-dione • 11α-Hydroxycurvularin Source: endophytic *Curvularia australiensis* from *Anthemis palestina* Amount of sample: 9.2 mg Percent yield: 0.20% Percent purity: 52.3% Physical description: White crystals Molecular formula: $C_{16}H_{20}O_6$ Molecular weight: 308.3264 g/mol Optical rotation: $[\alpha]_D^{20}$ = -3 (0.1 g/100 mL, EtOH)
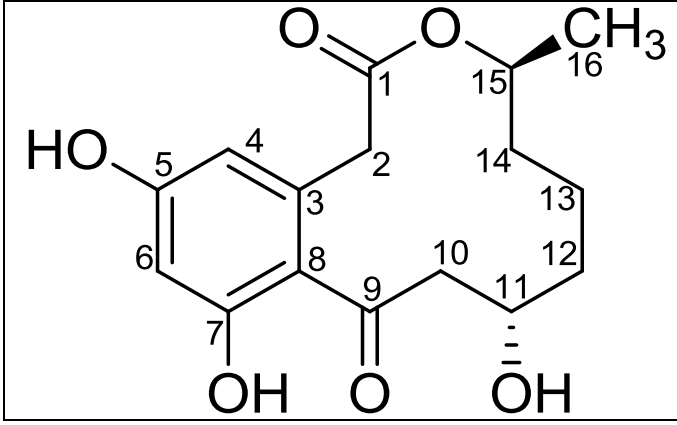

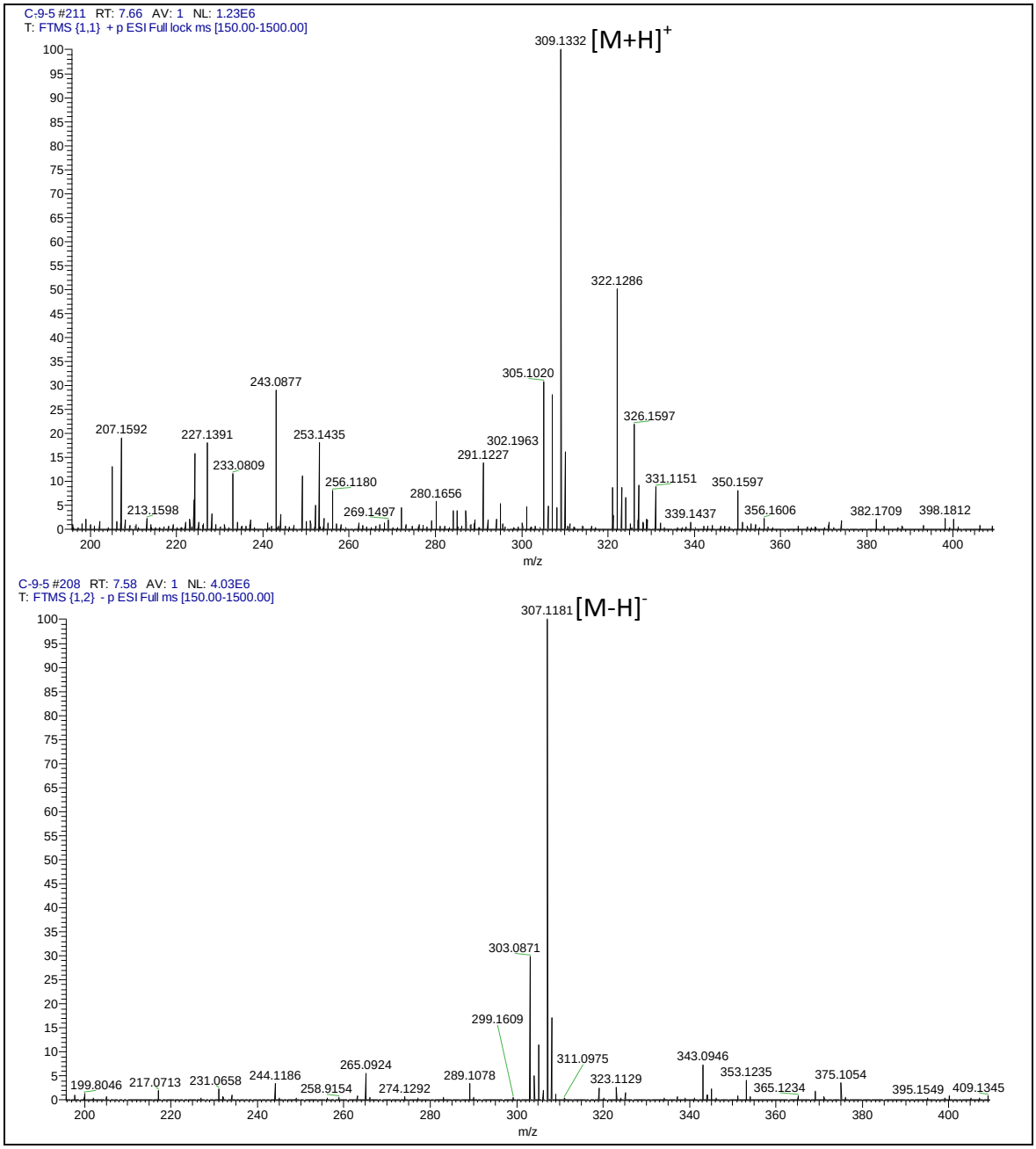

11α-Hydroxycurvularin was isolated as white crystals in a yield of 0.20% (9.2 mg). In LC-HRMS data, a pseudomolecular ion was observed at *m/z* 309.1322 $[M+H]^+$ and 307.1181 $[M-H]^-$, suggesting a molecular weight of 308.3264 g/mol. The molecular formula indicated by HRMS was $C_{16}H_{20}O_6$. However, this fraction was not completely pure as its fraction contained the compound dehydrocurvularin as well. The impurity could be detected in the chromatogram of

the LC-HRMS as depicted in Figure 4.29, eluting at 12.30 minutes. Moreover, ^{1}H peaks for dehydrocurvularin could be found in the NMR spectra as well (Figure 4.21 – 4.23).

As it name indicates, 11α-hydroxycurvularin is a derivative of (-)-(*S*)-curvularin, in which, hydroxylation process resulted in the addition of the hydroxyl group at position 11. Thus, both the ^{1}H and the ^{13}C NMR data for these two compounds are very similar (Table 4.12). Nevertheless, as position 11 in 11α-hydroxycurvularin was oxygenated, a deshielding effect by the oxygen took place. Thus, both proton and carbon NMR signals for position 11 are now shifted downfield to δ_H 3.90 and δ_C 65.5, respectively.

The identity of 11α-hydroxycurvularin was further confirmed by comparing both its ^{1}H and ^{13}C NMR data to those from the literature (Greve *et al*., 2008) (Table 4.13).

The optical rotation value for the obtained 11α-hydroxycurvularin was -3, $[\alpha]_D^{20}$ = -3 (0.1 g/100 mL, EtOH), so it was not considered enantiopure when compared to the literature, as its optical rotation value was -10.9 $[\alpha]_D^{24}$ = -10.9 (0.19 g/100 mL, EtOH) (Lai *et al*., 1989).

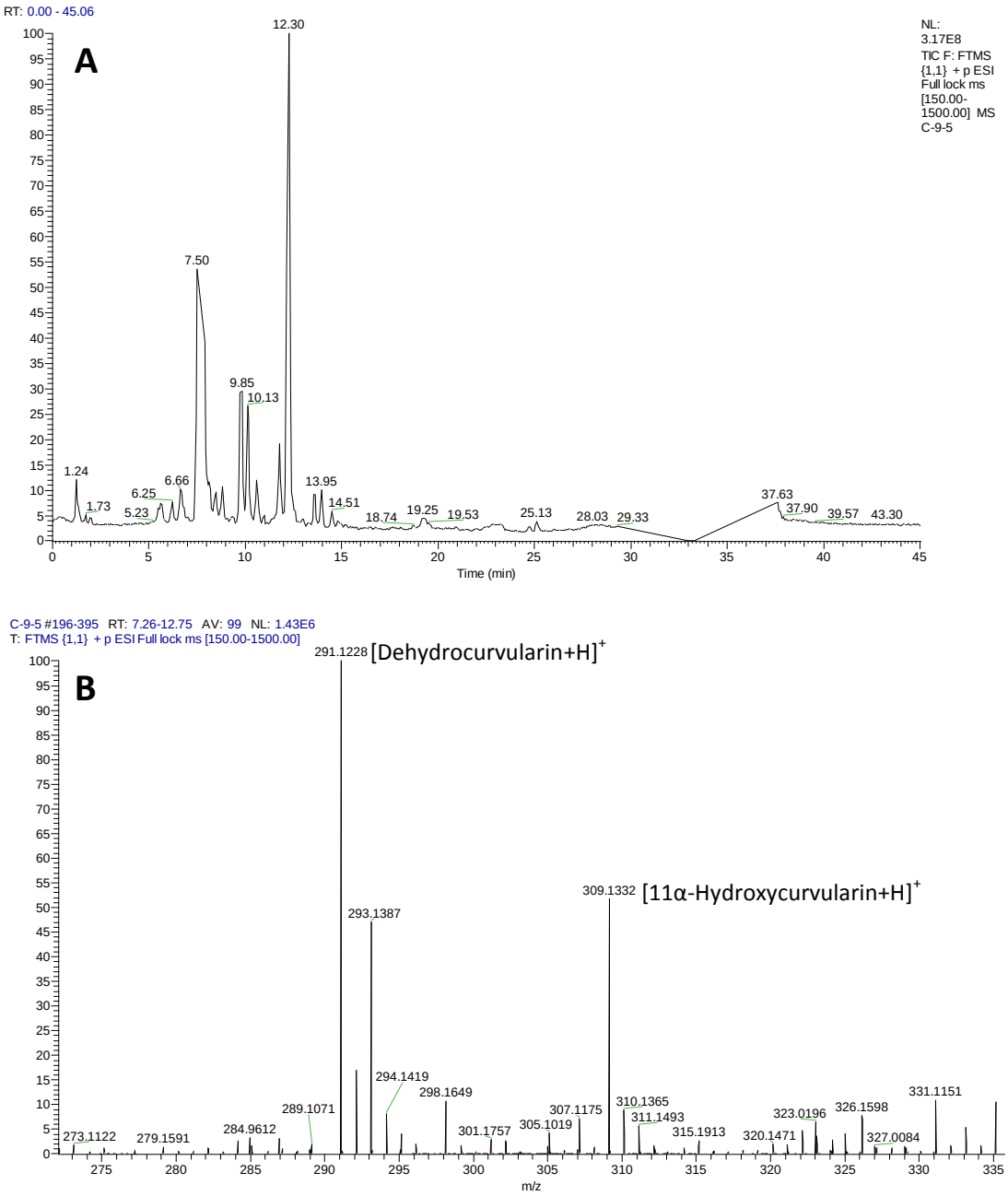

Figure 4.21: (A): The chromatogram of the fraction C.9.5, positive mode of ionisation and (B): mass spectrum for the peaks with t_R 7.26 – 12.75 minutes.

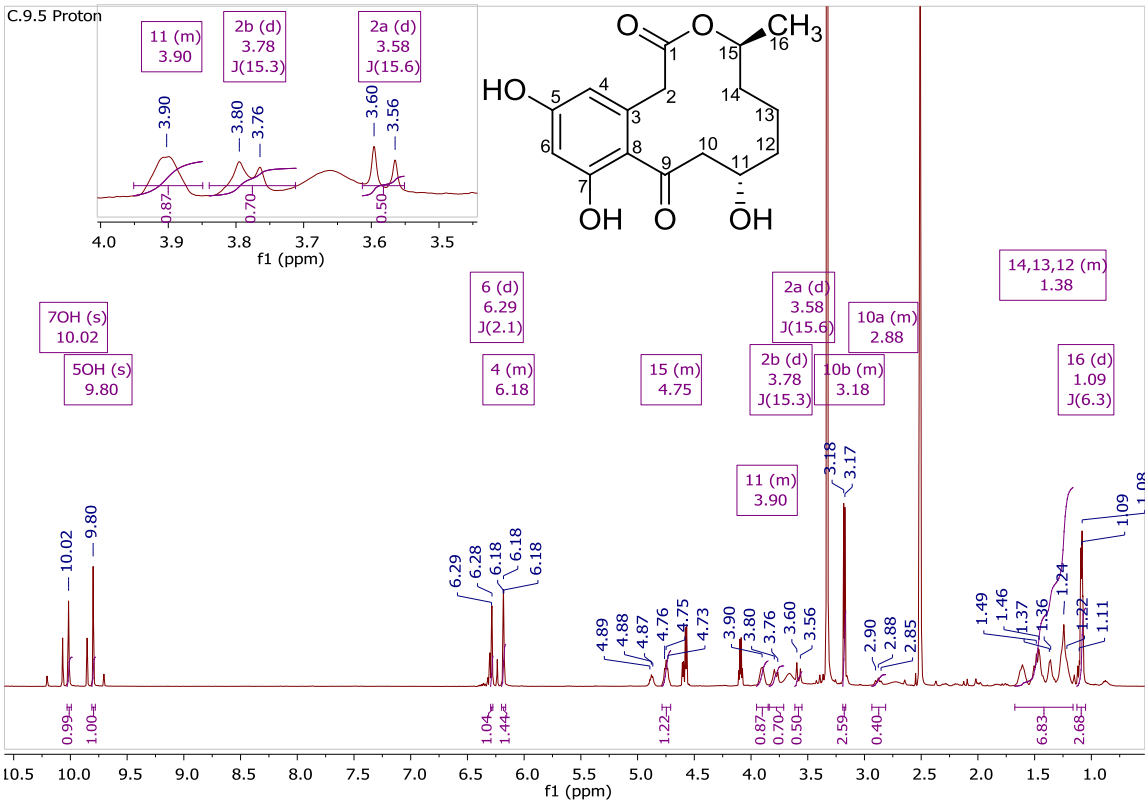

Figure 4.22: ^{1}H NMR (500 MHz) spectrum for 11α-hydroxycurvularin, measured in DMSO-d_6.

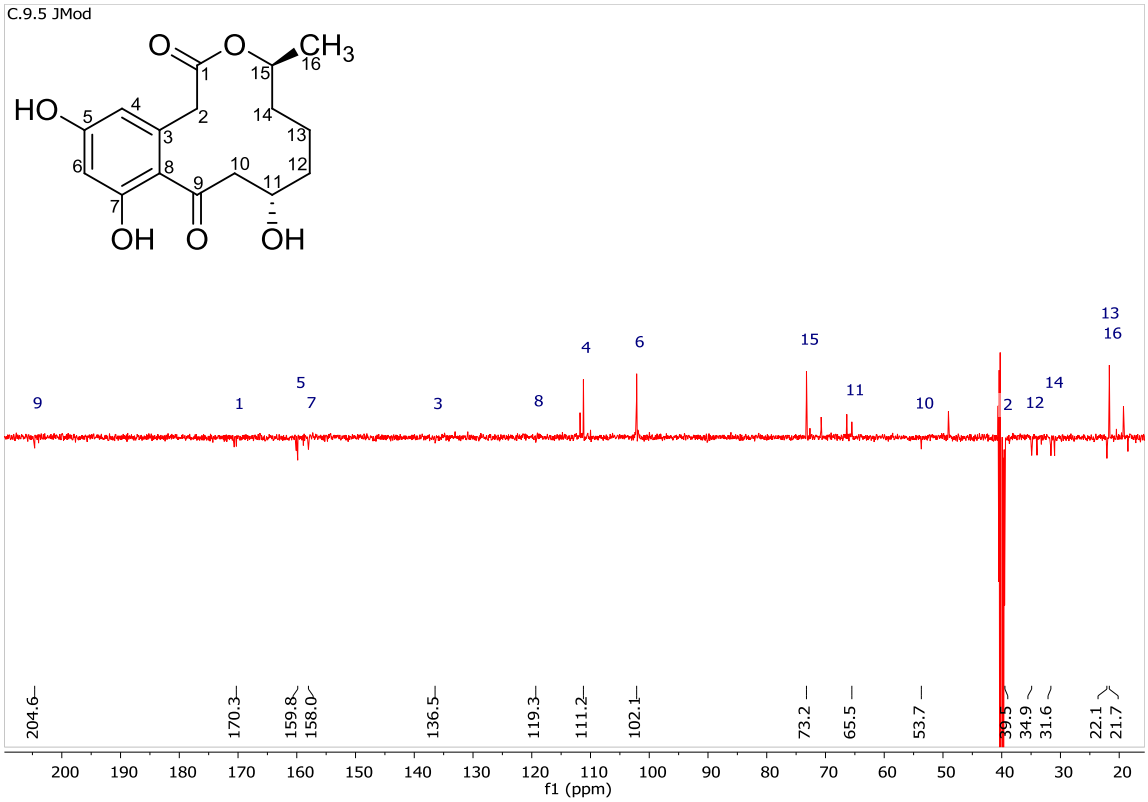

Figure 4.23: JMod NMR (125 MHz) spectrum for 11α-hydroxycurvularin, measured in DMSO-d_6.

Table 4.12: The ^{1}H and ^{13}C NMR data for 11α-hydroxycurvularin compared to (-)-(*S*)-curvularin.

	11α-hydroxycurvularin in DMSO-d_6						**(-)-(*S*)-curvularin in DMSO-d_6**				
	^{1}H NMR data, (500 MHz)				^{13}C NMR data, (125 MHz)		^{1}H NMR data, (400 MHz)				^{13}C NMR data, (100 MHz)
Atom no.	δ_H (ppm)	Integration	Multiplicity	*J* (Hz)	δ_C (ppm)	Multiplicity	δ_H (ppm)	Integration	Multiplicity	*J* (Hz)	δ_C (ppm)
1					170.3	C					170.8
2	3.78 3.58	1H 1H	d d	15.3 15.3	39.5	CH_2	3.71 3.60	1H 1H	d d	15.6 15.6	39.3
3					136.5	C					135.8
4	6.18	1H	m		111.2	CH	6.18	1H	d	2.2	111.5
5					159.8	C					159.7
6	6.29	1H	d	2.1	102.2	CH	6.27	1H	d	2.3	102.2
7					158.0	C					157.9
8					119.3	C					120.2
9					204.6	C					206.6
10	3.19 2.89	1H 1H	overlapped by impurity, m		53.7	CH_2	2.98, 2.68	1H 1H	m ddd	15.4, 9.5, 2.6	43.5
11	3.90	1H	m		65.5	CH	1.37 1.20	1H 1H	m m		23.9
12	1.16 – 1.68	2H	m		34.9	CH_2	1.29 1.17	1H 1H	m m		26.8
13	1.16 – 1.68	2H	m		22.1	CH_2	1.64 1.45	1H 1H	m m		22.8
14	1.16 – 1.68	2H	m		31.6	CH_2	1.54 1.33	1H 1H	m m		32.1
15	4.75	1H	m		73.2	CH	4.84	1H	ddt	9.0, 6.3, 3.9	72.0
16	1.08	3H	d	6.3	21.7	CH_3	1.08	3H	d	6.3	20.7
5-OH	9.80	1H	s				9.96	1H	s		
7-OH	10.02	1H	s				9.77	1H	s		

Table 4.13: The ^{1}H and ^{13}C NMR data for 11α-hydroxycurvularin compared to literature.

	11α-Hydroxycurvularin in DMSO-d_6						**11α-Hydroxycurvularin (Greve *et al.*, 2008) in acetone-d_6**				
	^{1}H NMR data, (500 MHz)				^{13}C NMR data, (125 MHz)		^{1}H NMR data, (300 MHz)				^{13}C NMR data, (75 MHz)
Atom no.	δ_H (ppm)	Integration	Multiplicity	*J* (Hz)	δ_C (ppm)	Multiplicity	δ_H (ppm)	Integration	Multiplicity	*J* (Hz)	δ_C (ppm)
1					170.3	C					170.8
2	3.78	1H	d	15.3	39.5	CH_2	3.82	1H	d	15.5	39.4
	3.58	1H	d	15.3			3.67	1H	d	15.5	
3					136.5	C					137.0
4	6.18	1H	m		111.2	CH	6.31	1H	d	2.2	112.0
5					159.8	C					160.4
6	6.29	1H	d	2.1	102.2	CH	6.41	1H	d	2.2	102.6
7					158.0	C					158.4
8					119.3	C					121.1
9					204.6	C					204.8
10	3.19	1H	overlapped by impurity,		53.7	CH_2	3.56	1H	dd	13.7, 10.0	54.5
	2.89	1H	m				2.86	1H	dd	13.7, 2.2	
11	3.90	1H	m		65.5	CH	4.10	1H	m		66.9
12	1.16 – 1.68	2H	m		34.9	CH_2	2.60	2H	m		35.5
13	1.16 – 1.68	2H	m		22.1	CH_2	1.69	1H	m		22.7
							1.31	1H	m		
14	1.16 – 1.68	2H	m		31.6	CH_2	1.56	1H	m		32.4
15	4.75	1H	m		73.2	CH	4.81	1H	m		73.4
16	1.08	3H	d	6.3	21.7	CH_3	1.09	3H	d	6.2	21.5
5-OH	9.80	1H	s								
7-OH	10.02	1H	s								

4.6.4 Cyclo(L-prolylglycyl) (4)

Cyclo(L-prolylglycyl)

Fraction: C.13.4

Synonym(s): 1.21

- (8a*S*)-Hexahydropyrrolo[1,2-*a*]pyrazine-1,4-dione
- Cyclo(glycyl-L-prolyl)
- (*S*)-3,6-Dioxohexahydropyrrolo[1,2-*a*]pyrazine

Source: *Curvularia australiensis*, isolated from *Anthemis palestina*

Amount of sample: 26.1 mg

Percent yield: 0.58%

Percent purity: 92.6%

Physical description: Brown crystals

Molecular formula: $C_7H_{10}N_2O_2$

Molecular weight: 154.1665 g/mol

Optical rotation: $[\alpha]_D^{20}$ = -49 (0.1 g/100 mL, EtOH)

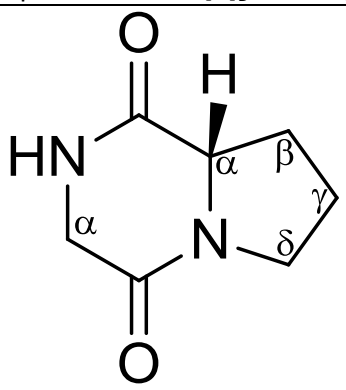

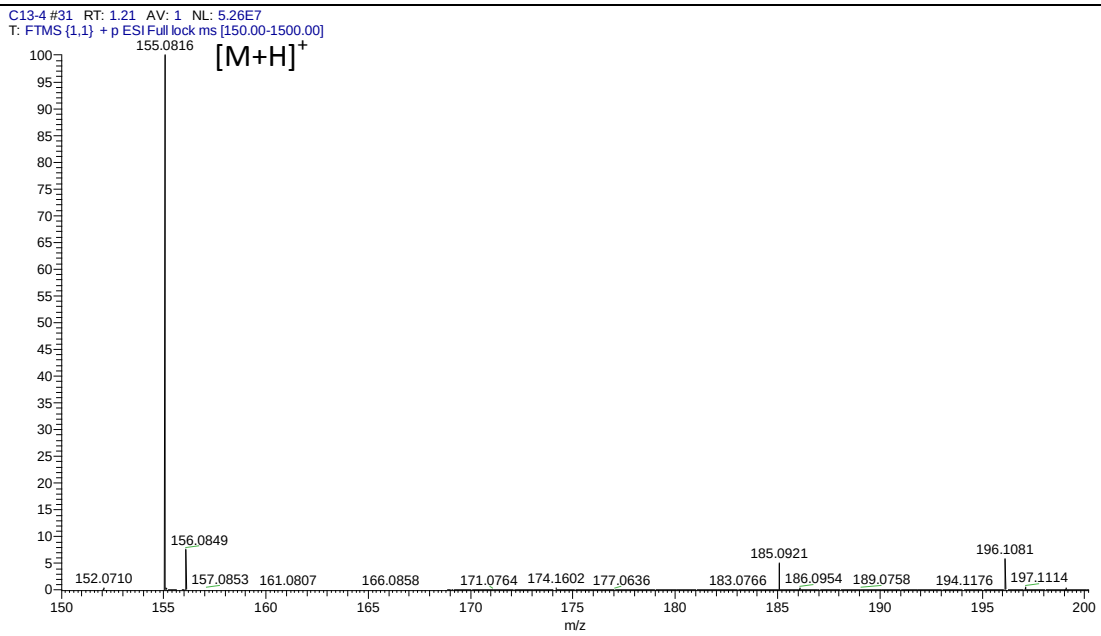

Cyclo(L-prolylglycyl) was isolated in the form of brown crystals, yielding of 26.1 mg (0.58%). LC-HRMS data afforded a pseudomolecular ion at *m/z* 155.0816 $[M+H]^+$. However, no $[M-H]^-$ was detected. This is referred to the two amidic goups that this compound possesses, that makes it a weak base. This leads to readily ionising it in the positive mode, but hinder its ionisation in the negative mode. The molecular weight of this compound is 154.1665 g/mol. The molecular formula established by HRMS as $C_7H_{10}N_2O_2$.

The cyclic peptide cyclo(L-prolylglycyl) is a 2,5-diketopiperazine that is composed of 2 amino acids, glycine and proline. The assignment of each proton signal to its corresponding amino acid could be done by utilising ^{1}H NMR and ^{1}H-^{1}H TOCSY NMR experiments (Figure 4.24 and Figure A.V.2). The proton H-α_1 of the glycyl moiety was detected as a doublet at δ_H 3.99 (*J*=16.4 Hz) and coupled through ^{1}H-^{1}H TOCSY to the doublet of doublet H-α_2 (δ_H 3.51, *J*=16.4, 4.6 Hz). These two protons were deshielded by the effect of the neighbouring carbonyl and nitrogen of the two amide groups of the compound. Moreover, both H-α_1 and H-α_2 are coupled via ^{1}H-^{1}H TOCSY to the amidic hydrogen that resonated as doublet at δ_H 8.06 (*J*=4.4 Hz). Furthermore, H-α_1 is coupled to H-α_2 as depicted by its ^{1}H-^{1}H COSY spectrum (Figure A.V.3). This caused both of their signals to split as doublets (*J*=16.4). In addition to that, H-α_2 is coupled to the doublet of N*H* (*J*=4.4 Hz). This resulted in splitting the signal of H-α_2 into another doublet. On the other hand, the alpha proton of the prolyl moiety (H-α) resonated as a triplet at δ_H 4.12 (*J*=7.8 Hz) and coupled through ^{1}H-^{1}H TOCSY to H-β_1 (δ_H 2.14), H-β_2 and H-γ (δ_H 1.84), H-δ_1 (δ_H 3.34) and H-δ_2 at (δ_H 3.42).

The carbon chemical shifts for the compound were obtained by a JMod NMR experiment (Figure 4.25). The aliphatic carbons C-β and C-γ were detected at δ_C 28.3 and δ_C 22.5 respectively. The carbons that are connected to nitrogen atoms resonated more downfield at δ_C 45.2 (C-δ), 46.4 (C-α of the glycyl moiety) and 58.5 (C-α of the prolyl moiety). Moreover, the amidic carbonyls could be detected at δ_C 164.3 and δ_C 169.7. All proton – carbon assignments were afforded by a ^{1}H-^{13}C HSQC experiment (Figure A.V.5).

A ^{1}H-^{13}C HMBC experiment was conducted to establish the connectivity of this compound (Figure A.V.6). Starting with the glycyl unit, ^3J correlations were noticed going from H-$\alpha_{1,2}$ to the carbonyl of the prolyl moiety and from the amidic proton to both the carbonyl of prolyl moiety

and to the C-α of the prolyl moiety. More correlations were detected for H-α_2, as it has ^2J correlation to the carbonyl of the glycyl moiety and a ^4J correlation (*W*) to C-δ of the prolyl moiety. Moving on to the protons of the prolyl unit, ^3J correlations were spotted going from H-$\beta_{1,2}$ protons to both the carbonyl and C-δ of the prolyl moiety, from H-$\gamma_{1,2}$ to C-α of the prolyl moiety and from H-$\delta_{1,2}$ to both C-α and C-β of the prolyl moiety. Furthermore, ^2J couplings were revealed correlating all protons to their neighbouring carbons and a ^4J coupling from H-$\gamma_{1,2}$ to the amidic carbonyl of the prolyl moiety.

The compound was confirmed as cyclo(L-prolylglycyl) by comparing both its ^{1}H and ^{13}C NMR data to the literature (Jiang *et al.*, 2000) (Table. 4.14). Cyclo(L-prolylglycyl) was synthesised by Fischer in 1909 and obtained in 1960 from the hydrolysis of *Streptomyces* sp. S-580 extract upon feeding on gelatine by using Streptomyces-protease (Fischer and Reif, 1909, Koaze, 1960).

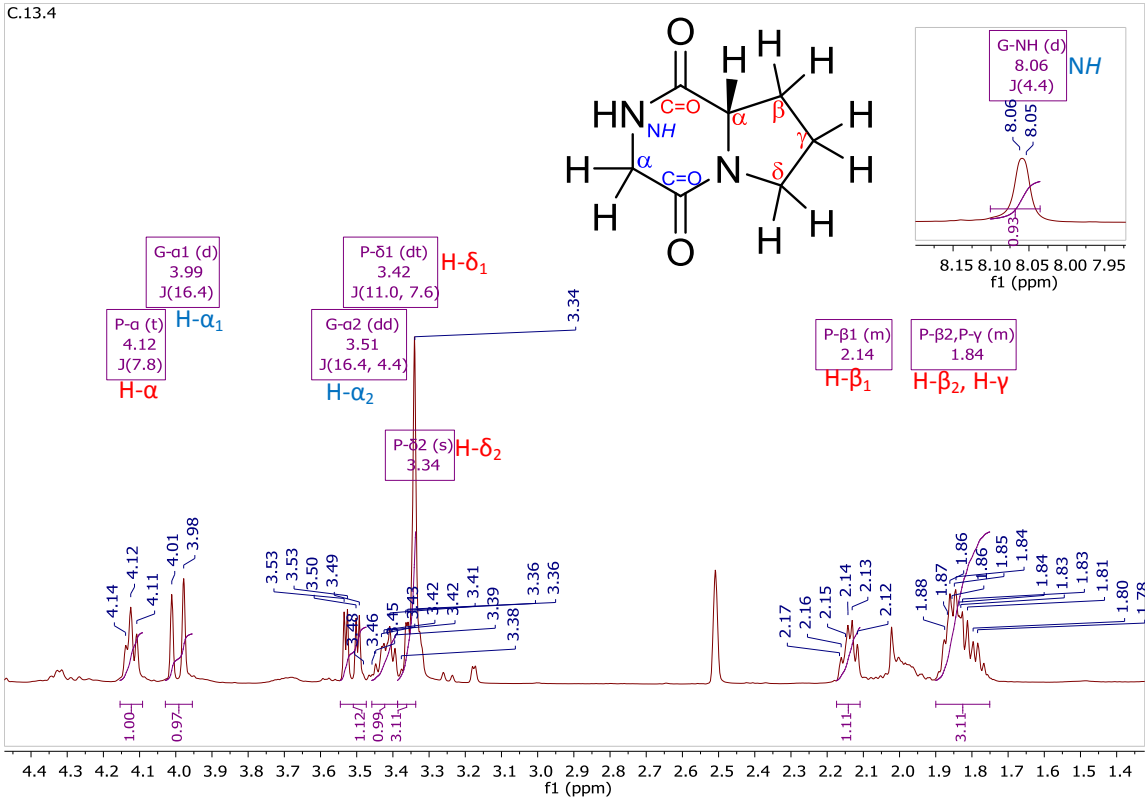

Figure 4.24: ^{1}H NMR (500 MHz) spectrum for cyclo(L-prolylglycyl), measured in DMSO-d_6. Red labels are for the signals that belong to the prolyl moiety (P) while blue labels are for the signals that belong to the gylcyl moiety (G).

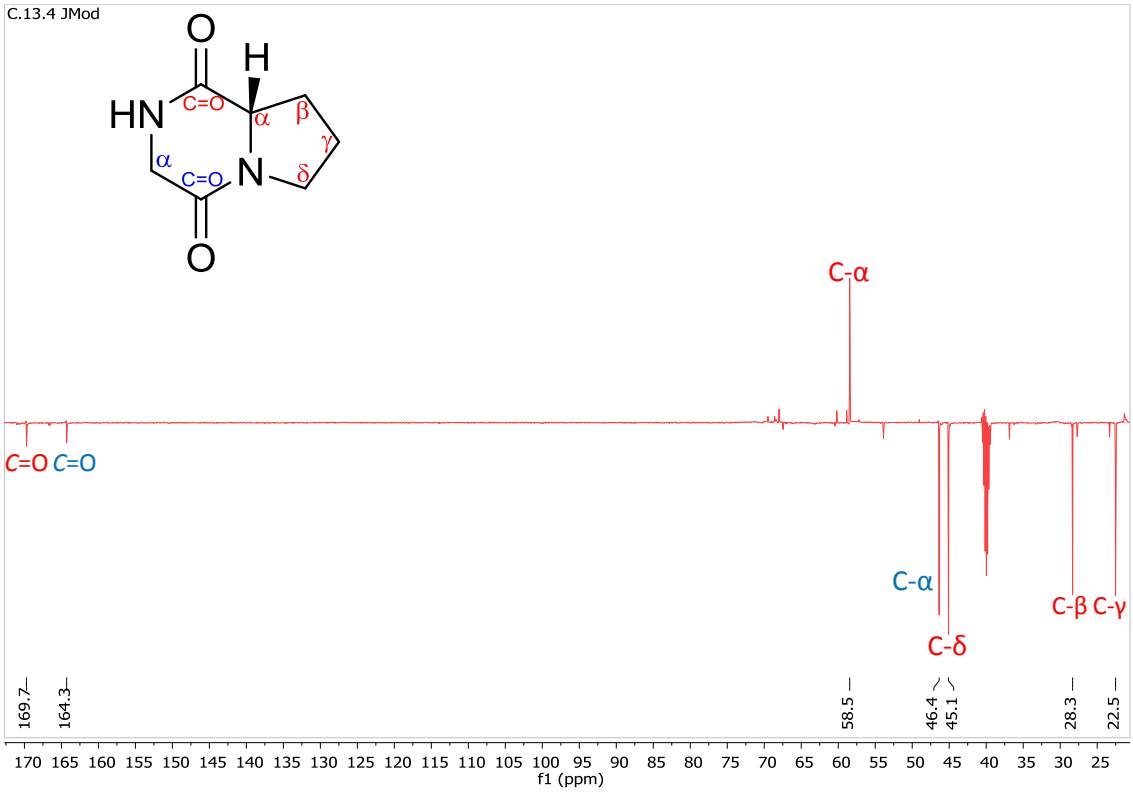

Figure 4.25: JMod NMR spectrum for cyclo(L-prolylglycyl), measured in DMSO-d_6. Red labels are for the signals that belong to the prolyl moiety while blue labels are for the signals that belong to the gylcyl moiety, (125 MHz).

Table 4.14: ^{1}H and ^{13}C NMR data for cyclo(L-prolylglycyl) compared to literature.

		cyclo(L-prolylglycyl) in DMSO-d_6						**cyclo(L-prolylglycyl) (Jiang *et al.*, 2000) in $CHCl_3$-*d***				
		^{1}H NMR data, (500 MHz)				^{13}C NMR data, (125 MHz)		^{1}H NMR data, (200 MHz)				^{13}C NMR data, (50 MHz)
	Position	δ_H (ppm)	Integration	Multiplicity	*J* (Hz)	δ_C (ppm)	Multiplicity	δ_H (ppm)	Integration	Multiplicity	*J* (Hz)	δ_C (ppm)
Prolyl residue	α	4.12	1H	t	7.8	58.5	CH	4.10	1H	d	7.9	58.4
	β	3.42 3.34	1H 1H	dt, overlapped by water	11.0 7.6	45.1	CH_2	3.58	2H	dd	8.5, 8.2	45.2
	γ	1.84	2H	m		22.5	CH_2	2.00 1.90	1H 1H	m m		22.3
	δ	2.14 1.84	1H 1H	m m		28.3	CH_2	2.35 2.00	1H 1H	m m		28.3
Glycyl residue	α	3.99, 3.51	1H 1H	d dd	16.4, 16.4, 4.6	46.3	CH_2	4.08 3.85	1H 1H	d dd	16.0 16.0, 4.3	46.6
	NH	8.06	1H	d	4.4			6.36	1H	brs		
2,5-Piperazinedione	C=O					164.3	C					163.3
	C=O					169.7	C					169.6

4.7 Biological activity of the isolated compounds from the endophyte *Curvularia australiensis*

The isolated compounds were tested for their anti-proliferative activity against both breast cancer (ZR-75) and lung cancer (A549) cell lines. (-)-(*S*)-curvularin and its derivatives were found active against breast cancer, while cyclo(L-prolylglycyl) was inactive (Table 4.15 and Figure 4.26). The IC_{50} of (-)-(*S*)-curvularin was 13 µM. It decreased to 8 µM for 11α-hydroxycurvularin and to 0.8 µM for dehydrocurvularin. The activity increased with hydroxylation of position 11 and the dehydrogenation at positions 10 and 11 that led to the creation of a double bond. Not only was this the case for breast cancer activity, but also for lung cancer bioactivity (Table 4.15 and Figure 4.27). Dehydrocurvularin was the most potent compound (IC_{50}=0.8 µM) followed by 11α-hydroxycurvularin (IC_{50}=28 µM), while (-)-(*S*)-curvularin and cyclo(L-prolylglycyl) possessed no activity (Figure 4.27). As a result, the curvularin-type isolated compounds dehydrocurvularin and 11α-hydroxycurvularin were active against both breast cancer and lung cancer, while (-)-(*S*)-curvularin was more selective as its activity was limited to breast cancer. Cyclo(L-prolylglycyl) possessed no activity against the tested cell lines. This confirmed the predicted activity for the metabolites that was obtained from the OPLS-DA models. The activity of (-)-(*S*)-curvularin could be certainly attributed to the identified compound as its purity was 100%, while the isolated dehydrocurvularin was of less purity (95.3%). However, the purity of 11α-hydroxycurvularin was 52.3% as its the fraction contained dehydrocurvularin as discussed under 4.6.3. Therefore, dehydrocurvularin could have affected the obtained activity of 11α-hydroxycurvularin either by synergy or it could be itself the active compound in this fraction.

Moreover, the isolated compounds were assayed for their toxicity against Human prostate normal cells (PNT2) and the results are shown in Table 4.15 and Figure 4.28. (-)-(*S*)-curvularin is more selective than its two other congeners because it was only found active against the tested breast cancer cell line and considered not toxic against normal cell line PNT2. The most toxic compound was dehydrocurvularin and 11α-hydroxycurvularin. Meanwhile, cyclo(L-prolylglycyl) possessed no toxicity.

Table 4.15: IC_{50} concentrations (µM) for the compounds isolated from *Curvularia australiensis* against the correspondent cell lines.

Compound	ZR-75	A549	PNT2A	% Purity
(-)-(*S*)-curvularin	13	> 30	> 30	100
dehydrocurvularin	0.8	3.6	10	95.3
11α-hydroxycurvularin	8	28	28	52.3
cyclo(L-prolylglycyl)	> 30	> 30	> 30	92.6

Furthermore, the selectivity indexes were calculated for the active compounds and mentioned in Table 4.16. All of the curvularin type compounds were selective in regard to their activity against breast cancer (ZR-75) cell line with an SI value greater than 2. However, of the active compounds against lung cancer (A549) cell line, only dehydrocurvularin was selective (SI=2.8), while 11α-hydroxycurvularin lacked the selectivity (SI=1.0).

Table 4.16: Selectivity indexes for the compounds isolated from *Curvularia australiensis* against the correspondent cell lines.

Compound	ZR-75	A549
(-)-(*S*)-curvularin	2.4	-
dehydrocurvularin	12.5	2.8
11α-hydroxycurvularin	3.5	1.0

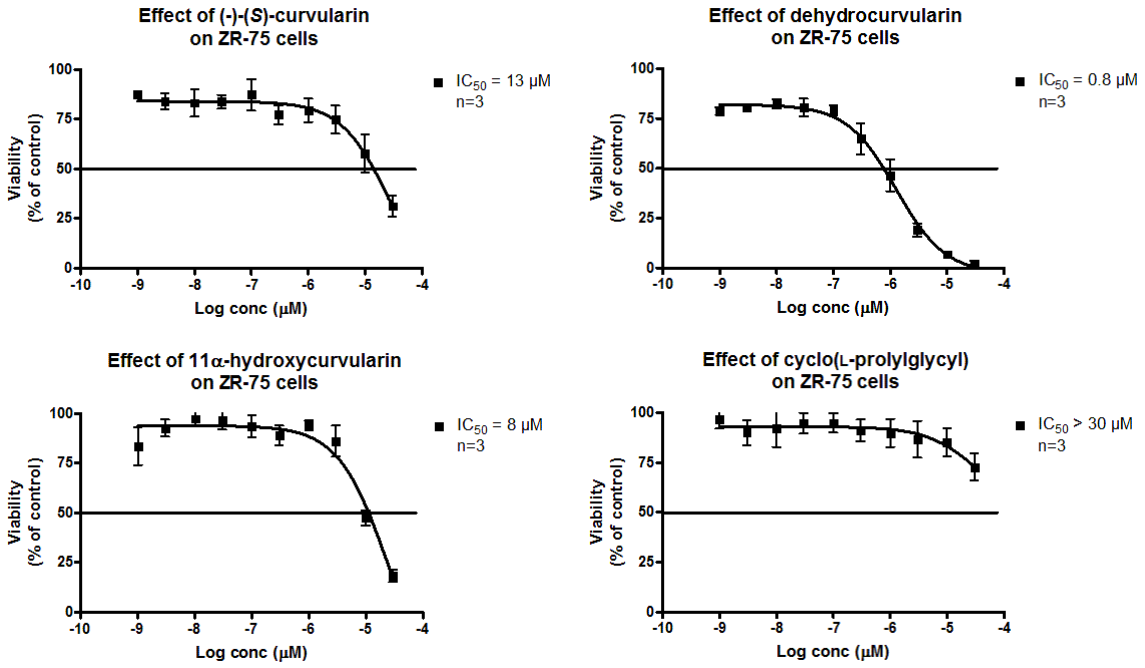

Figure 4.26: Dilution curves for the compounds isolated from *Curvularia australiensis* when tested against breast cancer (ZR-75) cell line to determine their IC_{50} values.

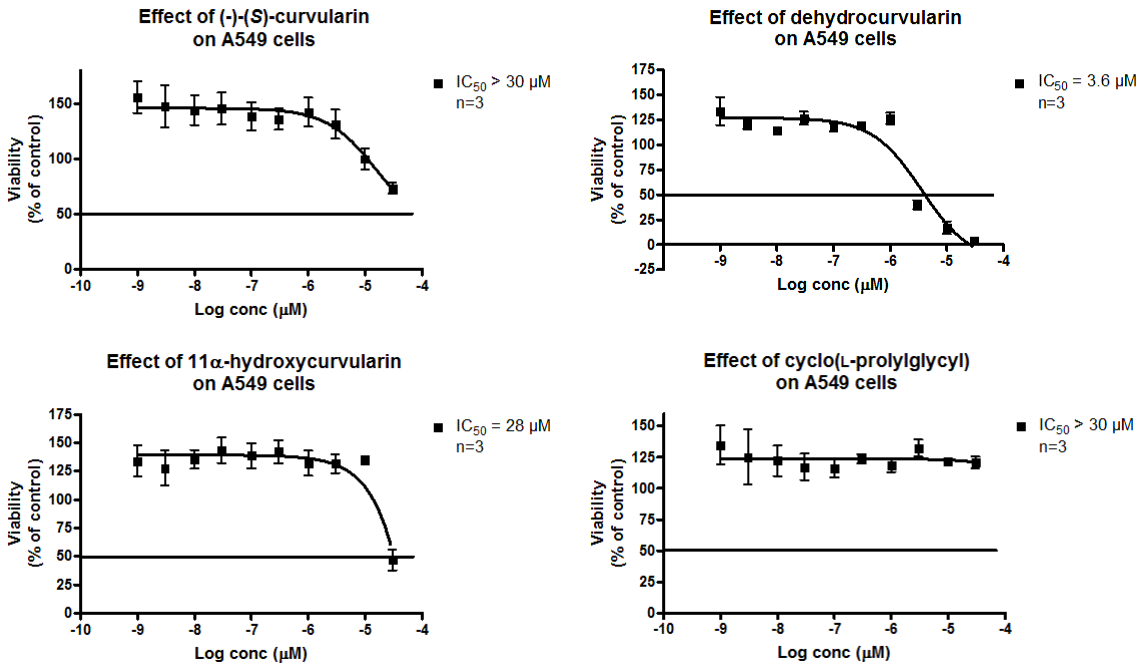

Figure 4.27: Dilution curves for the compounds isolated from *Curvularia australiensis* when tested against lung cancer (A549) cell line to determine their IC_{50} values.

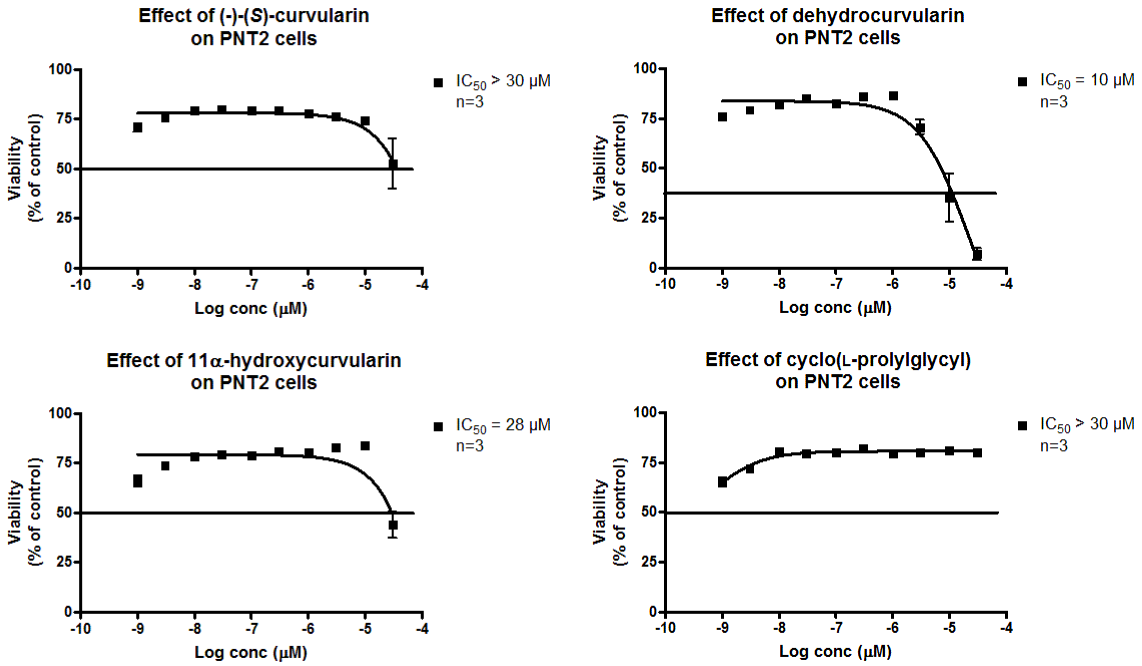

Figure 4.28: Dilution curves for the compounds isolated from *Curvularia australiensis* when tested against Human prostate normal (PNT2) cell line to determine their IC_{50} values.

Chapter 5: *Chaetomium subaffine*

5. *Chaetomium subaffine*

5.1. Introduction

5.1.1 Secondary metabolites isolated from *Chaetomium* spp

One of the largest genera of the family Chaetomiaceae (division Ascomycota) is *Chaetomium* (Zhang *et al*., 2012). There are more than 300 species that belong to this genus, from which, more than 200 secondary metabolites with wide bioactivity properties were isolated (Zhang *et al*., 2012, Li *et al*., 2015a). These metabolites belonged to different chemical classes including, chaetoglobosins, epipolythiodioxopiperazines, azaplilones, xanthones, anthraquinones, chromones, depsidones, terpenoids, and steroids. They exhibited antitumor, cytotoxic, antimalarial, enzyme inhibitory, antibiotic and other activities (Zhang *et al*., 2012).

Orsellides, globosumones A – C in addition to orsellinic acid and trichodion were isolated from the endophyte *Chaetomium globosum* that was obtained from the Mormon tea *Ephedra fasiculata* (Figure 5.1) (Bashyal *et al*., 2005). Globosumones A and B were found moderately active against four cancer cell lines, including non-small cell lung cancer (NCI-H460), breast cancer (MCF-7), central nervous system glioma (SF-268) and pancreatic carcinoma (MIA Pa Ca-2) (Bashyal *et al*., 2005). Moreover, antibacterial orsellides A – E, esters of orsellinic acid and 6-deoxyhexose, were isolated from *Chaetomium sp.* (Strain Gö 100/9), an endophyte from marine algae, in addition to the two known compounds globosumones A and B (Figure 5.1) (Schloerke and Zeeck, 2006). Furthermore, two mycotoxins, chaetoviridin A and chaetoglobosin F were isolated from *Chaetomium subaffine* (Figure 5.1) (Koyama *et al*., 1991). Three cytotoxic metabolites were also isolated from *Chaetomium sp.* obtained from the root of *Cymbidium goeringii* (Wang *et al*., 2017). These metabolites included the depsipeptide chaetomiamide A along with diketopiperazines chaetocochin A and C (Figure 5.1). These compounds were found to induce apoptosis in colon cancer cells. Furthermore, four spiro-azaplilone derivatives, cochliodones E – H, were isolated from *Chaetomium* sp. M336 that was obtained from *Huperzia serrata* (Figure 5.1). These cochliodones possessed antibacterial activities against *Escherichia coli*, *Staphylococcus aureus*, *Salmonella typhimurium* ATCC 6539 and *Enterococcus faecalis* (Yu *et al*., 2016). Moreover, 14 metabolites were isolated from *Chaetomium globosum* (Li *et al*., 2016). Some of these compounds inhibited the phytopathogenic fungi that cause root rot in

Panax notoginseng. The compounds flavipin, epicoccone, 3-methoxyepicoccone, epicoccolide A and epicoccolide B exhibited a significant 2,2-diphenyl-1-picrylhydrazyl (DPPH)-free radical scavenging activity while 3-methoxyepicoccone and epicoccolide B inhibited the enzyme acetylcholinesterase (Figure 5.1). In addition to that, nine metabolites were isolated from *Chaetomium gracile* (Bai *et al*., 2015). They included ergosterol, (22*E*,24*R*)-ergosta-7,22-diene-3*β*,5*α*,6*β*-triol, glycerol monopalmitate, eugenitol, *p*-hydroxybenzaldehyde, chaetochromin A, indole-3-carboxylic acid, adenosine and chaetoquadrin F, from which, chaetochromin A showed antibacterial activity against *Escherichia coli*, *Staphylococcu aureus*, and *Bacillus subtilis* (Figure 5.1). Additionally, three indole diketopiperazines, chaetocochins G, oidioperazines E and chetoseminudin E along with chetoseminudin C and N-acetyl-β-oxotryptamine were isolated from *Chaetomium* sp. 88194 (Figure 5.1) (Wang *et al*., 2015). Chaetocochins G exhibited a cytotoxic activity against the breast cancer cell line MCF-7.

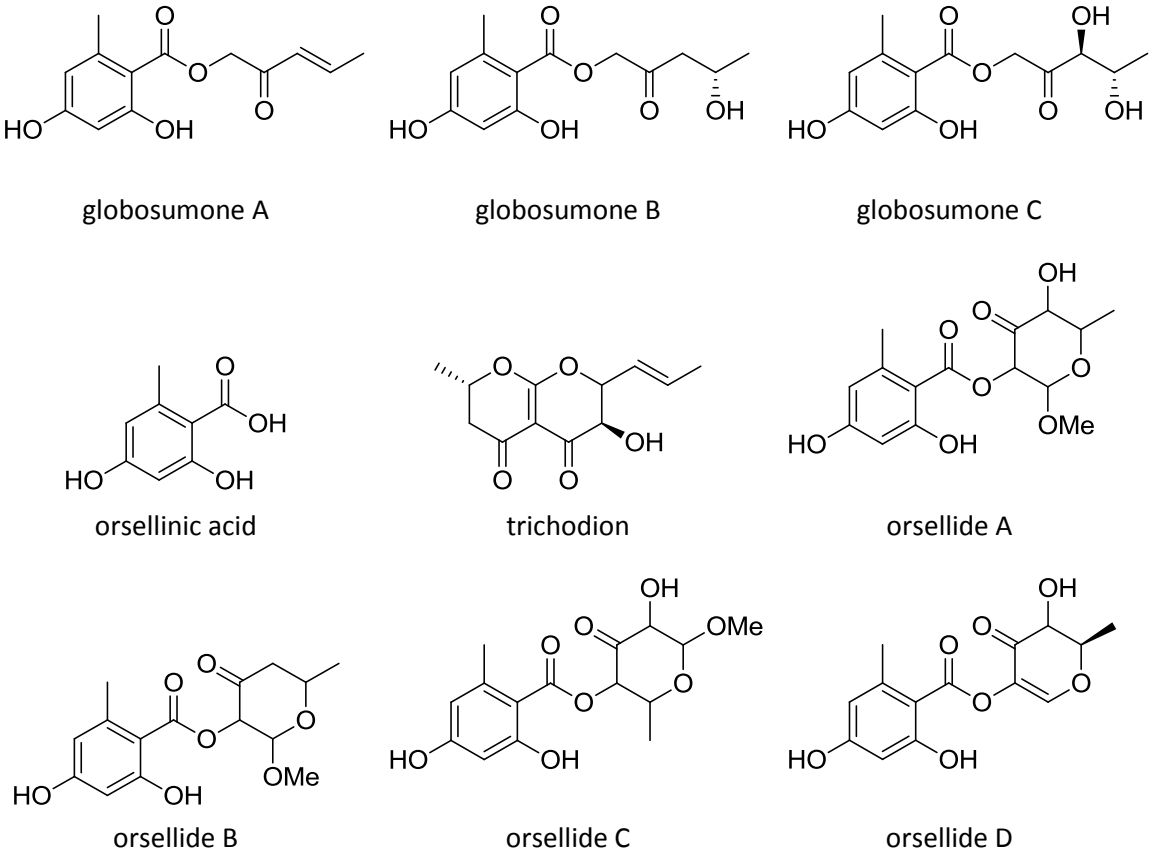

Figure 5.1: Secondary metabolites previously isolated from *Chaetomium* spp.

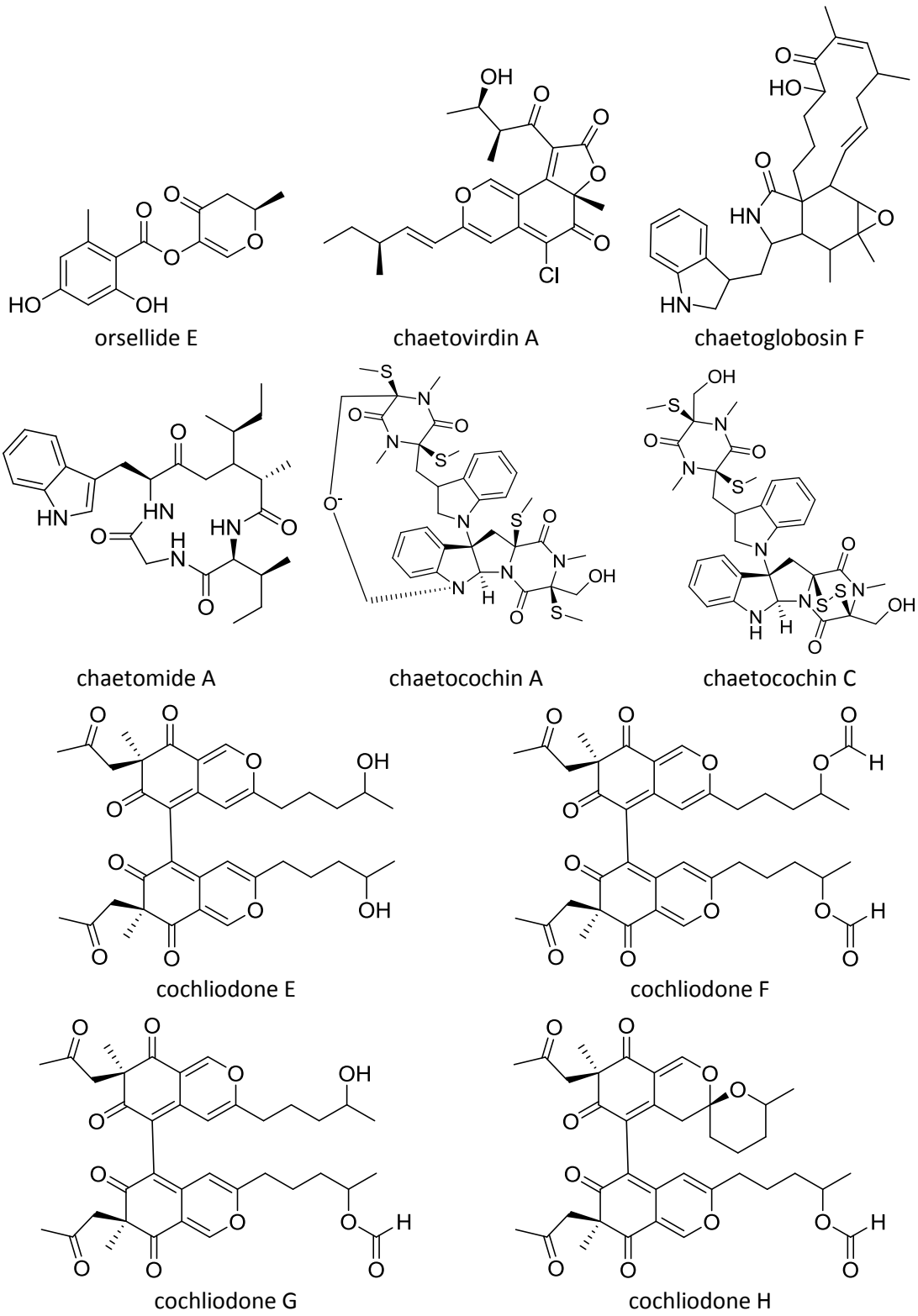

Figure 5.1 (continued): Secondary metabolites previously isolated from *Chaetomium* spp.

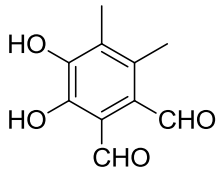

flavipin

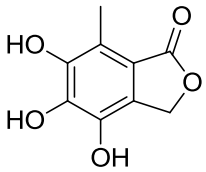

epicoccone

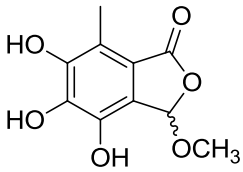

3-methoxyepicoccone

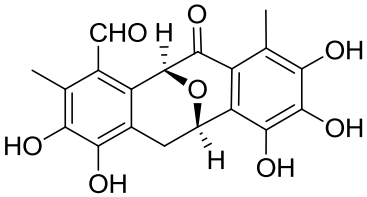

epicoccolide A

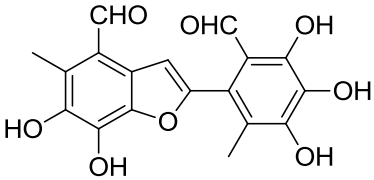

epicoccolide B

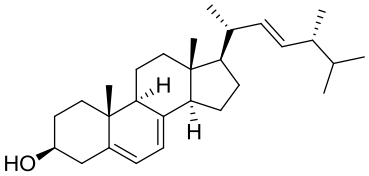

ergosterol

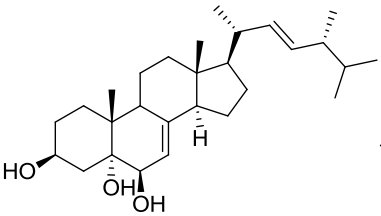

(22*E*,24*R*)-ergosta-7,22-diene-3*β*,5*α*,6*β*-triol

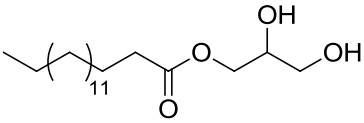

glycerol monopalmitate

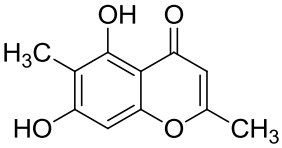

eugenitol

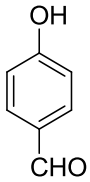

p-hydroxybenzaldehyde

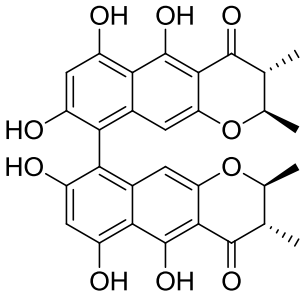

chaetochromin A

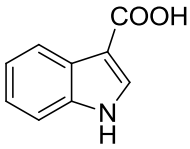

indole-3-carboxylic acid

Figure 5.1 (continued): Secondary metabolites previously isolated from *Chaetomium* spp.

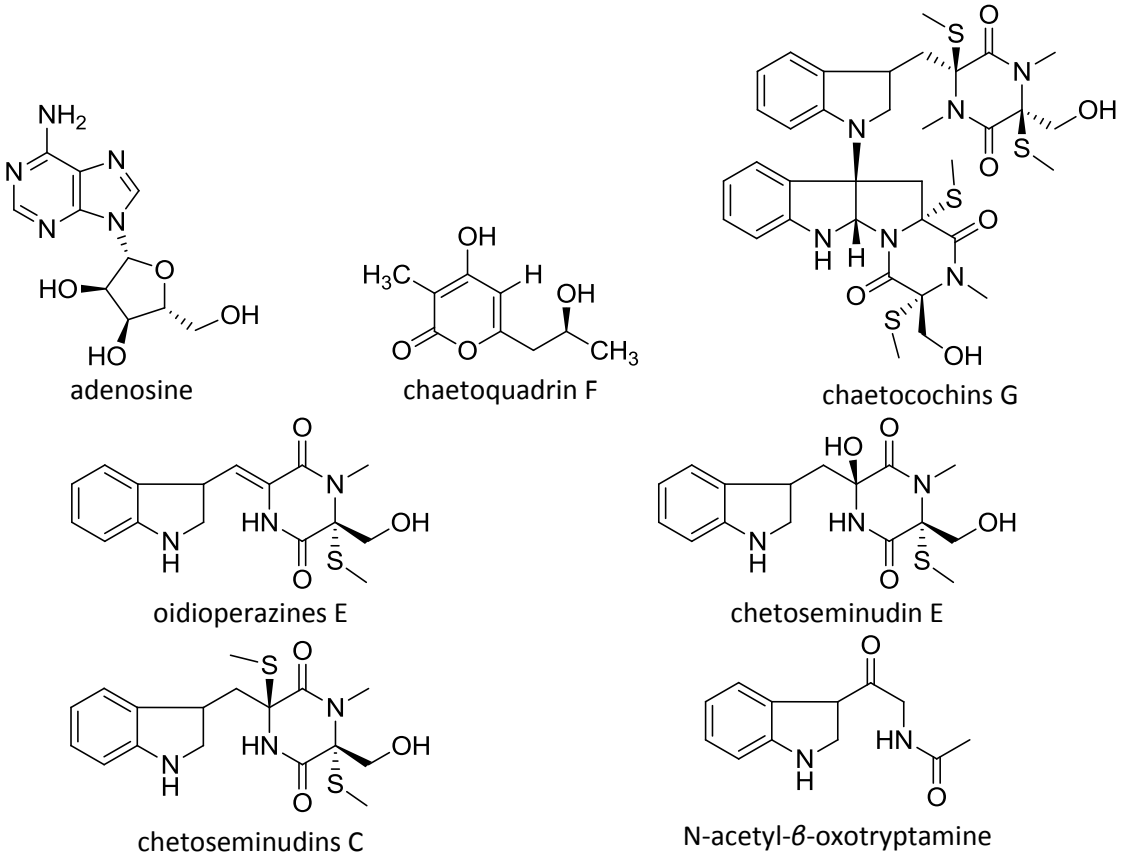

Figure 5.1 (continued): Secondary metabolites previously isolated from *Chaetomium* spp.

5.2 Medium optimisation to select the most suitable conditions for culturing *Chaetomium subaffine*, medium-scale fermentation

As shown in Table 5.1, the solid-rice medium gave higher yields than those of the liquid-Wickerham cultures, indicating better growth, which, in turn, suggested that the rice medium was a more suitable medium for scaling-up *Chaetomium subaffine.*

Table 5.1: Weights of *Chaetomium subaffine* extracts cultured in two types of media harvested at various incubation periods.

Medium	Incubation period (days)	Weight of extract (mg) per 100 mL (liquid) or 100 g (solid)
Liquid-Wickerham	7	17
Liquid-Wickerham	15	20
Liquid-Wickerham	30	30
Solid-Rice	7	348
Solid-Rice	15	391
Solid-Rice	30	421

Insights into the chemical composition of the respective extracts were deduced from their ^{1}H NMR and LC-HRMS data. The poor growth of the endophyte in the liquid cultures was confirmed by the ^{1}H NMR data (Figure 5.2). As depicted by the red boxes in the figure, most of the liquid-Wickerham medium peaks remained in the extract of the endophyte even after 30 days of incubation. This suggested the poor consumption of medium nutrients by the fungus, and hence, the poor growth and production of metabolites. However, this was not the case when the endophyte was incubated in the solid-rice medium (Figure 5.3), where a new set of aromatic peaks can be detected after 15 and 30 days of incubation (blue box). This set of aromatic peaks was referred to the aromatic protons of cochliodinol and its derivatives, amongst the major compounds that were later isolated from *Chaetomium subaffin*e.

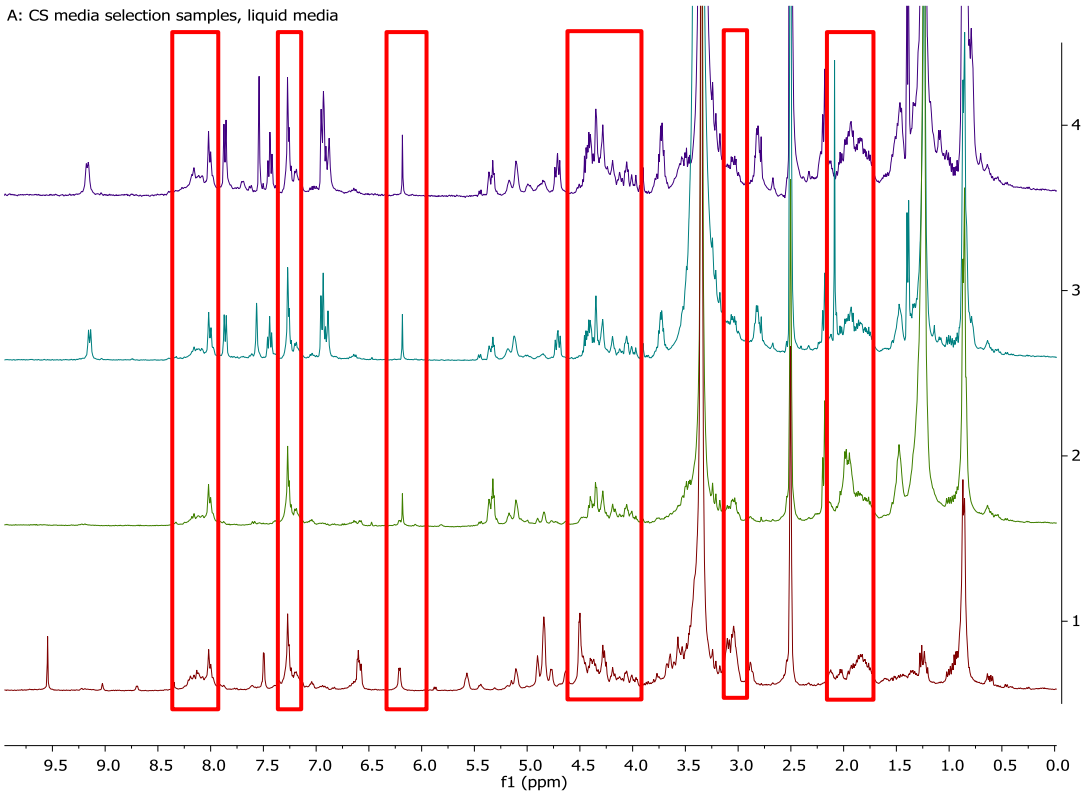

Figure 5.2: The ^{1}H NMR (400 MHz) data obtained from *Chaetomium subaffine* extracts after incubation in liquid-Wickerham medium. Spectrum 1 is the medium blank, 2 is 7 days incubation, 3 is 15 days and 4 is 30 days, measured in DMSO-d_6.

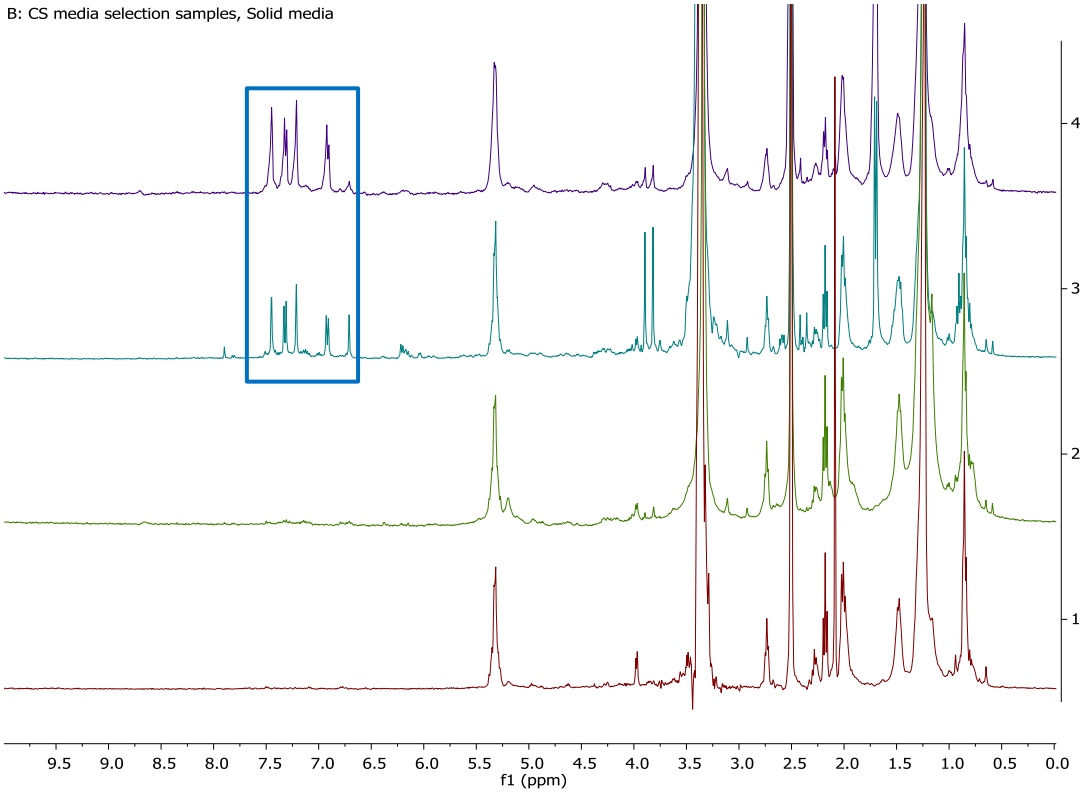

Figure 5.3: The ^{1}H NMR (400 MHz) data obtained from *Chaetomium subaffine* extracts after incubation in solid-rice medium. Spectrum 1 is the medium blank, 2 is 7 days incubation, 3 is 15 days and 4 is 30 days, measured in DMSO-d_6.

The ^{1}H NMR data gave only an indication of the major compounds of the respective extracts. A more detailed representation of the chemical composition of each of the extracts was construed from the LC-HRMS data. Scatter plots (Fig 5.4) of the LC-HRMS data confirmed the ^{1}H NMR findings. As shown by the scatter plots, the chemical composition of the 7 day-extract in liquid-Wickerham media was richer and more diverse than the extracts that were obtained after longer periods of incubation. This was indicated by the scattering pattern that is skewed in favour of the 7 days of incubation. This illustrated that the liquid-Wickerham medium remained more chemically complex and rich than the actual *Chaetomium subaffine* extracts.

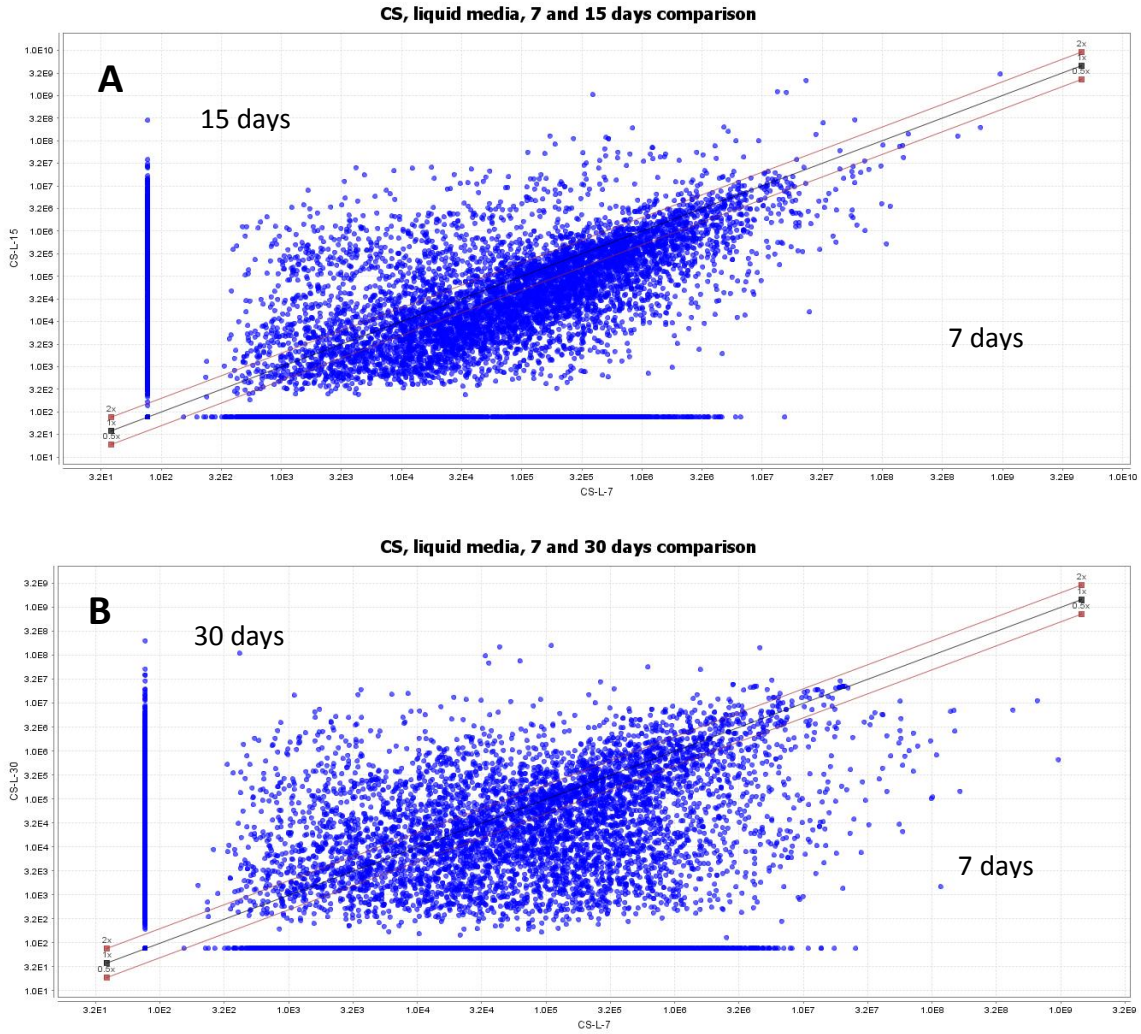

Figure 5.4: Scatter plots of the LC-HRMS data of *Chaetomium subaffine* extracts obtained at different incubation periods in liquid-Wickerham medium, (A): comparing 7 with 15 days and (B): 7 with 30 days of incubation.

On the other hand, it is totally the opposite in the case of the solid-rice medium, where incubating the endophyte for 15 and 30 days gave chemically richer extracts (Figure 5.5). This was confirmed by the obvious increase in the density of the scattering towards longer incubation periods.

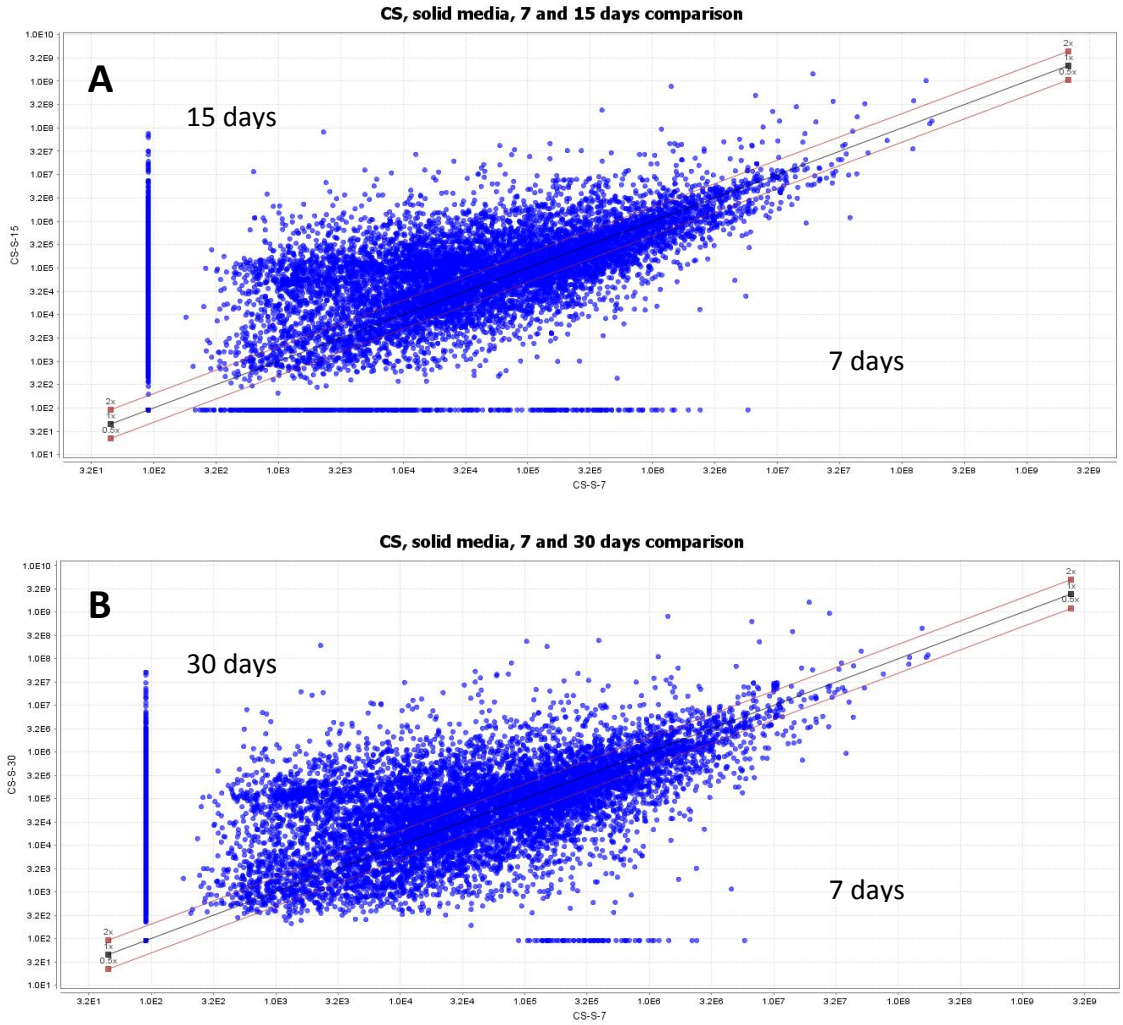

Figure 5.5: Scatter plots of the LC-HRMS data of *Chaetomium subaffine* extracts obtained at different incubation periods in solid-rice medium, comparing (A): 7 with 15 days and (B): 7 with 30 days of incubation.

An increased chemical diversity of the fungal metabolites in the solid-rice medium is illustrated in Figure 5.6. The scatter plot compared the production of the metabolites after 30 days of incubation in solid-rice medium to the same period of incubation in liquid-Wickerham medium. Not only the plot of 30 days of incubation in the solid-rice medium exhibited higher loadings, but also increased in scattering than the plot of 30 days of incubation in liquid-Wickerham medium. Thus, the fungal extract produced in a solid-rice medium after 30 days of incubation was more diverse and rich in terms of chemistry.

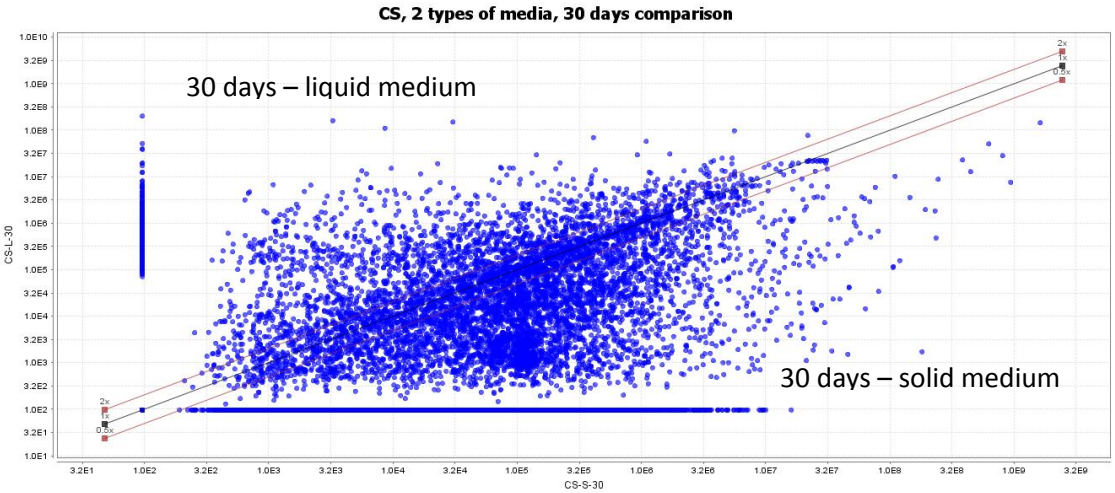

Figure 5.6: Scatter plot of LC-HRMS data of *Chaetomium subaffine* extracts, comparing 30 days of incubation in solid-rice medium to liquid-Wickerham medium.

Moreover, this explained the clustering pattern that was observed in the scores plot of the principal component analysis (PCA) of the LC-HRMS data of the different extracts (Figure 5.7). The red circle contained the more chemically diverse samples that clustered together, while the less chemically diverse samples are presented as outliers in the plot.

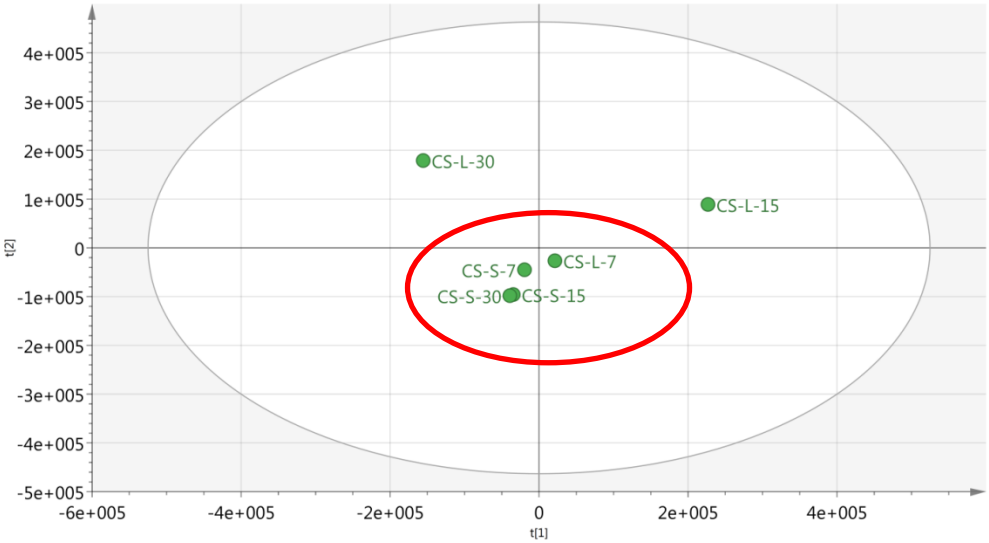

Figure 5.7: Scores plot based on the PCA of the LC-HRMS data for the various *Chaetomium subaffine* extracts. "CS" refers to the endophyte *Chaetomium subaffine*. The letter "S" is for the solid-rice medium and "L" is for the liquid-Wickerham medium. While the numbers "7, 15, and 30" indicate the incubation period. R2X=0.777, Q2=0.416.

The last parameter that was taken into consideration before choosing the most suitable fermentation conditions for the scale-up was the *in-vitro* biological activity of the extract against both breast cancer (ZR-75) and lung cancer (A549) cell lines (Figure 5.8).

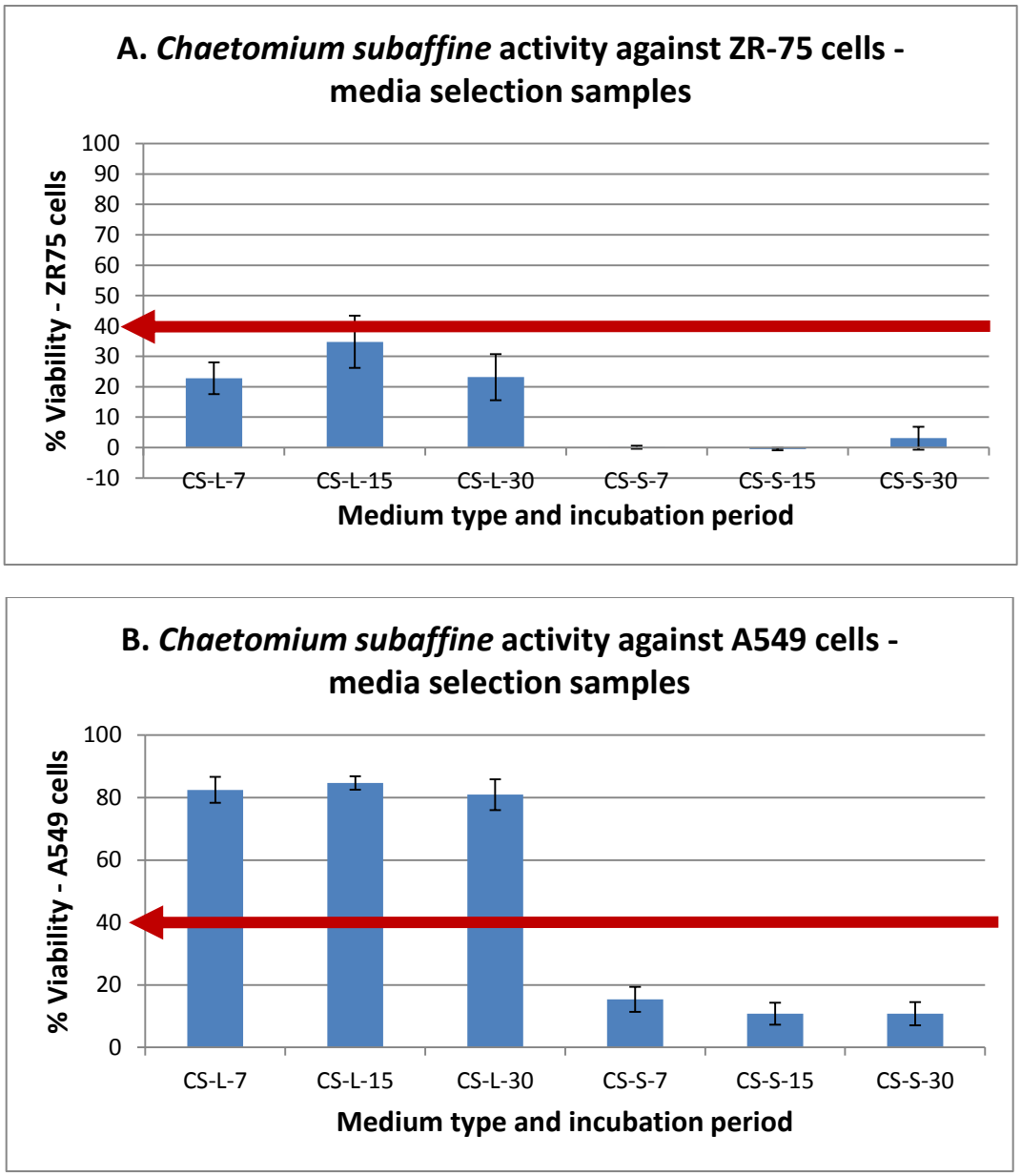

Figure 5.8: The biological activity of *Chaetomium subaffine* extracts at 30 µg/mL against (A): breast cancer (ZR-75) cell line and (B): lung cancer (A549) cell line. "CS" refers to the endophyte *Chaetomium subaffine*. The letter "S" is for the solid-rice medium and "L" is for the liquid-Wickerham medium. The numbers "7, 15, and 30" indicate the incubation period in days. The red line indicates the bioactivity threshold.

Causing cell viability on the cancer cells of less than 40%, all extracts were found active against ZR-75 cell line (Figure 5.8.A). However, the extracts obtained from the solid-rice media were more active as the cell viability was decreased to less than 10% for the three incubation periods, while the liquid-Wickerham samples exhibited 20% to 30% cell viability. However, against the A549 cell line, only the samples of the solid-rice media were active with less than 20% viability for the cells, while the liquid medium samples failed to give any decent cell growth inhibition.

To conclude, depending on both the chemistry and the biological activity, culturing the endophyte in solid-rice medium for either 15 or 30 days were the best options for the scale-up, with the richest chemical composition and the strongest biological activity. Nevertheless, 30 days of incubation was chosen for the large-scale fermentation because of the higher yield it provided.

5.3 Large scale fermentation and first fractionation of the extract of *Chaetomium subaffine*

Fifteen flasks were prepared for the large-scale fermentation. Each flask was prepared as described in 2.3.2.2. After 30 days of incubation, the mycelia were extracted with ethyl acetate as described in 2.3.2.5. The weight of the obtained total ethyl acetate extract was 39.4196 g. After liquid-liquid partitioning, the weight of the dried hexane extract was 12.1830 g, while the dried aqueous methanolic extract was 25.5970 g.

The polar methanolic extract was fractionated by gradient flash chromatography through a Büchi system as described in 2.5.2.3. A normal phase VersaPak^{TM} (48 g), spherical silica (20-45 µm) column was used with a flow rate of 100 mL/min. The mobile system is detailed in Table 5.2. The fractions were collected in conical flasks, as 100 mL of each and then pooled using TLC. A total of 12 fractions were obtained (Figure 5.9 and Table 5.3).

Table 5.2: Mobile phase used for the first fractionation of the polar extract of the endophyte *Chaetomium subaffine.*

Time (min)	% Hex	% EtOAc	% MeOH
0	100	0	0
10	100	0	0
70	0	100	0
75	0	100	0
105	0	50	50
120	0	50	50

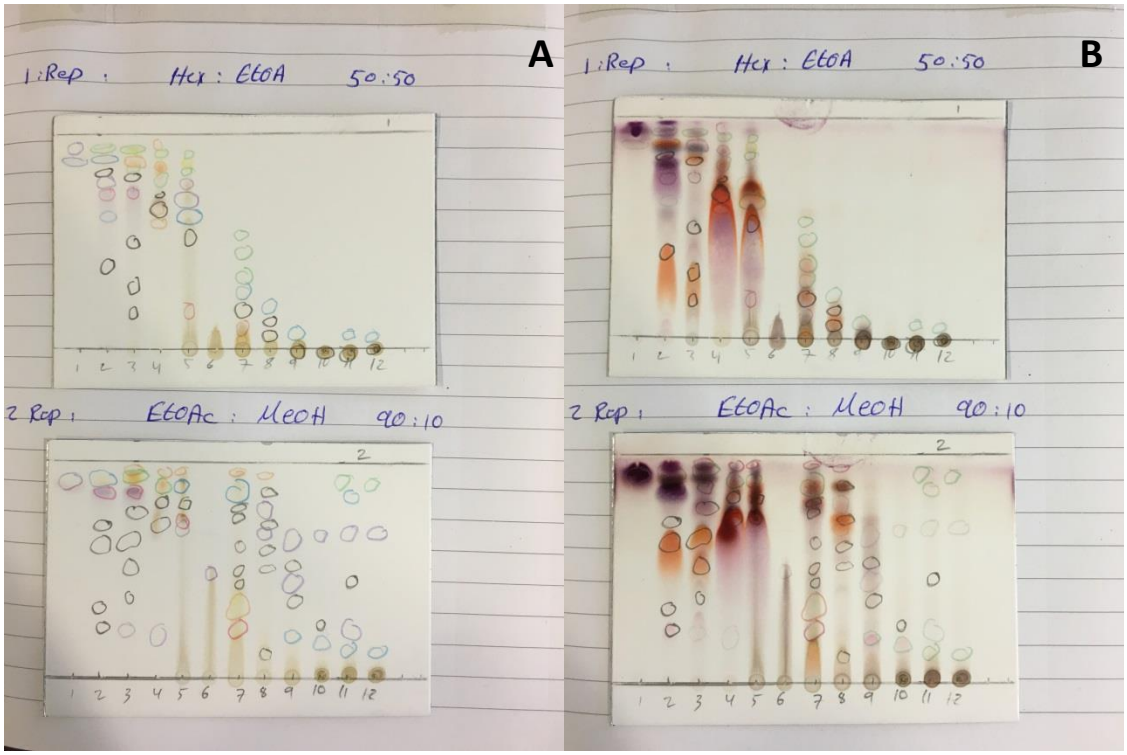

Figure 5.9: Summary TLC plates for the first fractionation step (H.n) of *Chaetomium subaffine,* (A): before and (B): after spraying with anisaldehyde spraying agent.

Table 5.3: Weights of fractions obtained from the first chromatographic fractionation of the methanolic extract of *Chaetomium subaffine*.

Fraction	Weight (mg)
H.1	28.5
H.2	113.2
H.3	84.8
H.4	2819.1
H.5	1705.2
H.6	3192.0
H.7	2895.7
H.8	4164.1
H.9	3807.8
H.10	2175.1
H.11	245.9
H.12	181.7

The fractions were subjected to ^{1}H NMR spectroscopy (Figure 5.10). Fractions H.1 to H.3 composed mainly of saturated fatty acids indicated by the presence of methylene resonances of an aliphatic chain observed at δ_H 1.00 – 1.50 along with α-proton signals at δ_H 2.00 – 2.40 (red box). However, fractions H.2 and H.3 were richer in unsaturated fatty acids indicated by the olefinic proton signals at δ_H 5.00 – 6.50 (orange box). In addition to that, the spectrum also possessed signals for the metabolite acremonisol A that was later isolated from fraction H.4. These were two methyl singlets at δ_H 4.00 that corresponded to the two methoxyl moieties of acremonisol A (green box). The characteristic peaks for the major compound, cochliodinol as detected in the crude extract were exhibited in the spectrum of fraction H.6 from which the compound was later purely isolated (blue box). Fractions H.7, H.8 and H.10 were considered to yield the most chemically interesting and diverse compounds. This was revealed by the complex spectrum where peaks were detected, particularly in the aromatic region, δ_H 6.00 – 9.00 (black boxes). The compounds of these fractions were also deemed to be glycosidic for peaks observed at δ_H 3.50 – 6.00 (grey boxes), characteristic signals for oxygenated protons of sugar units.

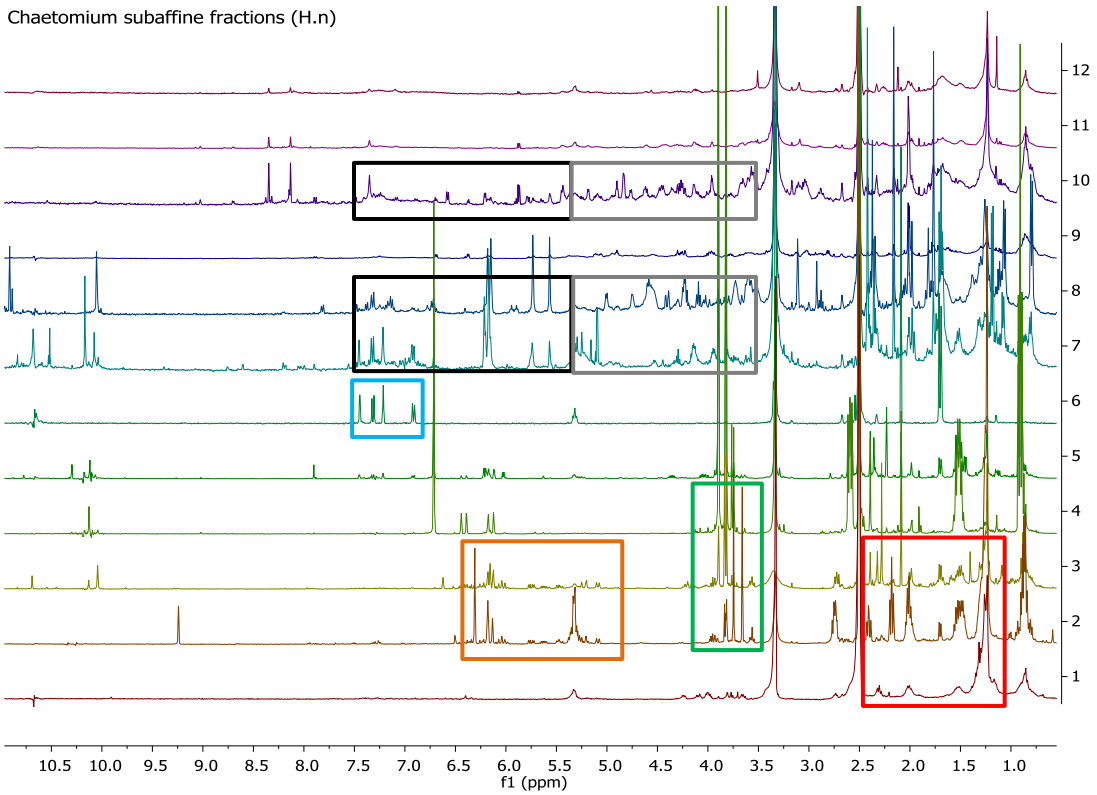

Figure 5.10: The ^{1}H NMR (400 MHz) data obtained from the first chromatographic fractionation of *Chaetomium subaffine* (H.n). Numbers on Y-axis indicate respective fractions. 5 mg of each sample was dissolved in DMSO-d_6.

Each of the fractions along with the hexane extract was again assayed against breast and lung cancer cell lines (Figure 5.11). Fractions H.5, H.6, H.7 and H.8 were found active against breast cancer cell line. However, more fractions exhibited activity against the lung cancer cell line, which included H.3, H.5, H.6, H.7, H.8, and H.9 along with the hexane extract.

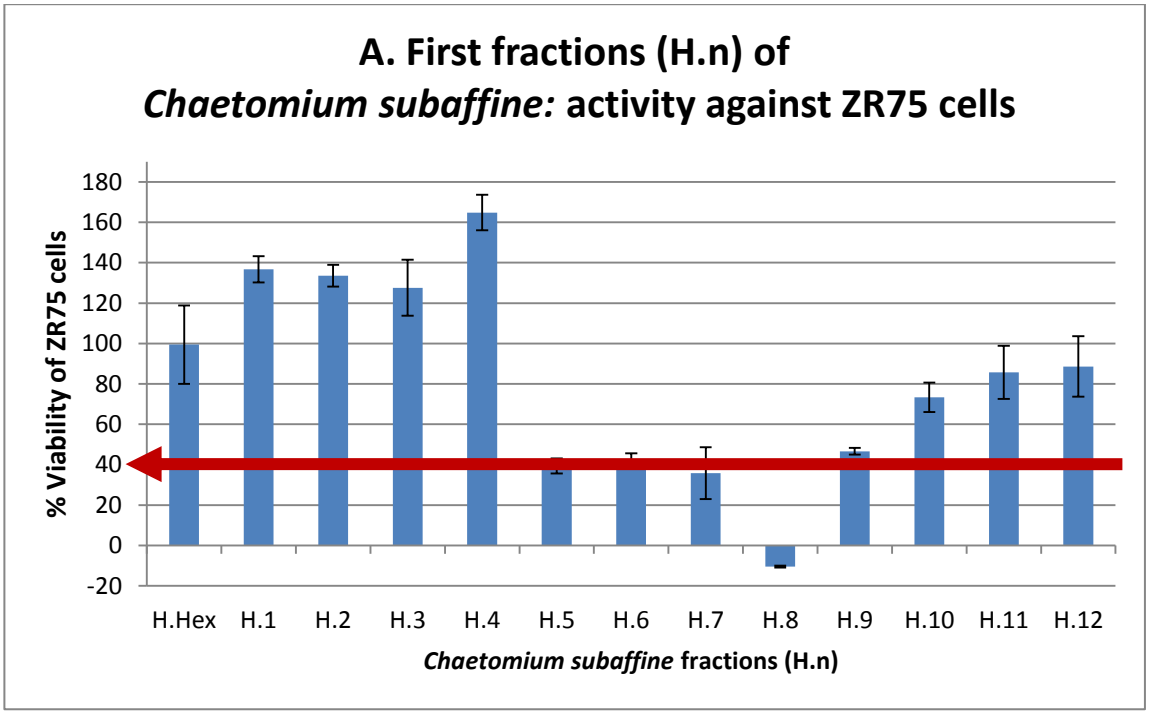

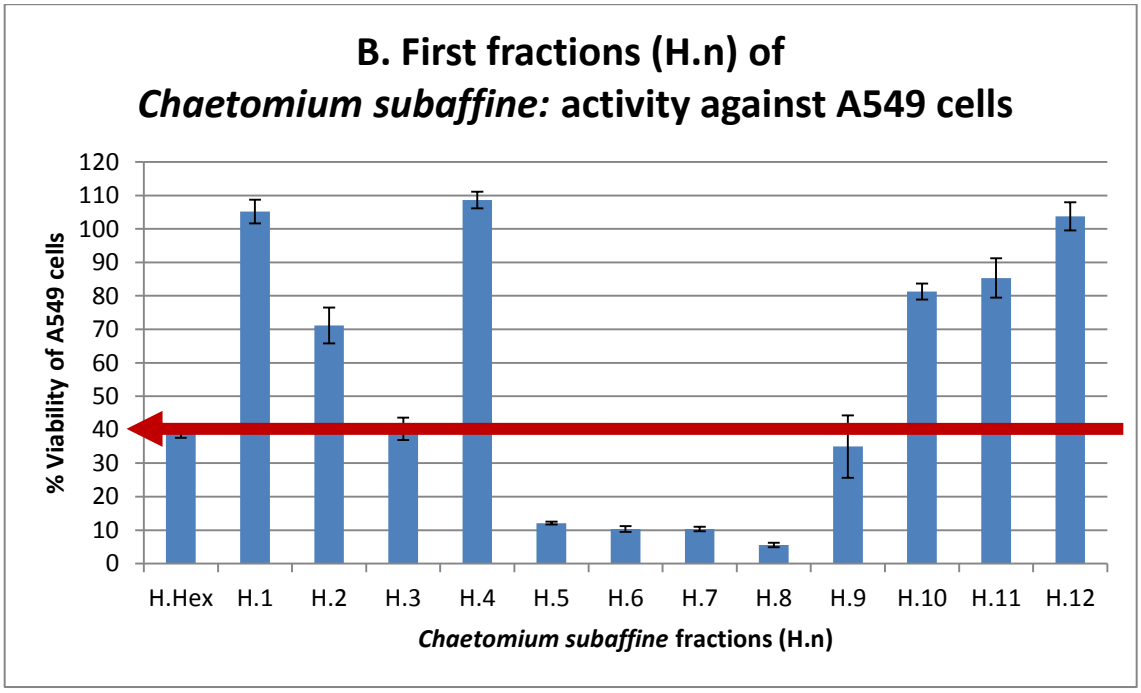

Figure 5.11: Biological activity for first fractions of *Chaetomium subaffine* (H.n) at 30 µg/mL against (A): breast cancer (ZR-75) and (B): lung cancer (A549) cell lines. The red line indicates the bioactivity threshold.

5.4 The creation of metabolomics-bioassay guided approach to pinpoint the bioactive metabolites of *Chaetomium subaffine* at the initial chromatographic separation step

For targeting the bioactive metabolites against breast cancer (ZR-75) cell line, the active fractions H.5, H.6, H.7 and H.8 were grouped together apart from the inactive fractions (Figure 5.12.A). However, as H.6 was closer to the inactive fractions and affecting both the fitting and predictive ability of the model (Permutation test: R2=0.80, Q2=0.28, R2Y=0.798 and Q2Y=0.0298), it was excluded and a new model was created (Figure 5.12.B). A permutation test was performed to test the validity of the model (Figure 5.13). R2 and Q2 values improved to 0.98 and 0.38, respectively, while the R2Y intercept was 0.832 and Q2Y intercept was 0.11. These values indicated excellent fitting as the R2 value is very close to 1. Furthermore, the prediction of this model was quite low at a Q2 value of 0.38. The quite huge difference between R2 and Q2 values could indicate that the model was "overfitted". The Q2Y value at 0.11 obtained from the permutation test is greater than zero. So, the result of the test does challenge the validity of the model, which could have been affected by the imbalanced number of samples between the active and inactive groups. The difference between R2Y and Q2 was 0.452 which is greater than 0.3, which may indicate the weakness of the model.

An S plot was generated from the OPLS-DA model (Figure 5.14). The "endpoint" target bioactive metabolites were found left of the Y-axis as shown in Figure 5.14.A. Those metabolites were dereplicated and listed in Table 5.4.

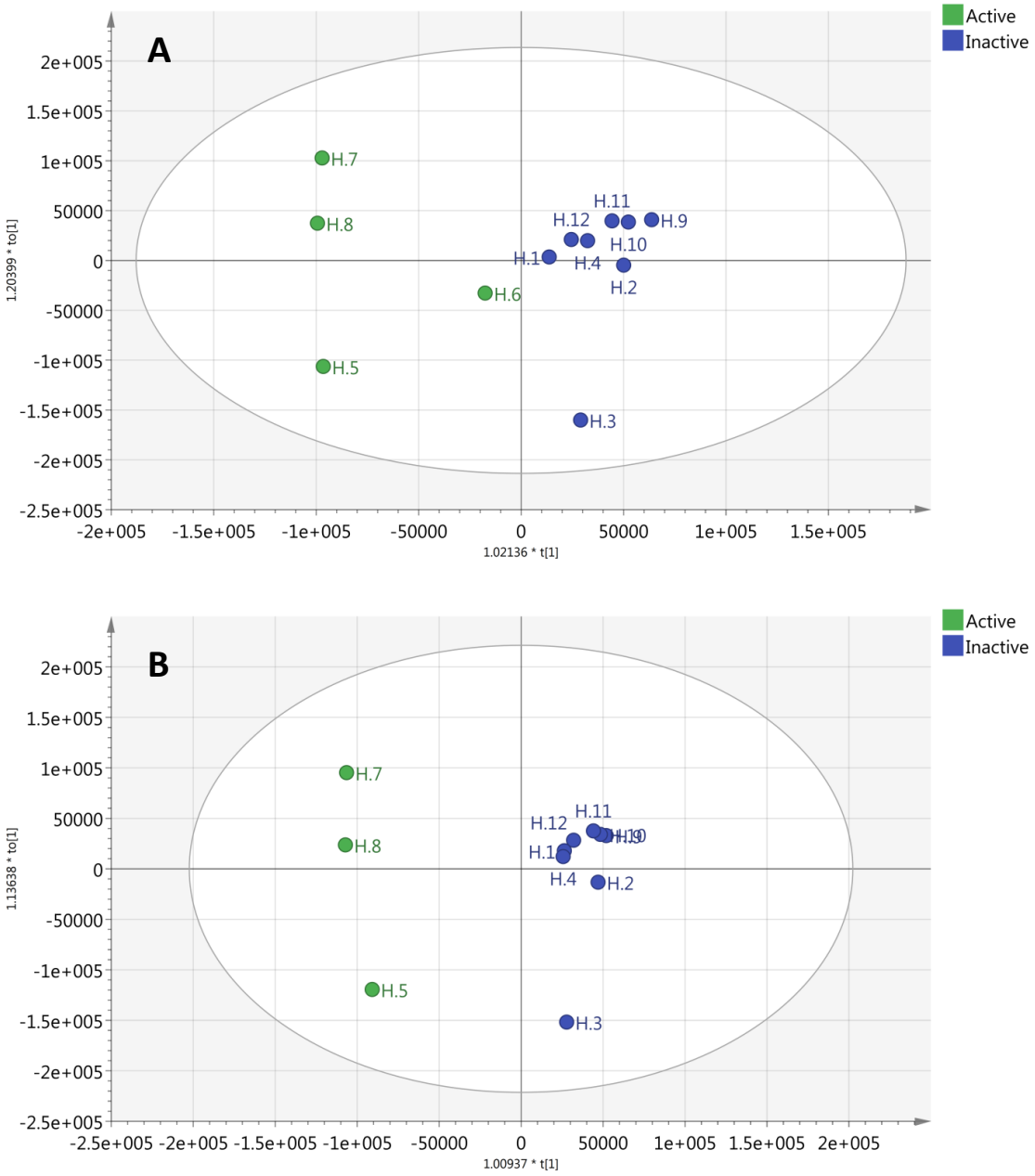

Figure 5.12: Scores plots of *Chaetomium subaffine* (H.n) fractions. Samples were grouped into active (green) and inactive (blue) according to their activity against breast cancer (ZR-75) cell line. (A): H.6 included in the model, R2X=0.293, R2Y=0.844, Q2=0.283. (B): H.6 excluded from the model, R2X=0.301, R2Y=0.976, Q2=0.378.

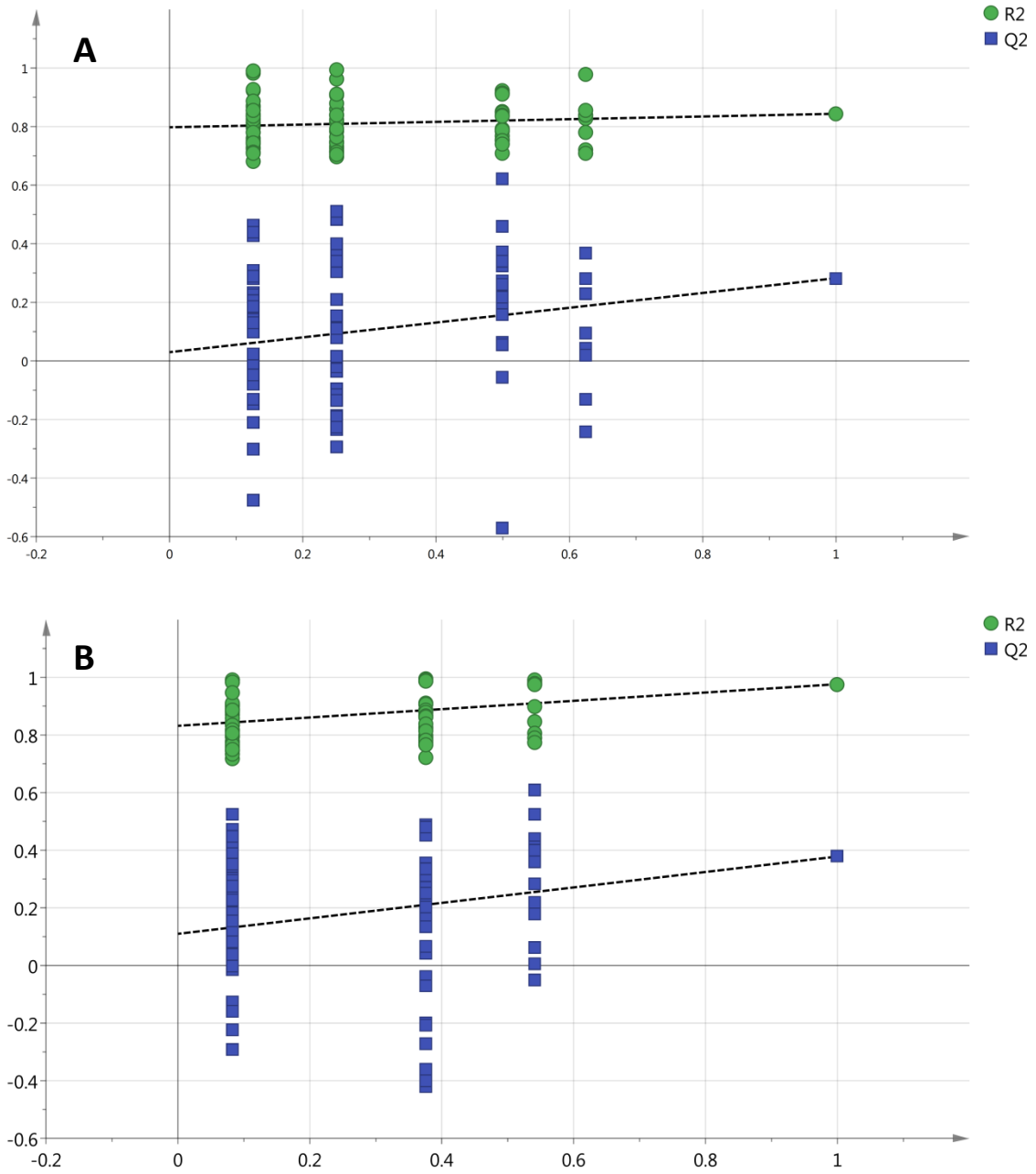

Figure 5.13: Permutation tests (100 permutations) for *Chaetomium subaffine* (H.n) fractions for the OPLS-DA model of their activity against breast cancer (ZR-75) cell line. (A): H.6 included in the model, (B): H.6 excluded from the model.

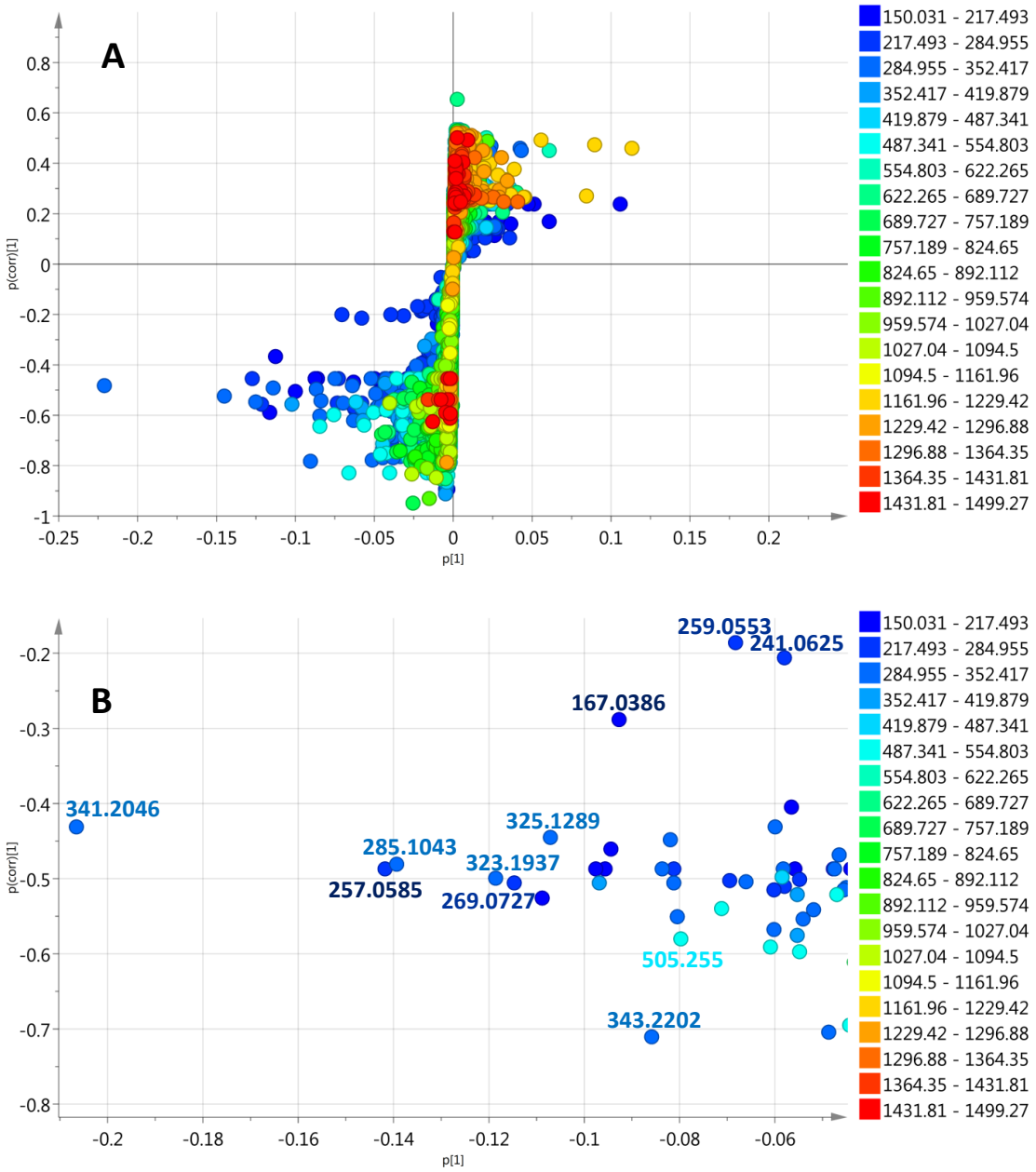

Figure 5.14: (A): S plot for *Chaetomium subaffine* (H.n) fractions acquired from an OPLS-DA model (Figure 5.12.B) for their activity against the breast cancer (ZR-75) cell line. (B): expanded view for the extreme left metabolites, the isolated metabolites and the outliers are labelled by their *m/z* value.

Table 5.4: Dereplication of target bioactive metabolites against both breast cancer (ZR-75) and lung cancer (A549) cell lines as predicted by OPLS-DA loadings S-plots. Highlighted rows represent compounds that were isolated from the fungal extracts.

t_R (min)	MZMine ID	*m/z*	Predicted Molecular formula	Fraction yielding highest peak intensity	Peak intensity	MWt	Name	Source
5.39	N_6276	285.1043	$C_{19}H_{14}N_2O$ $C_7H_{18}N_4O_8$	H.8	1.10E+09	286.1116	unknown	unknown
6.40	N_7410	269.0727	$C_{18}H_{10}N_2O$ $C_6H_{14}N_4O_8$	H.7	6.76E+08	270.0800	unknown	unknown
6.41	P_9469	258.1336	$C_{12}H_{19}NO_5$	H.8	1.7E+08	257.1263	5-hydroxy-3-methyl-2-pentenoic acid; (E)-form, Ac, (3-carboxypropyl)amide	mangrove-derived *Pestalotiopsis sp.* JCM2A4
							5-hydroxy-3-methyl-2-pentenoic acid; (E)-form, Ac, [3-(methoxycarbonyl)ethyl] amide	mangrove-derived *Pestalotiopsis sp.* JCM2A4
7.37	N_7411	167.0386	$C_{11}H_6NO$	H.7	5.64E+08	168.0459	unknown	unknown
7.41	P_2931	151.0390	$C_8H_6O_3$	H.7	51056203	150.0317	4-hydroxy-1,3-benzenedicarboxaldehyde	*Eriostemon myoporoides.* Isol. from *Heterobasidion annosum*

							8-hydroxy-2-octene-4,6-diynoic acid; (E)-form	*Camarophyllus virgineus* (snowy wax cap)
7.43	N_3320	283.0888	$C_{19}H_{12}N_2O$ $C_7H_{16}N_4O_8$	H.7	2.5E+08	284.0960	unknown	unknown
11.75	N_6030	325.1289	$C_{16}H_{22}O_7$	H.5	3.83E+08	326.1362	cyclocalopin A; 15-Methoxy	*Boletus calopus*
							3,4-dihydro-4,8-dihydroxy-3-(2-hydroxypentyl)-6,7-dimethoxy-1H-2-benzopyran-1-one; (3R,4R,10R)-form	*Colletotrichum* sp. CRI535-02 and *Microdochium bolleyi* strain 8880
							macrosphelide A; 9-Deoxy	*Microsphaeropsis sp*. FO-5050
							macrosphelide A; 4-Epimer, 9-deoxy	*Periconia byssoides* isol. from *Aplysia kurodai*
							macrosphelide A; 4-Epimer, 15-deoxy	*Periconia byssoides* isol. from *Aplysia kurodai*
							phomaligol A; Ac	a marine-derived *Purpureocillium lilacinum*

12.07	N_2668	341.2046	$C_{12}H_{30}N_4O_7$	H.9	3.01E+09	342.2118	unknown	unknown
12.08	P_9468	307.1901	$C_{18}H_{26}O_4$	H.8	2.54E+08	306.1828	7-(2-butenyl)-3,4-dihydro-6,8-dihydroxy-3-(3-pentenyl)-1H-2-benzopyran-1-one; (2''E,3R,3'E)-form, 2'',3',3'',4'-Tetrahydro	*Geotrichum sp.* isol. from *Crassocephalum crepidioides*
							ML 236A	*Eupenicillium javanicum* IFM 52670 and *Penicillium citrinum Sank* 18767
							ML 236A; 8-Deoxy, 3,5-dihydro, 3-oxo	*Eupenicillium javanicum* IFM 52670
							trisporic acid C	*Blakeslea trispora* and *Mucor mucedo*
							trisporic acid C; 9Z-Isomer	*Blakeslea trispora*
12.33	N_13669	339.1886	$C_9H_{20}N_{14}O$ $C_{13}H_{24}N_8O_3$ $C_{12}H_{28}N_4O_7$	H.8	1.24E+08	340.1959	unknown	unknown
13.17	N_1915	343.2202	$C_{13}H_{28}N_8O_3$	H.8	1.58E+08	344.2275	unknown	unknown
14.08	N_1761	221.0798	$C_{11}H_7ClO_3$	H.3	3.67E+08	222.0077	2-phenyl-4H-pyran-4-one; 3'-chloro, 5'-	*Polyporus sp.* PSU-ES44

							hydroxy	
14.08	N_1763	264.9914	$C_{12}H_7ClO_5$	H.3	3.21E+08	265.9987	8-chloro-2,3,5,6,7,8-hexahydro-5,6,7-trihydroxy-2,2-dimethyl-4H-1-benzopyran-4-one; (5R*,6R*,7S*,8S*)-form, 5-Me ether	a mangrove-derived *Pestalotiopsis sp.* PSU-MA69
14.09	N_1759	219.0033	$C_7H_2N_5O_4$	H.3	5.68E+08	220.0106	unknown	unknown
14.09	N_1760	262.9943	$C_8H_2N_5O_6$	H.3	4.91E+08	264.0016	unknown	unknown
14.53	N_6028	257.0585	$C_{12}H_{15}ClO_4$	H.5	1.10E+09	258.0657	acremine O	a marine-derived *Acremonium persicinum*
							acremonisol A; 3-Chloro-4,6-dihydroxy-2-propylbenzoic acid; Di-Me ether	a marine-derived *Acremonium sp.* (strain 273/H3 09) and *Chaetomium globosum* SNB-GTC2114
14.53	N_6029	213.0686	No predicted formula	H.5	5.22E+08	214.0759	unknown	unknown
14.53	N_6032	259.0553	$C_7H_{10}N_5O_6$ $C_6H_{14}NO_{10}$	H.5	3.61E+08	260.0625	unknown	unknown
14.53	N_6034	215.0656	$C_6H_{10}N_5O_4$	H.5	1.7E+08	216.0729	unknown	unknown

14.60	P_2090	241.0625	$C_{12}H_{13}ClO_3$	H.4	8.43E+08	240.0553	No hits produced by fungi	No hits produced by fungi
14.62	P_6279	367.2107	$C_{20}H_{30}O_6$	H.7	1.48E+08	366.2034	botcinin A; Deacetoxy, 3,4-didehydro	*Botrytis cinerea* AEM 211
							botryslactone; 1,2R,3,4-Tetrahydro, 4S-acetoxy	*Botrytis cinerea*
							gibberellin A42	*Gibberella fujikuroi*
							9,12,13,16,17-pentahydroxy-11-kauranone; (ent-12β,16βOH)-form, 17-Aldehyde	*Punctularia atropurpurascens*
							3,8,15-Scirpenetriol; (3α,8α)-form, 3-O-(3-Methylbutanoyl)	*Fusarium sporotrichioides*
							1,7,17-Trihydroxy-15-oxo-19-kauranoic acid; (ent-1β,7α,16βH)-form	*Geopyxis sp.* AZ0066 isol. from *Pseudevernia intensa*
14.65	N_7414	279.2028	$C_{11}H_{28}N_4O_4$	H.7	1.78E+08	280.2100	unknown	unknown
14.67	N_7409	383.2162	$C_{16}H_{34}NO_9$	H.7	4.77E+08	384.2235	unknown	unknown
15.59	N_5526	347.1942	$C_{15}H_{24}N_8O_2$	H.7	1.2E+08	348.2015	unknown	unknown
15.87	N_3071	323.1937	$C_{18}H_{28}O_5$	H.7	7.62E+08	324.1934	cytosporone A; 1'-	*Pestalotiopsis sp,* an

							Alcohol, 1'-Me ether, Me ester	endophytic fungus from *Taxus brevifolia*
								Dothiorella sp. HTF3
							2,4-dihydroxy-6-(6-hydroxyheptyl)benzoic acid; (R)-form, 2-methylpropyl ester	*Lasiodiplodia theobromae*
							14,18-dihydroxy-12-oxo-9,13,15-octadecatrienoic acid; (9Z,13Z,15E)-form	*Cantharellus cibarius*
							5,14-epoxy-5,7,8-marasmanetriol; (5β,7β,8β)-form, 5-Me ether, 8-Ac	*Lactarius piperatus*
							5,14-epoxy-5,7,8-marasmanetriol; (5α,7β,8β)-form, 5-Me ether, 8-Ac	*Lactarius piperatus*
							hymeglusin	*Cephalosporium* sp., *Scopulariopsis sp.* and *Fusarium sp.*
							hynapene A	*Penicillium sp.* FO-1611

							lachnellulone	*Lachnellula fuscosanguinea*
15.93	P_6845	307.1902	No predicted formula	H.7	2.78E+08	306.1829	unknown	unknown
16.56	N_10267	665.4061	$C_{40}H_{58}O_8$	H.9	3.39E+08	666.4134	No hits produced by fungi	No hits produced by fungi
16.90	N_7451	381.2367	$C_{18}H_{32}N_5O_4$ $C_{17}H_{36}NO_8$	H.8	1.2E+08	382.2440	unknown	unknown
18.81	N_7412	437.1606	$C_{25}H_{26}O_7$	H.7	1.82E+08	438.1679	albanin C	*Morus alba* infected with *Fusarium solani*
							butyrolactone I; Et ester analogue	*Aspergillus terreus* BCC 4651
							phomosine D; 1''-Benzyl ether	*Phomopsis sp.*
20.15	P_6249	523.2229	$C_{33}H_{26}N_6O$ $C_{32}H_{30}N_2O_5$	H.8	1.14E+08	522.2156	unknown	unknown
22.64	N_3036	505.2247	$C_{32}H_{30}N_2O_4$	H.7	2.35E+08	506.2319	cochliodinol	*Chaetomium globosum, Chaetomium cochliodes, Chaetomium elatum* and *Chaetomium abuense*

23.75	P_13459	1219.8870	$C_{69}H_{116}N_7O_{11}$	H.9	1.38E+09	1218.8700	unknown	unknown
23.80	P_11359	1204.8556	$C_{85}H_{109}N_3O_2$ $C_{76}H_{105}N_{11}O_2$ $C_{70}H_{105}N_{15}O_3$ $C_{80}H_{109}N_5O_4$ $C_{75}H_{109}N_7O_6$ $C_{69}H_{109}N_{11}O_7$ $C_{79}H_{113}NO_8$ $C_{73}H_{113}N_5O_9$ $C_{64}H_{109}N_{13}O_9$ $C_{68}H_{113}N_7O_{11}$ $C_{59}H_{109}N_{15}O_{11}$ $C_{72}H_{117}NO_{13}$ $C_{57}H_{113}N_{13}O_{14}$ $C_{52}H_{113}N_{15}O_{16}$ $C_{62}H_{117}N_5O_{17}$ $C_{56}H_{117}N_9O_{18}$ $C_{60}H_{121}N_3O_{20}$ $C_{61}H_{121}NO_{21}$	H.9	4.15E+08	1203.8484	unknown	unknown
23.97	P_11356	1205.8609	$C_{61}H_{112}N_{12}O_{12}$	H.9	3.98E+08	1204.8536	unknown	unknown
27.92	N_131	297.2500	No predicted formula	H.3	4.36E+08	298.2573	unknown	unknown

The same procedure that was done to determine the bioactive metabolites against breast cancer (ZR-75) cell line was done for lung cancer (A549) cell line as well (Figure 5.15). The active fractions, H.3, H.5, H.6, H.7, H.8 and H.9 were grouped together. H.6 was excluded again as it was closer to the inactive fractions and affecting both the fitting and predictive ability of the model (Permutation test: R2=0.88, Q2=0.03, R2Y=0.799 and Q2Y=0.113) and another model was created (Figure 5.15.B). The model's permutation test (Figure 5.16) gave an R2 of 0.99 and Q2 of 0.18, while the R2Y intercept was 0.818 and Q2Y intercept was 0.1653 indicating an excellent fitting but a weaker predictive model than the one that was generated for the activity of the fractions on breast cancer (ZR-75) cell line, as Q2 value was 0.18 which is less than 0.5. R2Y and Q2 values differed by 0.638, indicating the overfitting or weakness of the model itself.

Again, an S plot was generated from the previous OPLS-DA and presented in (Figure 5.17). The pinpointed loadings are the ones to left of the Y axis and are supposed to be with the most prominent activity. The metabolites were dereplicated and listed in Table 5.4.

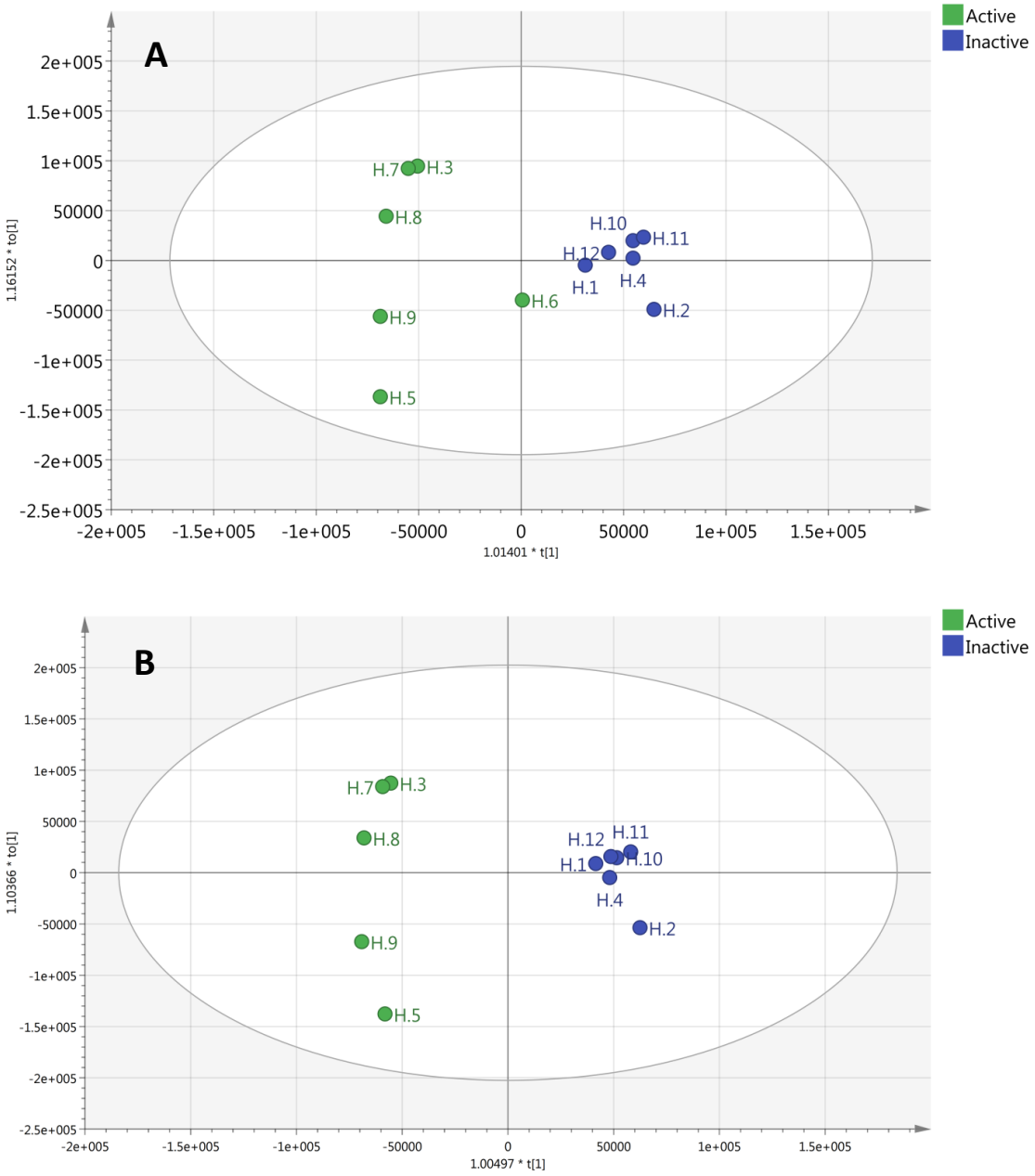

Figure 5.15: Scores plots of *Chaetomium subaffine* (H.n) fractions. Samples were grouped into active (green) and inactive (blue) according to their activity against lung cancer (A549) cell line. (A): H.6 included in the model, R2X=0.244, R2Y=0.880, Q2=0.027. (B): H.6 excluded from the model, R2X=0.250, R2Y=0.988, Q2=0.182.

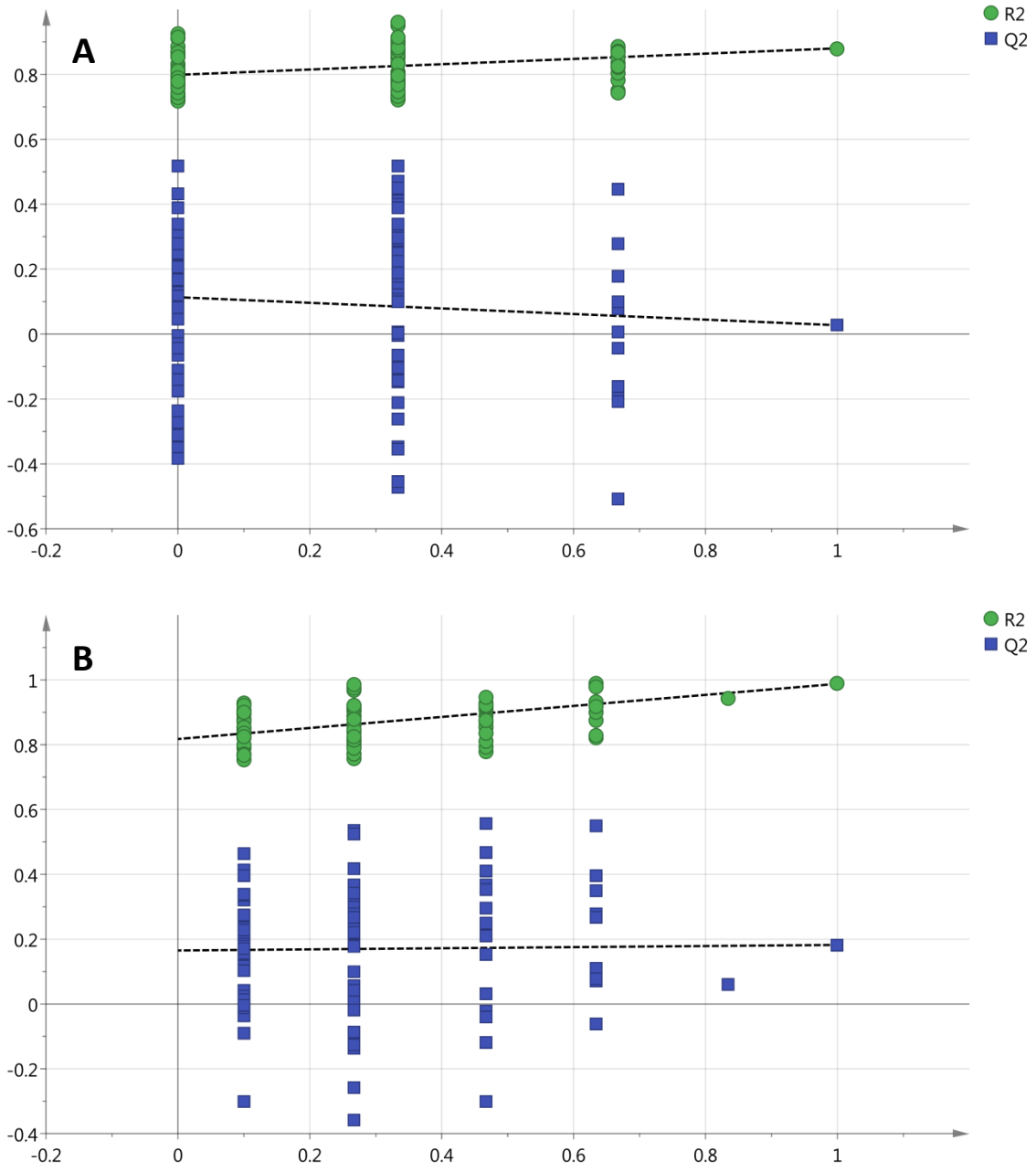

Figure 5.16: Permutation tests (100 permutations) for *Chaetomium subaffine* (H.n) fractions for the OPLS-DA model of their activity against lung cancer (A549) cell line. (A): H.6 included in the model, (B): H.6 excluded from the model.

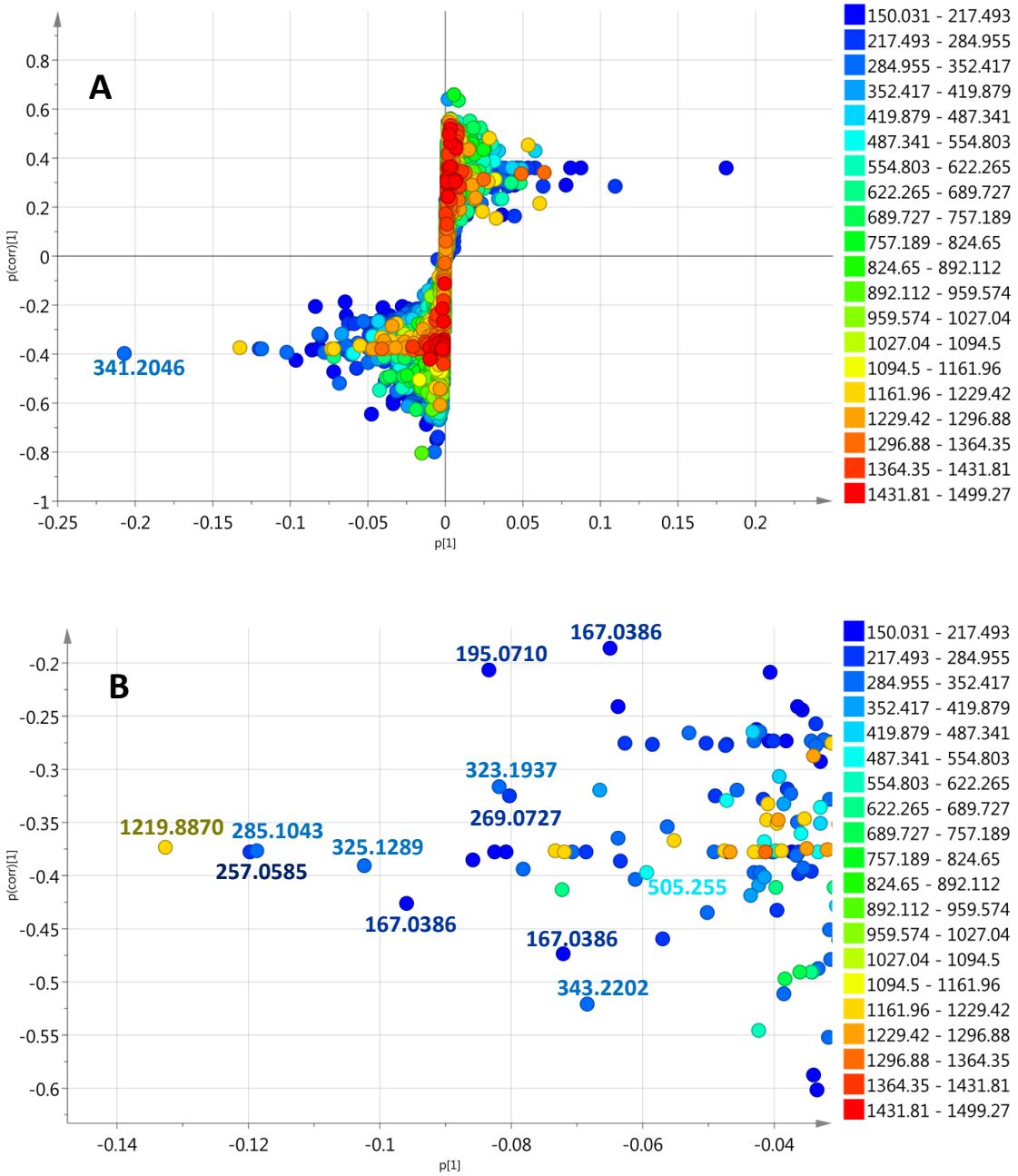

Figure 5.17: (A): S plot for *Chaetomium subaffine* (H.n) fractions acquired from an OPLS-DA model for their activity against the lung cancer (A549) cell line (Figure 5.15.B). (B): zoomed view for the extreme left metabolites, the isolated metabolites and the outliers are labelled by their *m/z* value.

5.5 Implementing metabolomics for the isolation of the pure secondary metabolites from the endophyte *Chaetomium subaffine*

The chromatographic work was planned to isolate the "pinpointed" metabolites that were presumed to possess the activity against both breast and lung cancer cell lines, ZR-75 and A549. The fractions that were subjected to further fractionation are the ones that contained the predicted target bioactive metabolites. This resulted in the isolation of seven pure compounds listed in Table 5.5.

Table 5.5: The metabolites that were isolated from *Chaetomium subaffine.*

Cpd No.	Name	New / Known	t_R (min)	*m/z*	MWt	Source	Weight (mg)	% Yield
1	acremonisol A	known	14.52	257.0644	258.0659	H.4	2819.1	7.15
2	cochliodinol	known	22.30	505.2154	506.2206	H.6	3192.0	8.10
3	chaetomi-pyrrolidinone	new	7.14	200.0735	201.1154	H.7	4.3	0.01
4	chaetomiside A	new	6.42	269.0662	270.0740	H.7	11.4	0.03
5	chaetomiside B	new	15.50	323.1179	324.1209	H.7	6.0	0.02
6	chaetomiside C	new	5.10	285.0971	286.1053	H.8	17.8	0.05
7	chaetomiside D	new	5.18	285.1019	286.1053	H.8	4.9	0.01

Both flash chromatography and preparative TLC were used as chromatographic techniques for the isolation of the pure compounds (Figure 5.18). The parameters and conditions applied for flash chromatography-1 (FC-1) are mentioned under section 5.3, while for all other flash chromatography experiments (2-6), the conditions used and parameters applied are mentioned in Table 5.6. The solvent systems that were used as mobile phases are mentioned in tables 5.7 to 5.11.

Table 5.6: The chromatographic conditions that were used in isolating the pure compounds from the extract of *Chaetomium subaffine.*

Column	Reveleris® Silica 12 - 48 g
Flow rate	15 mL/min
ELSD Threshold	20 mV
UV Threshold	0.05 AU
UV1 Wavelength	254 nm
UV2 Wavelength	280 nm

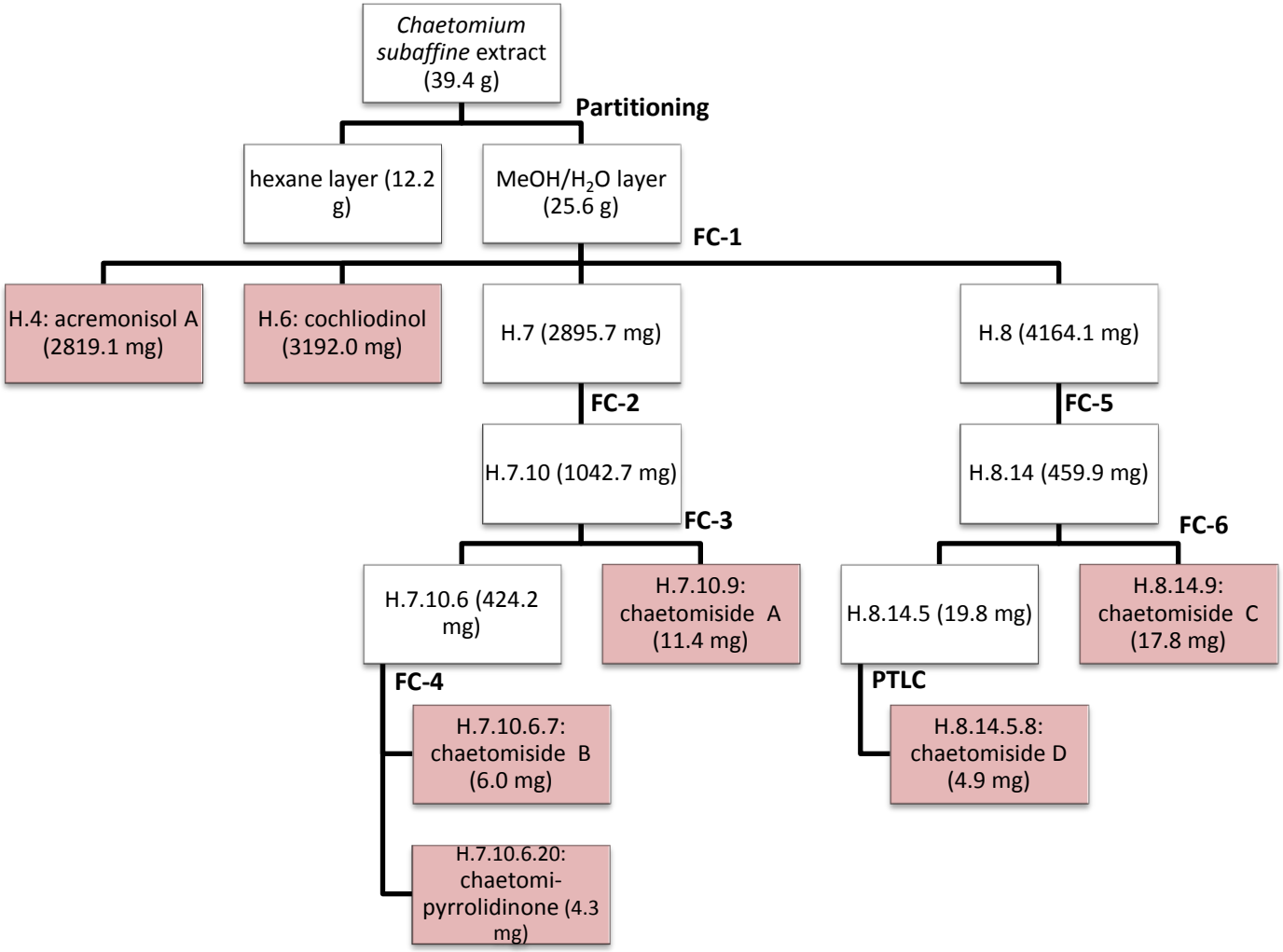

Figure 5.18: The workflow for isolating the pure compounds from *Chaetomium subaffine* extract.

Table 5.7: Mobile phase used for flash chromatography-2 (FC-2).

Time (min)	% Hex	% EtOAc	% DCM	% MeOH
0	80	20	0	0
20	80	20	0	0
140	20	80	0	0
160	20	80	0	0
161	0	0	100	0
165	0	0	100	0
185	0	0	90	10
205	0	0	90	10
225	0	0	70	30
230	0	0	70	30

Table 5.8: Mobile phase used for flash chromatography-3 (FC-3).

Time (min)	% DCM	% MeOH
0	100	0
40	95	5
60	95	5
70	93	7
80	93	7
90	90	10
100	90	10
110	80	20
120	80	20

Table 5.9: Mobile phase used for flash chromatography-4 (FC-4).

Time (min)	% Hex	% EtOAc	% ACN
0	90	10	0
10	90	10	0
20	70	30	0
35	70	30	0
50	50	50	0
65	50	50	0
80	20	80	0
90	20	80	0
100	0	100	0
110	0	100	0
120	0	80	20
130	0	80	20
140	0	50	50
150	0	50	50
160	0	0	100
170	0	0	100

Table 5.10: Mobile phase used for flash chromatography-5 (FC-5).

Time (min)	% Hex	% EtOAc	% MeOH
0	100	0	0
10	80	20	0
35	80	20	0
60	50	50	0
80	50	50	0
100	20	80	0
120	20	80	0
130	0	100	0
135	0	100	0
145	0	90	10
155	0	90	10
160	0	70	30
165	0	70	30

Table 5.11: Mobile phase used for flash chromatography-6 (FC-6).

Time (min)	% Hex	% EtOAc
0	60	40
10	50	50
40	50	50
70	30	70
90	30	70
110	0	100
120	0	100

For the fractionation of H.8.14.5, preparative TLC was utilised and prepared as described in 2.5.2.4. The mobile system used composed of 87% EtOAc and 13% hexane. The pure compound H.8.14.5.8 gave a violet colour under the long UV light (365 nm) and orange to red colour after spraying with anisaldehyde spraying reagent. Its R_f value was 0.38.

5.6 Structure elucidation of the pure secondary metabolites from the endophyte *Chaetomium subaffine*

5.6.1 Acremonisol A (1)

Acremonisol A
Fraction: H.4 Retenion time: 14.52 min Synonym(s): • 3-Chloro-4,6-dimethoxy-2-propyl-benzoic acid Source: *Chaetomium subaffine,* isolated from *Anthemis palestina* Amount of sample: 2819.1 mg Percent yield: 7.15% Percent purity: 85.9% Physical description: colourless oil Molecular formula: $C_{12}H_{15}ClO_4$ Molecular weight: 258.0659 g/mol
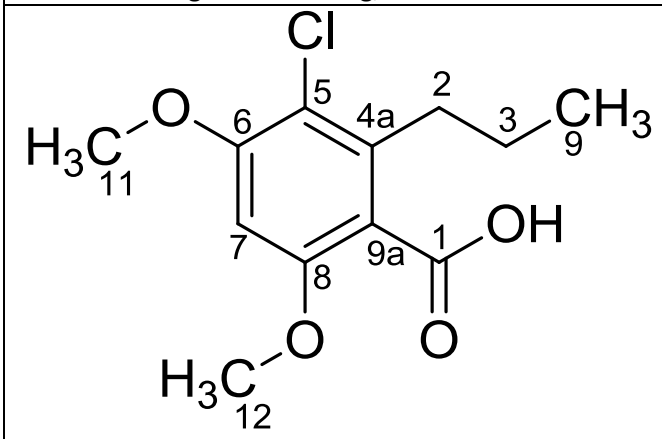

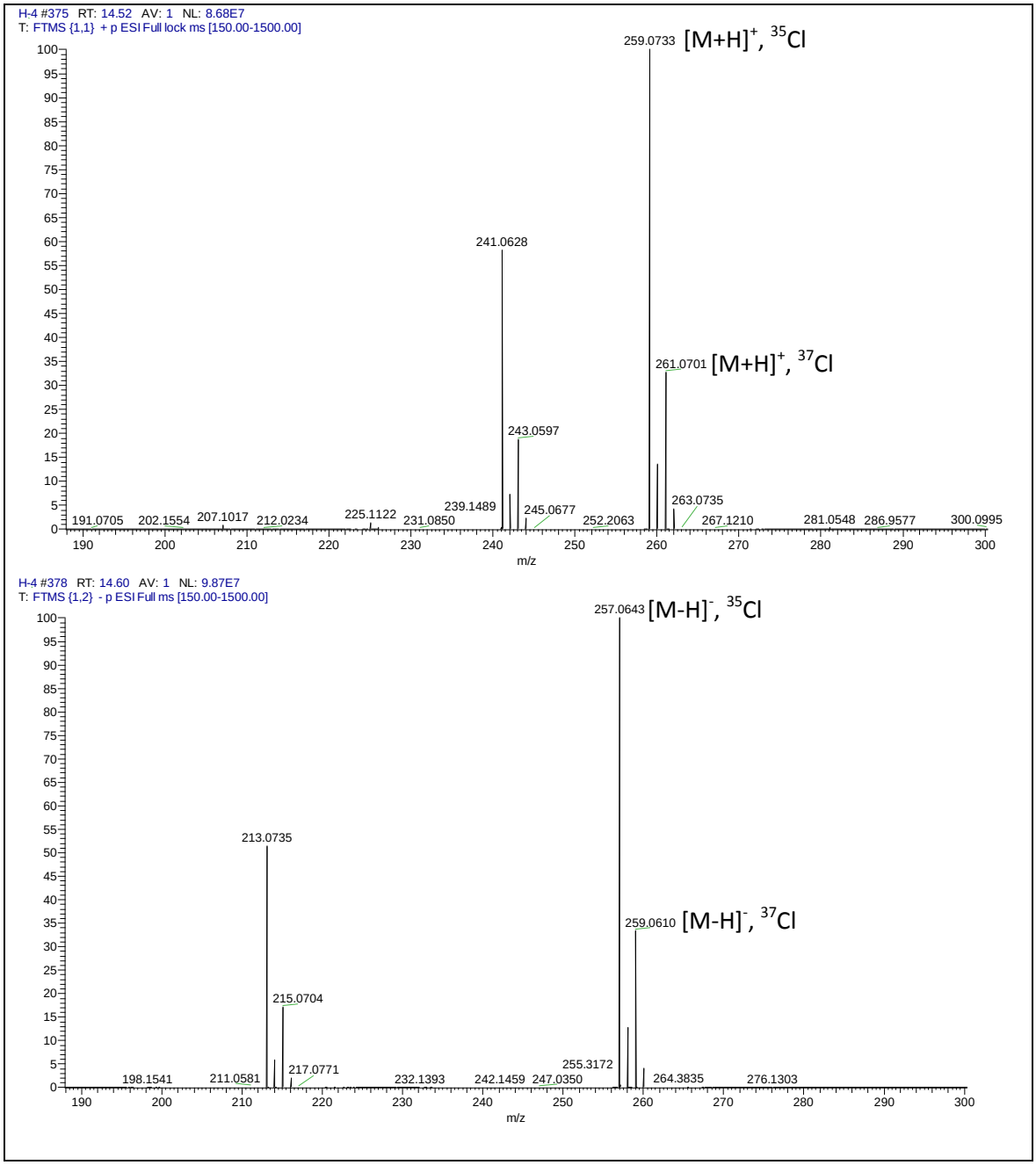

Acremonisol A was isolated in the form of a colourless oil with a yield of 7.15% (2819.1 mg). The LC-HRMS data gave pseudomolecular ion peaks at *m/z* of 259.0733 $[M+H]^+$ and 257.0644 $[M-H]^-$, suggesting that this compound has a molecular weight of 258.0659 g/mol. The molecular formula was established by HRMS as $C_{12}H_{15}ClO_4$. The presence of a chlorine atom in the molecule was confirmed by the presence of another two molecular ion peaks, the first one

was in the negative ionisation mode at *m/z* 259.0642 [X+2] while the second was in the positive ionisation mode at *m/z* 261.0701 [X+2]. Both of them have a relative abundance that is about one third of the relative abundance of the base peaks. The difference in the *m/z* ratio between these two peaks was referred to the difference in the weight of the two chlorine isotopes, ^{35}Cl and ^{37}Cl, at a ratio of 3:1 in their relative abundance in the favor of ^{35}Cl.

The ^{1}H NMR spectrum (Figure 5.19) showed a singlet at 6.71 ppm (H-7), indicating a shielding effect caused by an electron donating substituents. The electron donating groups involved two methoxy units, represented by singlets at δ_H 3.82 (CH_3-11) and δ_H 3.90 (CH_3-12). Both methoxy units are *ortho* to H-7 causing the H-7 singlet to be shifted upfield. The attachment of the methoxy units to C-6 and C-8 corresponded to ^{13}C NMR shifts at δ_c 155.6 and 156.3, respectvely, which also indicated that C-6 and C-8 are oxygenated aromatic carbons. Moreover, the positions of methoxy moieties were further confirmed by the ^{3}J HMBC correlation of the methoxy singlets at δ_H 3.82 (CH_3-11) and 3.90 (CH_3-12) to carbons C-6 and C-8, respectively (Figure A.VI.4). Furthermore, the COSY NMR spectrum showed a triplet at δ_H 0.91 ppm (CH_3-9, J=7.4 Hz) coupling to the multiplet at δ_H 1.52 (CH_2-3), which further coupled to the triplet at δ_H 2.59 ppm (CH_2-2, J=7.1 Hz). The COSY data constructed the propyl chain moiety attached to C-4a of the benzene ring, which was confirmed by the HMBC correlations of proton CH_2-2 to C-4a (^{2}J), C-9a (^{3}J) and C-5 (^{3}J) of the benzene ring (Figure A.VI.2). In addition, the position of the carboxyl group that is attached to C-9a was established by the ^{4}J (W) HMBC cross peak of H-7 to the carboxylic carbon at 168.7 ppm for C-1. The structure was further confirmed by comparing both of the ^{1}H and ^{13}C NMR data of the isolated compound to the literature (Table 5.12). Thus, this compound was identified as acremonisol A that was first reported from the marine-derived fungus *Acremonium* sp. (Pontius *et al*., 2008).

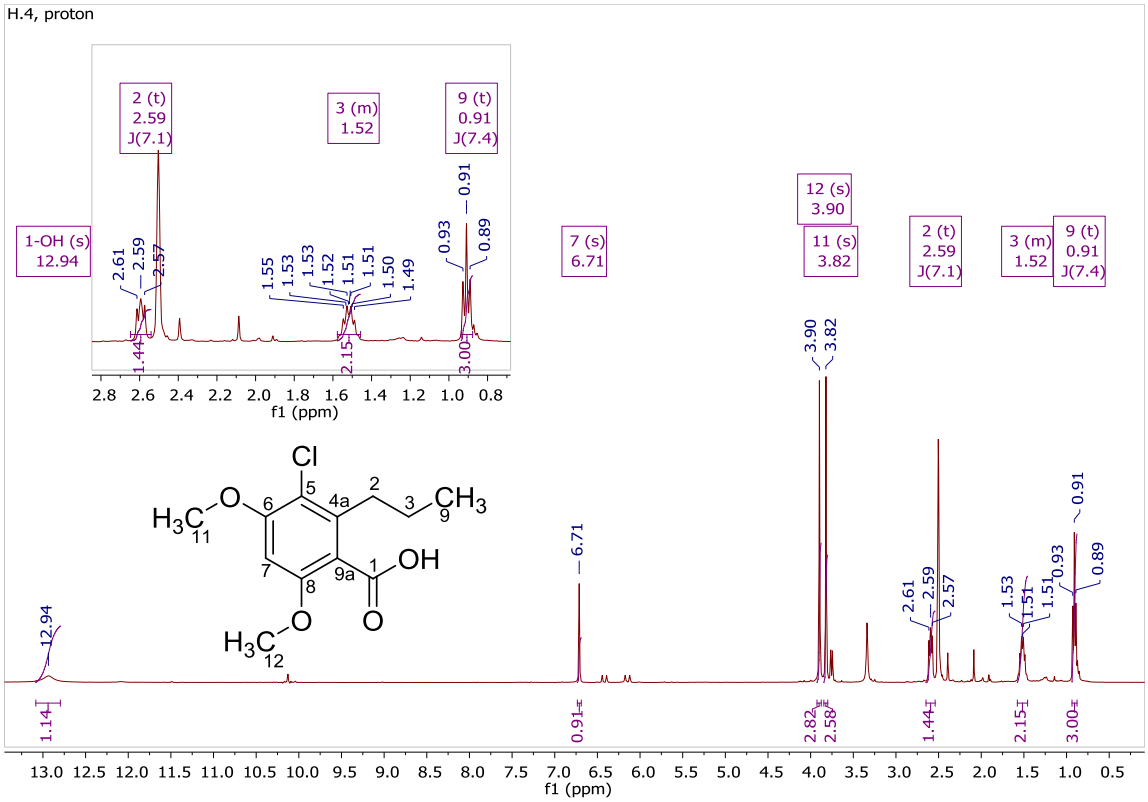

Figure 5.19: ^{1}H NMR (400 MHz) spectrum for acremonisol A, measured in DMSO-d_6.

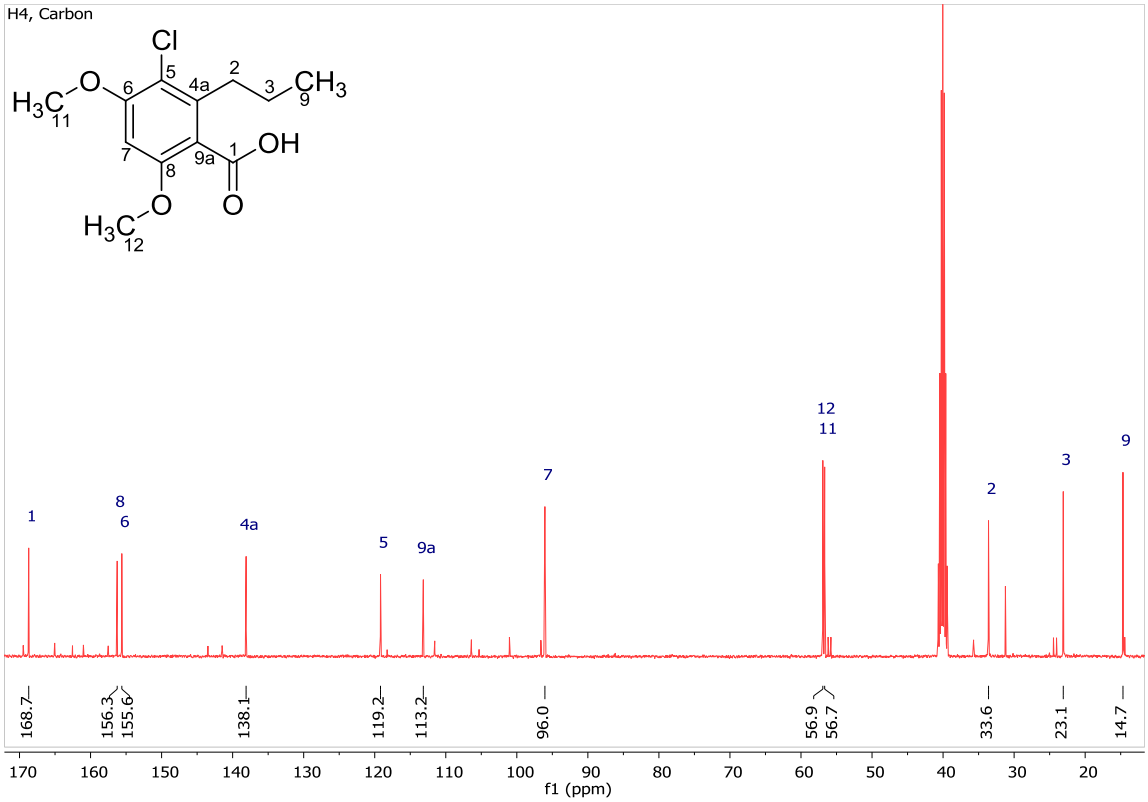

Figure 5.20: ^{13}C NMR (100 MHz) spectrum for acremonisol A, measured in DMSO-d_6.

Table 5.12: ^{1}H and ^{13}C NMR data for acremonisol A in comparison with the literature.

	acremonisol A in DMSO-d_6.						**acremonsiol A (Pontius *et al.*, 2008) in MeOH-d_4 .**				
	^{1}H NMR data (400 MHz)				^{13}C NMR data (100 MHz)		^{1}H NMR data (500 MHz)				^{13}C NMR data (75.5 MHz)
Atom no.	δ_H (ppm)	Integration	Multiplicity	*J* (Hz)	δ_C (ppm)	Multiplicity	δ_H (ppm)	Integration	Multiplicity	*J* (Hz)	δ_C (ppm)
1					168.7	C					171.4
2	2.59	2H	t	7.1	33.6	CH_2	2.74	2H	t	7.3	34.6
3	1.52	2H	m		23.1	CH_2	1.64	2H	sixt	7.3	24.0
4					138.1	C					140.0
5					119.2	C					119.0
6					155.6	C					157.0
7	6.71	1H	s		96.1	CH	6.68	1H	s		95.9
8					156.3	C					158.0
9	0.91	3H	t	7.3	14.7	CH_3	1.01	3H	t	7.3	14.6
10					113.2	C					115.1
11	3.82	3H	s		56.7	CH_3	3.90	3H	s		56.7
12	3.90	3H	s		56.9	CH_3	3.97	3H	s		56.8
OH	12.94		s								

5.6.2 Cochliodinol (2)

Cochliodinol
Fraction: H.6 Retenion time: 22.30 min Synonym(s): • 2,5-Dihydroxy-3,6-bis[5-(3-methyl-2-buten-1-yl)-1*H*-indol-3-yl]-2,5-Cyclohexadiene-1,4-dione Source: *Chaetomium subaffine*, isolated from *Anthemis palestina* Amount of sample: 3192.0 mg Percent yield: 8.10% Percent purity: 96.6% Physical description: Purple crystals Molecular formula: $C_{32}H_{30}N_2O_4$ Molecular weight: 506.2206 g/mol
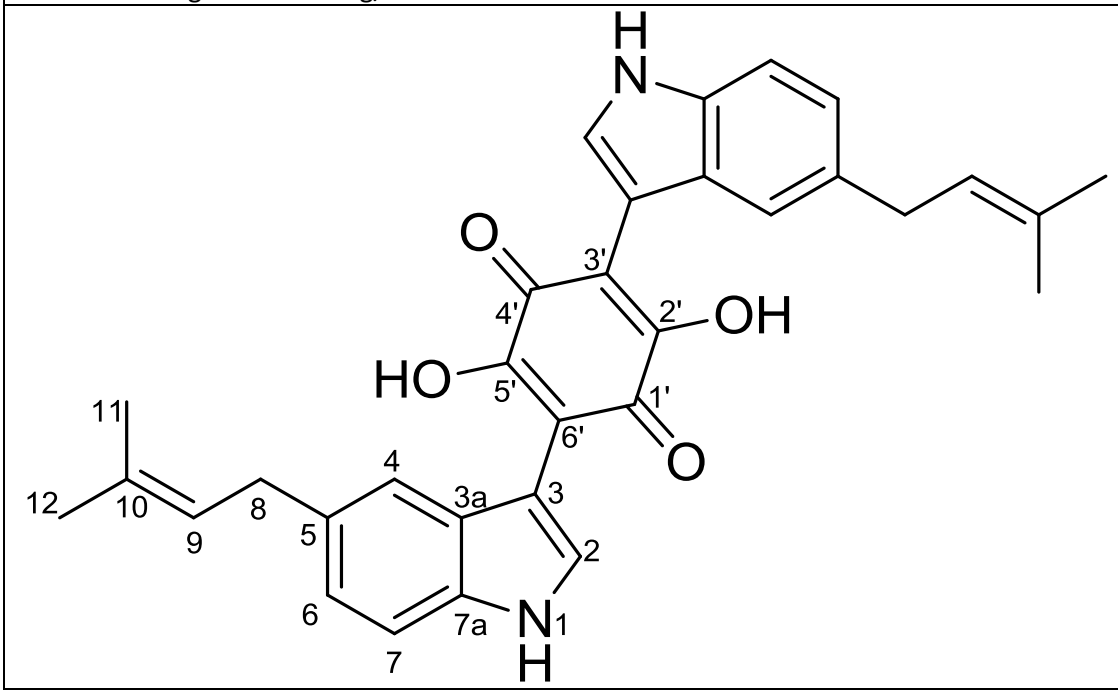

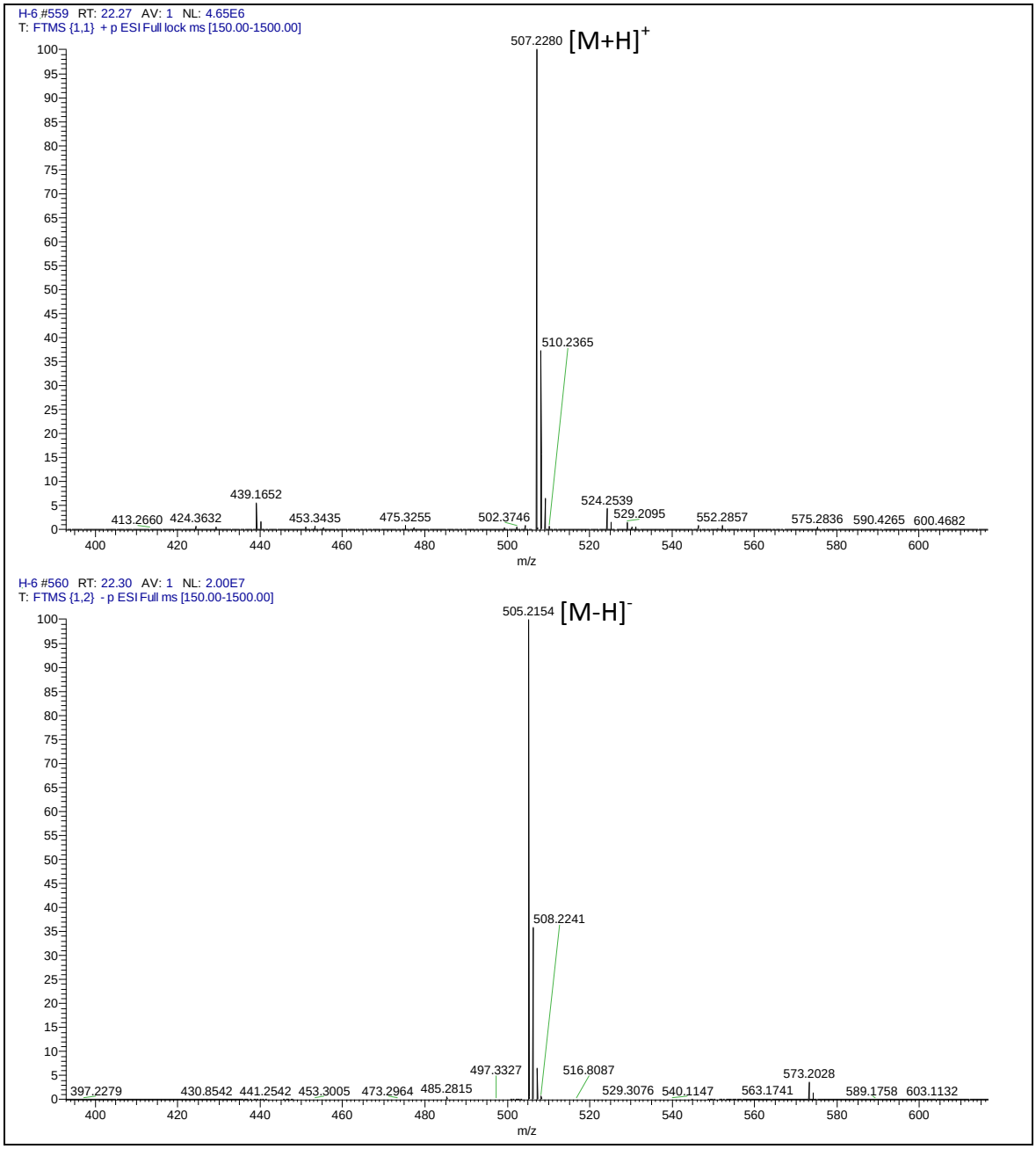

Cochliodinol was isolated as purple crystals with a yield of 8.10% (3192.0 mg). LC-HRMS data depicted a pseudomolecular ion at *m/z* 507.2281 $[M+H]^+$ and 505.2154 $[M-H]^-$, indicating a molecular weight of 506.2206 g/mol. The molecular formula established by HRMS as $C_{32}H_{30}N_2O_4$.

The ^{1}H NMR spectrum (Figure 5.21) displayed four signals in the aromatic region, from which, three signals coupled with each other indicating an ABX spin system. The *ortho* doublet at δ_H

7.33 (H-7, *J*=8.3 Hz) coupled with the doublet of doublet at δ_H 6.93 (H-6, *J*=8.3, 1.6 Hz) which, in turn, coupled to the *meta* proton at δ_H 7.23 (H-4, *J*=1 Hz). The presence of the ABX spin system was confirmed by a ^{1}H-^{1}H COSY experiment (Figure A.VII.2). The remaining aromatic signal was part of the adjacent pyrrole ring. It consisted of H-2 (δ_H 7.46 ppm, *J*=2.6 Hz) that coupled to 1-N*H* (δ_H 11.27, *J*=2.6 Hz). The presence of the pyrrole ring was signified by the value of coupling constant (*J*=2.6 Hz) between H-2 and 1-N*H* that is typical for 5-membered heterocyclic ring systems such as a pyrrole.

An olefinic proton was observed at δ_H 5.33 (H-9 ddq, *J*=7.4, 6.0, 1.6 Hz) that correlated in the ^{1}H-^{1}H COSY spectrum to methylene protons at δ_H 3.34 (CH_2-8). The methylene signals overlapped with the water peak. Moreover, two methyl groups were detected at δ_H 1.70 for CH_3-11 and δ_H 1.72 for CH_3-12.

The assignments of each proton to its corresponding carbon (^1J ^{1}H-^{13}C bond) was done by ^{1}H-^{13}C HSQC NMR (Figure A.VII.4) and the substructural units were connected to each other by implementing a ^{1}H-^{13}C HMBC NMR experiment (Figure A.VII.5). The ^{1}H-^{13}C HMBC spectrum exhibited correlations from CH_3-11 and CH_3-12 to both the olefinic methine at δ_c 125.3 (C-9, ^3J) and the quaternary carbon at δ_c 130.9 (C-10, ^2J), suggesting that the two methyl groups are geminal to each other, both attached on C-10. This was also confirmed by the ^3J correlations from CH_3-11 to C-12 and from CH_3-12 to C-11. Furthermore, this alkyl chain is connected to the benzene ring through C-5 at 131.9 ppm. This was shown by the ^3J correlation from the *meta* protons H-4 and H-6 to C-8 along with a ^2J correlation from CH_2-8 to C-5. Moreover, the pyrrole's position was confirmed by the ^3J correlations of its proton doublet H-2 to both C-3a and C-7a, as well as the cross peaks of 1-N*H* to the quaternary carbons at 134.7 ppm for C-7a (^2J) and 127.2 ppm for C-3a (^3J). Thus, forming an indole ring. The presence of half of the 2',5' dihydroxyquinone ring that connects the two 5-(3-methylbut-2-en-1-yl)-1H-indole moeities could be detected by its ^{13}C signals in the JMod spectrum (Figure 5.22) that showed C-6' signal at 111.7 ppm and both C-5' and C-4' at 168.6 ppm. The part established by the NMR experiments corresponded to half of the molecular weight obtained from the LC-HRMS data. Thus, the obtained compound was confirmed to be a dimer of two identical subunits that had the same NMR resonaces.

This compound was confirmed as cochliodinol. Its ^{1}H and ^{13}C NMR data were identical to those reported in the literature (Debbab *et al*., 2009) (Table 5.13).

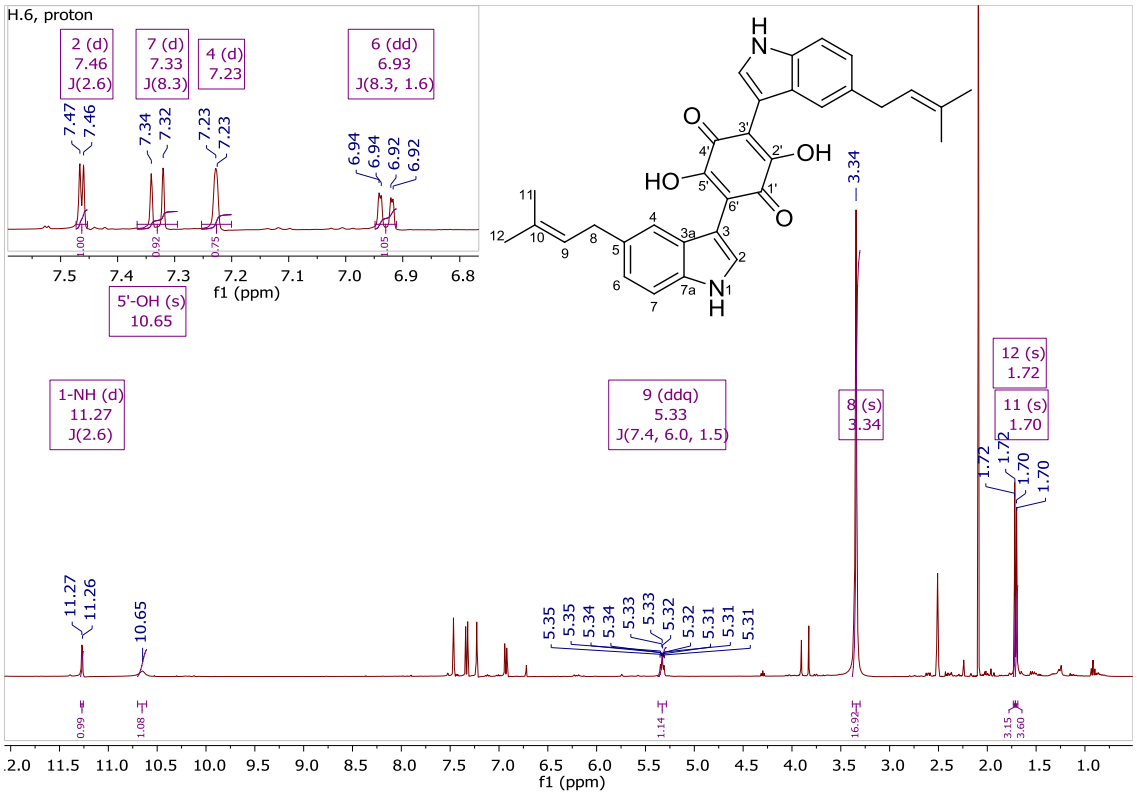

Figure 5.21: ^{1}H NMR (400 MHz) spectrum for cochliodinol, measured in DMSO-d_6.

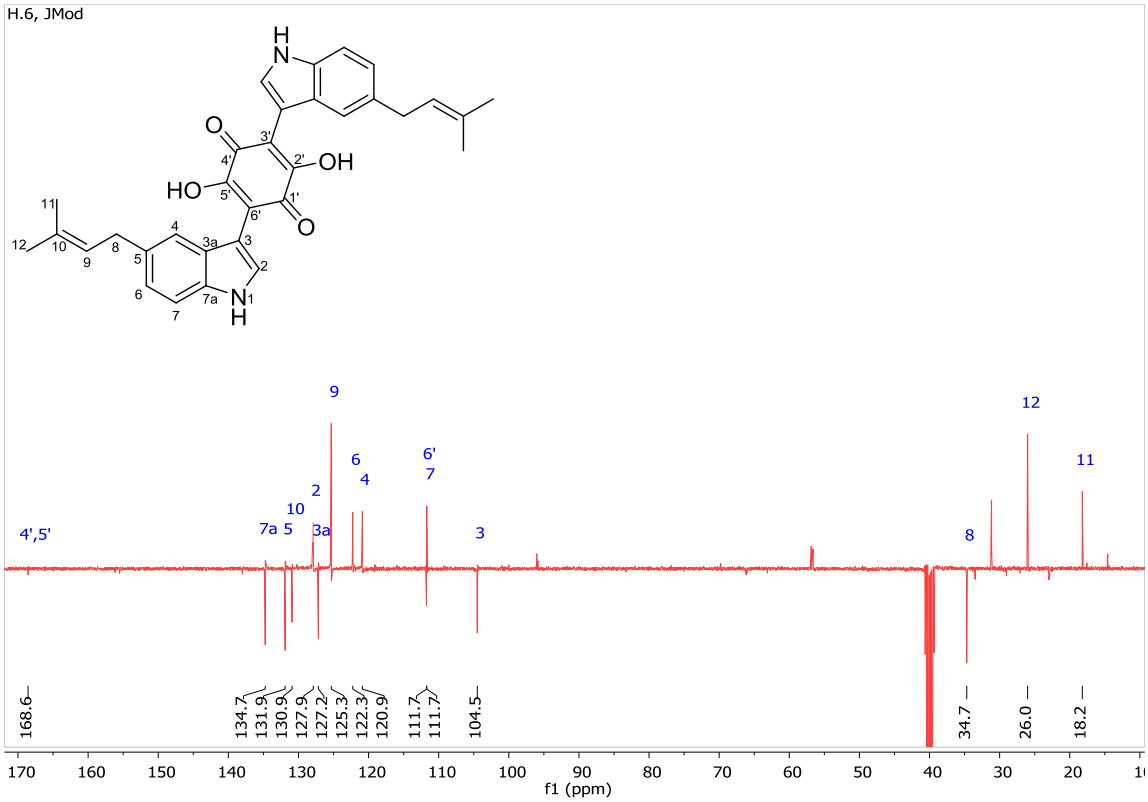

Figure 5.22: JMod NMR (100 MHz) spectrum for cochliodinol, measured in DMSO-d_6.

Table 5.13: ^{1}H and ^{13}C NMR data for cochliodinol compared to literature.

	Cochliodinol in DMSO-d_6						**Cochliodinol (Debbab *et al.*, 2009) in DMSO-d_6**				
	^{1}H NMR data (400 MHz)				^{13}C NMR data (100 MHz)		^{1}H NMR data (500 MHz)				^{13}C NMR data (125 MHz)
Atom no.	δ_H (ppm)	Integration	Multiplicity	*J* (Hz)	δ_C (ppm)	Multiplicity	δ_H (ppm)	Integration	Multiplicity	*J* (Hz)	δ_C (ppm)
1-NH	11.27	1H	d	2.6			11.21	1H	s		
2	7.46	1H	d	2.6	127.9	CH	7.51	1H	d	2.4	128.4
3					104.5	C					106.2
3a					127.2	C					129.9
4	7.23	1H	d	1	120.9	CH	7.37	1H	d	0.9	122.1
5					131.9	C					131.9
6	6.93	1H	dd	8.3, 1.6	122.3	CH	6.97	1H	dd	8.5, 1.5	122.9
7	7.33	1H	d	8.3	111.7	CH	7.31	1H	d	8.2	112.0
7a					134.7	C					135.7
8	3.34	2H	overlapped with water		34.7	CH_2	3.40	2H	d	7.2	35.8
9	5.33	1H	ddq	7.4, 6.0, 1.6	125.3	CH	5.40	1H	tq	7.2, 1.5	126.3
10					130.9	C					131.1
11	1.70	3H	s		18.2	CH_3	1.76	3H	br s		17.9
12	1.72	3H	s		26.0	CH_3	1.75	3H	d	7.2	25.9
4'					168.0	C					
5'					168.6	C					
6'					111.7	C					112.3
5'-OH	10.65	1H	s				9.72	1H	s		

5.6.3 Chaetomipyrrolidinone (3)

Chaetomipyrrolidinone (new compound)

Fraction: H.7.10.6.20
Retention time: 7.14 min
Synonym(s):

- 6-(3-Methylbut-2-en-1-yl)isoindolin-1-one

Source: *Chaetomium subaffine*, isolated from *Anthemis palestina*
Amount of sample: 4.3 mg
Percent yield: 0.01%
Percent purity: 80.3%
Physical description: yellow oil
Molecular formula: $C_{13}H_{15}NO$
Molecular weight: 201.1154 g/mol

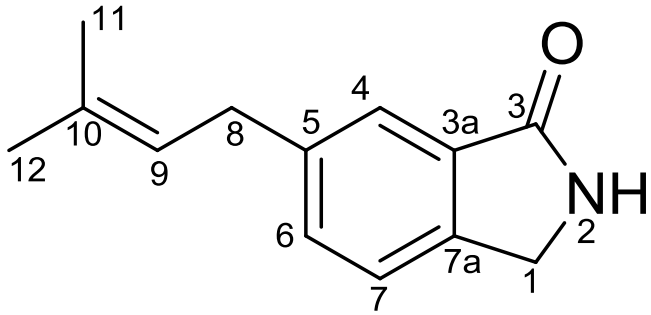

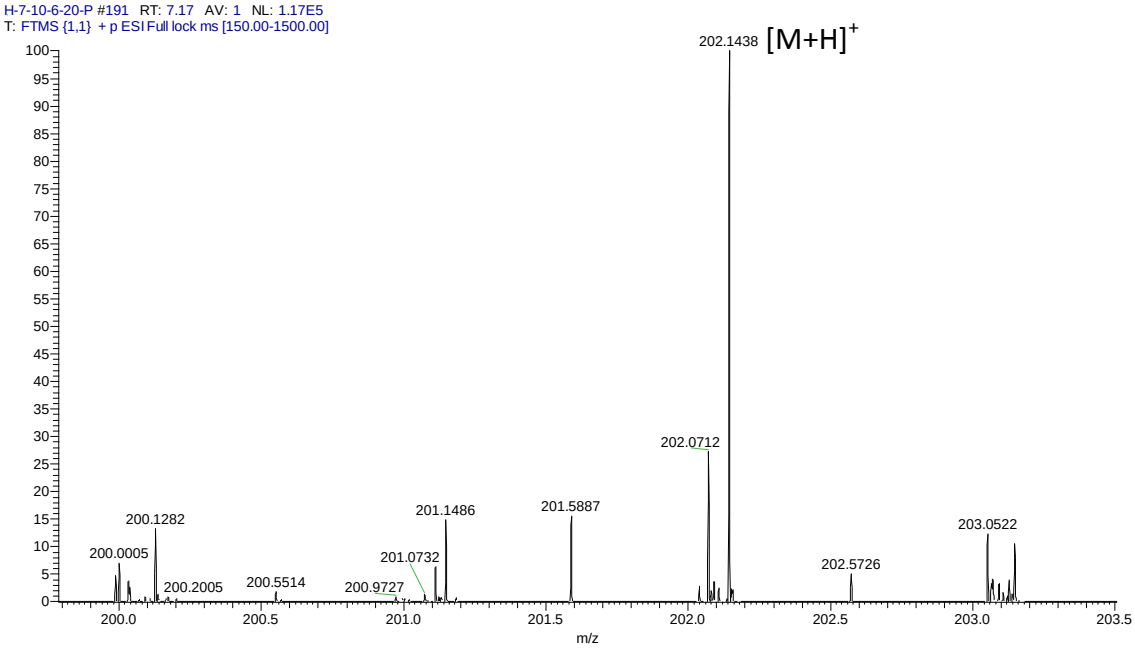

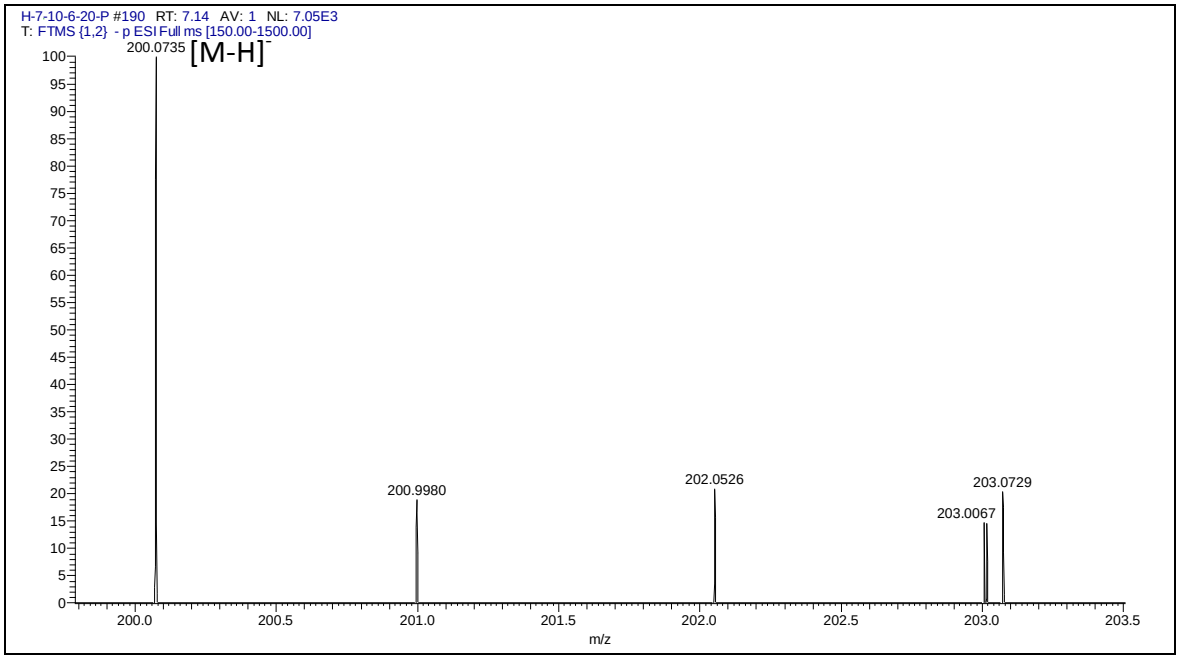

Chaetomipyrrolidinone was isolated in the form of a yellow oil with quite a low yield of 0.01% (4.3 mg). LC-HRMS provided a pseudomolecular ion at *m/z* of 202.1438 $[M+H]^+$ and 200.0735 $[M-H]^-$ indicating a molecular weight of 201.1154 g/mol. The molecular formula was established as $C_{13}H_{15}NO$.

Chaetomipyrrolidinone shared a similar 1,2-disubstituted-4-(3-methylbut-2-en-1-yl)benzene moeity as found in cochliodinol. This similarity was established by comparing both ^1H and ^{13}C NMR data for these two compounds as presented in Table 5.14. However, the pyrrole moeity of cochliodinol was replaced by a pyrrolidin-2-one. This replacement played a significant change in chemical shifts of both the *meta* (H-4) and *ortho* protons (H-7) in cochliodinol. H-4 and H-7 shifted upfield to δ_H 7.06 and 6.69 in chaetomipyrrolidinone (Figure 5.23 and Table 5.14). The shielding effect on H-4 and H-7 was due to the electron donating substituent. The presence of the pyrrolidin-2-one was further confirmed by the ^1H-^{13}C HMBC NMR spectrum (Figure 5.26). This afforded the ^3J correlation of the amide proton at 10.12 ppm (N*H*-2) to C-3a and C-7a at 131.8 and 140.7 ppm, respectively.

The carbons were assigned by utilising both the JMod and ^1H-^{13}C HSQC NMR spectra (Figure 5.24 and 5.25). The positions of the carbonyl group on C-3a and the methylene unit on C-7a

were confirmed by 1D NOE NMR experiments (Figure 5.27). Irradiating the meta doublet at δ_H 7.06 (H-4) gave an nOe signal on δ_H 3.23 (H-8) indicating that H-4 and CH_2-8 were positioned vicinal to each other. On the other hand, the ortho doublet at δ_H 6.69 (H-7) yielded nOes on δ_H 2.98 and 3.23 for CH_2-1 as well as at δ_H 6.97 (H-6) confirming that the methylene unit is adjacent to the ortho proton on H-7. Moreover, 1D nOe afforded the confirmation of the position of the methyl group at δ_H 1.70 (CH_3-12) to be *cis* to the olefinic proton H-9 at δ_H 5.25.

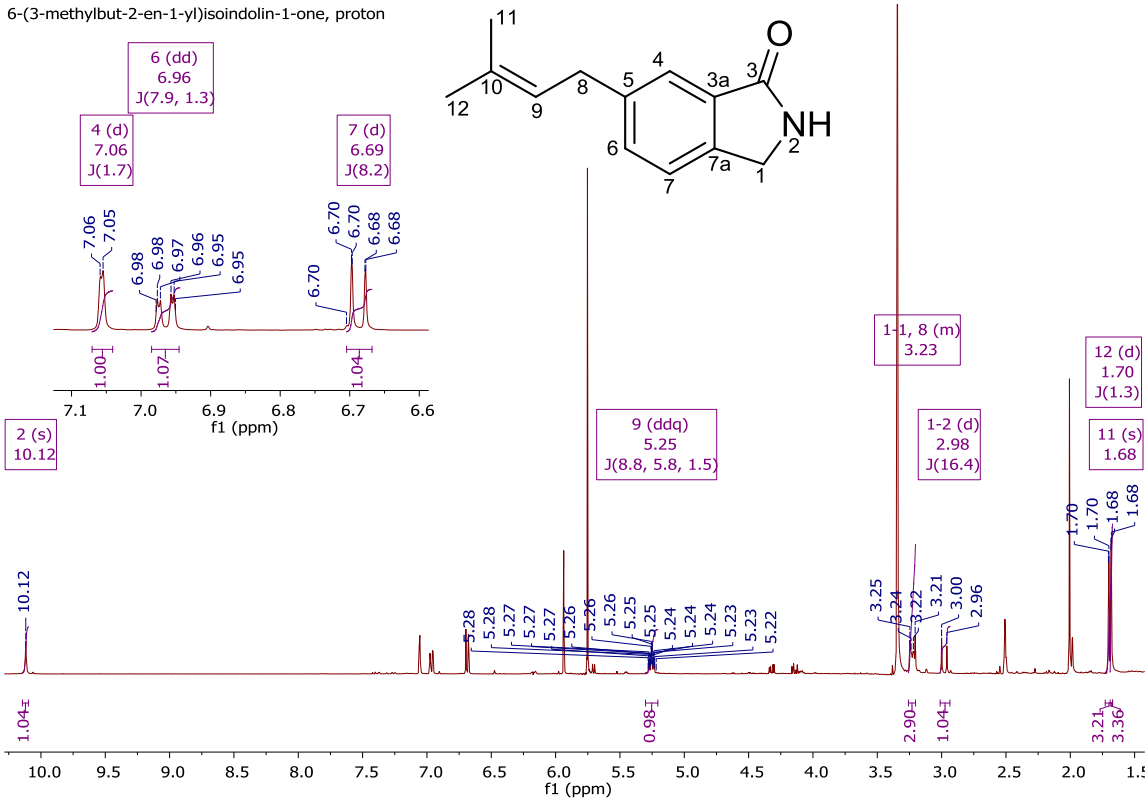

Figure 5.23: ^{1}H NMR (400 MHz) spectrum for chaetomipyrrolidinone, measured in DMSO-d_6.

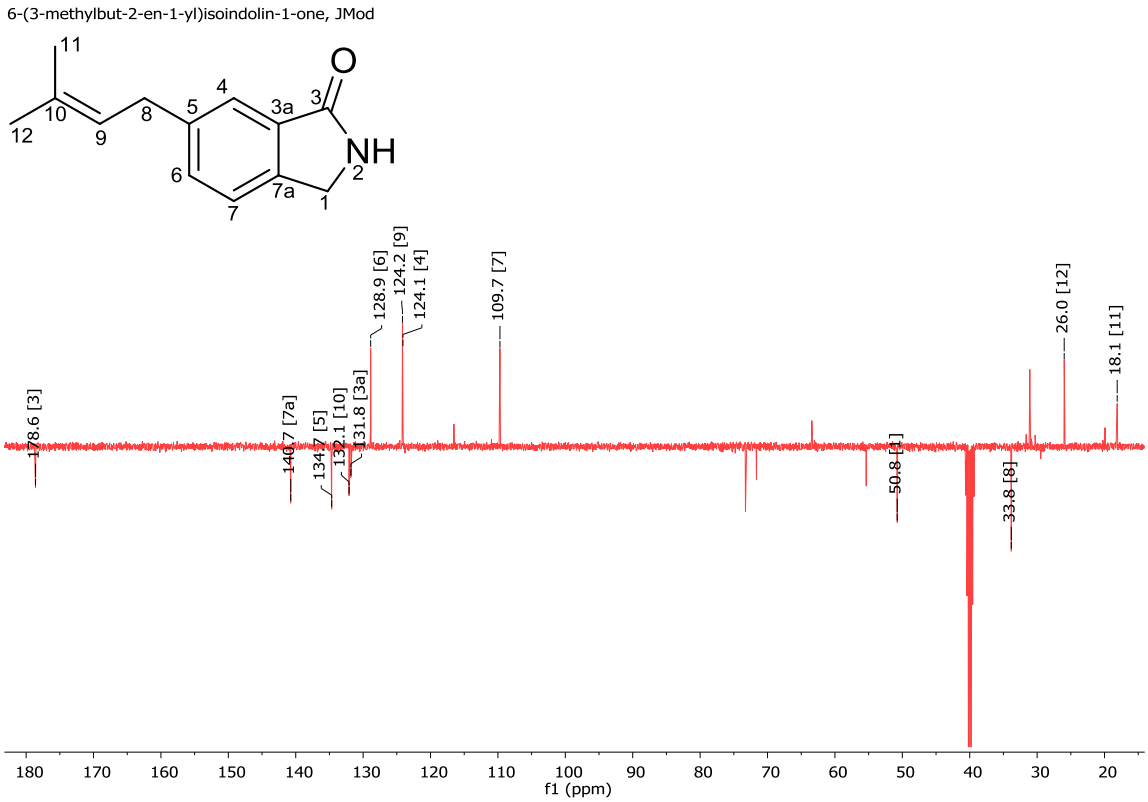

Figure 5.24: JMod NMR (100 MHz) spectrum for chaetomipyrrolidinone, measured in DMSO-d_6.

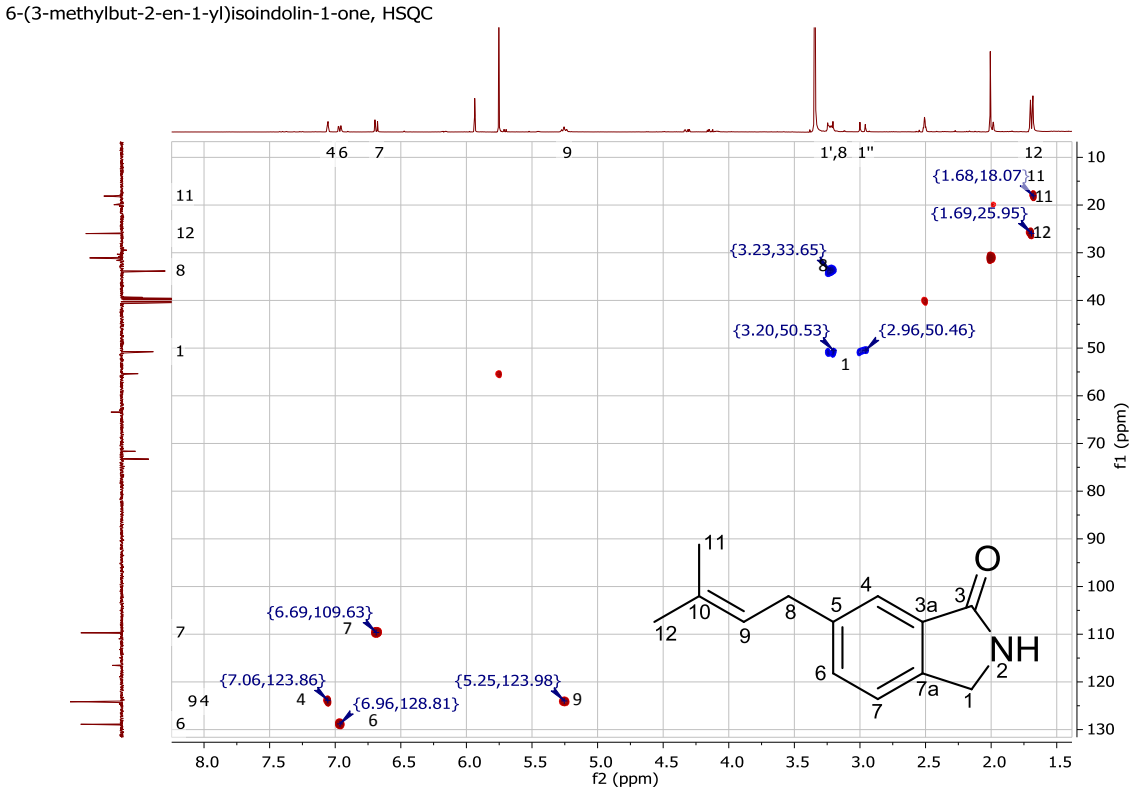

Figure 5.25: ^{1}H-^{13}C HSQC NMR (400 MHz) spectrum for chaetomipyrrolidinone, measured in DMSO-d_6.

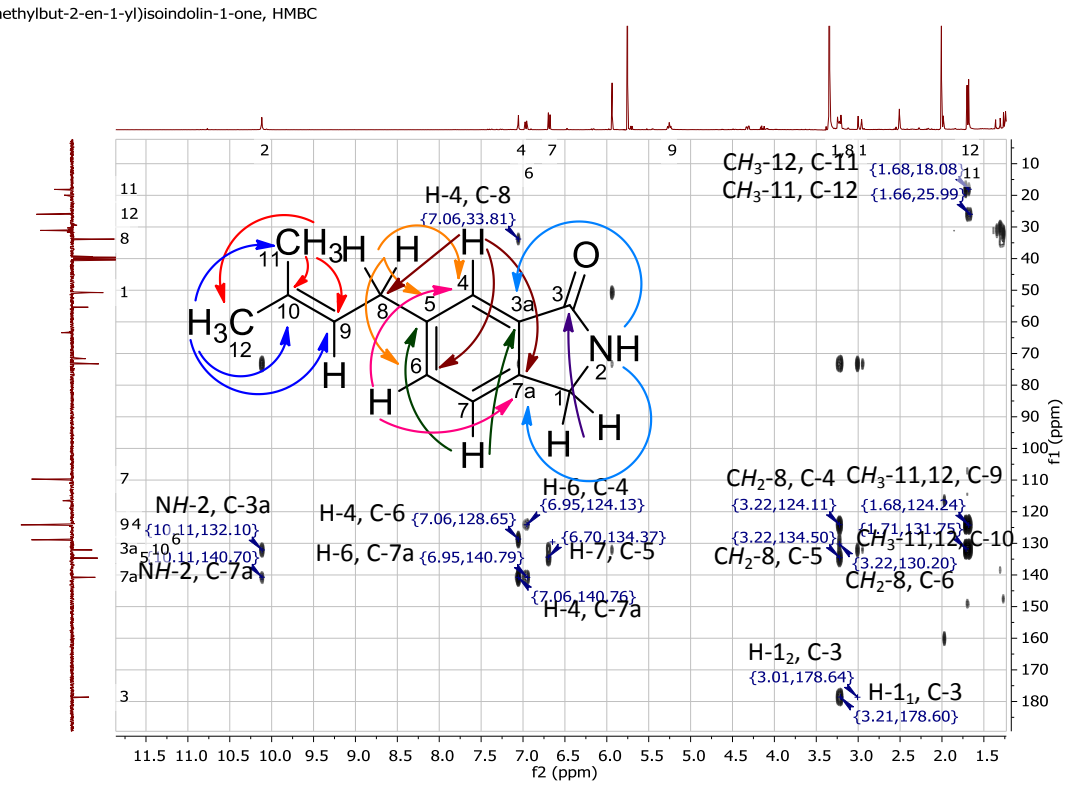

Figure 5.26: ^{1}H-^{13}C HMBC NMR (400 MHz) spectrum for chaetomipyrrolidinone, measured in DMSO-d_6.

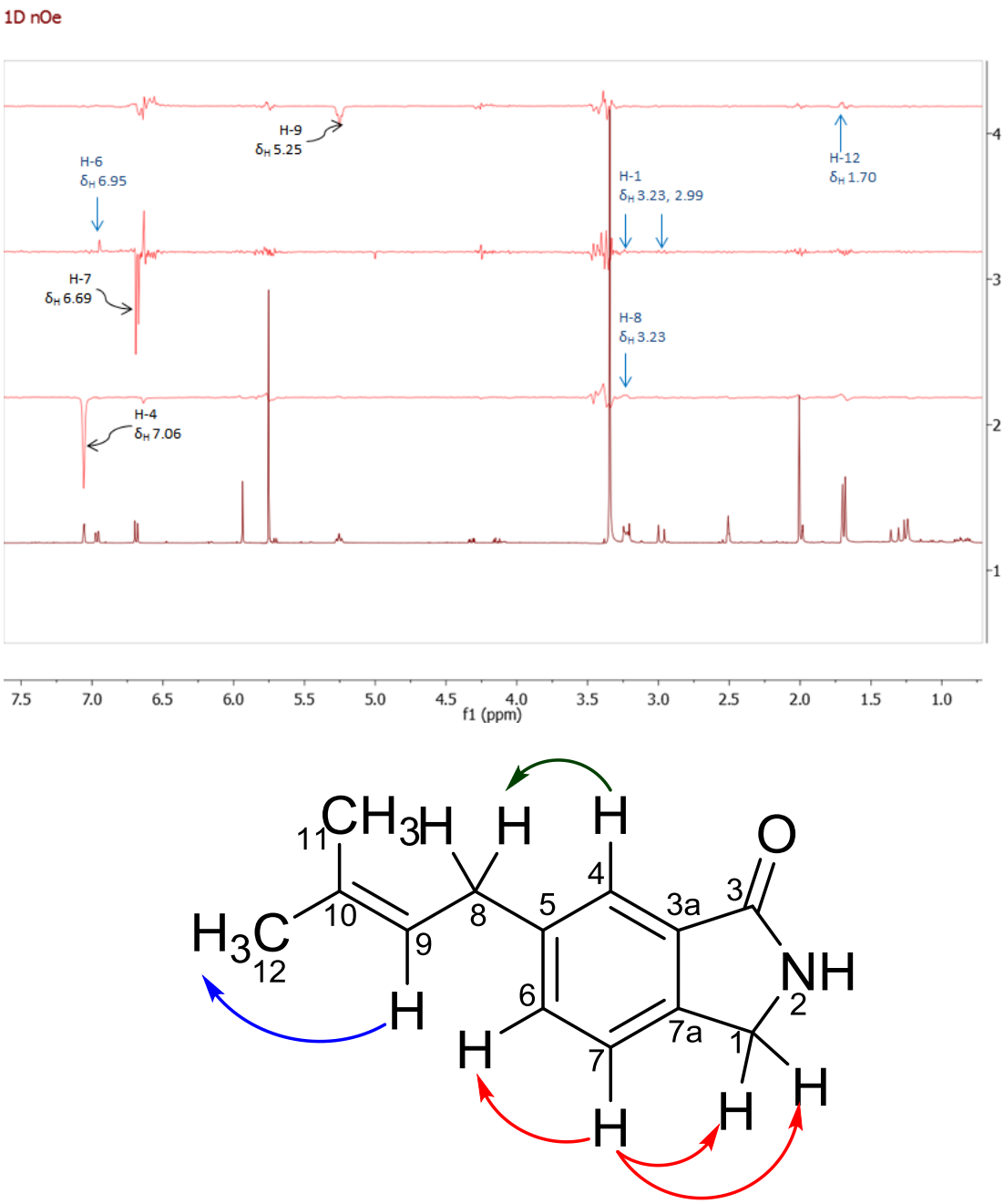

Figure 5.27: 1D nOe NMR (400 MHz) spectrum with irradiation of H-4, H-7 and H-9 for chaetomipyrrolidinone, measured in DMSO-d_6.

Table 5.14: ^{1}H and ^{13}C NMR data for chaetomipyrrolidinone compared to cochliodinol.

	Chaetomipyrrolidinone in DMSO-*d*$_6$						**Cochliodinol in DMSO-*d*$_6$**				
	^{1}H NMR data (400 MHz)				^{13}C NMR data (100 MHz)		^{1}H NMR data (400 MHz)				^{13}C NMR data (100 MHz)
Atom no.	δ_H (ppm)	Integration	Multiplicity	*J* (Hz)	δ_C (ppm)	Multiplicity	δ_H (ppm)	Integration	Multiplicity	*J* (Hz)	δ_C (ppm)
1	2.98 (1_2) 3.23 (1_1)	2H	d, overlapped by water	2.6	50.8	CH_2	11.27 (NH)	1H	d	2.6	
2	10.12 (NH)	1H	s				7.46	1H	d	2.6	127.9
3					178.6	C					104.5
3a					131.8	C					127.20
4	7.06	1H	d	1.7	124.1	CH	7.23	1H	d	1	120.9
5					134.7	C					131.9
6	6.97	1H	dd	7.9, 1.3	128.9	CH	6.93	1H	dd	8.3, 1.6	122.3
7	6.69	1H	d	8.2	109.7	CH	7.33	1H	d	8.3	111.7
7a					140.7	C					134.7
8	3.23	2H	overlapped by water	0	33.8	CH_2	3.34	2H	overlapped by water	0	34.7
9	5.25	1H	ddq	8.9, 5.8, 1.5	124.2	CH	5.33	1H	ddq	7.4, 6.0, 1.6	125.3
10					132.1	C					130.9
11	1.68	3H	s		18.1	CH_3	1.70	3H	s		18.2
12	1.70	3H	s		26.0	CH_3	1.72	3H	s		26.0

5.6.4 Chaetomiside A (4)

Chaetomiside A (new compound)

Fraction: H.7.10.9
Retention time: 6.42 min
Synonym(s):

- (2*S*)-3-((2,4-Dihydroxy-6-methylbenzoyl)oxy)-2-hydroxybutanoic acid

Source: *Chaetomium subaffine* isolated from *Anthemis palestina*
Amount of sample: 11.4 mg
Percent yield: 0.03%
Percent purity: 94.2%
Physical description: brown oil
Molecular formula: $C_{12}H_{14}O_7$
Molecular weight: 270.0740 g/mol
Optical rotation: $[\alpha]_D^{20}$ = -6 (0.1 g/100 mL, MeOH)

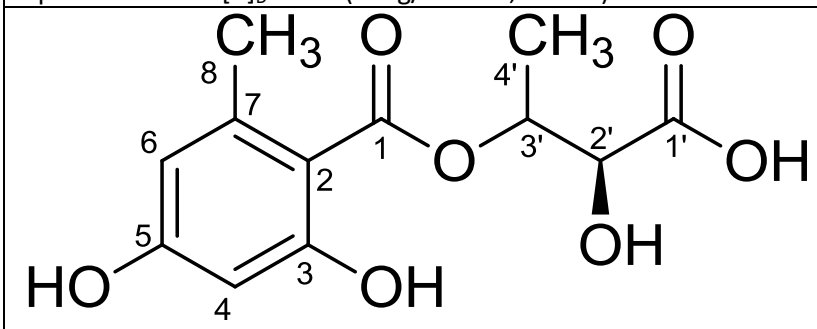

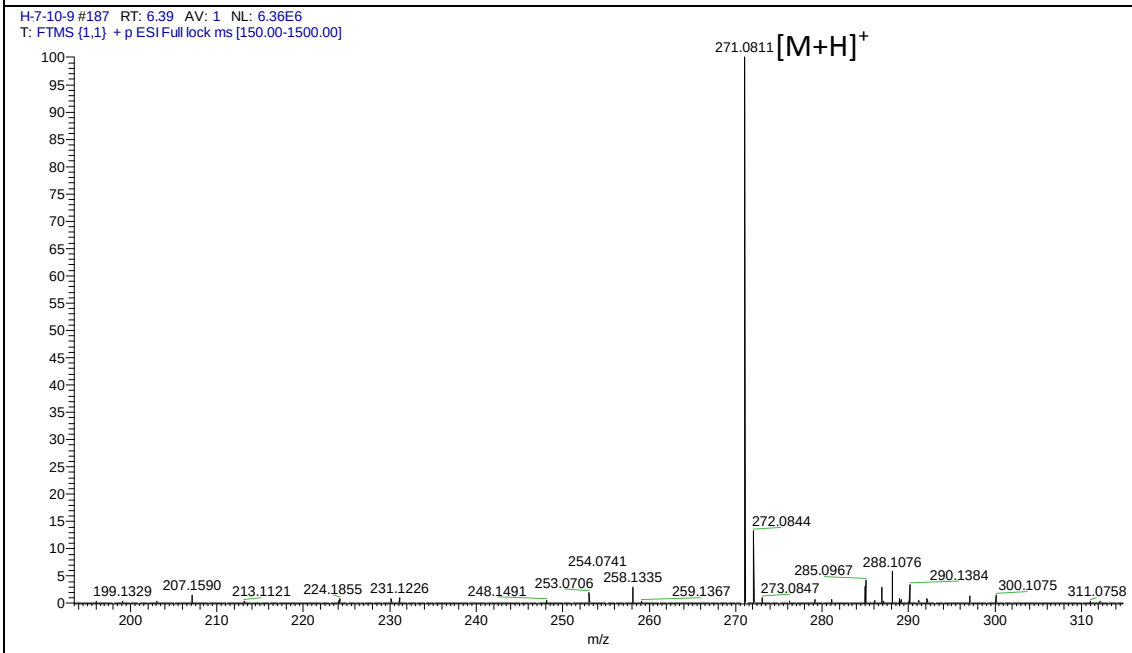

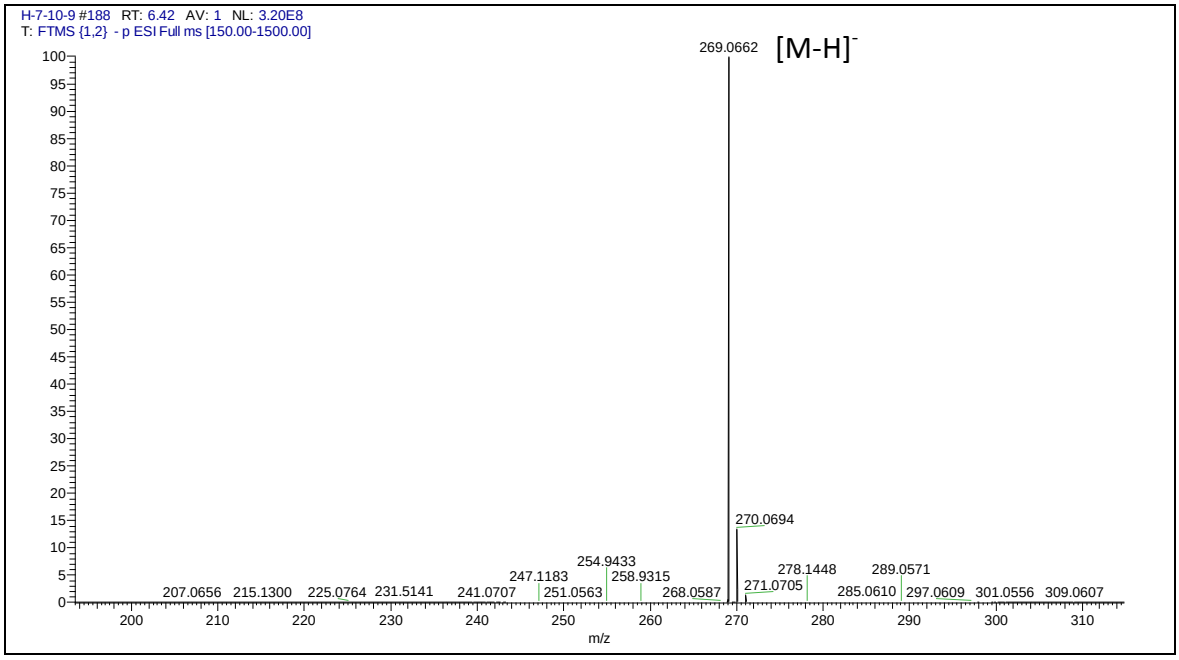

Chaetomiside A was isolated as brown oil with a yield of 0.03% (11.4 mg). LC-HRMS data granted a pseudomolecular ion at *m/z* 271.0811 $[M+H]^+$ and 269.0662 $[M-H]^-$, suggesting a molecular weight of 270.0740 g/mol. The molecular formula afforded by HRMS is $C_{12}H_{14}O_7$.

Chaetomiside A is composed of two substructural units, an orsellinate and a 2,3-dihydroxybutyric acid. The signals of the orsellinate's protons were identified in the ^{1}H NMR spectrum (Figure 5.28), in which, two doublets resonated at δ_H 6.18 and δ_H 6.22 that corresponded to H-4 and H-6, respectively. Both signals had a coupling constant of *J*=2.3 Hz, indicating their position as *meta* to each other. The singlet at δ_H 2.43 was assigned to the methyl C*H*$_3$-8 that is attached to the benzene ring via C-7.

JMod and ^{1}H-^{13}C HSQC experiments afforded both carbons and proton-carbon assignments (Figure 5.30 and 5.31). The presence of the carboxylate group was revealed by the value of its chemical shift at δ_C 169.6. The two signals at δ_C 162.3 and δ_C 162.7 were assigned to the two phenolic carbons C-3 and C-5, respectively. The methyl C*H*$_3$-8 (δ_C 23.3) is attached to the benzene ring via C-7 (δ_C 142.6). Moreover, the HSQC experiment revealed that H-4 is attached to C-4 (δ_C 101.0) and H-6 is attached to C-6 (δ_C 111.3).

The connectivity of orsellinate moiety was established by a ^{1}H-^{13}C HMBC experiment (Figure 5.32). It exhibited ^{3}J correlations from H-4 to both C-2 and C-6 in addition to ^{2}J correlations to C-3 and C-5. Moreover, ^{3}J correlations were observed from H-6 to C-2, C-4 and CH_3-8, from H-8 to both C-2 and C-6 and from 5-O*H* to both C-4 and C-6. The presence of orsellinate moeity in chaetomiside A was further confirmed by comparing both its ^{1}H and ^{13}C NMR data to those of orsellide A in literature (Schloerke and Zeeck, 2006) (Table 5.15).

The second substructural unit is 2,3-dihydroxybutyric acid. It is attached to the orsellinate by its hydroxyl unit at position 3'. The spin system of this unit is explained utlising the ^{1}H-^{1}H COSY NMR experiment (Figure 5.29). The protons of the methyl CH_3-4' (δ_H 1.19, *J*=6.4 Hz) coupled to a quartet of doublet H-3' (δ_H 4.15, *J*=6.4, 3.5 Hz) which further coupled to the doublet H-2' (δ_H 5.11, *J*=3.5 Hz). Moreover, these connectivities were confirmed by a ^{1}H-^{13}C HMBC experiment (Figure 5.32). The HMBC spectrum showed ^{2}J correlations from both H-2' and CH_3-4' to C-3', as well as from H-2' to the carboxyl carbon, C-1. Furthermore, the spectrum indicated ^{3}J correlations from H-2' to C-4' and, vice versa, from CH_3-4' to C-2'. The oxygenation occurred on both C-2' (δ_C 77.7) and C-3' (δ_C 66.1) as directed by their carbon chemical shift data from the JMod NMR spectrum (Figure 5.30).

The stereochemistry of the chiral centre C-2' was established by Mosher's method. This was attained by observing the changes in the chemical shifts of the neighbouring protons and by comparing the bis-*(R)*-MTPA-Cl and the bis-*(S)*-MTPA-Cl derivatives of the orsellide (Figure 5.33). The chemical shift of the methyl (CH_3-4') protons was shifted downfield to δ_H 1.71 upon reacting with the bis-*(R)*-MTPA-Cl reagent and to δ_H 1.61 ppm upon reacting with the bis-*(S)*-MTPA-Cl reagent. The $\Delta\delta^{S-R}$ value for CH_3-4' was calculated to be +0.1 ppm, bearing in mind that *R* Mosher acid chloride gives rise to the *S* Mosher ester and vice versa (Hoye *et al*., 2007).

The positive value marked the position of the methyl at C-4' at the right of the ester unit attached to the chiral centre C-2'. By assigning H-2' backwards while the carboxylate carbon C-1' was positioned left of the chiral centre, the *S* configuration was established.

Furthermore, the presence of 2,3-dihydroxybutyric acid was confirmed by comparing both its ^{1}H and ^{13}C NMR to 4-deoxyerythreonic, (2*S*,3*R*)-2,3-dihydroxybutanoic acid, from the literature (Appiah-Amponsah *et al*., 2009) (Table 5.16).

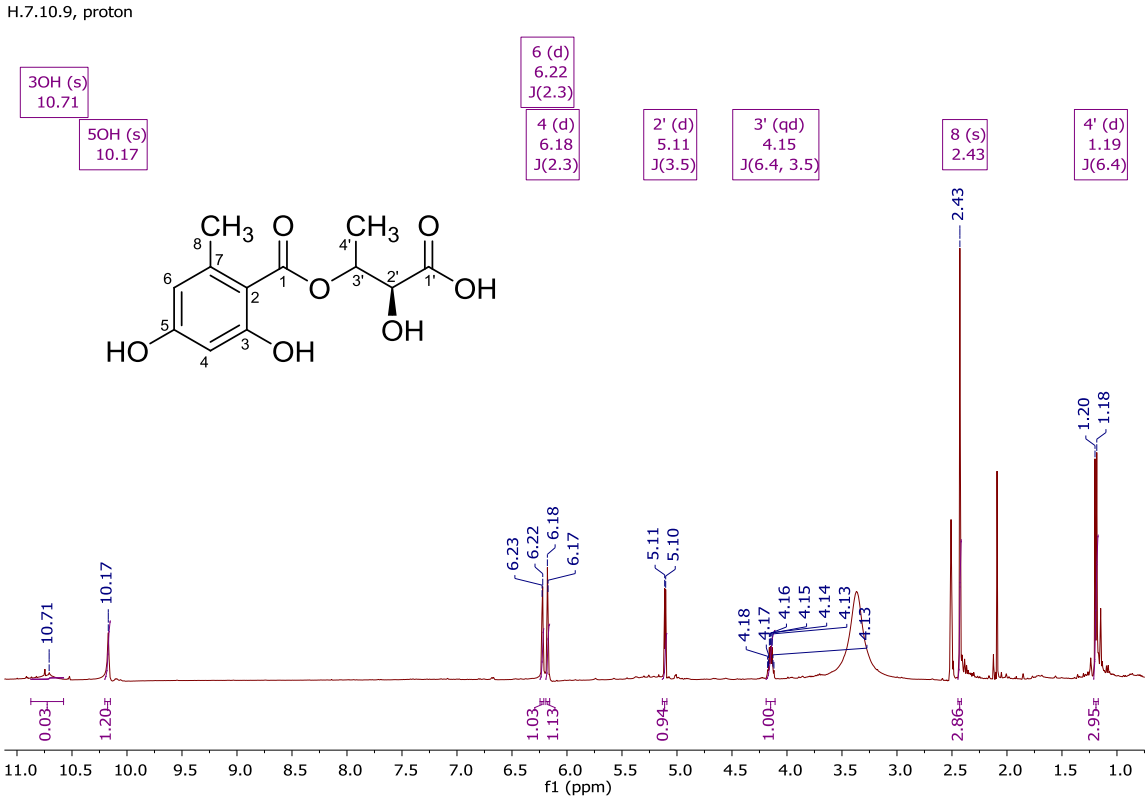

Figure 5.28: ^{1}H NMR (400 MHz) spectrum for chaetomiside A, measured in DMSO-d_6.

H.7.10.9, COSY

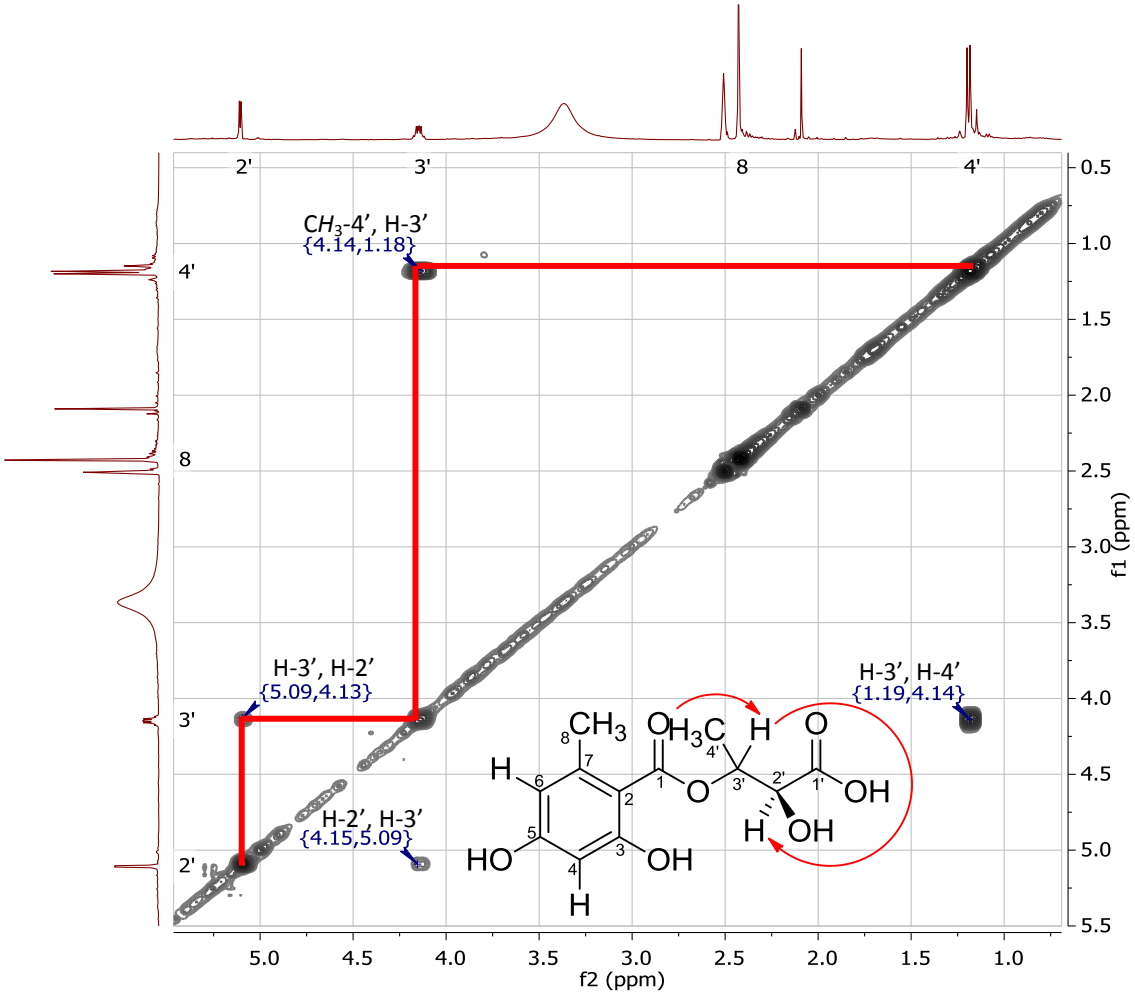

Figure 5.29: ^{1}H-^{1}H COSY NMR (400 MHz) spectrum for chaetomiside A, measured in DMSO-d_6.

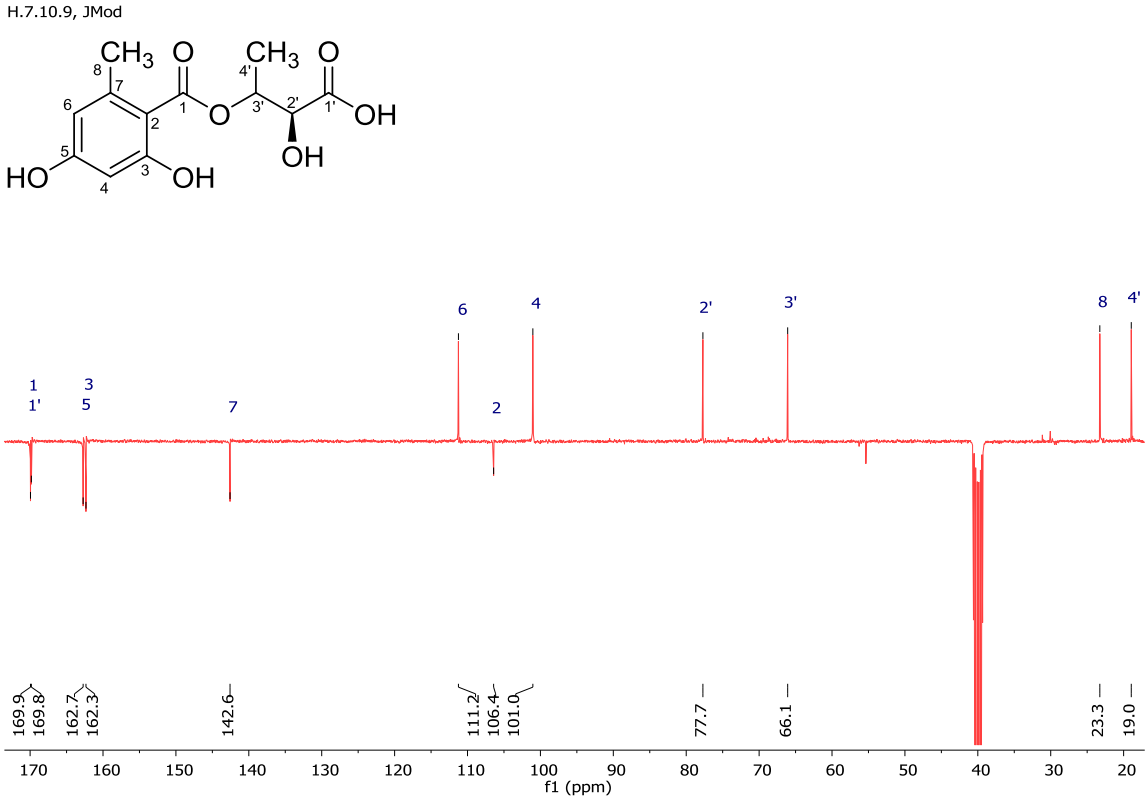

Figure 5.30: JMod NMR (100 MHz) spectrum for chaetomiside A, measured in DMSO-d_6.

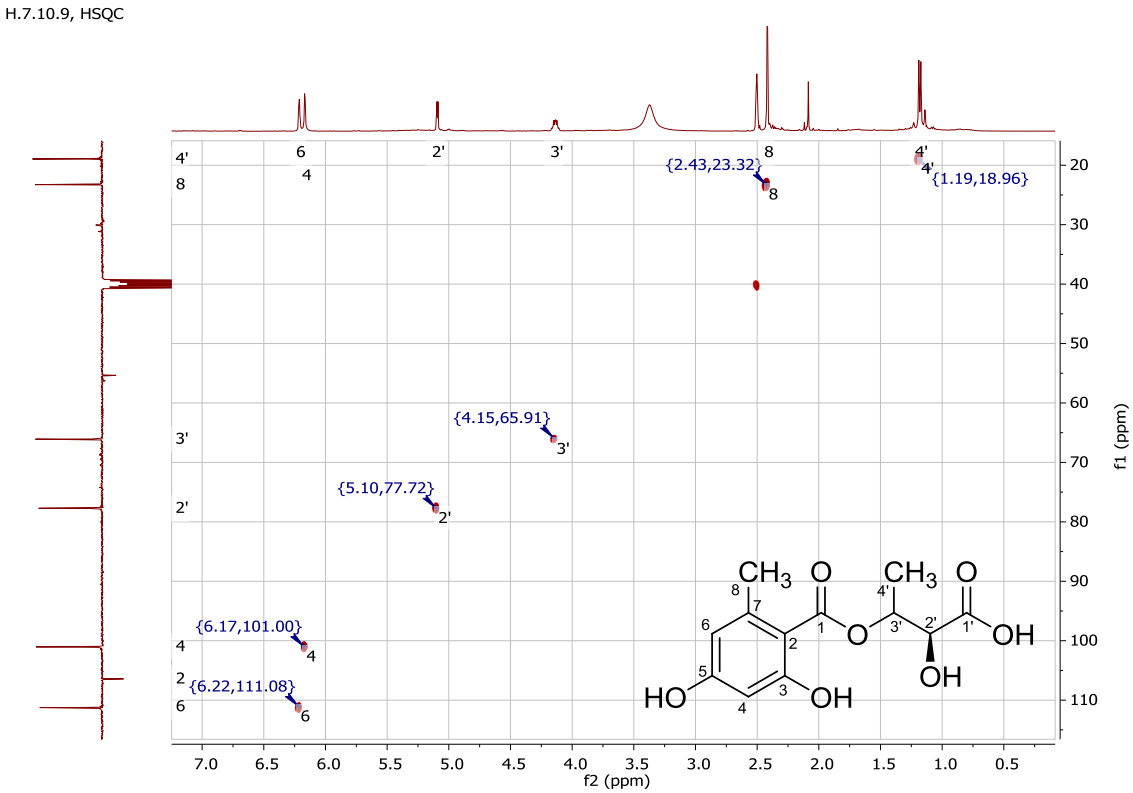

Figure 5.31: ^{1}H-^{13}C HSQC NMR (400 MHz) spectrum for chaetomiside A, measured in DMSO-d_6.

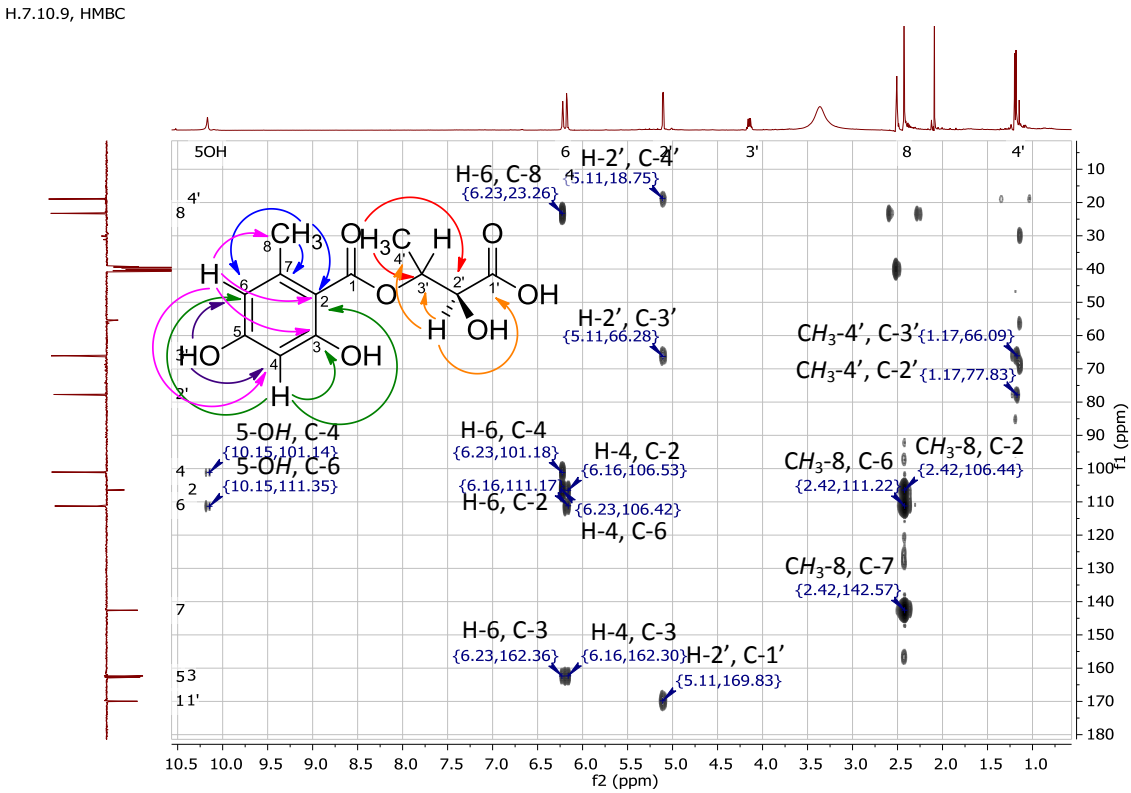

Figure 5.32: ^{1}H-^{13}C HMBC NMR (400 MHz) spectrum for chaetomiside A, measured in DMSO-d_6.

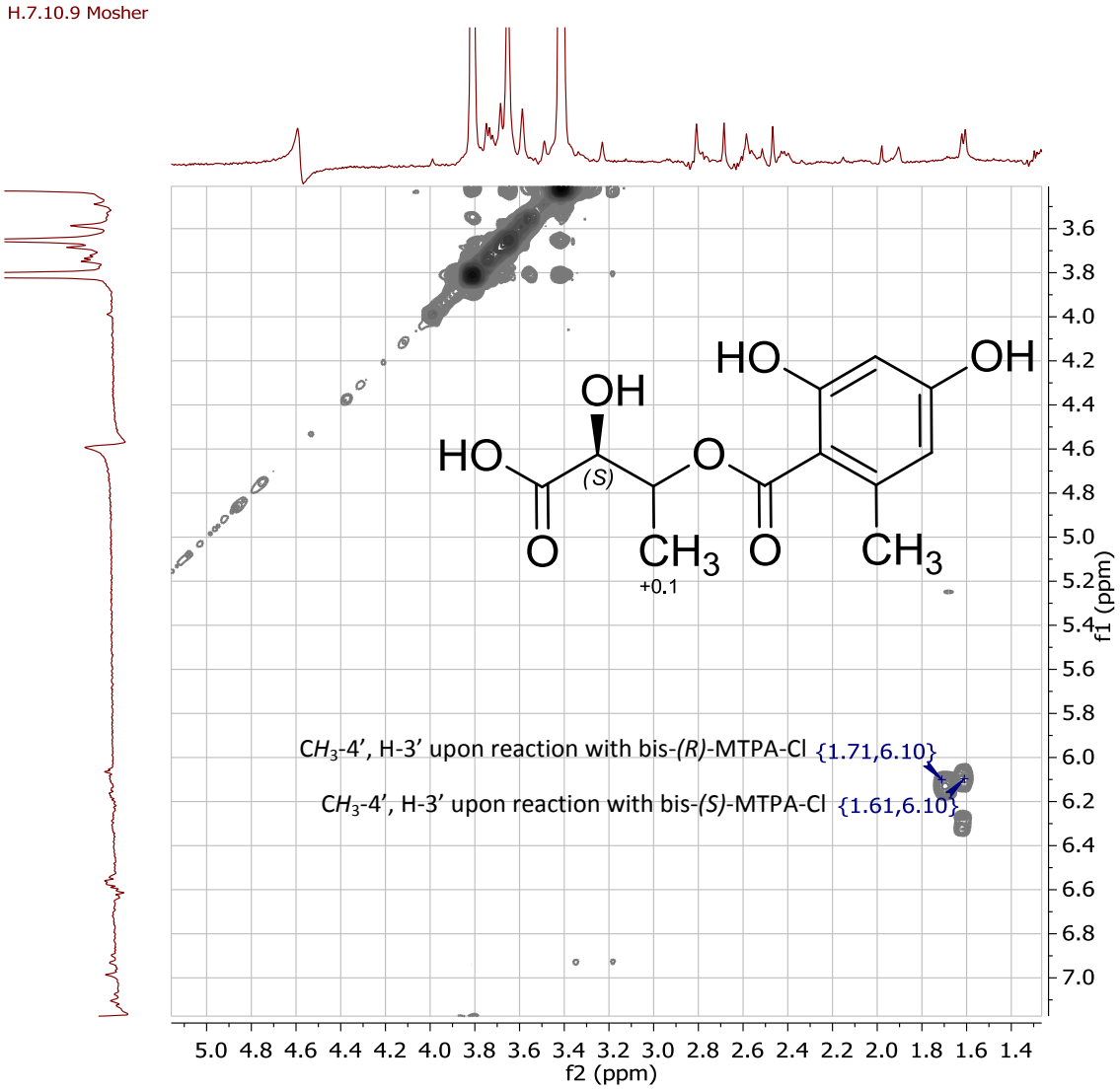

Figure 5.33: Superimposed ^{1}H-^{1}H COSY NMR (400 MHz) spectrum for chaetomiside A, measured 8 hours after it was reacted with both bis-*(R)*-MTPA-Cl and bis-*(S)*-MTPA-Cl reagents, measured in Pyridine-d_5.

Table 5.15: ^{1}H and ^{13}C NMR data for orsellinate part in chaetomiside A compared to oresellide A.

	Chaetomiside A in DMSO-d_6						**Orsellide A (Schloerke and Zeeck, 2006) in $CDCl_3$**					
	^{1}H NMR data (400 MHz)				^{13}C NMR data (100 MHz)		^{1}H NMR data (600 MHz)				^{13}C NMR data (150 MHz)	
Atom no.	δ_H (ppm)	Integration	Multiplicity	*J* (Hz)	δ_C (ppm)	Multiplicity	δ_H (ppm)	Integration	Multiplicity	*J* (Hz)	δ_C (ppm)	Multiplicity
1					169.6	C					169.4	C
2					106.4	C					104.6	C
3					162.3	C					165.2	C
4	6.18	1H	d	2.3	101.0	CH	6.22	1H	d	2.0	101.3	C
5					162.7	C					161.2	C
6	6.22	1H	d	2.3	111.3	CH	6.24	1H	d	2.0	111.9	CH
7					142.6	C					145.2	C
8	2.43	3H	s		23.3	CH_3	2.51	3H	s		24.2	CH_3
3-OH	10.79	1H	s				11.02	1H	s			
5-OH	10.17	1H	s									

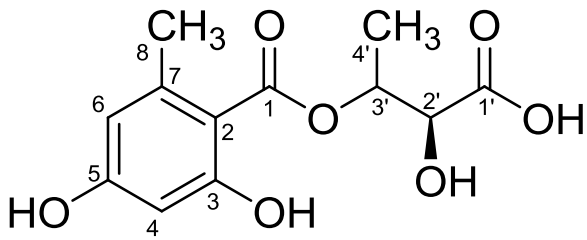

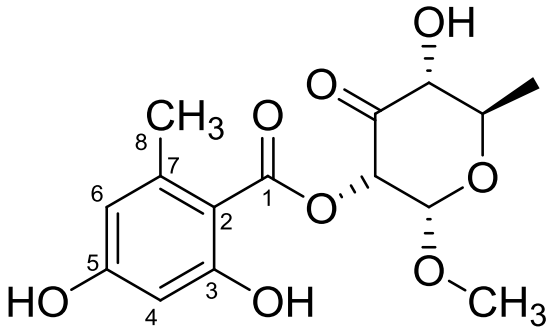

Table 5.16: ^{1}H and ^{13}C NMR data for the 2,3-dihydroxybutyric acid part in chaetomiside A compared to 4-deoxyerythreonic from the literature.

	Chaetomiside A in DMSO-d_6						**4-deoxyerythreonic acid (Appiah-Amponsah *et al.*, 2009) in D_2O**			
	^{1}H NMR data (400 MHz)				^{13}C NMR data (100 MHz)		^{1}H NMR data (500 MHz)		^{13}C NMR data	
Atom no.	δ_H (ppm)	Integration	Multiplicity	J (Hz)	δ_C (ppm)	Multiplicity	δ_H (ppm)	Integration	δ_C (ppm)	Multiplicity
1'					169.8	C			175.4	C
2'	5.11	1H	d	3.6	77.7	CH	4.22	1H	74.1	CH
3'	4.15	1H	qd	6.4, 3.6	66.1	CH	4.08	1H	68.3	CH
4'	1.19	3H	d	6.4	19.0	CH_3	1.14	3H	16.2	CH_3

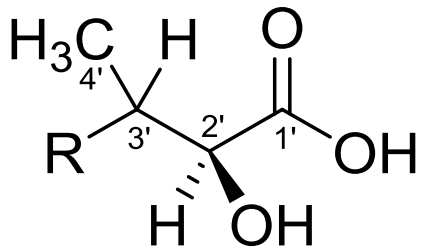

R = orsellinate, chaetomiside A
R = H, 4-deoxyerythreonic acid

5.6.5 Chaetomiside B (5)

Chaetomiside B (new compound)

Fraction: H.7.10.6.7
Retention time: 15.50 min
Synonym(s):

- 2-Oxo-2-((4*S*,5*S*)-2,2,5-trimethyl-1,3-dioxolan-4-yl)ethyl 2,4-dihydroxy-6-methylbenzoate

Source: *Chaetomium subaffine*, isolated from *Anthemis palestina*
Amount of sample: 6.0 mg
Percent yield: 0.02%
Percent purity: 99.0%
Physical description: brownish-yellow oil
Molecular formula: $C_{16}H_{20}O_7$
Molecular weight: 324.1209 g/mol
Optical rotation: $[\alpha]_D^{20}$ = +34 (0.1 g/100 mL, MeOH)

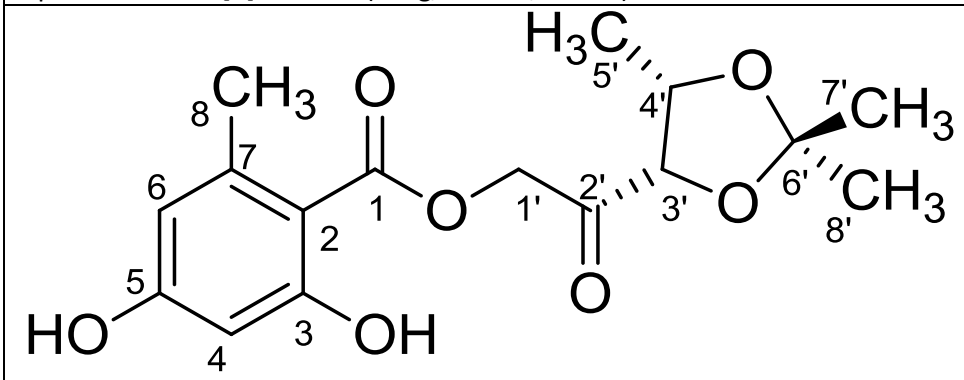

Stereochemistry is relative

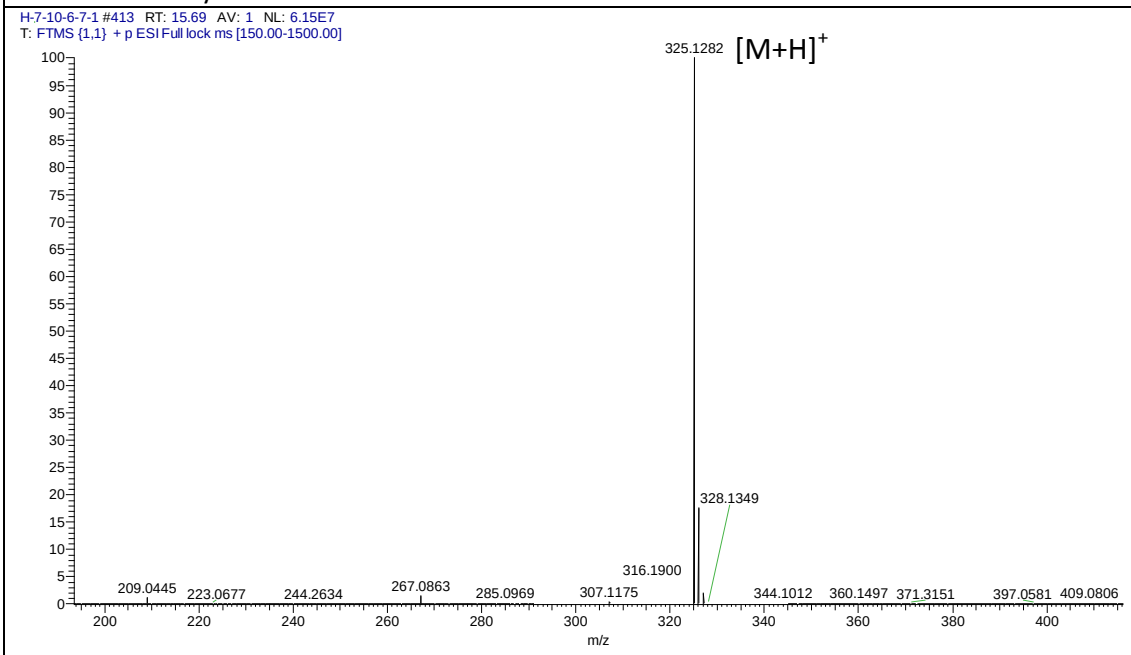

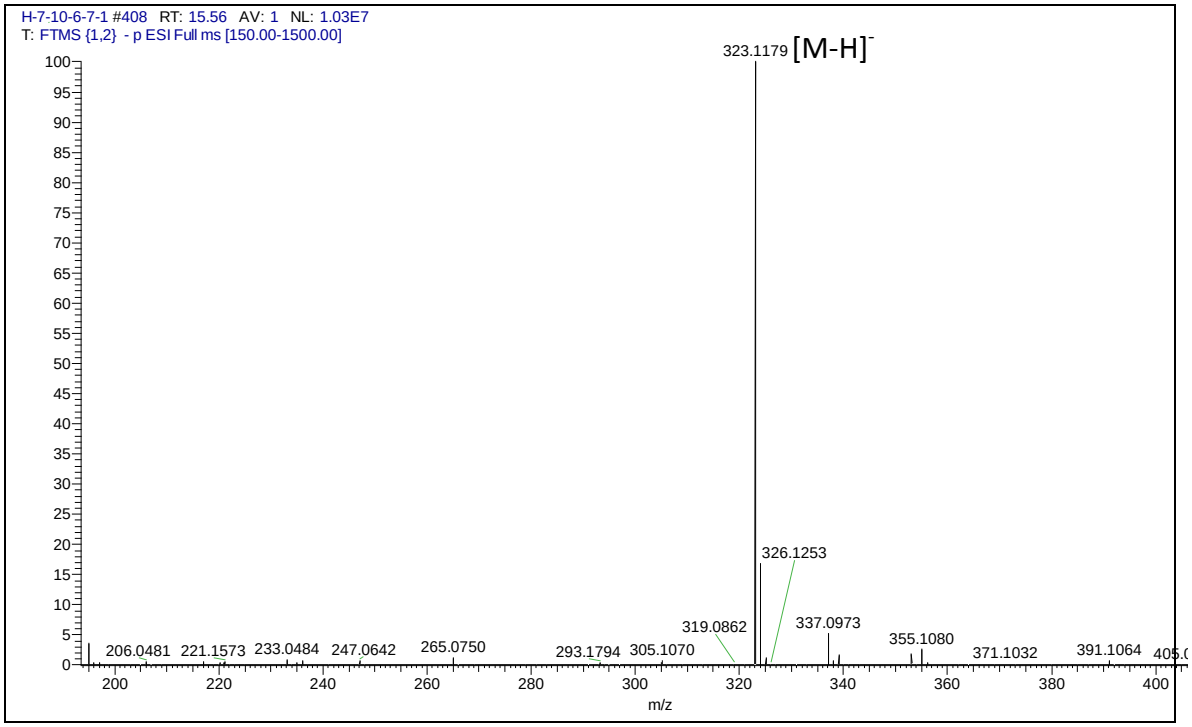

Chaetomiside B was isolated as a brownish yellow oil with a yield of 0.02% (6.0 mg). LC-HRMS data revealed a pseudomolecular ion at *m/z* 325.1282 $[M+H]^+$ and 323.1179 $[M-H]^-$. This concludes a molecular weight of 324.1209 g/mol. The molecular formula $C_{16}H_{20}O_7$ was established by HRMS.

As indicated by the typical NMR resonances for orsellides, orsellinate is one of the subunits that made up chaetomiside B. The occurrence of the orsellide unit was detected via ^{1}H and JMod NMR experiments and confirmed by comparing the data obtained from the mentioned experiments to those of chaetomiside A (Table 5.17).

The second subunit found in chaetomiside B is 2-oxo-2-((4*S*,5*S*)-2,2,5-trimethyl-1,3-dioxolan-4-yl)ethanolate. In the ^{1}H NMR spectrum (Figure 5.34), a doublet could be detected at δ_H 1.15 (*J*=6.2 Hz) resembling the protons of the methyl CH_3-5'. This doublet is coupled through ^{1}H-^{1}H COSY (Figure 5.35) to the H-4' pentet (δ_H 4.60, *J*=6.5 Hz, which coupled to the H-3' doublet (δ_H 4.64, *J*=7.7 Hz). The attachment of two oxygen atoms to both C-4' and C-3' is reponsible for the deshielding effect that caused the signals of their protons to be shifted downfield. Moreover, two singlets that represents the methyl units CH_3-7' and CH_3-8' resonated at δ_H 1.35 and 1.55,

respectively. The geminal protons of CH_2-1' could be found as two doublets at δ_H 5.10 and 5.20 with a coupling constant of 18.0 Hz. The position of the methylene unit between a ketone and an ester functional group caused their resonases to be shifted downfield.

Both JMod and ^{1}H-^{13}C HSQC experiments were conducted to establish both carbons and proton-carbon assignments (Figures 5.36 and 5.37). As oxygen bearing carbons, the chemical shift values of C-1' (δ_C 68.8 ppm), C-3' (δ_C 81.5 ppm), C-4' (δ_C 73.8 ppm), the highly oxygenated C-6' (δ_C 109.6 ppm) and the carbonyl C-2' (δ_C 204.2 ppm) were observed. The carbon signal for C-6' was detected at δ_C 109.6, more downfield than those of C-3' (δ_C 81.5), C-4' (δ_C 73.8) and C-1' (δ_C 68.8). The downfield shift for C-6' was due to the attachment of two geminal oxygen atoms. Furthermore, a signal was detected at δ_C 204.2 and assigned to the ketone group at C-2'

The connectivity of this unit was verified by a ^{1}H-^{13}C HMBC experiment (Figure 5.38). The spectrum exhibited ^2J correlations from both CH_3-7' and CH_3-8' to C-6'. Moreover, ^3J correlations were shown from CH_3-7' to C-8' and from CH_3-8' to C-7'. The attachment of C*H*-3' to the carbonyl C-2' afforded a ^3J correlations to both C-1' and C-6'. In addition to that, ^3J correlations were detected for CH_2-1' to C-1 and CH_3-5' to C-3'. The spectrum also exhibited ^2J correlations from CH_2-1' to C-2' and CH_3-5' to C-4'.

The presence of the 2-oxo-2-((4*S*,5*S*)-2,2,5-trimethyl-1,3-dioxolan-4-yl)ethanolate moeity in chaetomiside B was further confirmed by the comparison of its ^{1}H and ^{13}C NMR data to those found in the literature (Fronza *et al*., 2009) (Table 5.18). However, the oxygenation of CH_2-1' and its loss of a proton upon its attachment to orsellinate resulted in the changes in its ^{1}H and ^{13}C NMR chemical shifts, as well as its ^{1}H NMR's integration. The attachment of the oxygen deshielded CH_2-1', and the chemical shift of its protons went downdield from δ_H 2.21, as described in the literature, to δ_H 5.10 and 5.20 in chaetomiside B and the chemical shift of its carbon from δ_C 25.1 to δ_C 68.86.

The relative stereochemistry at positions 3', 4' and 6' was determined by running a ROESY experiment (Figure 5.39). The spectrum depicted two correlations from CH_3-7' to both C*H*-3' and C*H*-4'. This revealed that these protons are in *cis* position to each other while in *trans* position to CH_3-5' and CH_3-8'.

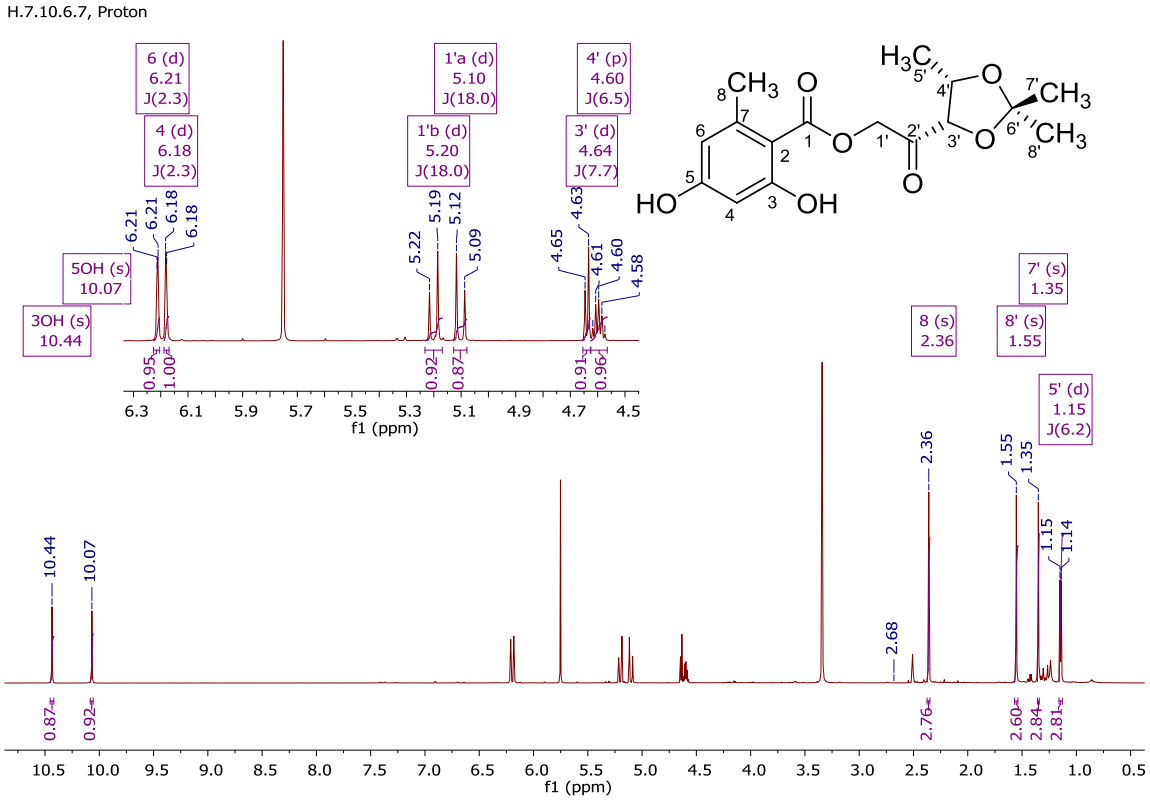

Figure 5.34: ^{1}H NMR (600 MHz) spectrum for chaetomiside B, measured in DMSO-d_6.

H.7.10.6 COSY

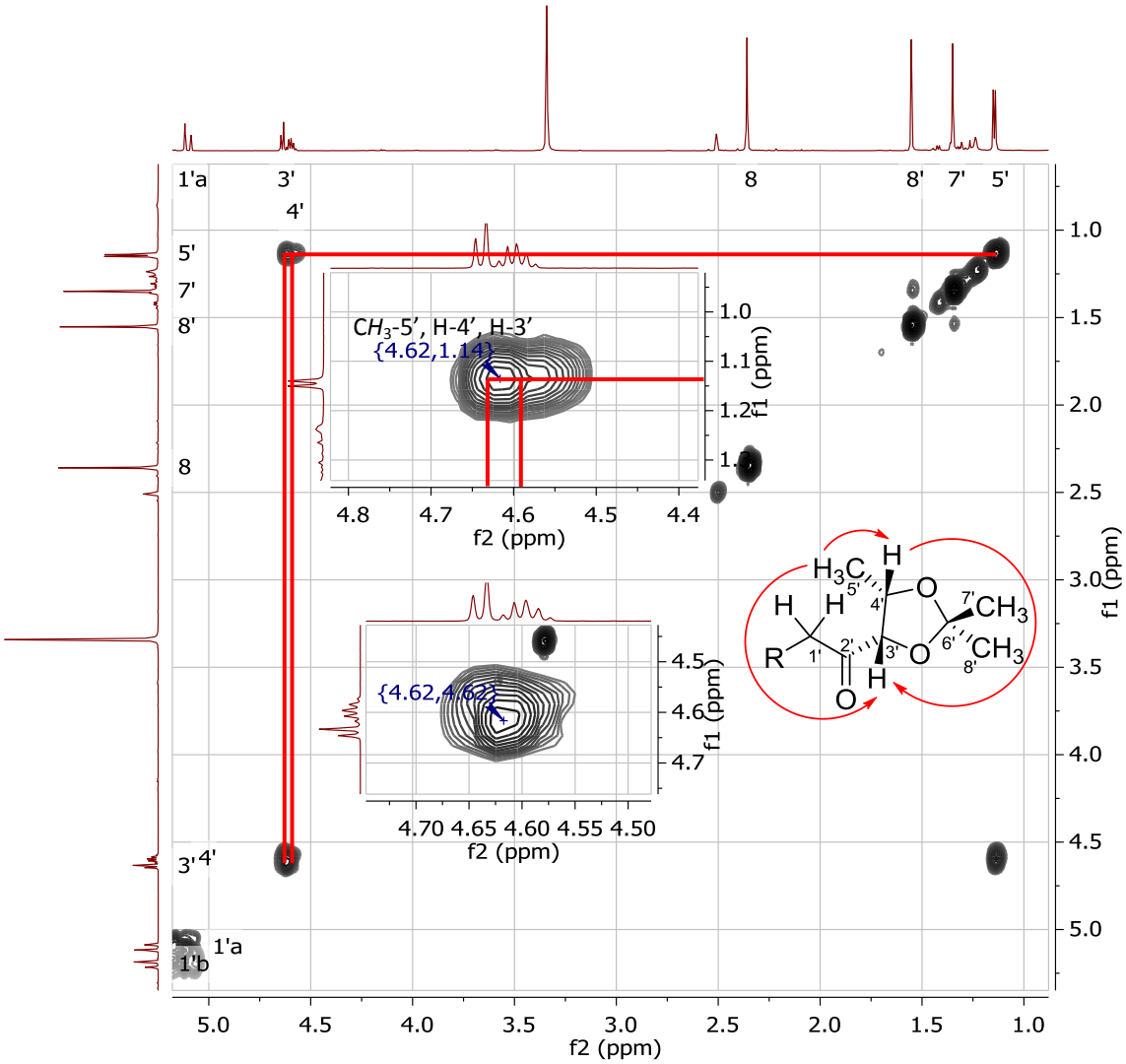

Figure 5.35: ^{1}H-^{1}H COSY (400 MHz) NMR spectrum for chaetomiside B, measured in DMSO-d_6.

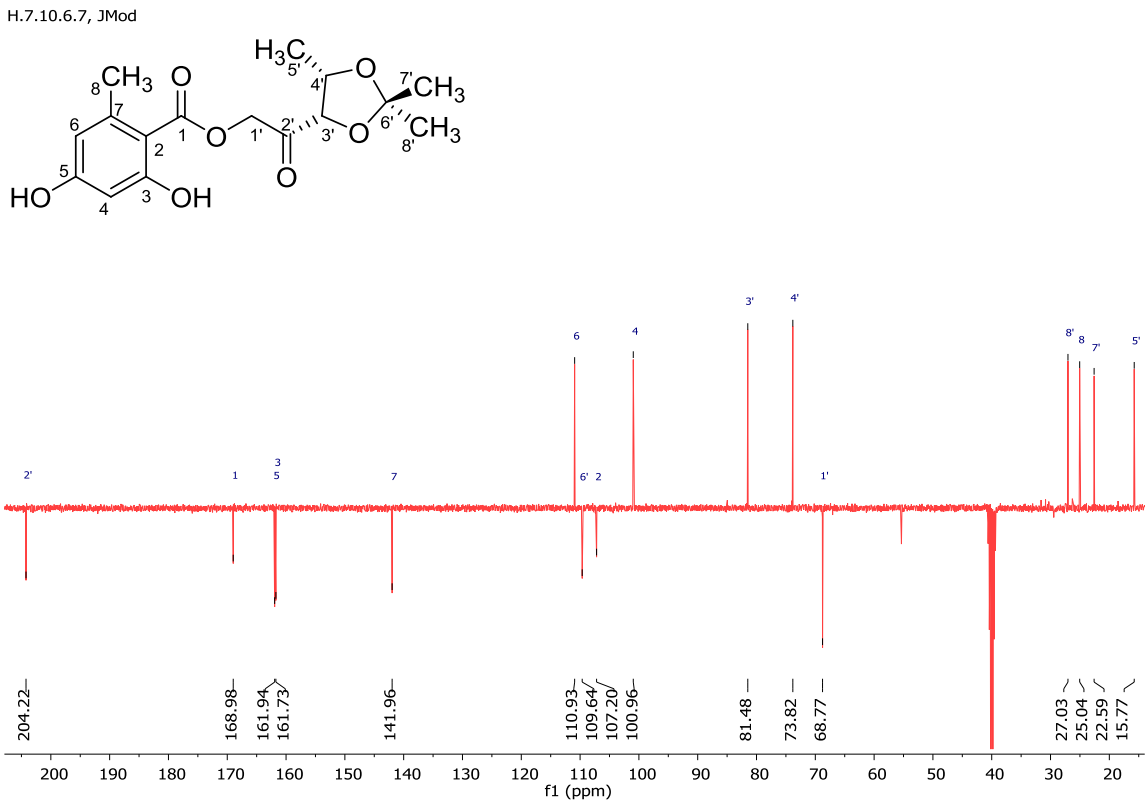

Figure 5.36: JMod NMR (100 MHz) spectrum for chaetomiside B, measured in DMSO-d_6.

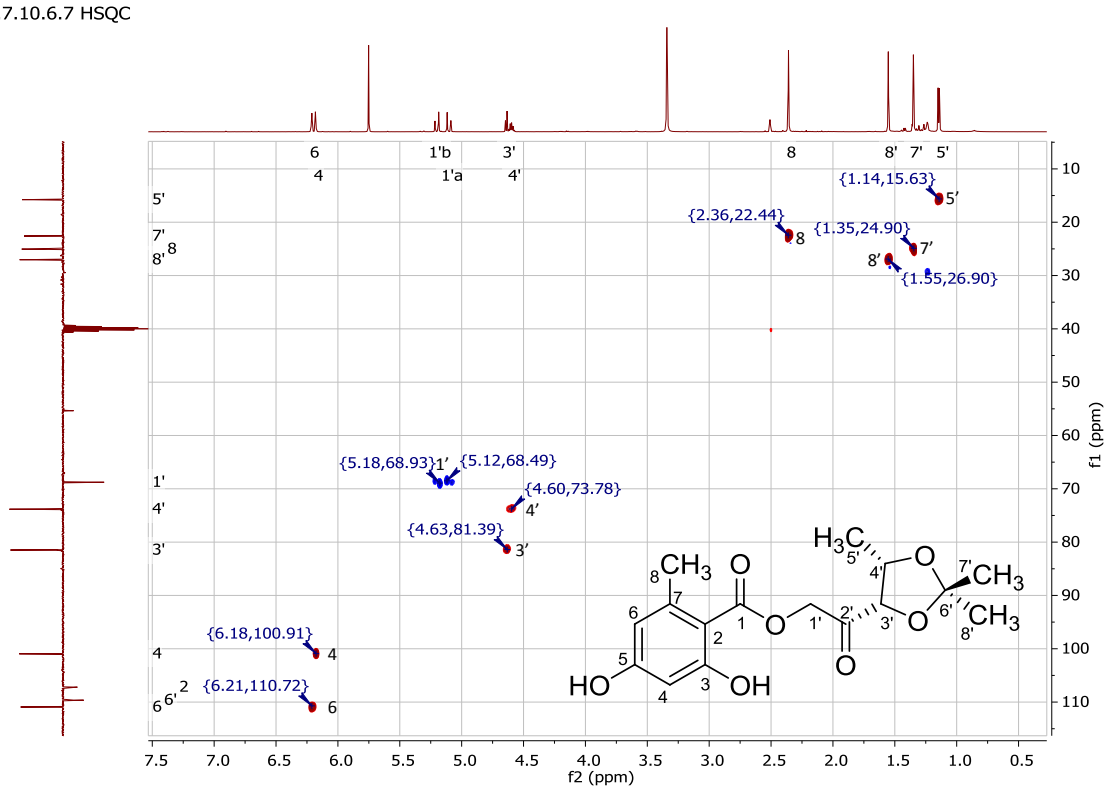

Figure 5.37: ^{1}H-^{13}C HSQC NMR (400 MHz) spectrum for chaetomiside B, measured in DMSO-d_6.

H.7.10.6.7 HMBC

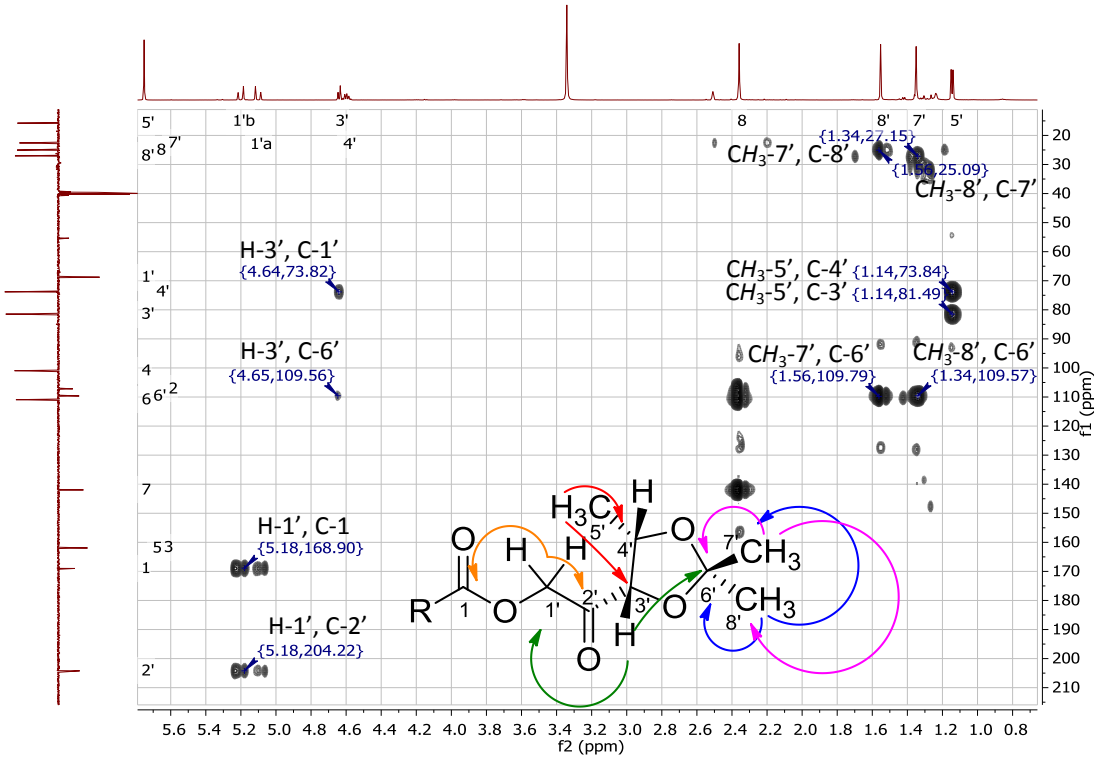

Figure 5.38: ^{1}H-^{13}C HMBC NMR (400 MHz) spectrum for chaetomiside B, measured in DMSO-d_6.

H.7.10.6.7, ROESY

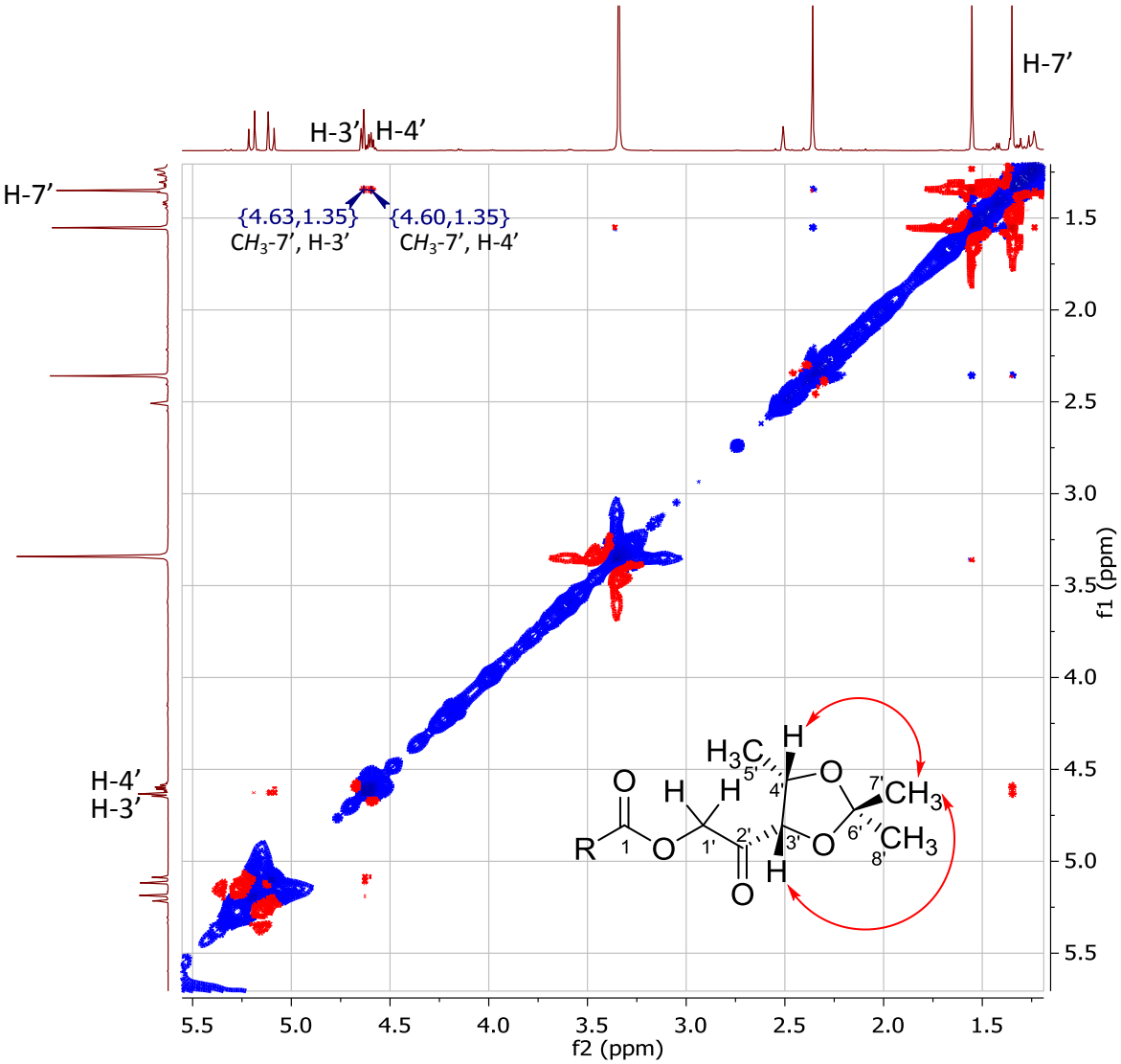

Figure 5.39: ^{1}H-^{1}H ROESY NMR (600 MHz) spectrum for chaetomiside B, measured in DMSO-d_6. Mixing time = 120 ms, spectral width (SWH) = 7211.5 Hz, free induction decay resolution (FIDRES) = 7.04 Hz, P1 = 7.93 µsec, D1= 2 sec, PLW1 = 9.6 W.

Table 5.17: ^{1}H and ^{13}C NMR data for orsellinate part in chaetomisides A – D, measured in DMSO-d_6.

	chaetomiside A		chaetomiside B		chaetomiside C		chaetomiside D	
Atom no.	δ_H (ppm), (integration, multiplicity, *J* (Hz)), (400 MHz)	δ_C (ppm), (100 MHz)	δ_H (ppm), (integration, multiplicity, *J* (Hz)), (600 MHz)	δ_C (ppm), (100 MHz)	δ_H (ppm), (integration, multiplicity, *J* (Hz)), (400 MHz)	δ_C (ppm), (100 MHz)	δ_H (ppm), (integration, multiplicity, *J* (Hz)), (400 MHz)	δ_C (ppm), (100 MHz)
1		169.6 (C)		169.0 (C)		170.1 (C)		170.1 (C)
2		106.4 (C)		107.2 (C)		107.4 (C)		107.2 (C)
3		162.3 (C)		161.7 (C)		162.0 (C)		162.0 (C)
4	6.18 (1H, d, 2.3)	101.0 (CH)	6.18 (1H, d, 2.3)	101.0 (CH)	6.15 (1H, d, 2.5)	101.0 (CH)	6.16 (1H, d, 2.4)	101.0 (CH)
5		162.7 (C)		161.9 (C)		162.3 (C)		162.5 (C)
6	6.22 (1H, d, 2.3)	111.3 (CH)	6.21 (1H, d, 2.3)	110.9 (CH)	6.19 (1H, d, 2.5)	111.2 (CH)	6.19 (1H, d, 2.4)	111.2 (CH)
7		142.6 (C)		142.0 (C)		142.0 (C)		142.4 (C)
8	2.43 (3H, s)	23.3 (CH_3)	2.36 (3H, s)	25.0 (CH_3)	2.39 (3H, s)	23.3 (CH_3)	2.38 (3H, s)	23.3 (CH_3)
3-OH	10.79 (1H, s)		10.43 (1H, s)		10.96 (1H, s)		10.92 (1H, s)	
5-OH	10.17 (1H, s)		10.07 (1H, s)		10.04 (1H, s)		10.05 (1H, s)	

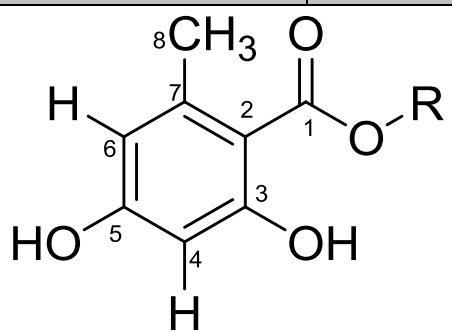

R = 4-deoxyerythreonic acid, chaetomiside A
R = 1-[(4*S*,5*S*)-2,2,5-trimethyl-1,3-dioxolan-4-yl]ethanone, chaetomiside B
R = 5-deoxy-D-ribitol, chaetomiside C
R = 1-deoxy-D-xylitol, chaetomiside D

Table 5.18: ^{1}H and ^{13}C NMR data for the 1,5-dideoxy-3,4-O-(1-methylethylidene)-L-erythro-2-pentulose part in chaetomiside B compared to literature.

	Chaetomiside B in DMSO-d_6						**1-[(4S,5S)-2,2,5-Trimethyl-1,3-dioxolan-4-yl]ethanone (Fronza *et al.*, 2009) in $CDCl_3$**					
	^{1}H NMR data (600 MHz)				^{13}C NMR data (100 MHz)		^{1}H NMR data (400 MHz)				^{13}C NMR data (100 MHz)	
Atom no.	δ_H (ppm)	Integration	Multiplicity	*J* (Hz)	δ_C (ppm)	Multiplicity	δ_H (ppm)	Integration	Multiplicity	*J* (Hz)	δ_C (ppm)	Multiplicity
1'	5.10, 5.20	1H, 1H	d, d	18.0, 18.0	68.8	CH_2	2.21	3H	s		25.1	CH_3
2'					204.2	C					209.5	C
3'	4.64	1H	d	7.7	81.5	CH	4.36	1H	d	7.7	83.1	CH
4'	4.60	1H	p	6.5	73.8	CH	4.52	1H	dq	7.7, 6.4	73.7	CH
5'	1.14	3H	d	6.3	15.8	CH_3	1.16	3H	d	6.4	15.8	CH_3
6'					109.6	C					109.7	C
7'	1.35	3H	s		22.6	CH_3	1.38	3H	s		24.8	CH_3
8'	1.55	3H	s		27.0	CH_3	1.60	3H	s		27.0	CH_3

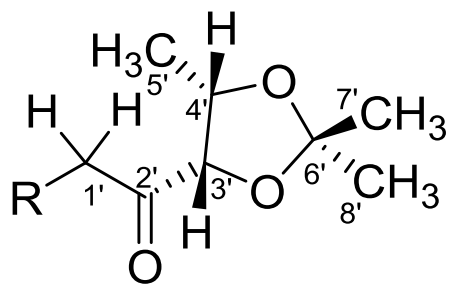

R = orsellinate, chaetomiside B

R = H, 1-[(4*S*,5*S*)-2,2,5-trimethyl-1,3-dioxolan-4-yl]ethanone

5.6.6 Chaetomiside C (6)

Chaetomiside C (new compound)

Fraction: H.8.14.9
Retention time: 5.10 min
Synonym(s):

- (3*S*,4*S*)-1,3,4-Trihydroxypentan-2-yl 2,4-dihydroxy-6-methylbenzoate

Source: *Chaetomium subaffine,* isolated from *Anthemis palestina*
Amount of sample: 17.8 mg
Percent yield: 0.05%
Percent purity: 77.7%
Physical description: brownish yellow oil
Molecular formula: $C_{13}H_{18}O_7$
Molecular weight: 286.1053 g/mol
Optical rotation: $[\alpha]_D^{20}$ = +5 (0.1 g/100 mL, MeOH)

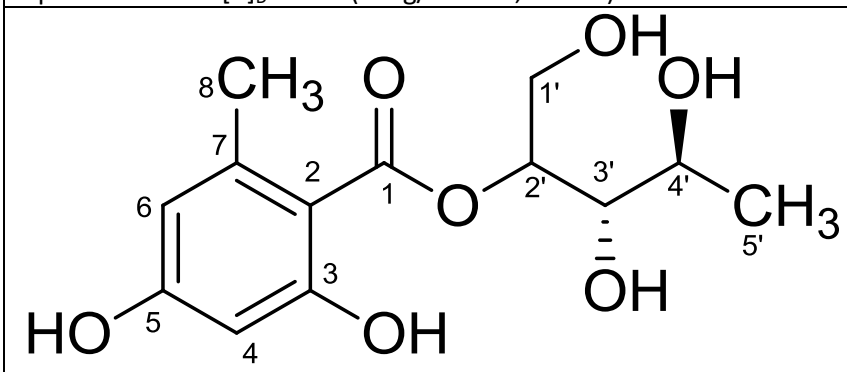

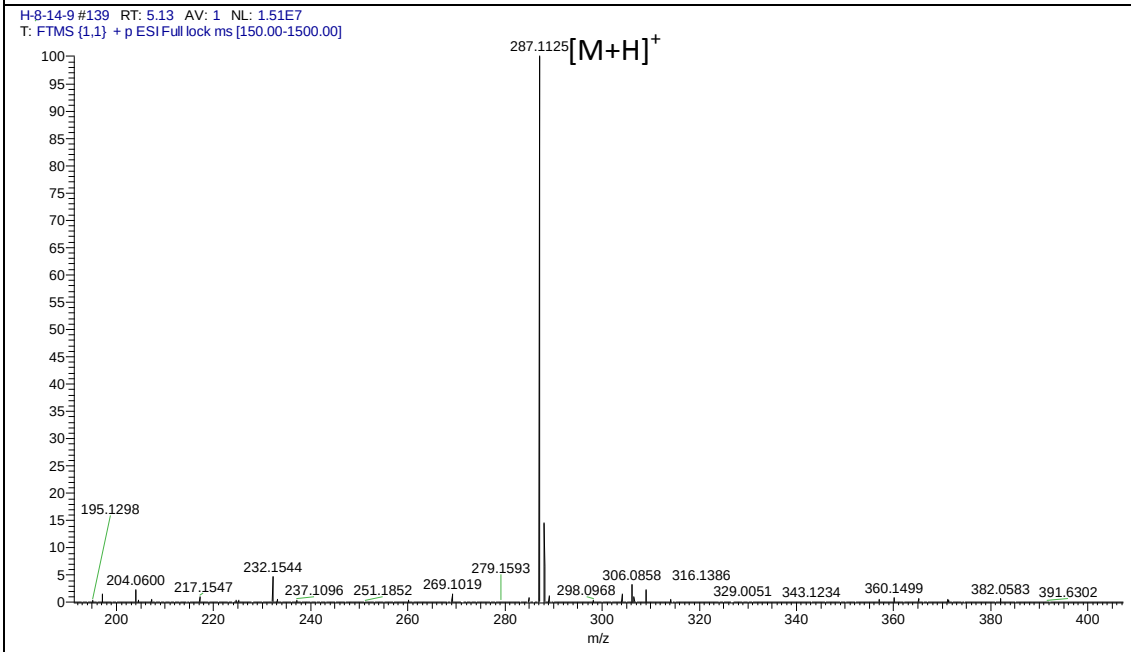

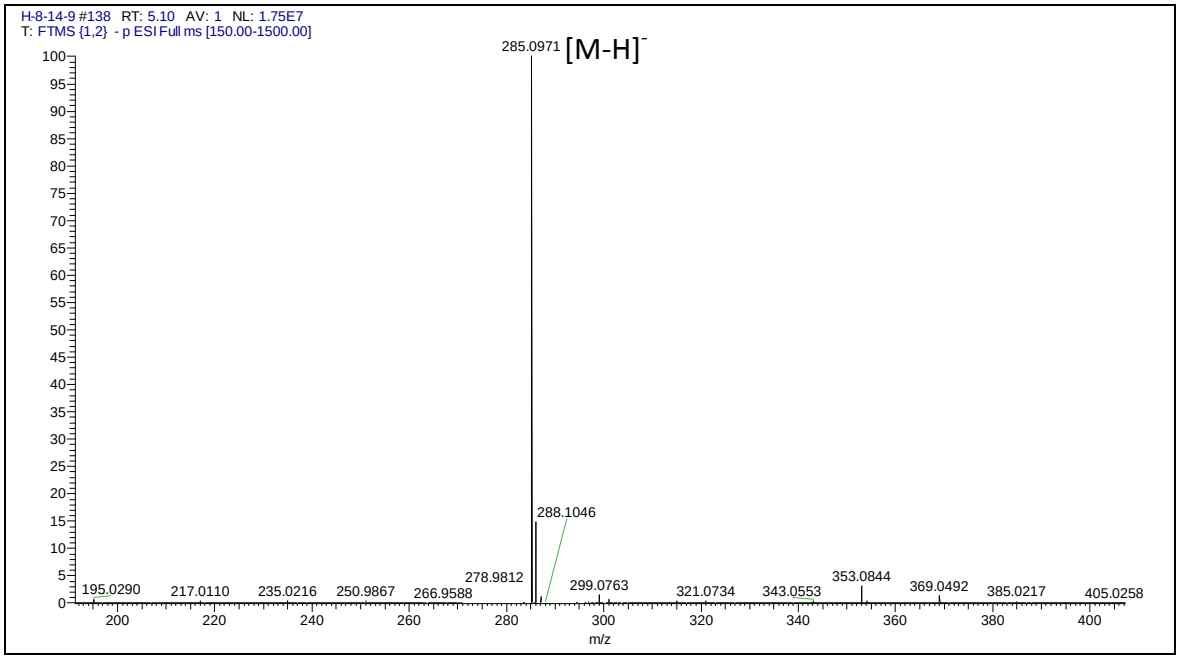

Chaetomiside C was isolated in the form of yellowish brown oil with a yield of 0.05% (17.8 mg). The LC-HRMS data afforded pseudomolecular ion peaks at *m/z* 287.11252 $[M+H]^+$ and 285.0971 $[M-H]^-$, resulting that this compound has a molecular weight of 286.1053 g/mol. The molecular formula $C_{13}H_{18}O_7$ was established by HRMS.

Chaetomiside C is a glycoside that consisted of an orsellinate moiety and an open-chain pentose sugar unit. The occurrence of orsellinate was also indicated by its characteristic ^{1}H and ^{13}C NMR resonances and was confirmed by comparing the data with its latter derivatives, chaetomiside A and B (Table 5.17).

The second subunit of chaetomiside C is 5-deoxy-D-ribitol. The ^{1}H NMR spectrum (Figure 5.40) showed a doublet that resonated at δ_H 1.10 (C*H*$_3$-5', *J*=6.1 Hz) and coupled through ^{1}H-^{1}H COSY (Figure 5.42) to the multiplet H-4' (δ_H 3.58). The attachment of hydroxyl groups to positions 1', 2', 3' and 4' deshielded their protons and pushed their chemical shifts downfield. Thus, the protons of C*H*$_2$-1' resonated at δ_H 3.70 and δ_H 3.77 and coupled through ^{1}H-^{1}H COSY to H-2' that was detected at δ_H 5.23 (*J*= 7.8, 4.7, 3.2 Hz), which further coupled with H-3' at δ_H 3.52 (*J*= 6.2, 4.8 Hz) (Figure 5.41 and Figure 5.43). Moreover, the signals for the hydroxyl protons were also identified from the ^{1}H NMR and COSY spectra. The 1'-O*H* triplet at δ_H 4.74 (*J*=5.8) coupled to

CH_2-1', the 3'-OH doublet at δ_H 4.96 (J=5.8) coupled to H-3', and the 4'-OH doublet at δ_H 4.66 (J=5.4) coupled to H-4'.

A ^{13}C NMR experiment was also conducted (Figure 5.44). The attachment of the hydroxyl substituents to carbons C1' to C4' made them resonated between 59.8 to 77.2 ppm. The carbon of the methyl C-5' was detected at δ_C 20.2. Moreover, ^{1}H-^{13}C HSQC experiment was conducted to obtain the proton-carbon assignments (Figure 5.45). The connectivity of this sugar was established by ^{1}H-^{13}C HMBC (Figure 5.46). As the HMBC spectrum indicated, ^2J and ^3J correlations were found from CH_3-5' to C-4' and C-3', respectively. Furthermore, ^3J correlations were also observed from the protons of the hydroxyl groups 3'-OH and 4'-OH to C-4' and C-3', respectively. Moreover, ^2J correlations were exhibited from the hydroxyl protons to its respective hydroxyl-bearing carbons and hence, from 3'-OH to C-3' and from 4'-OH to C-4'. In addition to that, a ^3J correlation was deteccted from H-3' to C-1'.

The stereochemistry at the chiral centres C-4' and C-3' was established by using Mosher ester derivatisation (Figure 5.47). The chemical shift of CH_3-5' proton was found at δ_H 1.29 in the (R) Mosher ester and 1.58 in the (S) Mosher ester. Thus, the $\Delta\delta^{S-R}$ value was +0.29, and hence, CH_3-5' was placed right of the chiral center C-4'. Moreover, the $\Delta\delta^{S-R}$ values were calculated for the other protons CH_2-1', H-2', H-3' and H-4' and were found to be -0.25, -0.56, -0.48 and +0.04, respectively. Assigning the protons with negative $\Delta\delta^{S-R}$ value were positioned left of both chiral centres C-4' and C-3' establishing the S configuration.

The occurrence and structure of 5-deoxy-D-ribitol was further confirmed by comparing both its ^{1}H and ^{13}C NMR data to those found in the literature (Ichihara *et al.*, 1985) (Table 5.19). However, the attachment of C-2' to the carboxylate group of the orsillinate moiety deshielded both the proton and the carbon of this position resulting to their downfield shifts δ_H and δ_C to 5.23 and 77.3, respectively.

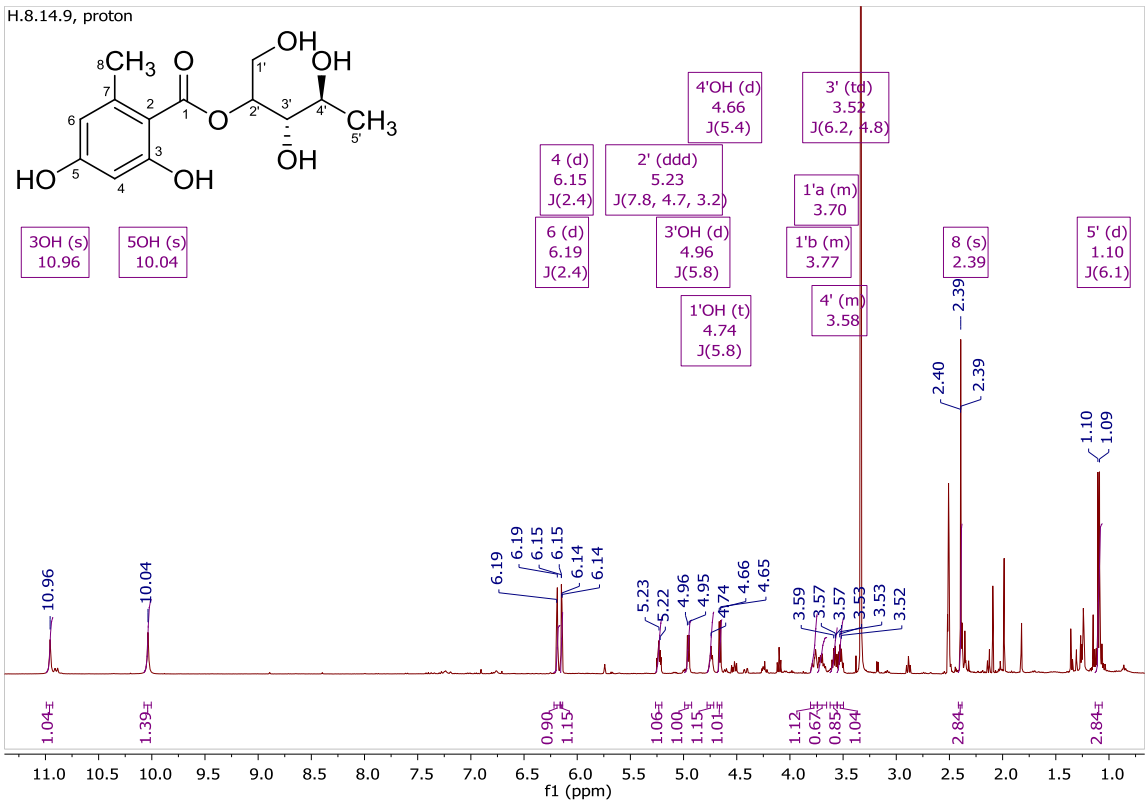

Figure 5.40: ^{1}H NMR (400 MHz) spectrum for chaetomiside C, measured in DMSO-d_6.

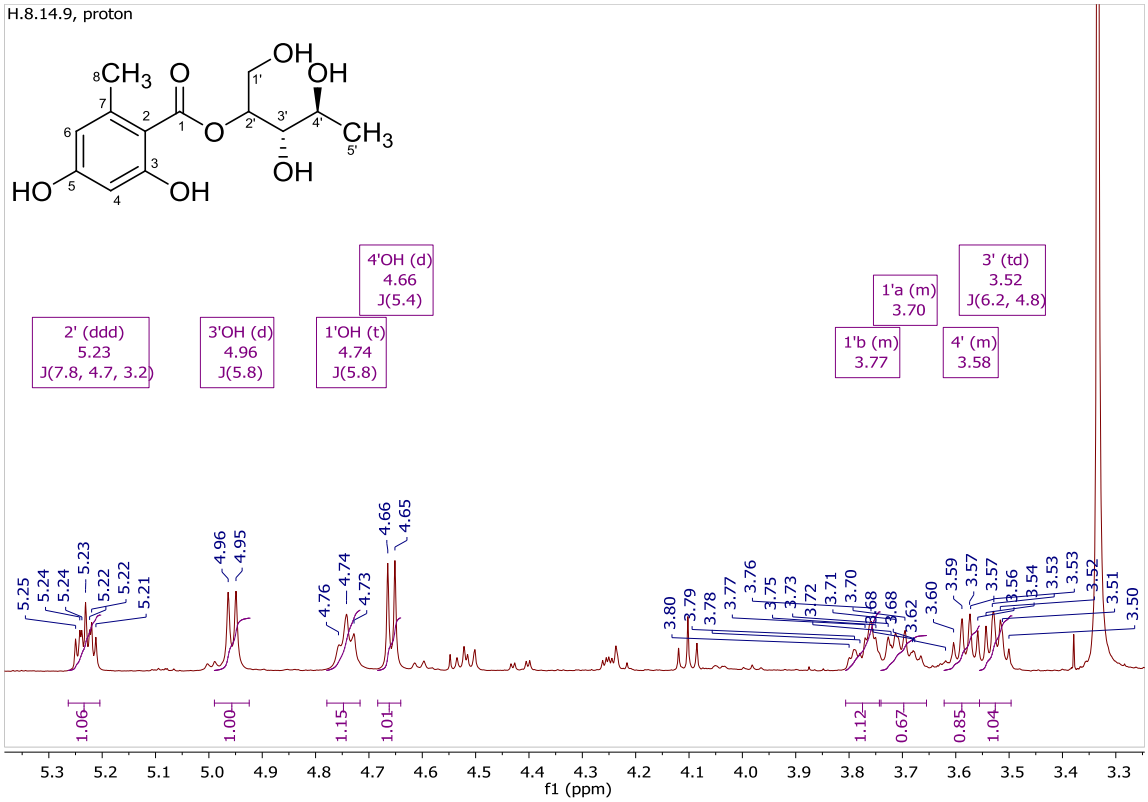

Figure 5.41: An expanded view for the region (3.30-5.30 ppm) of the ^{1}H NMR (400 MHz) spectrum for chaetomiside C, measured in DMSO-d_6.

H.8.14.9, COSY

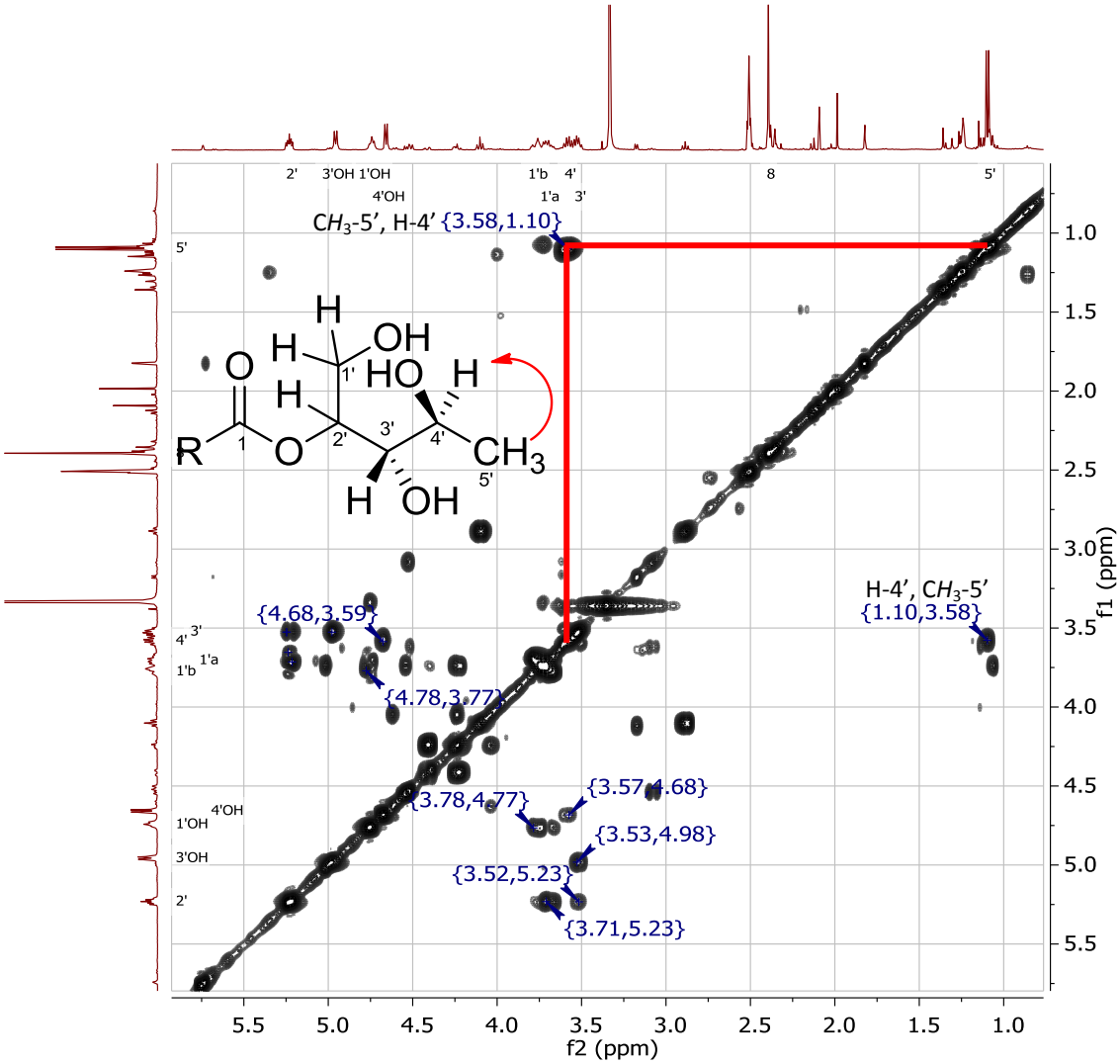

Figure 5.42: ^{1}H-^{1}H COSY NMR (400 MHz) spectrum for chaetomiside C, measured in DMSO-d_6.

H.8.14.9, COSY

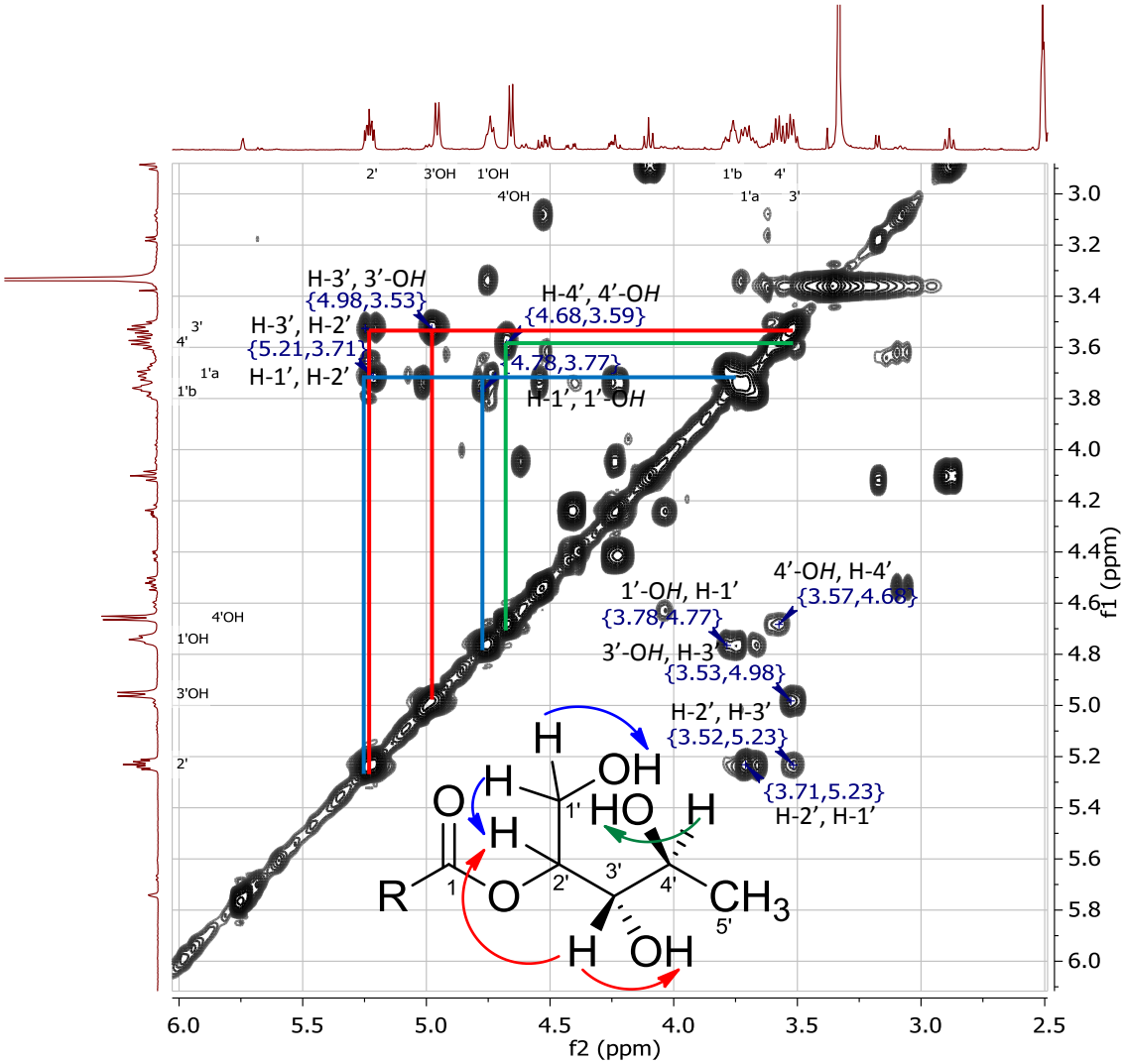

Figure 5.43: Expanded region for 3.00 – 6.00 ppm of the ^{1}H-^{1}H COSY NMR (400 MHz) spectrum for chaetomiside C, measured in DMSO-d_6.

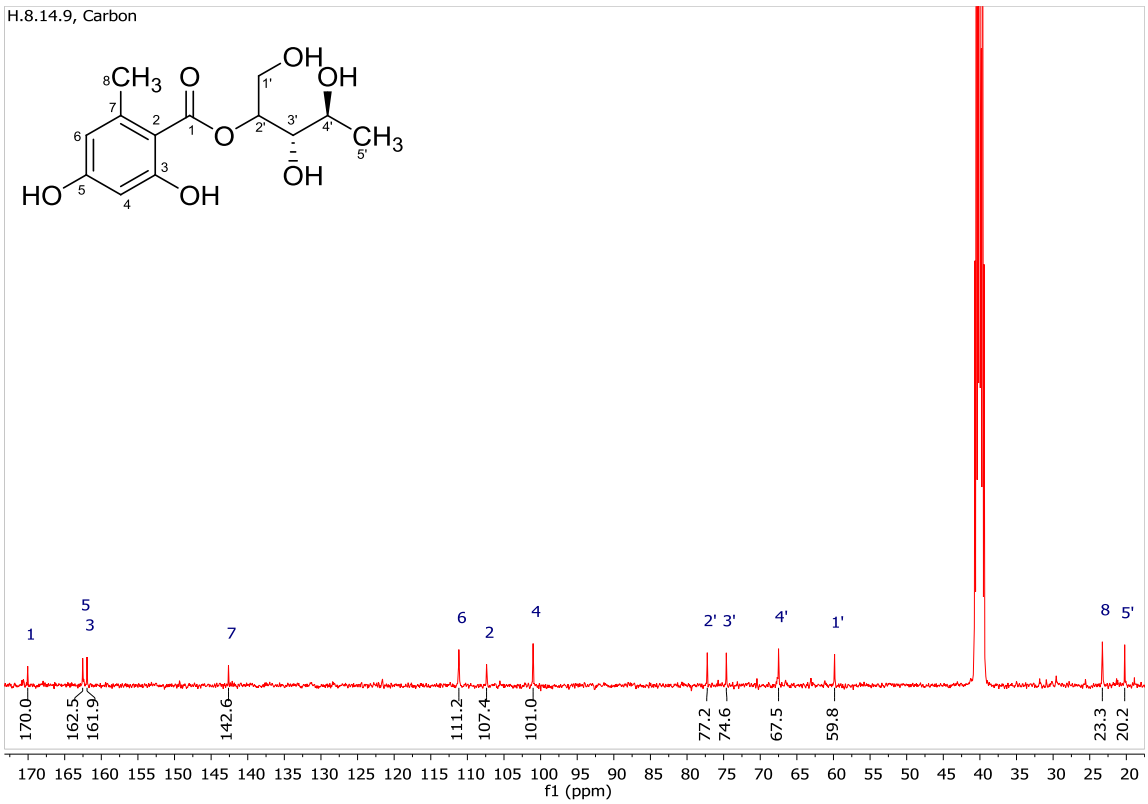

Figure 5.44: ^{13}C NMR (100 MHz) spectrum for chaetomiside C, measured in DMSO-d_6.

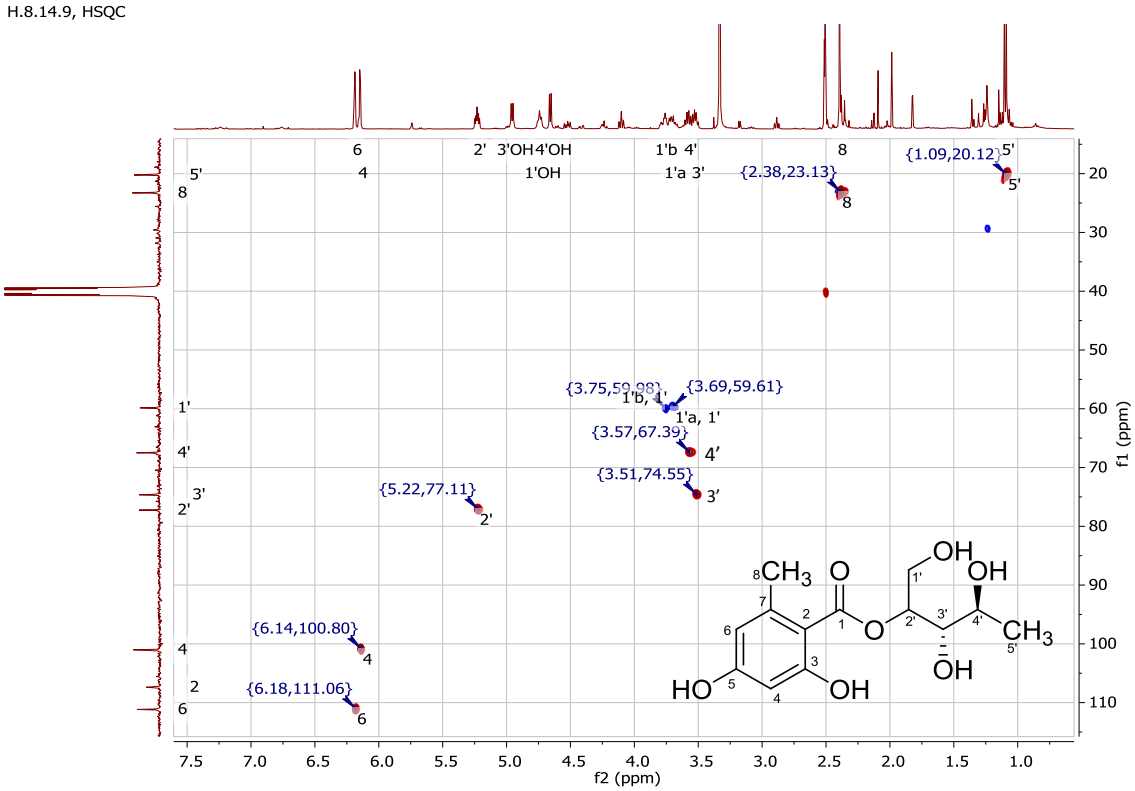

Figure 5.45: ^{1}H-^{13}C HSQC NMR (400 MHz) spectrum for chaetomiside C, measured in DMSO-$_{d6}$.

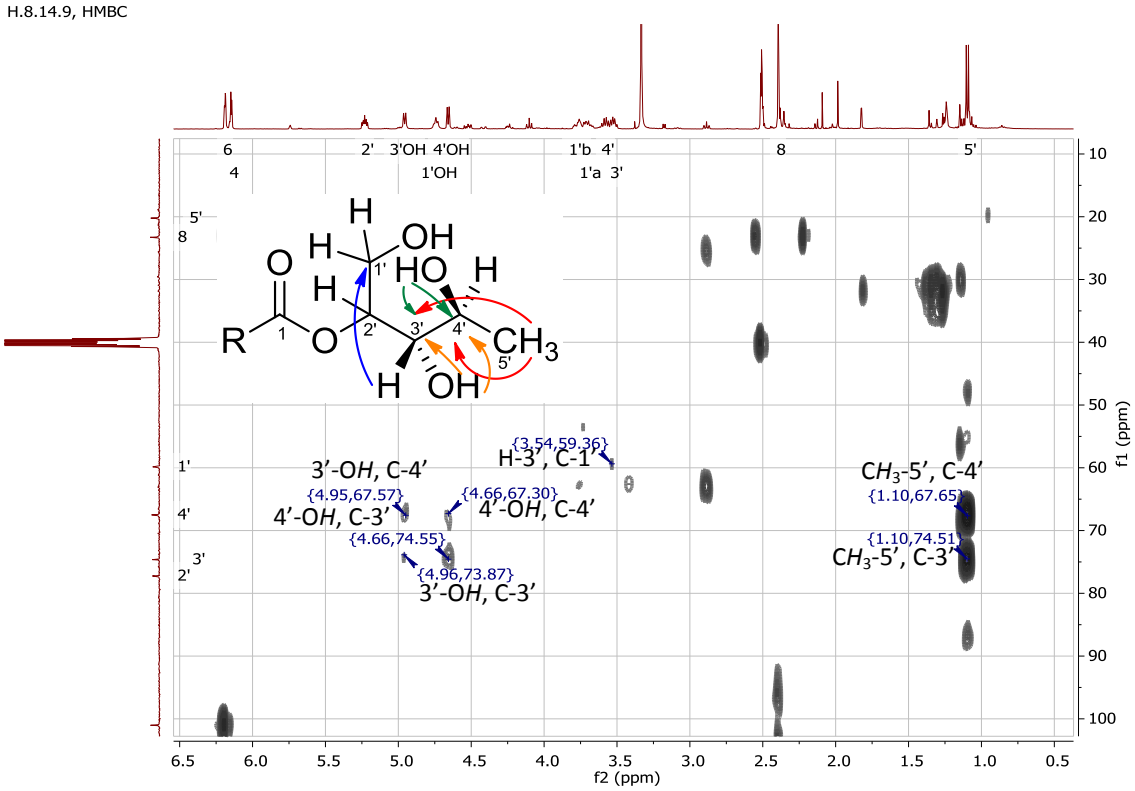

Figure 5.46: Expanded aliphatic region of the ^{1}H-^{13}C HMBC NMR (400 MHz) spectrum for chaetomiside C measured in DMSO-d_6.

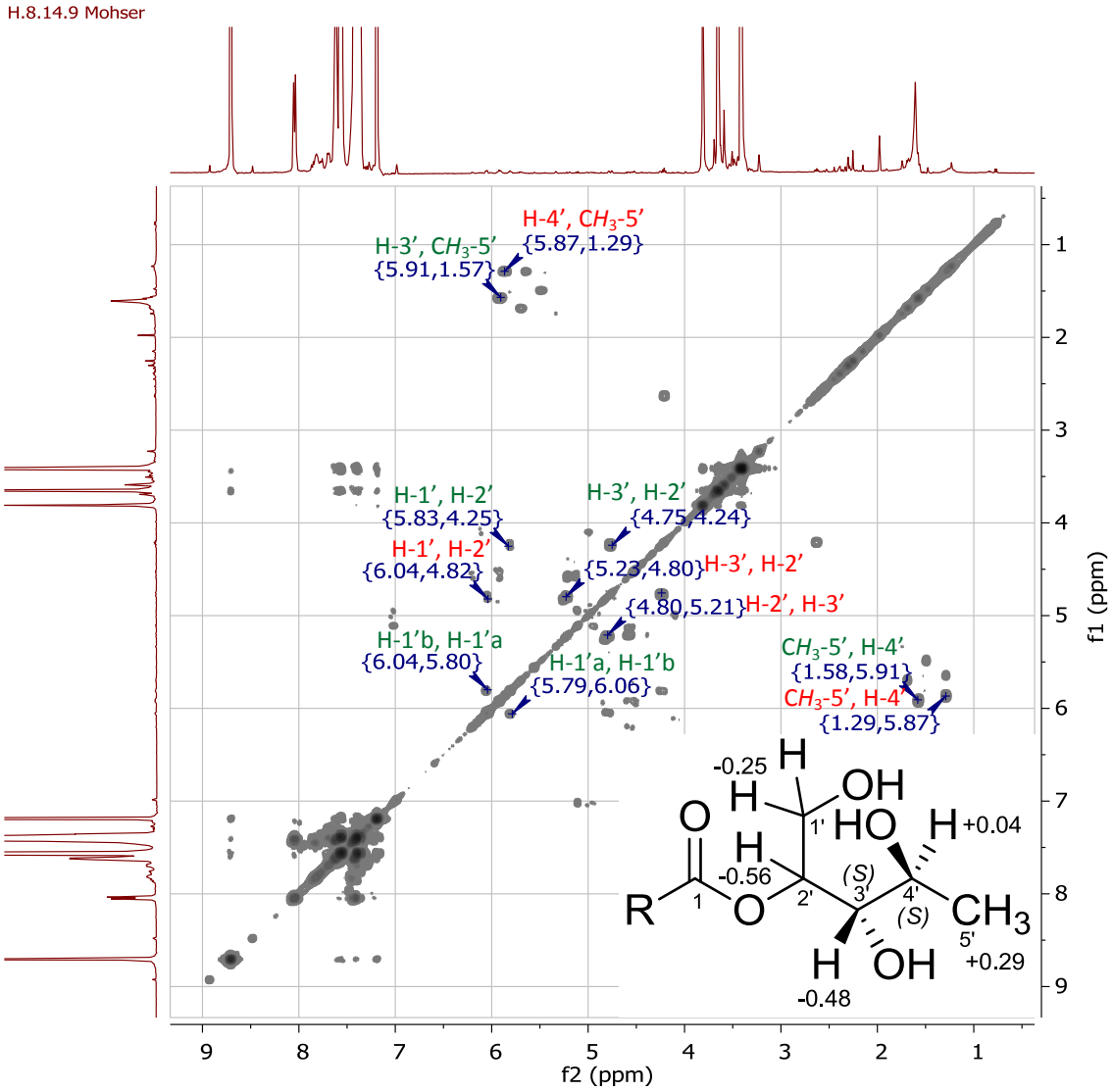

Figure 5.47: Superimposed ^{1}H-^{1}H COSY NMR spectrum for MPTA derivatives of chaetomiside C, measured 36 hours after it was reacted with both bis-*(R)*-MTPA-Cl and bis-*(S)*-MTPA-Cl reagents, measured in Pyridine-d_5, (400 MHz). Green labels are for the couplings upon reaction with bis-(*R*)-MTPA-Cl (*S* Mosher ester) while red labels are for the couplings upon reaction with bis-(*S*)-MTPA-Cl (*R* Mosher ester).

Table 5.19: ^{1}H and ^{13}C NMR data for the 5-deoxy-D-ribitol in chaetomiside C compared to the literature.

	Chaetomiside C in DMSO-*d6*		**5-deoxy-D-ribitol (Ichihara *et al.*, 1985) in D_2O**	
Atom no.	δ_H (ppm), (integration, multiplicity, *J* (Hz)), (400 MHz)	δ_C (ppm), (100 MHz)	δ_H (ppm), (integration, multiplicity, *J* (Hz))	δ_C (ppm)
1'	3.77 (1H, m), 3.70 (1H, m)	59.9 (CH_2)	3.90	63.0
2'	5.23 (1H, ddd, 7.8, 4.7, 3.2)	77.3 (CH)	3.00 – 4.00	72.4
3'	3.34 (1H, td, 6.2, 4.8)	74.6 (CH)	3.00 – 4.00	74.7
4'	3.58 (1H, m)	67.5 (CH)	3.00 – 4.00	67.8
5'	1.10 (3H, d, 6.1)	20.2 (CH_3)	1.15 (3H, d, 6.4)	16.4
1'-OH	4.74 (1H, t, 5.8)			
3'-OH	4.96 (1H, d, 5.8)			
4'-OH	4.66 (1H, d, 5.4)			

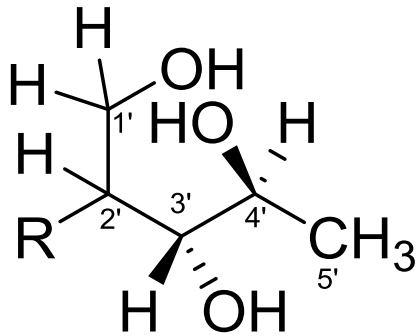

R = orsellinate, chaetomiside C
R = H, 5-deoxy-D-ribitol

5.6.7 Chaetomiside D (7)

Chaetomiside D (new compound)

Fraction: H.8.14.5.8
Retention time: 5.18 min
Synonym(s):

- (3*R*,4*R*)-3,4,5-Trihydroxypentan-2-yl 2,4-dihydroxy-6-methylbenzoate

Source: *Chaetomium subaffine,* isolated from *Anthemis palestina*
Amount of sample: 4.9 mg
Percent yield: 0.01%
Percent purity: 90.9%
Physical description: brownish yellow oil
Molecular formula: $C_{13}H_{18}O_7$
Molecular weight: 286.1053 g/mol
Optical rotation: $[\alpha]_D^{20}$ = -9 (0.1 g/100 mL, MeOH)

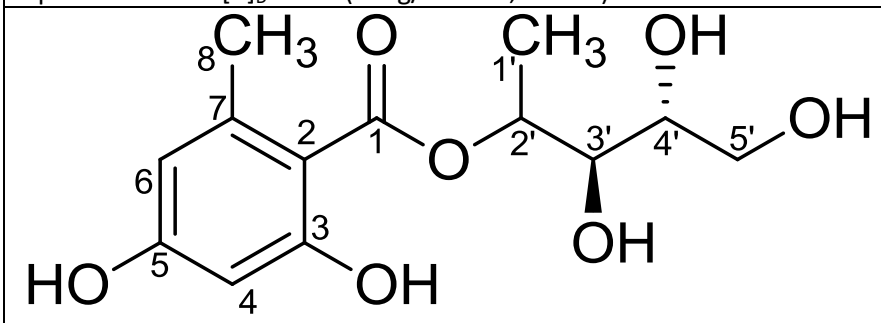

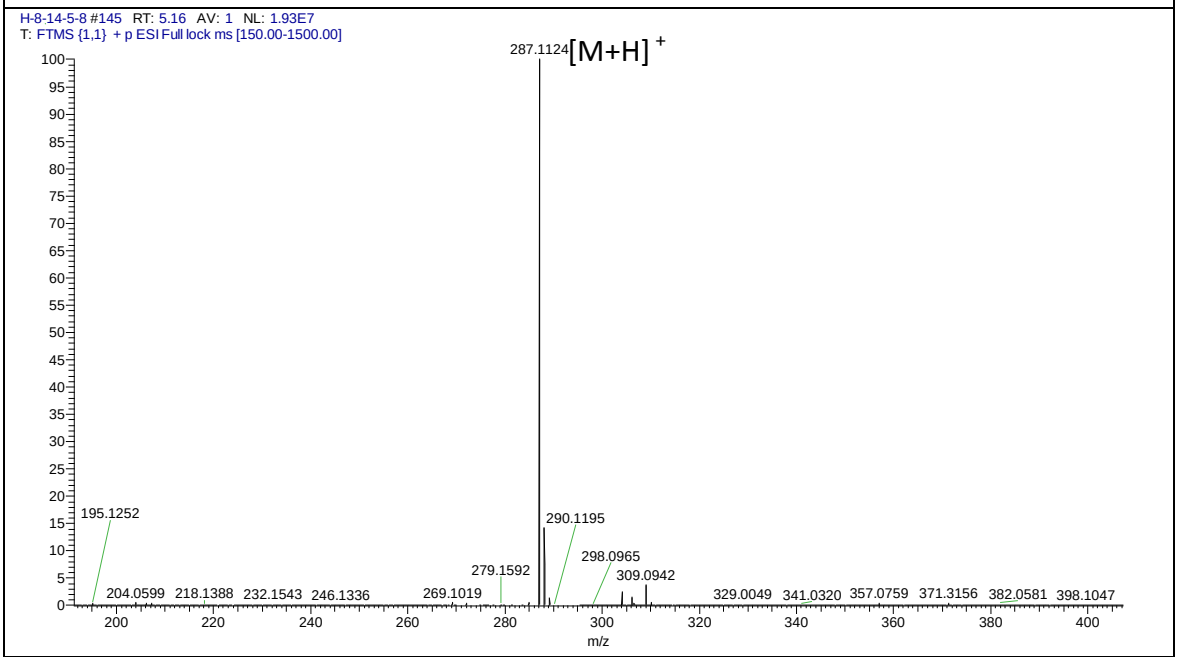

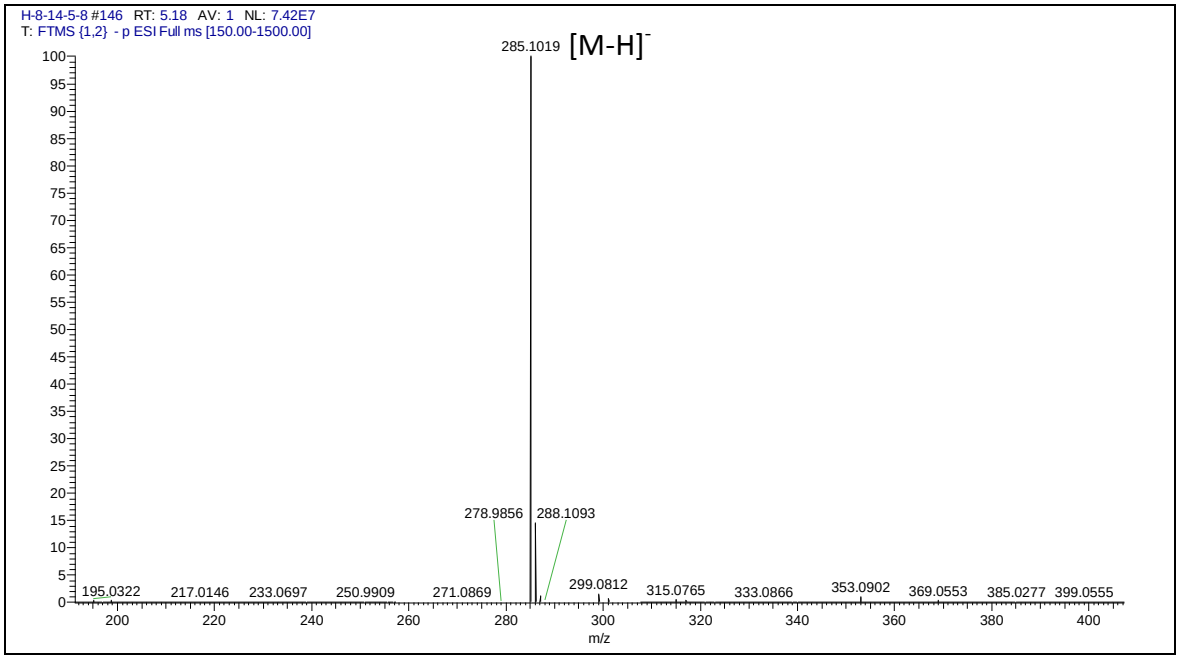

Chaetomiside D was isolated in the form of yellowish brown oil with a yield of 0.01% (4.9 mg). The LC-HRMS data afforded pseudomolecular ion peaks at *m/z* 287.1124 $[M+H]^+$ and 285.1019 $[M-H]^-$, suggesting that this compound has a molecular weight of 286.1053 g/mol. The molecular formula established by HRMS was $C_{13}H_{18}O_7$.

The occurrence of the orsellinate moiety was again indicated by ^{1}H and ^{13}C NMR spectral data, which were comparable to those of its congeners, chaetomiside A, B, and C (Table 5.17). Moreover, chaetomiside D shares an identical physical property, molecular weight and molecular formula with chaetomiside C. However, the change in the chemical shifts of some of its ^{1}H and ^{13}C signals indicated that chaetomiside C and chaetomiside D are positional isomers, as the sugar attached to the orsellinate in chaetomiside D was 1-deoxy-D-xylitol instead of 5-deoxy-D-ribitol as elucidated for chaetomiside C.

The protons of the methyl CH_3-1' resonated as doublet at δ_H 1.07 (*J*=6.3 Hz) and coupled through ^{1}H-^{1}H COSY to H-2' at δ_H 3.74. H-2' coupled to H-3' at δ_H 3.34 that further coupled to H-4' at δ_H 3.74 (Figures 5.48 – 5.50). The protons of CH_2-5' were detected as doublets of doublets at δ_H 4.24 (*J*=11.3, 6.9 Hz) and 4.53 (*J*=11.3, 2.7 Hz) coupling with 5'-OH at δ_H 4.53.

The ^{13}C NMR spectrum (Figure 5.51) indicated the presence of oxygen-bearing carbons (C2' to C5') resonating between δ_C 67.6 and 75.7. The C-1' methyl group was detected at δ_C 18.9. Furthermore, ^{1}H-^{13}C HSQC experiment was conducted to obtain the proton-carbon assignments (Figure 5.52). In addition to that, the connectivity of the sugar unit was established by ^{1}H-^{13}C HMBC experiment (Figure 5.53). As shown in figure 5.53, ^{3}J and ^{2}J correlations could be detected from CH_3-1' to C-3'and C-2', respectively. More ^{2}J correlations were found from H-3' to C-2' and from H-5' to C-4'.

The stereochemistry at the chiral centres C-3' and C-4' was determined by also implementing Mosher ester derivatisation (Figure 5.54). The proton chemical shift of CH_3-1' was detected at δ_H 1.49 in *R* Mosher ester and δ_H 1.68 in the *S* derivative. And so, its $\Delta\delta^{S-R}$ value was +0.19. Thus, CH_3-1' was placed right of the chiral centre C-3'. The $\Delta\delta^{S-R}$ values for protons H-2', H-3', H-4' and CH_2-5' were found to be +0.24, +0.05, -0.08 and -0.22, respectively. The protons with positive $\Delta\delta^{S-R}$ value were assigned at the right of the derivatised esters and protons with negative $\Delta\delta^{S-R}$ value were left of the derivatised esters, which concluded that both chiral centres C-3' and C-4' are in *R* configuration.

The elucidation of 1-deoxy-D-xylitol moiety was confirmed by comparing both its ^{1}H and ^{13}C NMR data to those found in the literature (Kitajima *et al*., 1999) (Table 5.20).

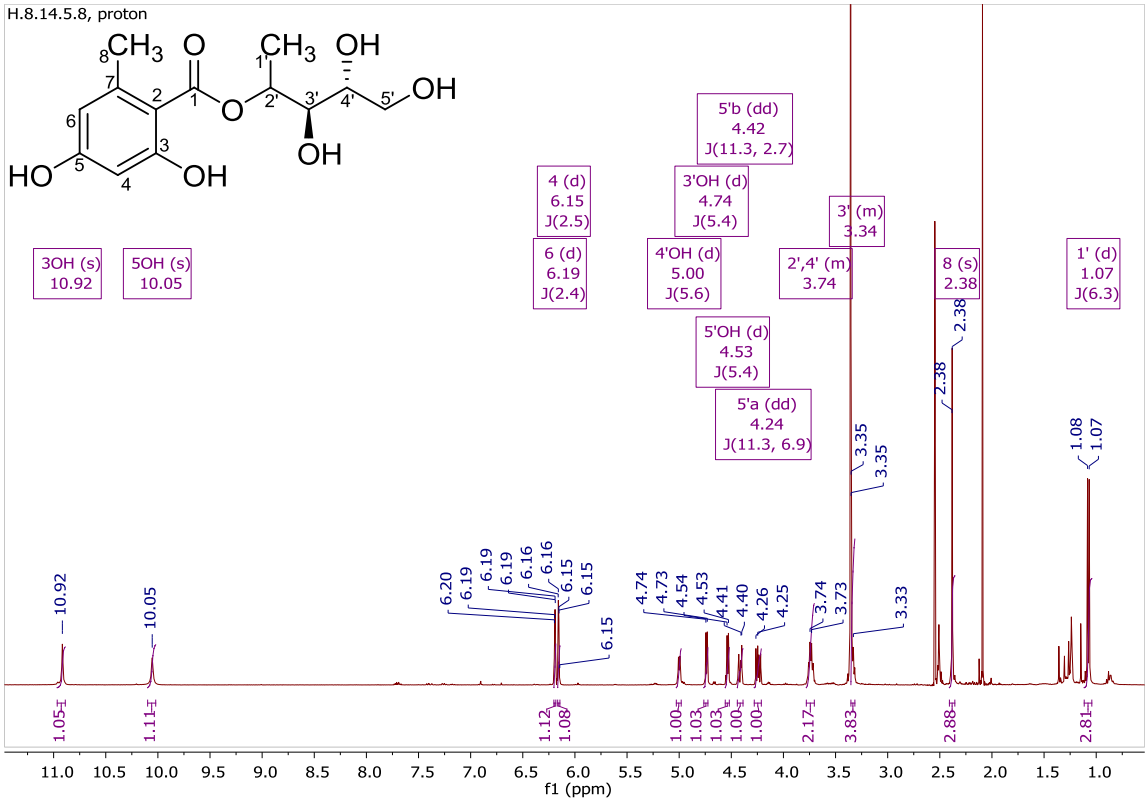

Figure 5.48: ^{1}H NMR (400 MHz) spectrum for chaetomiside D, measured in DMSO-d_6.

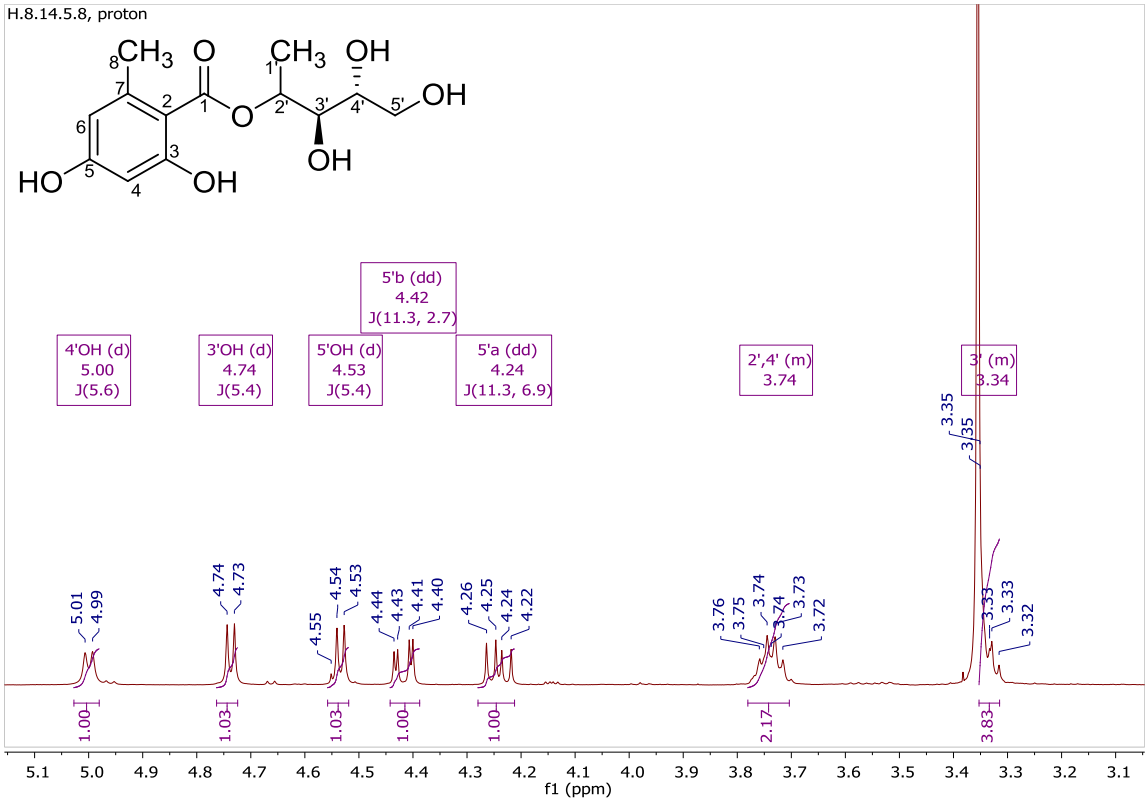

Figure 5.49: Expanded region between 3.10 – 5.10 ppm of the ^{1}H NMR (400 MHz) spectrum for chaetomiside D, measured in DMSO-d_6.

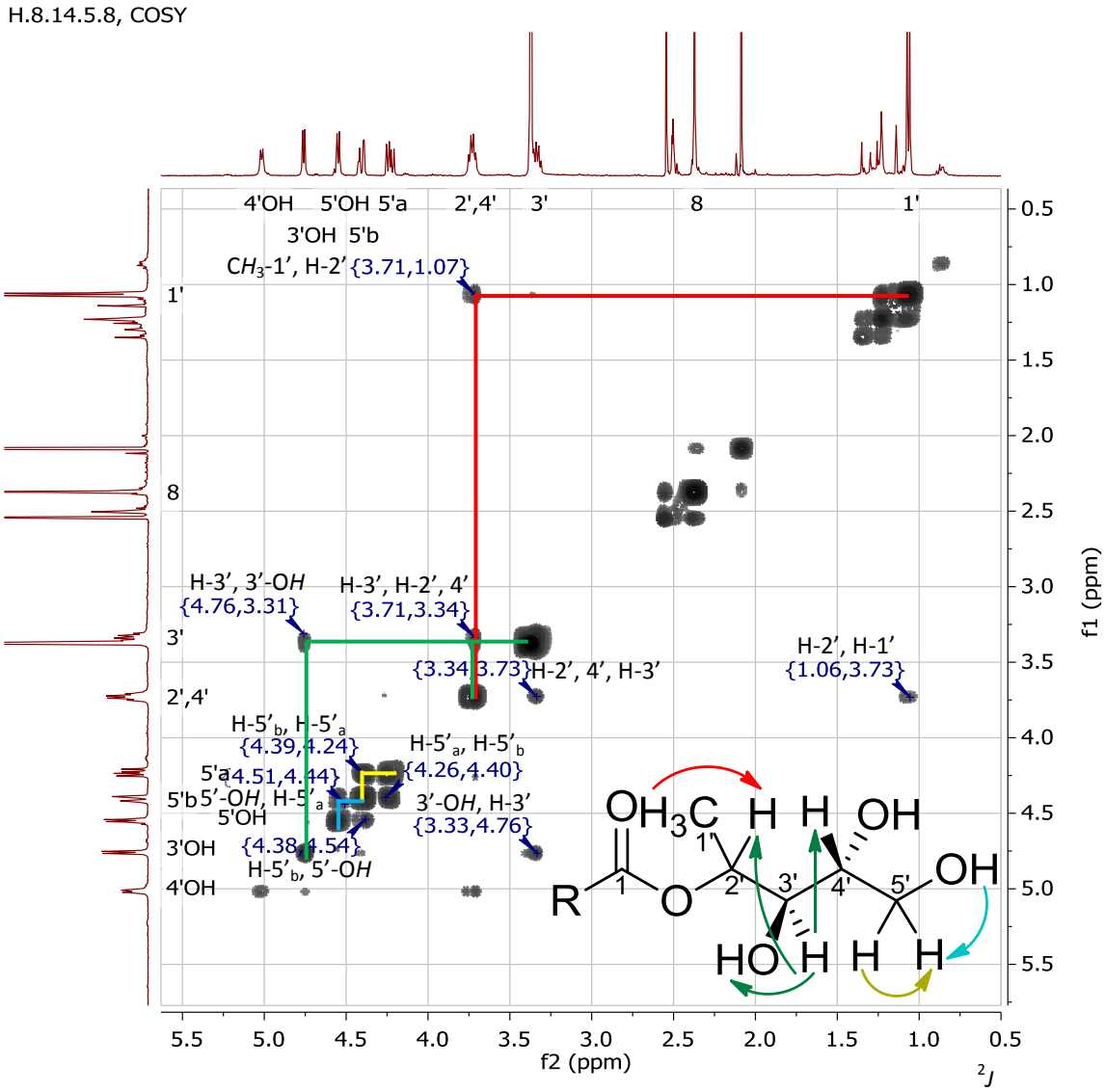

Figure 5.50: ^{1}H-^{1}H COSY NMR (400 MHz) spectrum for chaetomiside D, measured in DMSO-d_6.

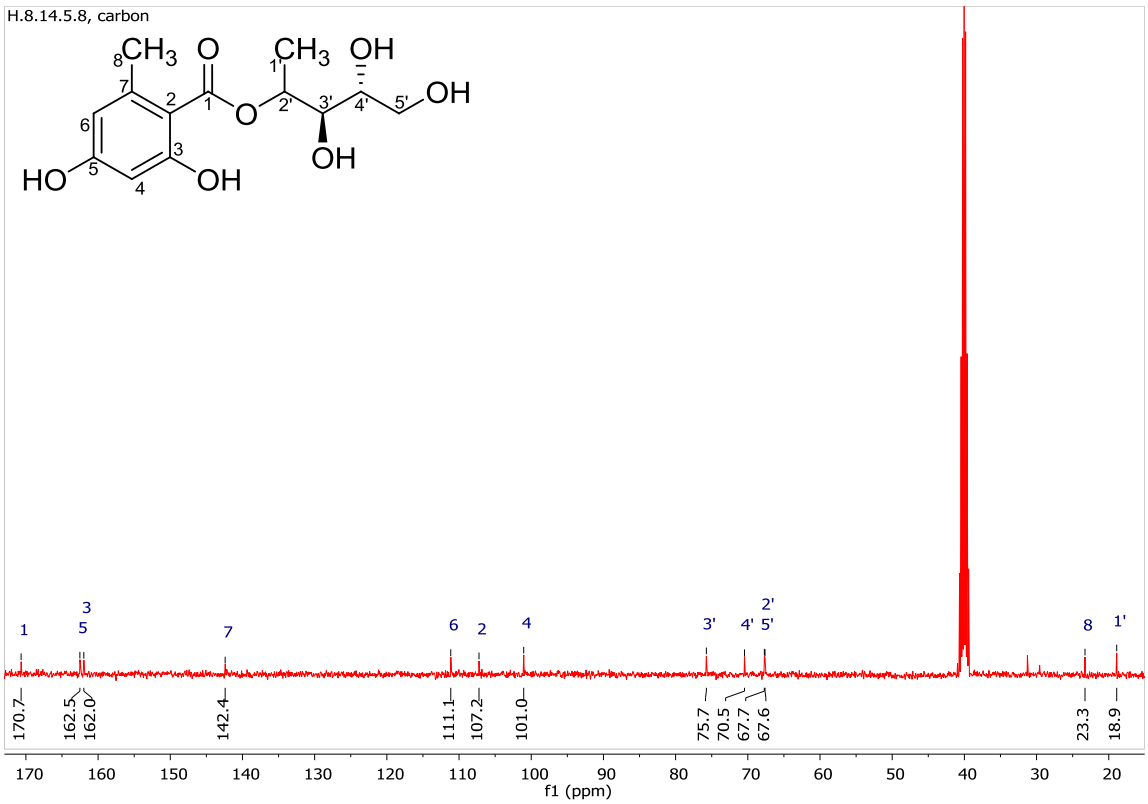

Figure 5.51: ^{13}C NMR (100 MHz) spectrum for chaetomiside D, measured in DMSO-d_6.

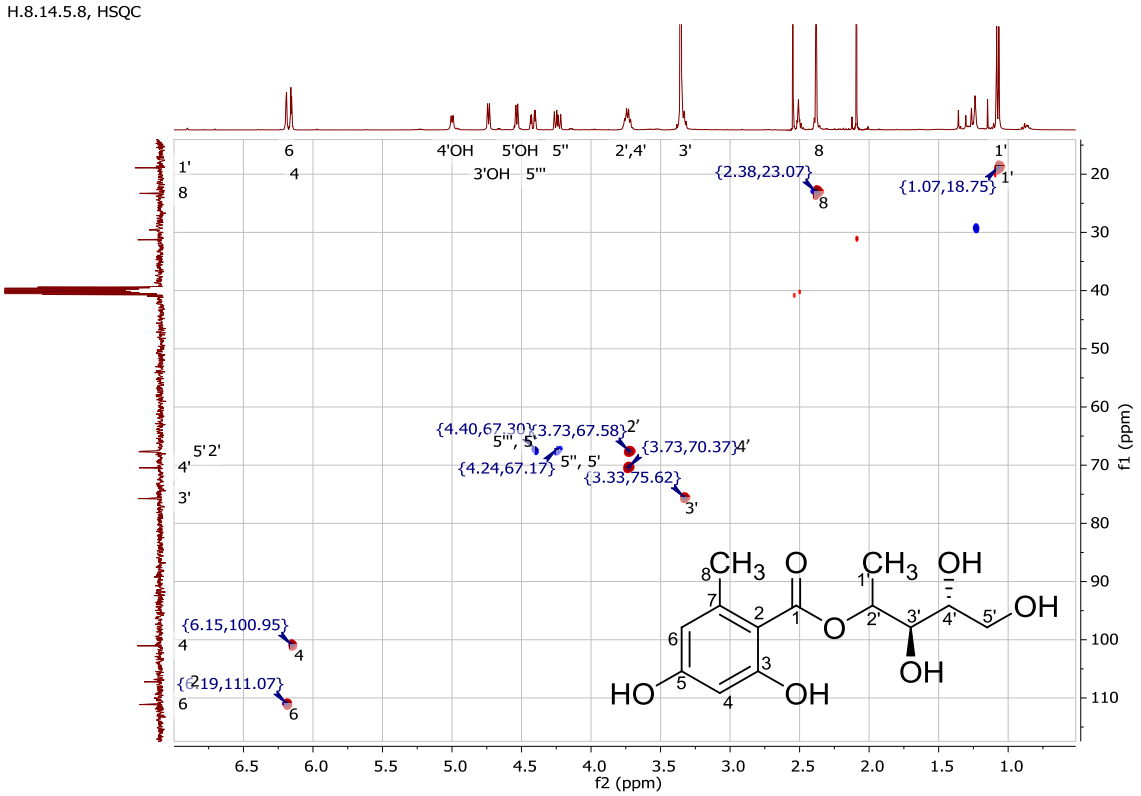

Figure 5.52: ^{1}H-^{13}C HSQC NMR (400 MHz) spectrum for chaetomiside D, measured in DMSO-d_6.

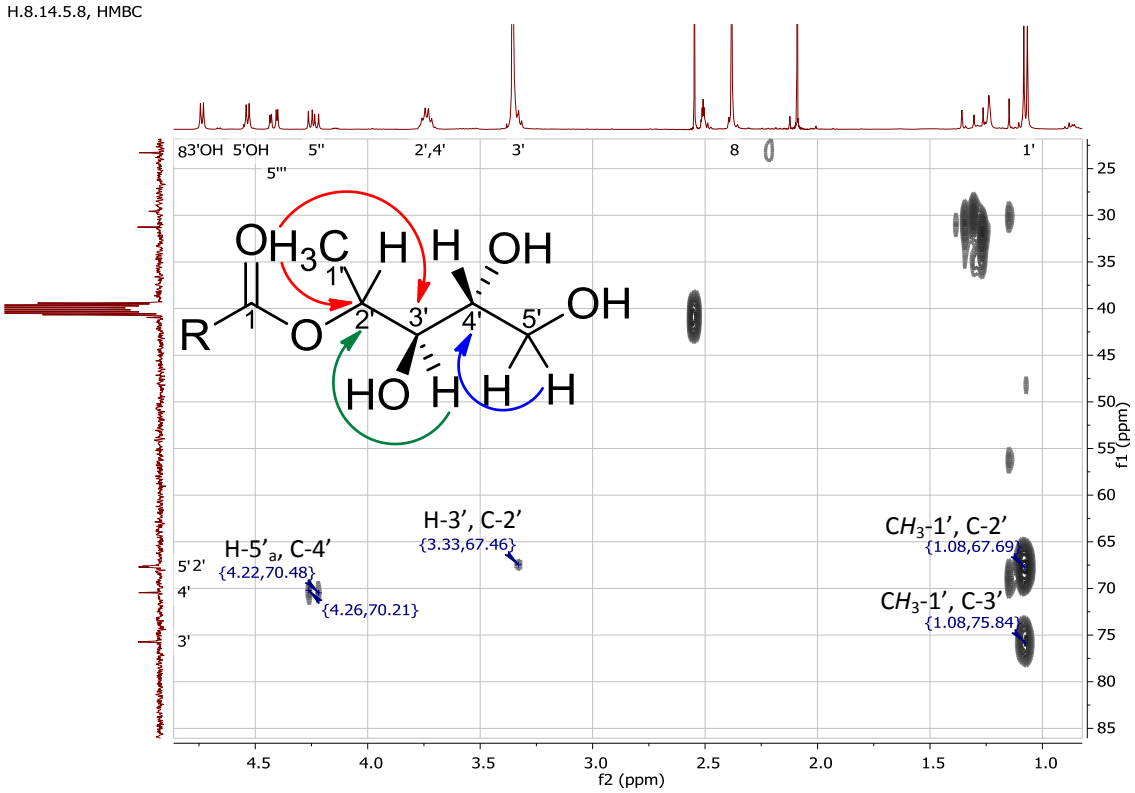

Figure 5.53: ^{1}H-^{13}C HMBC NMR (400 MHz) spectrum for chaetomiside D, measured in DMSO-d_6.

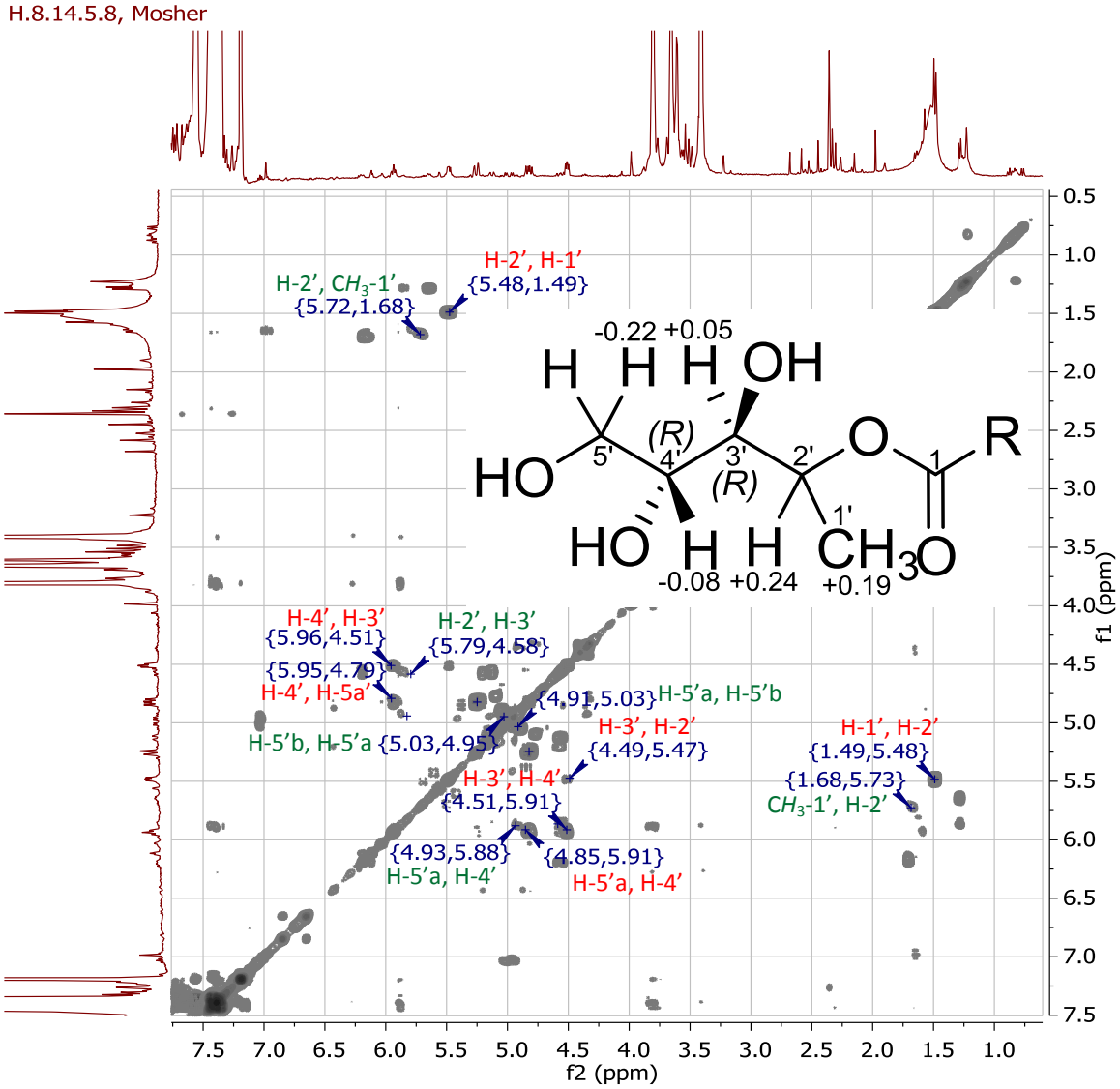

Figure 5.54: Superimposed ^{1}H-^{1}H COSY NMR spectrum for MPTA derivatives of chaetomiside D, measured 36 hours after it was reacted with both bis-*(R)*-MTPA-Cl and bis-*(S)*-MTPA-Cl reagents, measured in Pyridine-d_5, (400 MHz). Green labels are for the couplings upon reaction with bis-(R)-MTPA-Cl (*S* Mosher ester) while red labels are for the couplings upon reaction with bis-(S)-MTPA-Cl (*R* Mosher ester).

Table 5.20: ^{1}H and ^{13}C NMR data for the 1-deoxy-D-xylitol in chaetomiside D compared to the literature.

	Chaetomiside D in DMSO-*d6*		**1-deoxy-D-xylitol (Kitajima *et al.*, 1999) in Pyridine-*d5***	
Atom no.	δ_H (ppm), (integration, multiplicity, *J* (Hz)), (400 MHz)	δ_C (ppm), (100 MHz)	δ_H (ppm), (integration, multiplicity, *J* (Hz)), (500 MHz)	δ_C (ppm), (125 MHz)
1'	1.07 (3H, d, 6.3)	18.9 (CH_3)	1.56 (3H, d, 6.5)	20.4 (CH_3)
2'	3.74 (1 of 2H, m)	67.6 (CH)	4.52 (1H, dq, 4.0, 6.5)	69.2 (CH)
3'	3.33 (1H, overlapped with water)	75.7 (CH)	4.08 (1H, dd, 3.5, 6.5)	76.0 (CH)
4'	3.74 (1 of 2H, m)	70.5 (CH)	4.44 (1H, ddd, 3.5, 5.0, 6.0)	76.0 (CH)
5'	4.42 (1H, dd, 11.3, 2.7), 4.24 (1H, dd, 11.3, 6.9)	67.7 (CH_2)	4.33 (1H, dd, 6.0, 11.0), 4.36 (1H, dd, 5.0, 11.0)	64.8 (CH_2)
3'-OH	4.74 (1H, d, 5.4)			
4'-OH	5.00 (1H, d, 5.6)			
5'-OH	4.53 (1H, d, 5.4)			

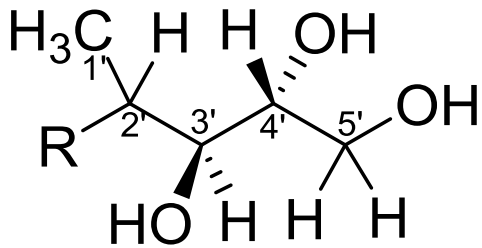

R = orsellinate, chaetomiside D
R = H, 1-deoxy-D-xylitol

5.7 Biological activity of the isolated compounds from the endophyte *Chaetomium subaffine*

All of the isolated compounds were analysed for their anti-proliferative activity against both breast cancer (ZR-75) and lung cancer (A549) cell lines. Six of the isolated compounds were found active against ZR-75 cell line (Table 5.21 and Figure 5.56). These compounds included cochliodinol, chaetomipyrrolidinone, the new chaetomiside derivatives A, B, C and D. Cochliodinol was the most potent compound with an IC_{50} value of 20 µM while the new chaetomiside B was the least active compound (IC_{50}=30 µM). For the new orsellides, it was observed that the activity increases for the compounds with the open-chain sugar unit, as well as when the side chain contains more hydroxyl groups. Therefore, chaetomiside D was the most active congener as it has a straight side chain with three hydroxyl units. Chaetomiside D was followed by chaetomiside A that also has an open-chain sugar unit but with two hydroxyl substituents. Despite having three hydroxyl groups, chaetomiside C, with its branched side chain, is less active than derivatives A and B. Chaetomiside B is the least active orsellide. This could be referred to the presence of the dioxlane ring and the absence of "free" hydroxyl groups.

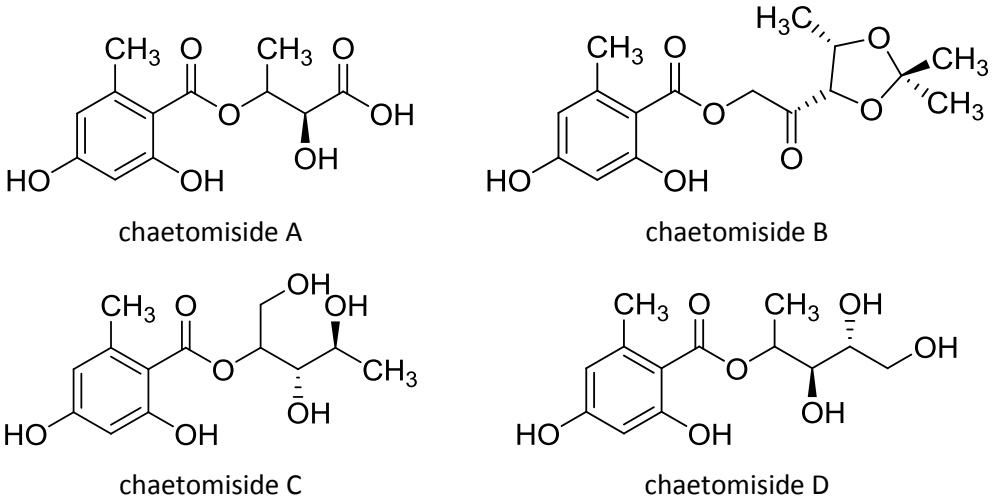

Figure 5.55: Chaetomisides A – D.

These results confirmed the findings of the established OPLS-DA model to pinpoint the active metabolites. However, acremonisol A was the only compound to have an IC_{50} >30 µM. On the contrary, only chaetomipyrrolidinone was found active against A549 cell line with an IC_{50} value of 25 µM (Table 5.21 and Figure 5.57). This could be referred to two reasons. First, the

difference between the concentrations used during first fractionation step, which were at 30 µg/mL while for constructing the dilution curves for pure compounds a concentration range of 0.001 – 30 µM were used. Second, the weakness of the obtained OPLS-DA model indicating a weak predictability at Q2=0.18. However, being not sufficiently pure for bioactivity determination, the activity of chaetomipyrrolidinone (80.3%) and chaetomiside C (77.7%) is still questionable. On the other hand, the purity of the other bioactive compounds exceeded 90%. Yet, the possibility of impurities having a role in the obtained activity shall not be overlooked. Moreover, the isolated compounds were analysed for their toxicity against PNT2 cell line (Human prostate normal cells). The results of this analysis showed that only two compounds were toxic (Table 5.21 and Fig 5.58). These compounds were cochliodinol (IC_{50}=19 µM) and chaetomipyrrolidinone (IC_{50}=30 µM). This toxicity might be caused by the (3-methylbut-2-en-1-yl)benzene moiety they both share.

Table 5.21: IC_{50} concentrations (µM) for the compounds isolated from *Chaetomium subaffine* against the correspondent cell lines.

Compound	ZR-75	A549	PNT2	% Purity
acremonisol A	> 30	> 30	> 30	85.9
cochliodinol	20	> 30	19	96.6
chaetomipyrrolidinone	25	25	30	80.3
chaetomiside A	25	> 30	> 30	94.2
chaetomiside B	30	> 30	> 30	99.0
chaetomiside C	28	> 30	> 30	77.7
chaetomiside D	22	> 30	> 30	90.9

Furthermore, the selectivity indexes were calculated for the active compounds that possessed toxicity against normal prostate (PNT2) cell line and mentioned in Table 5.22. Both cochliodinol and chaetomipyrrolidinone had poor selectivity with an SI value of less than 2. However, chaetomisides were considered selective as their IC_{50} values against PNT2 cells were out of the range that was used for constructing the dilution curves.

Table 5.22: Selectivity indexes for the compounds isolated from *Chaetomium subaffine* against the correspondent cell lines.

Compound	ZR-75	A549
cochliodinol	1.0	-
chaetomipyrrolidinone	1.2	1.2

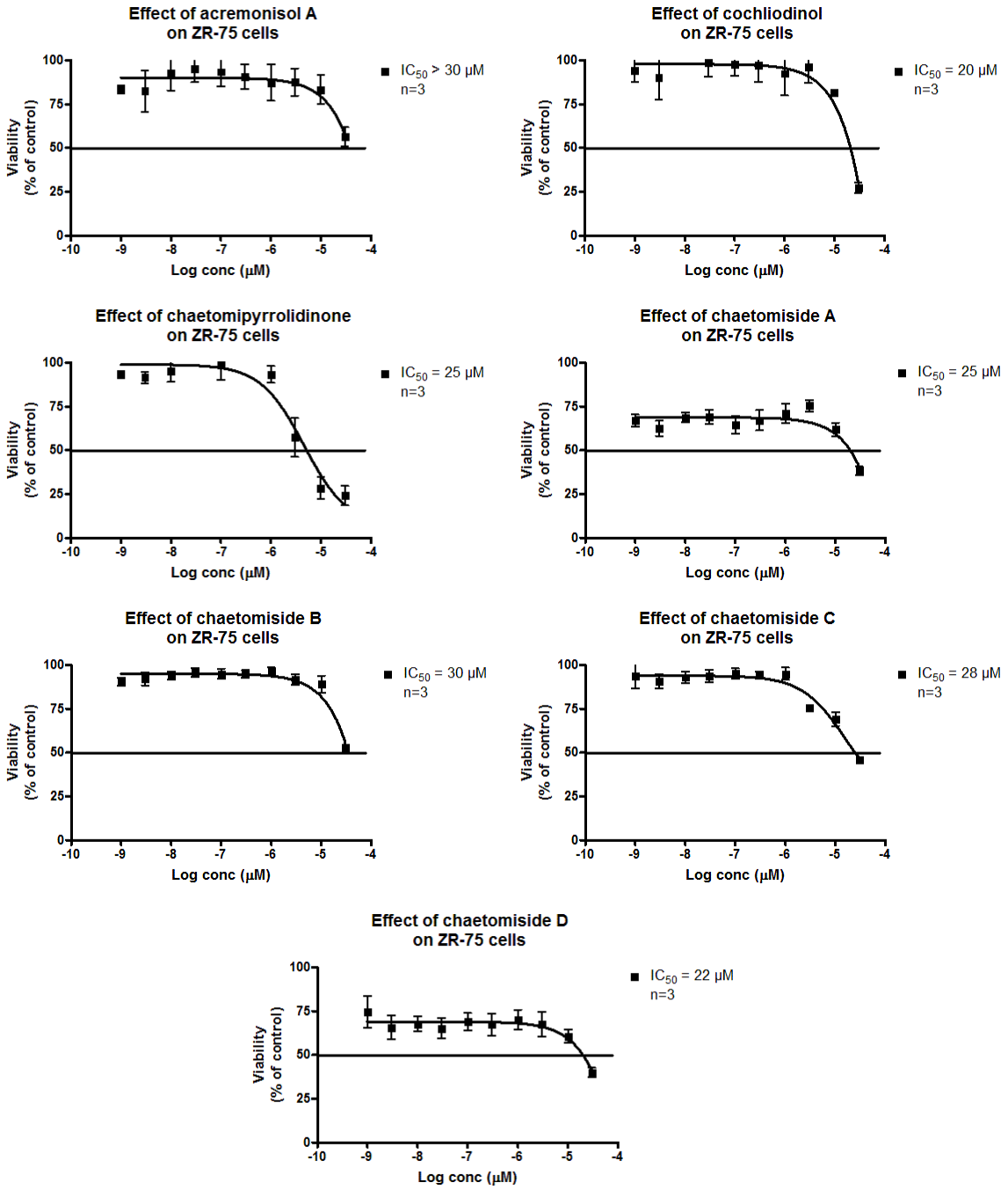

Figure 5.56: Dilution curves for the compounds isolated from *Chaetomium subaffine* when tested against ZR-75 cell line to determine their IC_{50} values.

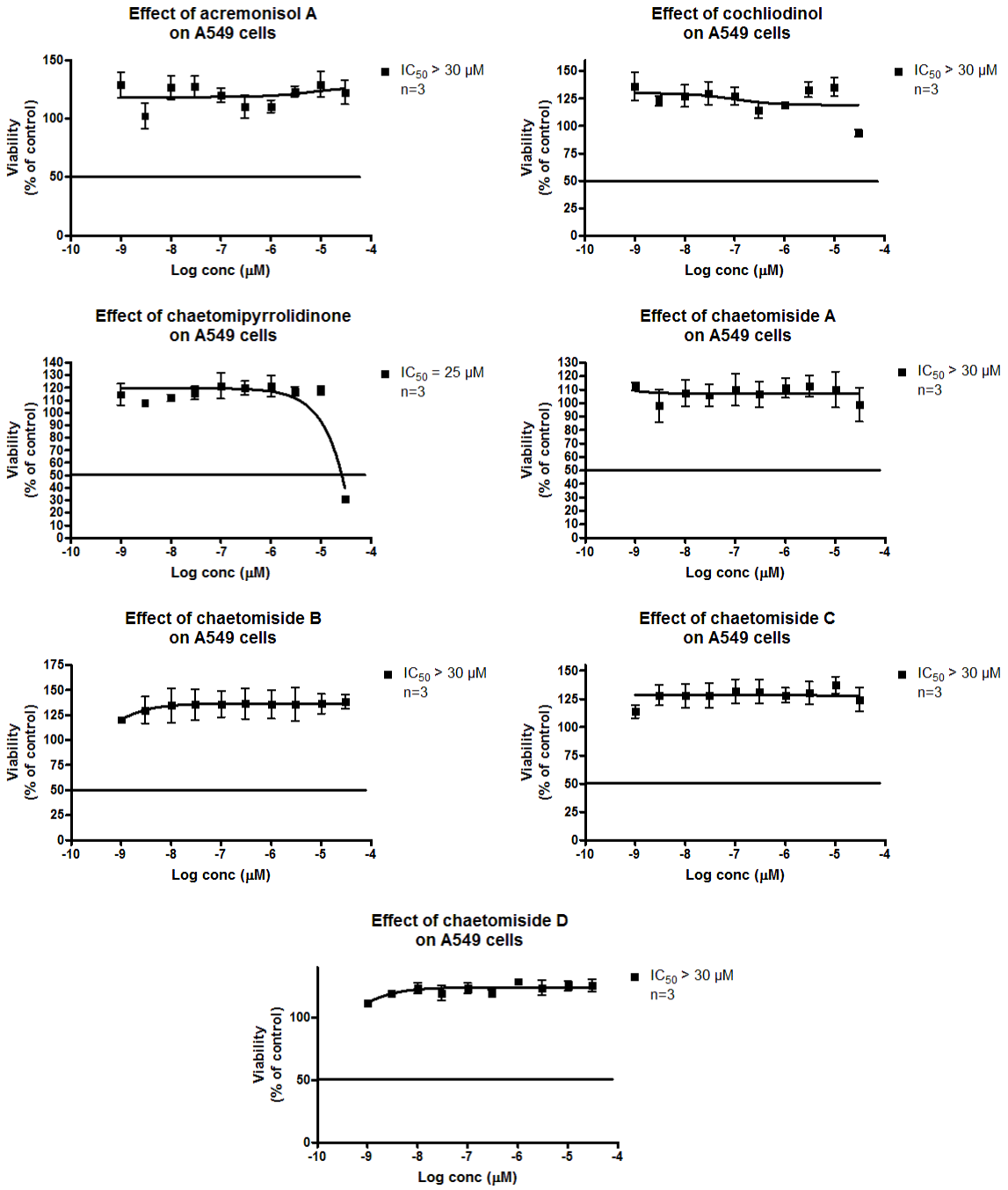

Figure 5.57: Dilution curves for the compounds isolated from *Chaetomium subaffine* when tested against A549 cell line to determine their IC_{50} values.

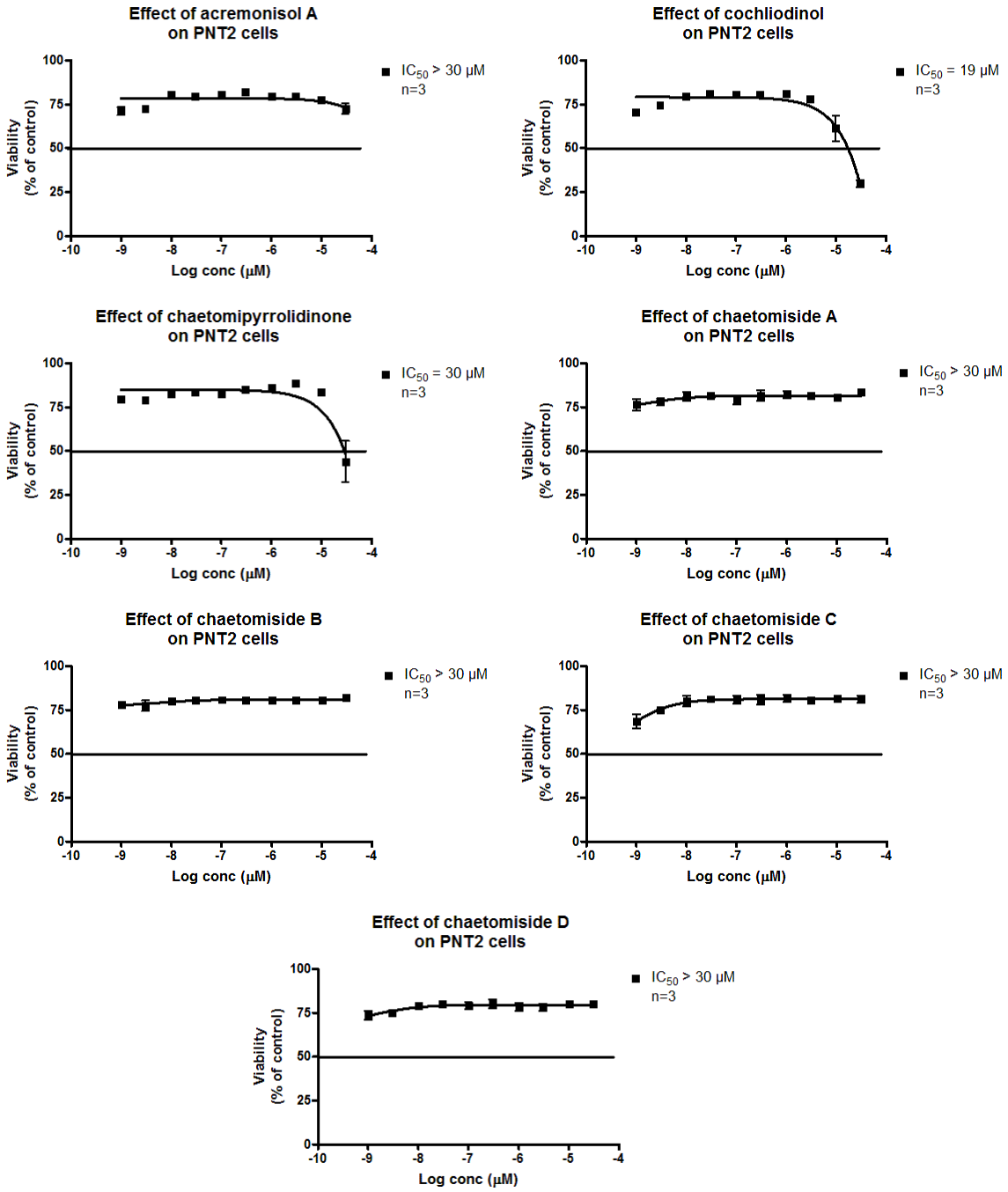

Figure 5.58: Dilution curves for the compounds isolated from *Chaetomium subaffine* when tested against PNT2 cell line to determine their IC_{50} values.

Chapter 6: *Fusarium acuminatum*

6 *Fusarium acuminatum*

6.1 Introduction

6.1.1 Secondary metabolites isolated from *Fusarium acuminatum and other Fusarium* spp

Fusarium is a genus of the family Nectriaceae (division: Ascomycota). Species of *Fusarium* inhibit soils in different climates and regions of earth, ranging from the Arctic to the Sahara desert. They are known plant pathogens and can even cause diseases on humans such as onychomycosis, keratomycosis of the cornea, ulcers, necroses, skin infections and infections in the internal organs (Webster and Weber, 2007). In terms of chemistry, they produce mycotoxins such as enniatins, beauvericin, moniliformin trichothecens and zearalenone (Firakova *et al*., 2007).

Fusarium acuminatum was obtained from the root of *Larrea tritentata* and yielded the furanopyrrolidone, 13α-hydroxylucilactaene in addition to NG-391, NG-393, enniatin A and enniatin B as shown in Figures 6.1 and 6.2, respectively (Bashyal *et al*., 2007). The isolated compounds were assayed against several human cancer cell lines, such as NCI-H460 (non-small cell lung), MCF-7 (breast cancer), SF-268 (CNS glioma), MIA Pa Ca-2 (pancreatic carcinoma) and PC-3M (metastatic prostate cancer). However, only enniatin A and enniatin B exhibited significant anti-proliferative activity. Moreover, two biologically inactive compounds, acuminatopyrone and chlamydosporol were isolated from the soil saprophytic *Fusariurm acuminatum* (Figure 6.1) (Grove and Hitchcock, 1991).

N-prenylated tryptophan metabolites were isolated from the rice pathogen *Fusarium fujikuroi* (Figure 6.1) (Arndt *et al*., 2017). The fungus afforded r-*N*-dimethylallyltryptophan (r-*N*-DMAT) and acetyl-r-*N*-dimethylallyltryptophan (ac-r-*N*-DMAT), which are products of dimethylallyltryptophan synthatases. Furthermore, *Fusarium solani* JK10 were obtained from the roots of *Chlorophora regia* and afforded seven derivatives of 7-desmehtyl fusarin C (DMFD 1 – 7) and five known compounds NG-391, NG-393 ,(+)–(S)–solaniol, 3–dihydro–5–hydrox-y–8–methoxy–2,4–dimethylnaphtho[1,2–b]furan–6,9–dione and N_b–acetyltryptamin (Figure 6.1) (Kyekyeku *et al*., 2017). The seven derivatives of 7-desmethyl fusarin C, along with NG-391 and NG-393 exhibited antibacterial activity against *Escherichia coli*. From the plant *Paepalanthus*

chiquitensis, 25 endophytic fungi were screened against *Staphylococcus aureus*, *Escherichia coli* and *Salmonella setubal* and the yeast *Candida albicans* (Hilario *et al*., 2017). The extract of the endophyte *Fusarium fujikuroi* was the most active. Therefore, it was scaled up in a liquid culture of potato dextrose broth and afforded the alkaloid 2-(4-butylpicolinamide) acetic acid along with the known metabolites fusaric acid, indole acetic acid and terpestacin (Figure 6.1). The compounds 2-(4-butylpicolinamide) acetic acid and fusaric acid possessed a moderate antibacterial activity against the tested bacteria and fusaric acid was active against the yeast *Candida albicans* (Hilario *et al*., 2017). Furthermore, the endophyte *Fusarium oxysporum* 162 cultivated in rice medium afforded indole-3-acetic acid, indole-3-acetic acid methyl ester, 4-hydroxybenzoic acid, methyl 4-hydroxybenzoate, methyl 2-(4-hydroxyphenyl)acetate and uridine, which were all isolated from *Fusarium* spp for the first time (Figure 6.1). Both indole-3-acetic acid and 4-hydroxybenzoic acid showed a strong nematocidal activity against *Meloidogyne incognita.* However, the other compounds possessed moderate to weak activity while uridine was not active at all (Bogner *et al*., 2017). Additionally, the one strain many compounds (OSMAC) approach was also employed on the endophyte *Fusarium tricinctum* yielding fusarielins A, B and J–L when cultivated on fruit and vegetable juice-supplemented solid rice media (Figure 6.1) (Hemphill *et al*., 2017). The obtained compounds were screened for their anti-proliferative activity and fusarielin J was found active against the human ovarian cancer cell line A2780 (Hemphill *et al*., 2017).

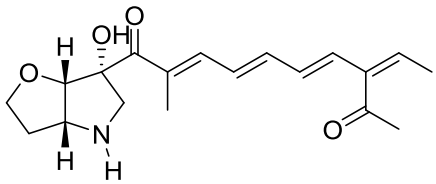

13α-hydroxylucilactaene

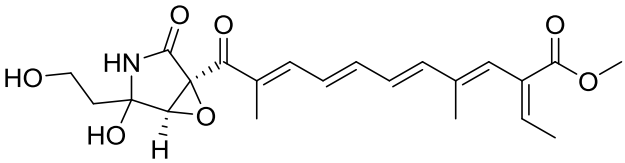

NG-391

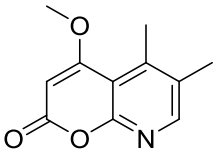

acuminatopyrone

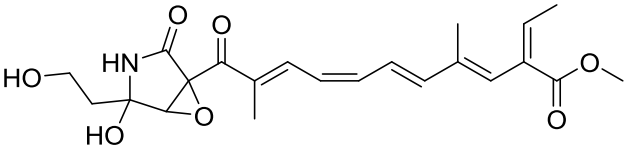

NG-393

Figure 6.1: Secondary metabolites isolated from *Fusarium acuminatum and other Fusarium* spp.

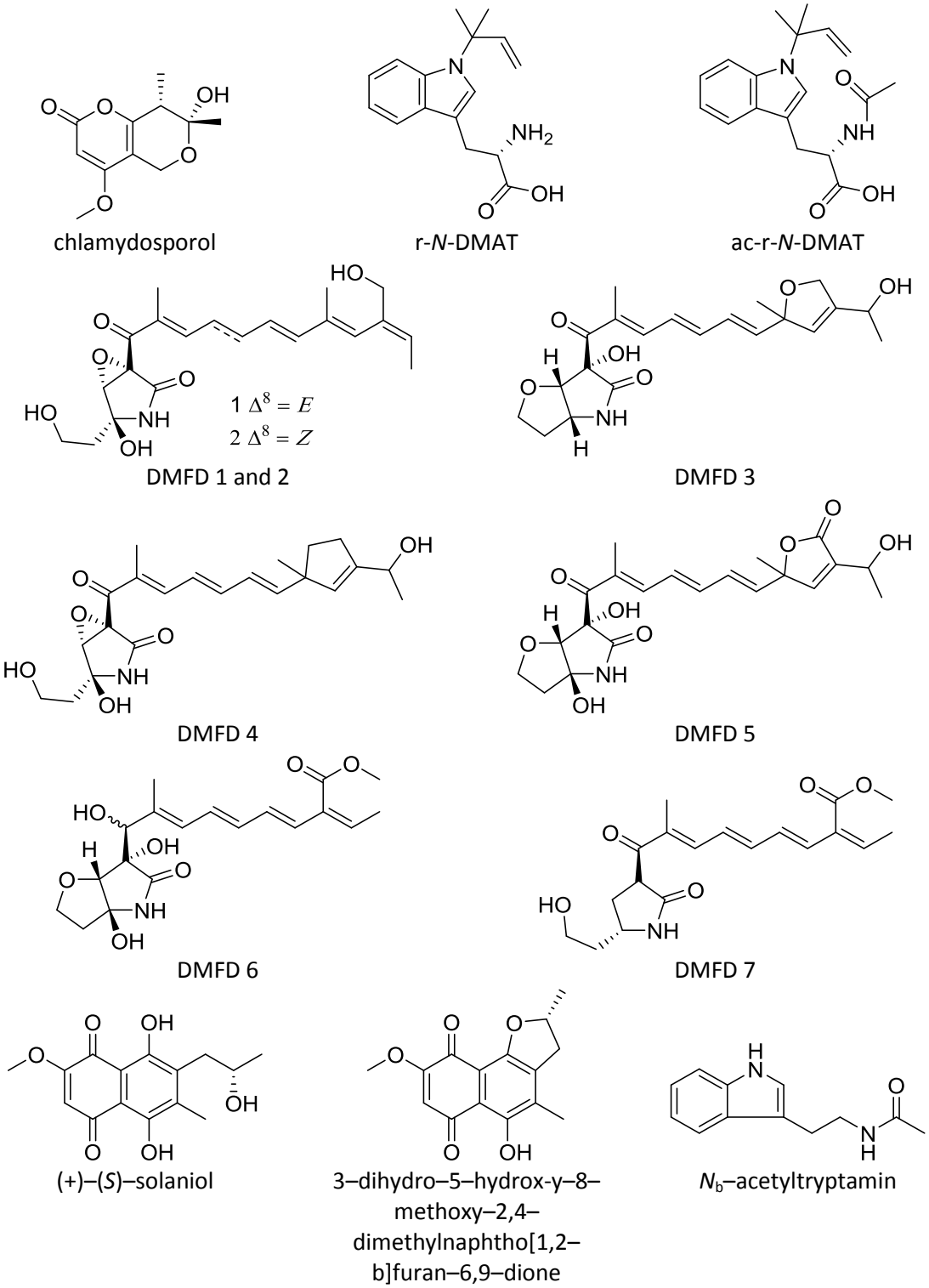

Figure 6.1 (continued): Secondary metabolites isolated from *Fusarium acuminatum and other Fusarium* spp.

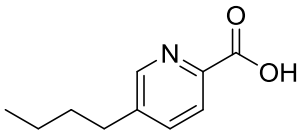

2-(4-butylpicolinamide)acetic acid

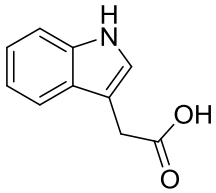

fusaric acid

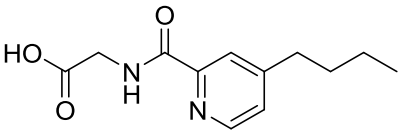

indole acetic acid

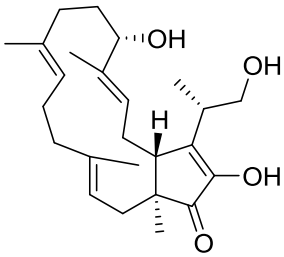

terpestacin

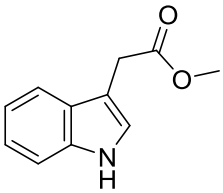

indole-3-acetic acid methyl ester

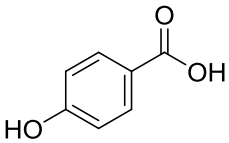

4-hydroxybenzoic acid

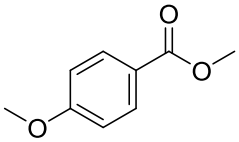

methyl 4-hydroxybenzoate

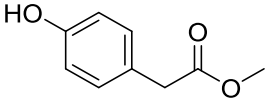

2-(4-hydroxyphenyl)acetate

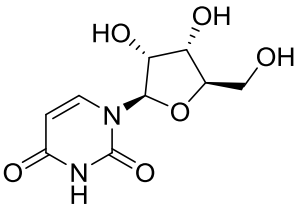

uridine

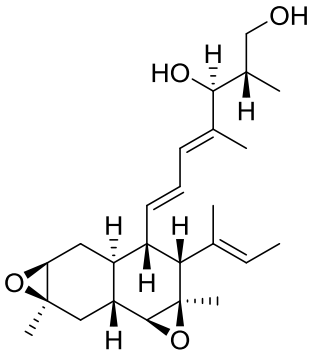

fusarielin A

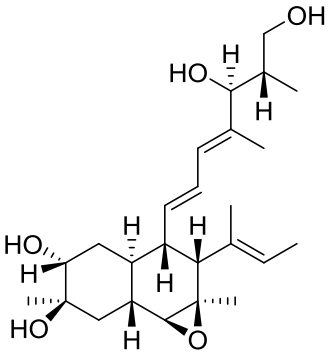

fusarielin B

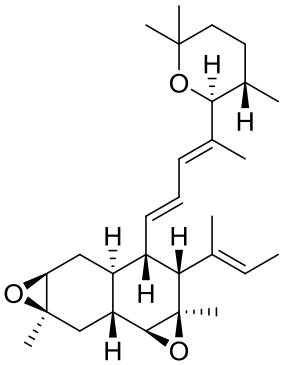

fusarielin L

Figure 6.1 (continued): Secondary metabolites isolated from *Fusarium acuminatum and other Fusarium* spp.

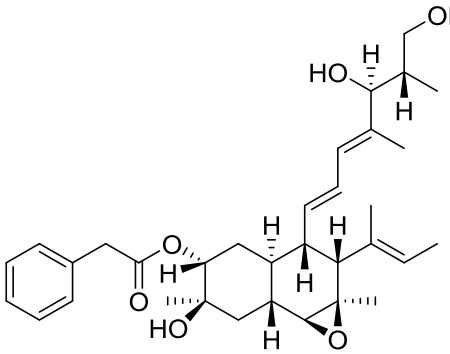

fusarielin J

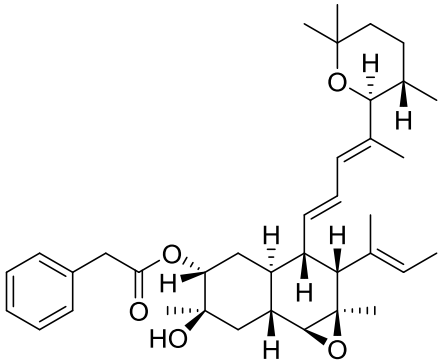

fusarielin K

Figure 6.1 (continued): Secondary metabolites isolated from *Fusarium acuminatum and other Fusarium* spp.

6.1.2 Enniatins isolated from *Fusarium* spp and other fungi

Enniatins are *N*-mehtylated cyclohexadepsipetides built of three units; each of these units is composed of *N*-methylated L-amino acid and D-α-hydroxy acid (Firakova *et al*., 2007). They are mycotoxins produced by the genus *Fusarium* that contaminate grains, including wheat, barley, rice and maize. Their production is catalysed by a group of enzymes known as enniatin synthatases in addition to the enzyme *N*-methyltransferase (Billich and Zocher, 1987). The active sites of these peptide synthatases are called modules and they catalyse one cycle of the polypeptide chain elongation and functional group alteration (Billich and Zocher, 1987). The modules of acyladenylates activate the subunits before they are covalently bonded as thioesters to the enzyme (Jestoi, 2008). After that, *N*-methylation takes place followed by the formation of peptide bonds and the cyclisation of the three dipeptidoles that construct the enniatin (Jestoi, 2008). The conversion of L-valine to D-α-hydroxyisovaleric acid is catalysed by the enzyme D-α-hydroxyisovalerate dehydrogenase (Hornbogen *et al*., 2002). Enniatins were isolated for the first time in 1947 by Gaumann and his colleagues from *Fusarium orthoceras* App. var. *enniatinum* (Gaumann and Roth, 1947).

The lipophilicity and the shape of the cyclodepsipeptide core of enniatins enable them to act as ionophores that can be easily incorporated into cell membranes, leading to the formation of cation selective pores. These pores are passive channels for K^+, Ca^{2+}, Na^+, Mg^{2+} and Li^+ that enter the cell changing the intracellular ion concentration, leading to the fragmentation of DNA

and inducing apoptosis (Firakova *et al*., 2007, Jestoi, 2008, Feudjio *et al*., 2010, Sy-Cordero *et al*., 2012, Luz *et al*., 2017). This leads to wide range of biological activities for enniatins, including cytotoxic activities towards several human cancer cell lines such as HCT116 (human colon carcinoma), Hep G2 (hepatocellular carcinoma), MRC-5 (fibroblast-like foetal lung normal cells), KB (human epidermoid carcinoma), BC-1 (human breast carcinoma) and Heps 7402 (hepatoma carcinoma) and antimicrobial activities against *Mycobacterium* spp., *Staphylococcus* spp., *Bacillus* spp., *Pseudomonas aeruginosa*, *Escherichia coli* and *Botrytis cinerea*. In addition to that, enniatins possess enzyme inhibition activities against acyl-CoA:cholesterol acyltransferase (ACAT), cyclic nucleotidase and protein kinases (Firakova *et al*., 2007, Sy-Cordero *et al*., 2012). Isolated enniatins are shown in Figure 6.2 while their sources and bioactivities are presented in Table 6.1, which was adopted from the reviews of Firakova *et al.* and Sy-Cordero *et al.* (Firakova *et al*., 2007, Sy-Cordero *et al*., 2012).

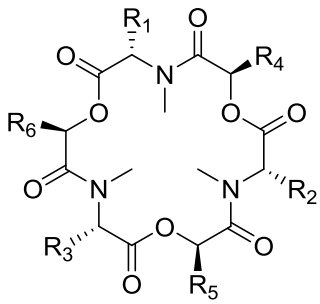

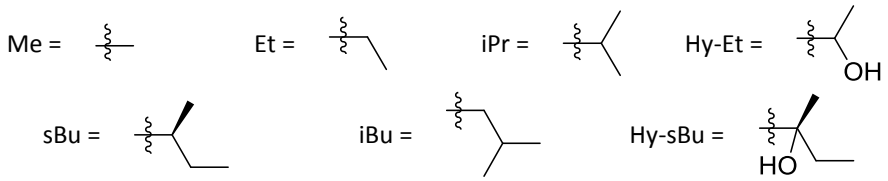

Compound	R_1	R_2	R_3	R_4	R_5	R_6
Enniatin A	sBu	sBu	sBu	iPr	iPr	iPr
Enniatin A_1	sBu	iPr	sBu	iPr	iPr	iPr
Enniatin A_2	sBu	iBu	sBu	iPr	iPr	iPr
Enniatin B	iPr	iPr	iPr	iPr	iPr	iPr
Enniatin B_1	iPr	sBu	iPr	iPr	iPr	iPr
Enniatin B_2*	iPr	iPr	iPr	iPr	iPr	iPr
Enniatin B_3*	iPr	iPr	iPr	iPr	iPr	iPr
Enniatin B_4 (D)	iPr	iPr	iBu	iPr	iPr	iPr
Enniatin C	iBu	iBu	iBu	iPr	iPr	iPr
Enniatin E_1	iPr	iBu	sBu	iPr	iPr	iPr
Enniatin E_2	iPr	sBu	iBu	iPr	iPr	iPr
Enniatin F	iBu	sBu	sBu	iPr	iPr	iPr
Enniatin G	iBu	iBu	iPr	iPr	iPr	iPr
Enniatin H	iPr	iPr	iPr	sBu	iPr	iPr
Enniatin I	iPr	iPr	iPr	sBu	sBu	iPr
MK 1688	iPr	iPr	iPr	sBu	sBu	sBu
Enniatin J_1	iPr	iPr	Me	iPr	iPr	iPr
Enniatin J_2	sBu	iPr	Me	iPr	iPr	iPr
Enniatin J_3	Me	iPr	sBu	iPr	iPr	iPr
Enniatin K_1	iPr	iPr	Et	iPr	iPr	iPr
Enniatin L	iPr	iPr	iPr	iPr	iPr	Hy-sBu
Enniatin M_1	iPr	iPr	iPr	iPr	sBu	Hy-sBu
Enniatin M_2	iPr	iPr	iPr	iPr	Hy-sBu	sBu
Enniatin N	iPr	iPr	iPr	sBu	sBu	Hy-sBu
Enniatin O_1	iBu	iPr	iPr	sBu	iPr	iPr
Enniatin O_2	iBu	iPr	iPr	iPr	sBu	iPr
Enniatin O_3	iBu	iPr	iPr	iPr	iPr	sBu
Enniatin P_1	iPr	iPr	Hy-Et	iPr	iPr	iPr
Enniatin P_2	iBu	iPr	Hy-Et	iPr	iPr	iPr

*B_2 and B_3 have one and two *N*-Methyls, respectively, in the R_1 and the R_1 and R_2 positions.

Figure 6.2: Enniatins (Sy-Cordero *et al*., 2012).

Table 6.1: Sources and bioactivities of enniatins (Firakova *et al*., 2007, Sy-Cordero *et al*., 2012).

Compound	Microbial producers	Bioactivities
Enniatin A	*Fusarium sambucinum* *Fusarium* sp. HA 43-88 *Fusarium oxysporum* *Fusarium avenaceum* Fusarium sp. FO-1305	Cytotoxic against Hep G2, MRC-5; ACAT inhibition
Enniatin A_1	*Fusarium* sp. HA 43-88 *Fusarium oxysporum* *Fusarium avenaceum* *Fusarium tricinctum* *Fusarium culmorum* *Fusarium poae* *Fusarium* sp. FO-1305	Cytotoxic against Hep G2, MRC-5; ACAT inhibition
Enniatin A_2	*Fusarium avenaceum*	Cytotoxic against Hep G2, MRC-5
Enniatin B	*Fusarium* sp. *Fusarium* sp. Y-53 *Fusarium* sp. F31 *Fusarium lateritium* var. *stiboides* *Fusarium avenaceum* *Fusarium sambucinum* *Fusarium scirpi* *Fusarium torulosum* *Fusarium tricinctum* *Fusarium culmorum* *Fusarium poae* *Verticillium hemipterigenum* *Halosarpheia* sp. 732 Unidentified fungus MOBCOF-1 Unidentified fungus BCC2629 *Fusarium* sp. FO-1305	Cytotoxic against Hep G2, MRC-5; ACAT inhibition
Enniatin B_1	*Fusarium* sp. HA 43-88 *Fusarium* sp. Y-53 *Fusarium* sp. F31 *Fusarium oxysporum* *Fusarium avenaceum* *Fusarium* sp. FO-1305	Cytotoxic against Hep G2, MRC-5; ACAT inhibition
Enniatin B_2	*Fusarium avenaceum* *Fusarium acuminatum*	Cytotoxic against Hep G2, MRC-5
Enniatin B_3	*Fusarium avenaceum* *Fusarium acuminatum*	Cytotoxic against Hep G2, MRC-5
Enniatin B_4 (D)	*Fusarium* sp. F31 *Fusarium* sp. FO-1305 *Verticillium hemipterigenum* *Halosarpheia* sp. 732 Unidentified fungus BCC2629 Unidentified fungus MOBCOF-1	ACAT inhibition

Table 6.1 (Continued): Sources and bioactivities of enniatins (Firakova *et al*., 2007, Sy-Cordero *et al*., 2012).

Compound	Microbial producers	Bioactivities
Enniatin C	*Fusarium* sp. *Verticillium hemipterigenum*	Antimalarial, antituberculous, cytotoxic
Enniatin E_1	*Fusarium* sp. FO-1305	ACAT inhibition
Enniatin E_2	*Fusarium* sp. FO-1305	ACAT inhibition
Enniatin F	*Fusarium* sp. FO-1305	ACAT inhibition
Enniatin G	*Verticillium hemipterigenum* *Halosarpheia* sp. 732	Heps 7402
Enniatin H	*Verticillium hemipterigenum* Unidentified fungus MOBCOF-1	Antimalarial, antituberculous, cytotoxic
Enniatin I	*Verticillium hemipterigenum* Unidentified fungus MOBCOF-1	Antimalarial, antituberculous, cytotoxic
MK 1688	*Verticillium hemipterigenum* Unidentified fungus MOBCOF-1	Antimalarial, antituberculous, cytotoxic
Enniatin J_1	*Fusarium* sp. F31	Against *Botrytis cinerea*
Enniatin J_2	*Fusarium* sp. F31	Against *Botrytis cinerea*
Enniatin J_3	*Fusarium* sp. F31	Against *Botrytis cinerea*
Enniatin K_1	*Fusarium* sp. F31	Against *Botrytis cinerea*
Enniatin L	Unidentified fungus BCC2629	Against *Botrytis cinerea*
Enniatin M_1	Unidentified fungus BCC2629	Antimalarial, antituberculous, cytotoxic
Enniatin M_2	Unidentified fungus BCC2629	Antimalarial, antituberculous, cytotoxic
Enniatin N	Unidentified fungus BCC2629	Antimalarial, antituberculous, cytotoxic
Enniatin O_1	*Verticillium hemipterigenum*	Antimalarial, antituberculous, cytotoxic
Enniatin O_2	*Verticillium hemipterigenum*	Antimalarial, antituberculous, cytotoxic
Enniatin O_3	*Verticillium hemipterigenum*	Antimalarial, antituberculous, cytotoxic
Enniatin P_1	*Fusarium* sp. Vi 03441	-
Enniatin P_2	*Fusarium* sp. Vi 03441	-

6.2 Medium optimisation to select the most suitable conditions for culturing *Fusarium acuminatum*, medium-scale fermentation

As shown in Table 6.1, it was perceived that by increasing the incubation period, the weight of the obtained extract increases in both media types. However, using the solid-rice medium resulted in a slight better growth for *Fusarium acuminatum* obtaining higher yields.

Table 6.1: Weights of *Fusarium acuminatum* extracts cultured in two types of media harvested at various incubation periods.

Medium Type	Incubation period (days)	Weight of extract (mg) per 100 mL (liquid) or 100 g (solid)
Liquid-Wickerham	7	35
Liquid-Wickerham	15	101
Liquid-Wickerham	30	122
Solid-Rice	7	77
Solid-Rice	15	114
Solid-Rice	30	207

To study the chemical composition of the extracts of *Fusarium acuminatum*, both ^{1}H NMR and LC-HRMS data were utilised. As depicted by the ^{1}H NMR spectra of the liquid-Wickerham samples (Figure 6.3.A), the incubation period did not affect the types of compounds produced, or at least, the major ones that were detected from the ^{1}H NMR spectra. The same pattern of peaks highlighted by the red boxes was observed for the three extracts obtained from different growth phases. This pattern is characteristic for enniatins, a cyclic depsipeptides that *Fusarium* species in general are known to produce. The doublets at δ_H 4.50 – 5.50 corresponded to the α-protons that are attached to both amide and ester functional groups. The large singlet at δ_H 3.00 indicated the presence of the *N*-methyl protons of the enniatin. Moreover, the protons of the aliphatic methyl units could be detected in the large overlapping doublets and triplets at δ_H 0.50 – 1.00 and δ_H 1.00 – 2.30 ppm.

For solid-rice samples (Figure 6.3.B), the extract of 7 days of incubation shared a very similar spectrum with the medium's blank (blue boxes), indicating a very weak production of metabolites. However, the extracts obtained after 15 and 30 days of incubation exhibited spectral pattern for enniatins (red boxes). The ^{1}H NMR spectral data for extracts from the 30 days of incubation in both liquid-Wickerham medium and solid-rice medium was identical (Figure 6.3.C). This concluded that the type of medium had no effect in determining the major compounds that the endophyte produces.

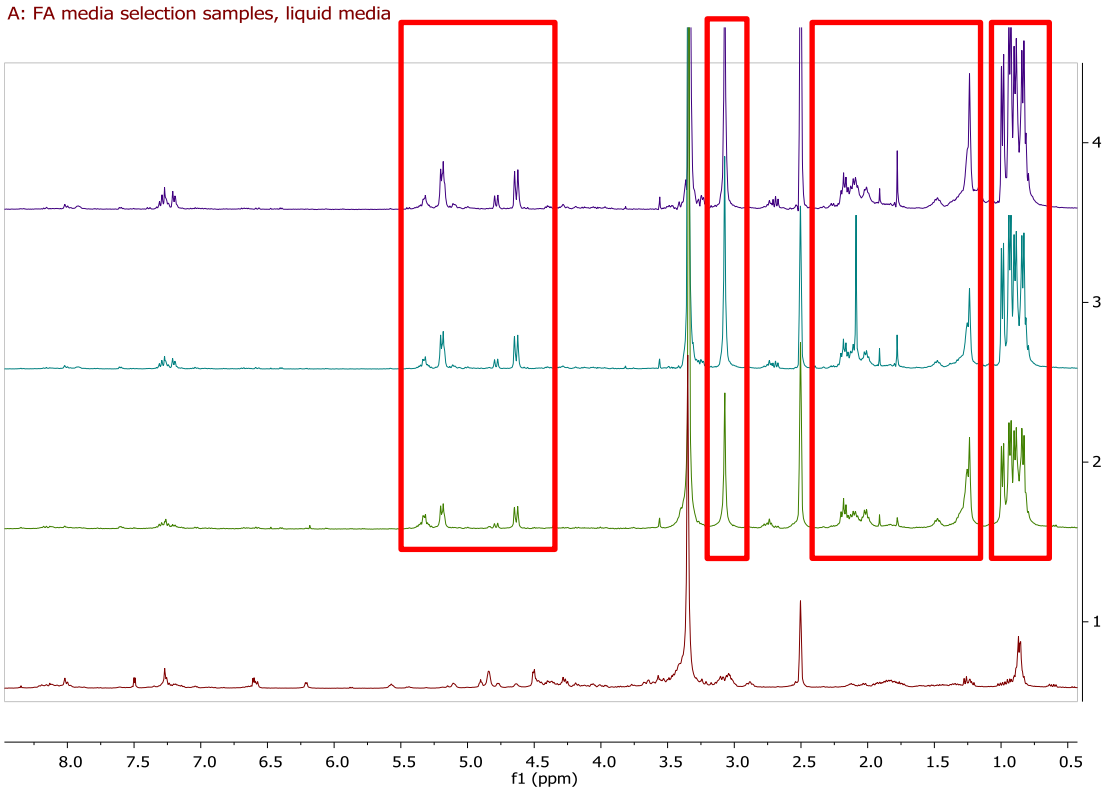

Figure 6.3: The ^{1}H NMR data obtained from *Fusarium acuminatum* extracts after incubation in (A): liquid media and (B): solid media. Spectrum 1 is the medium blank, 2 is 7 days incubation, 3 is 15 days and 4 is 30 days. (C): extracts' ^{1}H NMR data comparison in 1: liquid medium and 2: solid medium. All are measured in DMSO-d_6, (400 MHz).

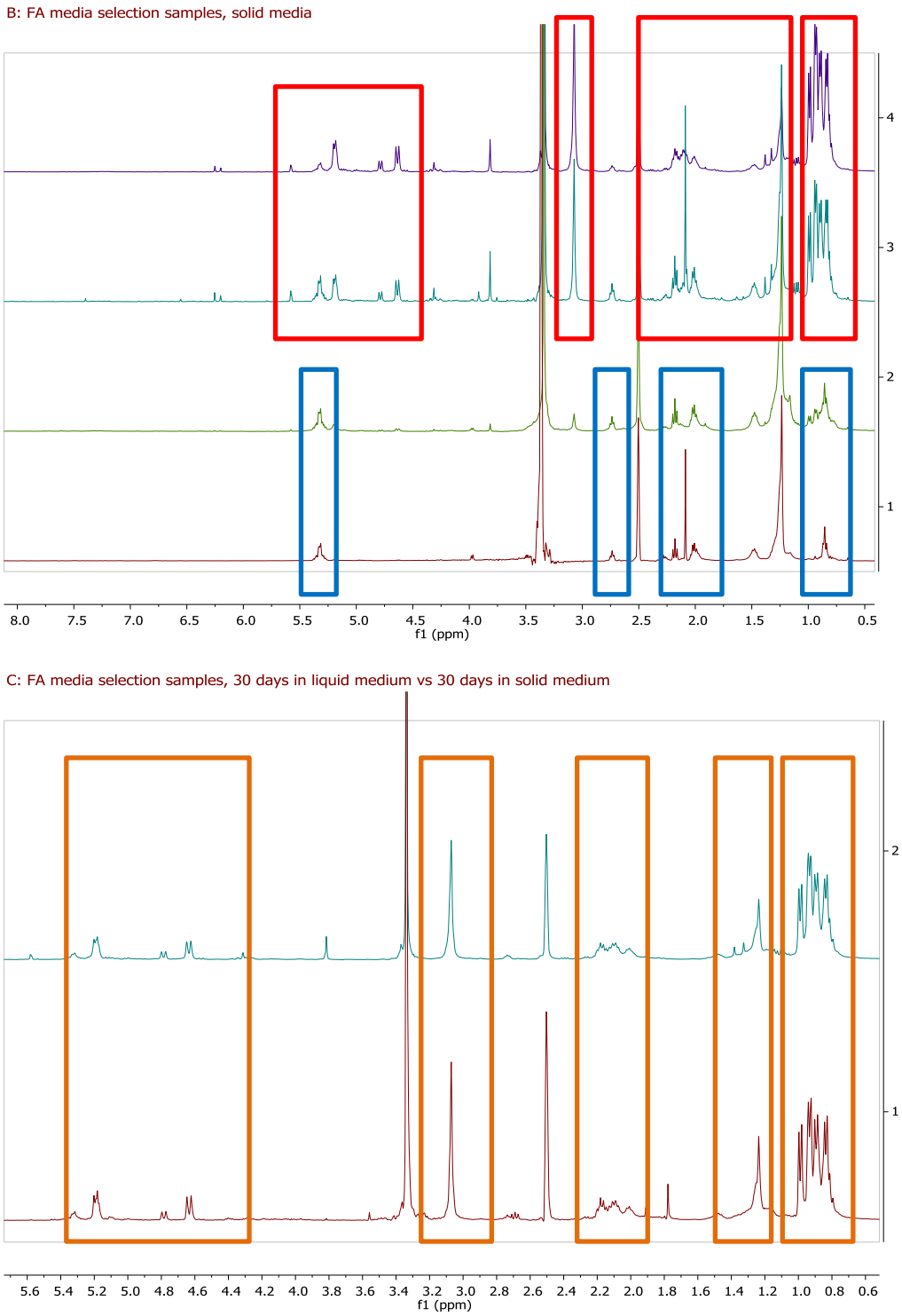

Figure 6.3 (continued): (B): solid media. Spectrum 1 is the medium blank, 2 is 7 days incubation, 3 is 15 days and 4 is 30 days. (C): extracts' ^{1}H NMR data comparison in 1: liquid medium and 2: solid medium. All are measured in DMSO-d_6, (400 MHz).

The LC-HRMS scatter plots that were obtained from the extracts of liquid-Wickerham cultures were presented in Figure 6.4. As shown in figure 6.4. , comparisons of the culture extracts obtained after 7 and 15 days of incubation as well as after 15 and 30 days indicated a similarities between all the extracts. This similarities denoted the closeness of the loadings to the equatorial line resulting in a reduced scattering, and hence, less variability and differences between the extracts.

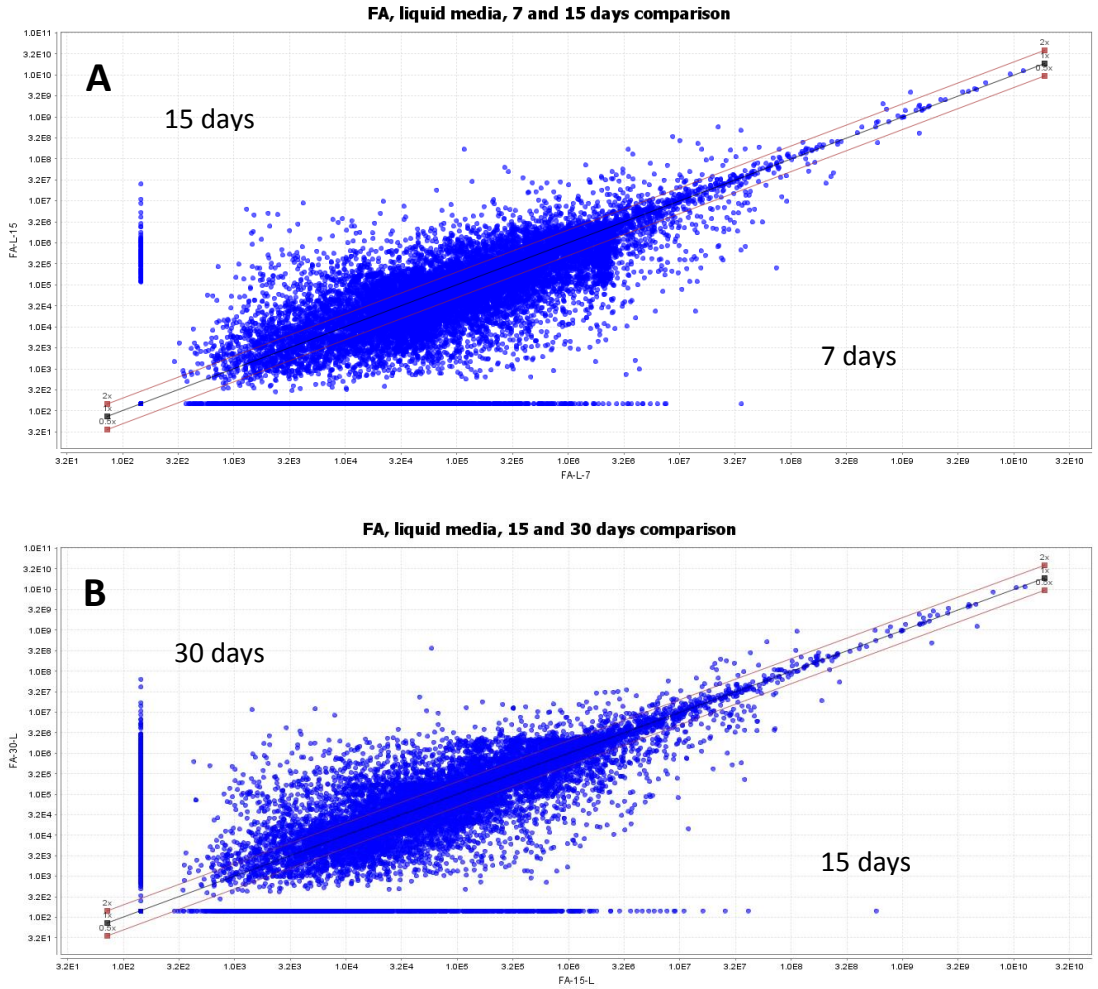

Figure 6.4: Scatter plots of the LC-HRMS data of *Fusarium acuminatum* extracts obtained at different incubation periods in liquid-Wickerham medium, comparing (A): 7 with 15 days and (B): 15 with 30 days of incubation.

For the solid-rice medium samples (Figure 6.5), similarity between samples was observed when comparing the extracts obtained after 7 and 15 days of incubation. However, a significant

difference in scattering was observed when comparing extracts obtained after 15 and 30 days of incubation, suggesting changes in the compounds produced between these two incubation periods. As the scattering was skewed in the favour of 30 days of incubation, this indicated more compounds to be produced if the endophyte was incubated in solid-rice medium for 30 days.

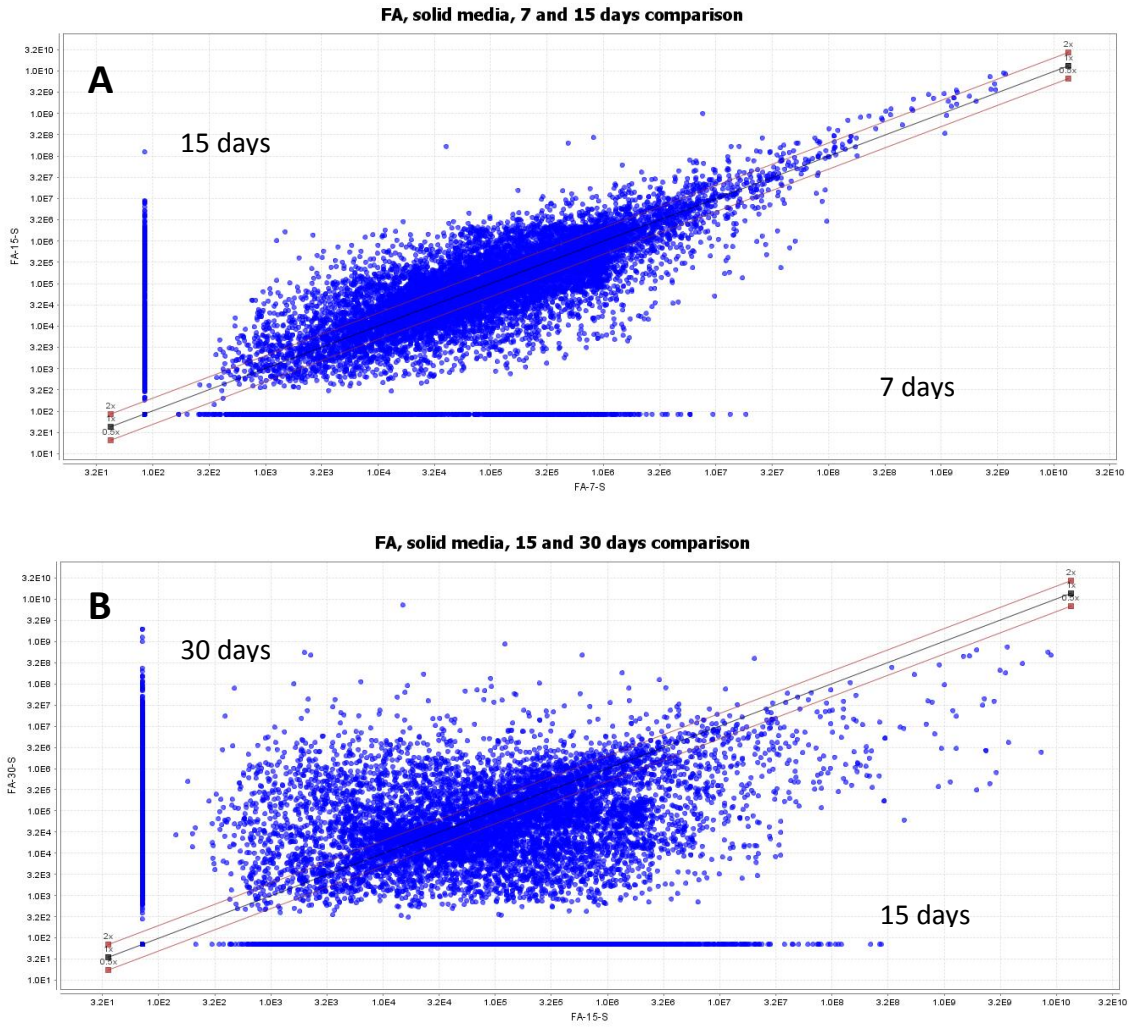

Figure 6.5: Scatter plots of the LC-HRMS data of *Fusarium acuminatum* extracts obtained at different incubation periods in solid-rice medium, comparing (A): 7 with 15 days and (B): 15 with 30 days of incubation.

Figure 6.6 compared 30 days of incubation in solid-rice medium to the same period of incubation in liquid-Wickerham medium. An increase in loadings and scattering was observed

for 30 days of incubation in solid-rice medium, resembling increased chemical diversity in the extract.

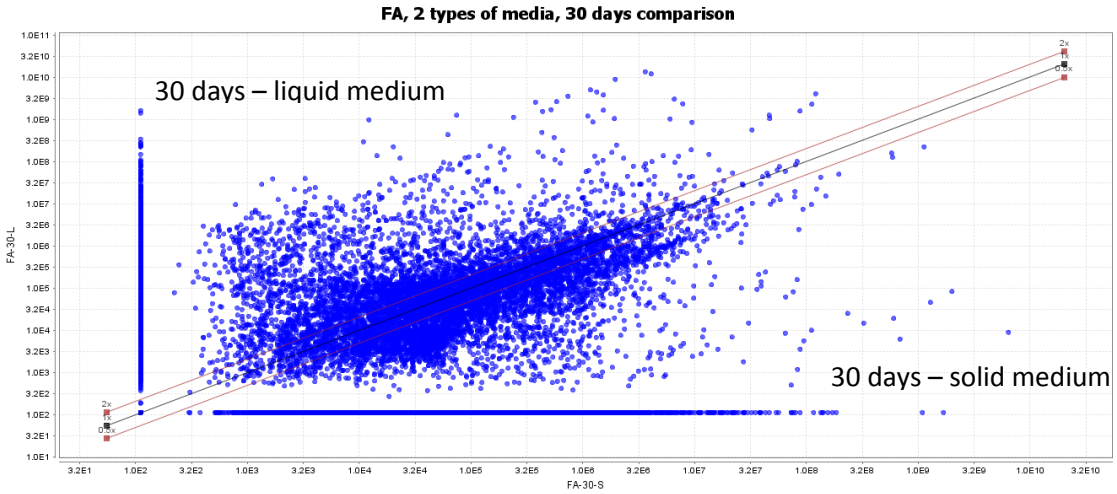

Figure 6.6: Scatter plot of LC-HRMS data of *Fusarium acuminatum* extracts, comparing 30 days of incubation in solid-rice medium to liquid-Wickerham medium.

The findings of the scatter plots explained the clustering pattern that was observed in the scores plot of the SIMCA-PCA of the LC-HRMS data of the medium optimisation samples (Figure 6.7.A). As depicted from the scatter plots, liquid-Wickerham samples were similar in terms of chemistry. As a result, they were clustered together in the PCA-scores plot and encircled in red in Figure 6.7. Moreover, extracts obtained after 7 and 15 days of incubation in solid-rice medium were similar as well as illustrated by the scatter plot. Thus, they were clustered together in the scores plot and contained in the blue circle. However, the extract obtained after 30 days of incubation in solid-rice medium was apart from the others, implying its chemical difference and richness that were observed in the scatter plots. The loadings plot was employed to study the uniqueness of the extract obtained after 30 days of incubation in solid-rice medium (Figure 6.7.B). The outliers marked in figure 6.7.B are listed in Table 6.2 and as described, most of these outliers are massetolides, which are cyclic depsipeptides, like the enniatins. Massetolides are known antimicrobial agents that are active against Mycobacteria (Gerard *et al*., 1997). The biosynthesis of enniatins in *Fusarium acuminatum* occurred quicker than that of the massetolides, which were only observed to be produced on the 30th day (Figure 6.7.B).

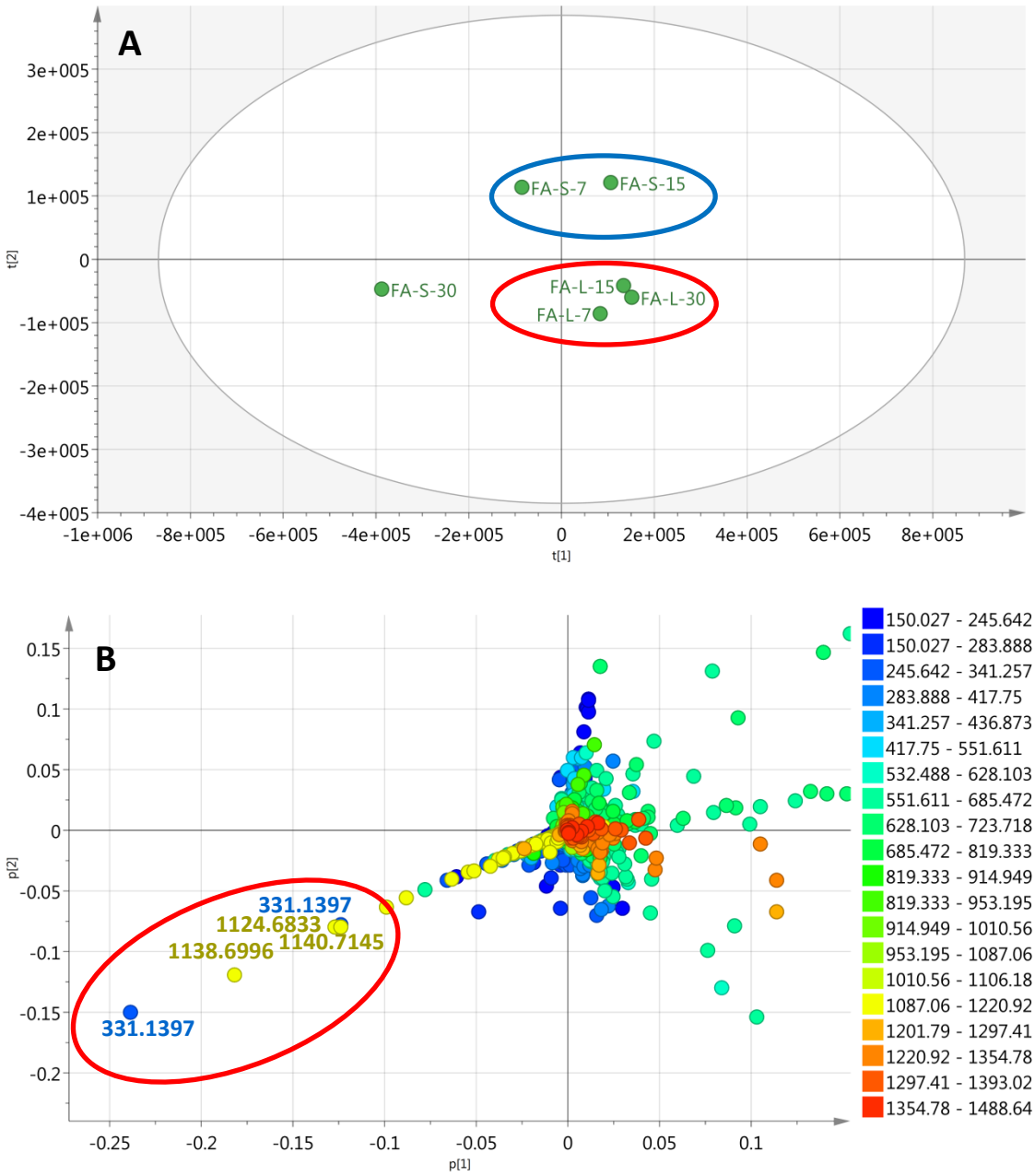

Figure 6.7: (A): Scores plot based on the PCA of the LC-HRMS data for the various *Fusarium acuminatum* extracts. "FA" refers to the endophyte *Fusarium acuminatum*. The letter "S" is for the solid-rice medium and "L" is for the liquid-Wickerham medium. While the numbers "7, 15, and 30" indicate the incubation period. R2X=0.816, Q2=0.411. (B): Loadings plot for media optimisation samples, acquired from the scores plot 6.7.A. The outliers are labelled by their *m/z* value.

Table 6.2: Dereplication of the outliers in the loadings plot of *Fusarium acuminatum* media optimisation samples (Figure 6.7).

t_R (min)	MZMine ID	*m/z*	Molecular formula	MWt	Name	Source
4.85	P_4230	331.1397	$C_{16}H_{18}N_4O_4$	330.1324	Preacinetobactin; 3'-Deoxy	*Pseudomonas* spp.
					Pseudomonine	*Pseudomonas fluorescens* AH2
26.70	N_6448	1124.6833	$C_{54}H_{95}N_9O_{16}$	1125.6906	Massetolide F	-
					Viscosin	*Pseudomonas viscosa* and *Pseudomonas fluorescens*
					Viscosin; 5-D-Leucyl epimer	*Pseudomonas reactans*
27.94	P_7556	1140.7145	$C_{55}H_{97}N_9O_{16}$	1139.7072	Massetolide A	-
					Massetolide A, Diastereoisomer	*Pseudomonas fluorescens* strain BRG100
					Massetolide D	-
					Massetolide G	-

Finally, the *in-vitro* biological activity of the extracts against both breast cancer (ZR-75) and lung cancer (A549) cell lines was tested and the results are shown in Figure 6.8.

All extracts constructed for media optimisation were found active against ZR-75 cell line (Figure 6.8.A). In Figure 6.8.A, less than 20% cell viability was achieved by all the tested extracts. This indicated the potency of the *Fusarium acuminatum* extracts and the potential of the fungus to be a source of anti-proliferative agents against breast cancer.

On the other hand, for the bioactivity against the A549 cell line as shown in Figure 6.8.B, the extracts from the liquid-Wickerham medium were generally more active and gave a percent viability between 15% and 25%. Less bioactivity was exhibited by the extracts obtained after 7 and 15 days of incubation in solid-rice medium, as about only 40% cell viability was achieved. Nonetheless, the sample that was obtained after 30 days of incubation on the solid culture had almost 0% viability of cells and was the most active amongst all the tested extracts.

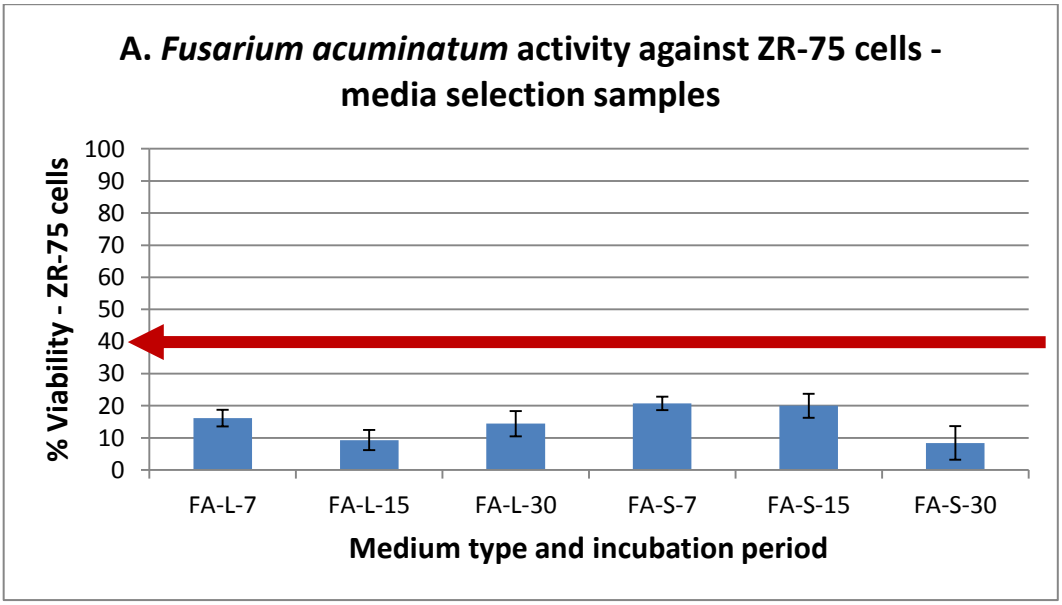

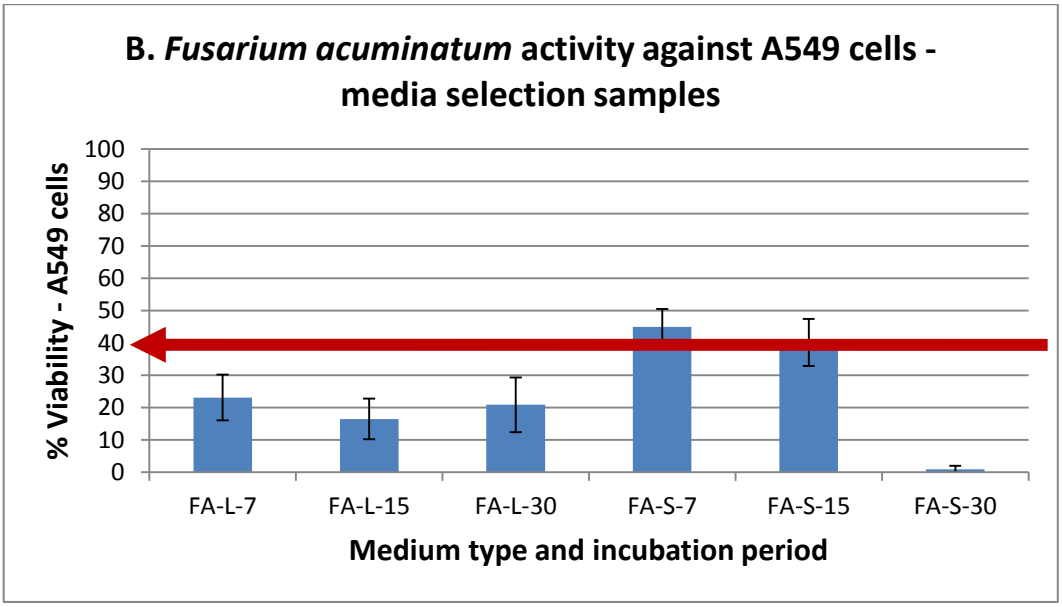

Figure 6.8: The biological activity for *Fusarium acuminatum* extracts at 30 µg/mL against (A): breast cancer (ZR-75) cell line and (B): lung cancer (A549) cell line. "FA" refers to the endophyte *Fusarium acuminatum*. The letter "S" is for the solid-rice medium and "L" is for the liquid-Wickerham medium. The numbers "7, 15 and 30" indicate the incubation period in days. The red line indicates the bioactivity threshold.

As an outcome for the three tested parameters, incubating *Fusarium acuminatum* in solid-rice medium for 30 days was the best option to scale-up the endophyte. Not only it obtained the highest yield, but also the most diverse and unique chemistry, even if its major compounds and

metabolites were similar to other extracts obtained from different incubation periods and media types. Moreover, its extract was the most active when tested *in vitro* on ZR-75 and particularly against A549 cell lines.

6.3 Large scale fermentation and first fractionation of the extract of *Fusarium acuminatum*

Eighteen 500 mL flasks were prepared for the large scale fermentation. The preparation was done as specified in 2.3.2.2. After 30 days of incubation, the metabolites were extracted by ethylacetate. The weight of the obtained extract was 28.7076 g. Liquid-liquid partitioning was done on the total crude extract as described in 2.3.2.5. The weight of the dried hexane extract was 14.7587 g and the weight of the dried aqueous methanolic extract was 13.4489 g.

The medium pressure liquid chromatography Büchi system as described in 2.5.2.3, was used to fractionate the methanolic extract. A normal phase VersaPak^{TM} (48 g), spherical silica (20-45 µm) column was used with a flow rate of 100 mL/min. The mobile system that was used is described in Table 6.3. The fractions were collected in conical flasks, at 100 mL of each and then pooled using TLC. A total of 24 fractions were obtained (Figure 6.9 and Table 6.4).

Table 6.3: Mobile phase used for the first fractionation of the methanolic extract of the endophyte *Fusarium acuminatum.*

Time (minutes)	% Hexane	% EtOAc	% MeOH
0	100	0	0
10	100	0	0
70	0	100	0
75	0	100	0
105	0	50	50
120	0	50	50

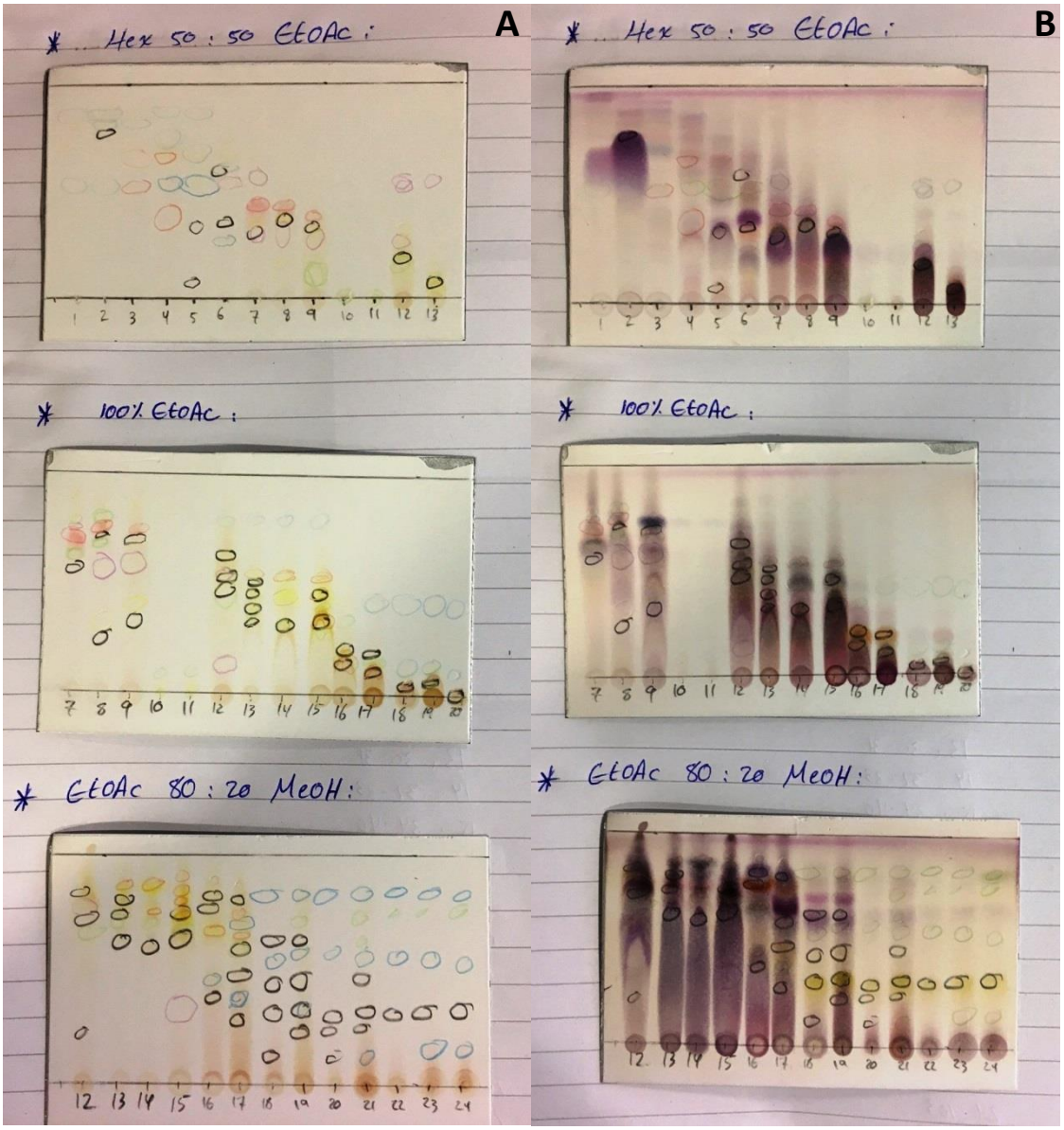

Figure 6.9: Summary TLC plate for the first fractionation step (F.n) of *Fusarium acuminatum,* (A): Before and (B): After spraying with anisaldehyde reagent.

The fractions were subjected to ^{1}H NMR analysis (Figure 6.10). As the figure depicts, this analysis afforded categorising fractions to six groups depending on the major compounds they possessed. The first category included fractions F.1 – F.5 that were mainly composed of fatty

Table 6.4: Fractions (F.n) obtained from first chromatographic separation of *Fusarium acuminatum* methanolic crude extract and their corresponding weight.

Fraction	Weight (mg)	Fraction	Weight (mg)
F.1	192.9	**F.13**	814.7
F.2	80.3	**F.14**	448.8
F.3	12.5	**F.15**	1206.8
F.4	38.3	**F.16**	736.3
F.5	66.5	**F.17**	1099.9
F.6	242.4	**F.18**	121.5
F.7	1238.0	**F.19**	569.5
F.8	590.8	**F.20**	45.9
F.9	864.2	**F.21**	396.0
F.10	7.1	**F.22**	45.2
F.11	5.0	**F.23**	194.9
F.12	767.2	**F.24**	64.7

acids. This was denoted to the methylene units observed at δ_H 1.00 – 1.50 and α-protons at δ_H 2.00 – 2.40 ppm (blue box). The second category was the enniatin-rich fractions F.6 – F.9. Their presence was noticed by detecting the α-protons as doublets at δ_H 4.50 – 5.50 ppm, the protons of the *N*-methyls as large singlet at δ_H 3.00 and the protons of the their aliphatic chains as large overlapping doublets and triplets at δ_H 0.50 – 1.00 (red boxes). The third group of fractions was composed of fractions F.10 and F.11. This group of compounds could contain either a pentasubstituted benzene rings, like those found in anthraquinones, or could represent an amide proton. This is referred to the singlets that resonated at δ_H 7.00 – 8.00 (green box). The fourth group of compounds contained fractions F.12 – F.15. These fractions constituted the major compound hymeglusin. The structure elucidation of its structure is discussed in section 6.6.1. The fifth group is represented by fraction F.16. This fraction composed mainly of aromatic compounds as the spectrum is quite busy at δ_H 6.50 – 8.00 (black box). The last category included fractions F.17 – F.24. These fractions are the most hydrophilic ones as they were the last ones to elute from the normal phase column. Moreover, most of their signals appeared at δ_H 4.00 – 6.00 (orange box) and δ_H 0.50 – 2.50 (brown box), indicating protons connected to oxygenated carbons and aliphatic protons, respectively. Thus, this category composed mainly of sugars. These sugars could be part of glyosidic aromatics as signals at δ_H 7.50 – 8.50 (yellow box) indicate.

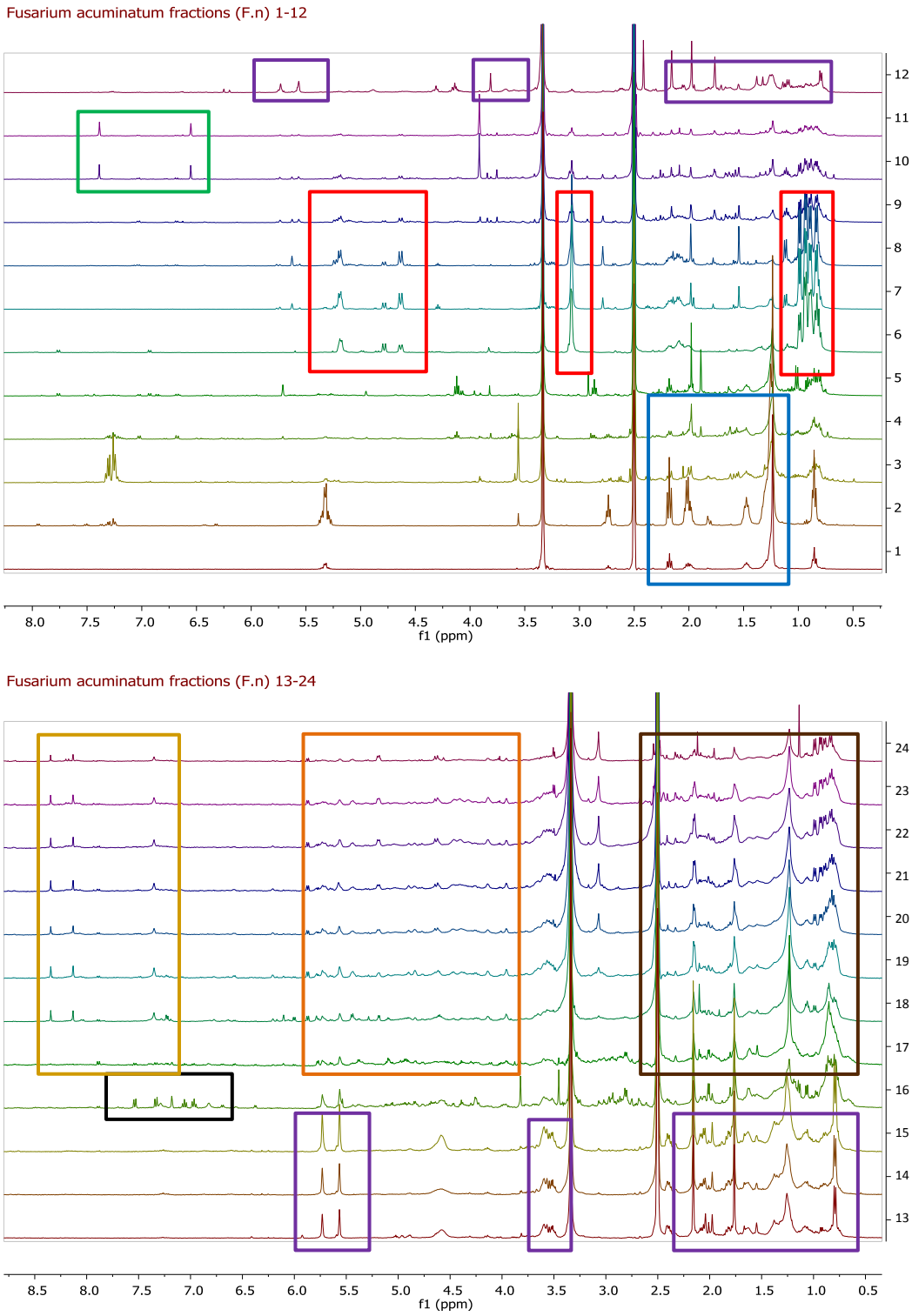

Figure 6.10: The ^{1}H NMR (400 MHz) data obtained from the first chromatographic fractionations of *Fusarium acuminatum* (F.n). Numbers on Y-axis indicate respective fractions. 5 mg of each sample was dissolved in DMSO-d_6.

Furthermore, the obtained fractions were tested *in-vitro* against both ZR-75 and A549 cell lines (Figure 6.11). Fractions F.3 – F.9 exhibited biological activity against ZR-75 cell line. These fractions consisted of enniatins. On the other hand, for A549 cell line, the activity was also observed for enniatin-containing fractions, F.6 – F.9 in addition to F.3.

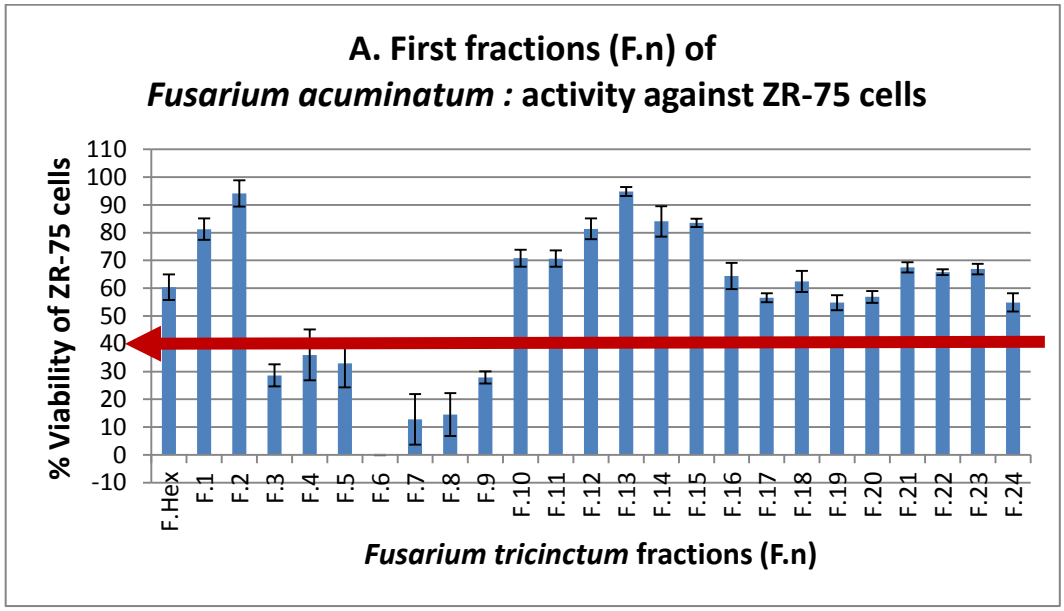

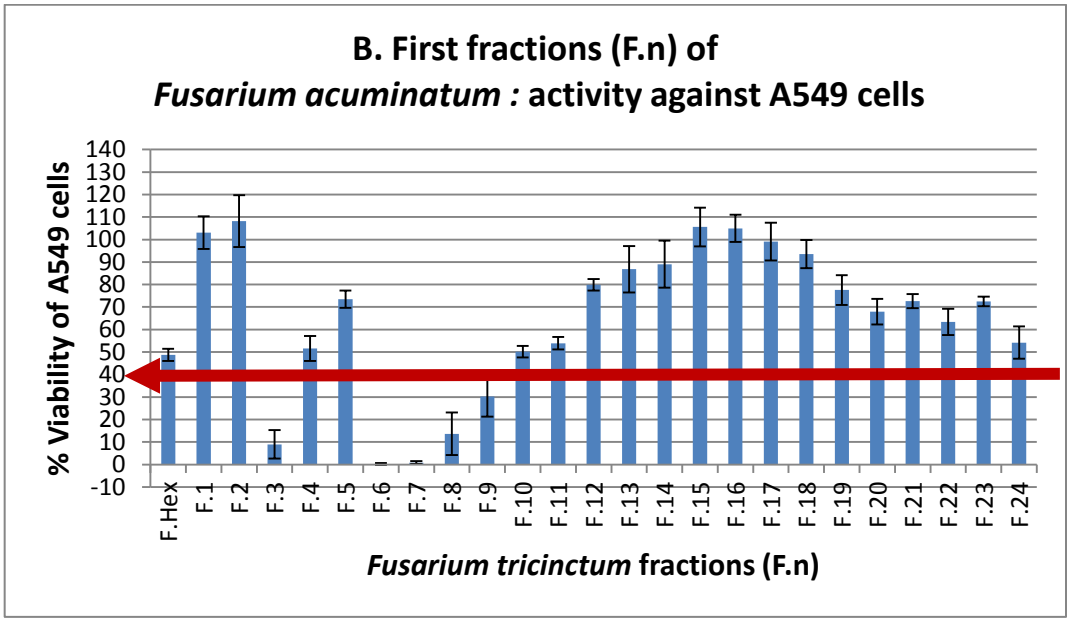

Figure 6.11: Biological activity for first fractions of *Fusarium acuminatum* (F.n) at 30 µg/mL against (A): breast cancer (ZR-75) and (B): lung cancer (A549) cell lines. The red line indicates the bioactivity threshold.

6.4 The creation of metabolomics-bioassay guided approach to pinpoint the bioactive metabolites of *Fusarium acuminatum* at the initial chromatographic separation step

The active fractions F.3 – F.9 were grouped together apart from the inactive fractions to target the bioactive metabolites against breast cancer (Figure 6.12). After that, a permutation test was conducted to test the validity of the model (Figure 6.13). In the generated model, the R2 was 0.89 and Q2 was 0.57, while the R2Y intercept was 0.6363 and the Q2Y intercept was -0.394. These values indicated both good fitting and good prediction as the R2 value was close to 1 and the Q2 value was greater than 0.5, respectively. The difference between R2Y and Q2 values was 0.0663, indicating that no overfitting occurred. The validity of the model was further confirmed by the negative value of Q2Y, being -0.394.

The OPLS-DA model led to the generation of an S plot (Figure 6.14). The metabolites that are on the right side of the Y axis of the S plot were those from the active fractions, while the ones to the left were those from the inactive fractions. Thus, the target bioactive metabolites were the ones to the right of the Y-axis in Figure 6.14.A. Those metabolites were dereplicated and listed in Table 6.5.

It is noted from the scores plot (Figure 6.12.A) that the active fractions are separated into two different groups. Therefore, a loadings plot was generated (Figure 6.12.B). As the loadings plot depicts, the separation of the two groups was an outcome for the difference in the compounds they contain. The main two compounds that caused the separation of group A were the two fatty acids $C_{18}H_{30}O_3$ and $C_{27}H_{40}O_3$, while group B (F.6 – F.9) was rich in enniatins that are responsible for its outliers in the loadings plot. This confirms the findings of ^{1}H NMR analysis of the fractions.

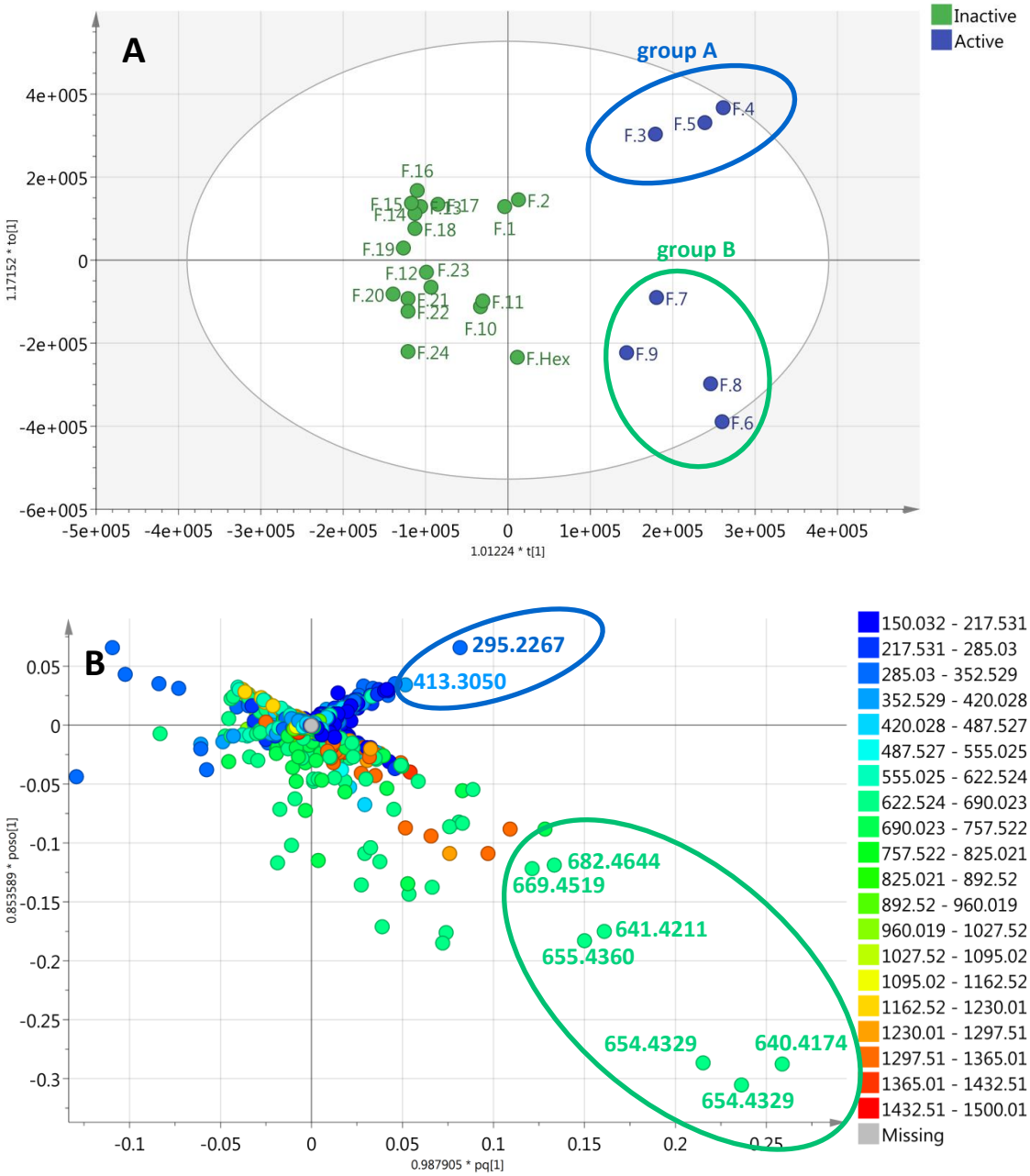

Figure 6.12: (A): Scores plot of *Fusarium acuminatum* (F.n) fractions. Samples were grouped into active (blue) and inactive (green) depending on their activity against breast cancer (ZR-75) cell line. R2X=0.349, R2Y=0.888, Q2=0.565. (B): Loadings plot for *Fusarium acuminatum* (F.n) fractions, acquired from the scores plot 6.12.A. The outliers are labelled by their *m/z* value and listed in table 6.5.

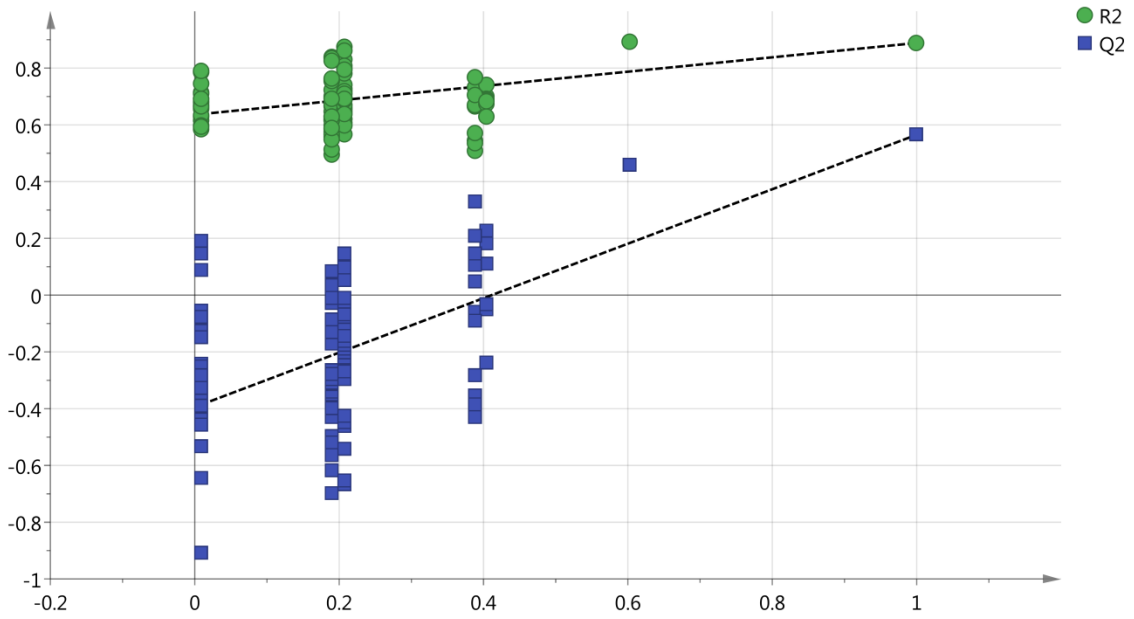

Figure 6.13: Permutation test (100 permutations) for *Fusarium acuminatum* (F.n) fractions for the OPLS-DA model of their activity against breast cancer (ZR-75) cell line.

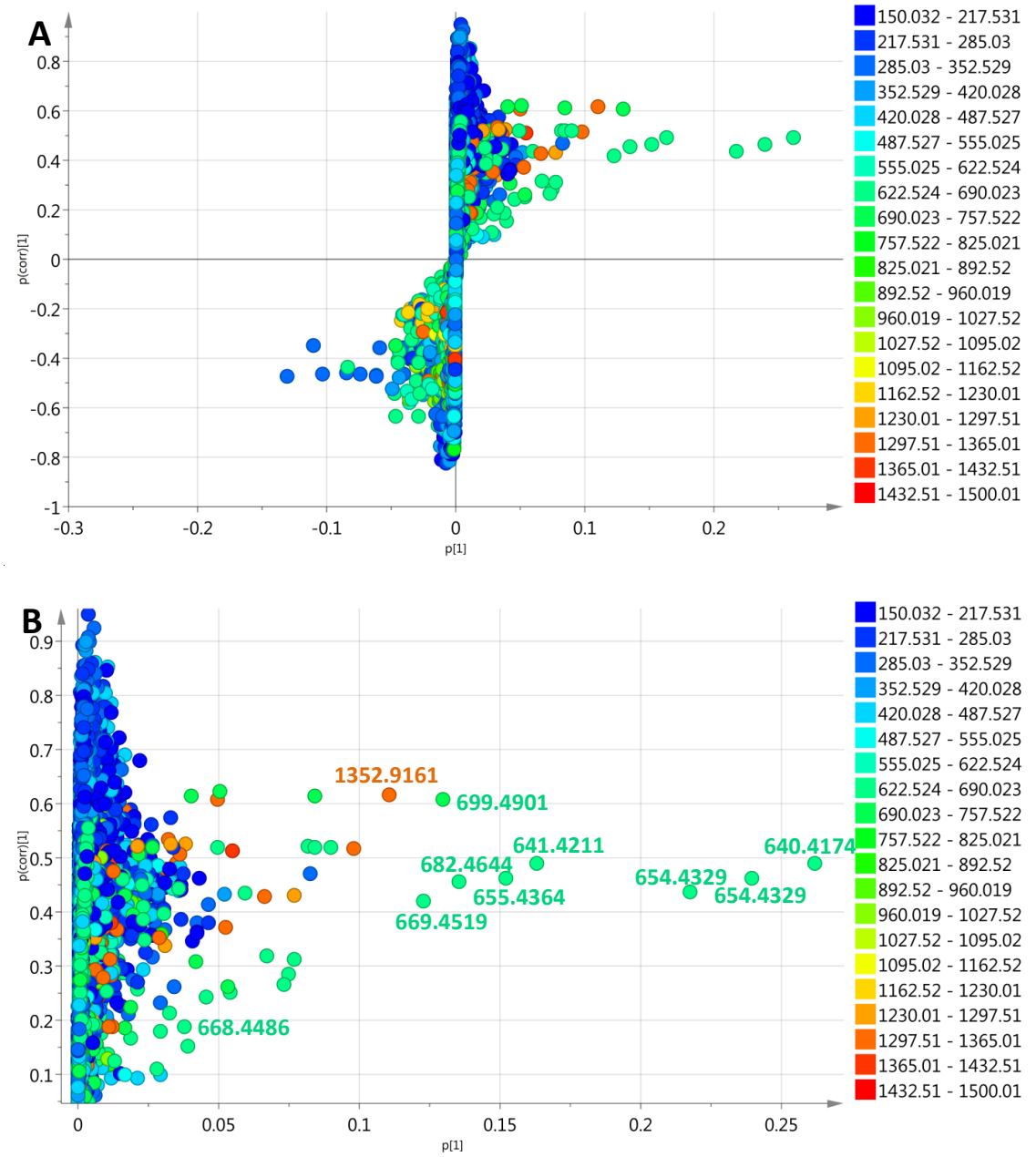

Figure 6.14: (A): S plot for *Fusarium acuminatum* (F.n) fractions acquired from an OPLS-DA model (Figure 4.12) for their activity against breast cancer (ZR-75) cell line. (B): expanded view for the end-points metabolites, the isolated metabolites and the outliers are labelled by their *m/z* value.

Table 6.5: Dereplication of target bioactive metabolites against both ZR-75 and A549 cell lines as predicted by OPLS-DA loadings S-plots. Highlighted rows represent compounds that were isolated from the fungal extracts.

t_R (min)	MZMine ID	m/z	Predicted Molecular formula	Fraction yielding highest peak intensity	Peak intensity	MWt	Name	Source
21.60	P_584	295.2267	$C_{18}H_{30}O_3$	F.4	2.69E+09	294.2194	hygrophorone F12	Isol. from *Hygrophorus persoonii*
							4-Oxo-2,9-octadecadienoic acid; (2*E*,9*E*)-form	Isol. from *Hygrophorus eburneus*
							4-oxo-2,11-octadecadienoic acid; (2*E*,11*Z*)-form	Isol. from *Hygrophorus eburneus*
							4-oxo-2,17-octadecadienoic acid; (*E*)-form	Isol. from *Hygrophorus eburneus*
							9-oxo-10,12-octadecadienoic acid; (10*E*,12*E*)-form	Constit. of the processed leaves of *Artemisia argyi*. Also from *Dimorphotheca sinuata* and the mushroom *Clitocybe clavipes*
							11-oxo-9,12-octadecadienoic acid; (*E,E*)-form	Prod. by *Trichoderma* sp. F5594
							tetrahydro-6-(3-hydroxy-4,7-tridecadienyl)-2H-pyran-2-one	Metab. of *Aspergillus nidulans*

22.71	P_493	626.4016	$C_{34}H_{47}N_{11}O$ $C_{33}H_{51}N_7O_5$ $C_{32}H_{55}N_3O_9$ $C_{34}H_{57}O_{10}$	F.6	6.36E+09	625.3943	unknown	unknown
23.11	P_489	642.4225	No predicted formula	F.8	1.75E+09	641.4153	unknown	unknown
23.29	P_24793	1297.8564	No predicted formula	F.8	1.49E+09	1296.8491	unknown	unknown
23.30	P_24791	641.4211	No predicted formula	F.7	7.91E+09	640.4138	unknown	unknown
23.33	P_487	1296.8529	$C_{67}H_{113}N_{11}O_{14}$ $C_{62}H_{113}N_{13}O_{16}$ $C_{66}H_{117}N_7O_{18}$	F.7	2.00E+09	1295.8457	unknown	unknown
23.49	P_10	640.4174	$C_{33}H_{57}N_3O_9$	F.8	1.95E+10	639.4102	enniatin B	Prod. by *Fusarium* spp. and *Halosarpheia* sp. 732
							verticilide B_1	Prod. by *Verticillium* sp. FKI-2679
24.37	P_21822	656.4388	$C_{50}H_{55}$ $C_{33}H_{49}N_{15}$ $C_{37}H_{53}N_9O_2$ $C_{36}H_{57}N_5O_6$ $C_{25}H_{57}N_{11}O_9$ $C_{35}H_{61}NO_{10}$	F.6	1.85E+09	655.4315	unknown	unknown
24.40	P_486	655.4364	No predicted formula	F.6	8.11E+09	654.4291	unknown	unknown
24.42	P_488	1324.8844	$C_{69}H_{117}N_{11}O_{14}$ $C_{64}H_{117}N_{13}O_{16}$ $C_{68}H_{121}N_7O_{18}$	F.8	2.38E+09	1323.8771	unknown	unknown
24.61	P_15	654.4329	$C_{34}H_{59}N_3O_9$	F.6	2.12E+10	653.4256	enniatin B_1	Prod. by *Fusarium roseum-acuminatum, Fusarium lateritium* and *Alternaria kikuchiana*

							enniatin D	Isol. from *Fusarium acuminatum* and other *Fusarium* spp. Also prod. by *Halosarpheia* sp. 732
							enniatin H	Prod. by *Verticillium hemipterigenum* BCC 1449
							pimaydolide	Metab. of *Pithomyces maydicus*
24.69	P_24794	686.4779	No predicted formula	F.8	2.16E+09	685.4706	unknown	unknown
25.31	P_115	487.3054	$C_{30}H_{38}N_4O_2$ $C_{29}H_{42}O_6$	F.9	6.97E+09	486.2982	unknown	unknown
25.65	P_491	1352.9161	$C_{71}H_{121}N_{11}O_{14}$ $C_{66}H_{121}N_{13}O_{16}$ $C_{70}H_{125}N_7O_{18}$	F.6	2.11E+09	1351.9088	unknown	unknown
25.73	P_24792	670.4551	$C_{51}H_{57}$ $C_{34}H_{51}N_{15}$ $C_{38}H_{55}N_9O_2$ $C_{42}H_{59}N_3O_4$ $C_{27}H_{55}N_{15}O_5$ $C_{37}H_{59}N_5O_6$	F.Hex	4.36E+08	669.4479	unknown	unknown
25.87	P_21820	669.4519	No predicted formula	F.6	8.75E+09	668.4446	unknown	unknown
25.88	P_490	690.4300	$C_{33}H_{55}N_9O_7$ $C_{32}H_{59}N_5O_{11}$ $C_{31}H_{63}NO_{15}$	F.7	2.62E+09	689.4228	unknown	unknown
25.95	P_30	685.4748	$C_{37}H_{56}N_{12}O$ $C_{36}H_{60}N_8O_5$	F.8	2.93E+09	684.4676	unknown	unknown
26.03	P_48	668.4486	$C_{35}H_{61}N_3O_9$	F.6	2.74E+09	667.4413	enniatin I	Prod. by *Verticillium hemipterigenum* BCC 1449

							enniatin A_1	Prod. by *Fusarium roseum-acuminatum, Fusarium avenaceum, Fusarium gibbosum* and *Alternaria kikuchiana*
							enniatin E	Isol. from *Fusarium* spp.
							enniatin G	Prod. by the mangrove fungus *Halosarpheia* sp. 732
							enniatin O_1	Prod. by *Verticillium hemipterigenum* BCC 1449
							enniatin O_2	Prod. by *Verticillium hemipterigenum* BCC 1449
							enniatin O_3	Prod. by *Verticillium hemipterigenum* BCC 1449
26.13	P_21824	700.4932	No predicted formula	F.6	1.50E+09	699.4859	unknown	unknown
26.33	P_28380	699.4901	$C_{38}H_{58}N_{12}O$ $C_{37}H_{62}N_8O_5$ $C_{36}H_{66}N_4O_9$ $C_{35}H_{70}O_{13}$	F.6	3.68E+09	698.4829	unknown	unknown
27.09	P_528	1380.9480	$C_{74}H_{121}N_{15}O_{10}$	F.6	1.13E+09	1379.9407	unknown	unknown
27.15	P_21821	682.4644	$C_{36}H_{63}N_3O_9$	F.6	9.00E+09	681.4571	enniatin A	Prod. by *Fusarium orthoceras, Fusarium sambucinum, Fusarium lateritium, Fusarium oxysporum, Fusarium roseum-acuminatum, Fusarium avenaceum, Fusarium gibbosum* and *Fusarium scirpi*

							enniatin C	Isol. from *Fusarium* spp.
							enniatin F	Isol. from *Fusarium* spp.
							enniatin MK 1688	Prod. by *Fusarium oxysporum* D 388
29.18	P_505	413.3050	$C_{27}H_{40}O_3$	F.5	1.49E+09	412.2977	no hits produced by fungi	-

The same OPLS-DA procedure was done to determine the bioactive metabolites against the lung cancer cell line. This resulted in the generation of a scores plot, in which, the active fractions, F.3 and F.6 – F. 9 were grouped together (Figure 6.15). The model's permutation test (Figure 5.16) afforded an R2 of 0.83 and Q2 of 0.51, while the R2Y intercept was 0.651 and Q2Y intercept was -0.333. This indicates a model with a good fitting and a good predictability, despite having lower Q2 value than what was achieved against breast cancer cell line. Since the Q2 values of the permuted Y models were mostly less than zero with a Q2Y intercept of -0. 333 on the permutation plot test, this was an indication that that the model was valid and not a coincidence. There was no overfitting in the model as the difference between R2Y and Q2 was 0.131.

Repeatedly, an S plot was generated from the previous OPLS-DA and depicted in (Figure 6.17). The pinpointed loadings are the ones to right of the Y axis and are supposed to be with the most prominent activity. The metabolites were dereplicated and listed in Table 6.5.

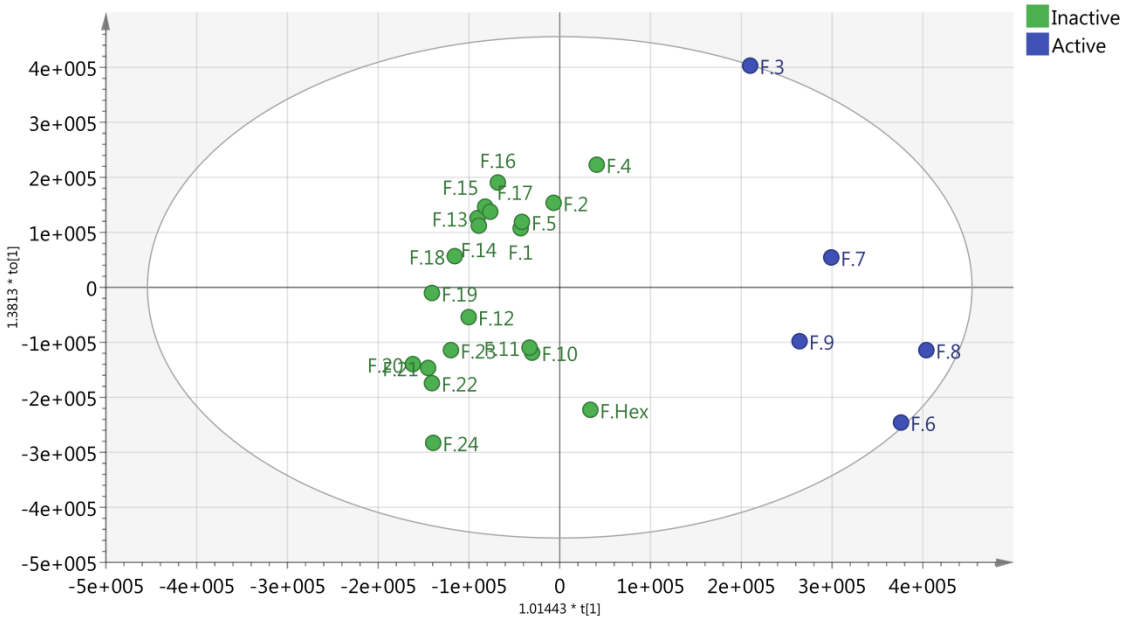

Figure 6.15: Scores plot of *Fusarium acuminatum* (F.n) fractions. Samples were grouped into active (blue) and inactive (green) depending on their activity against lung cancer (A549) cell line. R2X=0.337, R2Y=0.827, Q2=0.509.

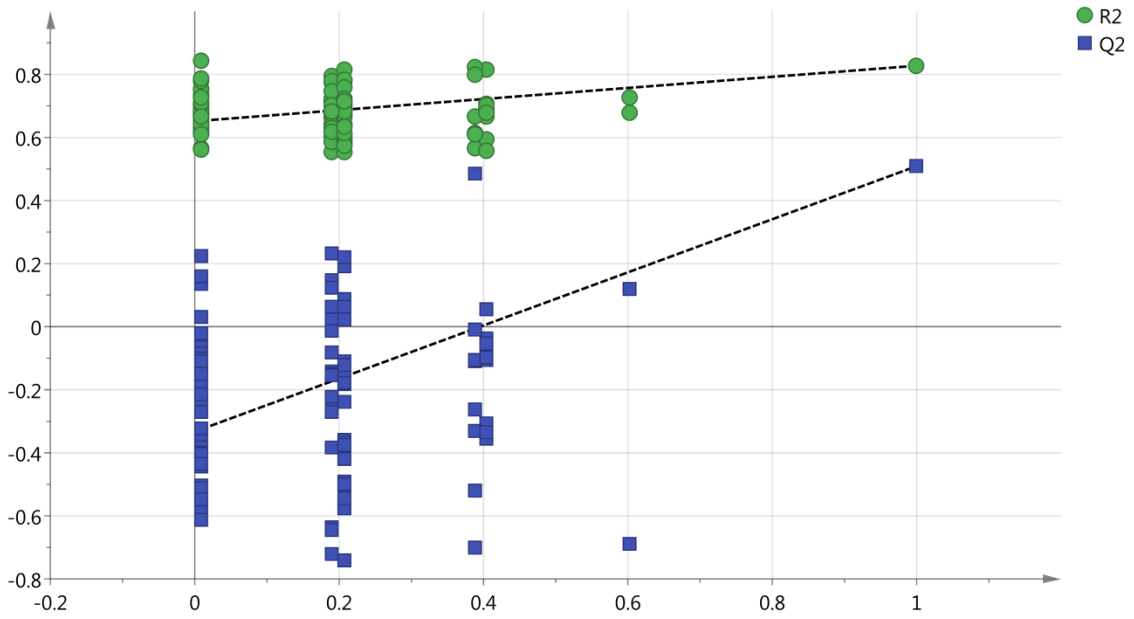

Figure 6.16: Permutation test (100 permutations) for *Fusarium acuminatum* (F.n) fractions for the OPLS-DA model of their activity against A549 cell line.

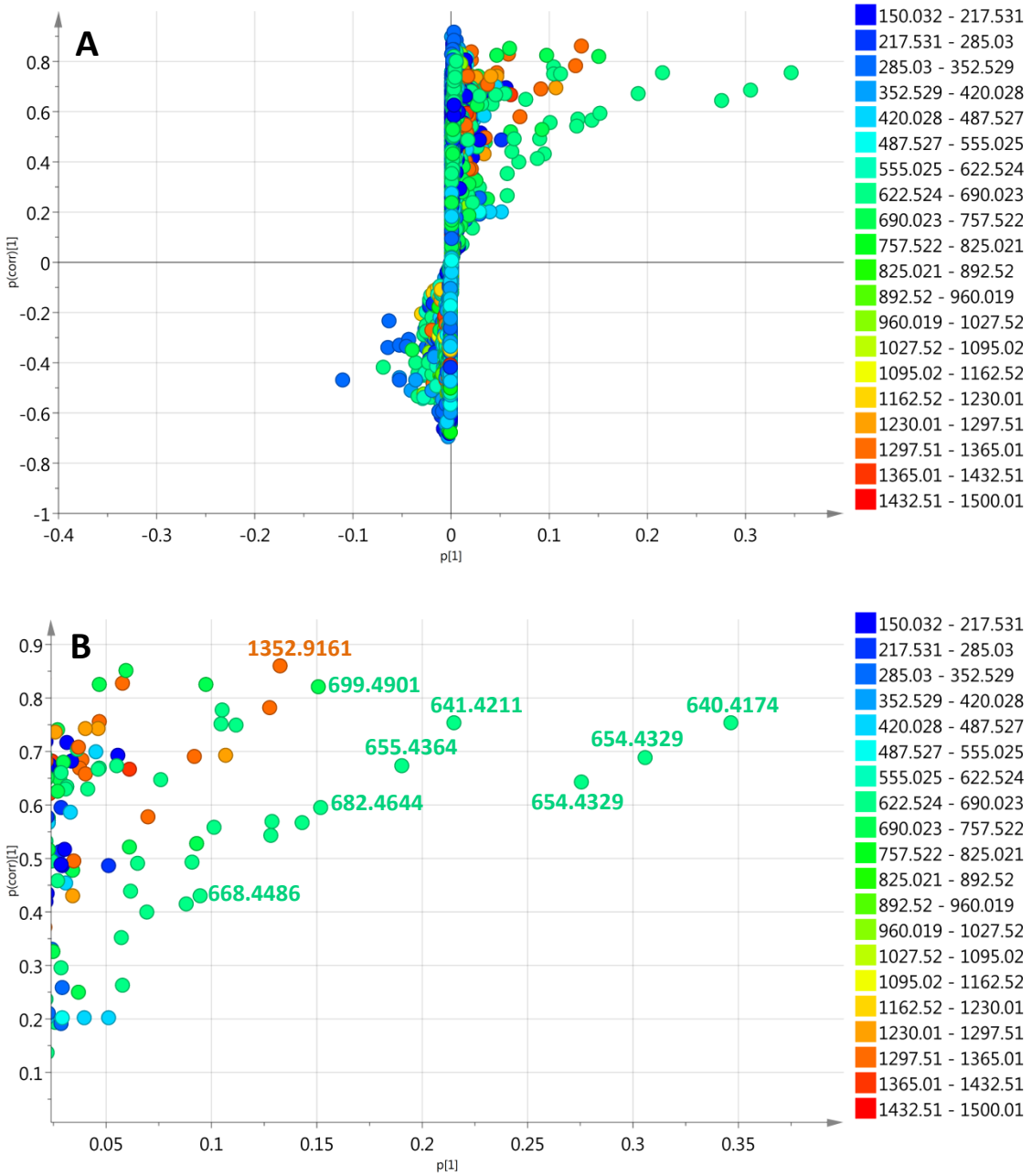

Figure 6.17: (A): S plot for *Fusarium acuminatum* (F.n) fractions acquired from an OPLS-DA model (Figure 4.15) for their activity against the lung cancer (A549) cell line. (B): Expanded view for the end-points metabolites, the isolated metabolites and the outliers are labelled by their *m/z* value.

6.5 Implementing metabolomics for the isolation of the pure secondary metabolites from the endophyte *Fusarium acuminatum*

The fractionation work was designed to isolate the "pinpointed" metabolites that were supposed to be responsible for the activity against both ZR-75 and A549 cell lines. Thus, the fractions that were subjected to further fractionation are the ones that contained the predicted target bioactive metabolites. As a result, three enniatins were isolated and listed in Table 6.6. Moreover, hymeglusin was isolated as a major compound from the first chromatographic separation step.

Table 6.6: The metabolites that were isolated from *Fusarium acuminatum.*

Cpd No.	Name	New / Known	t_R (min)	*m/z*	MWt	Source	Weight (mg)	% Yield
1	hymeglusin	known	11.84	325.2009	324.4119	F.15	1206.8	4.20
2	enniatin A	known	26.71	682.4616	681.9001	F.6	5.8	0.02
3	enniatin A_1	known	26.69	668.4481	667.8735	F.6	27.7	0.10
4	enniatin B	known	23.57	640.4170	639.8204	F.8	17.7	0.06

Both flash chromatography (FC) and semi-preparative HPLC (semiprep HPLC) were used as chromatographic techniques for the isolation of the pure compounds (Figure 6.18). The parameters and conditions that were applied for flash chromatography-1 (FC-1) are mentioned under section 6.2. The conditions used and parameters applied for flash chromatography for fractions 2 and 3 (FC-2 and FC-3) were enumerated in Table 6.7, while conditions for semi-preparative HPLC were listed in Table 6.8. The solvent systems that were used as mobile phases were presented in tables 6.9 – 6.11.

Table 6.7: The chromatographic conditions that were used for flash chromatography in isolating the pure compounds from the extract of *Fusarium acuminatum.*

Column	Reveleris® Silica 48 g
Flow rate	15 mL/min
ELSD Threshold	20 mV
UV Threshold	0.05 AU
UV1 Wavelength	254 nm
UV2 Wavelength	280 nm

Table 6.8: The chromatographic conditions that were used for semi-preparative HPLC in isolating the pure compounds from *Fusarium acuminatum* extract .

Column	VisionHT™ C18
Flow rate	5 mL/min
ELSD Threshold	20 mV
UV Threshold	0.05 AU
UV1 Wavelength	254 nm
UV2 Wavelength	265 nm
UV3 Wavelength	280 nm

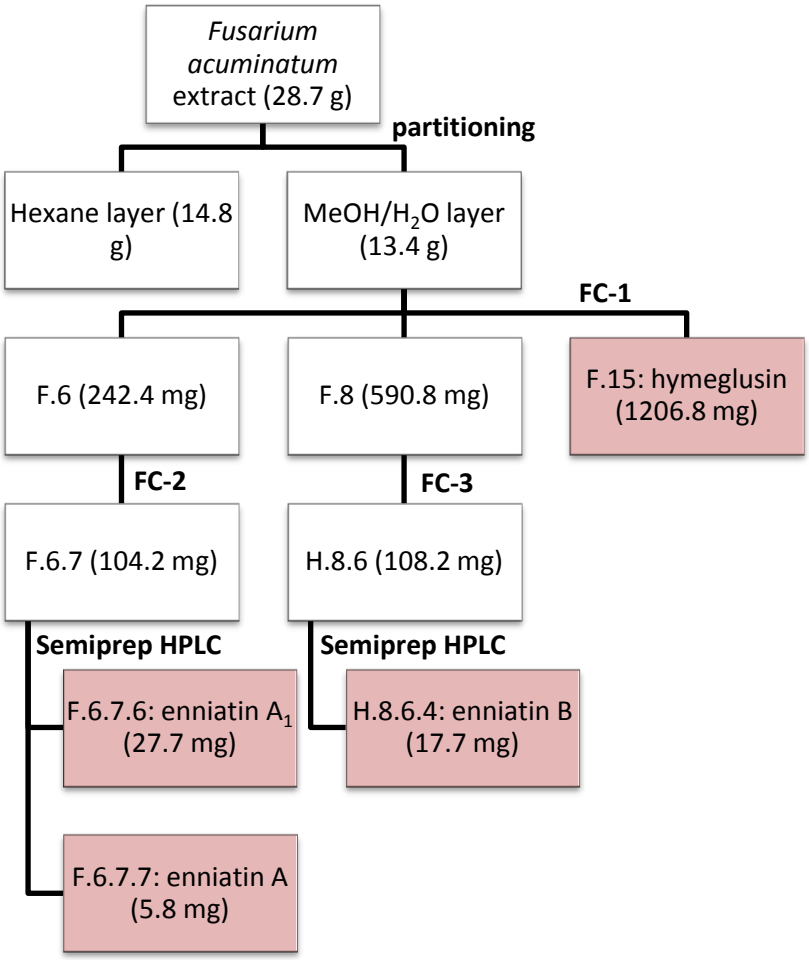

Figure 6.18: The workflow for isolating the pure compounds from *Fusarium acuminatum* extract. FC: Flash chromatography, Semiprep HPLC: Semi-preparative high performance liquid chromatography.

Table 6.9: Mobile phase used for flash chromatography-2 (FC-2).

Time (minutes)	% Hexane	% EtOAc
10	90	10
20	80	20
40	80	20
60	70	30
80	70	30
100	60	40
110	60	40
120	50	50
130	50	50
140	40	60
150	40	60

Table 6.10: Mobile phase used for flash chromatography-3 (FC-3).

Time (minutes)	% Hexane	% DCM	% ACN
10	80	20	0
15	60	40	0
25	60	40	0
30	40	60	0
40	40	60	0
50	20	80	0
60	20	80	0
70	0	100	0
80	0	100	0
90	0	90	10
100	0	90	10

Table 6.11: Mobile phase used for preparative HPLC.

Time (minutes)	% ACN	% Water
0	10	90
30	100	0
35	100	0
36	10	90
45	10	90

6.6 Structure elucidation of the pure secondary metabolites from the endophyte *Fusarium acuminatum*

6.6.1 Hymeglusin (1)

Hymeglusin (Known compound)
Fraction: F.15 Retention time: 11.84 min Synonym(s): • (2*E*,4*E*,7R)-11-[(2*R*,3*R*)-3-(Hydroxymethyl)-4-oxo-2-oxetanyl]-3,5,7-trimethyl-2,4-undecadienoic acid • 2,4-Undecadienoic acid, 11-[3-(hydroxymethyl)-4-oxo-2-oxetanyl]-3,5,7-trimethyl-, [2*R*-[2α(2*E*,4*E*,7*R**),3β]]- (8CI) Source: *Fusarium acuminatum,* isolated from *Anthemis palestina* Amount of sample: 1206.8 mg Percent yield: 4.20% Percent purity: 74.6% Physical description: brown prisms Molecular formula: $C_{18}H_{28}O_5$ Molecular weight: 324.4119 g/mol Optical rotation: $[\alpha]_D^{20}$ = +3 (0.1 g/100 mL, $CHCl_3$)
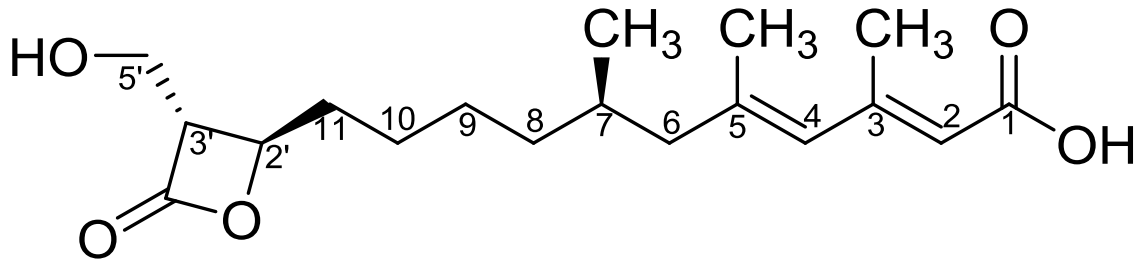

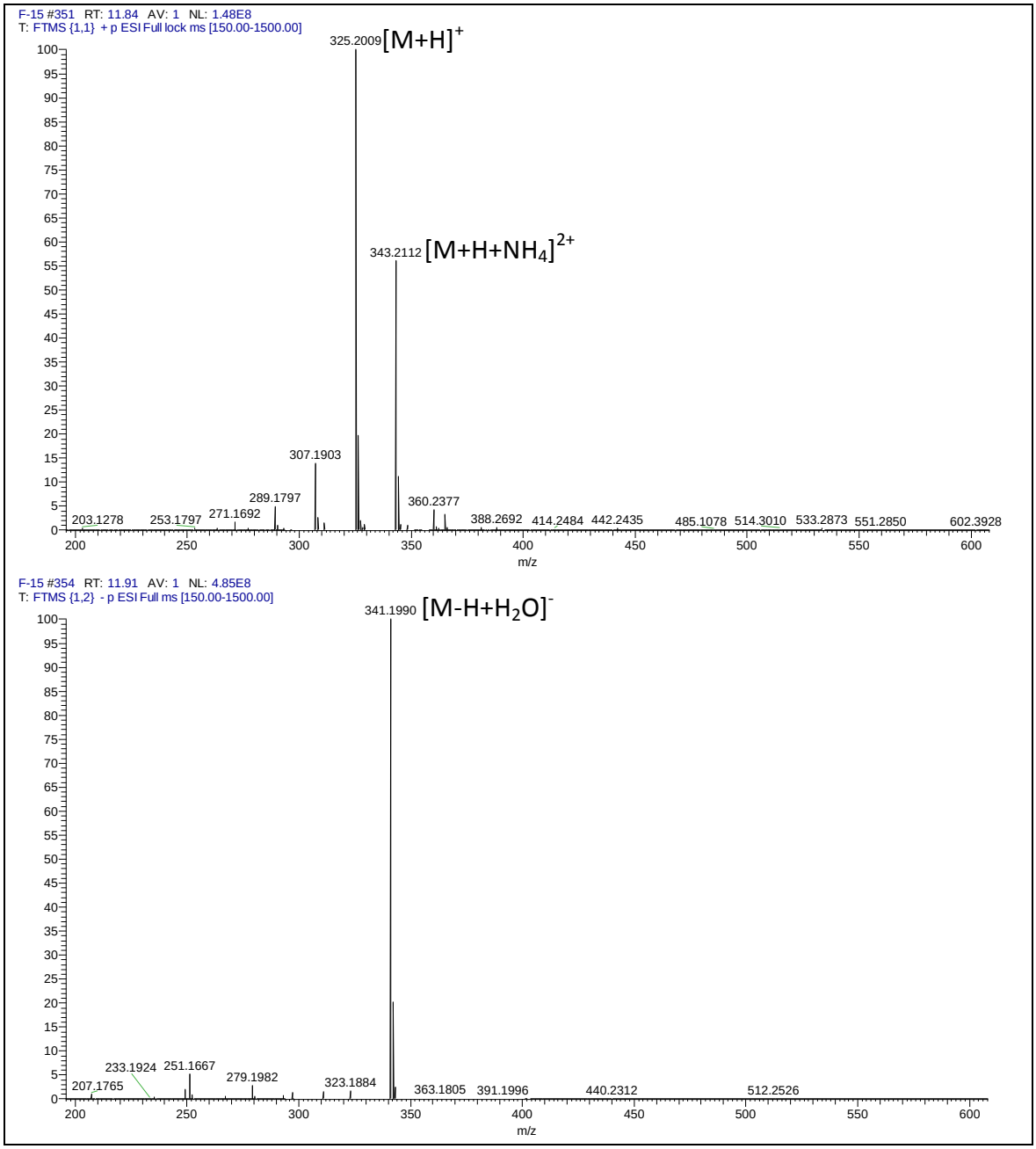

Hymeglusin was isolated in the form of brown crystals with a yield of 1206.8 mg (4.20%). The LC-HRMS data afforded pseudomolecular ion peaks at *m/z* 325.2009 $[M+H]^+$ and 341.1990 $[M-H+H_2O]^-$, resulting that this compound has a molecular weight of 324.4119 g/mol. The molecular formula suggested by HRMS was $C_{18}H_{28}O_5$.

The ^{1}H NMR spectrum (Figure 6.19) showed two singlets at δ_H 5.74 and δ_H 5.57, indicating the presence of the two olefinic protons H-4 and H-2, respectively. The protons that are attached to oxygenated carbons, C*H*$_2$-5' and H-2' were deshielded and could be detected at δ_H 3.52 and δ_H 3.59. Moreover, the proton H-3' resonated as a multiplet at δ_H 2.41. The two methyls 3-*Me* and 5-*Me* exhibited two singlets at δ_H 2.17 and δ_H 1.77, respectively. This was referred to their attachment to olefinic carbons that caused their resonances to be more downfield than 7-*Me,* which was detected as a doublet at δ_H 0.80. Its splitting was a result of its coupling with H-7 (δ_H 1.66) as detected via ^{1}H-^{1}H COSY experiment (Figure A.XIII.2). The aliphatic methylene protons H-8 to H-11 were detected at δ_H 1.02 – 1.47. Nevertheless, the other aliphatic protons, i.e. C*H*$_2$-6 exhibited signals more downfield at δ_H 2.08 (H-6$_b$) and δ_H 1.77 (H-6$_a$). This was a result of the connectivity of methylene C-6 to olefinic C-5.

The JMod NMR spectrum afforded a signal at δ_C 174.8 that corresponded for the β-lactone's carbonyl moiety. Morover, the carboxylate's carbon (C-1) was detected at δ_C 168.1 (Figure 6.20). Furthemore, all oleficnic carbons (C-2 – C-5) resonated downfield at δ_C 118.5 – 153.2. In addition to that, the oxygenated carbons (C-2' and C-5') exhibited their signals at δ_C 69.3 and 60.1, respectively. C-3' is connected to a carbonyl, and thus, it resonated at δ_C 55.4. Moreover, C-6 is connected to a methylene. So, its signal was detected at δ_C 48.9. All other aliphatic carbons were found upfield to δ_C 40.0. All proton – carbon assignments were afforded by an ^{1}H-^{13}C HSQC experiment (Figure A.XIII.4).

The connectivity of this compound was established by implementing an ^{1}H-^{13}C HMBC experiment (Figure A.XIII.5). ^{3}J correlations were found from the methyls to the corresponding carbons, and thus, from 3-*Me* to both C-2 and C-4, from 5-*Me* to both C-4 and C-6 and from 7-*Me* to both C-6 and C-8. Moreover, ^{2}J correlations could be detected from those methyls to where they are attached. As a result, ^{2}J correlations were exhibited from 3-*Me* to C-3, from 5-*Me* to C-5 and from 7-*Me* to C-7. Other ^{3}J correlations were noticed from H-2 to 3-Me, from H-4 to 5-Me and from H-6 to both 5-Me and 7-Me. In the β-lactone ring, ^{2}J correlations were detected from H-3' to C-2', C-5' and the carbonyl carbon.

The structure was confirmed as hymeglusin by comparing both its ^{1}H and ^{13}C NMR data to the literature (Bates *et al*., 1999) (Table 6.12). Hymeglusin is a β-lactone that was first isolated in

1971 from *Cephalosporium* sp. (Aldridge *et al*., 1971). It acts as an antibiotic and an inhibitor of both hydroxymethylglutaryl-CoA (HMG-CoA) synthatase and pancreatic lipase (Aldridge *et al*., 1971, Tomoda *et al*., 1999). Hymeglusin was not targeted by metabolomics as it possessed no activity against either breast nor lung cancer cell lines according to the created OPLS-DA models. However, it was isolated as a major product in the first chromatographic separation. This compound could be synthesised by *Fusarium acuminatum* as a chemical defence mechanism against bacteria. Hymeglusin was isolated from *Fusarium* sp. and *Fusarium* sp. ATCC 20788 previously (Omura *et al*., 1987, Saepudin and Harrison, 1995).

The optical rotation value for the obtained hymeglusin was +3, $[\alpha]_D^{20}$ = +3 (0.1 g/100 mL, $CHCl_3$), while it was found to be +29.0 in literature $[\alpha]_D^{20}$ = +29.0 (0.21 g/100 mL, $CHCl_3$) (Bates *et al*., 1999). Thus, the obtained hymeglusin was not considered enantiopure.

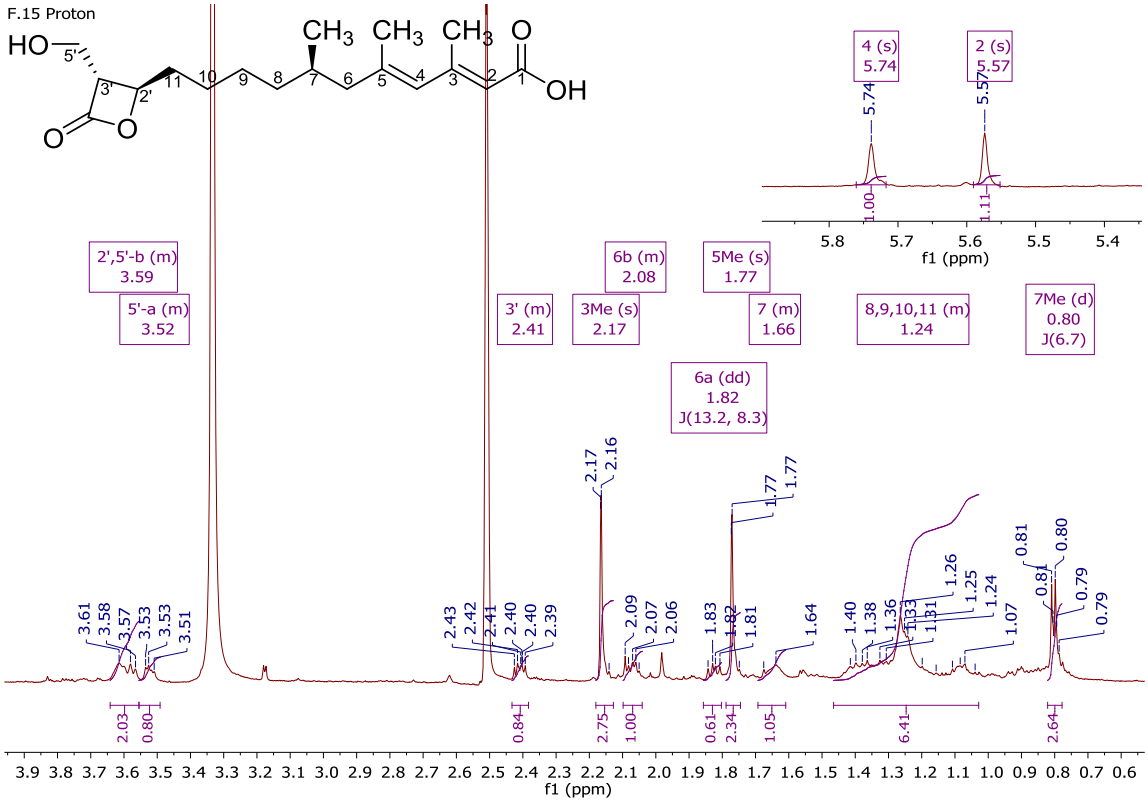

Figure 6.19: ^{1}H NMR (600 MHz) spectrum for hymeglusin, measured in DMSO-d_6.

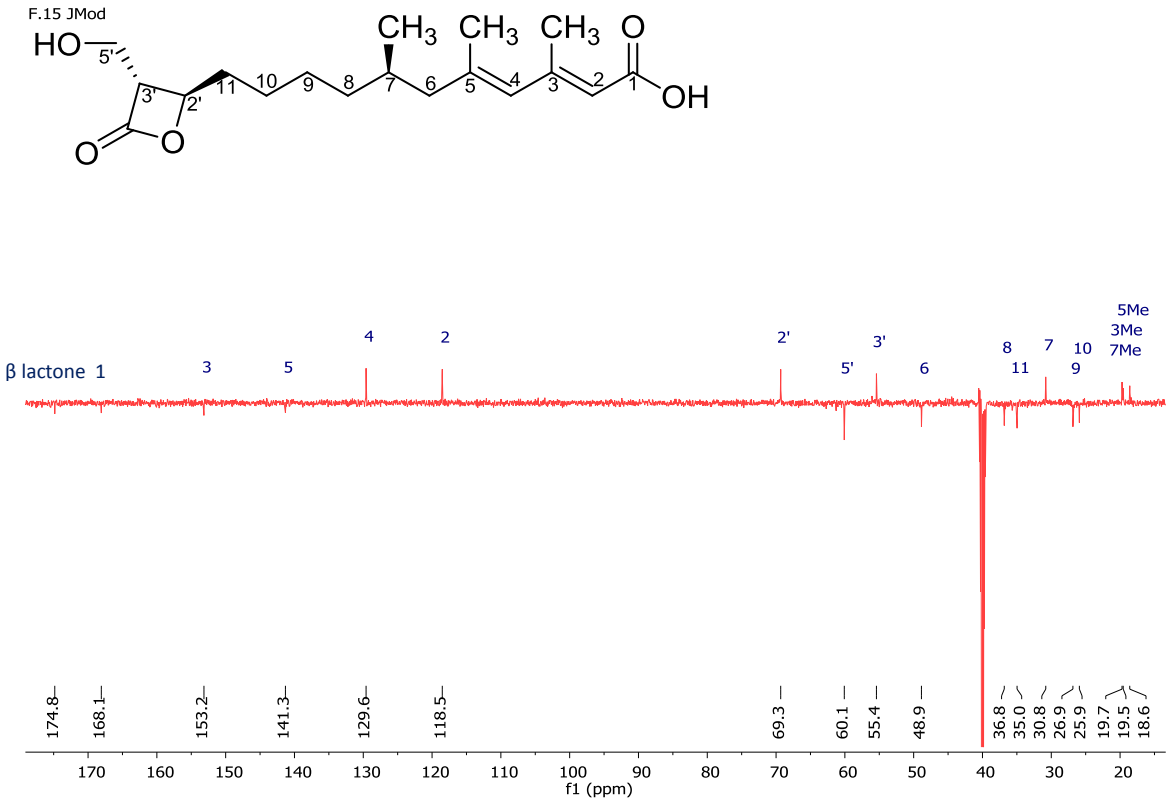

Figure 6.20: JMod NMR (150 MHz) spectrum for hymeglusin, measured in DMSO-d_6.

Table 6.12: ^{1}H and ^{13}C NMR data for hymeglusin compared to literature.

	Hymeglusin in DMSO-d_6						**Hymeglusin (Bates *et al.*, 1999) in $CDCl_3$**				
	^{1}H NMR data, (600 MHz)				^{13}C NMR data, (150 MHz)		^{1}H NMR data, (600 MHz)				^{13}C NMR data, (100 MHz)
Atom no.	δ_H (ppm)	Integration	Multiplicity	*J* (Hz)	δ_C (ppm)	Multiplicity	δ_H (ppm)	Integration	Multiplicity	*J* (Hz)	δ_C (ppm)
1					168.1	C					169.7
2	5.57	1H	s		118.5	CH	5.69	1H	s		116.6
3					153.2	C					157.0
4	5.74	1H	s		129.6	CH	5.73	1H	s		129.5
5					141.3	C					142.0
6	2.08, 1.82	1H, 1H	m, dd	13.2, 8.3	48.9	CH_2	2.06, 1.86	1H, 1H	dd, dd	13.3, 8.3, 13.3, 8.3	49.0
7	1.66	1H	m		30.8	CH	1.66	1H	dq	13.2, 6.7	30.9
8	1.02 – 1.47	2H	m		36.0	CH_2	1.30 – 1.46, 1.10 – 1.16	1H, 1H	m		36.6
9	1.02 – 1.47	2H	m		26.9	CH_2	1.30 – 1.46	2H	m		26.6
10	1.02 – 1.47	2H	m		25.9	CH_2	1.30 – 1.46	2H	m		25.2
11	1.02 – 1.47	2H	m		35.0	CH_2	1.89 – 1.81, 1.75 – 1.81	1H, 1H	m		34.0
3-Me	2.17	3H	s		19.6	CH_3	2.25	3H	s		19.9
5-Me	1.77	3H	s		18.6	CH_3	1.75 – 1.81	3H	m		18.5
7-Me	0.80	3H	d	6.7	19.7	CH_3	0.84	3H	d	6.6	19.4
2'	3.59	1H	m		69.3	CH	0.84	1H	ddd	7.3, 6.0, 4.2	74.9
3'	2.41	1H	m		55.4	CH	3.41	1H	q	4.4	58.6
5'	3.59, 3.52	1H, 1H	m, m		60.1	CH_2	4.05, 3.89	1H, 1H	dd, dd	11.6, 5.0, 11.6, 4.1	58.1
β-lactone					174.8	C					171.5

6.6.2 Enniatin A (2)

Enniatin A (Known compound)
Fraction: F.6.7.7 Retention time: 26.71 min Synonym(s): • Cyclo[(2*R*)-2-hydroxy-3-methylbutanoyl-*N*-methyl-L-isoleucyl-(2*R*)-2-hydroxy-3-methylbutanoyl-*N*-methyl-L-isoleucyl-(2*R*)-2-hydroxy-3-methylbutanoyl-*N*-methyl-L-isoleucyl] • Isoleucine, *N*-(D-2-hydroxy-3-methylbutyryl)-*N*-methyl-, trimol. cyclic ester (7CI) • 1,7,13-Trioxa-4,10,16-triazacyclooctadecane, cyclic peptide derivative • Cyclo(D-α-hydroxyisovaleryl-*N*-methyl-L-isoleucyl-D-α-hydroxyisovaleryl-*N*-methyl-L-isoleucyl-D-α-hydroxyisovaleryl-*N*-methyl-L-isoleucyl) Source: *Fusarium acuminatum* isolated from *Anthemis palestina* Amount of sample: 5.8 mg Percent yield: 0.02% Percent purity: 98.0% Physical description: Colourless crystals Molecular formula: $C_{36}H_{63}N_3O_9$ Molecular weight: 681.9001 g/mol Optical rotation: $[\alpha]_D^{20}$ = -57 (0.1 g/100 mL, $CHCl_3$)
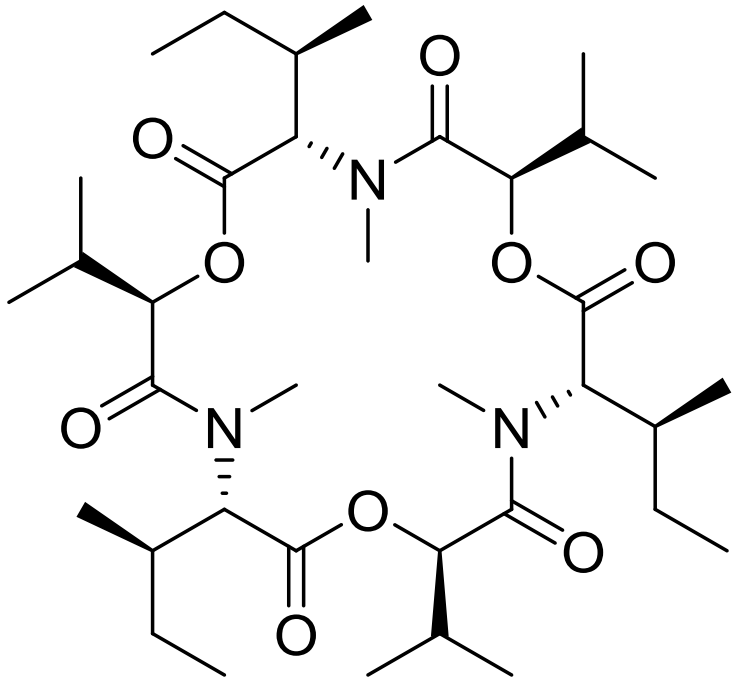

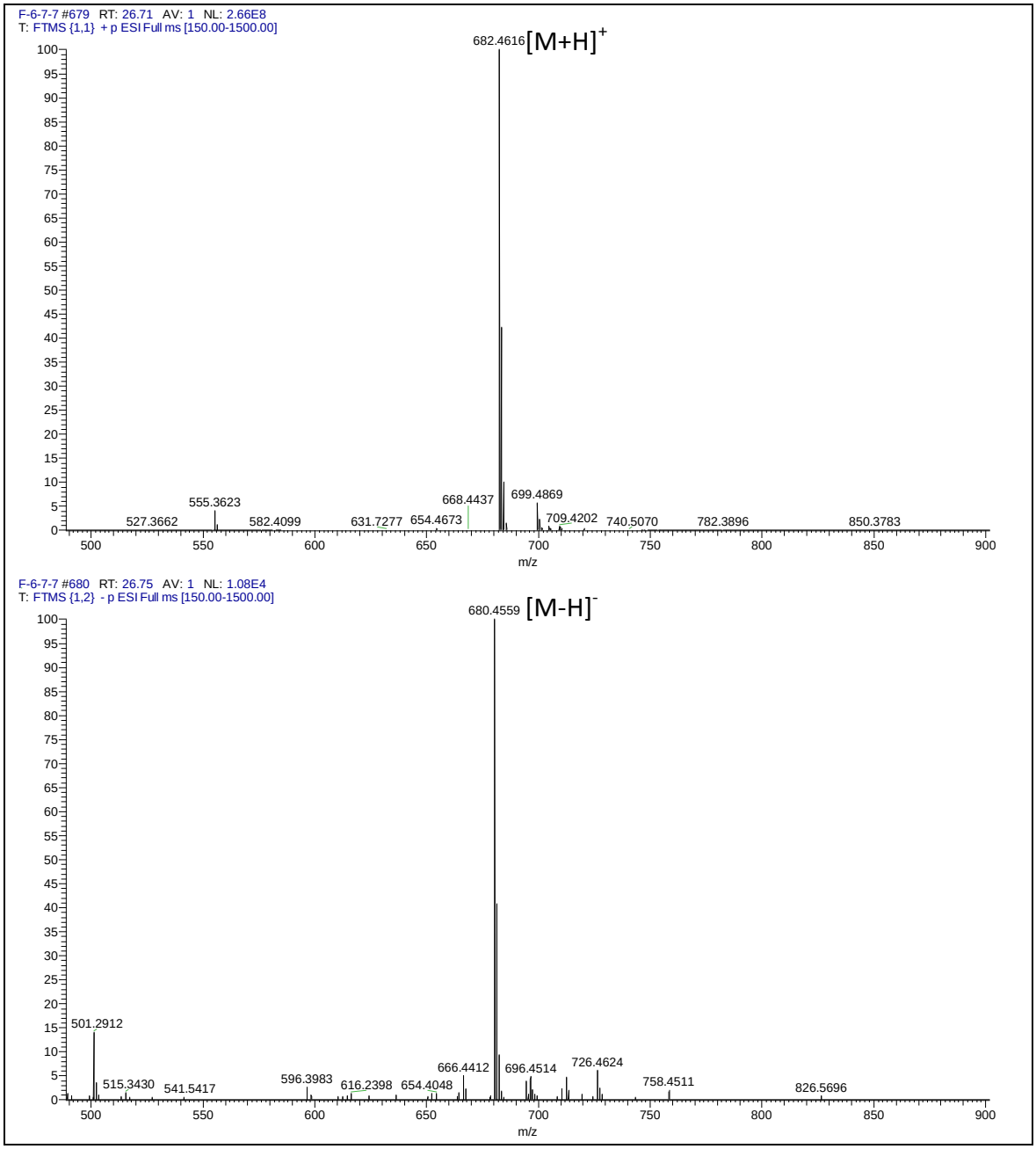

Enniatin A was isolated as colourless crystals with a yield of 5.8 mg (0.02%). The LC-HRMS data gave pseudomolecular ion peaks at *m/z* 682.4616 $[M+H]^+$ and 680.4559 $[M-H]^-$, suggesting that this compound has a molecular weight of 681.9001 g/mol. The molecular formula predicted by HRMS was $C_{36}H_{63}N_3O_9$.

Enniatin A is composed of three *N*-methylisoleucine (NMeIle) and three D-2-hydroxyisovaleric acid (HyIv) moeities. However, as these three moeties are chemically and magnetically equivalent, they were detected in NMR spectra as one set of signals and their integration was confirmed by the molecular weight and formula that were obtained by HRMS.

The α proton of HyIv (HyIv-α, δ_H 5.20, d, *J*=7.7 Hz) was detected more downfield than that of NMeIle (NMeIle-α, δ_H 4.81, d, *J*=9.6 Hz) in the ^{1}H NMR spectrum (Figure 6.21). This allowed the attachment of both an oxygen and a carbonyl to HyIv-α position. This caused it to be more deshielded than NMeIle-α where a less electronegative nitrogen and a carbonyl were attached. The doublet splitting pattern of the previous α protons was caused by the effect of β protons that resonated upfield at δ_H 2.14 (HyIv-β, m) and δ_H 2.02 (NMeIle-β, m) and coupled to HyIv-α and NMeIle-α respectively as depected in the ^{1}H-^{1}H COSY spectrum (Figure A.XIV.2). Furthermore, CH_2-γ_1 protons of NMeIle were deteted more upfield (δ_H 1.39 and δ_H 1.10) as multiplets coupled through ^{1}H-^{1}H COSY to the multiplet NMeIle-β and the triplet NMeIle-δ that resonated at δ_H 0.84 (*J*=7.3 Hz). In addition to that, the protons of CH_3-γ_2 of NMeIle exhibited a doublet at δ_H 1.10 (*J*=5.7 Hz) corresponding to its ^{1}H-^{1}H COSY correlation to NMeIle-β. On the other hand, the protons CH_3-γ of HyIv were detected as two doublets at δ_H 0.96 (*J*=5.7 Hz) and δ_H 0.92 (*J*=6.6 Hz), both correlated through ^{1}H-^{1}H COSY to HyIv-β. Moreover, the protons of the N-CH_3 were detected as a singlet at δ_H 3.10.

The amidic carbonyl could be detected at δ_C 169.3 in the JMod NMR spectrum (Figure 6.22), just a little bit upfield to the esteric carbonyl that was detected at δ_C 170.6 ppm. As the C-α of the HyIv moeity is oxygenated, its δ_C was found downfield to the nitrogenated C-α of NMeIle that was detected at δ_C 59.6. All other aliphatic carbons were detected upfield to δ_C 50.0 and all proton – carbon assignments were provided by running an ^{1}H-^{13}C HSQC NMR experiment (Figure A.XIV.4).

The connectivity of the structure was established by utilising an ^{1}H-^{13}C HMBC experiment (Figure A.XIV.5). For the NMeIle moeity, ^3J correlations could be found going from CH_3-δ to C-β, from H-γ_1 to C-γ_2, from CH_3-γ_2 to both C-γ_1 and C-α, from H-α to both the *N*-methyl and the amidic carbonyl and from the protons of the *N*-methyl to both the amidic carbonyl and the adjacent C-α positions. Moreover, in the HyIv moeity, ^3J correlations were detected through its

correlation from CH_3-γ to C-α and H-α to both C-γ and the esteric carbonyl. Furthermore, many ^2J correlations could be found as illustrated in figure A.XIV.5.

The structure was confirmed by comparing both its ^{1}H and ^{13}C NMR data to the literature and was identified as Enniatin A (Blais *et al.*, 1992) (Tables 6.13 and 6.14).

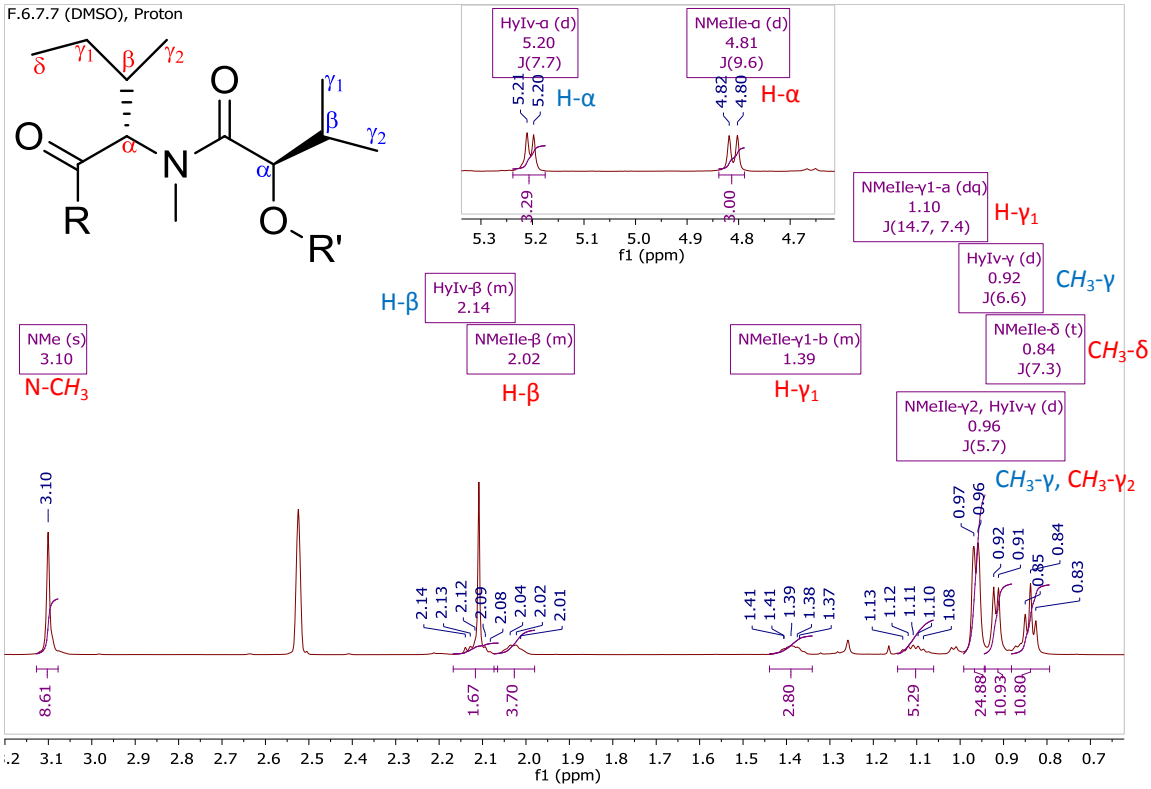

Figure 6.21: ^{1}H NMR (600 MHz) spectrum for enniatin A, measured in DMSO-d_6. Red-labelled signals belong to the NMeIle moiety while blue-labelled signals belong to the HyIv moiety.

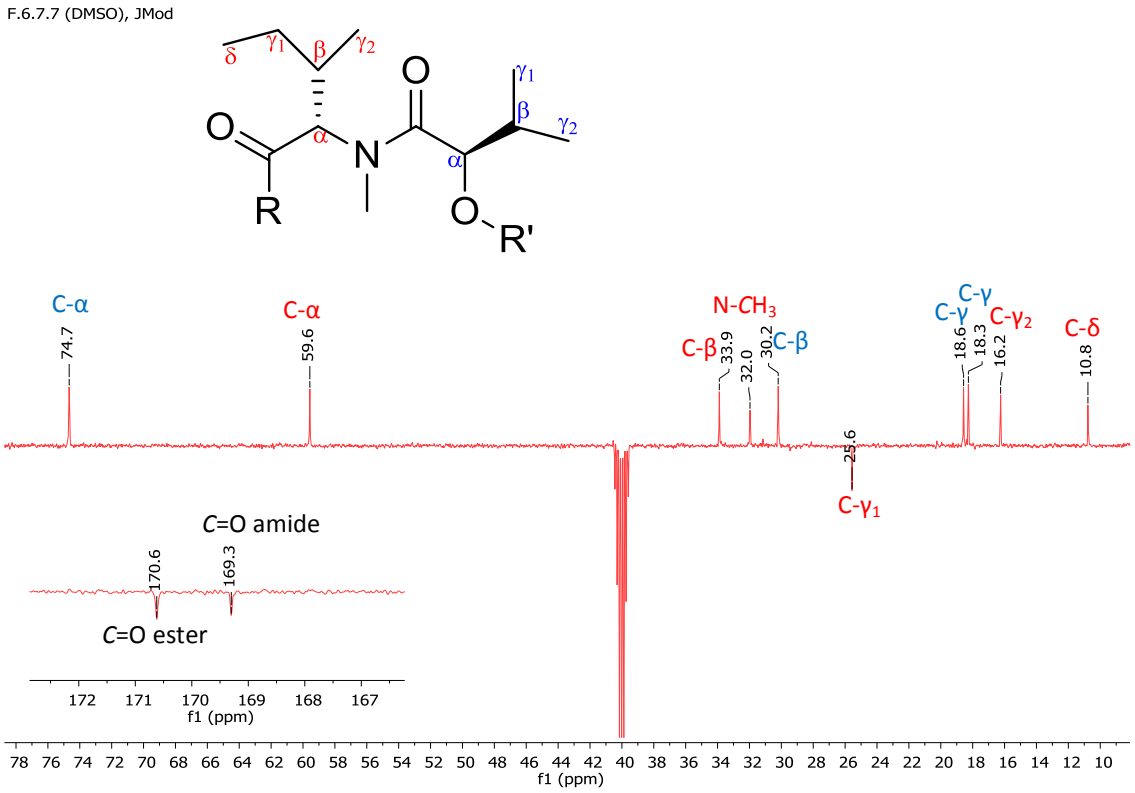

Figure 6.22: JMod NMR (150 Hz) spectrum for enniatin A, measured in DMSO-d_6. Red-labelled signals belong to the NMeIle moiety while blue-labelled signals belong to the HyIv moiety.

Table 6.13: ^{1}H NMR data for enniatins compared to the literature.

Compound		enniatin A		enniatin A_1		enniatin B	
Fraction		F.6.7.7	(Blais *et al.*, 1992)	F.6.7.6	(Blais *et al.*, 1992)	F.8.15	(Visconti *et al.*, 1992)
Solvent		DMSO-d_6	$CHCl_3$-*d*	DMSO-d_6	$CHCl_3$-*d*	DMSO-d_6	$CHCl_3$-*d*
Spectrometer frequency (MHz)		600	500	600	500	600	500
Moiety	**Proton**	**δ_H (ppm) (multiplicity, *J* (Hz))**					
NMeIle	α (C*H*)	4.81 (d, 9.6)	4.65 ($J_{\alpha,\beta}$=9.2)	4.81 (d, 9.4)	4.62 ($J_{\alpha,\beta}$=9.2), 4.66 ($J_{\alpha,\beta}$=9.2)		
	β (C*H*)	2.03 (m)	2.04 ($J_{\beta,\alpha}$=9.2; $J_{\beta,\gamma}$=3.2)	2.02 (m)	2.01		
	γ_1(CH_2)	1.11 (dq, 14.4, 7.4)	1.04 (J_{AB}=13.2; $J_{\gamma1,\delta}$=7.5)	1.11 (m)	1.04		
	γ_1(CH_2)	1.39 (m)	1.42 ($J_{\gamma1,\delta}$=7.4; $J_{\gamma1,\beta}$=3.2)	1.39 (m)	1.42 ($J_{\gamma1,\delta}$=7.2)		
	γ_2(CH_3)	0.96 (o)	1.00 ($J_{\gamma2,\beta}$=8.3)	0.96 (o)	0.98		
	δ (CH_3)	0.84 (d, 7.3)	0.84 ($J_{\delta,\gamma1}$=7.4)	0.83 (d, 7.4)	0.83 ($J_{\delta,\gamma1}$=7.5)		
	N-CH_3	3.10 (s)	3.09	3.10	3.08		
NMeVal	α (C*H*)			4.66 (d, 9.7)	4.42 ($J_{\alpha,\beta}$=10.3)	4.65 (d, 10.0)	4.42
	β (C*H*)			2.20 (m)	2.28	2.18 (m)	2.27
	γ (CH_3)			1.02 (d, 6.6)	1.03 ($J_{\gamma,\beta}$=6.2)	1.00 (d, 6.7)	1.03
	γ (CH_3)			0.87 (d, 6.6)	0.87	0.84 (d, 6.7)	0.86
	N-CH_3			3.10	3.10	3.08	3.09
HyIv	α (C*H*)	5.20 (d, 7.7)	5.10 ($J_{\alpha,\beta}$=7.8)	5.21 (d, 7.47)	5.10 ($J_{\alpha,\beta}$=8.8, 9.1, 7.0)	5.20 (d, 7.8)	5.11
	β (C*H*)	2.14 (o)	2.25 ($J_{\beta,\gamma}$=6.8)	2.11 (m)	2.26	2.11 (m)	2.27
	γ (CH_3)	0.92 (d, 6.6)	0.92 ($J_{\gamma,\beta}$=6.8)	0.92	0.92 – 0.99	0.90 (d, 6.7)	0.93
	γ (CH_3)	0.96 (o)	0.98 ($J_{\gamma,\beta}$=7.2)	0.96 (o)		0.94 (d, 6.7)	0.96

Table 6.14: ^{13}C NMR data for enniatins compared to the literature.

Compound		enniatin A		enniatin A_1		enniatin B	
Fraction		F.6.7.7	(Blais *et al.*, 1992)	F.6.7.6	(Blais *et al.*, 1992)	F.8.15	(Visconti *et al.*, 1992)
Solvent		DMSO-d_6	$CHCl_3$-*d*	DMSO-d_6	$CHCl_3$-*d*	DMSO-d_6	$CHCl_3$-*d*
Spectrometer frequency (MHz)		150	62.5	150	62.5	150	62.5
Moiety	**Carbon**	**δ_C (ppm)**					
NMelle	α (CH)	59.6	61.8	59.6	61.4, 61.4		
	β (CH)	33.9	34	33.8, 33.9	33.9, 34.0		
	γ_1(CH_2)	22.6	25.4	25.4, 22.5	25.5		
	γ_2(CH_3)	16.3	16.2	16.2	16.2		
	δ (CH_3)	10.8	10.9	10.8	10.9		
	N-CH_3	32.0	33.0	31.9	32.7, 32.8		
	C=O (ester)	170.6	170.4	170.6	170.5		
	C=O (amide)	169.3	169.3	169.3	169.5		
NMeVal	α (CH)			61.5	63.4	61.4	63.2
	β (CH)			28.1	28.1	28.0	27.9
	γ (CH_3)			19.9, 20.2	19.5, 20.5	19.8, 20.2	19.3, 20.4
	N-CH_3			32.1	33.4	32.1	33.2
	C=O (ester)			170.5	170.4	170.4	170.3
	C=O (amide)			169.3	169.5	169.2	169.3
Hylv	α (CH)	74.7	75.6	74.6, 74.7	75.4, 75.2, 76.0	74.7	75.7
	β (CH)	30.2	29.8	30.2	29.8	30.1	29.9
	γ (CH_3)	18.3, 18.6	18.3, 18.4	18.3, 18.4, 18.5, 18.6	18.4 – 18.7	18.4, 18.6	18.5, 18.6

6.6.3 Enniatin A_1 (3)

Enniatin A_1 (Known compound)
Fraction: F.6.7.6 Retention time: 26.69 min Synonym(s): • 1,7,13-Trioxa-4,10,16-triazacyclooctadecane-2,5,8,11,14,17-hexone, 3,9-di-*sec*-butyl-6,12,15,18-tetraisopropyl-4,10,16-trimethyl- (7CI) • 1,7,13-Trioxa-4,10,16-triazacyclooctadecane, enniatin A derivative • Cyclo(D-α-hydroxyisovaleryl-*N*-methyl-L-isoleucyl-D-α-hydroxyisovaleryl-*N*-methyl-L-isoleucyl-D-α-hydroxyisovaleryl-*N*-methyl-L-valyl) Source: *Fusarium acuminatum,* isolated from *Anthemis palestina* Amount of sample: 27.7 mg Percent yield: 0.10% Percent purity: 89.1% Physical description: Colourless crystals Molecular formula: $C_{35}H_{61}N_3O_9$ Molecular weight: 667.8735 g/mol Optical rotation: $[\alpha]_D^{20}$ = -61 (0.1 g/100 mL, $CHCl_3$)
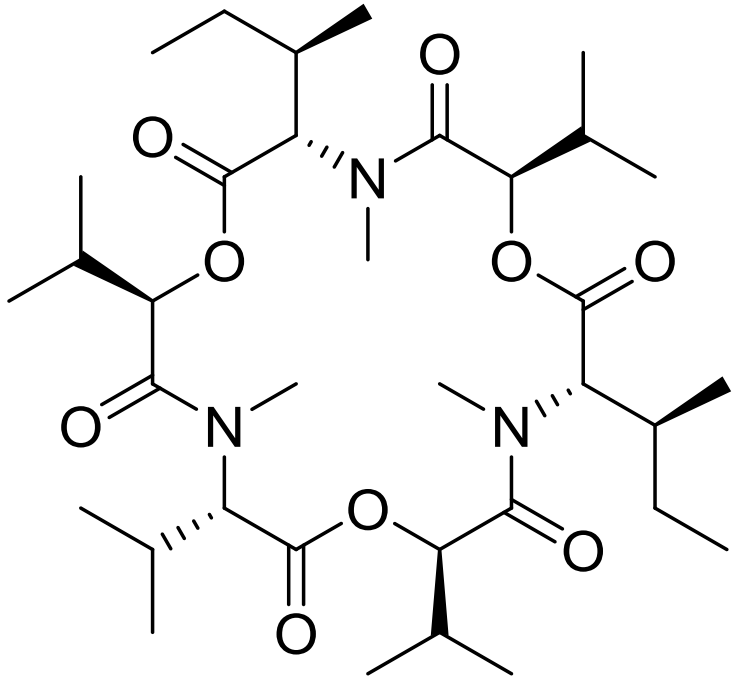

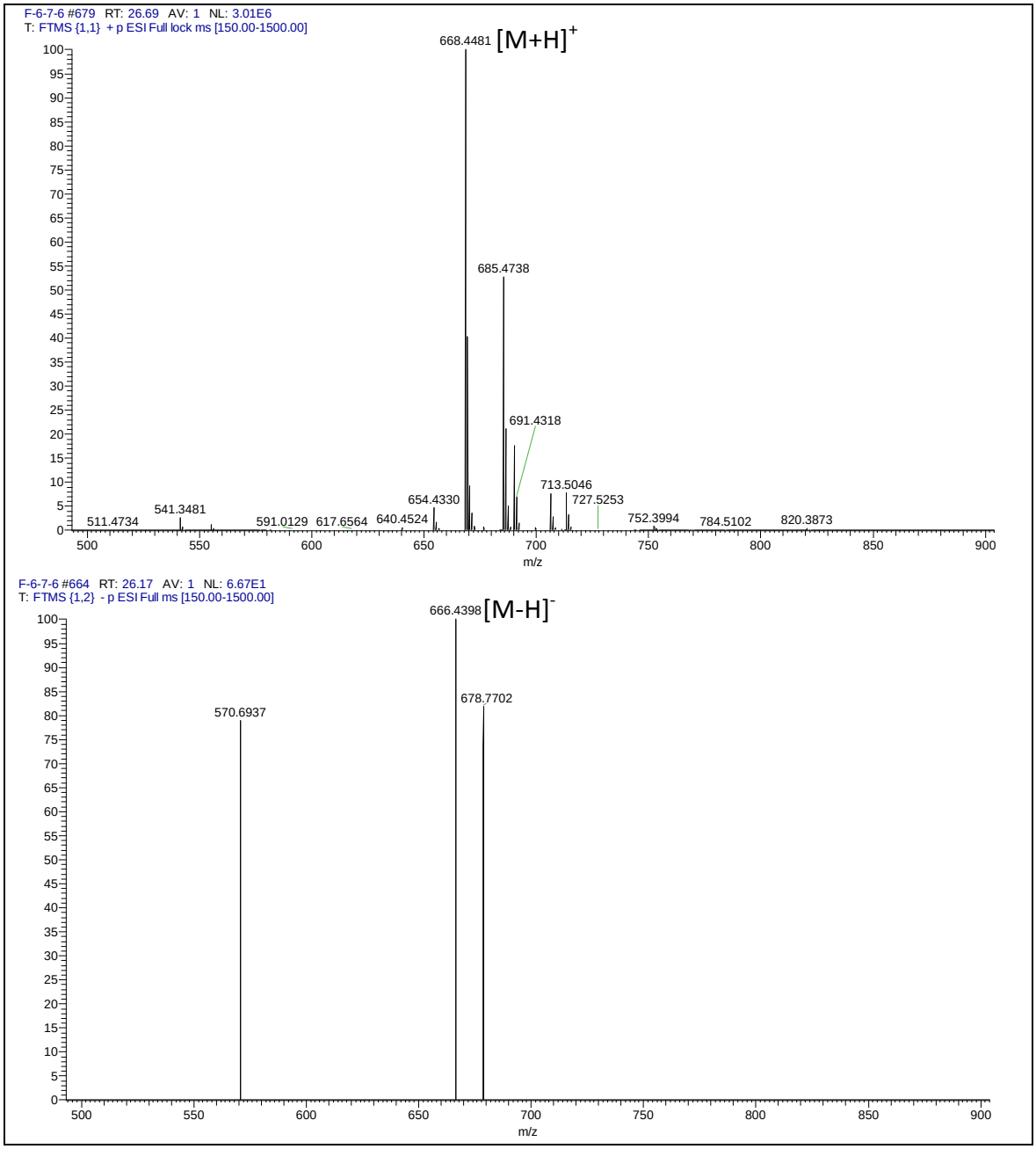

Enniatin A_1 was isolated in the form of colourless crystals. Its yield was 0.10% (27.7 mg). The LC-HRMS data afforded pseudomolecular ion peaks at *m/z* 668.4481 $[M+H]^+$ and 666.4398 $[M-H]^-$, indicating a molecular weight of 667.8735 g/mol. The molecular formula established by HRMS was $C_{35}H_{61}N_3O_9$.

Enniatin A_1 consisted of two *N*-methylisoleucine (NMeIle) moieties, three D-2-hydroxyisovaleric acid (HyIv) moeities and one *N*-methylvaline (NMeVal) moiety. Thus, it closely resembles enniatin A, where one NMeIle moieties is replaced by NMeVal. As a result, all signals of NMeIle and HyIv that were detected in the NMR spectra of enniatin A were also detected in the NMR spectra of enniatin A_1. The presence of these two amino acid moeities was confirmed by comparing the data obtained from ^{1}H and JMod NMR experiments of enniatin A_1 to those of enniatin A (Table 6.13 and Table 6.14). Nevertheless, additional signals resembling the NMeVal moeity were detected in the NMR spectra of enniatin A_1. The following discussion will cover the additional signals corresponding for NMeVal only.

In the ^{1}H NMR spectrum (Figure 6.23), H-α was detected as doublet at δ_H 4.66 (*J*=9.7 Hz) and coupled through ^{1}H-^{1}H COSY experiment to H-β at δ_H 2.20 (Figure A.XV.2). This coupling was responsible for splitting the signal of H-α to a doublet. Moreover, H-β was, in turn, coupled via ^{1}H-^{1}H COSY to the two doublets of CH_3-γ at δ_H 1.02 and δ_H 0.87. In addition to that, the protons of N-CH_3 resonated at δ_H 3.10 along with those of the NMeIle moiety.

The JMod NMR spectrum afforded information about the carbons that constructed the compound (Figure 6.24). The carbonyl ester was detected at δ_C 170.5, while the amidic carbon was detected a little upfield, at δ_C 169.3. As C-α is located between a nitrogen and a carbonyl, it was detected at δ_C 61.5. C-β was detected at δ_C 28.1 and the two methyls C-γ were detected at δ_C 20.2 and δ_C 19.9. Furthermore, the carbon of *N*-methyl resonated at δ_C 32.1. A ^{1}H-^{13}C HSQC experiment was run to assign all protons to their corresponding carbons (Figure A.XV.4).

The connectivity of the NMeVal moeity was attained by implementing an ^{1}H-^{13}C HMBC spectrum (Figure A.XV.5). ^3J correlations were detected going from H-α to the carbon of N-CH$_3$ and vice versa, from the protons of N-CH_3 to C-α. In addition to that, more ^3J correlations were detected from the protons of two methyls CH_3-γ to C-α and to the carbon of the other methyl. Furthermore, ^2J correlations were detected from H-α to C-β, from H-β to both C-α and the two methyls C-γ and form both methyls CH_3-γ to C-β.

The structure was confirmed as enniatin A_1 by comparing both its ^{1}H and ^{13}C NMR data to the literature (Blais *et al*., 1992) (Tables 6.13 and 6.14).

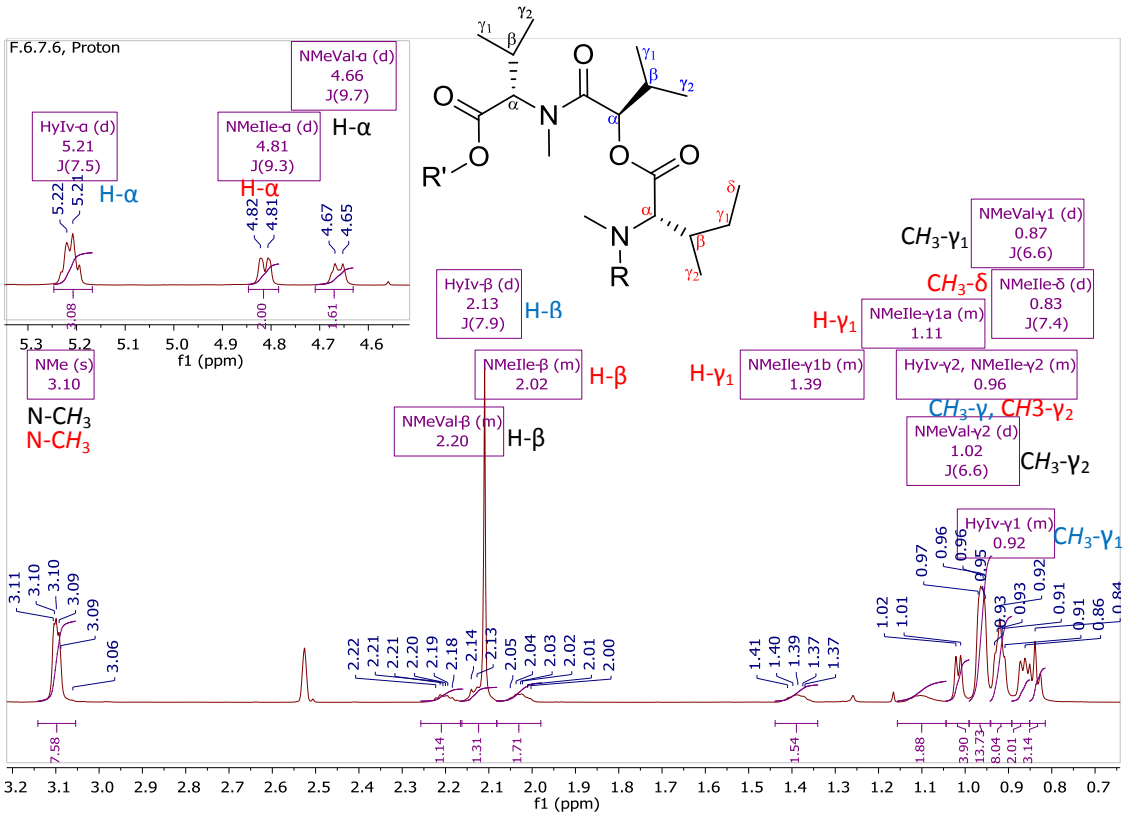

Figure 6.23: ^{1}H NMR (600 MHz) spectrum for enniatin A_1, measured in DMSO-d_6. Red-labelled signals belong to the NMeIle moiety, blue-labelled signals belong to the HyIv moiety and black-labelled signals belong to the NMeVal moiety.

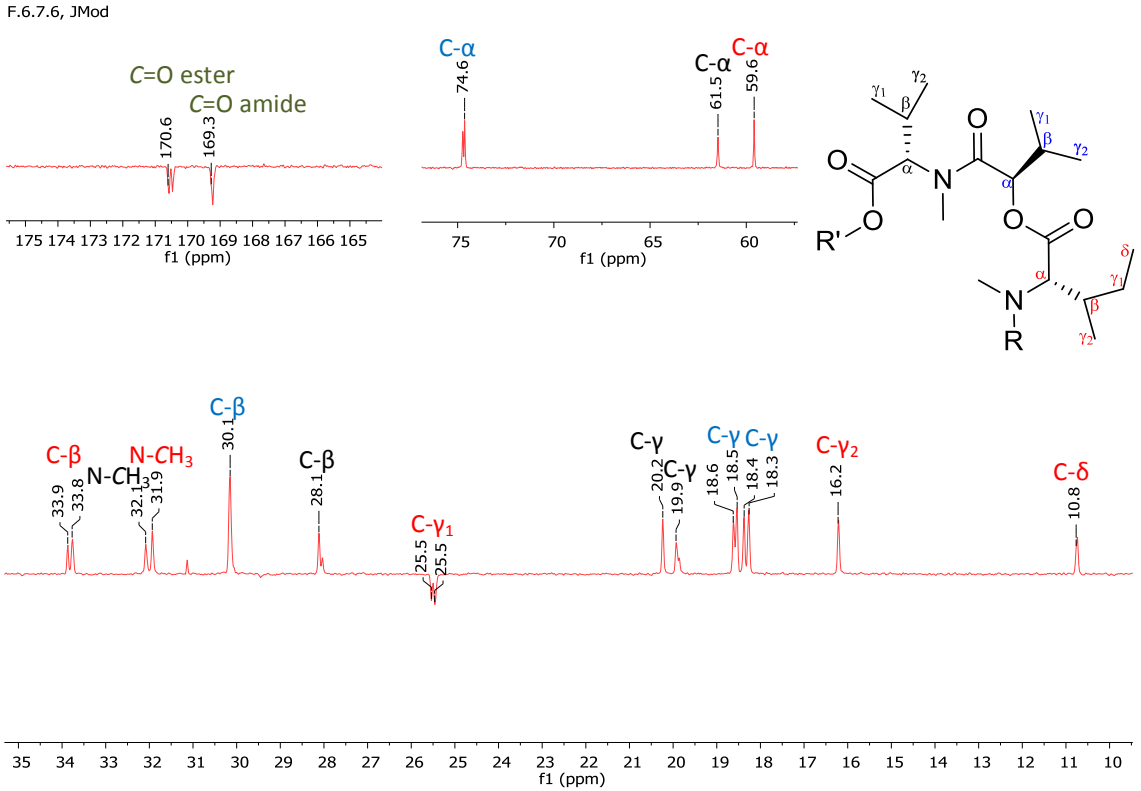

Figure 6.24: JMod NMR (150 MHz) spectrum for enniatin A_1, measured in DMSO-d_6. Red-labelled signals belong to the NMeIle moiety, blue-labelled signals belong to the HyIv moiety and black-labelled signals belong to the NMeVal moiety.

6.6.4 Enniatin B (4)

Enniatin B (Known compound)
Fraction: F.8.15 Retention time: 23.57 min Synonym(s): • Cyclo[(2*R*)-2-hydroxy-3-methylbutanoyl-*N*-methyl-L-valyl-(2*R*)-2-hydroxy-3-methylbutanoyl-*N*-methyl-L-valyl-(2*R*)-2-hydroxy-3-methylbutanoyl-*N*-methyl-L-valyl] • 1,7,13-Trioxa-4,10,16-triazacyclooctadecane, cyclic peptide derivative • Cyclo(3-methyl-D-2-hydroxybutanoyl-*N*-methyl-L-valyl-3-methyl-D-2-hydroxybutanoyl-*N*-methyl-L-valyl-3-methyl-D-2-hydroxybutanoyl-*N*-methyl-L-valyl) Source: *Fusarium acuminatum,* isolated from *Anthemis palestina* Amount of sample: 4.9 mg Percent yield: 0.06% Percent purity: 86.2% Physical description: Colourless crystals Molecular formula: $C_{33}H_{57}N_3O_9$ Molecular weight: 639.8204 g/mol Optical rotation: $[\alpha]_D^{20}$ = -37 (0.1 g/100 mL, $CHCl_3$)
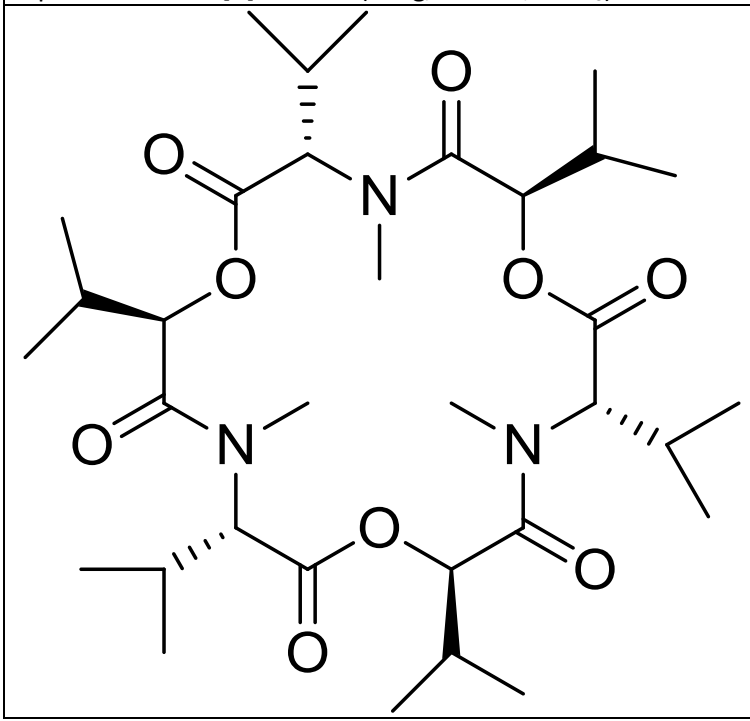

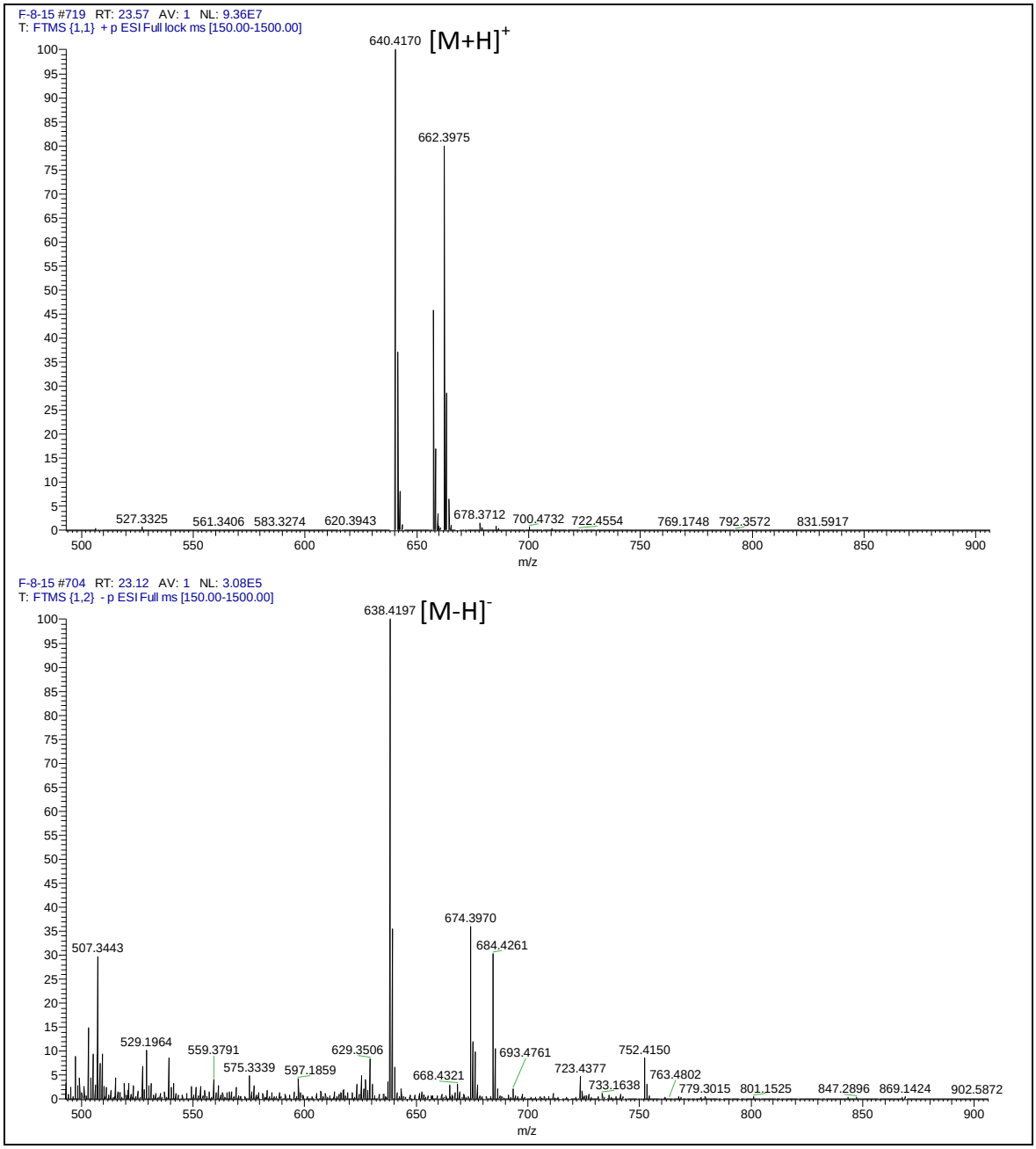

Enniatin B was isolated as colourless crystals, yielding 0.06% (4.9 mg). In the LC-HRMS data, pseudomolecular ion peaks were detected at *m/z* 640.4170 $[M+H]^+$ and 638.4197 $[M-H]^-$, suggesting a molecular weight of 639.8204 g/mol. The molecular formula predicted by HRMS was $C_{33}H_{57}N_3O_9$.

Enniatin B is made of three *N*-methylvaline (NMeVal) moieties and three D-2-hydroxyisovaleric acid (HyIv). And so, it's similar to both enniatin A and enniatin A_1, where the NMeIle units are replaced by NMeVal.

As a result, all signals of HyIv and NMeVal which were detected in the NMR spectra of enniatin A and enniatin A_1 were detected in the NMR spectra of enniatin B as well. The presence of these two moeities was confirmed by comparing the data obtained from ^{1}H and JMod NMR experiments of enniatin B to those of enniatin A and enniatin A_1 (Table 6.13 and Table 6.14). However, as there are three NMeVal moeities in enniatin B, their ^{1}H NMR signals' integration values are different than those of enniatin A_1 (Figure 6.25).

In the ^{1}H NMR spectrum, a doublet was detected at δ_H 4.65 (*J*=10.0 Hz), it coresponded to H-α and coupled through ^{1}H-^{1}H COSY to the multiplet H-β (δ_H 2.18). This coupling caused H-α to be splitted to doublet. The multiplet H-β was also coupled via ^{1}H-^{1}H COSY to the two methyl doublets CH_3-γ_1 (δ_H 0.84, *J*=6.7 Hz) and CH_3-γ_2 (δ_H 1.00, *J*=6.7 Hz).

The proton H-β was also responsible for splitting the signals of the methyls H-γ to doublets that are noticed at δ_H 0.84 ppm and δ_H 1.00 ppm. The singlet at δ_H 3.08 corresponded to the protons of the *N*-methyl. Moreover, the protons of N-CH_3 resonated at δ_H 3.08.

A JMod NMR experiment was run to detect the carbons of this compound (Figure 6.26). As C-α was attached to both nitrogen and carbonyl, it resonated at δ_C 61.5. Moreover, C-β resonated at δ_C 28.0 and the two C-γ methyls at δ_C 20.2 and δ_C 19.8. All proton-carbon connections were assigned by running an ^{1}H-^{13}C HSQC experiment (Figure A.XVI.4).

The connectivity of NMeVal moeity was established by utilising an ^{1}H-^{13}C HMBC experiment (Figure A.XVI.5). ^3J correlations were detected going from H-α to both the carbon of N-*C*H_3 and the amidic carbonyl, from the protons of N-CH_3 to C-α and the amidic carbonyl, as well as from the protons of the two methyls CH_3-γ to C-α and to the carbon of the other methyl. Furthermore, ^2J correlations were detected from H-α to both C-β and the carbonyl ester and form both methyl units CH_3-γ to C-β.

The structure was further confirmed as enniatin B by comparing both its ^{1}H and ^{13}C NMR data to the literature (Visconti *et al*., 1992) (Tables 6.13 and 6.14).

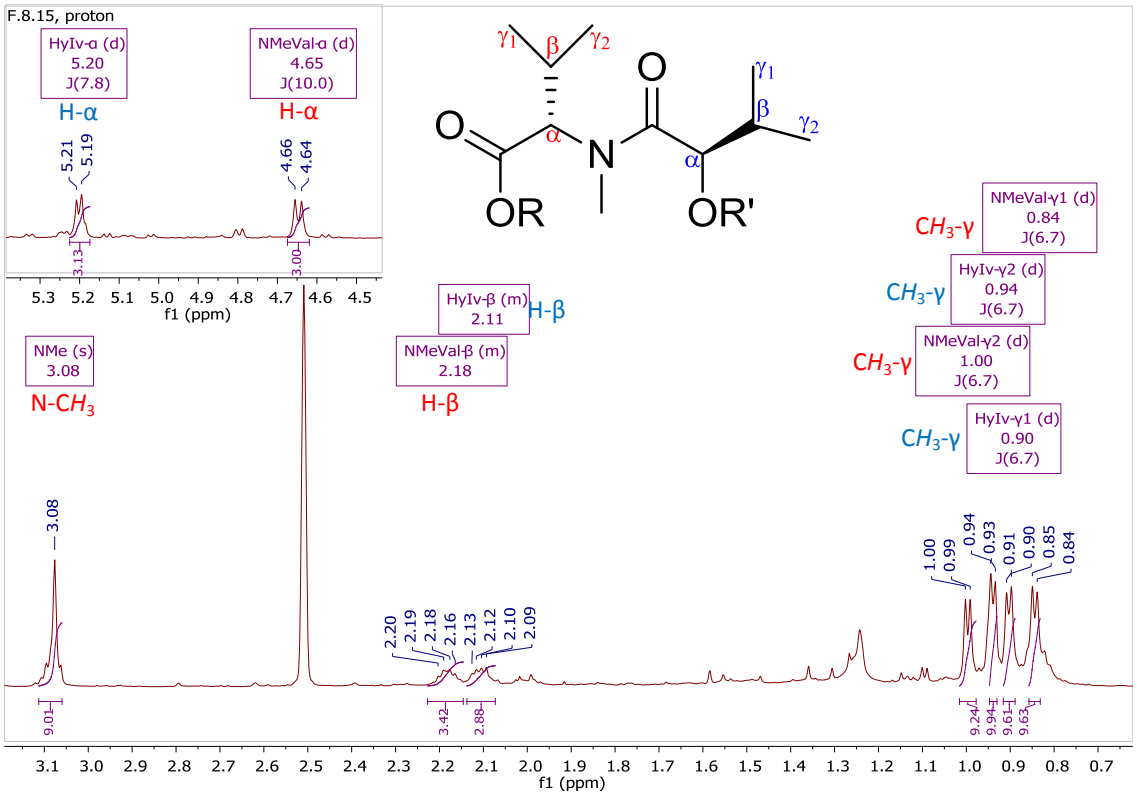

Figure 6.25: ^{1}H NMR spectrum for enniatin B, measured in DMSO-d_6, (600 MHz). Red-labelled signals belong to the NMeVal moiety while blue-labelled signals belong to the HyIv moiety.

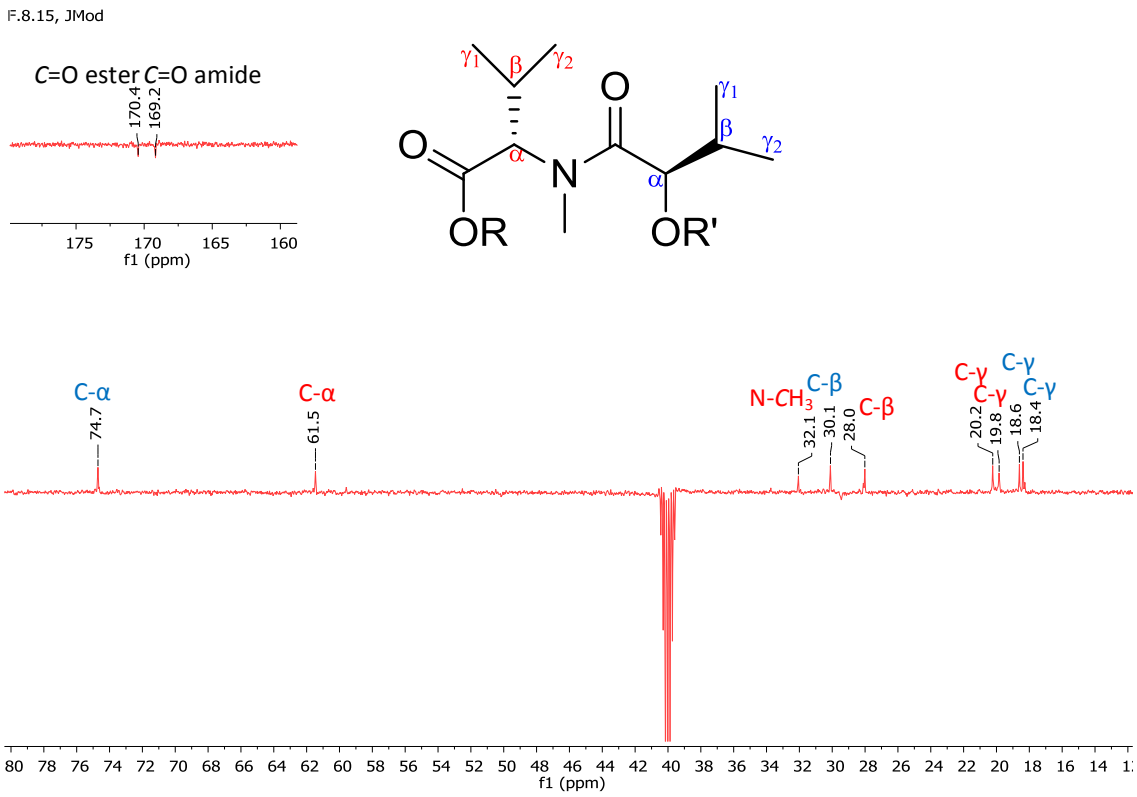

Figure 6.26: JMod NMR (150 MHz) spectrum for enniatin B, measured in DMSO-d_6. Red-labelled signals belong to the NMeVal moiety while blue-labelled signals belong to the HyIv moiety.

6.7 Biological activity of the isolated compounds from the endophyte *Fusarium acuminatum*

The anti-proliferative activity of the isolated compounds against both breast cancer (ZR-75) and lung cancer (A549) cell lines was tested. Three isolated compounds, *i.e.* the three enniatins, possessed potent activity against both ZR-75 and A549 cell lines (Table 6.15, Figure 6.27 and Figure 6.28).

For breast cancer, enniatin A_1 was the most active compound with an IC_{50} value of 7 µM. Other enniatins were not far from enniatin A_1 with an IC_{50} values of 9 µM for enniatin A and 8 µM for enniatin B. On the other hand, enniatin B was the most potent compound against lung cancer (IC_{50}=7 µM), while the IC_{50} values for the other enniatins A and A_1 were 13 µM and 9 µM, respectively. The major compound hymeglusin was not active against any of the tested cell lines with an (IC_{50} > 30 µM). These findings matched the predicted activity for the metabolites that was obtained from the created OPLS-DA models. Yet, the purity of enniatin A_1 and enniatin B was 89.1% and 86.2%, respectively. Thus, the activity they possessed could have been affected by the presence of impurities.

Furthermore, the isolated compounds were assayed for their toxicity against Human prostate normal (PNT2) cell line. The results of this assay revealed that none of them was toxic as the IC_{50} value was more than 30 µM for all of the compounds (Table 6.14 and Figure 6.29).

Table 6.15: IC_{50} concentrations (µM) for the compounds isolated from *Fusarium acuminatum* against the correspondent cell lines.

Compound	ZR-75	A549	PNT2	% Purity
Hymeglusin	> 30	> 30	> 30	74.6
Enniatin A	9	13	> 30	98.0
Enniatin A_1	7	9	> 30	89.1
Enniatin B	8	7	> 30	86.2

Furthermore, the selectivity indexes were calculated for the active compounds, enniatins, and listed in Table 6.16. The selectivity index values for the isolated enniatins against both of the tested cell lines were more than 2, indicating the selective activity of enniatins.

Table 6.16: Selectivity indexes for the compounds isolated from *Fusarium acuminatum* against the correspondent cell lines.

Compound	ZR-75	A549
Enniatin A	11.1	7.7
Enniatin A_1	14.3	11.1
Enniatin B	12.5	14.3

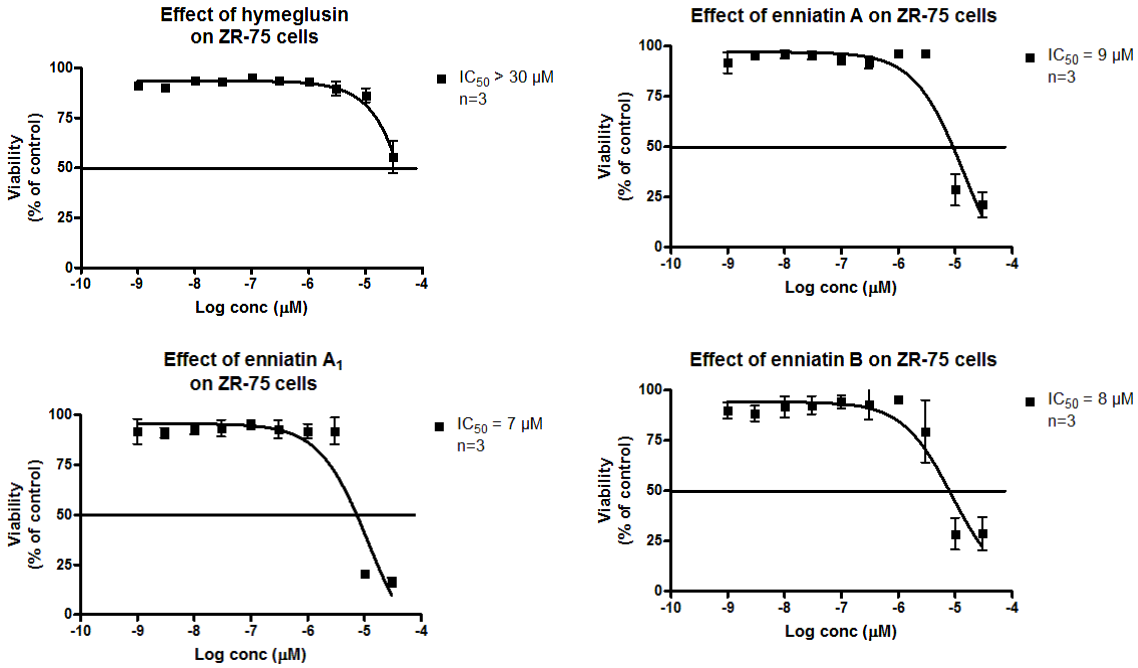

Figure 6.27: Dilution curves for the compounds isolated from *Fusarium acuminatum* when tested against breast cancer (ZR-75) cell line to determine their IC_{50} values.

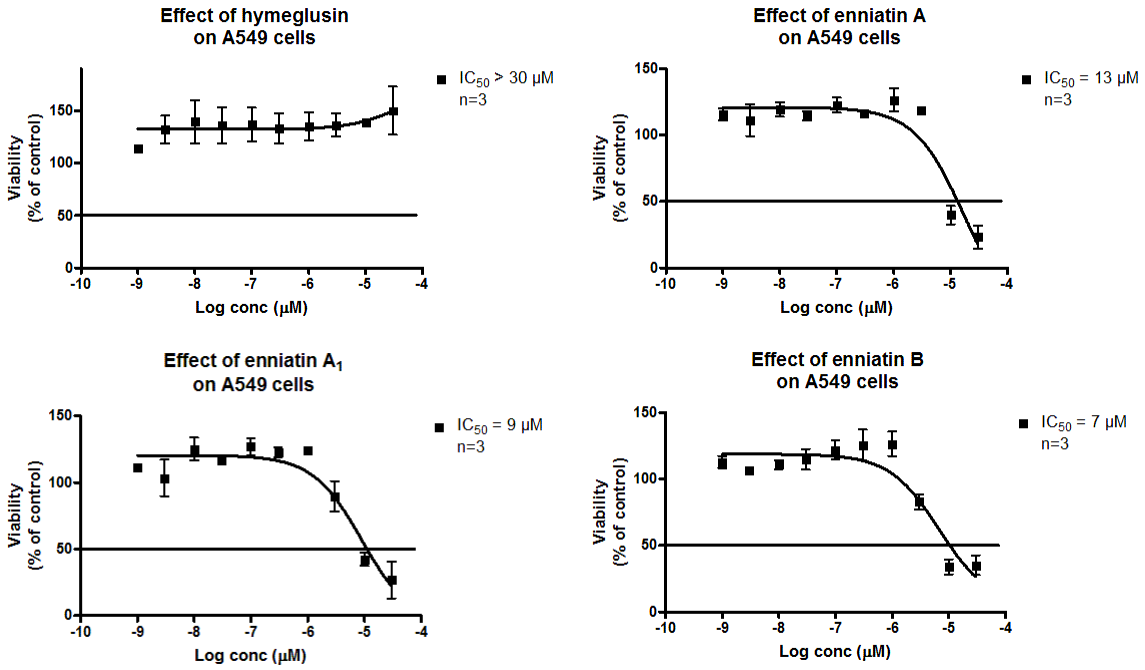

Figure 5.28: Dilution curves for the compounds isolated from *Fusarium acuminatum* when tested against lung cancer (A549) cell line to determine their IC_{50} values.

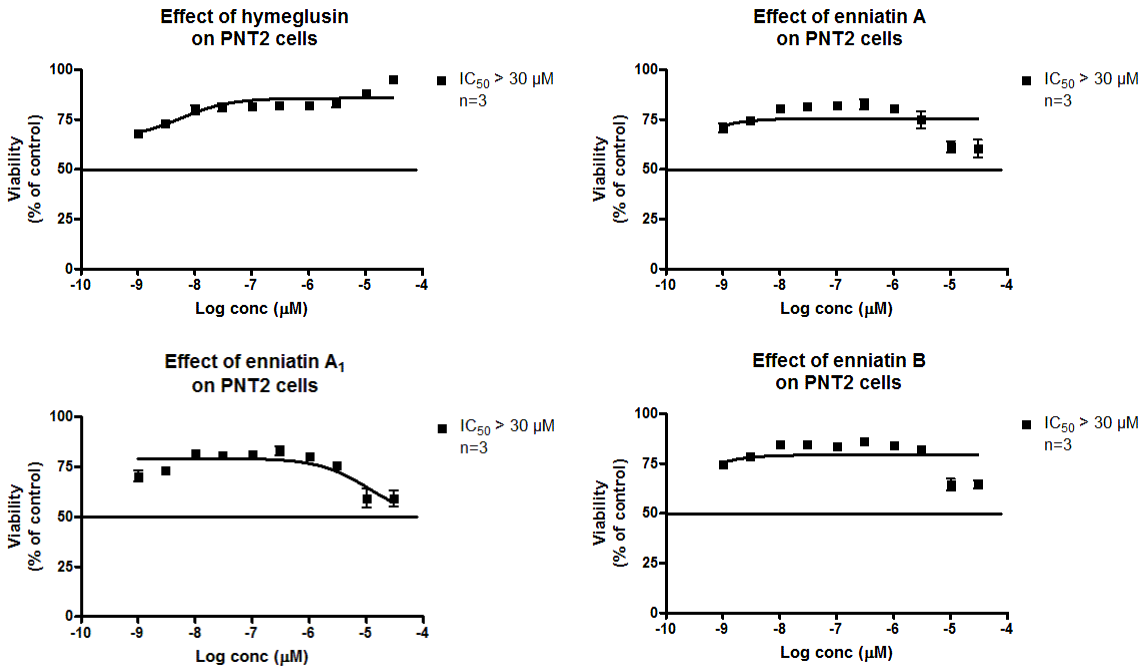

Figure 5.29: Dilution curves for the compounds isolated from *Fusarium acuminatum* when tested against Human prostate normal (PNT2) cell line to determine their IC_{50} values.

Chapter 7: Summary, conclusions and future recommendations

7. Summary, conclusions and future recommendations

7.1 Isolation of endophytes from the obtained plants

Twenty six (26) fungal endophytes were obtained from four chosen Jordanian medicinal plants. Amongst, the four chosen plants, the best sources of endophytes were *Anthemis palestina* (family: Asteraceae) that yielded eleven (11) endophytes and *Euphorbia peplus* (family: Euphorbiaceae) affording nine (9) endophytes. This agreed with the fact that species of the Asteraceae family are among the most to associate endophytes in their tissues (Martinez-Klimova *et al*., 2017). Moreover, all of the identified endophytes belonged to the phylum Ascomycota, as earlier described in the literature, 31 out of each 36 isolated endophytes belonged to this phylum (Martinez-Klimova *et al*., 2017).

The obtained endophytes were preliminarily screened for biological activity against breast cancer (ZR-75) cell line and six of the endophytes exhibited bioactivity. Out of those six, *Curvularia australiensis, Chaetomium subaffine* and *Fusarium acuminatum* obtained from *Anthemis palestina,* were chosen to be scaled-up, based on the chemistry of their extracts. Liquid-Wickerham and solid-rice media were employed for media optimisation in the production of the bioactive metabolites. The scaled-up extracts were fractionated and screened by ^{1}H NMR to reveal the major metabolites. The fractions were subjected to LC-HRMS analysis and bioassay *in vitro* screening against both breast cancer (ZR-75) and lung cancer (A549) to pinpoint the biologically active compounds as “targets” to guide the isolations work by multivariate analysis (MVA) using OPLS-DA. The isolated compounds are listed in Table 7.1.

Table 7.1: The isolated compounds.

No.	Name	New/known	MWt	Molecular formula	%Purity	Structure	IC_{50} (µM)	
							Breast cancer	Lung cancer
Compounds isolated from endophytic *Curvularia australiensis*, obtained from *Anthemis palestina*								
4.1	(-)-(*S*)-curvularin	known	292.3270	$C_{16}H_{20}O_5$	100	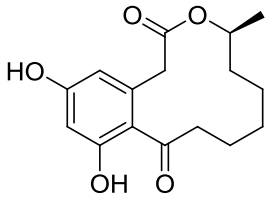	13	> 30
4.2	dehydrocurvularin	known	290.3111	$C_{16}H_{18}O_5$	95.3	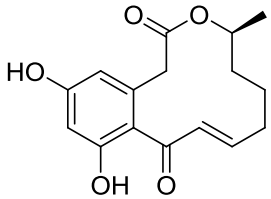	0.8	3.6
4.3	11α-hydroxycurvularin	known	308.3264	$C_{16}H_{20}O_6$	52.3	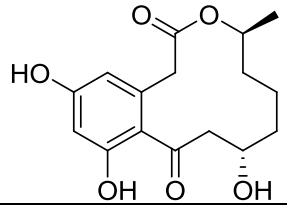	8	28
4.4	cyclo(L-prolylglycyl)	known	154.1665	$C_7H_{10}N_2O_2$	92.6	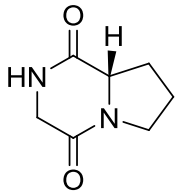	> 30	> 30

Compounds isolated from endophytic *Chaetomium subaffine*, obtained from *Anthemis palestina*								
5.1	acremonisol A	known	258.0659	$C_{12}H_{15}ClO_4$	85.9	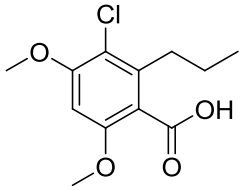	> 30	> 30
5.2	cochliodinol	known	506.2206	$C_{32}H_{30}N_2O_4$	96.6	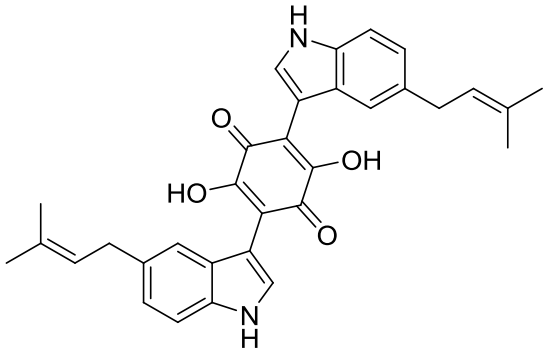	20	> 30
5.3	chaetomipyrrolidinone	new	201.1154	$C_{13}H_{15}NO$	80.3	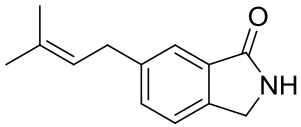	25	25
5.4	chaetomiside A	new	270.0740	$C_{12}H_{14}O_7$	94.2	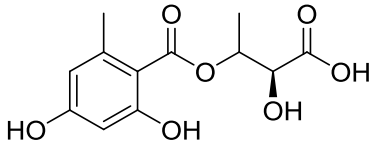	25	> 30
5.5	chaetomiside B	new	324.1209	$C_{16}H_{20}O_7$	99.0	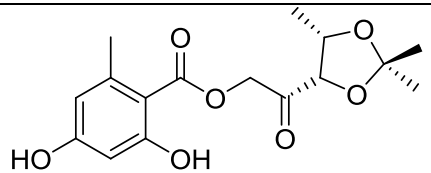	30	> 30

5.6	chaetomiside C	new	286.1053	$C_{13}H_{18}O_7$	77.7	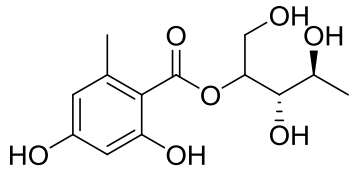	28	> 30
5.7	chaetomiside D	new	286.1053	$C_{13}H_{18}O_7$	90.9	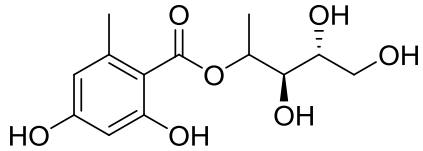	22	> 30
Compounds isolated from endophytic *Fusarium acuminatum*, obtained from *Anthemis palestina*								
6.1	hymeglusin	known	324.4119	$C_{18}H_{28}O_5$	74.6	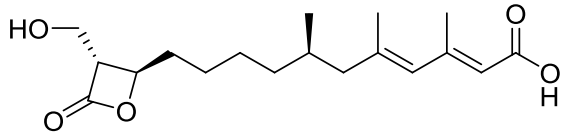	> 30	> 30
6.2	enniatin A	known	681.9001	$C_{36}H_{63}N_3O_9$	98.0	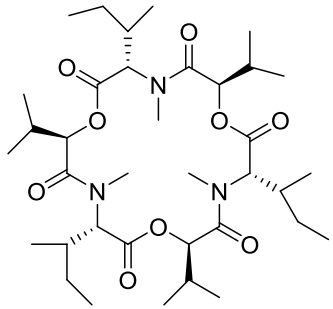	9	13

6.3	enniatin A_1	known	667.8735	$C_{35}H_{61}N_3O_9$	89.1	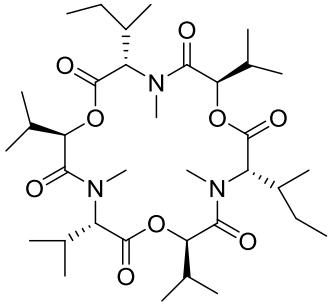	7	9
6.4	enniatin B	known	639.8204	$C_{33}H_{57}N_3O_9$	86.2	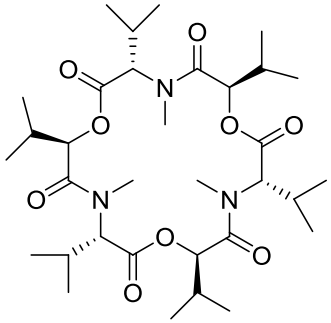	8	7

7.2 Isolation of bioactive compounds from *Curvularia australiensis*

Cultures of *Curvularia australiensis* are best grown in liquid-Wickerham medium as indicated by the extracts' ^{1}H NMR and LC-HRMCS spectral data. The findings proved the ability of the fungus cultured in liquid-Wickerham medium to provide a more chemically complex extracts of this endophyte. Moreover, the extract obtained from the liquid-Wickerham medium-culture was active against the two tested cell lines, breast and lung cancer. The extract obtained from the rice medium-culture was active against breast cancer only. The three polyketides; (-)-(*S*)-curvularin (**4.1**), dehydrocurvularin (**4.2**) and 11α-hydroxycurvularin (**4.3**), in addition to the dipeptide cyclo(L-prolylglycyl) (**4.4**) were isolated. All of the obtained compounds were isolated for the first time from *Curvularia australiensis* and were assayed for the first time against ZR-75 and A549 cell lines.

The curvularin-type derivatives were all found active against breast cancer (ZR-75) cell line, while only dehydrocurvularin and 11α-hydroxycurvularin were active against lung cancer (A549) cell line. The dipeptide cyclo(L-prolylglycyl) (**4.4**) was not a target metabolite, so it exhibited no activity against the tested cell lines. This confirmed the findings of the metabolomics-bioassay guided approach. The isolated metabolites were assayed against normal prostate (PNT2) cell line to determine their toxicity and calculate their selectivity indexes. As a result, all three polyketides demonstrated selective activity against breast cancer cell line, while only dehydrocurvularin was selectively active against lung cancer cell line.

As appeared from the IC_{50} values of the polyketides, the dehydrogenation of positions 10 and 11 increased the potency of the curvularin-type derivative. Moreover the attachment of hydroxyl group to position 11 resulted in reducing the selectivity. Curvularin was successfully obtained as a result of total synthesis that utilised the compound methyl-[2,4-bis(methoxycarbonyl)-3,5-dihydroxyphenyl]acetate as a starter. This was achieved through a series of decarboxylation, methylation, addition and condensations (Elzner *et al*., 2008).

7.3 Isolation of bioactive compounds from *Chaetomium subaffine*

The most ideal condition for the large scale fermentation of *Chaetomium subaffine* was achieved at 30 days of incubation in solid-rice medium. Scatter plots obtained after LC-HRMS

screening showed that the extracts obtained from the rice cultures were more chemically complex and diverse. Moreover, the rice culture extracts exhibited activity against both breast cancer and lung cancer cell lines, while the liquid-Wickerham culture extracts were only active against the breast cancer cell line. Further isolation works yielded seven compounds, six of which were pinpointed by multivariate analysis to exhibit the putative bioactivity. The isolated target compounds included two known target compounds, which were acremonisol A (**5.1**) and cochliodinol (**5.2**); in addition, four new orsellinic acid derivatives; chaetomisides A (**5.4**), B (**5.5**), C (**5.6**), and D (**5.7**). The new compound chaetomipyrrolidinone (**5.3**) was also isolated but was not detected amongst the predicted target metabolites from the multivariate analysis. Both acremonisol A and cochliodinol were isolated for the first time from the fungus *Chaetomium subaffine*. On the other hand, chaetomipyrrolidinone and chaetomisides were not reported previously in literature, and thus, they were characterised and isolated for the first time. All of the isolated compounds were assayed for the first time against ZR-75 and A549 cell lines.

Except for acremonisol A, all other compounds exhibited very good bioactivity against the tested breast cancer (ZR-75) cell line, with IC_{50} values between 20 and 30 µM. Nonetheless, the only compound that was active against the tested lung cancer (A549) cell line was chaetomipyrrolidinone, while the other compounds were rendered inactive when tested at lower concentrations of <30 µM. Preliminary screens done on the extracts and fractions used a concentration of 30 µg/mL that was way above the 30 µM concentration that was employed for pure compounds. Either the difference in concentration used between the preliminary screening of the extracts and the pure compounds or the weakness and low predictability score of the OPLS-DA model in defining the putative target bioactive compounds against the lung cancer cell line tested could have contributed to the absence of the activity when the isolated compounds were tested. The toxicity of the isolated compounds was investigated by testing their effect on normal prostate (PNT2) cells. Acremonisol A and chaetomisides showed no anti-proliferative activity. However, both cochliodinol and chaetomipyrrolidinone lacked selectivity against both breast cancer and lung cancer cell lines. This could be attributed to the (3-methylbut-2-en-1-yl)benzene moiety that they possess.

In spite of their weak activity against breast cancer cell line, chaetomisides lacked activity against both lung cancer and normal prostate cells. Thus, they could be utilised as a starting point to develop specific breast cancer drugs. The IC_{50} values showed that the antiproliferative activity of chaetomisides against breast cancer increased if the side chain was straight and contained more hydroxyl groups (Figure 7.1). Therefore, the activity of chaetomisides could be strengthened by synthesising more optimum side chains and attaching them to orsellinic acid via an esterification reaction.

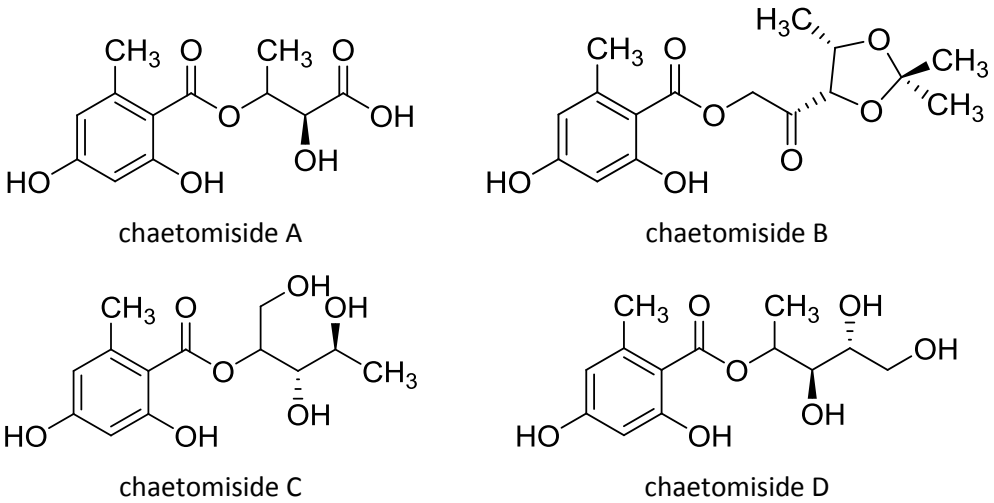

Figure 7.1: Chaetomisides A – D.

7.4 Isolation of bioactive compounds from *Fusarium acuminatum*

Incubating *Fusarium acuminatum* in solid-rice and liquid-Wickerham medium afforded the same type of major compounds, which were the enniatins, as indicated by ^{1}H NMR spectral data. Moreover, the extracts of both media exhibited good activity against both breast and lung cancer cell lines. However, incubating *Fusarium acuminatum* for 30 days in rice medium afforded the highest yield and the most diverse chemistry as indicated by the scatter plots of the LC-HRMS data. Therefore, the 30-day rice culture was chosen for the scaling-up. The isolation work yielded the major compound hymeglusin (**6.1**), along with three enniatin derivatives; enniatin A (**6.2**), enniatin A_1 (**6.3**) and enniatin B (**6.4**). Both hymeglusin and enniatin A_1 were isolated for the first time from *Fusarium acuminatum*. However, enniatin A and enniatin B were isolated before from the same organism as stated under 6.1.1. The activity

of any of the isolated compounds against ZR-75 and A549 cell lines was not reported previously.

All of the pinpointed compounds as target metabolites, *i.e.* the enniatins, were active against both the tested breast and lung cancer cell lines. Hymeglusin was inactive against neither breast nor lung cancer cell lines. Moreover, Human prostate normal cells (PNT2) were employed to study the toxicity of and the selectivity of the isolated compounds. All of the isolated compounds were considered safe. In addition to that, the active enniatins were selectively active against both breast and lung cancer cell lines as demonstrated by their SI values.

All of enniatins were weakly active as anticancers against breast and lung cancer. However, they were inactive against normal prostate cells. Therefore, their selectivity could be advantageous in terms of their development as drugs. The activity of enniatins is a result of their cyclodepsipeptide core that enables them to incorporate into cell membranes and act as ionophores (Figure 7.2). Thus, this cyclodepsipeptide core should remain intact to retain the activity. Yet, the alkyl side chains could be manipulated and its effect on the activity could be studied.

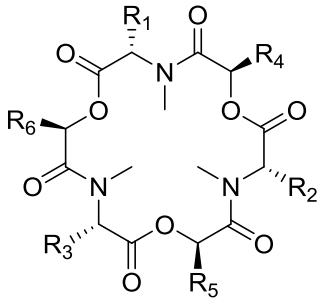

Figure 7.2: General structure of enniatins.

Enniatin B was the only enniatin that could be obtained by total synthesis. This was acheived by Ley and his research group who utilised Benzyl (2*R*)-2-hydroxy-3-methylbutanoate and *N*-methyl-*N*-butoxycarbonyl D-valine starting reactants (Hu *et al*., 2012).

7.5 Conclusions and future recommendations

Implementing metabolomics approaches in pinpointing and targeting the bioactive compounds for isolation work presented a good approach in the search for new biologically active compounds from natural sources. The metabolomics-guided isolation approach resulted in the isolation of 11 compounds that exhibited good activity against the tested breast cancer cell line, which included four new orsellinic acid derivatives, while five compounds exhibited good activity against the tested lung cancer cell line. However, performing the permutation test on the OPLS-DA models is essential to ensure their strength and validity. Moreover, it should be noted that some new compounds may share the same molecular formulae, and thus, the molecular weight with known natural products. Therefore, in the dereplication step, hits that appeared to be known should not be overlooked; especially, when they are outliers in the active region of the S-plot.

Furthermore, some of the putative active target compounds were not isolated due to their occurrence at extremely low concentrations in the crude extracts. Thus, the fermentation volume or mass employed for the scale-up should be increased. Furthermore, as some of the important and valuable secondary metabolites that are used as drugs like taxol and camptothecin were discovered to be produced by endophytes (Aly *et al*., 2011), studies should be carried on the plant sources of biologically active secondary metabolites that are either used in ethnopharmacology or have a commercial value to detect whether these compounds could be produced by the endophytes that these plant sources host or not. Therefore, the biosynthetic relationship between endophytes and their host plants should be further investigated. Precursors or intermediates for the biosynthesis of biologically active compounds could be provided from the host plant to the endophyte or vice versa (Kusari *et al*., 2016). Moreover, horizontal transfer of genetic information might take place between the host plant and the endophyte, leading to the production of similar secondary metabolites (Taghavi *et al*., 2005, Bomke and Tudzynski, 2009, Alvin *et al*., 2014). Additionally, co-cultivation approach that could apply stress conditions between fungi or fungi and bacteria could be used as a strategy in scaling-up the yield of the target metabolite (Kalaitzis, 2013, Nah *et al*., 2013, Stevens *et al*., 2013, Zhang *et al*., 2017). In a co-culture system, the two species will grow either in symbiosis or they will compete until an equilibrium state is achieved. This will include interactions

between the two species that might switch on the production of certain metabolites that are not produced when single strain is cultivated (Zhang *et al*., 2017). Moreover, the unfavourable conditions may activate cryptic genes which may lead to more diverse metabolomes (Ola *et al*., 2013).

As hypothesised, the application of metabolomics in the search for anti-proliferative agents against breast and lung cancers from plant-associated endophytes facilitated in pinpointing the biologically active compounds in the first fractionation step which targeted their further isolation and chromatographic purification.

References

References

ABDELMOHSEN, U. R., CHENG, C., VIEGELMANN, C., ZHANG, T., GRKOVIC, T., AHMED, S., QUINN, R. J., HENTSCHEL, U. & EDRADA-EBEL, R. 2014. Dereplication strategies for targeted isolation of new antitrypanosomal actinosporins A and B from a marine sponge associated-*Actinokineospora* sp. EG49. *Mar. Drugs,* 12**,** 1220-1244, 25.

ABDELWAHAB, M. F., SANGI, S., ARAFAT, H. H. & RAGAB, E. A. 2016. New Phytochemical Constituent and Bioactivities of Horwoodia dicksoniae and *Rumex cyprius*. *Pharmacogn. Mag.,* 12**,** 165-70.

ABEL, U., KOCH, C., SPEITLING, M. & HANSSKE, F. G. 2002. Modern methods to produce natural-product libraries. *Curr. Opin. Chem. Biol.,* 6**,** 453-8.

ABUEREISH, G. M. 1998. Pepsin inhibitor from roots of *Anchusa strigosa*. *Phytochemistry,* 48**,** 217-221.

AL-KHALIL, S. 1995. A Survey of Plants Used in Jordanian Traditional Medicine. *Int. J. Pharmacogn.,* 33**,** 317-323.

AL-NURI, M. A., ZA'TAR, N. A., ABU-EID, M. A., HANNOUN, M. A., AL-JONDI, W. J., HUSSEIN, A. I. & AL-SHTAYEH, M. S. 1996. Emodin, a naturally occurring anthraquinone: its isolation and spectrophotometric determination in *Rumex cyprius* plant. *Spectrosc. Lett.,* 29**,** 1539-1543.

AL-SAYAIDEH, A., NIMRI, O., ARQOUB, K., AL-ZAGHAL, M. & HALASA, W. 2012. Cancer Incidence in Jordan - 2012. Non communicable diseases Directorate, Cancer Prevention Department, Jordan Cancer Registry.

AL KHATEEB, W., ALU'DATT, M., AL ZGHOUL, H., KANAAN, R., EL-OQLAH, A. & LAHHAM, J. 2017. Enhancement of phenolic compounds production in in vitro grown *Rumex cyprius* Murb. *Acta Physiol. Plant.,* 39**,** 1-13.

ALALI, F. Q., TAWAHA, K., EL-ELIMAT, T., SYOUF, M., EL-FAYAD, M., ABULAILA, K., NIELSEN, S. J., WHEATON, W. D., FALKINHAM, J. O., III & OBERLIES, N. H. 2007. Antioxidant activity and total phenolic content of aqueous and methanolic extracts of Jordanian plants: an ICBG project. *Nat. Prod. Res.,* 21**,** 1121-1131.

ALDRIDGE, D. C., GILES, D. & TURNER, W. B. 1971. Antibiotic 1233A: a fungal β-lactone. *J. Chem. Soc. C*, 0**,** 3888-3891.

ALI, K., IQBAL, M., YULIANA, N. D., LEE, Y.-J., PARK, S., HAN, S., LEE, J.-W., LEE, H.-S., VERPOORTE, R. & CHOI, Y. H. 2013. Identification of bioactive metabolites against adenosine A1 receptor using NMR-based metabolomics. *Metabolomics,* 9**,** 778-785.

ALVIN, A., MILLER, K. I. & NEILAN, B. A. 2014. Exploring the potential of endophytes from medicinal plants as sources of antimycobacterial compounds. *Microbiol. Res.,* 169**,** 483-495.

ALWAN, A. H., AL-GAILLANY, K. A. S. & NAJI, A. 1989. Inhibition of the binding of 3H-benzo[a]pyrene to rat liver microsomal protein by plant extracts. *Int. J. Crude Drug Res.,* 27**,** 33-7.

ALY, A. H., DEBBAB, A., CLEMENTS, C., EDRADA-EBEL, R., ORLIKOVA, B., DIEDERICH, M., WRAY, V., LIN, W. & PROKSCH, P. 2011. NF kappa B inhibitors and antitrypanosomal metabolites from endophytic fungus *Penicillium* sp. isolated from *Limonium tubiflorum*. *Bioorg. Med. Chem.,* 19**,** 414-421.

ALY, A. H., DEBBAB, A., KJER, J. & PROKSCH, P. 2010. Fungal endophytes from higher plants: a prolific source of phytochemicals and other bioactive natural products. *Fungal Diversity,* 41**,** 1-16.

AMIN, E., MOAWAD, A. & HASSAN, H. 2017. Biologically-guided isolation of leishmanicidal secondary metabolites from *Euphorbia peplus* L. *Saudi Pharm. J.,* 25**,** 236-240.

APPIAH-AMPONSAH, E., SHANAIAH, N., NAGANA GOWDA, G. A., OWUSU-SARFO, K., YE, T. & RAFTERY, D. 2009. Identification of 4-deoxythreonic acid present in human urine using HPLC and NMR techniques. *J. Pharm. Biomed. Anal.,* 50**,** 878-885.

ARAFA, R. F. 2005. Some polyphenolic compounds from Egyptian plant of family Polygonaceae. *Egypt. J. Biomed. Sci.,* 18**,** 29-34.

ARNDT, B., SCHMID, R., HUBNER, F., HUMPF, H.-U., JANEVSKA, S. & TUDZYNSKI, B. 2017. A Fungal *N*-Dimethylallyltryptophan Metabolite from *Fusarium fujikuroi*. *Chembiochem.,* 18**,** 899-904.

BACON, C. W. & WHITE, J. 2000. *Microbial Endophytes*.

BAI, H., WU, L., YANG, T. & LI, G. 2015. Isolation and identification of secondary metabolites from fungus *Chaetomium gracile* and their antimicrobial activities. *Chin. .J Appl. Environ. Biol.,* 21**,** 274-278.

BAKER, D., MOCEK, U. & GARR, C. 2000. Natural products vs. combinatorials: a case study. *Spec. Publ. - R. Soc. Chem.,* 257**,** 66-72.

BAKER, D. D., CHU, M., OZA, U. & RAJGARHIA, V. 2007. The value of natural products to future pharmaceutical discovery. *Nat. Prod. Rep.,* 24**,** 1225-1244.

BARDAWEEL, S. K., TAWAHA, K. A. & HUDAIB, M. M. 2014. Antioxidant, antimicrobial and antiproliferative activities of *Anthemis palestina* essential oil. *BMC Complement. Altern. Med.,* 14**,** 297-305.

BARRY, C. E., III & BLANCHARD, J. S. 2010. The chemical biology of new drugs in the development for tuberculosis. *Curr. Opin. Chem. Biol.,* 14**,** 456-466.

BASHYAL, B. P., FAETH, S. H. & GUNATILAKA, A. A. L. 2007. 13α-hydroxylucilactaene and other metabolites of an endophytic strain of *Fusarium acuminatum*. *Nat. Prod. Commun.,* 2**,** 547-550.

BASHYAL, B. P. & LESLIE GUNATILAKA, A. A. 2010. Tricinonoic acid and tricindiol, two new irregular sesquiterpenes from an endophytic strain of *Fusarium tricinctum*. *Nat. Prod. Res.,* 24**,** 349-356.

BASHYAL, B. P., WIJERATNE, E. M. K., FAETH, S. H. & GUNATILAKA, A. A. L. 2005. Globosumones A-C, cytotoxic orsellinic acid esters from the Sonoran Desert endophytic fungus *Chaetomium globosum*. *J. Nat. Prod.,* 68**,** 724-728.

BATES, R. W., FERNANDEZ-MEGIA, E., LEY, S. V., RUCK-BRAUN, K. & TILBROOK, D. M. G. 1999. Total synthesis of the cholesterol biosynthesis inhibitor 1233A via a (π-allyl)tricarbonyliron lactone complex. *J. Chem. Soc., Perkin Trans. 1*, 0**,** 1917-1925.

BEHIE, S. W., MOREIRA, C. C., SEMENTCHOUKOVA, I., BARELLI, L., ZELISKO, P. M. & BIDOCHKA, M. J. 2017. Carbon translocation from a plant to an insect-pathogenic endophytic fungus. *Nat. Commun.,* 8**,** 14245.

BERES, T., DRAGULL, K., DOLEZAL, K., BERES, T., TARKOWSKI, P., POSPISIL, J., TARKOWSKA, D., BIBA, O., STRNAD, M. & DANCAK, M. 2017. Quantitative Analysis of Ingenol in *Euphorbia* species via Validated Isotope Dilution Ultra-high Performance Liquid Chromatography Tandem Mass Spectrometry. *Phytochem Anal*., 29**,** 23-29.

BERG, G. & HALLMANN, J. 2006. Control of Plant Pathogenic Fungi with Bacterial Endophytes. *In:* SCHULZ, B. J. E., BOYLE, C. J. C. & SIEBER, T. N. (eds.) *Microbial Root Endophytes.* Berlin, Heidelberg: Springer Berlin Heidelberg., 53-69.

BHIMBA, B. V., AGNEL, D. F. D. A., MATHEW, J. M., JOSE, G. M., JOEL, E. L. & THANGARAJ, M. 2012. Anticancer and antimicrobial activity of mangrove derived fungi *Hypocrea lixii* VB1. *Chin. J. Nat. Med.,* 10**,** 77-80.

BILLICH, A. & ZOCHER, R. 1987. *N*-Methyltransferase function of the multifunctional enzyme enniatin synthetase. *Biochemistry,* 26**,** 8417-23.

BIRCH, A. J., MUSGRAVE, O. C., RICHARDS, R. W. & SMITH, H. 1959. Studies in relation to biosynthesis. XX. Structure and biosynthesis of curvularin. *J. Chem. Soc.*, 0**,** 3146-52.

BLAIS, L. A., APSIMON, J. W., BLACKWELL, B. A., GREENHALGH, R. & MILLER, J. D. 1992. Isolation and characterization of enniatins from *Fusarium avenaceum* DAOM 196490. *Can. J. Chem.,* 70**,** 1281-7.

BOCHNER, B. R. 2009. Global phenotypic characterization of bacteria. *FEMS Microbiol. Rev.,* 33**,** 191-205.

BOGNER, C. W., SICHTERMANN, G., GRUNDLER, F. M. W., SCHOUTEN, A., KAMDEM, R. S. T., PROKSCH, P., MATTHAUS, C., POPP, J., MATTHAUS, C., POPP, J. & HOLSCHER, D. 2017. Bioactive secondary metabolites with multiple activities from a fungal endophyte. *Microb. Biotechnol.,* 10**,** 175-188.

BOMKE, C. & TUDZYNSKI, B. 2009. Diversity, regulation, and evolution of the gibberellin biosynthetic pathway in fungi compared to plants and bacteria. *Phytochemistry,* 70**,** 1876-93.

BORRAS-LINARES, I., FERNANDEZ-ARROYO, S., ARRAEZ-ROMAN, D., PALMEROS-SUAREZ, P. A., DEL VAL-DIAZ, R., ANDRADE-GONZALES, I., FERNANDEZ-GUTIERREZ, A., GOMEZ-LEYVA, J. F. & SEGURA-CARRETERO, A. 2015. Characterization of phenolic compounds, anthocyanidin, antioxidant and antimicrobial activity of 25 varieties of Mexican Roselle (*Hibiscus sabdariffa*). *Ind. Crops Prod.,* 69**,** 385-394.

BRACA, A., BADER, A., SICILIANO, T., MORELLI, I. & DE TOMMASI, N. 2003. New pyrrolizidine alkaloids and glycosides from *Anchusa strigosa*. *Planta Med.,* 69**,** 835-841.

BUSTANJI, Y., ISSA, A., MOULAY, A., HUDAIB, M., TAWAHA, K., MOHAMMAD, M., HAMED, S., MASRI, I. & ALALI, F. Q. 2011. Hormone sensitive lipase inhibition by selected medicinal plants. *J. Med. Plants Res.,* 5**,** 4405-4410.

BYLESJOE, M., RANTALAINEN, M., CLOAREC, O., NICHOLSON, J. K., HOLMES, E. & TRYGG, J. 2007. OPLS discriminant analysis: combining the strengths of PLS-DA and SIMCA classification. *J. Chemom.,* 20**,** 341-351.

Cancer Research UK. 2018. Cancer Statistics for the UK [Online]. Available: http://www.cancerresearchuk.org/health-professional/cancer-statistics-for-the-uk [Accessed 19.03.2018 2018].

CASTILLO, U. F., STROBEL, G. A., FORD, E. J., HESS, W. M., PORTER, H., JENSEN, J. B., ALBERT, H., ROBISON, R., CONDRON, M. A. M., TEPLOW, D. B., STEVENS, D. & YAVER, D. 2002. Munumbicins, wide-spectrum antibiotics produced by *Streptomyce*s NRRL 30562, endophytic on *Kennedia nigriscans*. *Microbiology,* 148**,** 2675-85.

CATENI, F., ZILIC, J., ZACCHIGNA, M. & PROCIDA, G. 2010. Cerebrosides with antiproliferative activity from *Euphorbia peplis* L. *Fitoterapia,* 81**,** 97-103.

CHADHA, N., MISHRA, M., RAJPAL, K., BAJAJ, R., CHOUDHARY, D. K. & VARMA, A. 2015. An ecological role of fungal endophytes to ameliorate plants under biotic stress. *Arch. Microbiol.,* 197**,** 869-881.

CHANG, J. & KWON, H. J. 2016. Discovery of novel drug targets and their functions using phenotypic screening of natural products. *J. Ind. Microbiol. Biotechnol.,* 43**,** 221-231.

CHANG, M. C. Y. & KEASLING, J. D. 2006. Production of isoprenoid pharmaceuticals by engineered microbes. *Nat. Chem. Biol.,* 2**,** 674-681.

CHATZIKONSTANTINOU, A. V., CHATZIATHANASIADOU, M. V., RAVERA, E., FRAGAI, M., PARIGI, G., GEROTHANASSIS, I. P., LUCHINAT, C., STAMATIS, H. & TZAKOS, A. G. 2017. Enriching the biological space of natural products and charting drug metabolites, through real time biotransformation monitoring: The NMR tube bioreactor. *Biochim. Biophys. Acta, Gen. Subj.*, 1862(1)**,** 1-8.

CHEN, J., LI, W., YAO, H. & XU, J. 2015. Insights into drug discovery from natural products through structural modification. *Fitoterapia***,** 103**,** 231-241.

CHEN, Y., DE BRUYN KOPS, C. & KIRCHMAIR, J. 2017. Data Resources for the Computer-Guided Discovery of Bioactive Natural Products. *J. Chem. Inf. Model.,* 57**,** 2099-2111.

CHOW, Y. & TING, A. S. Y. 2014. Endophytic l-asparaginase-producing fungi from plants associated with anticancer properties. *J. Adv. Res.*, 6**,** 869-876.

COVINGTON, B. C., MCLEAN, J. A. & BACHMANN, B. O. 2017. Comparative mass spectrometry-based metabolomics strategies for the investigation of microbial secondary metabolites. *Nat. Prod. Rep.,* 34**,** 6-24.

DA CUNHA, K. C., SUTTON, D. A., FOTHERGILL, A. W., GENE, J., CANO, J., MADRID, H., HOOG, S. D., CROUS, P. W. & GUARRO, J. 2013. In vitro antifungal susceptibility and molecular identity of 99 clinical isolates of the opportunistic fungal genus *Curvularia*. *Diagn. Microbiol. Infect. Dis.,* 76**,** 168-174.

DAI, J., KROHN, K., FLOERKE, U., PESCITELLI, G., KERTI, G., PAPP, T., KOEVER, K. E., BENYEI, A. C., DRAEGER, S., SCHULZ, B. & KURTAN, T. 2010. Curvularin-type metabolites from the fungus *Curvularia* sp. isolated from a marine alga. *Eur. J. Org. Chem.*, 5**,** 6928-6937.

DEBBAB, A., ALY, A. H., EDRADA-EBEL, R. A., MUELLER, W. E. G., MOSADDAK, M., HAKIKI, A., EBEL, R. & PROKSCH, P. 2009. Bioactive secondary metabolites from the endophytic fungus *Chaetomium* sp. isolated from *Salvia officinalis* growing in Morocco. *Biotechnol., Agron., Soc. Environ.,* 13**,** 229-234.

DETTMER, K., ARONOV, P. A. & HAMMOCK, B. D. 2007. Mass spectrometry-based metabolomics. *Mass Spectrom. Rev.,* 26**,** 51-78.

DILUVIO, L., BAVETTA, M., DI, P. M., BIANCHI, L., CAMPIONE, E. & ORLANDI, A. 2017. Dermoscopic monitoring of efficacy of ingenol mebutate in the treatment of pigmented and non-pigmented basal cell carcinomas. *Dermatol. Ther.,* 30**,** e12438.

DISI, A. M., TAMIMI, S. O. & ABUEREISH, G. M. 1998. Effects of *Anchusa strigosa* root aqueous extract on gastric ethanol-induced ulcer in laboratory animals. *J. Ethnopharmacol,* 60**,** 189-198.

DREWRY, D. H. & MACARRON, R. 2010. Enhancements of screening collections to address areas of unmet medical need: an industry perspective. *Curr. Opin. Chem. Biol.,* 14**,** 289-298.

EL-FATTAH, H. A. 1989. Anthraquinones and C-flavonoids of *Rumex cyprius* Murb. *Mansoura J. Pharm. Sci.,* 6**,** 141-148.

EL-MEKKAWY, S., MESELHY, M., KUSUMOTO, I. T., KADOTA, S., HATTORI, M. & NAMBA, T. 1995. Inhibitory effects of Egyptian folk medicines on human immunodeficiency virus (HIV) reverse transcriptase. *Chem. Pharm. Bull.,* 43**,** 641-648.

ELZNER, S., SCHMIDT, D., SCHOLLMEYER, D., ERKEL, G., ANKE, T., KLEINERT, H., FOERSTERMANN, U. & KUNZ, H. 2008. Inhibitors of inducible NO synthase expression: total synthesis of (S)-curvularin and its ring homologues. *Chem. Med. Chem.,* 3**,** 924-939.

ERIKSSON, L., JOHANSSON, E., KETTANEH-WOLD, N. & WOLD, S. 2006. *Multi and megavariate data analysis*, Umea˚: Umetrics AB.

ERNST, M., GRACE, O. M., SASLIS-LAGOUDAKIS, C. H., RONSTED, N., NILSSON, N. & SIMONSEN, H. T. 2015. Global medicinal uses of *Euphorbia* L. (Euphorbiaceae). *J. Ethnopharmacol.,* 176**,** 90-101.

FEUDJIO, F. T., DORNETSHUBER, R., LEMMENS, M., HOFFMANN, O., LEMMENS-GRUBER, R. & BERGER, W. 2010. Beauvericin and enniatin: emerging toxins and/or remedies? *World Mycotoxin J.,* 3**,** 415-430.

FIRAKOVA, S., PROKSA, B. & STURDIKOVA, M. 2007. Biosynthesis and biological activity of enniatins. *Pharmazie,* 62**,** 563-568.

FISCHER, E. & REIF, G. 1909. Synthesis of Polypeptides. XXVII. 2. Derivatives of Proline. *Justus Liebigs Ann. Chem.,* 363**,** 118-135.

FRONZA, G., FUGANTI, C. & SERRA, S. 2009. Stereochemical course of Baker's yeast mediated reduction of the tri- and tetrasubstituted double bonds of substituted cinnamaldehydes. *Eur. J. Org. Chem.*, 2009**,** 6160-6171.

GALLOP, M. A., BARRETT, R. W., DOWER, W. J., FODOR, S. P. A. & GORDON, E. M. 1994. Applications of Combinatorial Technologies to Drug Discovery. 1. Background and Peptide Combinatorial Libraries. *J. Med. Chem.,* 37**,** 1233-1251.

GARDES, M. & BRUNS, T. D. 1993. ITS primers with enhanced specificity for basidiomycetes - application to the identification of mycorrhizae and rusts. *Molecular Ecology,* 2**,** 113-118.

GARG, B. D., GUPTA, S. K., KRISHNASWAMY, N. R. & ARORA, R. B. 1970. Phytochemical and pharmacological investigations of *Anchusa strigosa* (Gaozban), and Indian medicinal plant. *J. Res. Indian Med.,* 4**,** 185-192.

GAUMANN, E. & ROTH, S. 1947. Enniatin, ein neues, gegen Mykobakterien wirksames Antibiotikum. *Experientia,* 3**,** 202-203.

GELADI, P. 2003. Chemometrics in spectroscopy. Part 1. Classical chemometrics. *Spectrochim. Acta, Part B,* 58B**,** 767-782.

GERARD, J., LLOYD, R., BARSBY, T., HADEN, P., KELLY, M. T. & ANDERSEN, R. J. 1997. Massetolides A−H, Antimycobacterial Cyclic Depsipeptides Produced by Two Pseudomonads Isolated from Marine Habitats. *J. Nat. Prod.,* 60**,** 223-229.

GERIS DOS SANTOS, R. M., RODRIGUES-FO, E., CALDAS ROCHA, W. & SIMAS TEIXEIRA, M. F. 2003. Endophytic fungi from *Melia azedarach*. *World J. Microbiol. Biotechnol.,* 19**,** 767-770.

GILLESPIE, D. E., BRADY, S. F., BETTERMANN, A. D., CIANCIOTTO, N. P., LILES, M. R., RONDON, M. R., CLARDY, J., GOODMAN, R. M. & HANDELSMAN, J. 2002. Isolation of antibiotics turbomycin A and B from a metagenomic library of soil microbial DNA. *Appl. Environ. Microbiol.,* 68**,** 4301-4306.

GIORDANO, L., GONTHIER, P., VARESE, G., MISERERE, L. & NICOLOTTI, G. 2009. Mycobiota inhabiting sapwood of healthy and declining Scots pine (*Pinus sylvestris* L.) trees in the Alps. *Fungal Diversity,* 38**,** 69-83.

GLOER, J. B. 2007. Applications of Fungal Ecology in the Search for New Bioactive Natural Products. *In:* KUBICEK, C. P. & DRUZHININA, I. S. (eds.) *Environmental and Microbial Relationships.* Springer Berlin Heidelberg.

GRAY, A. I., IGOLI, J. O. & EDRADA-EBEL, R. 2012. Natural products isolation in modern drug discovery programs. *Methods Mol. Biol. (N. Y., NY, U. S.),* 864**,** 515-534.

GRAYER, R. J. & KOKUBUN, T. 2001. Plant-fungal interactions: The search for phytoalexins and other antifungal compounds from higher plants. *Phytochemistry,* 56**,** 253-263.

GREEN, A. C. & BEARDMORE, G. L. 1988. Home treatment of skin cancer and solar keratoses. *Australas. J. Dermatol.,* 29**,** 127-30.

GREVE, H., SCHUPP, P. J., EGUEREVA, E., KEHRAUS, S., KELTER, G., MAIER, A., FIEBIG, H.-H. & KONIG, G. M. 2008. Apralactone A and a new stereochemical class of curvularins from the marine fungus *Curvularia* sp. *Eur. J. Org. Chem.*, 2008**,** 5085-5092.

GRIFFITHS, W. J., KOAL, T., WANG, Y., KOHL, M., ENOT, D. P. & DEIGNER, H.-P. 2010. Targeted Metabolomics for Biomarker Discovery. *Angew. Chem., Int. Ed.,* 49**,** 5426-5445.

GROVE, J. F. & HITCHCOCK, P. B. 1991. Metabolic products of *Fusarium acuminatum*: acuminatopyrone and chlamydosporol. *J. Chem. Soc., Perkin Trans. 1*, 0**,** 997-999.

GUO, M., WANG, Q.-B., WANG, Z.-W., JIA, L.-W. & WANG, Z.-Y. 2014. Screening and determination of anthraquinones secondary metabolites from endophytic fungi of *Rumex gmelini* Turcz. *Tianran Chanwu Yanjiu Yu Kaifa,* 26**,** 1634-1637.

HAMDAN, I. I. & AFIFI, F. U. 2008. Screening of Jordanian flora for α -Amylase inhibitory activity. *Pharm. Biol. (N. Y., NY, U. S.),* 46**,** 746-750.

HARDOIM, P. R. & VAN ELSAS, J. D. Properties of bacterial endophytes leading to maximized host fitness. 2013. Wiley-Blackwell, 405-411.

HARVEY, A. L. 2008. Natural products in drug discovery. *Drug Discov. Today,* 13**,** 894-901.

HARVEY, A. L., EDRADA-EBEL, R. & QUINN, R. J. 2015. The re-emergence of natural products for drug discovery in the genomics era. *Nat. Rev. Drug Discov.,* 14**,** 111-129.

HEMPHILL, C. F. P., DALETOS, G., PROKSCH, P., SUREECHATCHAIYAN, P., KASSACK, M. U., ORFALI, R. S. & LIN, W. 2017. OSMAC approach leads to new fusarielin metabolites from *Fusarium tricinctum*. *J. Antibiot. (Tokyo),* 70**,** 726-732.

HENTSCHEL, U., SCHMID, M., WAGNER, M., FIESELER, L., GERNERT, C. & HACKER, J. 2001. Isolation and phylogenetic analysis of bacteria with antimicrobial activities from the Mediterranean sponges *Aplysina aerophoba* and *Aplysina cavernicola*. *FEMS Microbiol. Ecol.,* 35**,** 305-312.

HILARIO, F., CHAPLA, V. M., ARAUJO, A. R., SANO, P. T., BAUAB, T. M. & DOS SANTOS, L. C. 2017. Antimicrobial screening of endophytic fungi isolated from the aerial parts of *Paepalanthus chiquitensis* (Eriocaulaceae) led to the isolation of secondary metabolites produced by *Fusarium fujikuroi*. *J. Braz. Chem. Soc.,* 28**,** 1389-1395.

HORAKOVA, K. & BETINA, V. 1977. Cytotoxic activity of macrocyclic substances from fungi. *Neoplasma,* 24**,** 21-27.

HORNBOGEN, T., GLINSKI, M. & ZOCHER, R. 2002. Biosynthesis of depsipeptide mycotoxins in *Fusarium*. *Eur. J. Plant Pathol.,* 108**,** 713-718.

HORTON, T. R. & BRUNS, T. D. 2001. The molecular revolution in ectomycorrhizal ecology: peeking into the black-box. *Mol. Ecol.,* 10**,** 1855-1871.

HOU, D.-X., FUJII, M., TERAHARA, N. & YOSHIMOTO, M. 2004. Molecular mechanisms behind the chemopreventive effects of anthocyanidins. *J. Biomed. Biotechnol.*, 5**,** 321-325.

HOYE, T. R., JEFFREY, C. S. & SHAO, F. 2007. Mosher ester analysis for the determination of absolute configuration of stereogenic (chiral) carbinol carbons. *Nat. Protoc.,* 2**,** 2451-2458.

HU, D. X., BIELITZA, M., KOOS, P. & LEY, S. V. 2012. A total synthesis of the ammonium ionophore, (-)-enniatin B. *Tetrahedron Lett.,* 53**,** 4077-4079.

HUA, J., XIAO, C.-J., LIU, Y., JING, S.-X., LUO, S.-H. & LI, S.-H. 2017. Chemical profile and defensive function of the latex of *Euphorbia peplus*. *Phytochemistry,* 136**,** 56-64.

HUBERT, J., NUZILLARD, J.-M., PURSON, S., HAMZAOUI, M., BORIE, N., REYNAUD, R. & RENAULT, J.-H. 2014. Identification of Natural Metabolites in Mixture: A Pattern Recognition Strategy Based on 13C NMR. *Anal. Chem. (Washington, DC, U. S.),* 86**,** 2955-2962.

HUDAIB, M. M., TAWAHA, K. A., MOHAMMAD, M. K., ASSAF, A. M., ISSA, A. Y., ALALI, F. Q., ABURJAI, T. A. & BUSTANJI, Y. K. 2011. Xanthine oxidase inhibitory activity of the methanolic extracts of selected Jordanian medicinal plants. *Pharmacogn. Mag.,* 7**,** 320-324.

HUSEIN, A. I., AL-NURI, M. A., ZATAR, N. A., JONDI, W., SALEEM, M. & ALI, S. 2012. Isolation and antifungal evaluation of *Rumex cyprius* Murb extracts. *J. Chem. Chem. Eng.,* 6**,** 547-550.

HYEON, S.-B., OZAKI, A., SUZUKI, A. & TAMURA, S. 1976. Isolation of αβ-dehydrocurvularin and β-hydroxycurvularin from Alternaria tomato as sporulation-suppressing factors. *Agric. Biol. Chem.,* 40**,** 1663-1664.

ICHIHARA, S., ICHIHARA, Y., TOMISAWA, H., FUKAZAWA, H. & TATEISHI, M. 1985. Identification of 5-deoxy-D-ribitol as a major metabolite of 5'-deoxy-5-fluorouridine in rats. *Drug Metab. Dispos.,* 13**,** 520-521.

JARADAT, N. A., AYESH, O. I. & ANDERSON, C. 2016a. Ethnopharmacological survey about medicinal plants utilized by herbalists and traditional practitioner healers for treatments of diarrhea in the West Bank/Palestine. *J. Ethnopharmacol.,* 182**,** 57-66.

JARADAT, N. A., DAMIRI, B. & ABUALHASAN, M. N. 2016b. Antioxidant evaluation for *Urtica urens, Rumex cyprius* and *Borago officinalis* edible wild plants in Palestine. *Pak. J. Pharm. Sci.,* 29**,** 325-330.

JESTOI, M. 2008. Emerging Fusarium-Mycotoxins Fusaproliferin, Beauvericin, Enniatins, And Moniliformin - A Review. *Crit. Rev. Food Sci. Nutr.,* 48**,** 21-49.

JI, Z., WU, W., WANG, M. & GU, A. 2005. Identification of fungicidal compounds from endophytic fungi *Fusarium proliferatum* in *Celastrus angulatus*. *J. Northwest Sci. Tech. Univer. Agric. Forest. (Natural Science Edition),* 33**,** 61-64.

JIANG, Z., BOYD, K. G., MEARNS-SPRAGG, A., ADAMS, D. R., WRIGHT, P. C. & BURGESS, J. G. 2000. Two diketopiperazines and one halogenated phenol from cultures of the marine bacterium, *Pseudoalteromonas luteoviolacea*. *Nat. Prod. Lett.,* 14**,** 435-440.

JORDA, J., JOUHTEN, P., CAMARA, E., MAAHEIMO, H., ALBIOL, J. & FERRER, P. 2012. Metabolic flux profiling of recombinant protein secreting *Pichia pastoris* growing on glucose:methanol mixtures. *Microb. Cell Fact.,* 11**,** 57-71.

KALAITZIS, J. A. 2013. Discovery, biosynthesis, and rational engineering of novel enterocin and wailupemycin polyketide analogues. *Methods Mol. Biol. (N. Y., NY, U. S.),* 1055**,** 171-189.

KAMAL, A., AHMAD, N., KHAN, M. A. & QURESHI, I. H. 1962. Biochemistry of microorganisms. I. Curvulin and curvulinic acid, metabolic products of *Curvalaria siddiquii*. *Tetrahedron,* 18**,** 433-436.

KITAJIMA, J., ISHIKAWA, T., TANAKA, Y. & IDA, Y. 1999. Water-soluble constituents of fennel. IX. Glucides and nucleosides. *Chem. Pharm. Bull.,* 47**,** 988-992.

KLOEPPER, J. W. & RYU, C.-M. 2006. Bacterial Endophytes as Elicitors of Induced Systemic Resistance. *In:* SCHULZ, B. J. E., BOYLE, C. J. C. & SIEBER, T. N. (eds.) *Microbial Root Endophytes.* Berlin, Heidelberg: Springer Berlin Heidelberg.

KNOBLOCH, T., DRAGER, G., COLLISI, W., SASSE, F. & KIRSCHNING, A. 2012. Unprecedented deoxygenation at C-7 of the ansamitocin core during mutasynthetic biotransformations. *Beilstein J. Org. Chem.,* 8**,** 861-869.

KOAZE, Y. 1960. Mechanism of L-prolyldioxopiperazine formation by *Streptomyces*. *Bull. Agric. Chem. Soc. Jpn.,* 24**,** 449-458.

KOBAYASHI, A., HINO, T., UNEYAMA, K. & KAWAZU, K. 1985. Chemical studies on microtuble assembly regulators of microbial origin. *Tennen Yuki Kagobutsu Toronkai Koen Yoshishu,* 27**,** 343-350.

KOBERL, M., WHITE, R. A., 3RD, JANSSON, J. K., ERSCHEN, S., BERG, G. & EL-ARABI, T. F. 2015. Draft Genome Sequence of *Paenibacillus polymyxa* Strain Mc5Re-14, an Antagonistic Root Endophyte of *Matricaria chamomilla*. *Genome Announc.,* 3.

KOHLI, K. & ALI, M. 2003. Phytochemical studies of Iranian *Anchusa strigosa* Linn. *Recent Progress in Medicinal Plants,* 2**,** 247-251.

KOPP, F. & MARAHIEL, M. A. 2007. Where chemistry meets biology: the chemoenzymatic synthesis of nonribosomal peptides and polyketides. *Curr. Opin. Biotechnol.,* 18**,** 513-520.

KOYAMA, K., TAKAHASHI, K., NATORI, S. & UDAGAWA, S. 1991. Production of mycotoxins by *Chaetomium* species. *Maikotokishin (Tokyo),* 33**,** 40-43.

KRUG, D. & MULLER, R. 2014. Secondary metabolomics: the impact of mass spectrometry-based approaches on the discovery and characterization of microbial natural products. *Nat. Prod. Rep.,* 31**,** 768-783.

KUSARI, P., KUSARI, S., ECKELMANN, D., ZUEHLKE, S., KAYSER, O. & SPITELLER, M. 2016. Cross-species biosynthesis of maytansine in *Maytenus serrata*. *RSC Adv.,* 6**,** 10011-10016.

KUSARI, S., SINGH, S. & JAYABASKARAN, C. 2014. Biotechnological potential of plant-associated endophytic fungi: hope versus hype. *Trends Biotechnol.,* 32**,** 297-303.

KUSARI, S. & SPITELLER, M. 2011. Are we ready for industrial production of bioactive plant secondary metabolites utilizing endophytes? *Nat. Prod. Rep.,* 28**,** 1203-1207.

KYEKYEKU, J. O., KUSARI, S., SPITELLER, M., ADOSRAKU, R. K., BULLACH, A., GOLZ, C. & STROHMANN, C. 2017. Antibacterial secondary metabolites from an endophytic fungus, *Fusarium solani* JK10. *Fitoterapia,* 119**,** 108-114.

LAI, S., SHIZURI, Y., YAMAMURA, S., KAWAI, K. & FURUKAWA, H. 1991. New curvularin-type metabolites from the hybrid strain ME 0005 derived from *Penicillium citreo-viride* B. IFO 4692 and 6200. *Bull. Chem. Soc. Jpn.,* 64**,** 1048-1050.

LAI, S., SHIZURI, Y., YAMAMURA, S., KAWAI, K., TERADA, Y. & FURUKAWA, H. 1989. Novel curvularin-type metabolites of a hybrid strain ME 0005 derived from *Penicillium citreo-viride B*. IFO 6200 and 4692. *Tetrahedron Lett.,* 30**,** 2241-2244.

LI, H., TIAN, J.-M., TANG, H.-Y., PAN, S.-Y., ZHANG, A.-L. & GAO, J.-M. 2015a. Chaetosemins A-E, new chromones isolated from an ascomycete *Chaetomium seminudum* and their biological activities. *RSC Adv.,* 5**,** 29185-29192.

LI, T.-X., YANG, M.-H., WANG, X.-B., WANG, Y. & KONG, L.-Y. 2015b. Synergistic antifungal meroterpenes and dioxolanone derivatives from the endophytic fungus *Guignardia* sp. *J. Nat. Prod.,* 78**,** 2511-2520.

LI, W., YANG, X., YANG, Y., DUANG, R., CHEN, G., LI, X., LI, Q., QIN, S., LI, S., ZHAO, L. & DING, Z. 2016. Anti-phytopathogen, multi-target acetylcholinesterase inhibitory and antioxidant activities of metabolites from endophytic *Chaetomium globosum*. *Nat. Prod. Res.,* 30**,** 2616-2619.

LIU, L.-F., TAN, G.-S., LIU, L.-F., ZHANG, H., QI, H., WANG, X.-M. & WANG, J.-D. 2017a. A new androstanoid metabolite from a soil fungus *Curvularia borreriae* strain HS-FG-237. *Nat. Prod. Res.,* 31**,** 1080-1084.

LIU, R., LI, X. & LAM, K. S. 2017b. Combinatorial chemistry in drug discovery. *Curr. Opin. Chem. Biol.,* 38**,** 117-126.

LUDWIG-MULLER, J. 2015. Plants and endophytes: equal partners in secondary metabolite production? *Biotechnol. Lett.,* 37**,** 1325-1334.

LUGTENBERG, B. J. J., CHIN-A-WOENG, T. F. C. & BLOEMBERG, G. V. 2002. Microbe-plant interactions: principles and mechanisms. *A. Van. Leeuw.,* 81**,** 373-383.

LUO, J., YAN, Z.-Y., GUO, X.-H. & WANG, Y.-L. 2007. Isolation, identification and the antibacterial activity of endophytic fungi in *Euphorbia nematocypha* Hand.-Mazz. *Huaxi Yaoxue Zazhi,* 22**,** 380-382.

LUZ, C., SALADINO, F., LUCIANO, F. B., MANES, J. & MECA, G. 2017. Occurrence, toxicity, bioaccessibility and mitigation strategies of beauvericin, a minor *Fusarium* mycotoxin. *Food Chem. Toxicol.,* 107**,** 430-439.

MACHAVARIANI, N. G., IVANKOVA, T. D., SINEVA, O. N. & TEREKHOVA, L. P. 2014. Isolation of endophytic actinomycetes from medicinal plants of the Moscow region, Russia. *World Appl. Sci. J.,* 30**,** 1599-1604.

MACINTYRE, L., ZHANG, T., VIEGELMANN, C., JUAREZ MARTINEZ, I., CHENG, C., DOWDELLS, C., ABDELMOHSEN, U. R., GERNERT, C., HENTSCHEL, U. & EDRADA-EBEL, R. 2014. Metabolomic Tools for Secondary Metabolite Discovery from Marine Microbial Symbionts. *Mar. Drugs,* 12**,** 3416-3448.

MANDAL, S., MOUDGIL, M. N. & MANDAL, S. K. 2009. Rational drug design. *Eur. J. Pharmacol.,* 625**,** 90-100.

MAREE, J., KAMATOU, G., GIBBONS, S., VILJOEN, A. & VAN VUUREN, S. 2014. The application of GC-MS combined with chemometrics for the identification of antimicrobial compounds from selected commercial essential oils. *Chemom. Intell. Lab. Syst.,* 130**,** 172-181.

MARTINEZ-KLIMOVA, E., RODRÍGUEZ-PEÑA, K. & SÁNCHEZ, S. 2017. Endophytes as sources of antibiotics. *Biochem. Pharmacol.,* 134**,** 1-17.

MAYS, T. D. & MAZAN, K. D. 1996. Legal issues in sharing the benefits of biodiversity prospecting. *J. Ethnopharmacol.,* 51**,** 93-109.

MCCHESNEY, J. D., VENKATARAMAN, S. K. & HENRI, J. T. 2007. Plant natural products: Back to the future or into extinction? *Phytochemistry,* 68**,** 2015-2022.

MOK, D. K. W. & CHAU, F.-T. 2006. Chemical information of Chinese medicines: A challenge to chemist. *Chemom. Intell. Lab. Syst.,* 82**,** 210-217.

MONDOL, M. A. M., LAATSCH, H., FARTHOUSE, J., ISLAM, M. T. & SCHUFFLER, A. 2017. Metabolites from the Endophytic Fungus *Curvularia* sp. M12 Act as Motility Inhibitors against P*hytophthora capsici* Zoospores. *J. Nat. Prod.,* 80**,** 347-355.

MONGE, A., CHORGHADE, M., ERHARDT, P. W., GANELLIN, C. R., KOGA, N., LINDBERG, P., PERUN, T. J., TOPLISS, J. G., TRIVEDI, B. K. & WERMUTH, C. G. 2000. Medicinal chemistry in the development of societies, biodiversity and natural products. *Ing. Cienc. Quim.,* 19**,** 50-53.

MUCCIARELLI, M., SCANNERINI, S., BERTEA, C. & MAFFEI, M. 2003. In vitro and in vivo Peppermint (*Mentha piperita*) Growth Promotion by Nonmycorrhizal Fungal Colonization. *New Phytol.,* 158**,** 579-591.

MUELLER, B. A. 2009. Imatinib and its successors - how modern chemistry has changed drug development. *Curr. Pharm. Des.,* 15**,** 120-133.

MUNRO, H. D., MUSGRAVE, O. C. & TEMPLETON, R. 1967. Curvularian. V. Compound C16H18O5, α,β-dehydrocurvularin. *J. Chem. Soc. C***,** 947-948.

MUSGRAVE, O. C. 1956. Curvularin. I. Isolation and partial characterization of a metabolic product from a new species of *Curvularia*. *J. Chem. Soc.***,** 4301-4305.

NAH, J.-H., KIM, H.-J., LEE, H.-N., LEE, M.-J., CHOI, S.-S. & KIM, E.-S. 2013. Identification and Biotechnological Application of Novel Regulatory Genes Involved in Streptomyces Polyketide Overproduction through Reverse Engineering Strategy. *BioMed. Res. Int.,* 2013**,** 549737.

NANBA, T., KADOTA, S., SHIMOMURA, K., IIDA, K. & YAMABE, Y. 1996. *Cosmetics containing extracts of Rumex cyprius*. Copyright (C) 2015 American Chemical Society (ACS). All Rights Reserved.

NEWMAN, D. J. & CRAGG, G. M. 2012. Natural Products As Sources of New Drugs over the 30 Years from 1981 to 2010. *J. Nat. Prod.,* 75**,** 311-335.

NEWMAN, D. J. & CRAGG, G. M. 2016. Natural Products as Sources of New Drugs from 1981 to 2014. *J. Nat. Prod.,* 79**,** 629-661.

NISA, H., KAMILI, A. N., NAWCHOO, I. A., SHAFI, S., SHAMEEM, N. & BANDH, S. A. 2015. Fungal endophytes as prolific source of phytochemicals and other bioactive natural products: A review. *Microb. Pathogenesis,* 82**,** 50-59.

NOBELI, I. & THORNTON, J. M. 2006. A bioinformatician's view of the metabolome. *Bioessays,* 28**,** 534-545.

OLA, A. R. B., THOMY, D., LAI, D., BROETZ-OESTERHELT, H. & PROKSCH, P. 2013. Inducing Secondary Metabolite Production by the Endophytic Fungus *Fusarium tricinctum* through Coculture with *Bacillus subtilis*. *J. Nat. Prod.,* 76**,** 2094-2099.

OMURA, S., TOMODA, H. & KUMAGAI, H. 1987. Potent inhibitory effect of antibiotic 1233A, which specifically blocks 3-hydroxy-3-methylglutaryl coenzyme A synthase, on cholesterol biosynthesis. *J. Antibiot.,* 40**,** 1356-1357.

OWEN, N. L. & HUNDLEY, N. 2004. Endophytes: The chemical synthesizers inside plants. *Sci. Prog.,* 87**,** 79-99.

PANG, Y.-W., ZHANG, L.-J., FANG, J.-S., LIU, Q.-F., ZHANG, H., XIANG, W.-S., WANG, J.-D. & WANG, X.-J. 2013. Two new antitumor constituents from a soil fungus *Curvularia inaequalis* (strain HS-FG-257). *J. Antibiot.,* 66**,** 287-289.

PEAY, K. G., KENNEDY, P. G. & BRUNS, T. D. 2008. Fungal Community Ecology: A Hybrid Beast with a Molecular Master. *BioScience,* 58**,** 799-810.

PLUSKAL, T., CASTILLO, S., VILLAR-BRIONES, A. & OREŠIČ, M. 2010. MZmine 2: Modular framework for processing, visualizing, and analyzing mass spectrometry-based molecular profile data. *BMC Bioinformatics,* 11**,** 395-406.

PONTIUS, A., MOHAMED, I., KRICK, A., KEHRAUS, S. & KOENIG, G. M. 2008. Aromatic Polyketides from Marine Algicolous Fungi. *J. Nat. Prod.,* 71**,** 272-274.

QASEM, J. R. 2015. Prospects of wild medicinal and industrial plants of saline habitats in the Jordan valley. *Pak. J. Bot.,* 47**,** 551-570.

QUINN, R. J., CARROLL, A. R., PHAM, N. B., BARON, P., PALFRAMAN, M. E., SURAWEERA, L., PIERENS, G. K. & MURESAN, S. 2008. Developing a drug-like natural product library. *J. Nat. Prod.,* 71**,** 464-468.

RAJALAHTI, T. & KVALHEIM, O. M. 2011. Multivariate data analysis in pharmaceutics: A tutorial review. *Int. J. Pharm.,* 417**,** 280-290.

REINHOLD-HUREK, B. & HUREK, T. 2011. Living inside plants: bacterial endophytes. *Curr. Opin. Plant Biol.,* 14**,** 435-43.

RISHTON, G. M. 2008. Natural products as a robust source of new drugs and drug leads: past successes and present day issues. *Am. J. Cardiol.,* 101**,** 43-49.

ROCHA, R., DA, L. D. E., ENGELS, C., PILEGGI, S. A. V., DE, S. J. F. D., MATIELLO, R. R. & PILEGGI, M. 2009. Selection of endophytic fungi from comfrey (*Symphytum officinale* L.) for in vitro biological control of the phytopathogen *Sclerotinia sclerotiorum* (Lib.). *Braz. J. Microbiol,* 40**,** 73-78.

ROCHFORT, S. 2005. Metabolomics Reviewed: A New "Omics" Platform Technology for Systems Biology and Implications for Natural Products Research. *J. Nat. Prod.,* 68**,** 1813-1820.

RODRIGUES DE CARVALHO, C., VIEIRA, M. D. L. A., CANTRELL, C. L., WEDGE, D. E., ALVES, T. M. A., ZANI, C. L., PIMENTA, R. S., SALES, P. A., JR., MURTA, S. M. F., ROMANHA, A. J., ROSA, C. A. & ROSA, L. H. 2015. Biological activities of ophiobolin K and 6-epi-ophiobolin K produced by the endophytic fungus *Aspergillus calidoustus*. *Nat. Prod. Res.*, 30, 478-481.

SAEPUDIN, E. & HARRISON, P. 1995. The biosynthesis of antibiotic F-244 in *Fusarium* sp. ATCC 20788: origin of the carbon, hydrogen, and oxygen atoms. *Can. J. Chem.,* 73**,** 1-5.

SAIKKONEN, K., FAETH, S. H., HELANDER, M. & SULLIVAN, T. J. 1998. FUNGAL ENDOPHYTES: A Continuum of Interactions with Host Plants. *Annu. Rev. Ecol. Evol. Syst.,* 29**,** 319-343.

SAIKKONEN, K., WALI, P., HELANDER, M. & FAETH, S. H. 2004. Evolution of endophyte-plant symbioses. *Trends Plant Sci.,* 9**,** 275-280.

SALIM, M. L., AMMAR, H. A., ABDERRUHMAN, S. & EL-REMAWY, H. A. 1996. Phytochemical screening and antimicrobial activity of wild Jordanian plants from Al-Balq'a. *Bull. Fac. Pharm.,* 34**,** 235-238.

SAMAGA, P. V. & RAI, V. R. 2016. Diversity and bioactive potential of endophytic fungi from *Nothapodytes foetida*, *Hypericum mysorense* and *Hypericum japonicum* collected from Western Ghats of India. *Ann. Microbiol.,* 66**,** 229-244.

SANKA LOGANATHACHETTI, D. & MUTHURAMAN, S. 2015. Biomedical potential of natural products derived through metagenomic approaches. *RSC Adv.,* 5**,** 101200-101213.

SARKER, S. D. & NAHAR, L. 2012. An introduction to natural products isolation. *Methods Mol. Biol.,* 864**,** 1-25.

SCHERLACH, K. & HERTWECK, C. 2009. Triggering cryptic natural product biosynthesis in microorganisms. *Org. Biomol. Chem.,* 7**,** 1753-1760.

SCHLOERKE, O. & ZEECK, A. 2006. Orsellides A-E: an example for 6-deoxyhexose derivatives produced by fungi. *Eur. J. Org. Chem.*, 1043-1049.

SCHULZ, B. & BOYLE, C. 2005. The endophytic continuum. *Mycol. Res.,* 109, 661-686.

SCHULZ, B., BOYLE, C., DRAEGER, S., ROEMMERT, A.-K. & KROHN, K. 2002. Endophytic fungi: a source of novel biologically active secondary metabolites. *Mycol. Res.,* 106, 996-1004.

SHAH, A., HASSAN, Q. P., MUSHTAQ, S., SHAH, A. M., HUSSAIN, A., SHAH, A., HASSAN, Q. P., SHAH, A. M. & HUSSAIN, A. 2017. Chemoprofile and functional diversity of fungal and bacterial endophytes and role of ecofactors - A review. *J. Basic Microbiol.,* 57, 814-826.

SHERAMETI, I., SHAHOLLARI, B., VENUS, Y., ALTSCHMIED, L., VARMA, A. & OELMUELLER, R. 2005. The Endophytic Fungus Piriformospora indica Stimulates the Expression of Nitrate Reductase and the Starch-degrading Enzyme Glucan-water Dikinase in Tobacco and Arabidopsis Roots through a Homeodomain Transcription Factor That Binds to a Conserved Motif in Their Promoters. *J. Biol. Chem.,* 280, 26241-26247.

SICILIANO, T., DE LEO, M., BADER, A., DE TOMMASI, N., VRIELING, K., BRACA, A. & MORELLI, I. 2005. Pyrrolizidine alkaloids from *Anchusa strigosa* and their antifeedant activity. *Phytochemistry,* 66, 1593-1600.

SIEBER, T. N. 2007. Endophytic fungi in forest trees: are they mutualists? *Fungal Biol. Rev.,* 21, 75-89.

SIEGEL, R. L., MILLER, K. D. & JEMAL, A. 2017. Cancer Statistics, 2017. *CA Cancer J. Clin.,* 67, 7-30.

SONG, Z.-Q., MU, S.-Z., DI, Y.-T. & HAO, X.-J. 2010. A new jatrophane diterpenoid from *Euphorbia peplus*. *Zhongguo Tianran Yaowu,* 8, 81-83.

STEVENS, D. C., CONWAY, K. R., PEARCE, N., VILLEGAS-PEÑARANDA, L. R., GARZA, A. G. & BODDY, C. N. 2013. Alternative Sigma Factor Over-Expression Enables Heterologous Expression of a Type II Polyketide Biosynthetic Pathway in *Escherichia coli*. *PLOS ONE,* 8, e64858.

STIERLE, A., STROBEL, G. & STIERLE, D. 1993a. Taxol and taxane production by *Taxomyces andreanae*, an endophytic fungus of Pacific yew. *Science,* 260, 214-217.

STIERLE, A., STROBEL, G. & STIERLE, D. 1993b. Taxol and taxane production by *Taxomyces andreanae*, an endophytic fungus of Pacific yew. *Science,* 260, 214-216.

STIERLE, A., STROBEL, G., STIERLE, D., GROTHAUS, P. & BIGNAMI, G. 1995. The search for a taxol-producing microorganism among the endophytic fungi of the Pacific yew, *Taxus brevifolia*. *J. Nat. Prod.,* 58, 1315-1324.

STROBEL, G. & DAISY, B. 2003. Bioprospecting for microbial endophytes and their natural products. *Microbiol. Mol. Biol. Rev.,* 67, 491-502.

STROBEL, G., DAISY, B., CASTILLO, U. & HARPER, J. 2004. Natural products from endophytic microorganisms. *J. Nat. Prod.,* 67, 257-268.

STROBEL, G. A. 2003. Endophytes as sources of bioactive products. *Microbes Infect.,* 5, 535-544.

STROBEL, G. A., MILLER, R. V., MARTINEZ-MILLER, C., CONDRON, M. M., TEPLOW, D. B. & HESS, W. M. 1999. Cryptocandin, a potent antimycotic from the endophytic fungus *Cryptosporiopsis cf. quercina*. *Microbiology,* 145, 1919-1926.

SUDHA, V., GOVINDARAJ, R., BASKAR, K., AL-DHABI, N. A. & DURAIPANDIYAN, V. 2016. Biological properties of endophytic fungi. *Braz. Arch. Biol. Technol.,* 59, 1-7.

SUMNER, L. W., MENDES, P. & DIXON, R. A. 2003. Plant metabolomics: large-scale phytochemistry in the functional genomics era. *Phytochemistry,* 62, 817-836.

SWINNEY, D. C. & ANTHONY, J. 2011. How were new medicines discovered? *Nat. Rev. Drug Discov.,* 10**,** 507-19.

SY-CORDERO, A. A., PEARCE, C. J. & OBERLIES, N. H. 2012. Revisiting the enniatins: a review of their isolation, biosynthesis, structure determination and biological activities. *J. Antibiot.,* 65**,** 541-549.

SYED, B., PRASAD, M. N. N., RAO, H. C. Y., RAKSHITH, D., MAITHRI, B., KAVITHA, K. S., AZMATH, P., KAVITHA, H. U., HARINI, B. P., KUMAR, K., ZAREI, M. & SATISH, S. 2015. Actinomycetic Symbionts Inhabiting *Euphorbia hirta* L. with Antimicrobial Potentials. *J. Biol. Act. Prod. Nat.,* 5**,** 419-426.

TAGHAVI, S., BARAC, T., GREENBERG, B., BORREMANS, B., VANGRONSVELD, J. & VAN DER LELIE, D. 2005. Horizontal gene transfer to endogenous endophytic bacteria from poplar improves phytoremediation of toluene. *Appl. Environ. Microbiol.,* 71**,** 8500-8505.

TAWAHA, K., ALALI, F. Q., GHARAIBEH, M., MOHAMMAD, M. & EL-ELIMAT, T. 2007. Antioxidant activity and total phenolic content of selected Jordanian plant species. *Food Chem.,* 104**,** 1372-1378.

TAWAHA, K. A., ALALI, F. Q. & HUDAIB, M. M. 2015. Chemical Composition and General Cytotoxicity Evaluation of Essential Oil from the Flowers of *Anthemis palestina* Reut. ex Boiss., Growing in Jordan. *J. Essent. Oil-Bear. Plants,* 18**,** 1070-1077.

TAWFIKE, A. F., ABBOTT, G., YOUNG, L. & EDRADA-EBEL, R. 2017. Metabolomic-Guided Isolation of Bioactive Natural Products from *Curvularia* sp., an Endophytic Fungus of *Terminalia laxiflora*. *Planta Med.*, 84**,** 182-190.

TAWFIKE, A. F., VIEGELMANN, C. & EDRADA-EBEL, R. 2013. Metabolomics and dereplication strategies in natural products. *Methods Mol. Biol.,* 1055**,** 227-244.

TAYLOR, T. N. & TAYLOR, E. L. 2000. The Rhynie chert ecosystem: a model for understanding fungal interactions. *In:* BACON, C. W. & WHITE JR., J. F. (eds.) *Microbial Endophytes.* New York: Marcel Dekker, Inc.

THOMASSET, S., TELLER, N., CAI, H., MARKO, D., BERRY, D. P., STEWARD, W. P. & GESCHER, A. J. 2009. Do anthocyanins and anthocyanidins, cancer chemopreventive pigments in the diet, merit development as potential drugs? *Cancer Chemother. Pharmacol.,* 64**,** 201-211.

TOMODA, H., OHBAYASHI, N., KUMAGAI, H., HASHIZUME, H., SUNAZUKA, T. & OMURA, S. 1999. Differential inhibition of HMG-CoA synthase and pancreatic lipase by the specific chiral isomers of beta-lactone DU-6622. *Biochem. Biophys. Res. Commun.,* 265**,** 536-40.

TORRE, L. A., BRAY, F., SIEGEL, R. L., FERLAY, J., LORTET-TIEULENT, J. & JEMAL, A. 2015. Global cancer statistics, 2012. *CA Cancer J. Clin.,* 65**,** 87-108.

TOYA, Y. & SHIMIZU, H. 2013. Flux analysis and metabolomics for systematic metabolic engineering of microorganisms. *Biotechnol. Adv.,* 31**,** 818-826.

TRIBA, M. N., LE MOYEC, L., AMATHIEU, R., GOOSSENS, C., BOUCHEMAL, N., NAHON, P., RUTLEDGE, D. N. & SAVARIN, P. 2015. PLS/OPLS models in metabolomics: the impact of permutation of dataset rows on the K-fold cross-validation quality parameters. *Mol. Biosyst.,* 11**,** 13-19.

TUNTIWACHWUTTIKUL, P., TAECHOWISAN, T., WANBANJOB, A., THADANITI, S. & TAYLOR, W. C. 2008. Lansai A-D, secondary metabolites from *Streptomyces* sp. SUC1. *Tetrahedron,* 64**,** 7583-7586.

UMA, A. K. P. G. & MYTHILI, S. 2017. Antioxidant and hepatoprotective potentials of novel endophytic fungus *Achaetomium* sp., from *Euphorbia hirta*. *Asian. Pac. J. Trop. Med.,* 10**,** 588-593.

VERMA, V. C., KHARWAR, R. N. & STROBEL, G. A. 2009. Chemical and functional diversity of natural products from plant associated endophytic fungi. *Nat. Prod. Commun.,* 4**,** 1511-1532.

VIEIRA, M. L. A., JOHANN, S., HUGHES, F. M., ROSA, C. A. & ROSA, L. H. 2014. The diversity and antimicrobial activity of endophytic fungi associated with medicinal plant *Baccharis trimera* (Asteraceae) from the Brazilian savannah. *Can. J. Microbiol.,* 60**,** 847-856.

VISCONTI, A., BLAIS, L. A., APSIMON, J. W., GREENHALGH, R. & MILLER, J. D. 1992. Production of enniatins by *Fusarium acuminatum* and *Fusarium compactum* in liquid culture: isolation and characterization of three new enniatins, B2, B3, and B4. *J. Agric. Food Chem.,* 40**,** 1076-1082.

WAGENAAR, M. M. 2008. Pre-fractionated microbial samples--the second generation natural products library at Wyeth. *Molecules,* 13**,** 1406-1426.

WALL, P. E. 2005. *Thin-Layer Chromatography: A Modern Practical Approach,* Cambridge, UK, The Royal Society of Chemistry.

WAN, J. 2015. *A topical Chinese medicine for treating sore, furuncle and pyogenic infections*. Copyright (C) 2015 American Chemical Society (ACS). All Rights Reserved.

WAN, L.-S., CHU, R., PENG, X.-R., ZHU, G.-L., YU, M.-Y., LI, L., ZHOU, L., LU, S.-Y., DONG, J.-R., ZHANG, Z.-R., LI, Y., QIU, M.-H., CHU, R., ZHU, G.-L., YU, M.-Y., LI, L., LU, S.-Y., DONG, J.-R. & QIU, M.-H. 2016. Pepluane and Paraliane Diterpenoids from *Euphorbia peplu*s with Potential Anti-inflammatory Activity. *J. Nat. Prod.,* 79**,** 1628-1634.

WANG, B., WANG, Z.-Y., WANG, X.-X., ZHENG, C.-L. & WEI, L.-M. 2012. Studies on chemical constituents of RGT-S11 mycelium from *Rumex gmelini* turcz. *Yaowu Shengwu Jishu,* 19**,** 332-333.

WANG, F.-Q., TONG, Q.-Y., MA, H.-R., XU, H.-F., HU, S., MA, W., XUE, Y.-B., LIU, J.-J., WANG, J.-P., SONG, H.-P., ZHANG, J.-W., ZHANG, G. & ZHANG, Y.-H. 2015. Indole diketopiperazines from endophytic *Chaetomium* sp. 88194 induce breast cancer cell apoptotic death. *Sci. Rep.,* 5**,** 9294.

WANG, F., JIANG, J., HU, S., MA, H., ZHU, H., TONG, Q., CHENG, L., HAO, X., ZHANG, G. & ZHANG, Y. 2017. Secondary metabolites from endophytic fungus *Chaetomium* sp. induce colon cancer cell apoptotic death. *Fitoterapia,* 121**,** 86-93.

WANI, K., SABOO, S., SOLANKE, P. & TIDK, P. 2016. Production of novel secondary metabolites from endophytic fungi by using fermentation process. *Indo Am. J. Pharm. Res.,* 6**,** 4957-4961.

WANI, M. C., TAYLOR, H. L., WALL, M. E., COGGON, P. & MCPHAIL, A. T. 1971. Plant antitumor agents. VI. Isolation and structure of taxol, a novel antileukemic and antitumor agent from Taxus brevifolia. *J. Amer. Chem. Soc.,* 93**,** 2325-2327.

WANI, Z. A., ASHRAF, N., MOHIUDDIN, T. & RIYAZ-UL-HASSAN, S. 2015. Plant-endophyte symbiosis, an ecological perspective. *Appl. Microbiol. Biotechnol.,* 99**,** 2955-2965.

WATANABE, K. & OIKAWA, H. 2007. Robust platform for de novo production of heterologous polyketides and nonribosomal peptides in *Escherichia coli*. *Org. Biomol. Chem.,* 5**,** 593-602.

WEBSTER, J. & WEBER, R. 2007. *Introduction to Fungi*, Cambridge University Press.

WIKLUND, S. 2008. *Multivariate Data Analysis for Omics*, Umetrics.

WOLD, S. & SJOSTROM, M. 1998. Chemometrics, present and future success. *Chemom. Intell. Lab. Syst.,* 44**,** 3-14.

WU, C., KIM, H. K., VAN WEZEL, G. P. & CHOI, Y. H. 2015. Metabolomics in the natural products field – a gateway to novel antibiotics. *Drug Discov. Today: Technologies*, 13**,** 1-46.

YU, F.-X., CHEN, Y., YANG, Y.-H. & ZHAO, P.-J. 2016. Four new dimeric spiro-azaplilone derivatives cochliodones E-H from the entophytic fungus *Chaetomium* sp. M336. *Phytochem. Lett.,* 16**,** 263-267.

YU, H., ZHANG, L., LI, L., ZHENG, C., GUO, L., LI, W., SUN, P. & QIN, L. 2010. Recent developments and future prospects of antimicrobial metabolites produced by endophytes. *Microbiol. Res.,* 165**,** 437-449.

YUAN, Z.-L., DAI, C.-C. & CHEN, L.-Q. 2007. Regulation and accumulation of secondary metabolites in plant-fungus symbiotic system. *Afr. J. Biotechnol.,* 6**,** 1266-1271.

YULIANA, N. D., KHATIB, A., CHOI, Y. H. & VERPOORTE, R. 2011. Metabolomic for bioactivity assessment of natural products. *Phytother. Res.,* 25**,** 157-169.

YURCHENKO, A. N., SMETANINA, O. F., KHUDYAKOVA, Y. V., KIRICHUK, N. N., YURCHENKO, E. A. & AFIYATULLOV, S. S. 2013. Metabolites of the marine isolate of the fungus *Curvularia inaequalis*. *Chem. Nat. Compd.,* 49**,** 163-164.

ZARCHI, K. & JEMEC, G. B. E. 2015. Ingenol mebutate: from common weed to cancer cure. *Curr. Probl. Dermatol.,* 46**,** 136-42.

ZHAN, J., WIJERATNE, E. M. K., SELIGA, C. J., ZHANG, J., PIERSON, E. E., PIERSON, L. S., III, VANETTEN, H. D. & GUNATILAKA, A. A. L. 2004. A new anthraquinone and cytotoxic curvularins of a *Penicillium* sp. from the rhizosphere of *Fallugia paradox*a of the Sonoran desert. *J. Antibiot.,* 57**,** 341-344.

ZHANG, P., LI, X. & WANG, B.-G. 2016. Secondary Metabolites from the Marine Algal-Derived Endophytic Fungi: Chemical Diversity and Biological Activity. *Planta Med.,* 82**,** 832-842.

ZHANG, Q., LI, H. Q., ZONG, S. C., GAO, J. M. & ZHANG, A. L. 2012. Chemical and bioactive diversities of the genus *Chaetomium* secondary metabolites. *Mini-Rev. Med. Chem.,* 12**,** 127-148.

ZHANG, Z., HE, X., ZHANG, G., CHE, Q., ZHU, T., GU, Q. & LI, D. 2017. Inducing Secondary Metabolite Production by Combined Culture of Talaromyces aculeatus and *Penicillium variabile*. *J. Nat. Prod.,* 80**,** 3167-3171.

ZHU, F., CAI, J., WU, X., HUANG, J., HUANG, L., ZHU, J., ZHENG, Q., CEN, P. & XU, Z. 2013. The main byproducts and metabolic flux profiling of γ-PGA-producing strain B. subtilis ZJU-7 under different pH values. *J. Biotechnol.,* 164**,** 67-74.

Appendices

Appendix I: BLAST results for *Curvularia australiensis*, *Chaetomium subaffine* and *Fusarium acuminatum*

A. *Curvularia australiensis*

Score	Expect	Identities	Gaps	Strand
966 bits(523)	0.0	523/523(100%)	0/523(0%)	Plus/Plus

```
Query  1    GCCGTTCGCGGCTGGACTATTTATTACCCTTGTCTTTTGCGCACTTGTTGTTTCCTGGGC  60
            ||||||||||||||||||||||||||||||||||||||||||||||||||||||||||||
Sbjct  49   GCCGTTCGCGGCTGGACTATTTATTACCCTTGTCTTTTGCGCACTTGTTGTTTCCTGGGC  108

Query  61   GGGTTCGCTCGCCACCAGGACCACAATATAAACCTTTTTTATGCAGTTGCAATCAGCGTC  120
            ||||||||||||||||||||||||||||||||||||||||||||||||||||||||||||
Sbjct  109  GGGTTCGCTCGCCACCAGGACCACAATATAAACCTTTTTTATGCAGTTGCAATCAGCGTC  168

Query  121  AGTATAACAAATGTAAATCATTTACAACTTTCAACAACGGATCTCTTGGTTCTGGCATCG  180
            ||||||||||||||||||||||||||||||||||||||||||||||||||||||||||||
Sbjct  169  AGTATAACAAATGTAAATCATTTACAACTTTCAACAACGGATCTCTTGGTTCTGGCATCG  228

Query  181  ATGAAGAACGCAGCGAAATGCGATACGTAGTGTGAATTGCAGAATTCAGTGAATCATCGA  240
            ||||||||||||||||||||||||||||||||||||||||||||||||||||||||||||
Sbjct  229  ATGAAGAACGCAGCGAAATGCGATACGTAGTGTGAATTGCAGAATTCAGTGAATCATCGA  288

Query  241  ATCTTTGAACGCACATTGCGCCCTTTGGTATTCCAAAGGGCATGCCTGTTCGAGCGTCAT  300
            ||||||||||||||||||||||||||||||||||||||||||||||||||||||||||||
Sbjct  289  ATCTTTGAACGCACATTGCGCCCTTTGGTATTCCAAAGGGCATGCCTGTTCGAGCGTCAT  348

Query  301  TTGTACCCTCAAGCTTTGCTTGGTGTTGGGCGTTTTTGTCTTTGGCCCGCCAAAGACTCG  360
            ||||||||||||||||||||||||||||||||||||||||||||||||||||||||||||
Sbjct  349  TTGTACCCTCAAGCTTTGCTTGGTGTTGGGCGTTTTTGTCTTTGGCCCGCCAAAGACTCG  408

Query  361  CCTTAAAATGATTGGCAGCCGGCCTACTGGTTTCGCAGCGCAGCACATTTTTGCGCTTGC  420
            ||||||||||||||||||||||||||||||||||||||||||||||||||||||||||||
Sbjct  409  CCTTAAAATGATTGGCAGCCGGCCTACTGGTTTCGCAGCGCAGCACATTTTTGCGCTTGC  468

Query  421  AATCAGCAAAAGAGGACGGCAATCCATCAAGACTCCTTCTCACGTTTGACCTCGGATCAG  480
            ||||||||||||||||||||||||||||||||||||||||||||||||||||||||||||
Sbjct  469  AATCAGCAAAAGAGGACGGCAATCCATCAAGACTCCTTCTCACGTTTGACCTCGGATCAG  528

Query  481  GTAGGGATACCCGCTGAACTTAAGCATATCAATAAGCGGAGGA  523
            |||||||||||||||||||||||||||||||||||||||||||
Sbjct  529  GTAGGGATACCCGCTGAACTTAAGCATATCAATAAGCGGAGGA  571
```

B. *Chaetomium subaffine*

Score	Expect	Identities	Gaps	Strand
970 bits(525)	0.0	530/532(99%)	2/532(0%)	Plus/Plus

```
Query  1    CTCCCT-AACCATTGTG-ACGTTACCTAAACCGTTGCTTcggcggcggccccggggttt  58
            |||||| |||||||||| |||||||||||||||||||||||||||||||||||||||||
Sbjct  18   CTCCCTAAACCATTGTGAACGTTACCTAAACCGTTGCTTCGGCGGGCGGCCCCGGGGTTT  77

Query  59   acccccccggcgcccctgggccccaccgcgggcgcccgcccggAGGTCACCAAACTCTTGA  118
            ||||||||||||||||||||||||||||||||||||||||||||||||||||||||||||
Sbjct  78   ACCCCCCGGGCGCCCCTGGGCCCCACCGCGGGCGCCCGCCGGAGGTCACCAAACTCTTGA  137

Query  119  TAATTTATGGCCTCTCTGAGTCTTCTGTACTGAATAAGTCAAAACTTTCAACAACGGATC  178
            ||||||||||||||||||||||||||||||||||||||||||||||||||||||||||||
Sbjct  138  TAATTTATGGCCTCTCTGAGTCTTCTGTACTGAATAAGTCAAAACTTTCAACAACGGATC  197

Query  179  TCTTGGTTCTGGCATCGATGAAGAACGCAGCGAAATGCGATAAGTAATGTGAATTGCAGA  238
            ||||||||||||||||||||||||||||||||||||||||||||||||||||||||||||
Sbjct  198  TCTTGGTTCTGGCATCGATGAAGAACGCAGCGAAATGCGATAAGTAATGTGAATTGCAGA  257

Query  239  ATTCAGTGAATCATCGAATCTTTGAACGCACATTGCGCCCGCCAGTATTCTGGCGGGCAT  298
            ||||||||||||||||||||||||||||||||||||||||||||||||||||||||||||
Sbjct  258  ATTCAGTGAATCATCGAATCTTTGAACGCACATTGCGCCCGCCAGTATTCTGGCGGGCAT  317

Query  299  GCCTGTTCGAGCGTCATTTCAACCATCAAGCCCCGGGCTTGTGTTGGGGACCTGCGGCTG  358
            ||||||||||||||||||||||||||||||||||||||||||||||||||||||||||||
Sbjct  318  GCCTGTTCGAGCGTCATTTCAACCATCAAGCCCCGGGCTTGTGTTGGGGACCTGCGGCTG  377

Query  359  CCGCAGGCCCTGAAAAGCAGTGGCGGGCTCGCTGTCACACCGAGCGTAGTAGCATATATC  418
            ||||||||||||||||||||||||||||||||||||||||||||||||||||||||||||
Sbjct  378  CCGCAGGCCCTGAAAAGCAGTGGCGGGCTCGCTGTCACACCGAGCGTAGTAGCATATATC  437

Query  419  TCGCTCTGGGCGTGCTGCGGGTTCCGGCCGTTAAACCACCTTTTAACCCAAGGTTGACCT  478
            ||||||||||||||||||||||||||||||||||||||||||||||||||||||||||||
Sbjct  438  TCGCTCTGGGCGTGCTGCGGGTTCCGGCCGTTAAACCACCTTTTAACCCAAGGTTGACCT  497

Query  479  CGGATCAGGTAGGAAGACCCGCTGAACTTAAGCATATCAATAAGCGGAGGAA  530
            ||||||||||||||||||||||||||||||||||||||||||||||||||||
Sbjct  498  CGGATCAGGTAGGAAGACCCGCTGAACTTAAGCATATCAATAAGCGGAGGAA  549
```

C. *Fusarium acuminatum*

Score	Expect	Identities	Gaps	Strand
952 bits(515)	0.0	515/515(100%)	0/515(0%)	Plus/Plus

```
Query  1    AACCCCTGTGACATACCTTAATGTTGCCTCGGCGGATCAGCCCGCGCCCCGTAAAACGGG  60
            ||||||||||||||||||||||||||||||||||||||||||||||||||||||||||||
Sbjct  100  AACCCCTGTGACATACCTTAATGTTGCCTCGGCGGATCAGCCCGCGCCCCGTAAAACGGG  159

Query  61   ACGGCCCGCCAGAGGACCCAAACTCTAATGTTTCTTATTGTAACTTCTGAGTAAAACAAA  120
            ||||||||||||||||||||||||||||||||||||||||||||||||||||||||||||
Sbjct  160  ACGGCCCGCCAGAGGACCCAAACTCTAATGTTTCTTATTGTAACTTCTGAGTAAAACAAA  219

Query  121  CAAATAAATCAAAACTTTCAACAACGGATCTCTTGGTTCTGGCATCGATGAAGAACGCAG  180
            ||||||||||||||||||||||||||||||||||||||||||||||||||||||||||||
Sbjct  220  CAAATAAATCAAAACTTTCAACAACGGATCTCTTGGTTCTGGCATCGATGAAGAACGCAG  279

Query  181  CAAAATGCGATAAGTAATGTGAATTGCAGAATTCAGTGAATCATCGAATCTTTGAACGCA  240
            ||||||||||||||||||||||||||||||||||||||||||||||||||||||||||||
Sbjct  280  CAAAATGCGATAAGTAATGTGAATTGCAGAATTCAGTGAATCATCGAATCTTTGAACGCA  339

Query  241  CATTGCGCCCGCTGGTATTCCGGCGGGCATGCCTGTTCGAGCGTCATTTCAACCCTCAAG  300
            ||||||||||||||||||||||||||||||||||||||||||||||||||||||||||||
Sbjct  340  CATTGCGCCCGCTGGTATTCCGGCGGGCATGCCTGTTCGAGCGTCATTTCAACCCTCAAG  399

Query  301  CCCCCGGGTTTGGTGTTGGGGATCGGCTCTGCCCTTCTGGGCGGTGCCGCCCCCGAAATA  360
            ||||||||||||||||||||||||||||||||||||||||||||||||||||||||||||
Sbjct  400  CCCCCGGGTTTGGTGTTGGGGATCGGCTCTGCCCTTCTGGGCGGTGCCGCCCCCGAAATA  459

Query  361  CATTGGCGGTCTCGCTGCAGCCTCCATTGCGTAGTAGCTAACACCTCGCAACTGGAACGC  420
            ||||||||||||||||||||||||||||||||||||||||||||||||||||||||||||
Sbjct  460  CATTGGCGGTCTCGCTGCAGCCTCCATTGCGTAGTAGCTAACACCTCGCAACTGGAACGC  519

Query  421  GGCGCGGCCATGCCGTAAAACCCCAACTTCTGAATGTTGACCTCGGATCAGGTAGGAATA  480
            ||||||||||||||||||||||||||||||||||||||||||||||||||||||||||||
Sbjct  520  GGCGCGGCCATGCCGTAAAACCCCAACTTCTGAATGTTGACCTCGGATCAGGTAGGAATA  579

Query  481  CCCGCTGAACTTAAGCATATCAATAAGCGGAGGAA  515
            |||||||||||||||||||||||||||||||||||
Sbjct  580  CCCGCTGAACTTAAGCATATCAATAAGCGGAGGAA  614
```

Appendix II: NMR data of (-)-(*S*)-curvularin

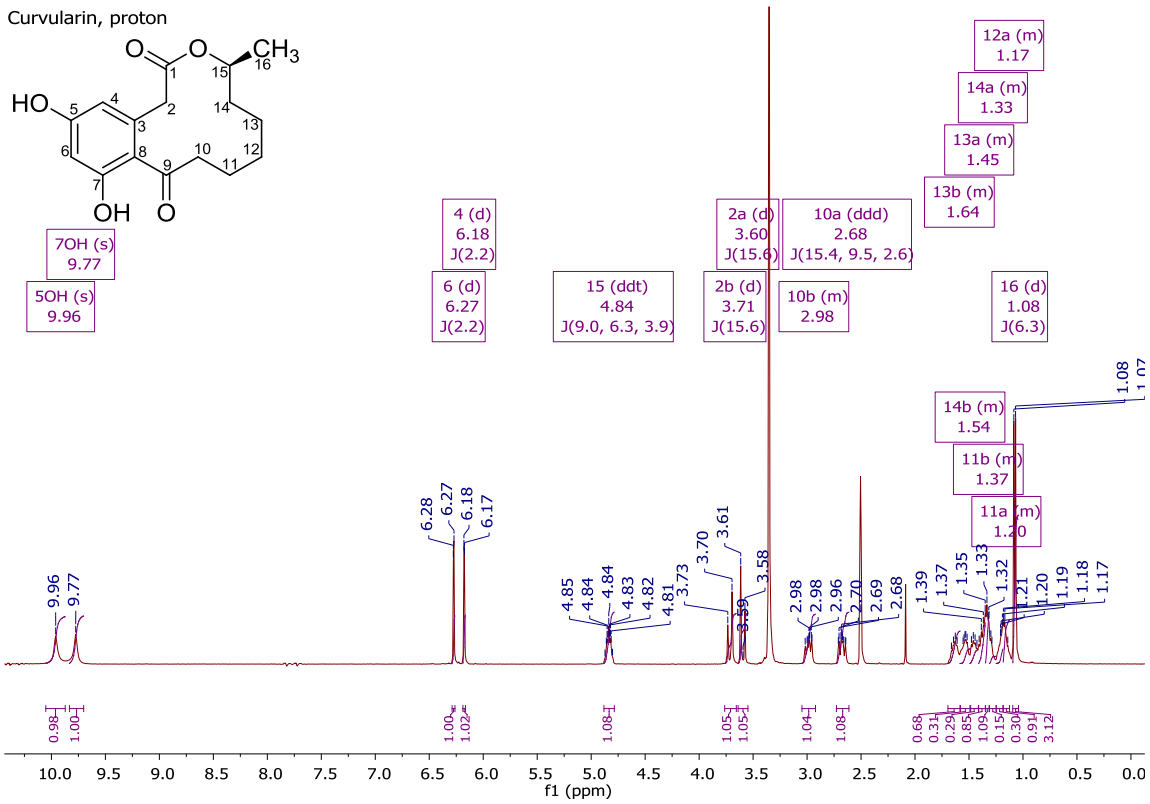

Figure A.II.1: ^{1}H NMR (400 MHz) spectrum for (-)-(*S*)-curvularin, measured in DMSO-d_6.

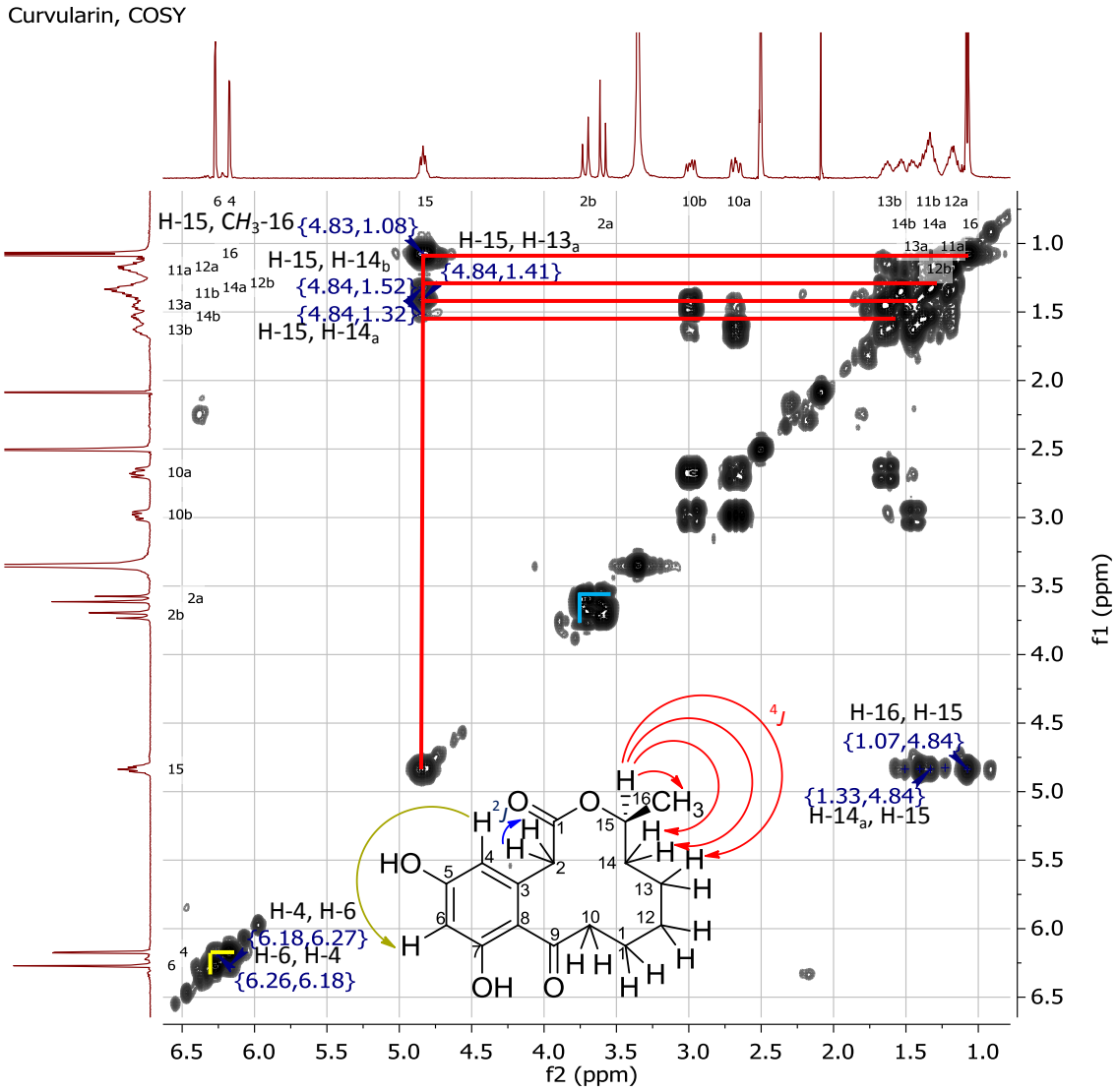

Figure A.II.2: ^{1}H-^{1}H COSY NMR (400 MHz) spectrum for (-)-(*S*)-curvularin, measured in DMSO-d_6.

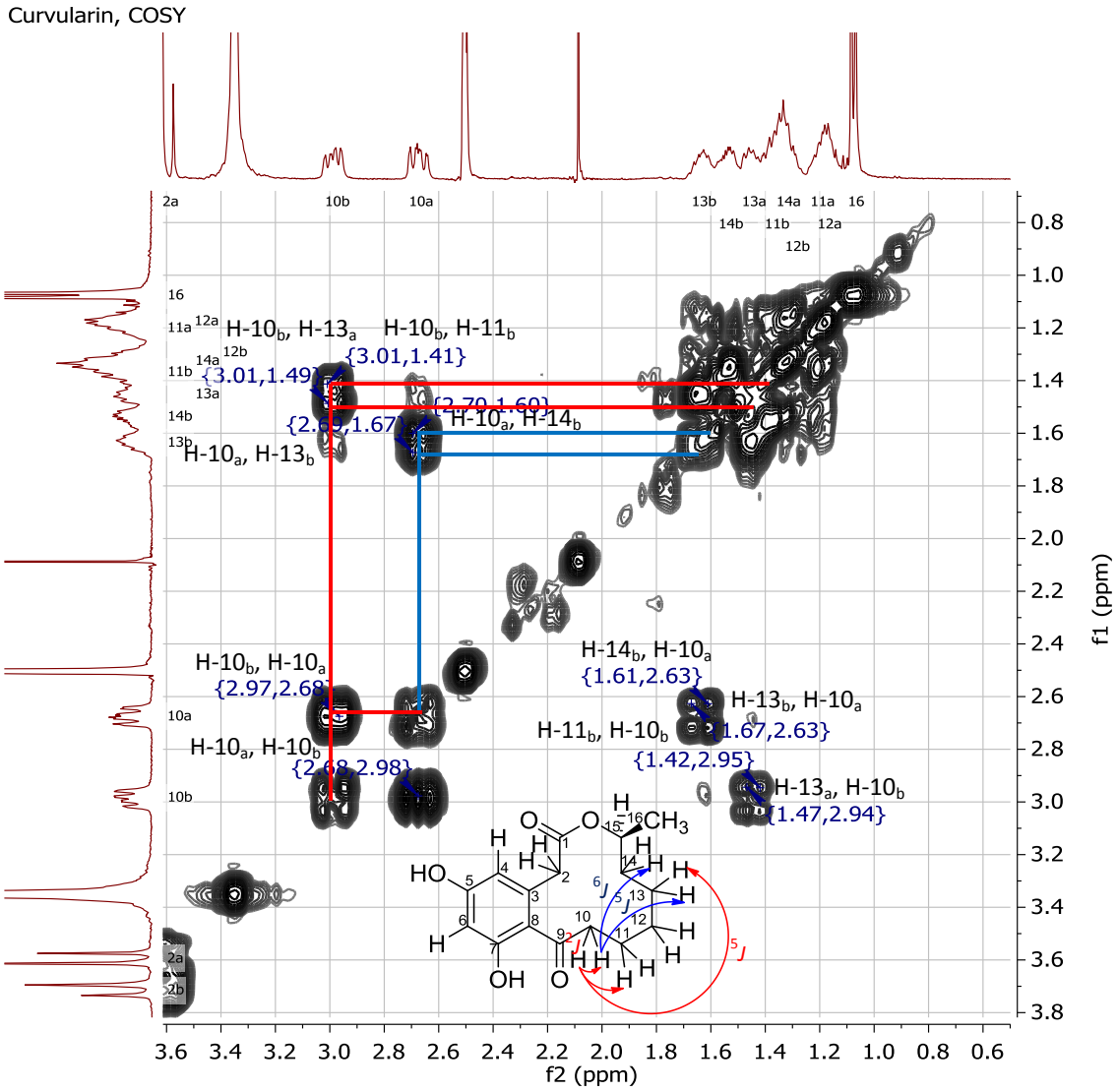

Figure A.II.3: Expanded view for the region δ_H 0.80 – 3.80 ppm of the ^{1}H-^{1}H COSY NMR (400 MHz) spectrum for (-)-(*S*)-curvularin, measured in DMSO-d_6.

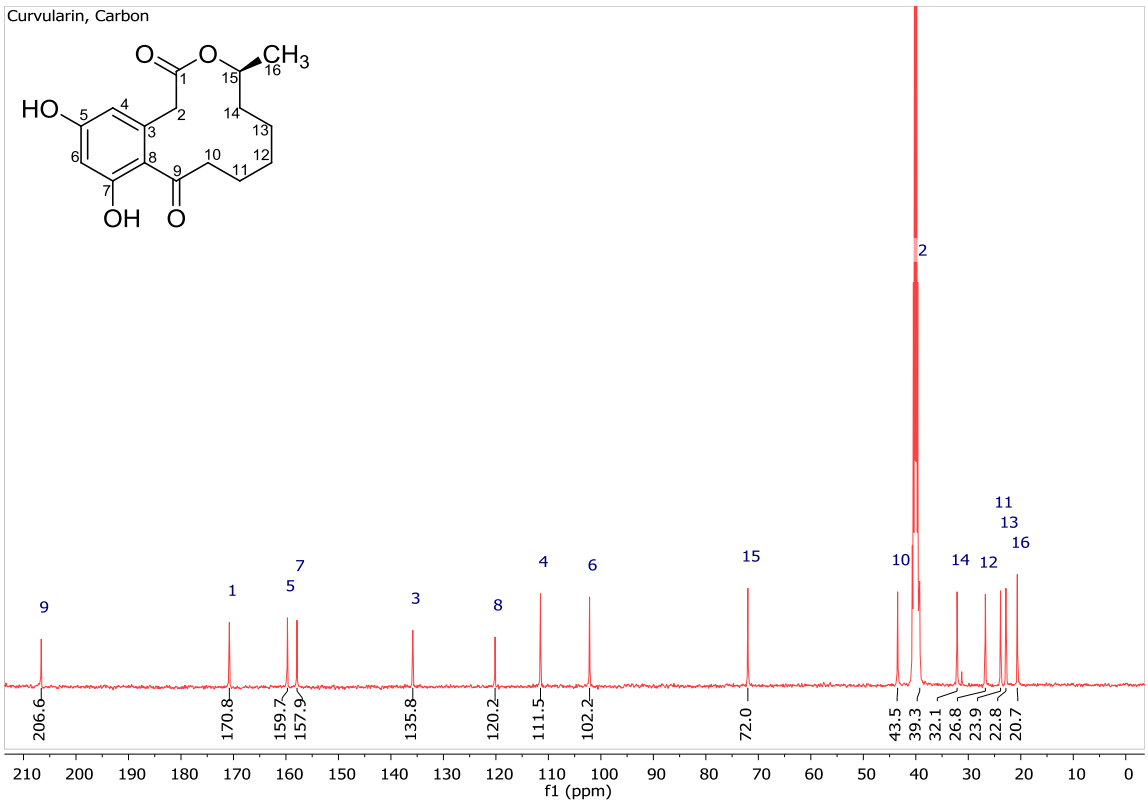

Figure A.II.4: ^{13}C NMR (100 MHz) spectrum for (-)-(*S*)-curvularin, measured in DMSO-d_6.

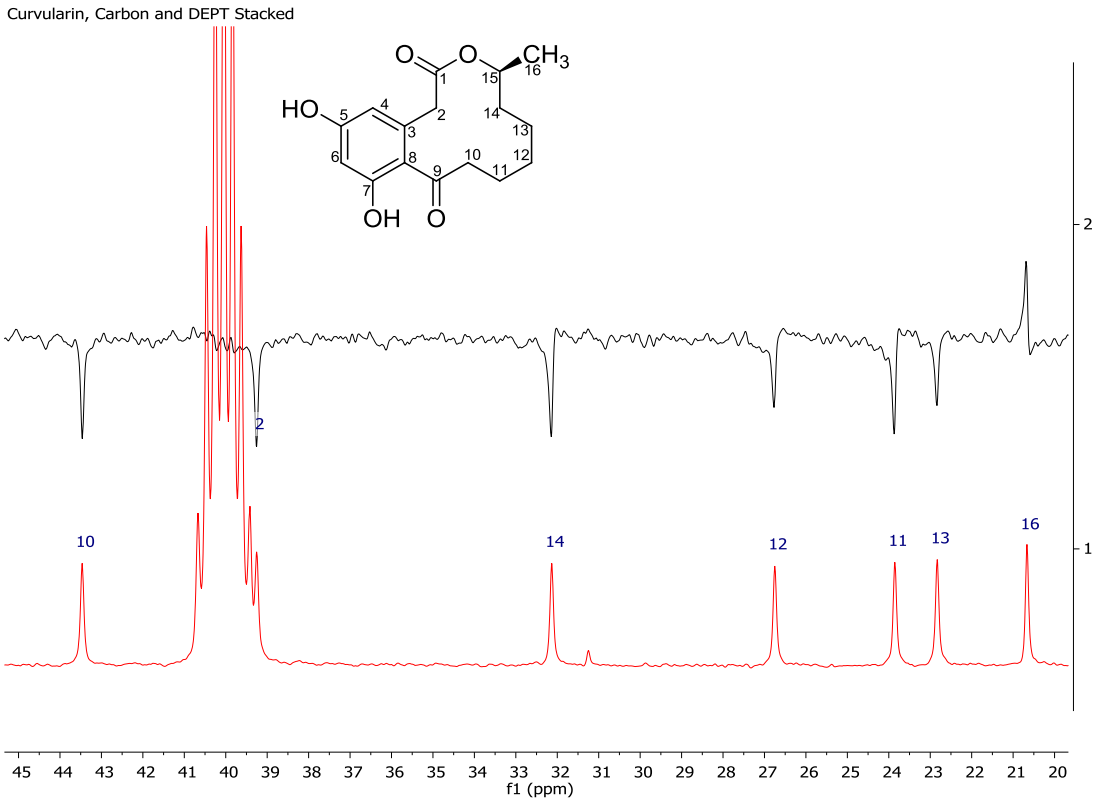

Figure A.II.5: Stacked ^{13}C (1) and DEPT (2) NMR (100 MHz) spectra for (-)-(*S*)-curvularin, measured in DMSO-d_6.

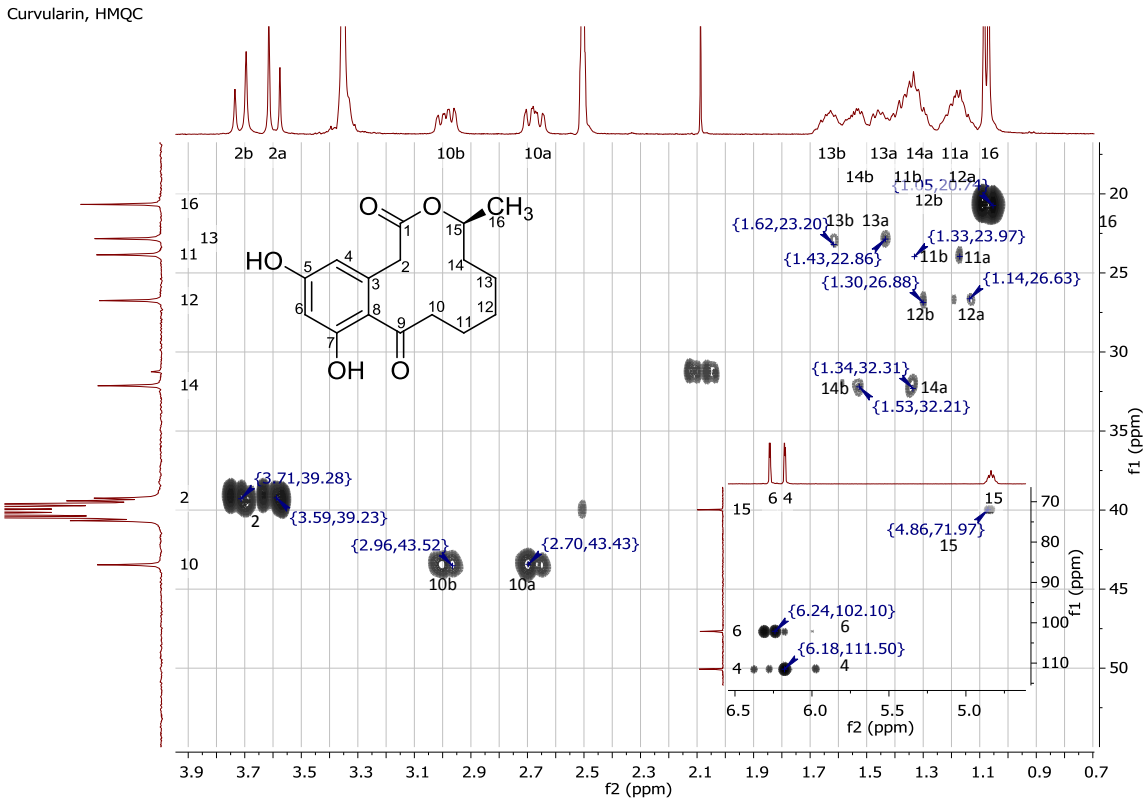

Figure A.II.6: ^{1}H-^{13}C HMQC NMR (400 MHz) spectrum for (-)-(*S*)-curvularin, measured in DMSO-d_6.

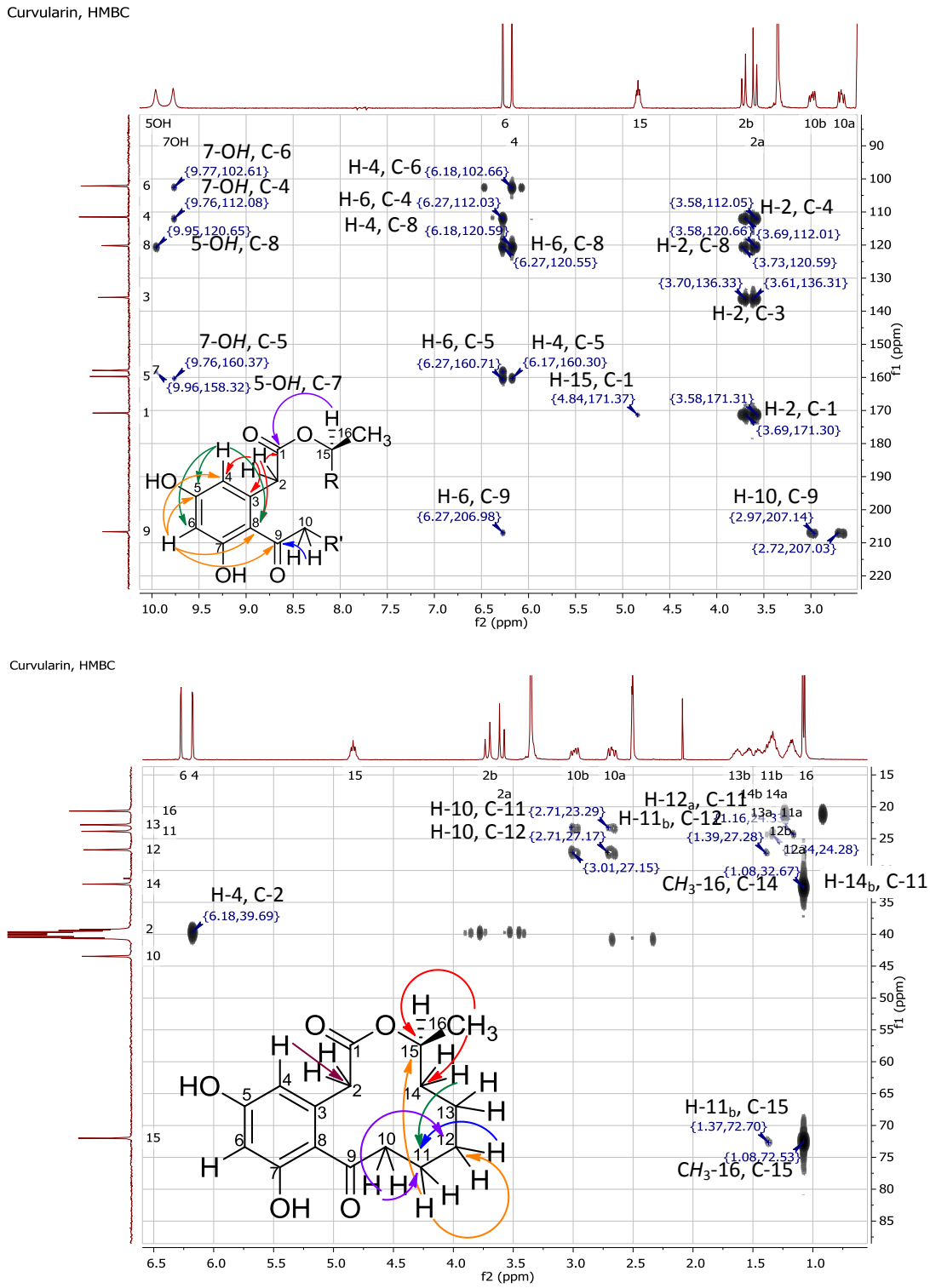

Figure A.II.7: ^{1}H-^{13}C HMBC NMR (400 MHz) spectrum for (-)-(*S*)-curvularin, measured in DMSO-d_6.

Appendix III: NMR data of dehydrocurvularin

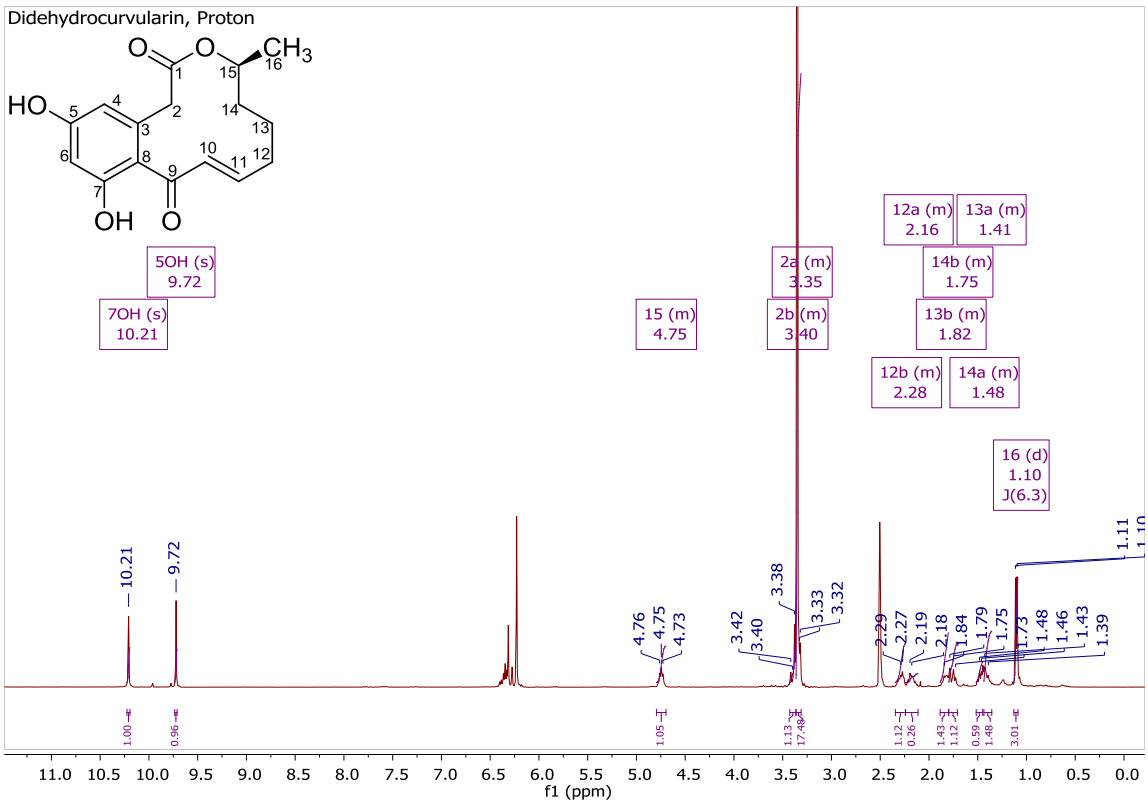

Figure A.III.1: ^{1}H NMR spectrum (400 MHz) for dehydrocurvularin, measured in DMSO-d_6.

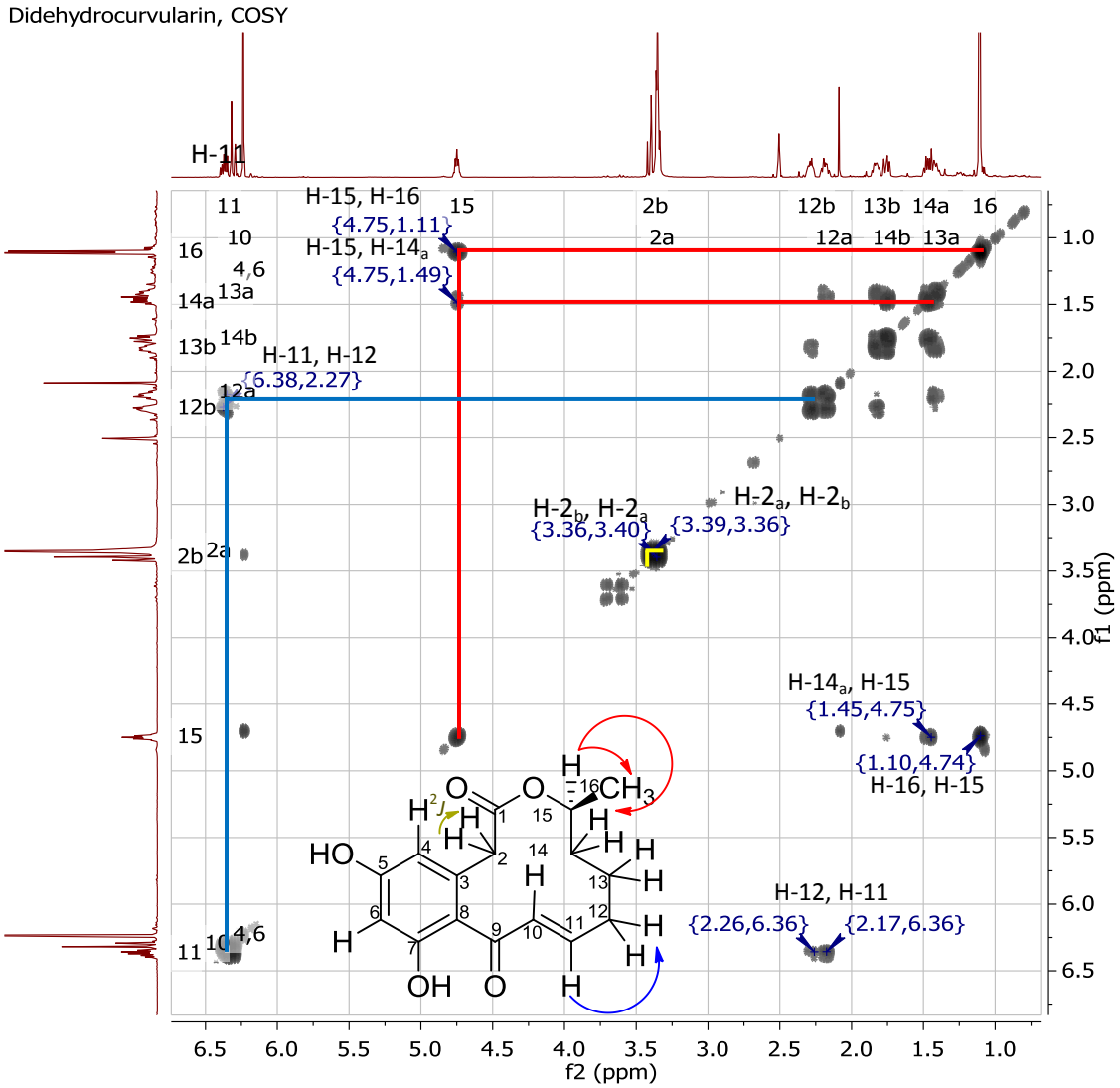

Figure A.III.2: ^{1}H-^{1}H COSY NMR (400 MHz) spectrum for dehydrocurvularin, measured in DMSO-d_6.

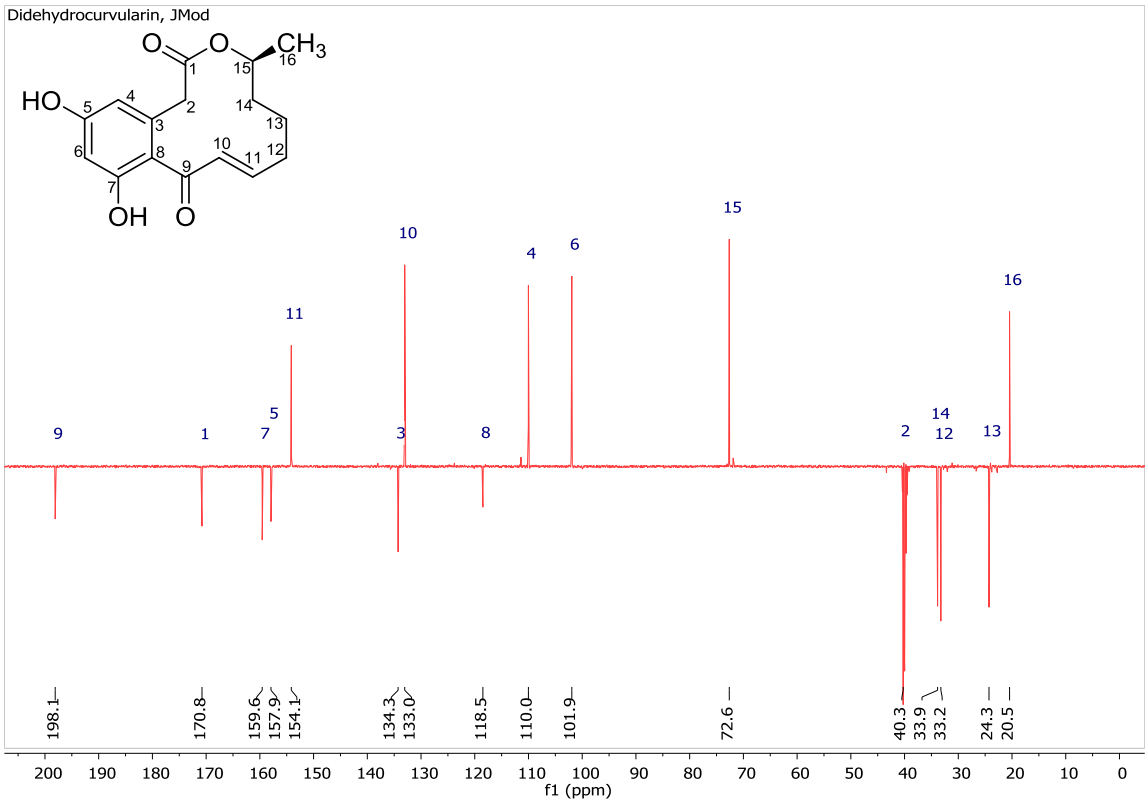

Figure A.III.3: JMod NMR (100 MHz) spectrum for dehydrocurvularin, measured in DMSO-d_6.

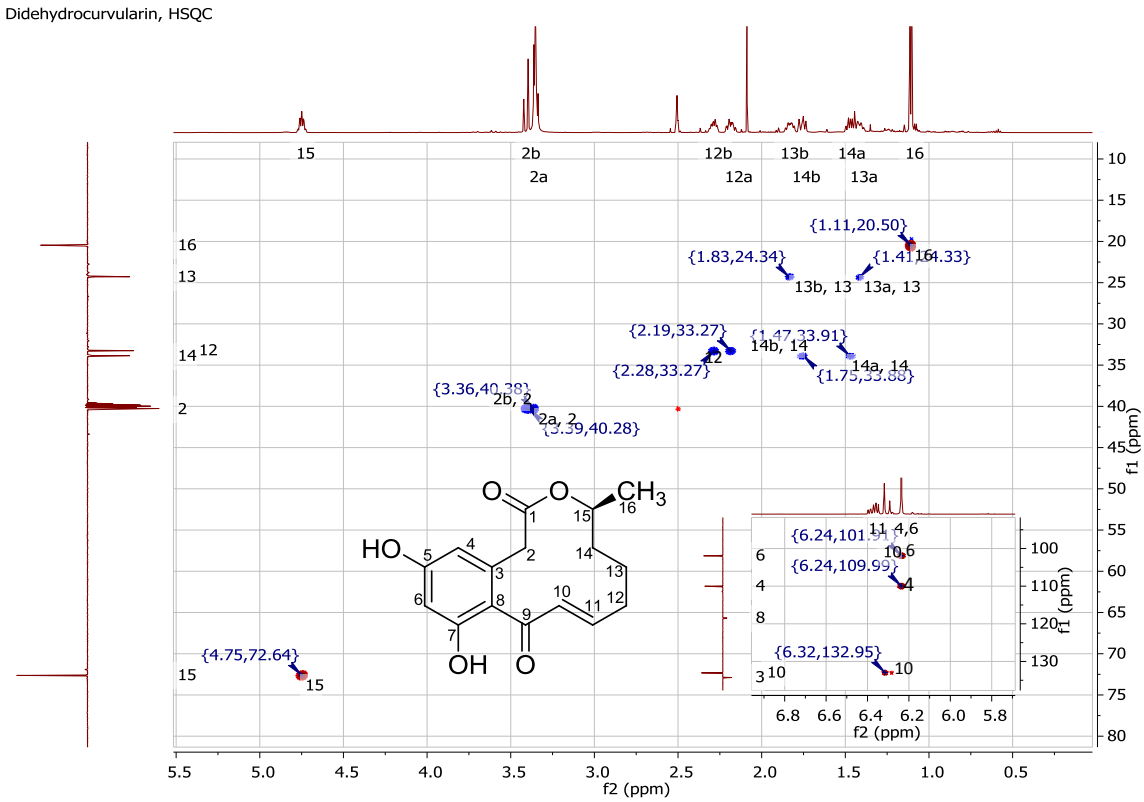

Figure A.III.4: ^{1}H-^{13}C HSQC NMR (400 MHz) spectrum for dehydrocurvularin, measured in DMSO-d_6.

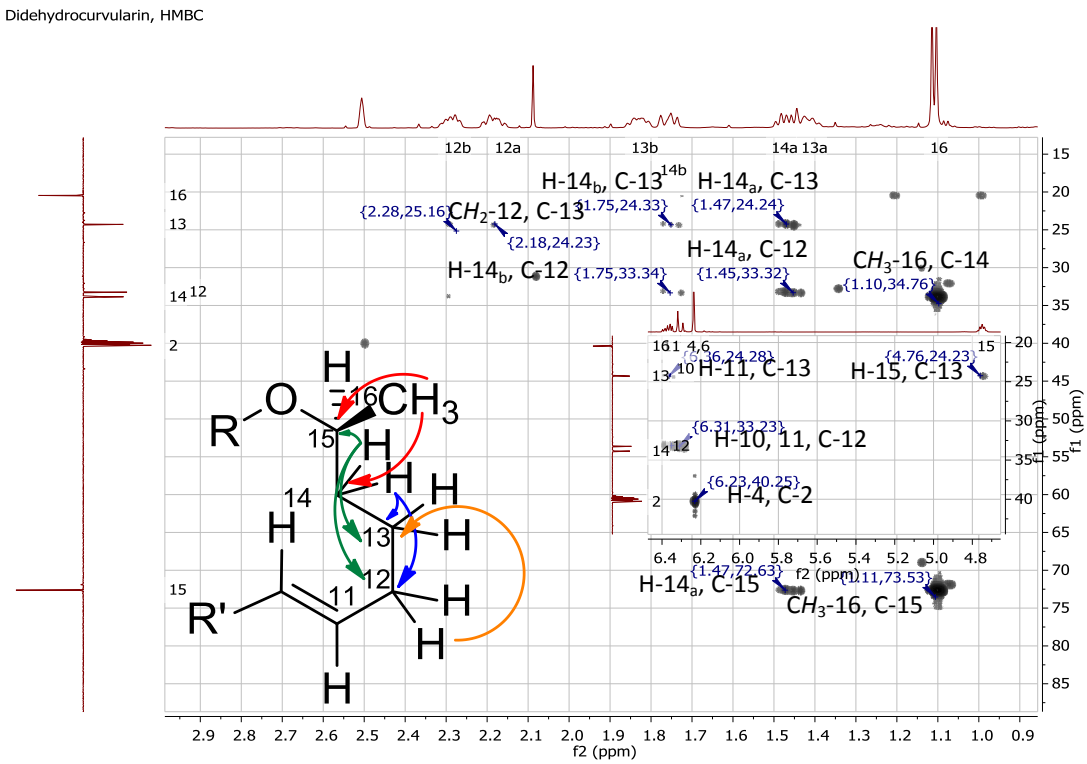

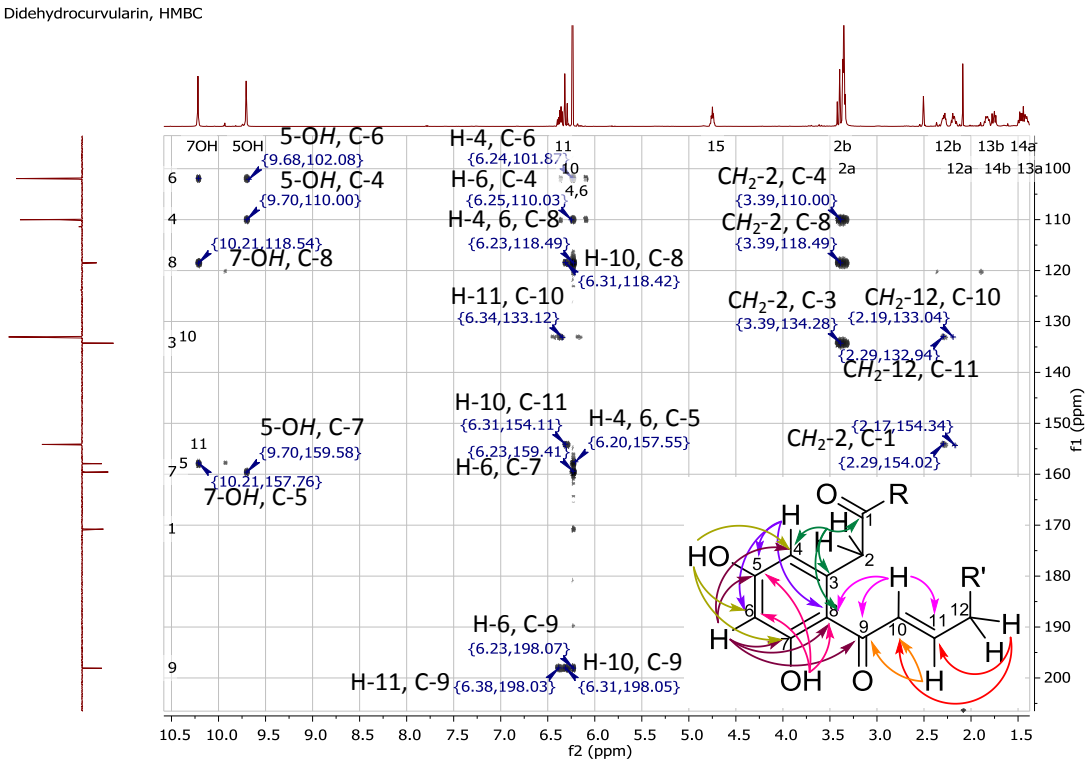

Figure A.III.5: ^{1}H-^{13}C HMBC NMR (400 MHz) spectrum for dehydrocurvularin, measured in DMSO-$_{d6}$.

Appendix IV: NMR data of 11α-hydroxycurvularin

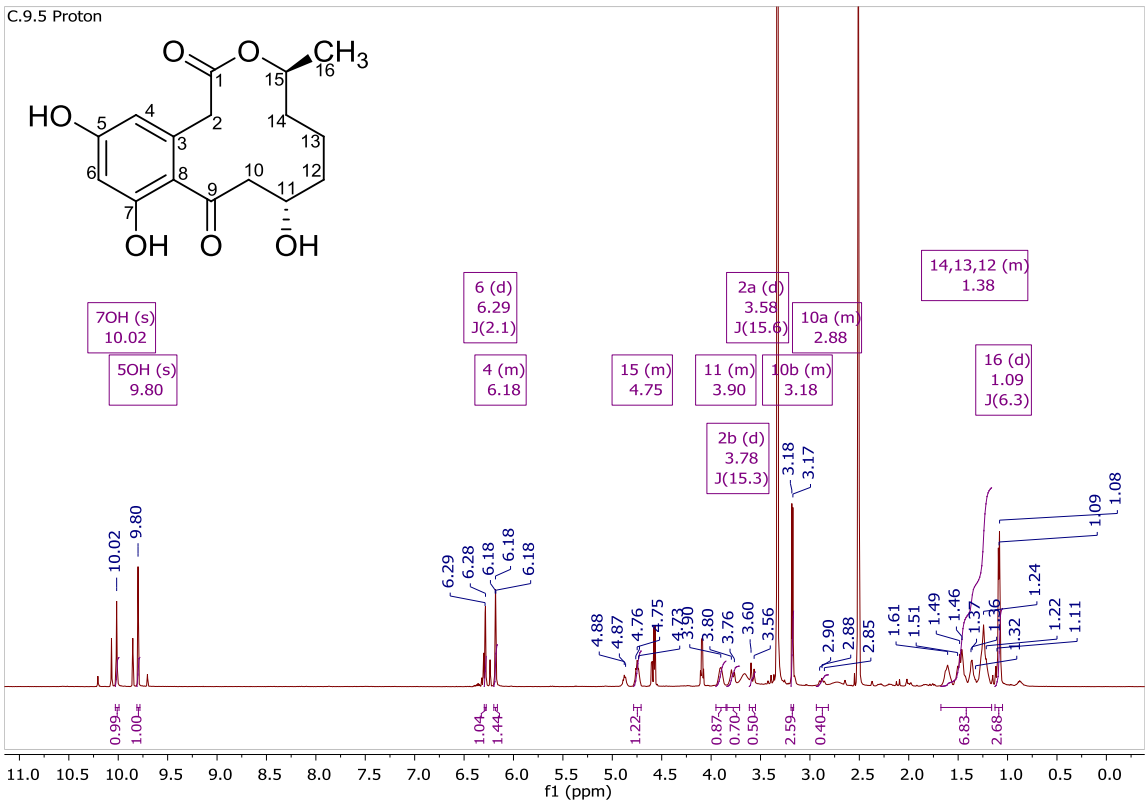

Figure A.IV.1: ^{1}H NMR (500 MHz) spectrum for 11α-hydroxycurvularin, measured in DMSO-d_6.

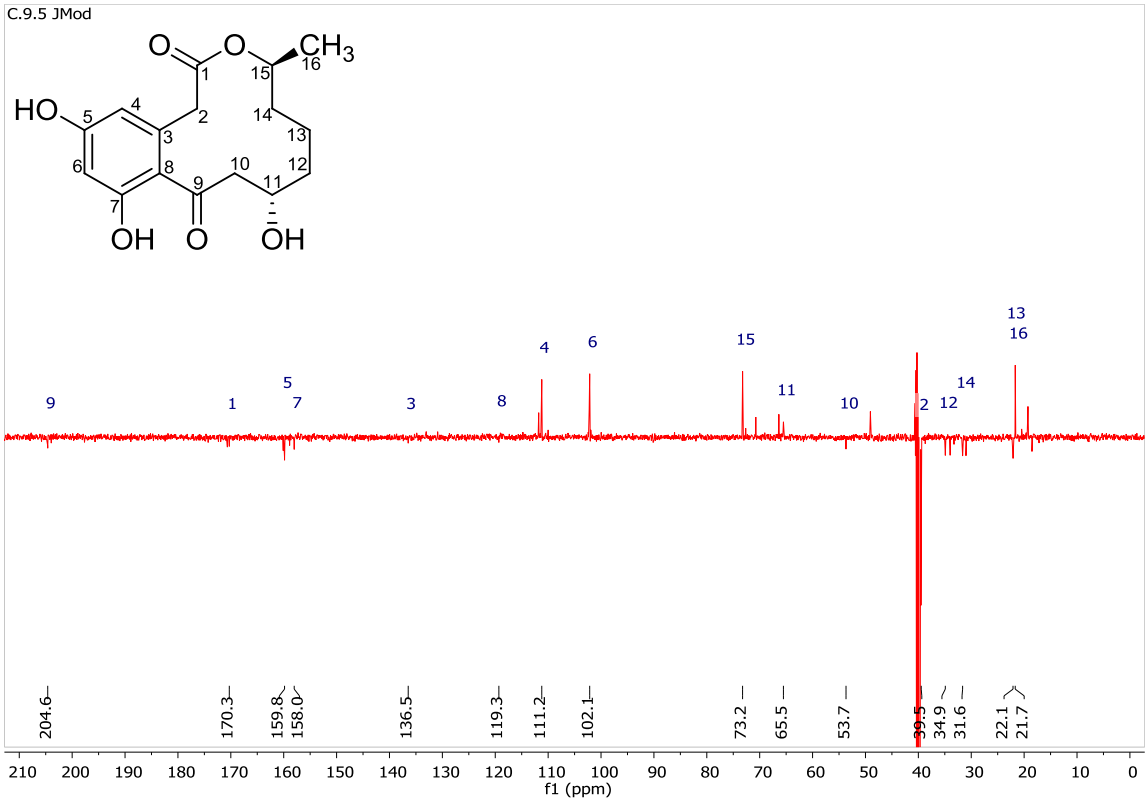

Figure A.IV.2: JMod NMR (125 MHz) spectrum for 11α-hydroxycurvularin, measured in DMSO-d_6.

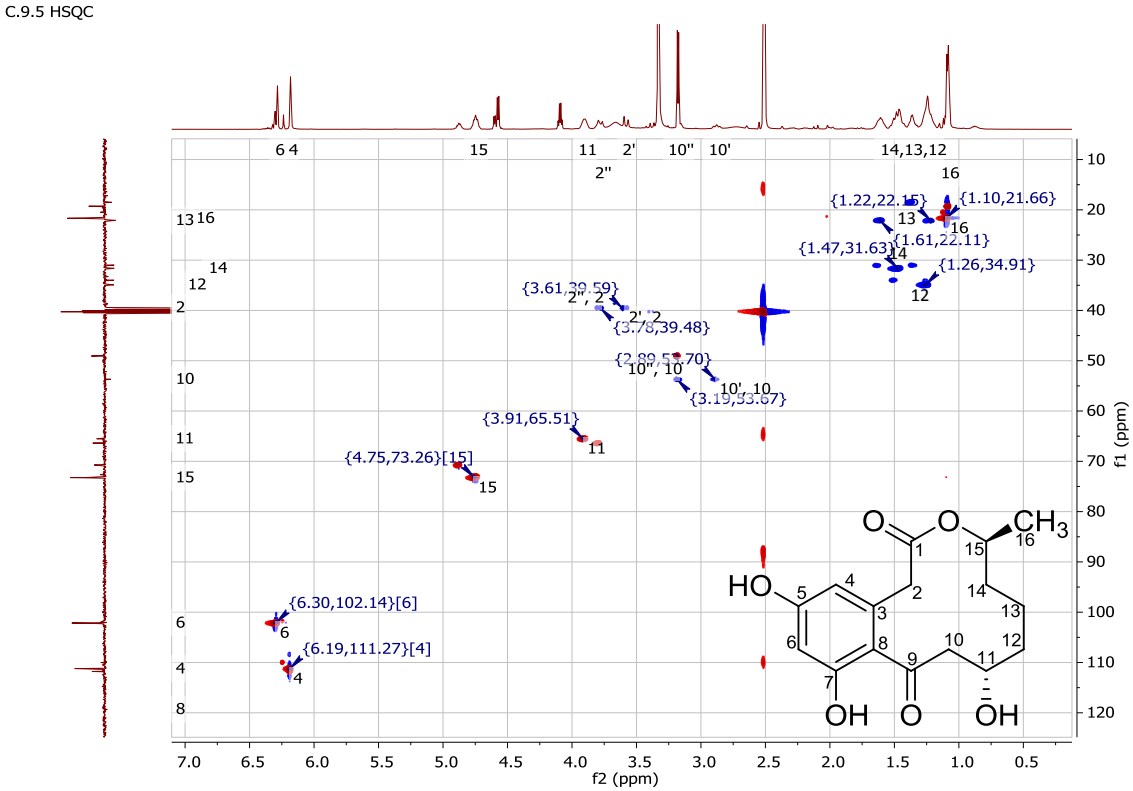

Figure A.IV.3: ^{1}H-^{13}C HSQC NMR (500 MHz) spectrum for 11α-hydroxycurvularin, measured in DMSO-$_{d6}$.

Appendix V: NMR data of cyclo(L-prolylglycyl)

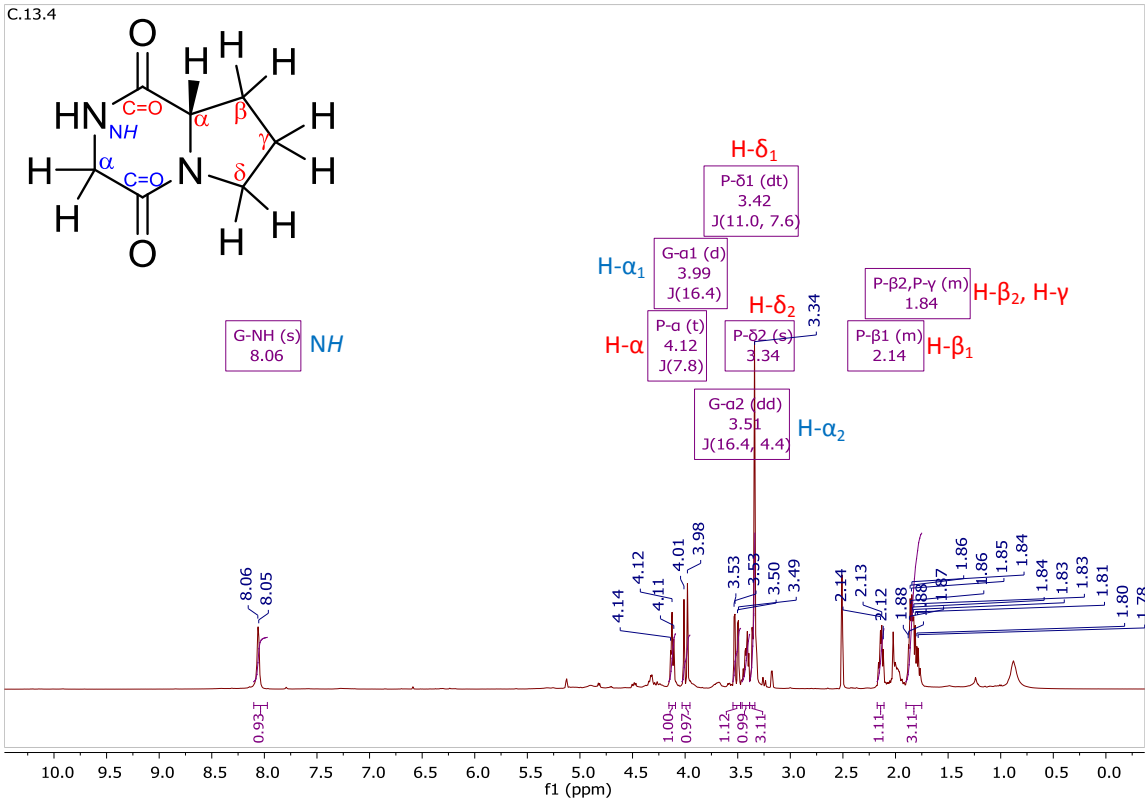

Figure A.V.1: ^{1}H NMR (500 MHz) spectrum for cyclo(L-prolylglycyl), measured in DMSO-d_6. Red labels are for the signals that belong to the prolyl moiety (P) while blue labels are for the signals that belong to the gylcyl moiety (G).

C.13.4 TOCSY

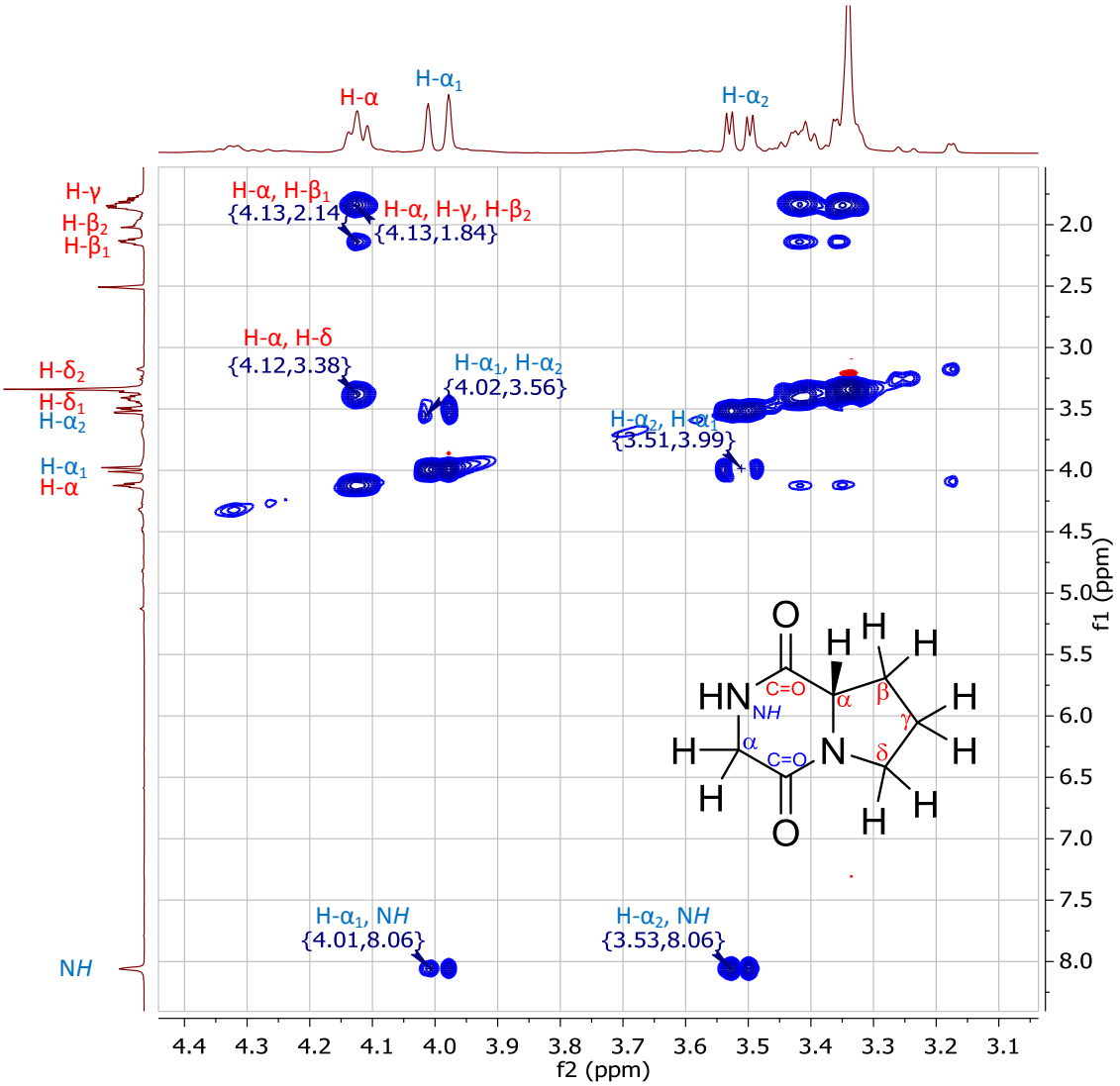

Figure A.V.2: ^{1}H-^{1}H TOCSY NMR (500 MHz) spectrum for cyclo(L-prolylglycyl), measured in DMSO-$_{d6}$. Red labels are for the signals that belong to the prolyl moiety (P) while blue labels are for the signals that belong to the gylcyl moiety (G).

C.13.4 COSY

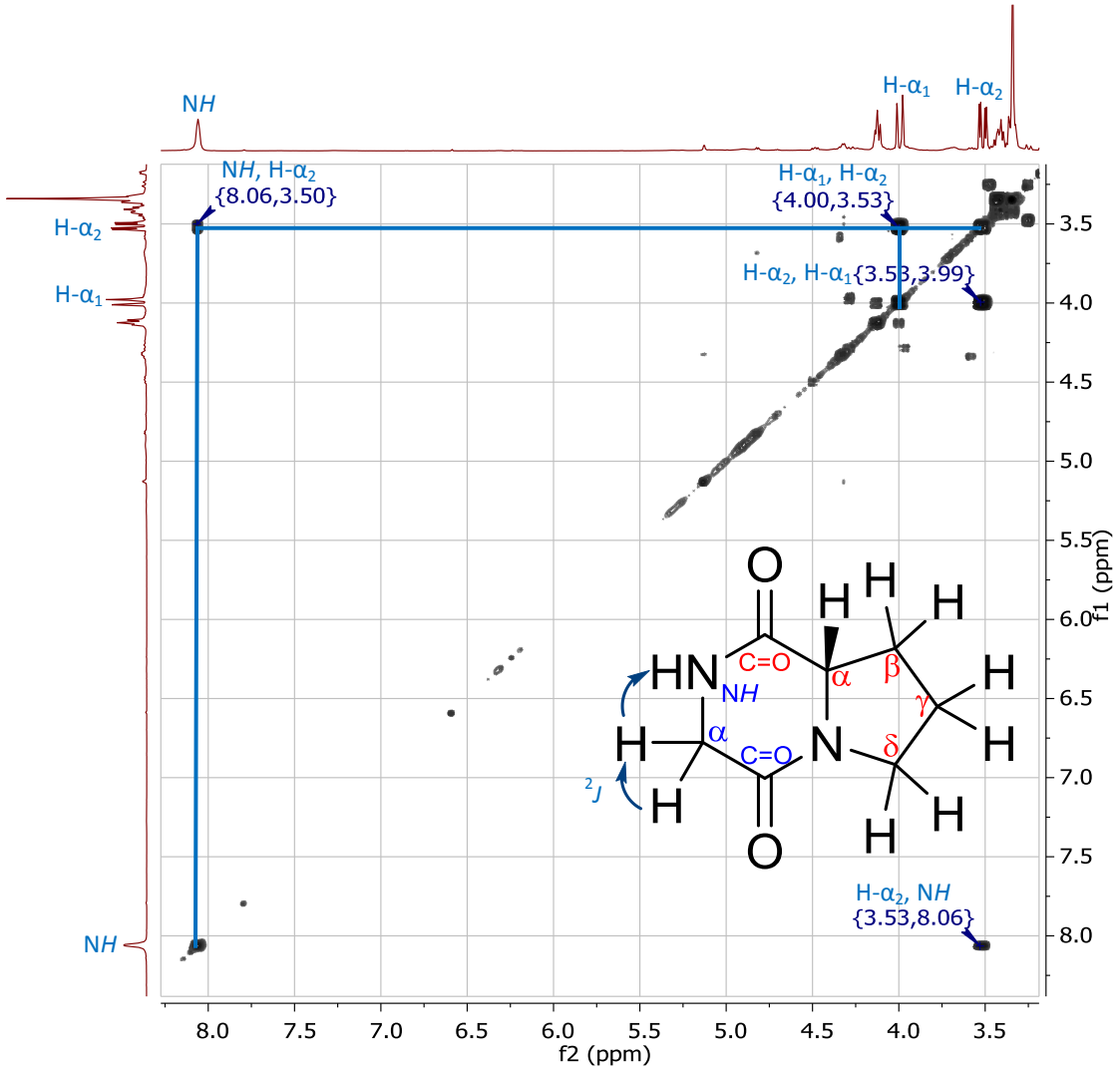

Figure A.V.3: ^{1}H-^{1}H COSY NMR (500 MHz) spectrum for cyclo(L-prolylglycyl), measured in DMSO-d_6. Red labels are for the signals that belong to the prolyl moiety (P) while blue labels are for the signals that belong to the gylcyl moiety (G).

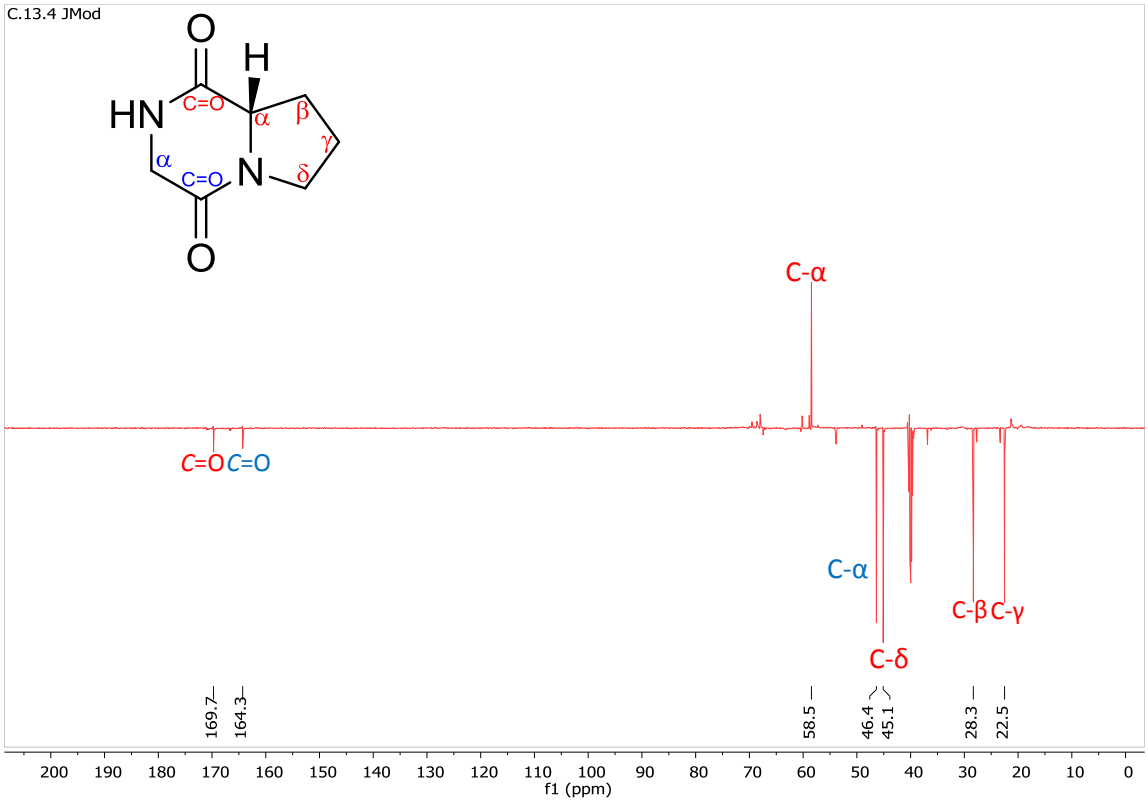

Figure A.V.4: JMod NMR spectrum for cyclo(L-prolylglycyl), measured in DMSO-d_6. Red labels are for the signals that belong to the prolyl moiety while blue labels are for the signals that belong to the gylcyl moiety, (125 MHz).

C.13.4 HSQC

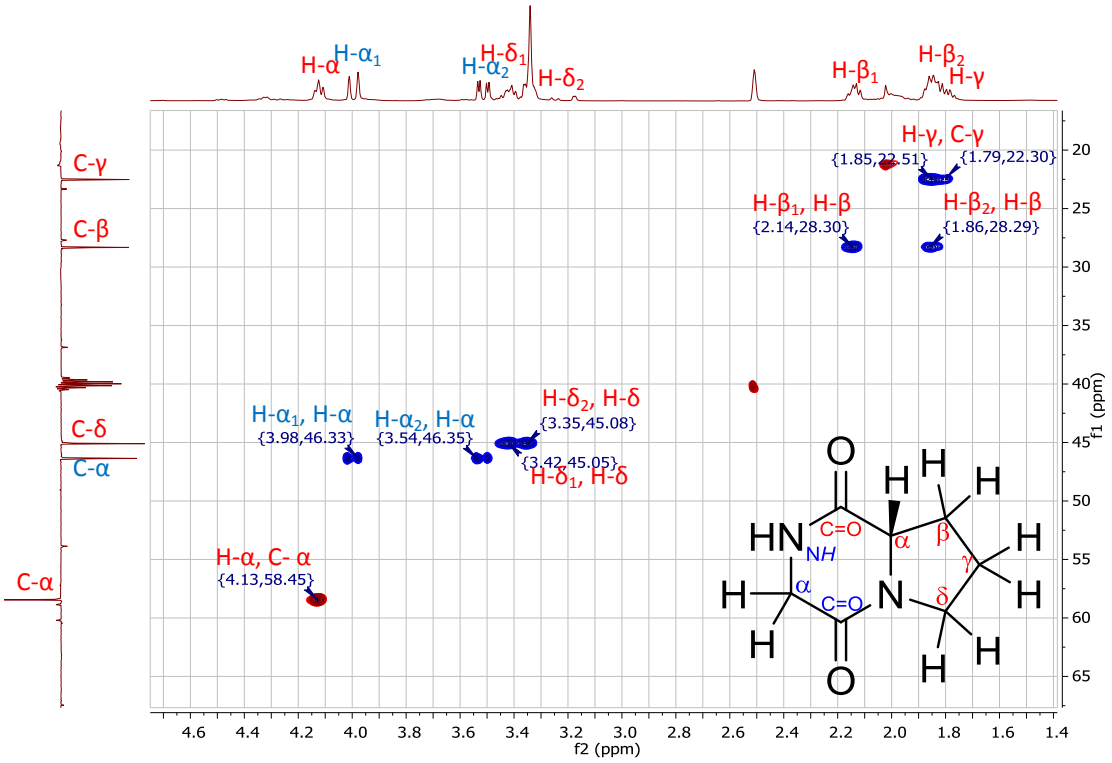

Figure A.V.5: ^{1}H-^{13}C HSQC NMR (500 MHz) spectrum for cyclo(L-prolylglycyl), measured in DMSO-d_6. Red labels are for the signals that belong to the prolyl moiety while blue labels are for the signals that belong to the gylcyl moiety.

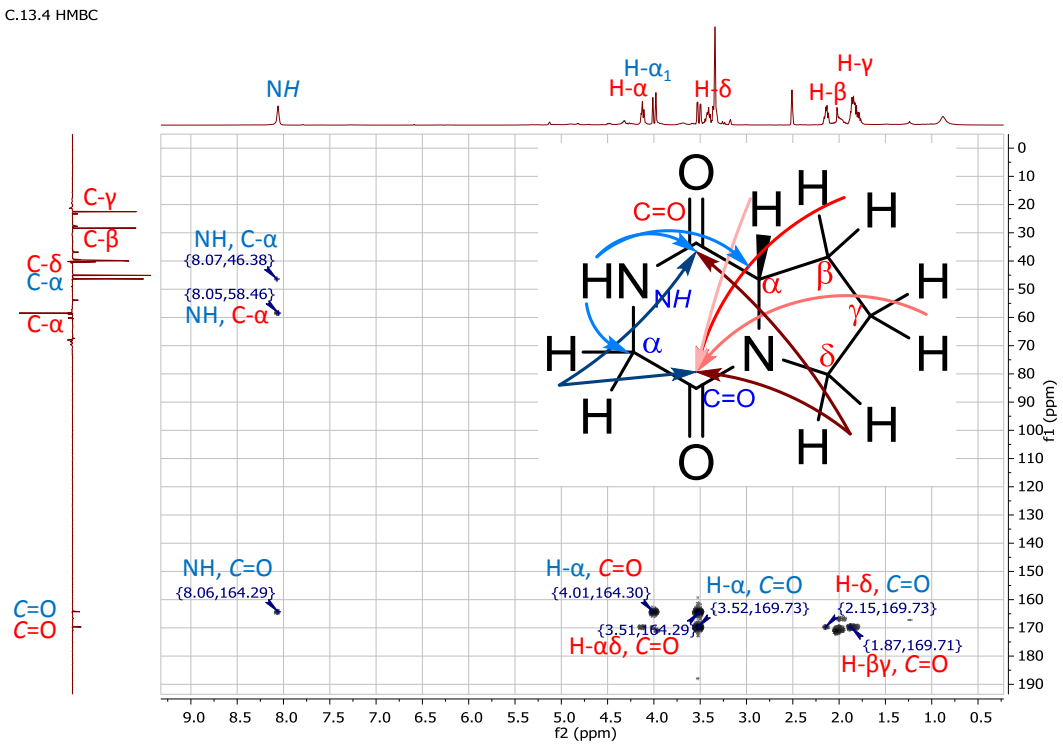

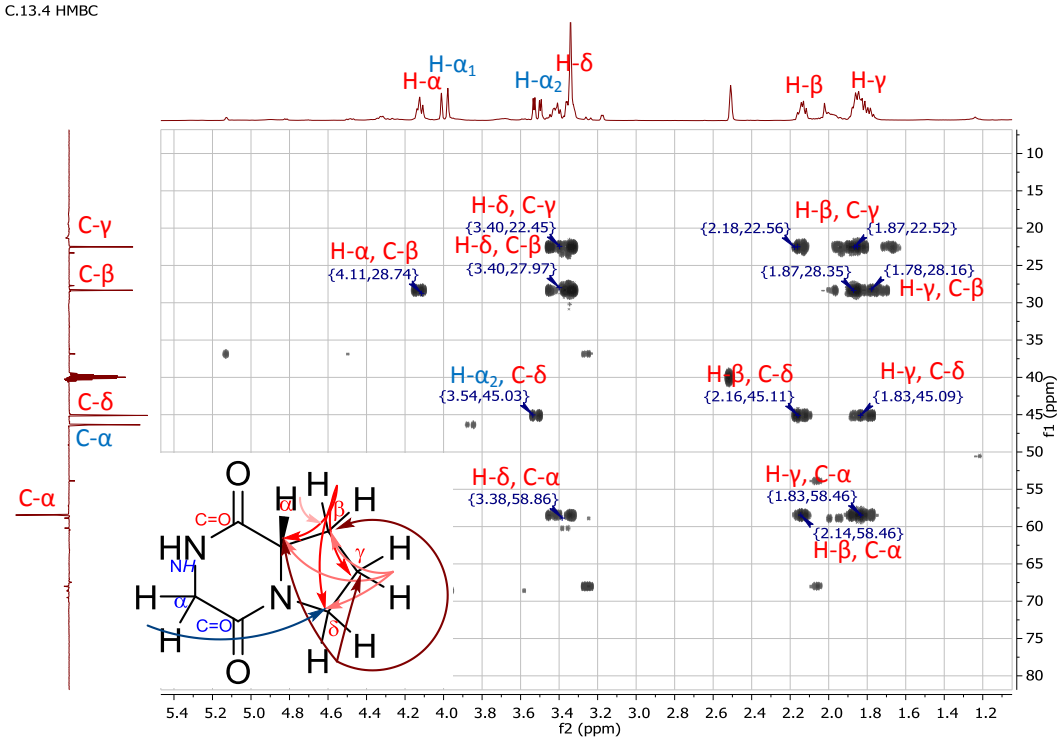

Figure A.V.6: ^{1}H-^{13}C HMBC NMR (500 MHz) spectrum for cyclo(L-prolylglycyl), measured in DMSO-d_6. Red labels are for the signals that belong to the prolyl moiety while blue labels are for the signals that belong to the gylcyl moiety.

Appendix VI: NMR data of acremonisol A

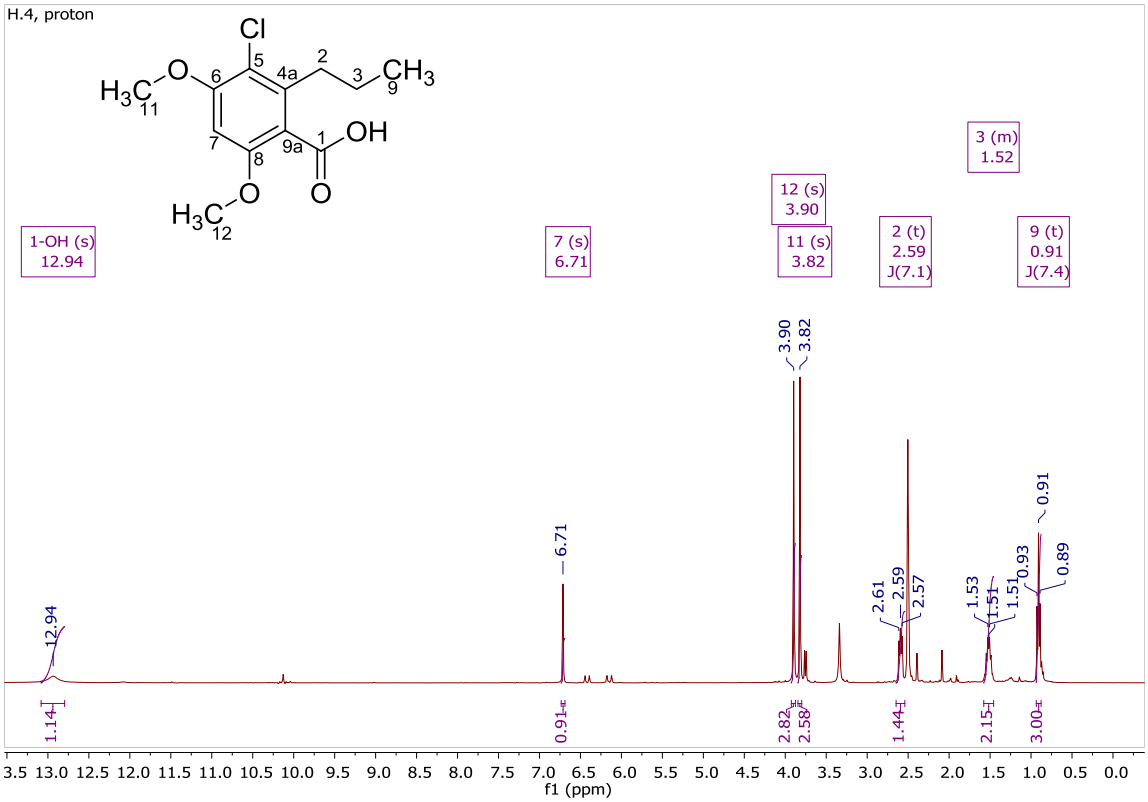

Figure A.VI.1: ^{1}H NMR (400 MHz) spectrum for acremonisol A, measured in DMSO-d_6.

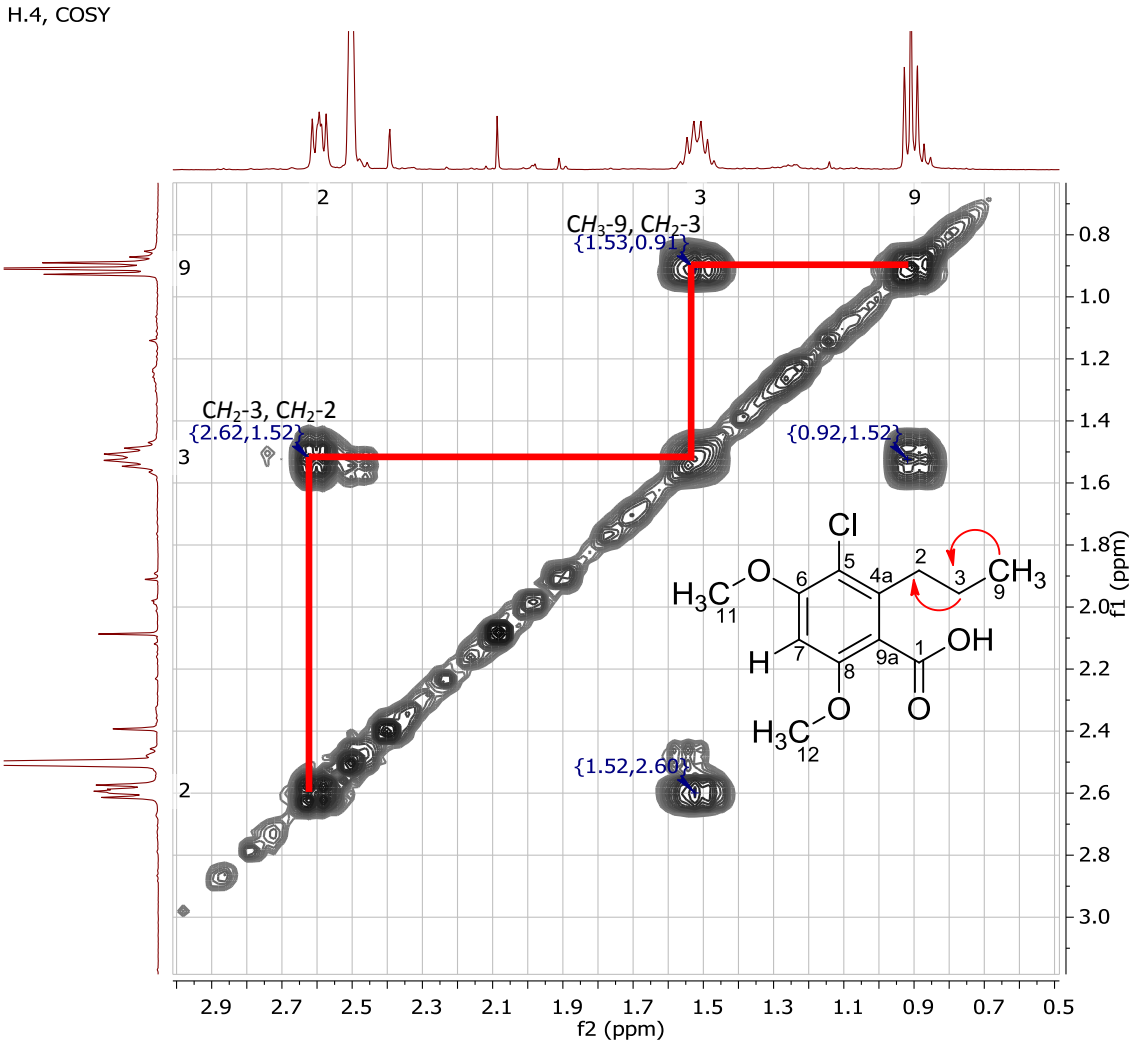

Figure A.VI.2: ^{1}H-^{1}H COSY NMR (400 MHz) spectrum for acremonisol A, measured in DMSO-d_6.

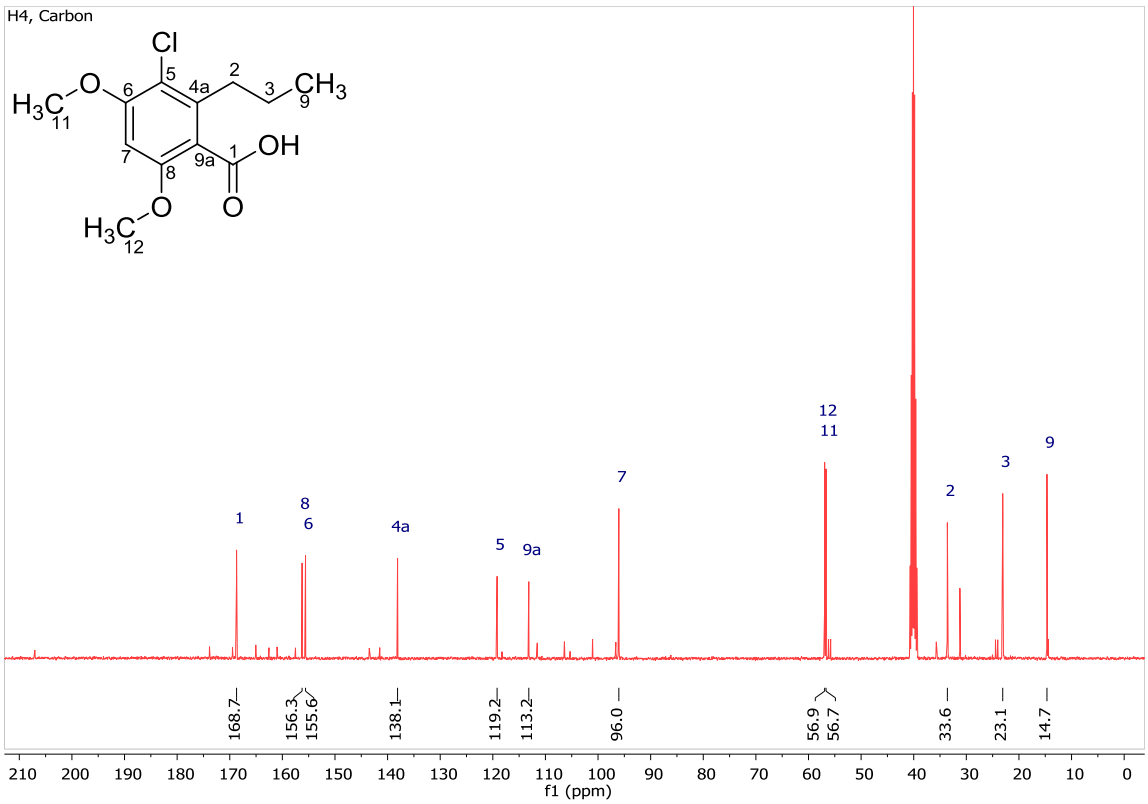

Figure A.VI.3: ^{13}C NMR (100 MHz) spectrum for acremonisol A, measured in DMSO-d_6.

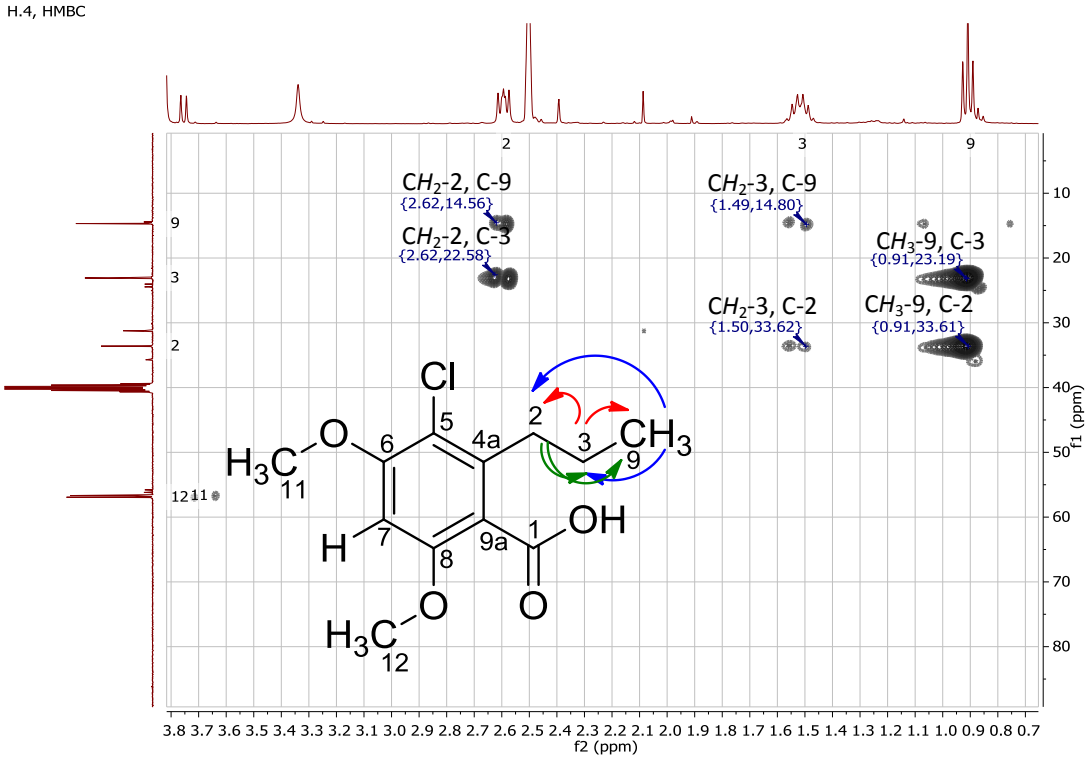

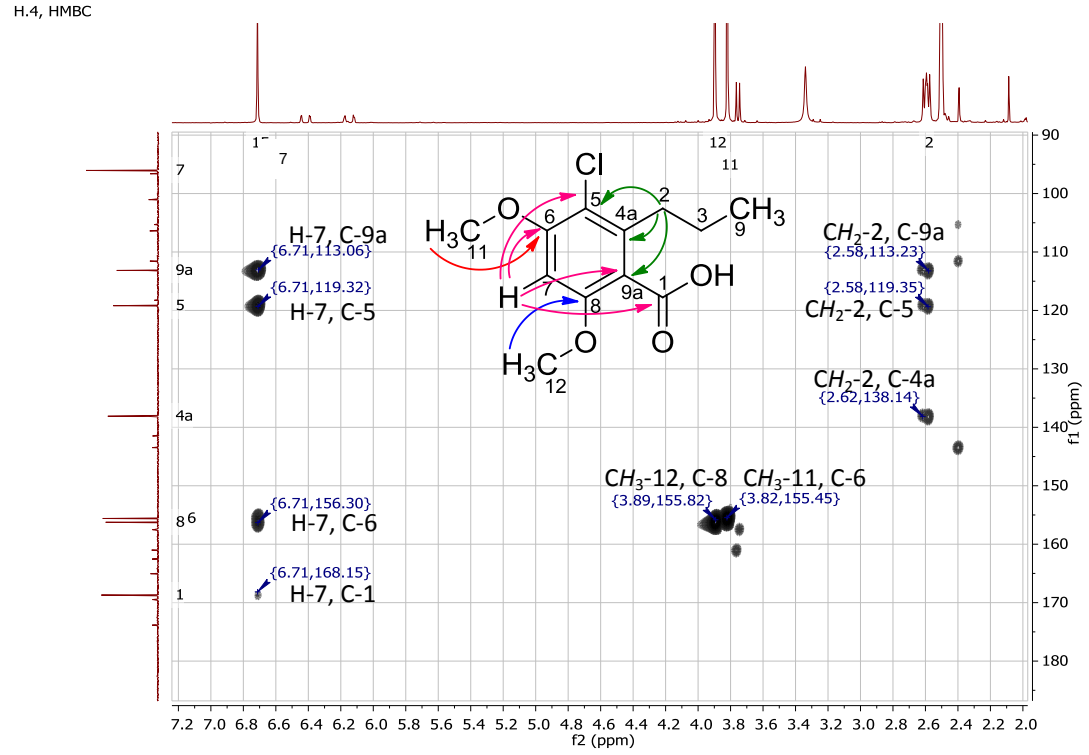

Figure A.VI.4: ^{1}H-^{13}C HMBC NMR (400 MHz) spectrum for acremonisol A, measured in DMSO-d_6.

Appendix VII: NMR data of cochliodinol

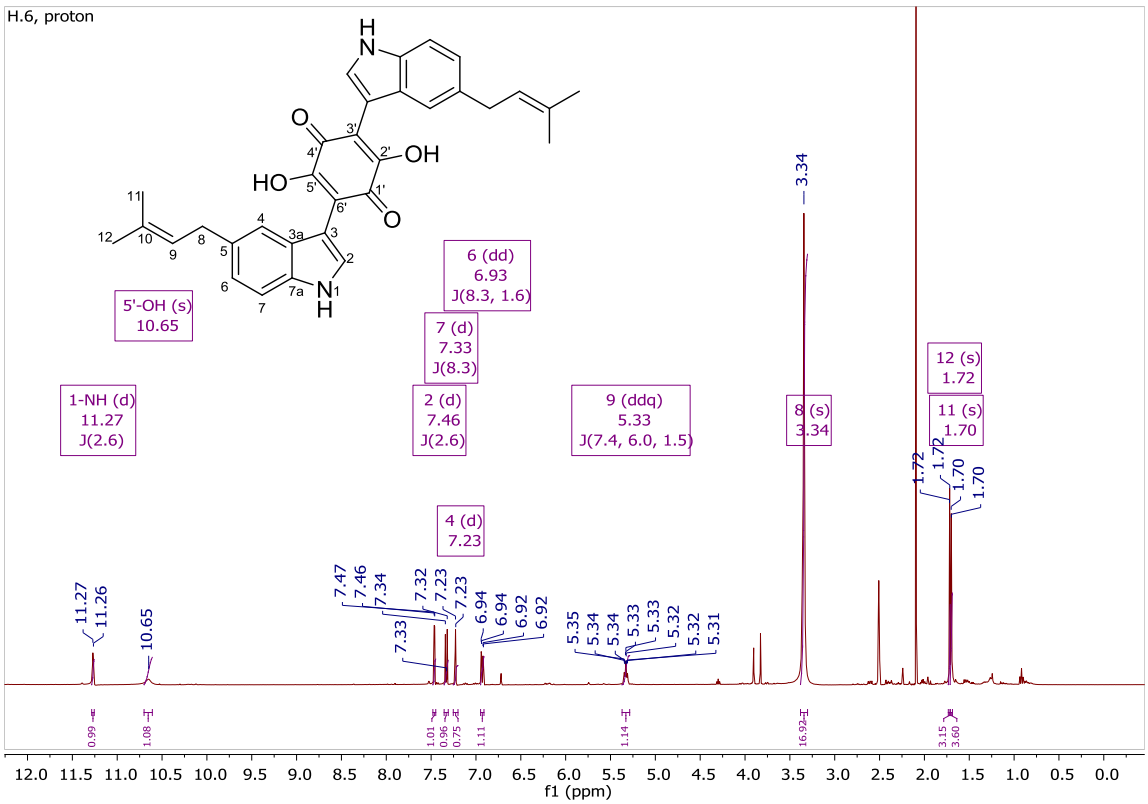

Figure A.VII.1: ^{1}H NMR (400 MHz) spectrum for cochliodinol, measured in DMSO-d_6.

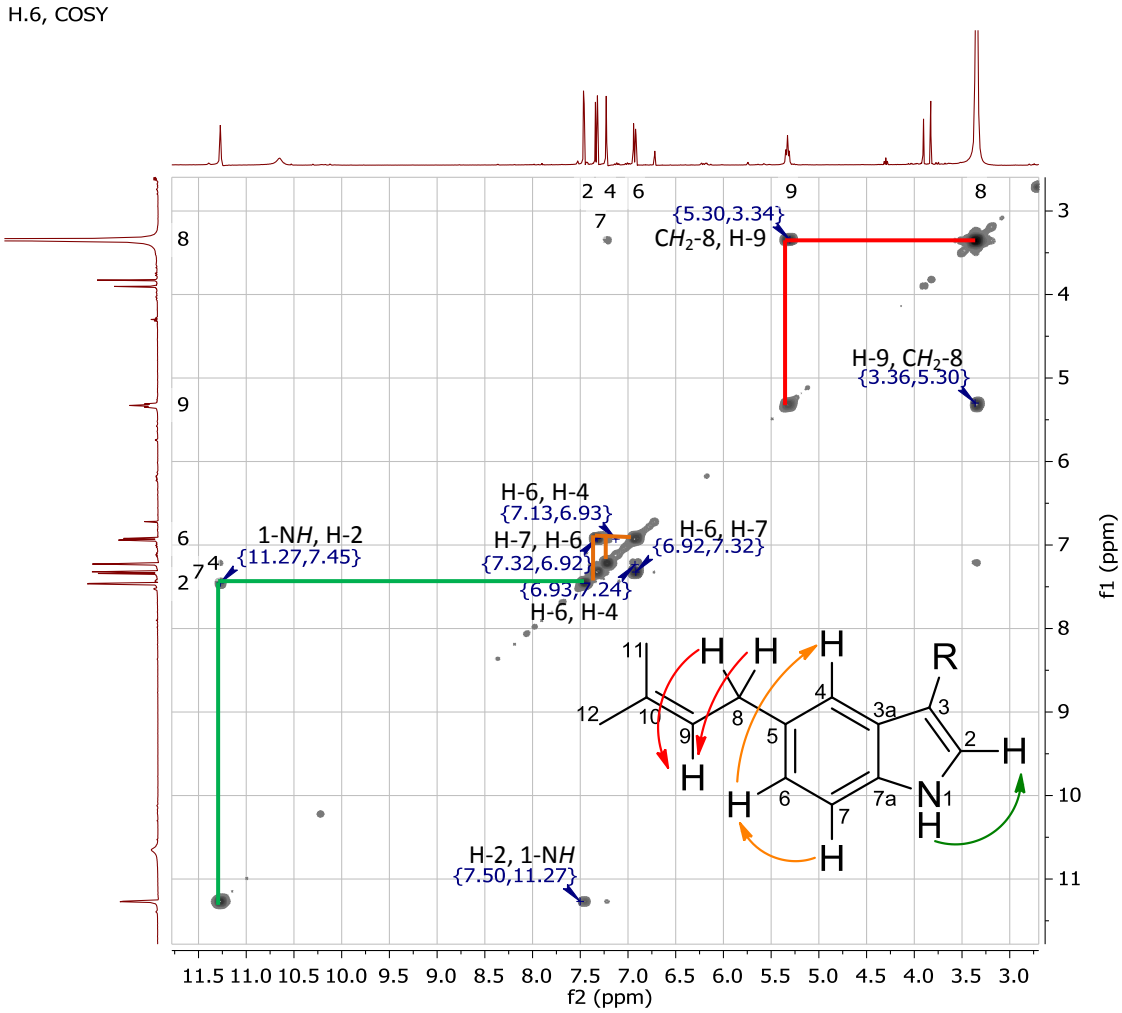

Figure A.VII.2: ^{1}H-^{1}H COSY NMR (400 MHz) spectrum for cochliodinol, measured in DMSO-d_6.

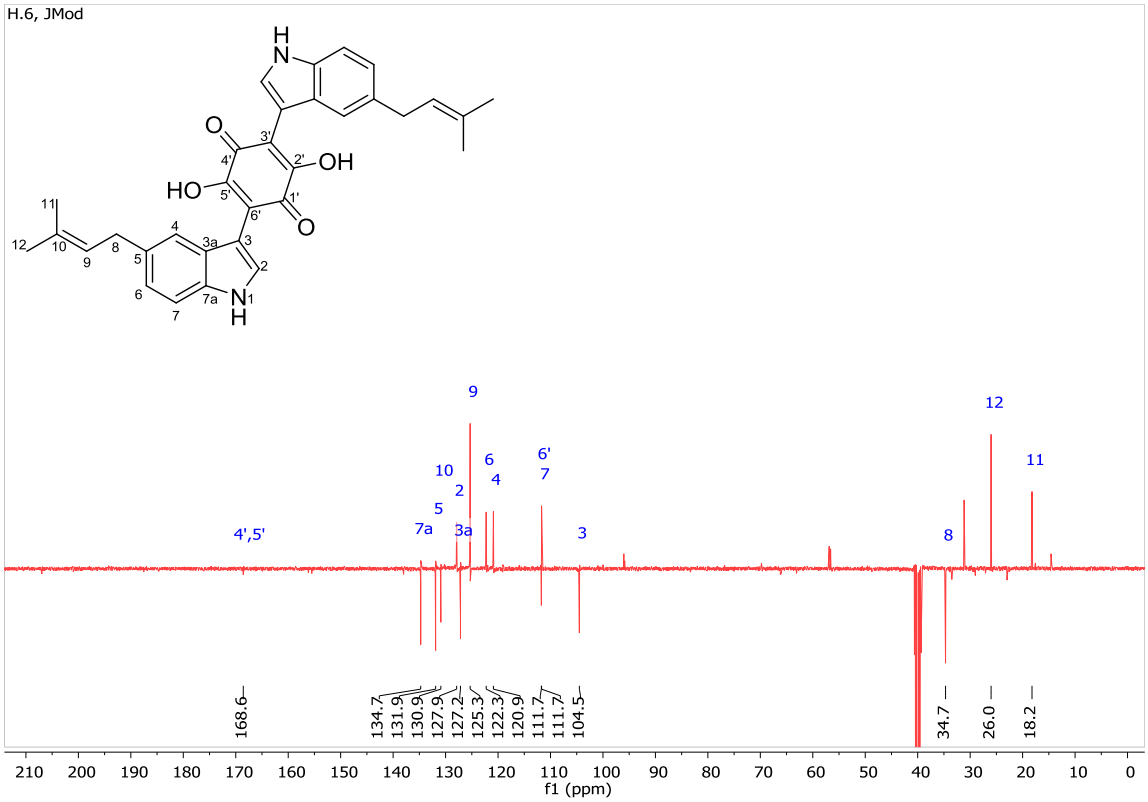

Figure A.VII.3: JMod NMR (100 MHz) spectrum for cochliodinol, measured in DMSO-d_6.

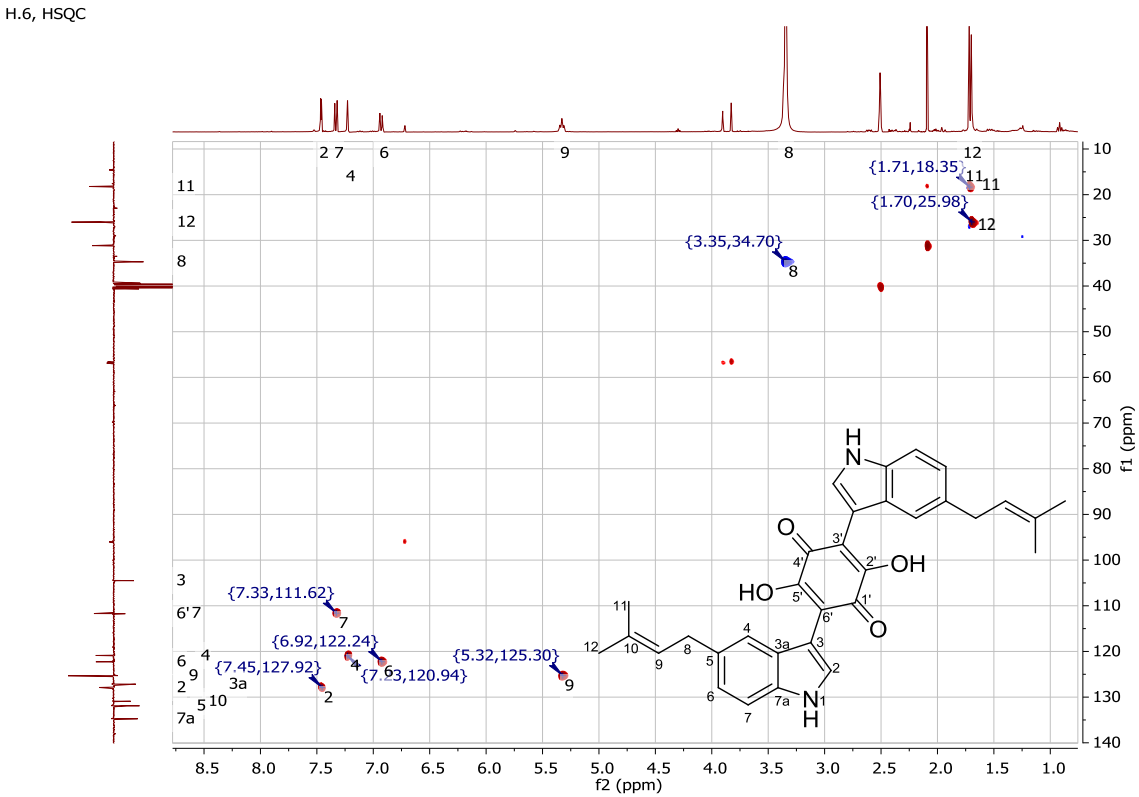

Figure A.VII.4: ^{1}H-^{13}C HSQC NMR (400 MHz) spectrum for cochliodinol, measured in DMSO-d_6.

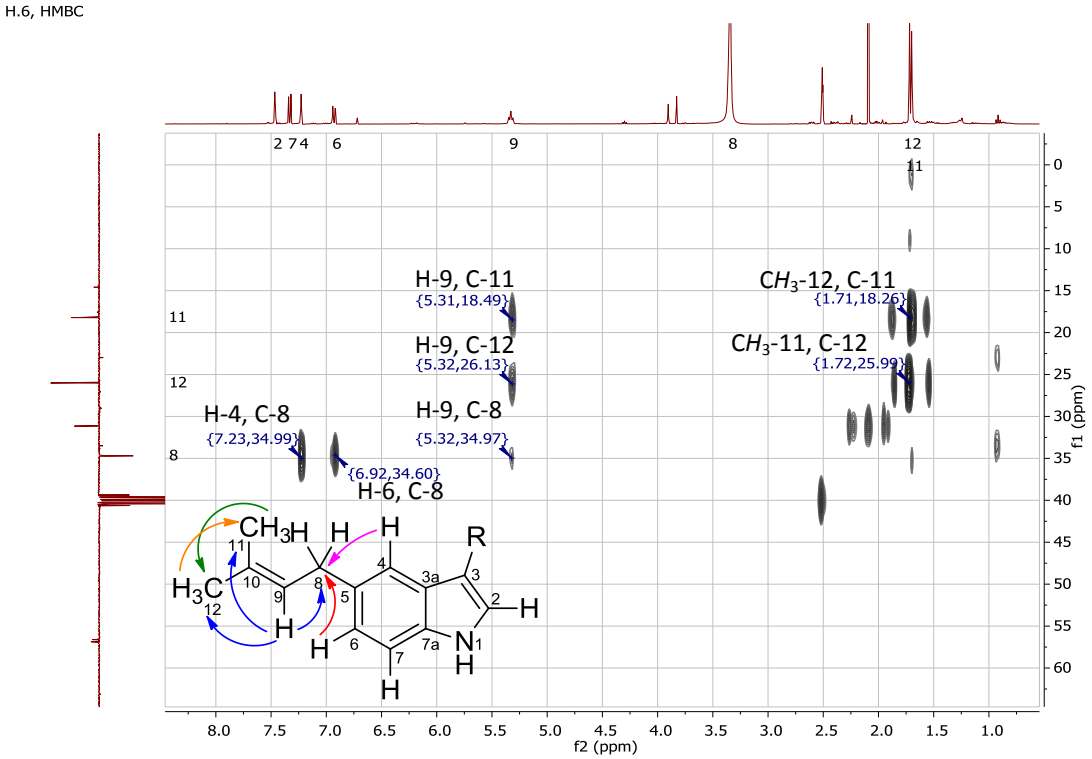

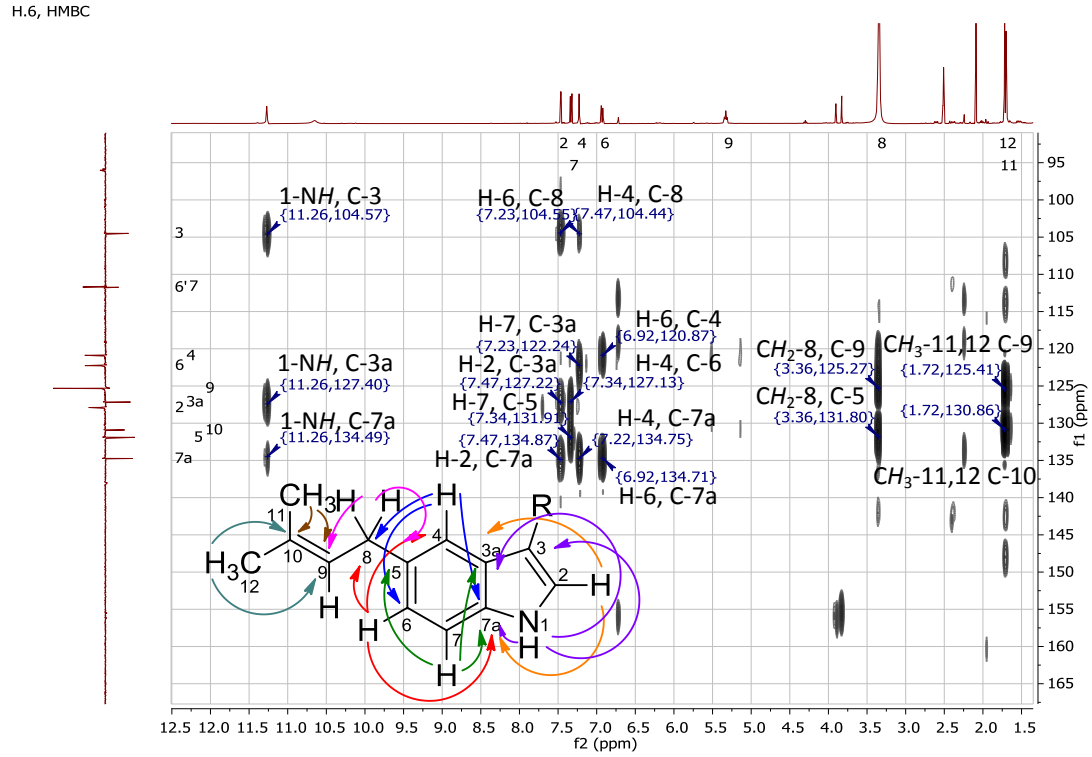

Figure A.VII.5: ^{1}H-^{13}C HMBC NMR (400 MHz) spectrum for cochliodinol, measured in DMSO-d_6.

Appendix VIII: NMR data of chaetomipyrrolidinone

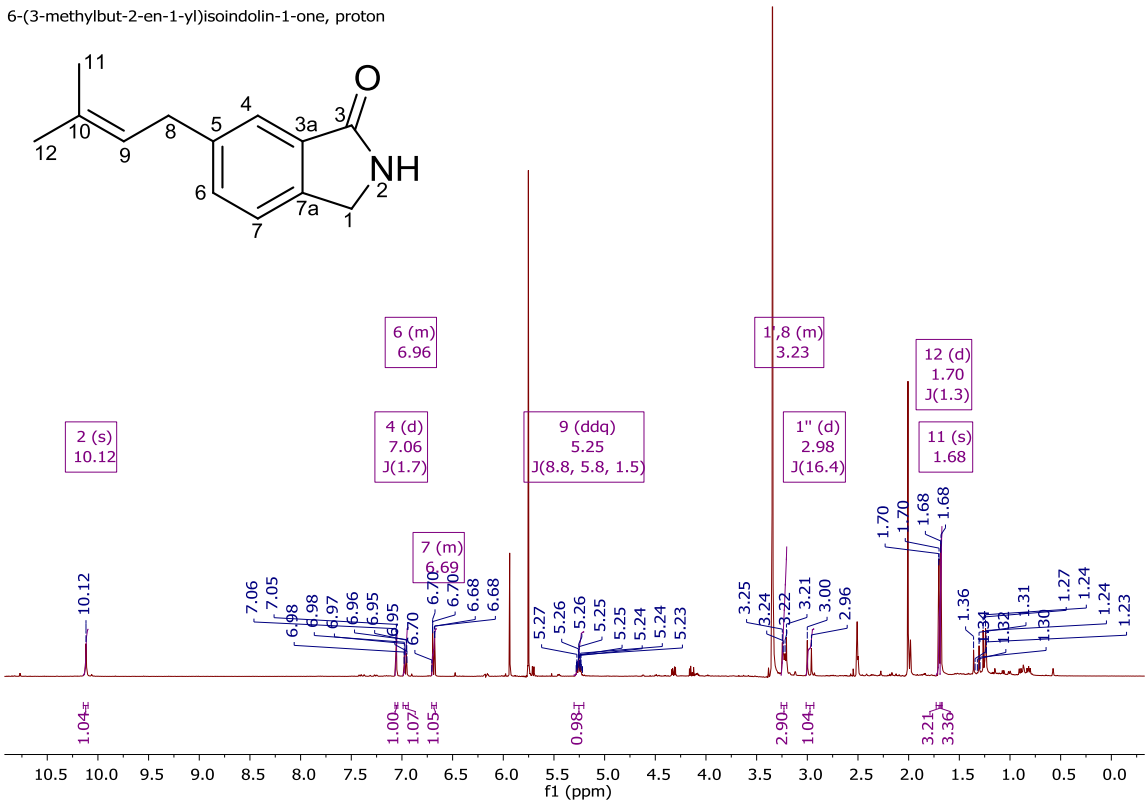

Figure A.VIII.1: ^{1}H NMR (400 MHz) spectrum for chaetomipyrrolidinone, measured in DMSO-d_6.

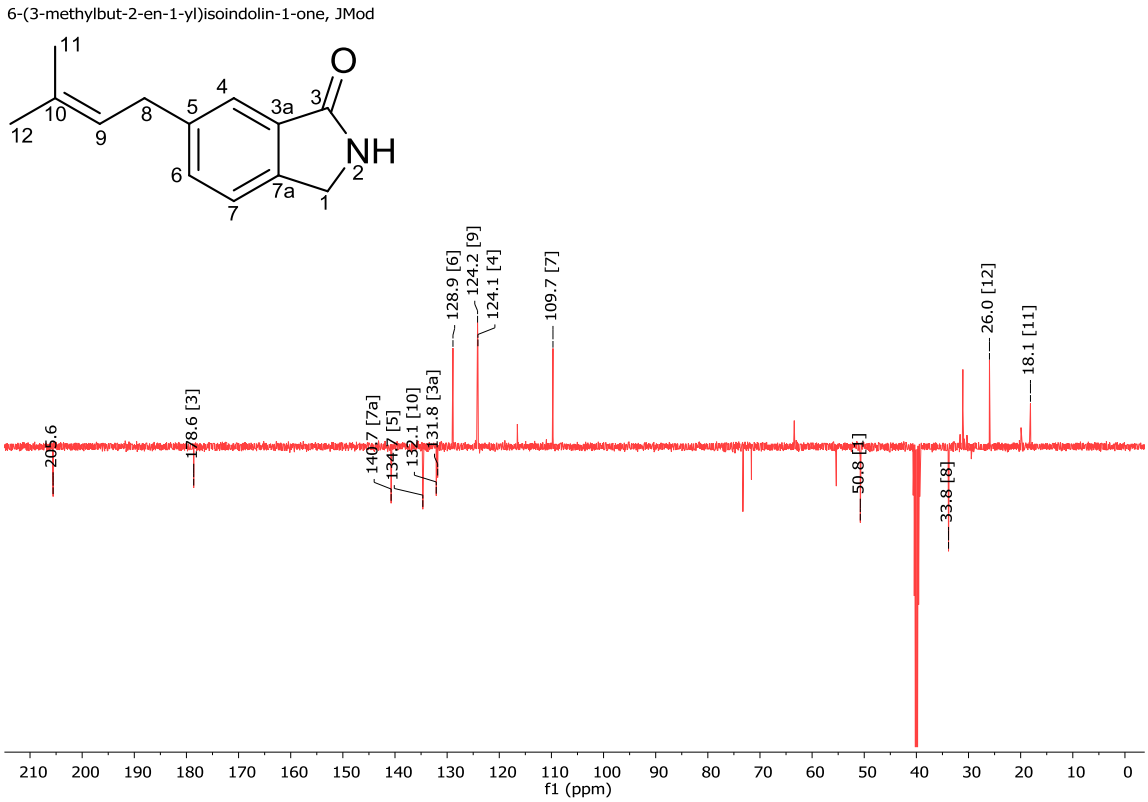

Figure A.VIII.2: JMod NMR (100 MHz) spectrum for chaetomipyrrolidinone, measured in DMSO-d_6.

Appendix IX: NMR data of chaetomiside A

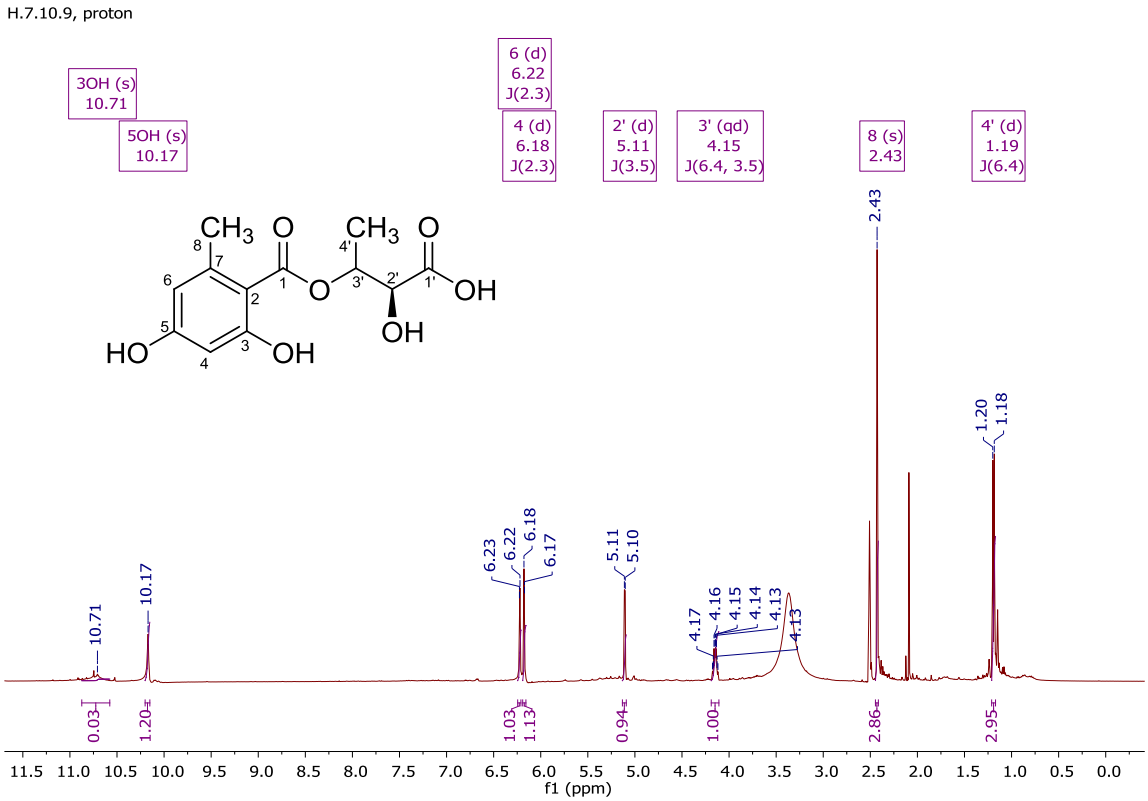

Figure A.IX.1: ^{1}H NMR (400 MHz) spectrum for chaetomiside A, measured in DMSO-d_6.

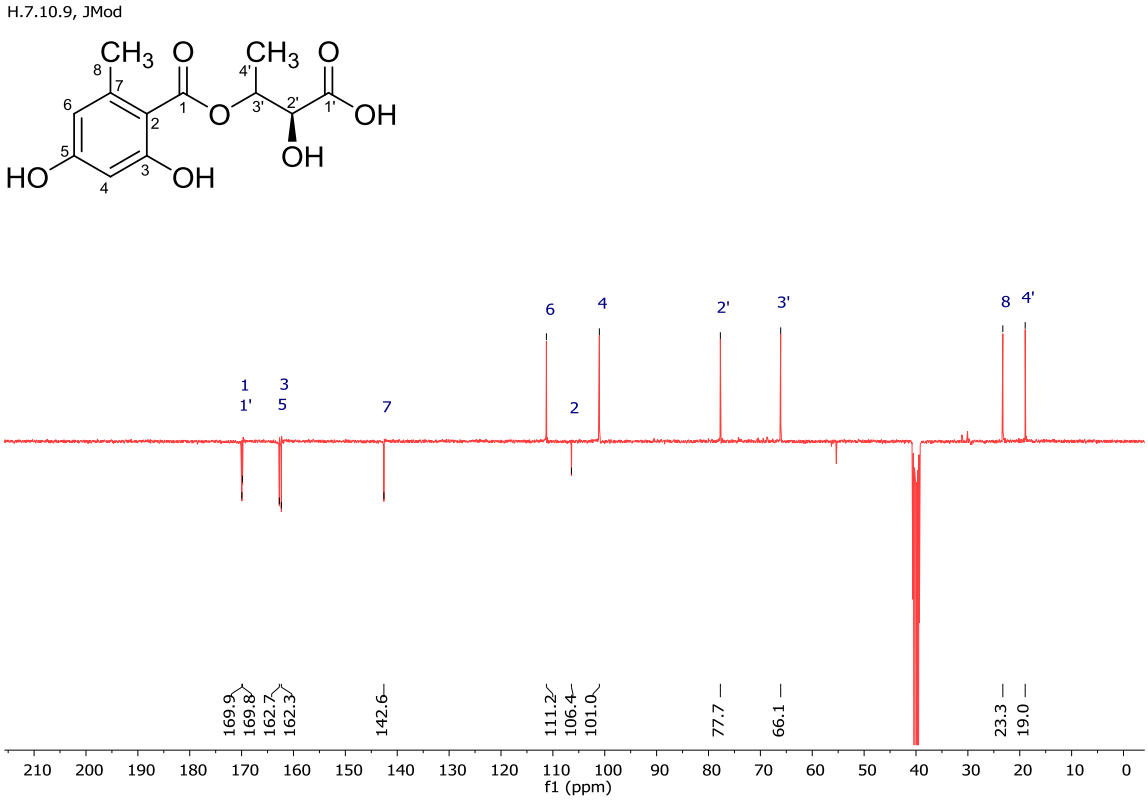

Figure A.IX.2: JMod NMR (100 MHz) spectrum for chaetomiside A, measured in DMSO-d_6.

Appendix X: NMR data of chaetomiside B

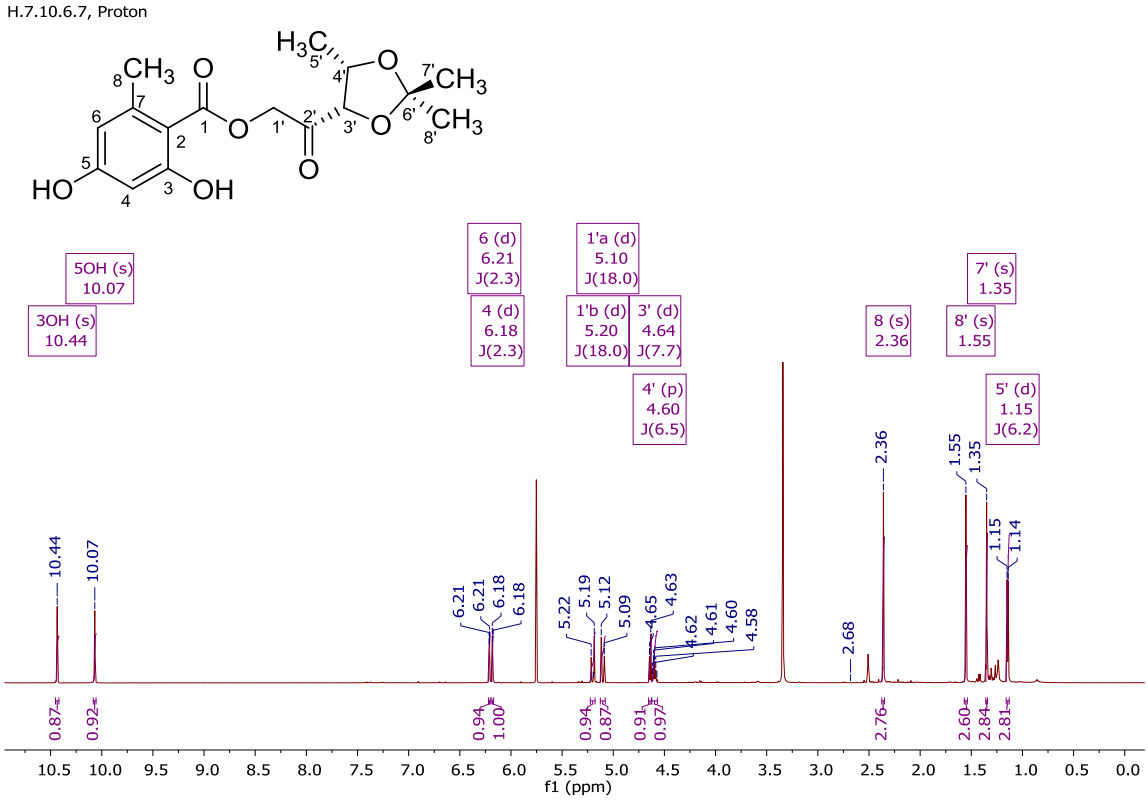

Figure A.X.1: ^{1}H NMR (600 MHz) spectrum for chaetomiside B, measured in DMSO-d_6.

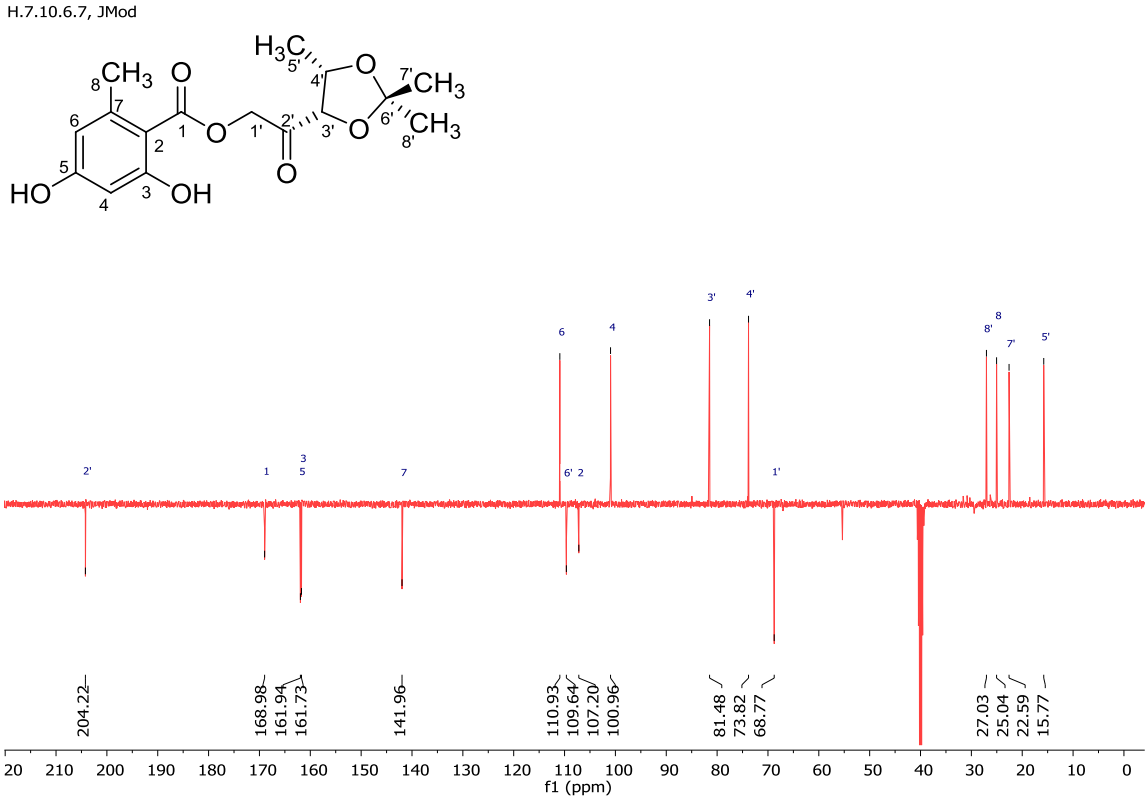

Figure A.X.2: JMod NMR (100 MHz) spectrum for chaetomiside B, measured in DMSO-d_6.

Appendix XI: NMR data of chaetomiside C

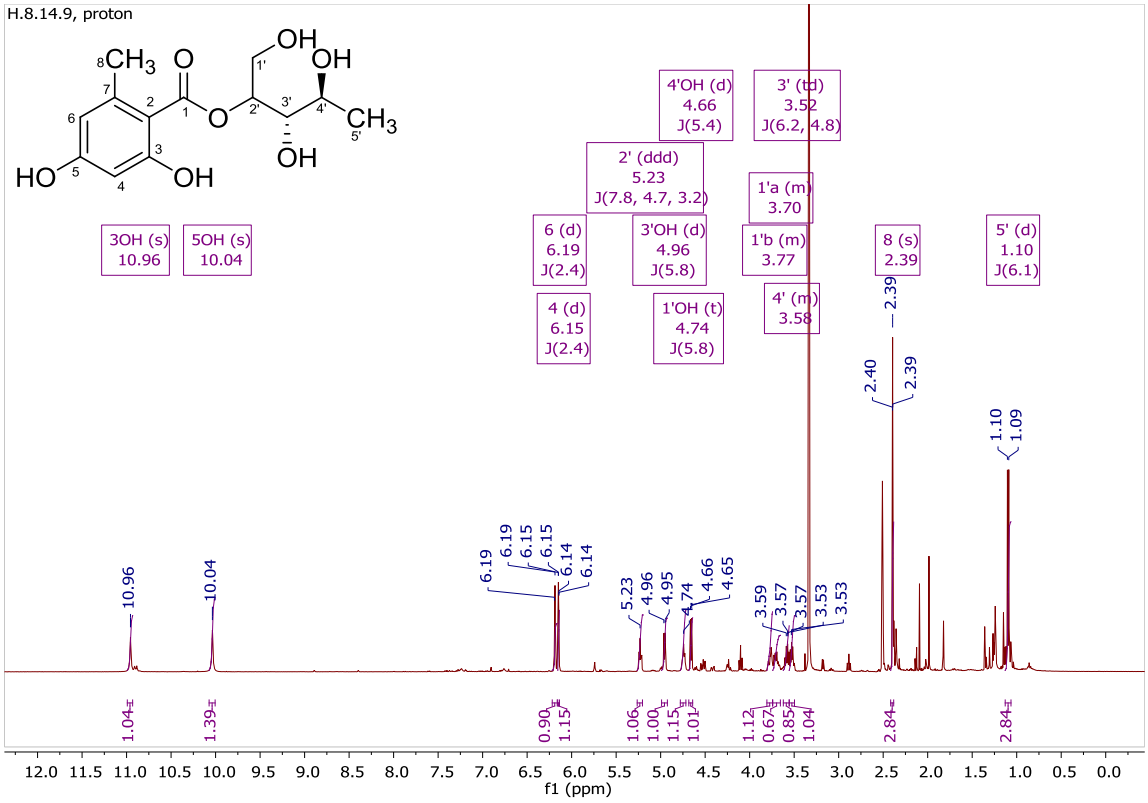

Figure A.XI.1: ^{1}H NMR (400 MHz) spectrum for chaetomiside C, measured in DMSO-d_6.

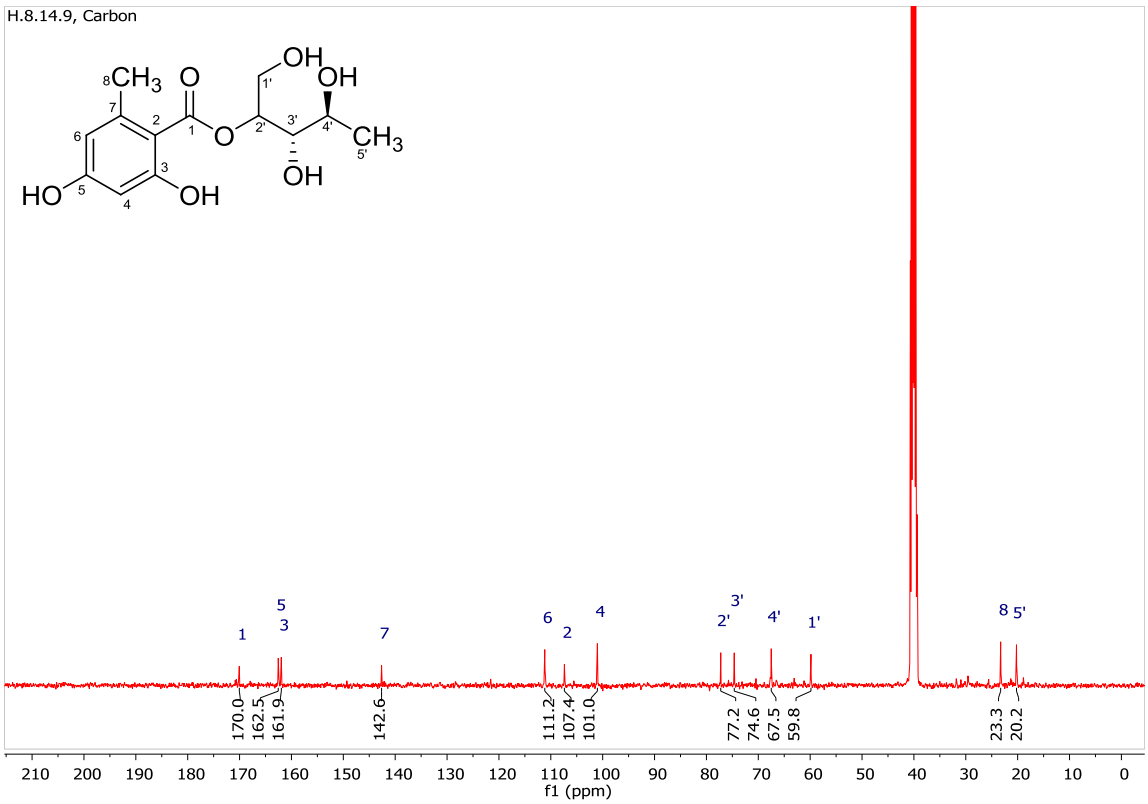

Figure A.XI.2: ^{13}C NMR (100 MHz) spectrum for chaetomiside C, measured in DMSO-d_6.

Appendix XII: NMR data of chaetomiside D

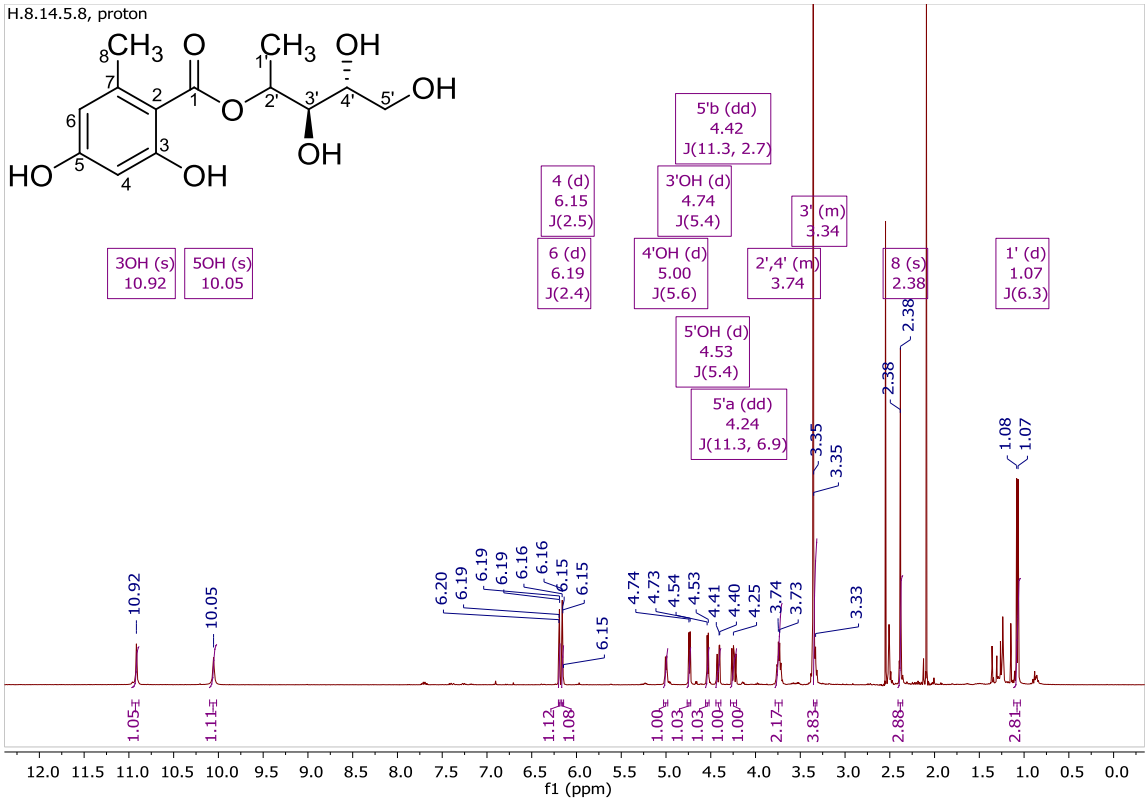

Figure A.XII.1: ^{1}H NMR (400 MHz) spectrum for chaetomiside D, measured in DMSO-d_6.

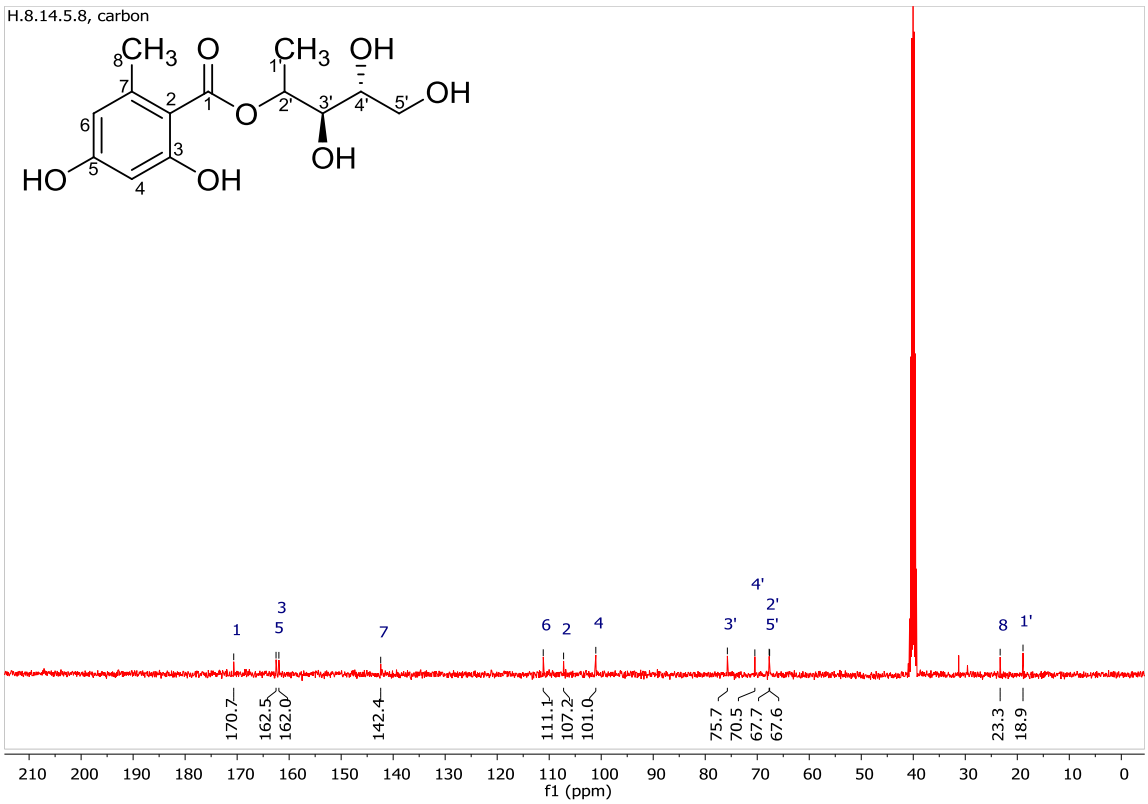

Figure A.XII.2: ^{13}C NMR (100 MHz) spectrum for chaetomiside D, measured in DMSO-d_6.

Appendix XIII: NMR data of hymeglusin

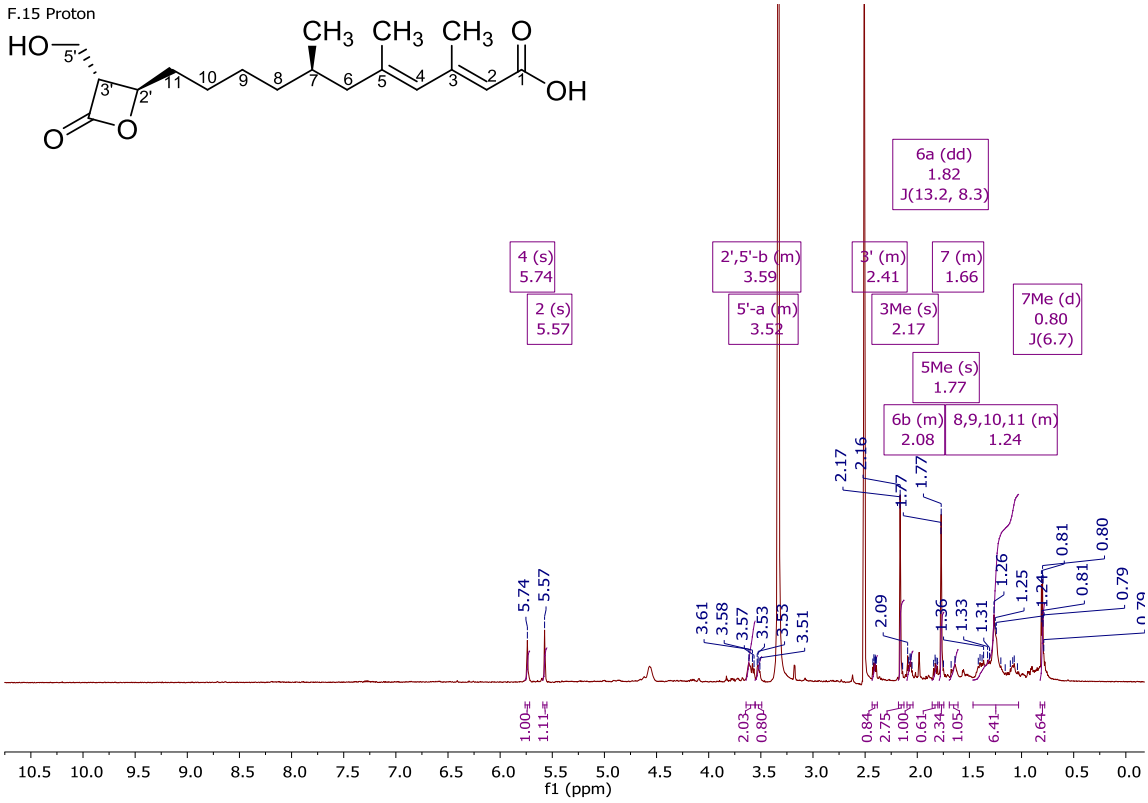

Figure A.XIII.1: ^{1}H NMR (600 MHz) spectrum for hymeglusin, measured in DMSO-d_6.

F.15 COSY

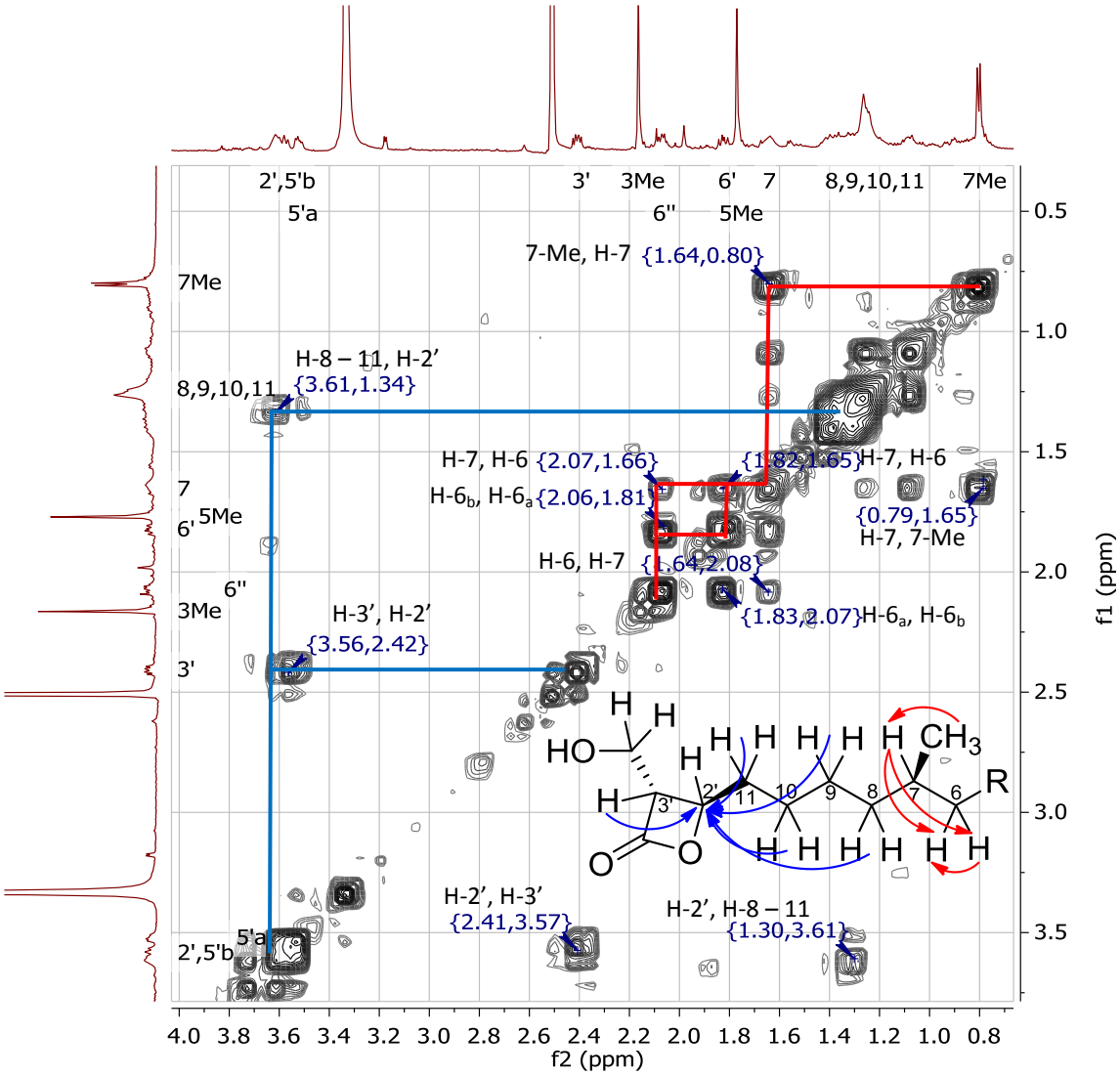

Figure A.XIII.2: ^{1}H-^{1}H COSY NMR (600 MHz) spectrum for hymeglusin, measured in DMSO-d_6.

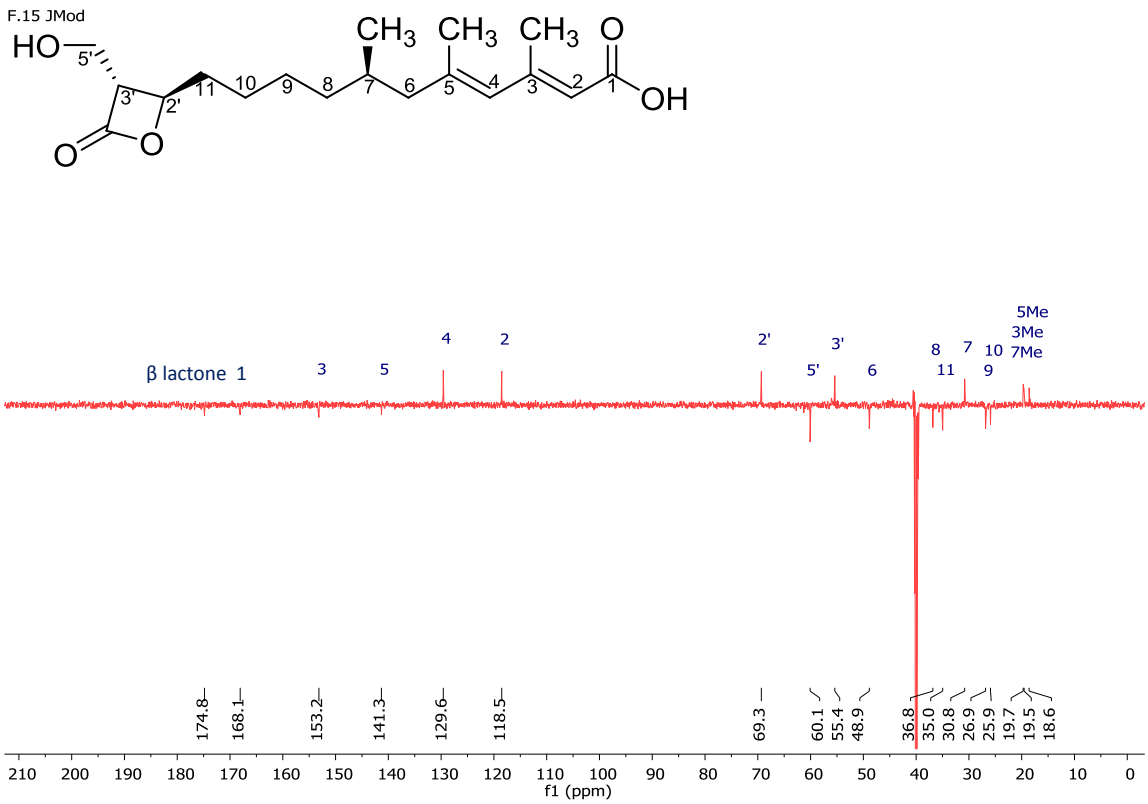

Figure A.XIII.3: JMod NMR (150 MHz) spectrum for hymeglusin, measured in DMSO-d_6.

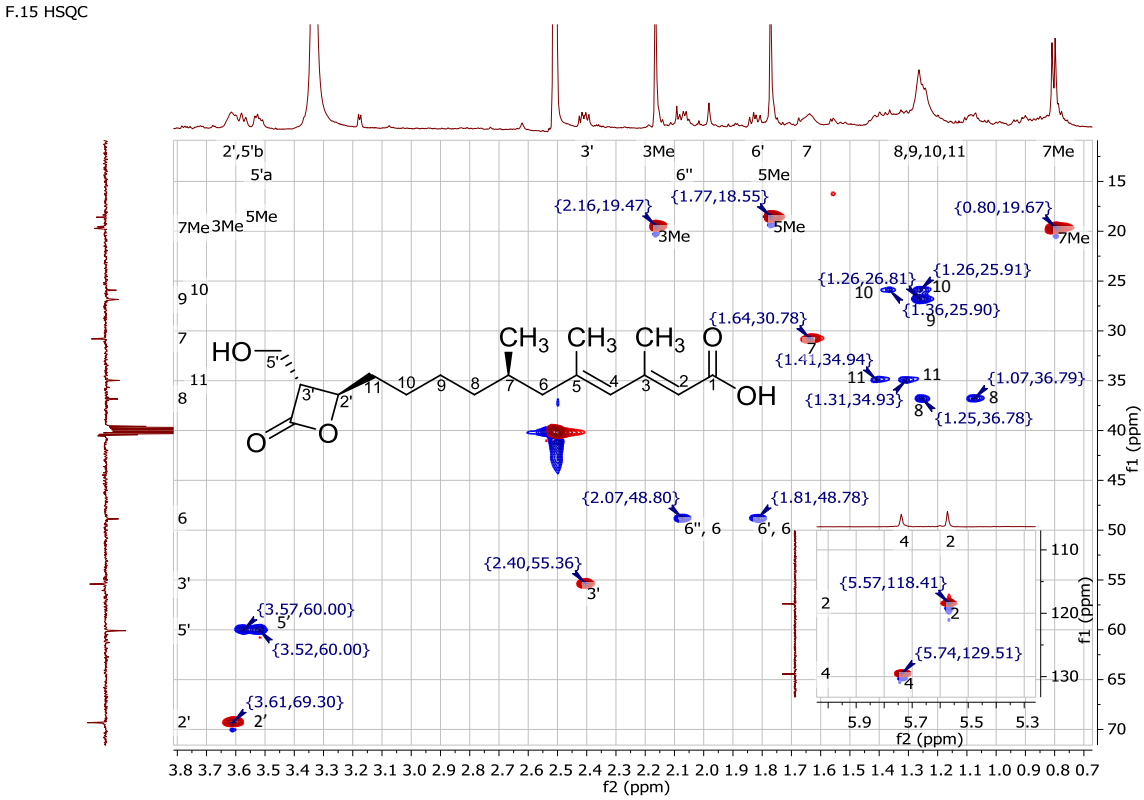

Figure A.XIII.4: ^{1}H-^{13}C HSQC NMR (600 MHz) spectrum for hymeglusin, measured in DMSO-d_6.

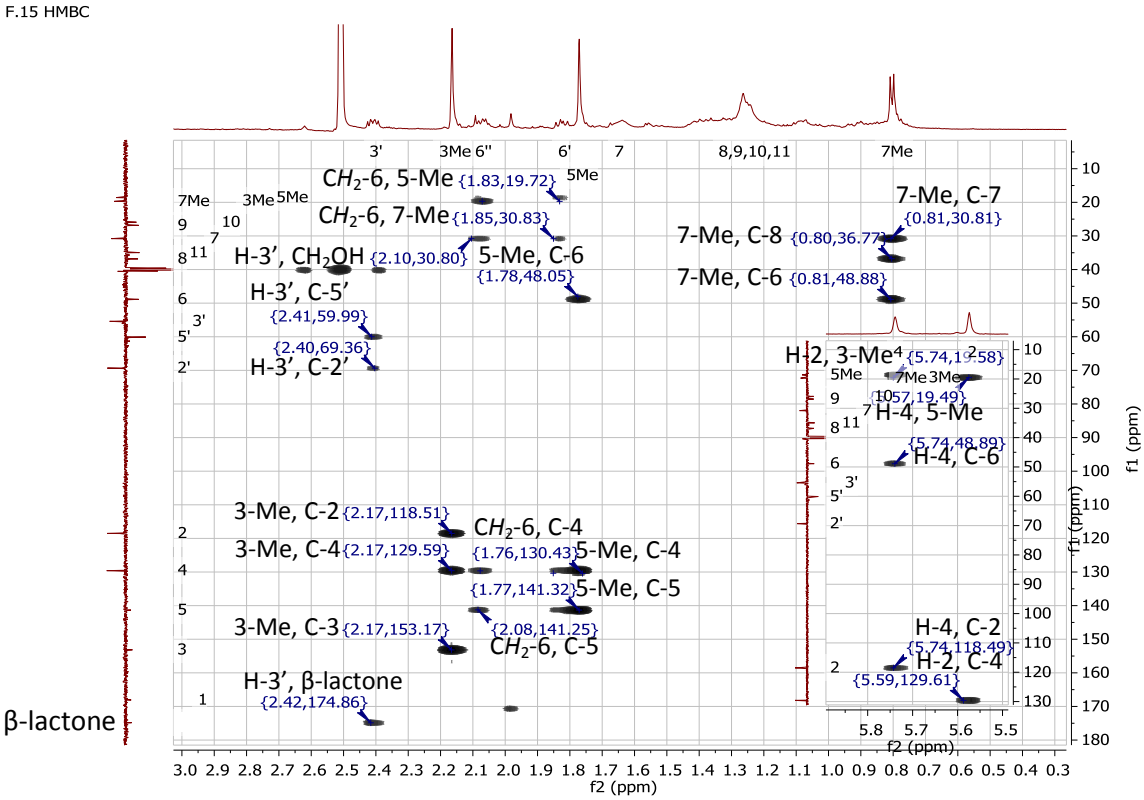

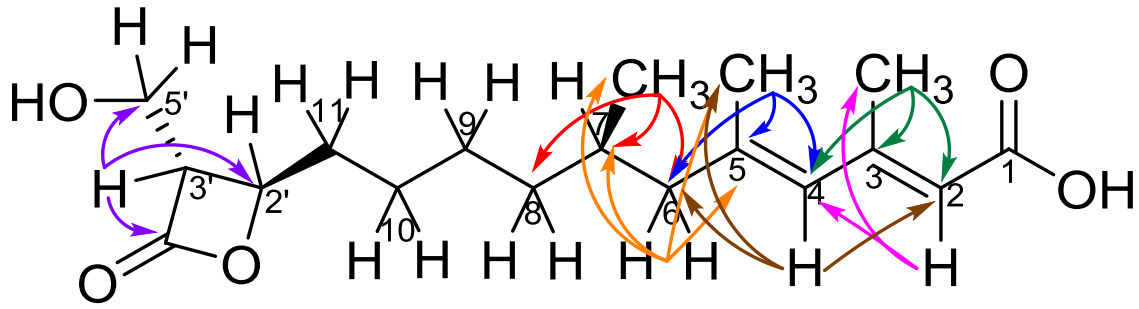

Figure A.XIII.5: ^{1}H-^{13}C HMBC NMR (600 MHz) spectrum for hymeglusin, measured in DMSO-d_6.

Appendix XIV: NMR data of enniatin A

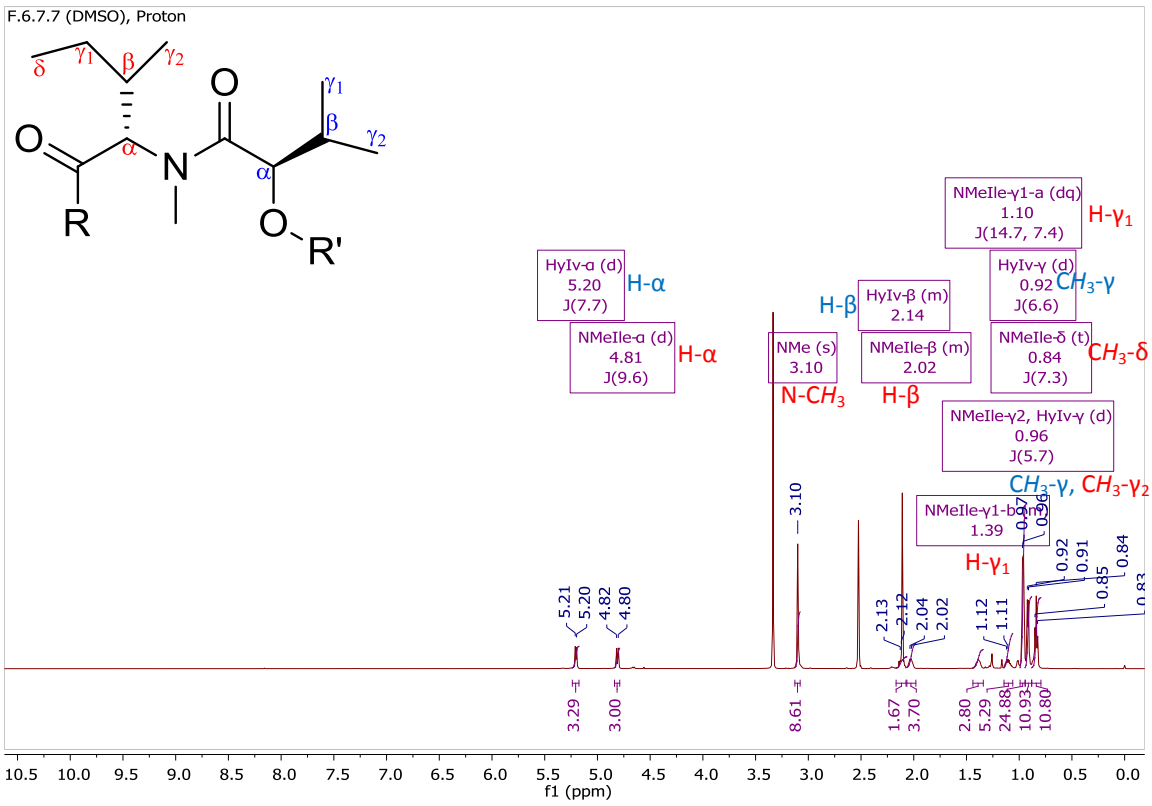

Figure A.XIV.1: ^{1}H NMR (600 MHz) spectrum for enniatin A, measured in DMSO-d_6. Red-labelled signals belong to the NMeIle moiety while blue-labelled signals belong to the HyIv moiety.

F.6.7.7 (DMSO), COSY

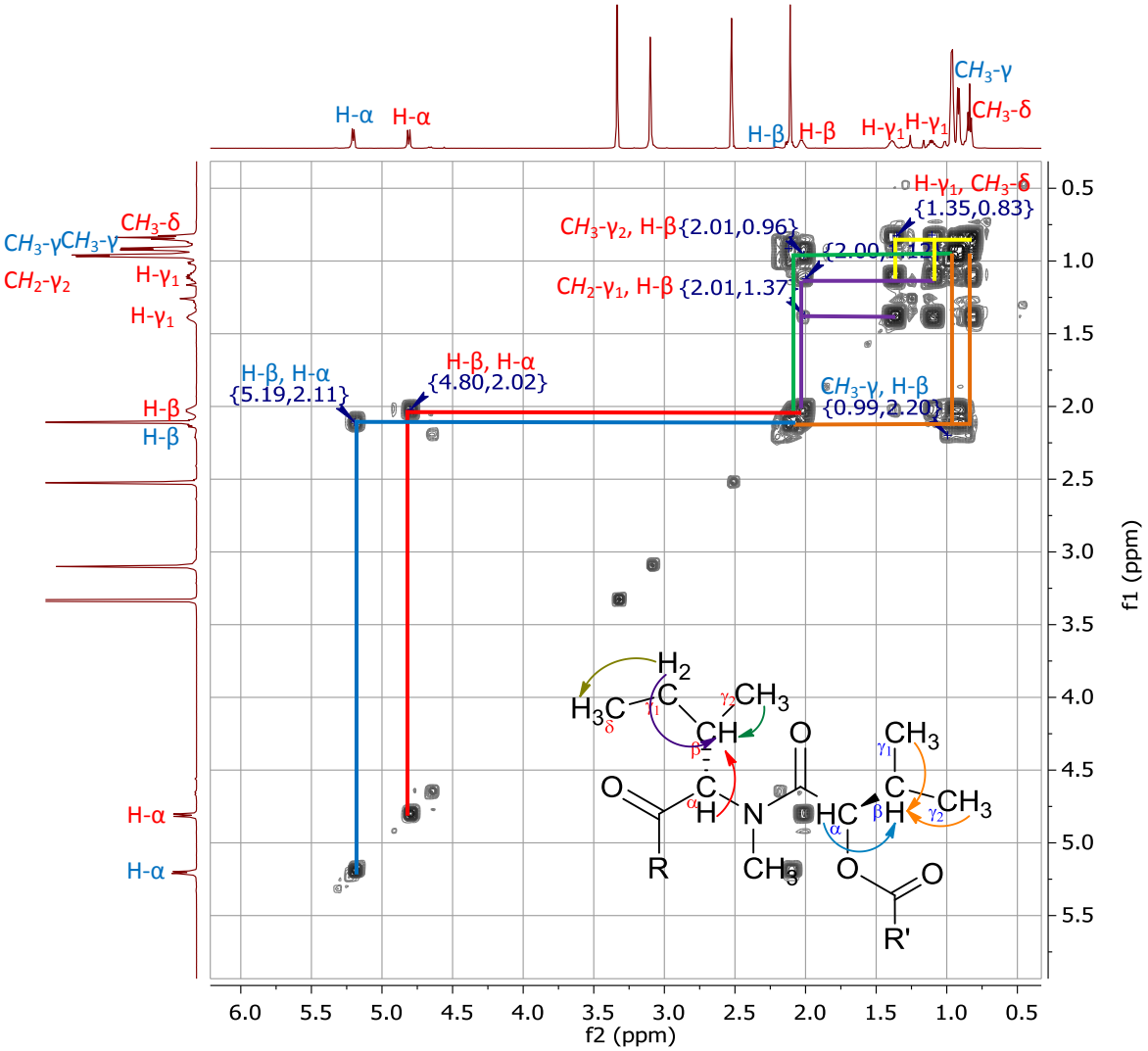

Figure A.XIV.2: ^{1}H-^{1}H COSY NMR (600 MHz) spectrum for enniatin A, measured in DMSO-d_6. Red-labelled signals belong to the NMeIle moiety while blue-labelled signals belong to the Hylv moiety.

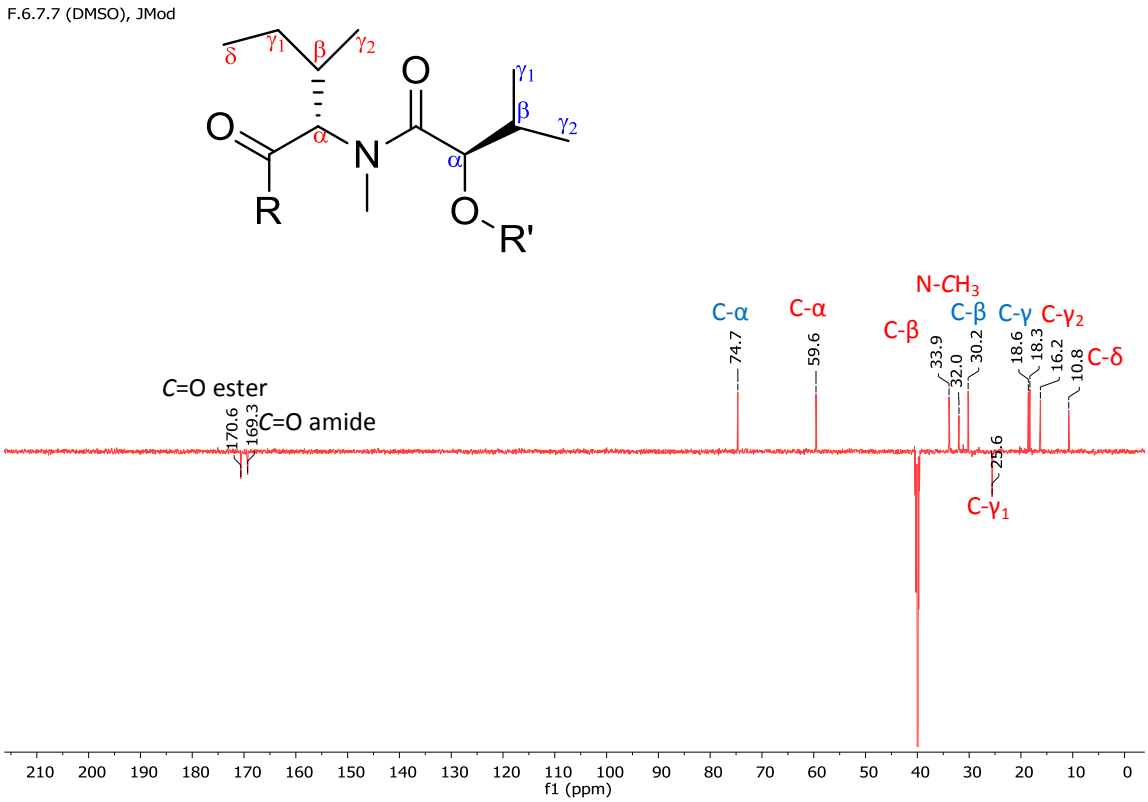

Figure A.XIV.3: JMod NMR (150 Hz) spectrum for enniatin A, measured in DMSO-d_6. Red-labelled signals belong to the NMeIle moiety while blue-labelled signals belong to the HyIv moiety.

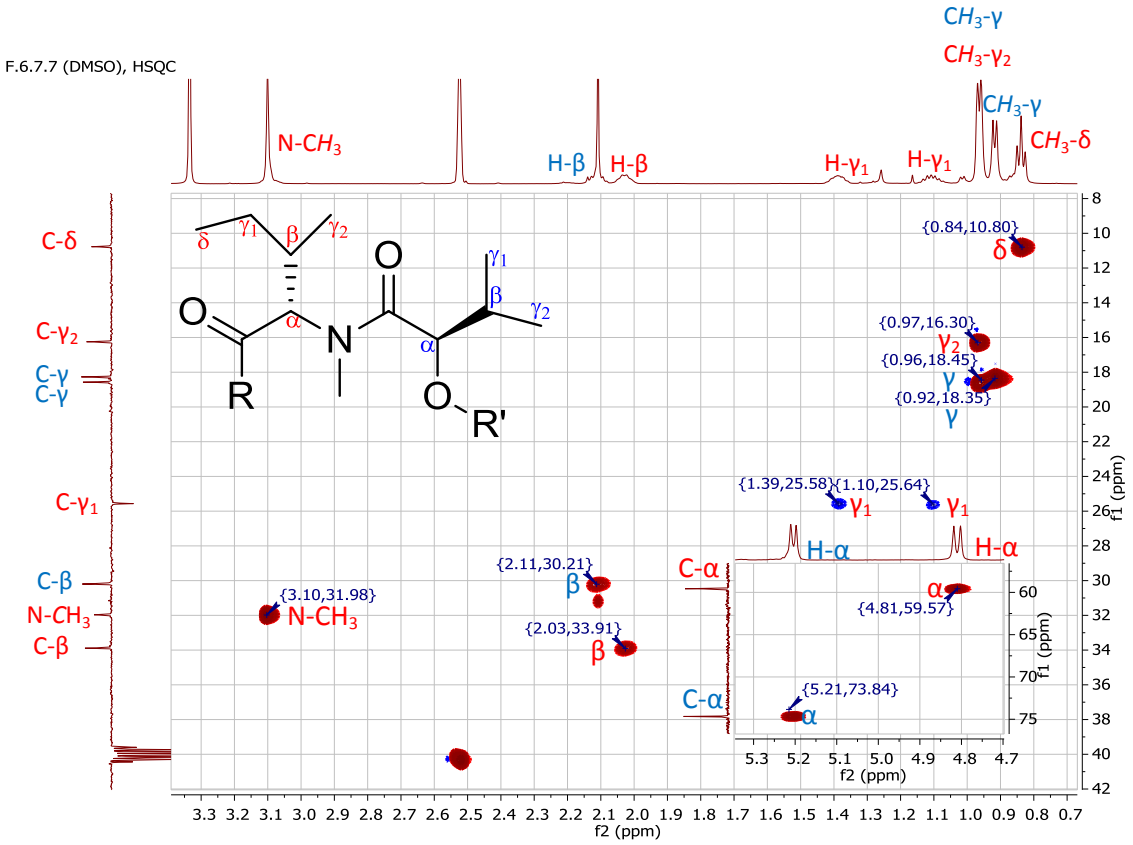

Figure A.XIV.4: ^{1}H-^{13}C HSQC NMR (600 MHz) spectrum for enniatin A, measured in DMSO-d_6. Red-labelled signals belong to the NMeIle moiety while blue-labelled signals belong to the HyIv moiety.

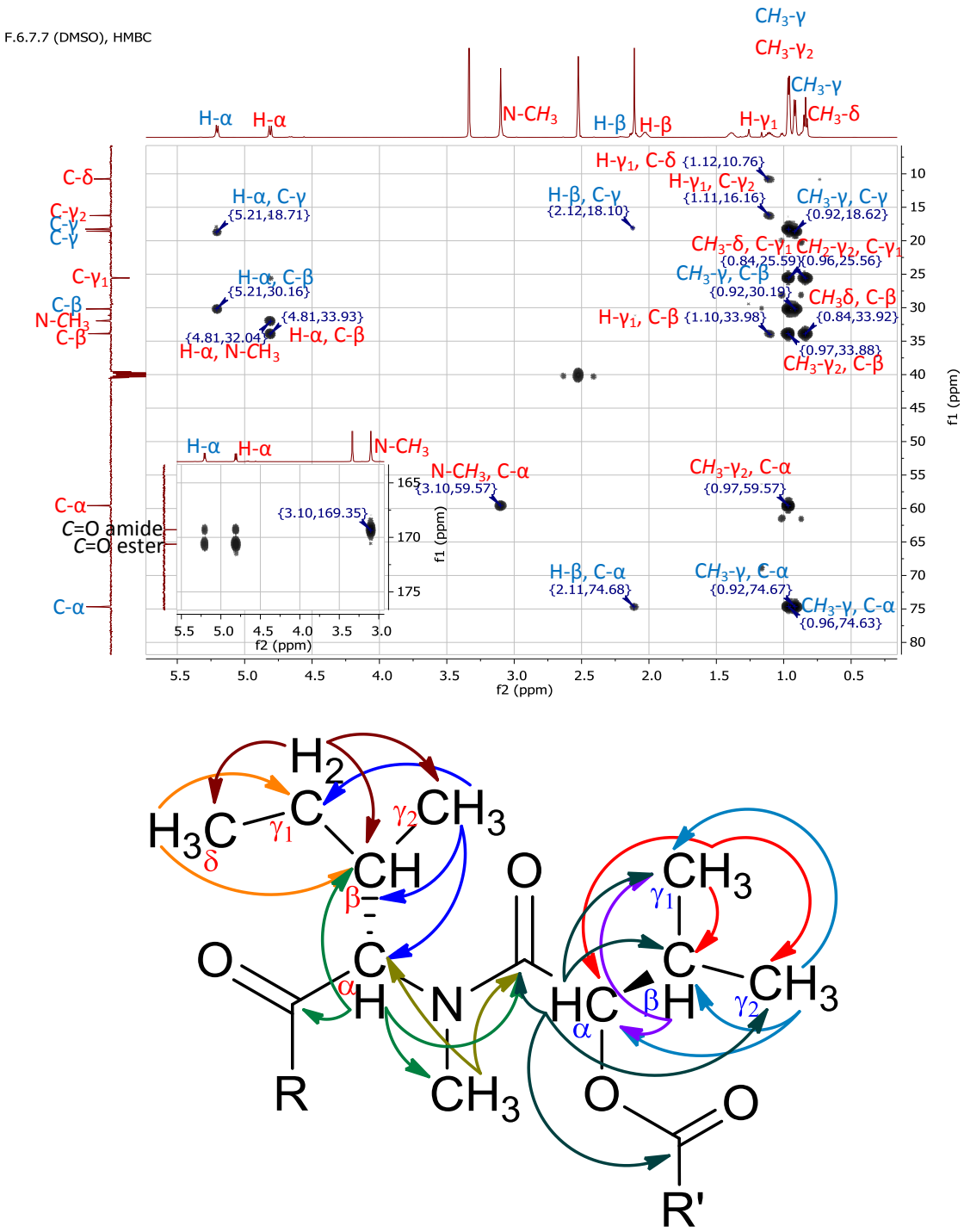

Figure A.XIV.5: ^{1}H-^{13}C HMBC (600 MHz) NMR spectrum for enniatin A, measured in DMSO-d_6. Red-labelled signals belong to the NMeIle moiety while blue-labelled signals belong to the HyIv moiety.

Appendix XV: NMR data of enniatin A_1

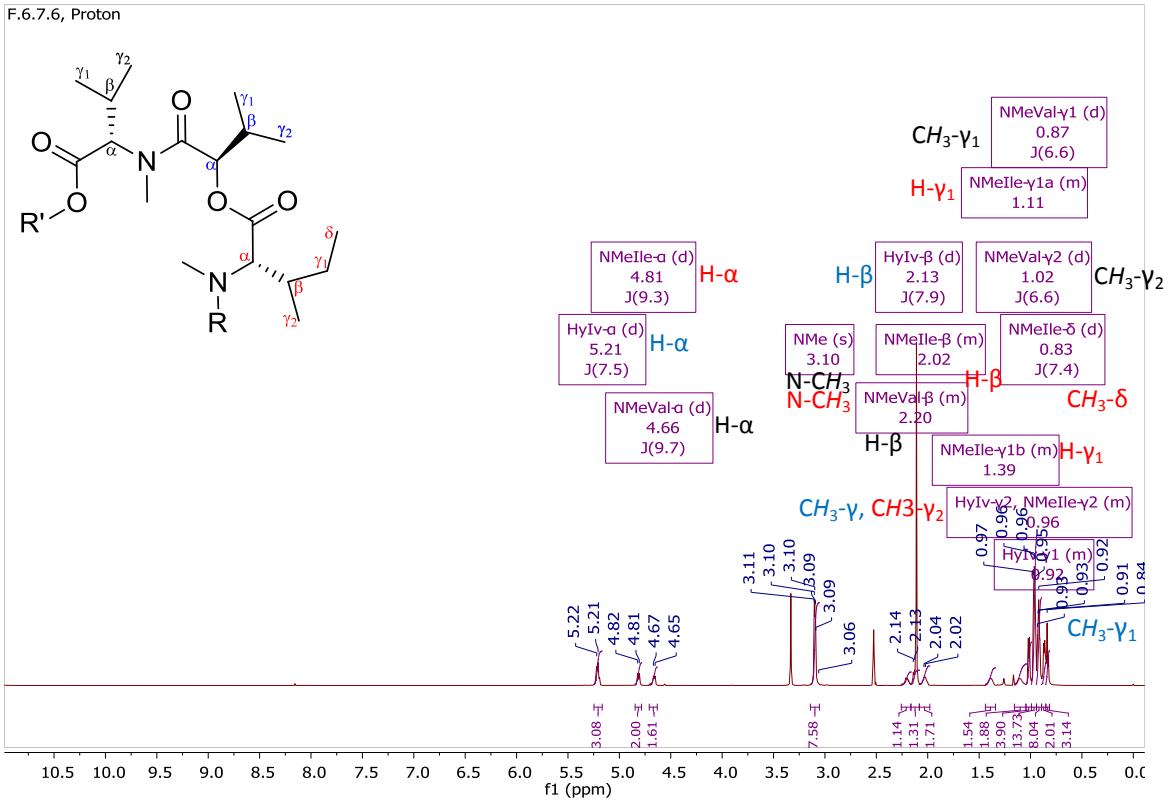

Figure A.XV.1: ^{1}H NMR (600 MHz) spectrum for enniatin A_1, measured in DMSO-d_6. Red-labelled signals belong to the NMeIle moiety, blue-labelled signals belong to the HyIv moiety and black-labelled signals belong to the NMeVal moiety.

F.6.7.6, COSY

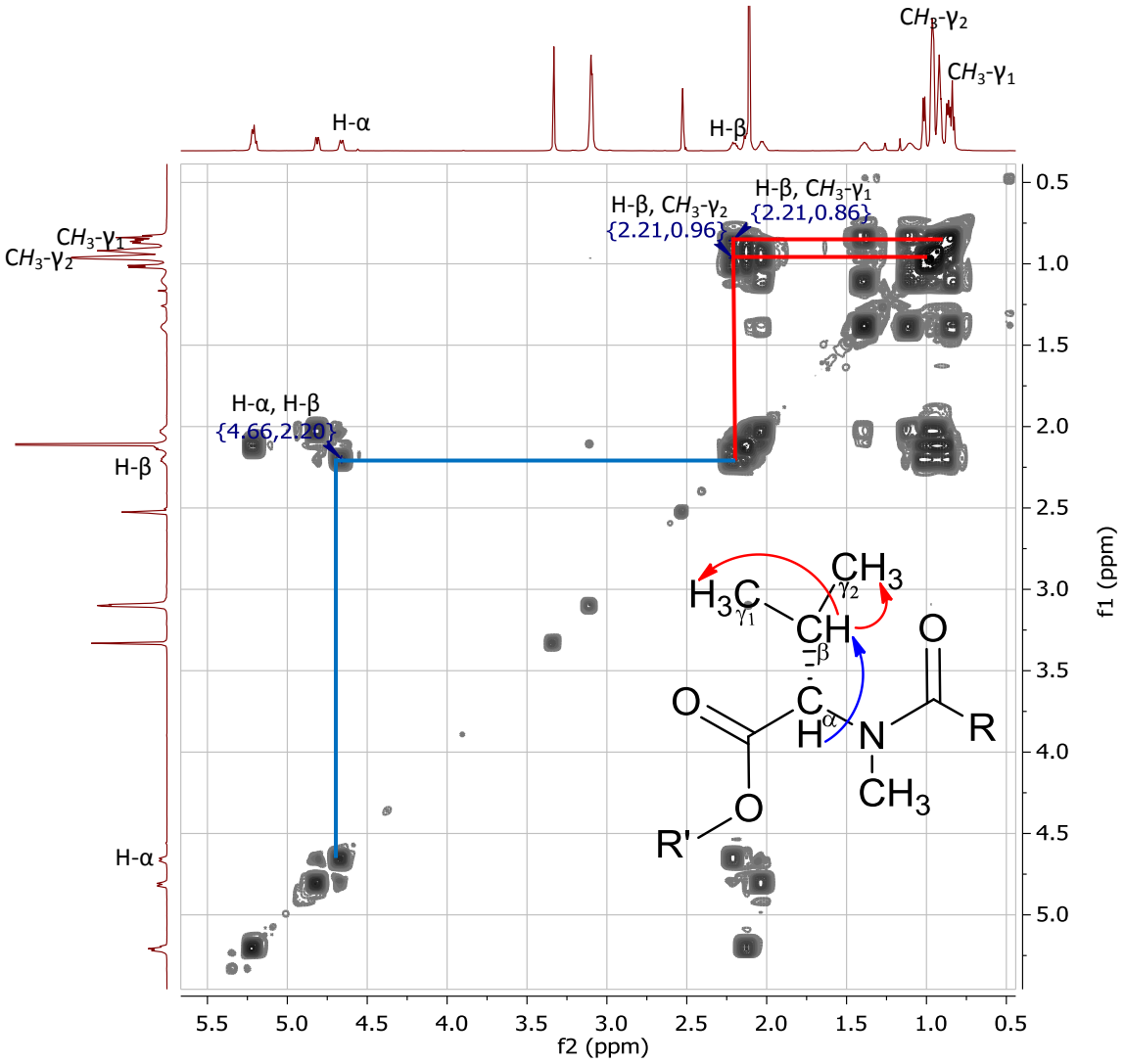

Figure A.XV.2: ^{1}H-^{1}H COSY NMR (600 MHz) spectrum for enniatin A_1, measured in DMSO-d_6. Red-labelled signals belong to the NMeIle moiety, blue-labelled signals belong to the HyIv moiety and black-labelled signals belong to the NMeVal moiety.

F.6.7.6, JMod

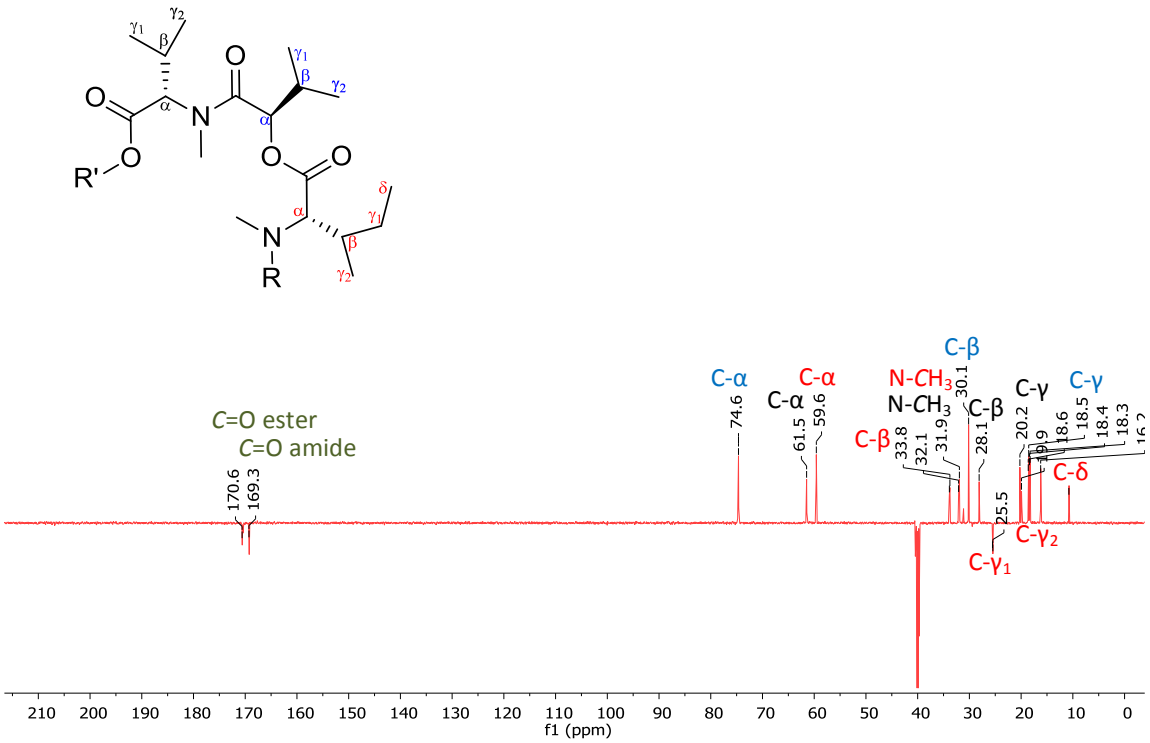

Figure A.XV.3: JMod NMR (150 MHz) spectrum for enniatin A_1, measured in DMSO-d_6. Red-labelled signals belong to the NMeIle moiety, blue-labelled signals belong to the HyIv moiety and black-labelled signals belong to the NMeVal moiety.

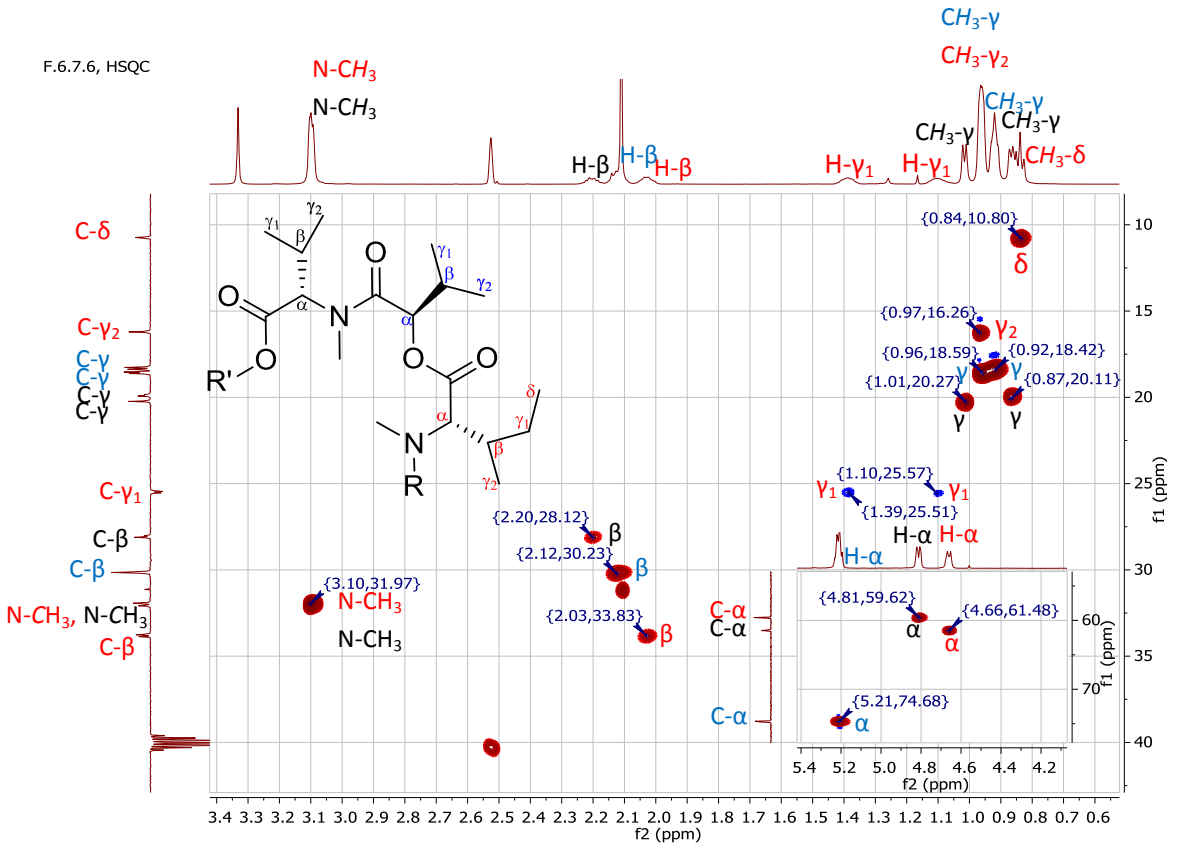

Figure A.XV.4: ^{1}H-^{13}C HSQC NMR (600 MHz) spectrum for enniatin A_1, measured in DMSO-d_6. Red-labelled signals belong to the NMeIle moiety, blue-labelled signals belong to the Hylv moiety and black-labelled signals belong to the NMeVal moiety.

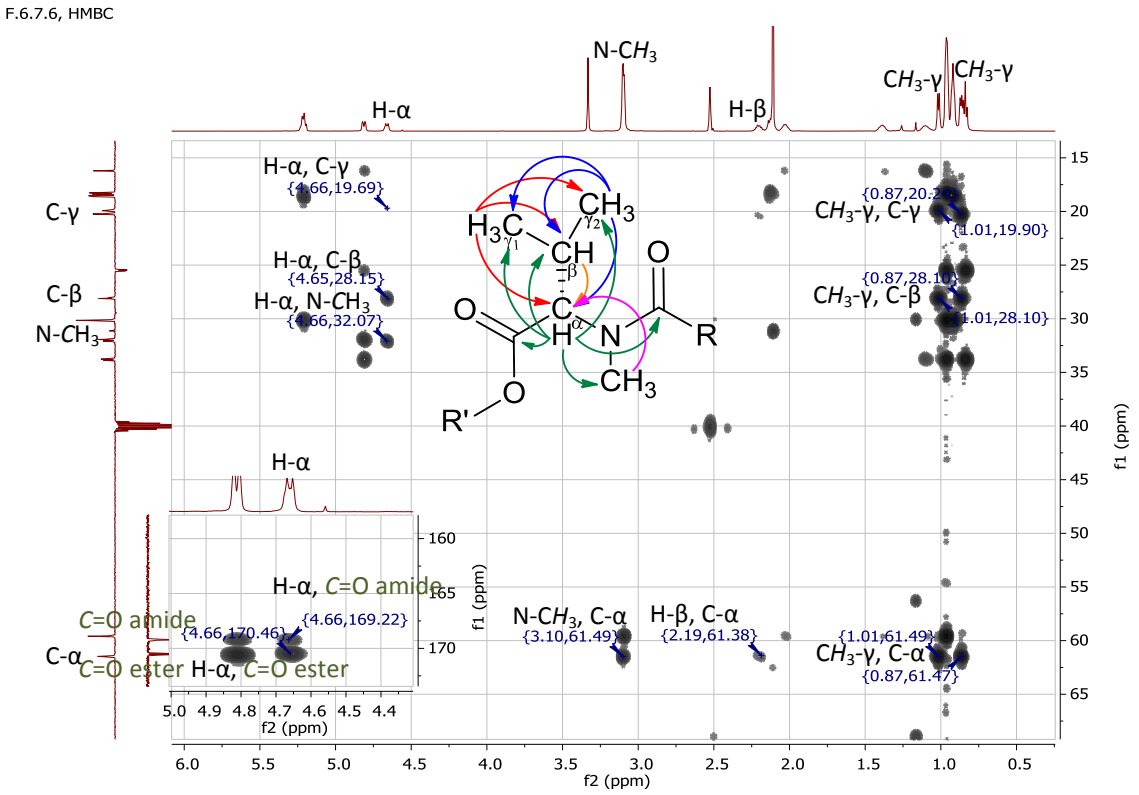

Figure A.XV.5: ^{1}H-^{13}C HMBC NMR (600 MHz) spectrum for enniatin A_1, measured in DMSO-d_6. Red-labelled signals belong to the NMeIle moiety, blue-labelled signals belong to the Hylv moiety and black-labelled signals belong to the NMeVal moiety.

Appendix XVI: NMR data of enniatin B

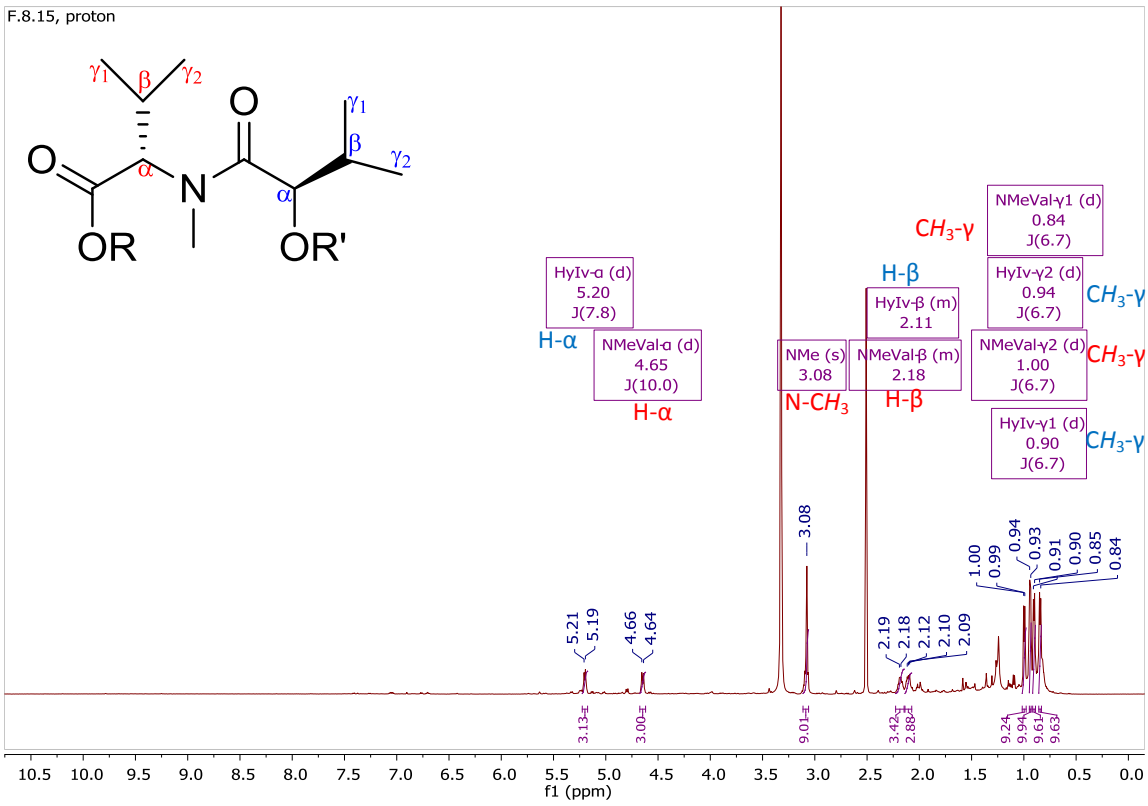

Figure A.XVI.1: ^{1}H NMR spectrum for enniatin B, measured in DMSO-d_6, (600 MHz). Red-labelled signals belong to the NMeVal moiety while blue-labelled signals belong to the HyIv moiety.

F.8.15, COSY

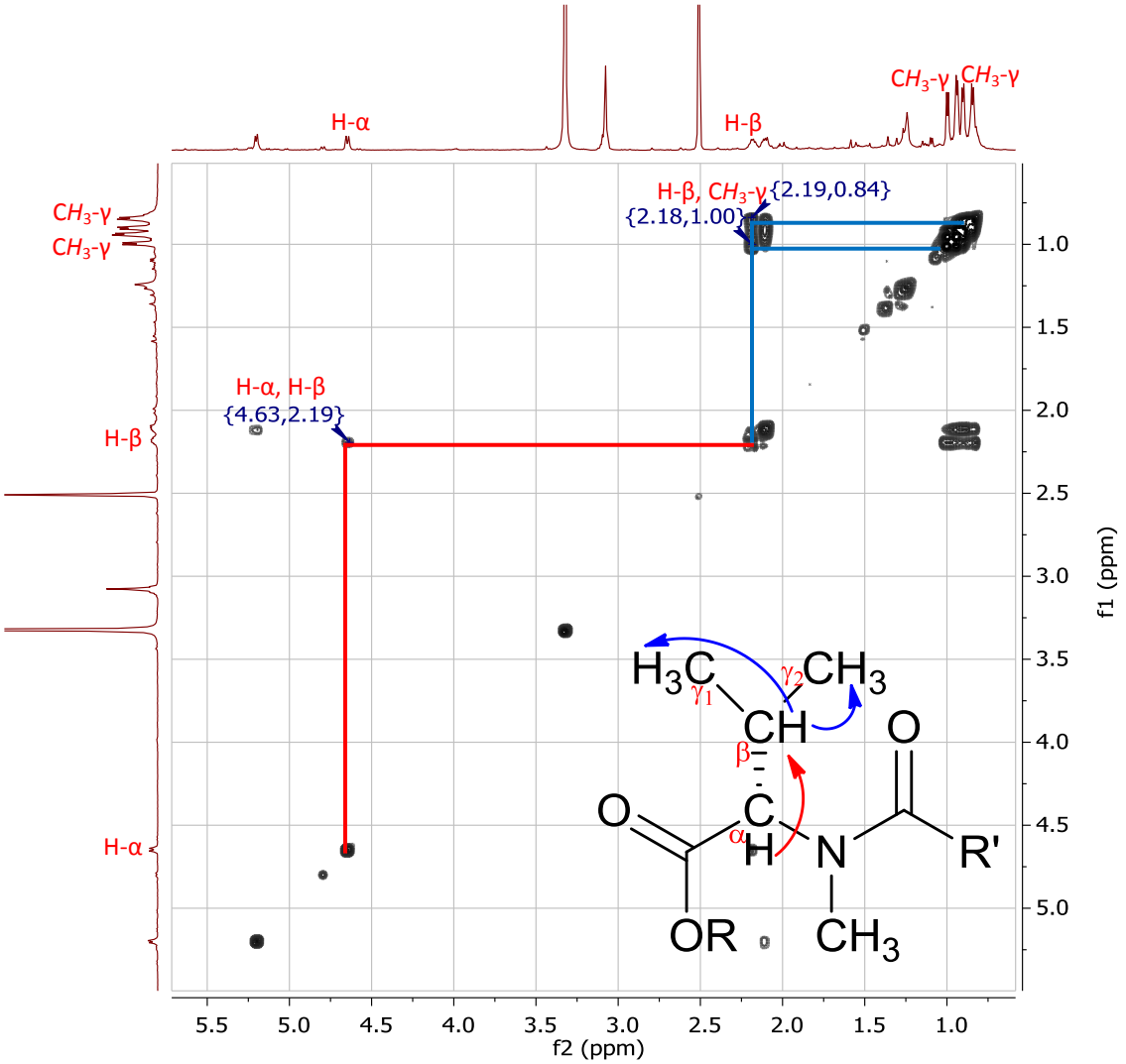

Figure A.XVI.2: ^{1}H-^{1}H COSY NMR (600 MHz) spectrum for enniatin B, measured in DMSO-d_6. Red-labelled signals belong to the NMeVal moiety while blue-labelled signals belong to the Hylv moiety.

F.8.15, JMod

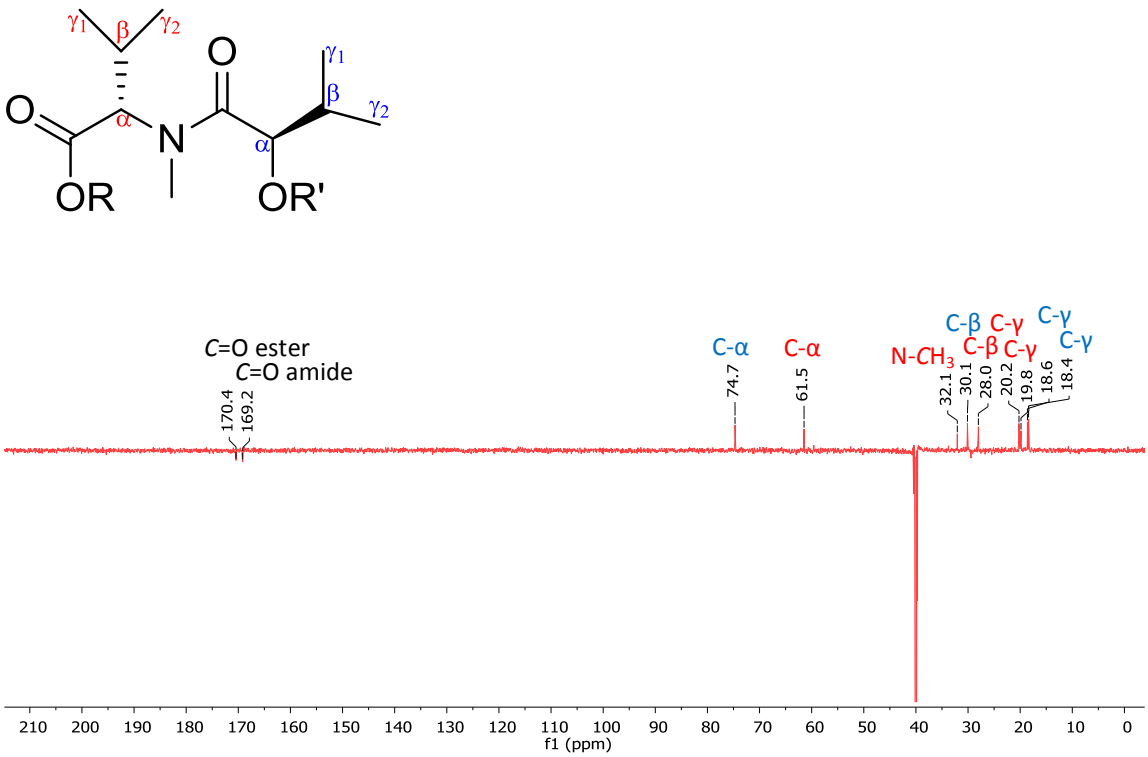

Figure A.XVI.3: JMod NMR (150 MHz) spectrum for enniatin B, measured in DMSO-d_6. Red-labelled signals belong to the NMeVal moiety while blue-labelled signals belong to the HyIv moiety.

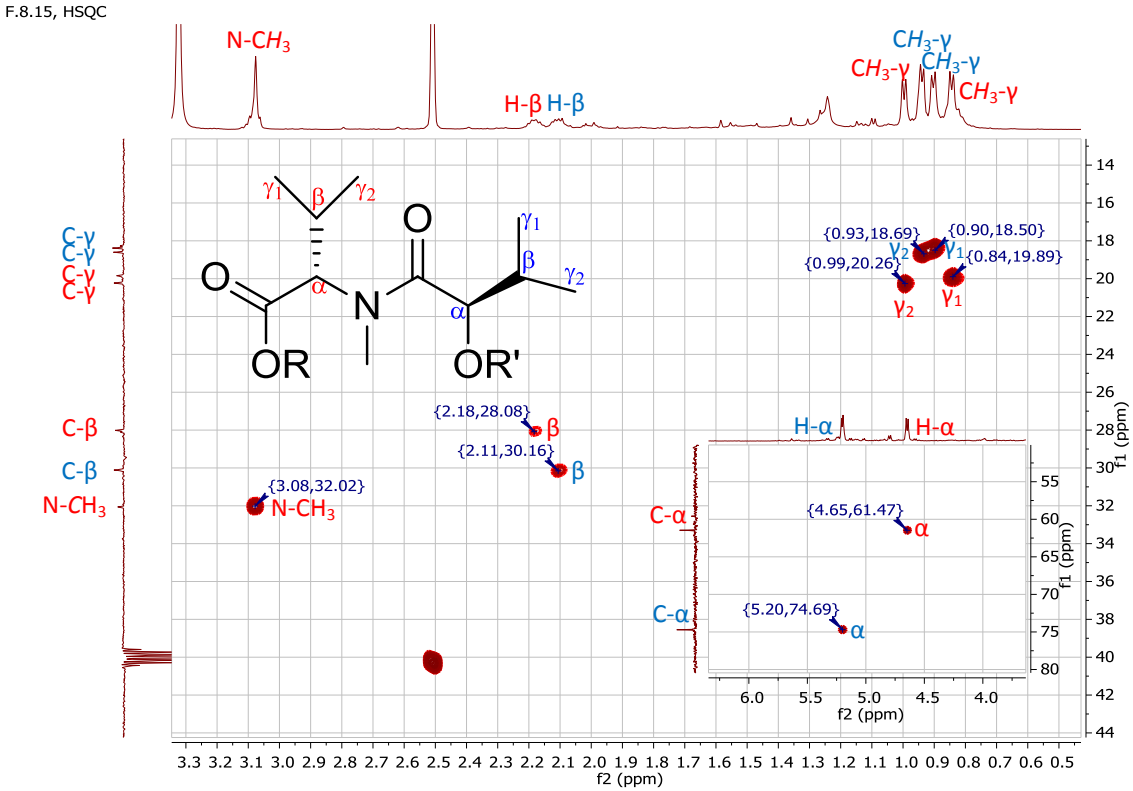

Figure A.XVI.4: ^{1}H-^{13}C HSQC NMR (600 MHz) spectrum for enniatin B, measured in DMSO-d_6. Red-labelled signals belong to the NMeVal moiety while blue-labelled signals belong to the Hylv moiety.

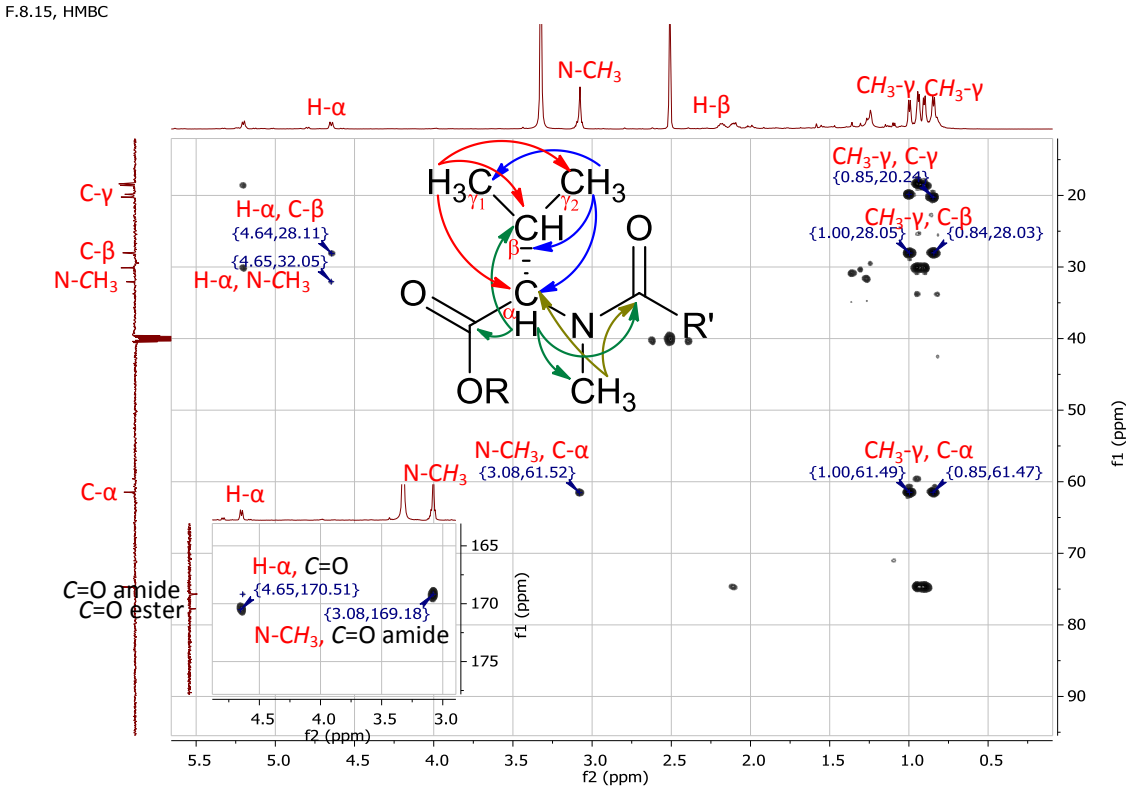

Figure A.XVI.5: ^{1}H-^{13}C HMBC NMR (600 MHz) spectrum for enniatin B, measured in DMSO-d_6. Red-labelled signals belong to the NMeVal moiety while blue-labelled signals belong to the Hylv moiety.